



Universitat Autònoma de Barcelona

ADVERTIMENT. L'accés als continguts d'aquesta tesi queda condicionat a l'acceptació de les condicions d'ús establertes per la següent llicència Creative Commons:  http://cat.creativecommons.org/?page_id=184

ADVERTENCIA. El acceso a los contenidos de esta tesis queda condicionado a la aceptación de las condiciones de uso establecidas por la siguiente licencia Creative Commons:  <http://es.creativecommons.org/blog/licencias/>

WARNING. The access to the contents of this doctoral thesis it is limited to the acceptance of the use conditions set by the following Creative Commons license:  <https://creativecommons.org/licenses/?lang=en>



Universitat Autònoma de Barcelona

**Evaluating inorganic nanoparticles in the
living organism *Caenorhabditis elegans***

Laura González Moragas

DOCTORAL THESIS

Doctoral Studies in Materials Science

Directors: Dr. Anna Roig and Dr. Anna Laromaine

Tutor: Dr. Gemma Garcia

Departament de Física,
Facultat de Ciències

2016

Dra. Anna Roig Serra, Investigadora Científica del CSIC, la **Dra. Anna Laromaine Sagué**, Investigadora Científica del CSIC, i la **Dra. Gemma Garcia Alonso**, Professora de la UAB

CERTIFIQUEN:

Que la Laura González Moragas, Graduada en Farmàcia per la Universitat de Barcelona, ha dut a terme aquesta tesis doctoral sota la seva direcció i que porta per títol “Evaluating inorganic nanoparticles in the living organism *Caenorhabditis elegans*”, la qual queda recollida en aquesta memòria per optar al grau de Doctor en Ciència en el Programa de Ciència de Materials amb Menció Internacional.

I perquè així consti, signen el present certificat

Dra. Anna Roig

Dra. Anna Laromaine

Dra. Gemma Garcia

Bellaterra, 19 de Setembre 2016

*Als meus pares Elisabet i Raimundo
i al meu estimat marit Alfonso.*

“Equipped with his five senses,
man explores the universe around him
and calls the adventure Science.”

Edwin Powell Hubble,
American astronomer

Acknowledgements

Before 2012, the year I graduated in Pharmacy at the Universitat de Barcelona, I was not aware of the possibility of pursuing a PhD. Pharmacy has a long list of “appealing” job positions to apply for: in pharmacies, hospitals, laboratories, “big pharma” companies, etc. I guess this is the reason why we were not very encouraged to pursue any further studies other than Master’s degrees. During my research into ‘what next?’ after my degree, I fulfilled my desire of working in the pharmaceutical industry first as an intern and then securing a job position, but I did never meet my desire of researching into biomedicine, which was actually my very initial motivation for enrolling in Pharmacy. Hence, I decided to look for a PhD position in a field that complemented my knowledge on health sciences with a more technical focus. Nanotechnology seemed to meet all the requirements. I contacted several groups and was really keen on Dr. Anna Roig’s group from the very beginning. The project that Anna Roig and Anna Laromaine proposed sounded very exciting and challenging, the perfect combination between biology and materials science that I was looking for. Moreover, I was really impressed by their CVs and international experience. I really want to thank both Annas for their great support since I first contacted them and throughout all this time. Their balance of patience, ambition, focus on quality and orientation to results helped me to progress in my research and also in my personal life. I also have to thank previous colleagues from ICMAB who I really miss these days and who I shared many memorable moments with: Elisa, Muling, Maria, Nerea, Wojtek, Pengfei, Siming, Rafa, Raluca, Elizabeth, Dejan, Laura; and my current ICMAB colleagues: Anna May, Roxana, Cica, Cristiano, Mengdi, Jike, Qhianze, Ivan, Deyaa...

I would like to thank our collaborators: Dr. Yannick Schwab from EMBL and his great Electron Microscopy team; Dr. Stephen Stürzenbaum from KCL and the kind members of the Toxicogenomics group, who welcomed and helped me during a 3-month stay in his lab; Dr. Romain Quidant and his group at ICFO for their collaboration and support; Dr. Jesús de la Fuente and his group at INA-UNIZAR for their interest in the hyperthermia experiments in *C. elegans*; and Dr. Lorenzo Albertazzi from IBEC for his motivation to combine our expertise. I also thank all the other ‘worm’ labs with who we have been in touch during these years (Cerón lab from IDIBELL, Marta Artal lab from CABD, Natascia Ventura lab from IUF, Juan Cabello lab from CIBIR, Esther Dalfo lab from UAB...).

I would also like to acknowledge my previous colleagues and bosses from Laboratorios Salvat, especially Albert, Lourdes, Xavier and Daniel. They advised me to leave the company and undertake a PhD so I could progress in my professional career. Their support comforted me when I still had some doubts about whether to go for the PhD adventure or to stay in the industry.

Above all, I have to thank my beloved husband Alfonso and my dear parents Elisabet and Raimundo for their patience, support and true love. *Us mereixeu molt més que 'quatre ratlles'. Avui jo no estaria aquí sense vosaltres, no seria qui sóc sense vosaltres.*

Finally, I acknowledge the funding sources during these years: the 4-year PhD fellowship Formación al Profesorado Universitario 2012 (ref. FPU12/05549) awarded by the Spanish Ministry of Education and Culture; the following travel grants: Estancias breves FPU 2015 (ref. EST15/00188) awarded by the Spanish Ministry of Education and Culture; Christian Boulton Fellowship 2015 awarded by EMBL; and Short Term Scientific Mission (ECOST-STSM-BM1408-301115-070015) awarded by the GENIE COST Action BM1408. I was also privileged with a travel grant to attend the 64th Lindau Nobel Laureate Meeting in Physiology/Medicine 2014 and a summer school at UIMP (Santander) in 2014.

Foreword and aim of this thesis

In the last decades, a range of nano-sized materials have been approved by the regulatory agencies worldwide to be commercialized as drugs, contrast agents for medical imaging or medical devices. Many other nanomaterials are currently under clinical investigation. In general, these materials are well-characterised regarding their physicochemical properties; however their biological evaluations tend to be delayed as they require the transition from the chemical to the biological laboratory. A preliminary biological screening within the synthetic laboratory of the nanomaterial being developed could provide initial biological data very quickly, with special focus on the biocompatibility of the material and the suitability of its design for a particular application. Upon collection of this worthy information, material scientists could optimize the material's design and investigate the effects of its modifications. With this purpose, it is required to find a biological system whose maintenance requirements can be met in any synthetic lab.

Initial biological experiments are usually performed using cell cultures; however they demand a rather complex infrastructure and hence dedicated labs are required. In contrast, simple model organisms such as zebra fish, the fruit fly *Drosophila* or the tiny worm *Caenorhabditis elegans* (*C. elegans*) can be easily grown in synthetic laboratories. Among them, *C. elegans* has been long used to study development and the nervous system; however it is also highly promising in toxicology, to validate drug targets, to study biochemical pathways, and even to model human metabolic and neurodegenerative diseases. Hence, *C. elegans* holds great potential in many fields. Moreover, *C. elegans* shows significant advantages compared to cells. As a multicellular organism, it is more physiologically relevant and its body offers a three-dimensional biological space where interactions with the nanomaterials occur and can be studied. In contrast, most cell culture assays are performed using monolayers (2D assays). The complex anatomy of the *C. elegans*, which is composed of ~1000 cells, also allows us studying the transport of nanomaterials across biological barriers (i.e. the intestine or the dermis) and the mechanisms responsible for such NP crossing. These possibilities open avenues to easily investigate routes of administration of nano-drugs other than the intravenous route, in particular using the *C. elegans* intestine as a model to study oral delivery. Furthermore, *C. elegans* is also a very interesting system to perform molecular biology studies and also allows scientists to study whether the toxicity mechanisms of NPs that have been reported in cells are conserved in whole organisms.

In 2013, we implemented in our chemical laboratory at the Institut de Ciència de Materials de Barcelona (ICMAB-CSIC) a facility to host and grow *C. elegans* consisting on a laminar flow cabinet, a stereoscope, an incubator and a nutating rotator. We were approved to use this model organism in the Institute and worked in compliance with the waste disposal regulations for biological waste. Our main purpose was to use *C. elegans* as an *in vivo* biological system to monitor NPs with biomedical uses in a living organism

with complex anatomy. Previous work in the field of *C. elegans* and NPs had been mainly done by biologists focusing on the toxicological evaluation of the nanomaterial, with little attention to the nanomaterial status upon contact with *C. elegans* was reported. In contrast, we, as material scientists, were also interested in the study of NP status inside the body of *C. elegans* to correlate it with the biological effects observed. Some of our initial questions were: Do NPs enter the *C. elegans* body? By which entrance routes do they enter? Where are they located? Are they able to cross biological barriers? How many nanoparticles are ingested by the worm? Are they accumulated in the body or excreted? Do they aggregate inside *C. elegans*? Do they maintain their initial properties? Do the material properties (i.e. size, composition, surface properties) determine the biological effects of the material? During the development of this thesis we have tried to give answer to these questions.

This thesis aims to screen biomedical inorganic nanoparticles in the model organism *C. elegans* and to characterise their nano-bio interactions with special focus on the study of the material's properties *in vivo* including their status, uptake, fate, biological effects and mechanisms.

The specific objectives of this thesis were the following:

- 1- Review of previous studies of nanoparticles in *C. elegans* to define the state-of-the-art and to propose and adopt novel techniques to advance in the study of nano-bio interactions.
- 2- Synthesis and characterisation of in-house fabricated high quality superparamagnetic iron oxide nanoparticles with different surface coatings (citrate and bovine serum albumin) and gold nanoparticles of two different sizes (11 and 150 nm) using robust and scalable reactions.
- 3- Evaluation of the uptake, fate, metabolism, biological effects and molecular mechanisms of the as-synthesised nanoparticles in *C. elegans*.
- 4- Evaluation of the relevance of the initial properties of the nanoparticles (size, surface coating and composition) in their *in vivo* behaviour in *C. elegans*.

This thesis has been divided the following sections:

- *Chapter 1* introduces the applications of nanomaterials in medicine and describes the most widely used biological systems to screen those materials at early stages of development. Finally, it presents *C. elegans* as a model organism for nanoparticle assessment.
- *Chapter 2* reviews relevant literature of nanoparticle assessment in *C. elegans* and describes the potential of combining materials science and *C. elegans* in the study of nano-bio interactions.

- *Chapter 3* describes the properties and biomedical applications of iron oxide and gold nanoparticles, presents the synthetic routes used to produce nanoparticles, the characterisation of the as synthesised materials, and studies their colloidal stability in *C. elegans* media.
- *Chapter 4* includes the protocols adopted in this thesis to characterise the interaction between nanoparticles and *C. elegans*.
- *Chapter 5* contains a detailed study of the interaction between iron oxide nanoparticles and *C. elegans* combining toxicity assessments, materials science and imaging techniques, and gene expression analysis. The effect of NP coating (citrate *versus* bovine serum albumin) is explored.
- *Chapter 6* contains a detailed study of the interaction between gold nanoparticles and *C. elegans* combining toxicity assessments, materials science and imaging techniques, and gene expression analysis. The effect of NP size (11 nm *versus* 150 nm) and the effect of NP composition (gold *versus* iron oxide) are explored.
- *Chapter 7* summarises the main findings of this thesis and proposes some future work.
- *References* lists the journal articles, books, book chapters and other sources of information cited in the thesis.
- *Appendix 1* describes the protocols to maintain and grow *C. elegans*.
- *Appendix 2* presents preliminary trials using materials science techniques in *C. elegans*, not included in the main body of the thesis, and describes their potential.
- *Appendix 3* contains the primers and probe combinations used in the qPCR analysis.
- *CV and Publications* includes the curriculum vitae of the author and the list of publications resulting from this thesis.

Presentación y objetivos de la tesis

En las últimas décadas, agencias reguladoras de todo el mundo han aprobado la comercialización de varios materiales de tamaño nanométrico como medicamento, agente de contraste o producto sanitario. Actualmente hay una amplia variedad de nanomateriales en fase de investigación clínica. En general, estos materiales han sido bien caracterizados a nivel fisicoquímico, sin embargo los ensayos biológicos se suelen ver retrasados en el tiempo ya que requieren la transición desde el laboratorio químico al laboratorio biológico. Una caracterización preliminar del material dentro del mismo laboratorio donde se desarrolla podría proporcionar una información biológica inicial rápida, enfocada sobre todo a la biocompatibilidad del material y valorar la idoneidad de su diseño para una aplicación particular. Disponer de esta valiosa información permitiría a los científicos de materiales optimizar el diseño del material e investigar los efectos de sus modificaciones. Sin embargo, para lograr este propósito se necesita un sistema biológico que pueda ser conservado dentro del laboratorio químico.

En general, los ensayos biológicos iniciales se realizan usando cultivos celulares en laboratorios biológicos que disponen de una infraestructura más compleja. En cambio, existen organismos modelo simples como el pez cebra, la mosca *Drosophila* o el nematodo *Caenorhabditis elegans* (*C. elegans*) que pueden mantenerse fácilmente en el laboratorio sintético. Entre ellos, *C. elegans* ha sido ampliamente usado en el estudio del desarrollo y del sistema nervioso, y se considera muy prometedor en toxicología, para validar nuevos fármacos, estudiar rutas bioquímicas e incluso para modelizar enfermedades metabólicas y neurodegenerativas humanas. Es por todo ello que *C. elegans* ofrece un gran potencial en muchos campos. Además, presenta ventajas considerables respecto al uso de células. Como organismo pluricelular que es, presenta una relevancia fisiológica superior y su cuerpo ofrece un modelo biológico tridimensional donde estudiar la interacción con nanomateriales. En cambio, la mayoría de experimentos en células se realizan usando monocapas, es decir, en 2D. La anatomía de *C. elegans*, formada por unas 1000 células, también facilita el estudio de los mecanismos de transporte de nanomateriales a través de barreras biológicas como el intestino o la dermis). Estas posibilidades permiten investigar rutas de administración de nanomedicinas diferentes de la administración intravenosa, en concreto, usando el intestino *C. elegans* como un modelo para el estudio de la vía oral. Asimismo, *C. elegans* también resulta un sistema muy interesante para estudios de biología molecular y permite estudiar si los mecanismos de toxicidad de nanopartículas reportados en células están conservados en organismos completos.

En 2013 implementamos en nuestro laboratorio químico en el Institut de Ciència de Materials de Barcelona (ICMAB-CSIC) una instalación para mantener y crecer *C. elegans*. En concreto, adquirimos una cabina de flujo laminar, un estereoscopio, un incubador y un agitador. Un comité del CSIC aprobó el uso de este organismo modelo en

el instituto en cumplimiento con las normas específicas de eliminación de residuos biológicos. Nuestro principal objetivo era usar *C. elegans* como un sistema biológico *in vivo* para evaluar nanopartículas con finalidades biomédicas en un organismo simple. La mayoría de estudios previos realizados en el campo de *C. elegans* y NPs habían sido realizados por biólogos y con mayor énfasis en la evaluación toxicológica del nanomaterial, prestando menor atención al estado de los nanomateriales en contacto con *C. elegans*. En cambio, nosotras como científicas de materiales estamos muy interesadas en caracterizar el estado de las nanopartículas dentro del cuerpo del gusano para intentar correlacionarlo con los efectos observados. Algunas de nuestras preguntas iniciales eran: ¿Entran las NPs al cuerpo de *C. elegans*? ¿Cuál es la vía de entrada? ¿Dónde se localizan las NPs dentro del gusano? ¿Son capaces de cruzar barreras biológicas? ¿Cuántas nanopartículas son ingeridas? ¿Las NPs se acumulan en el cuerpo del gusano o son excretadas? ¿Se agregan dentro del *C. elegans*? ¿Se mantienen sus propiedades iniciales? ¿Influyen las propiedades del material (ej. tamaño, composición, propiedades de superficie) en los efectos *in vivo*? Durante el desarrollo de esta tesis hemos tratado de dar respuesta a estas cuestiones.

El objetivo de esta tesis es evaluar nanopartículas inorgánicas en el organismo modelo *C. elegans* y caracterizar *in vivo* la interacción nano-bio centrándonos especialmente en las propiedades del material incluyendo su estado, ingesta y localización, y sus efectos y mecanismos biológicos.

Los objetivos específicos de esta tesis son los siguientes:

- 1- Revisar estudios previos de nanopartículas en *C. elegans* para definir el punto de partida de la tesis y proponer y adoptar nuevas técnicas para avanzar en el campo de las nano-bio interacciones.
- 2- Sintetizar y caracterizar nanopartículas inorgánicas de alta calidad de óxido de hierro con diferentes recubrimientos superficiales (citrato y albúmina sérica bovina) y nanopartículas de oro de dos tamaños diferentes (11 y 150 nm) empleando reacciones sintéticas robustas y escalables.
- 3- Evaluar la ingesta, la localización, el metabolismo y los efectos biológicos y mecanismos moleculares de las nanopartículas sintetizadas en *C. elegans*.
- 4- Estudiar la importancia de las propiedades iniciales de las nanopartículas (tamaño, recubrimiento superficial y composición) en su comportamiento *in vivo* en *C. elegans*.

Esta tesis se divide en los siguientes apartados:

- El *Capítulo 1* introduce las aplicaciones de los nanomateriales en medicina y describe los sistemas biológicos más utilizados para evaluar nuevos materiales en las fases iniciales de desarrollo. Finalmente, se presenta *C. elegans* como organismo modelo para la evaluación de nanopartículas.

- El *Capítulo 2* revisa bibliografía relevante de investigación de nanopartículas en *C. elegans* y describe el potencial de combinar la ciencia de materiales con *este organismo modelo* para el estudio de la interacción nano-bio.
- El *Capítulo 3* describe las propiedades y las aplicaciones biomédicas de las nanopartículas de óxido de hierro y de oro, y presenta los procedimientos sintéticos usados para su fabricación en nuestro laboratorio, su caracterización y estudios de estabilidad coloidal en medios para *C. elegans*.
- El *Capítulo 4* presenta los protocolos adoptados en esta tesis para estudiar la interacción entre las nanopartículas y *C. elegans*.
- El *Capítulo 5* contiene un estudio detallado de la interacción de las nanopartículas de óxido de hierro con *C. elegans* combinando ensayos de toxicidad, técnicas de ciencia de materiales y de imagen, y análisis de la expresión génica. Asimismo, se investiga el efecto del recubrimiento superficial (citrato *versus* albúmina sérica bovina).
- El *Capítulo 6* contiene un estudio detallado de la interacción de las nanopartículas de oro con *C. elegans* combinando ensayos de toxicidad, técnicas de ciencia de materiales y de imagen, y análisis de la expresión génica. Asimismo, se investiga el efecto del tamaño (11 nm *versus* 150 nm) y el efecto de la composición (oro *versus* óxido de hierro).
- El *Capítulo 7* resume los principales hallazgos de esta tesis y propone futuros experimentos para complementar los resultados presentes.
- Las *Referencias* listan los artículos de revista, los libros, los capítulos de libros y demás fuentes de información utilizadas en esta tesis.
- El *Apéndice 1* describe los protocolos usados para mantener y crecer *C. elegans*.
- El *Apéndice 2* presenta ensayos preliminares del empleo de técnicas experimentales de ciencia de materiales en *C. elegans*, no incluidos en capítulos anteriores, y describe su potencial.
- El *Apéndice 3* contiene los cebadores y las combinaciones de sondas usados en los experimentos de qPCR.
- El *CV y Publicaciones* incluye el currículum vitae del autor y la lista de publicaciones resultantes de esta tesis.

Presentació i objectius de la tesi

En les darreres dècades, agències reguladores d'arreu del món han aprovat la comercialització de diversos materials de mida nanomètrica per ús com a medicament, agent de contrast o producte sanitari. Actualment hi ha una àmplia varietat de nanomaterials en fase d'investigació clínica. En general, aquests materials estan ben caracteritzats a nivell fisicoquímic però la seva avaluació biològica es sol retardar en el temps ja que requereix la transició des del laboratori químic al biològic. Una caracterització preliminar del material dins del mateix laboratori on s'està desenvolupant proporcionaria una informació biològica inicial molt ràpida, enfocada sobretot a l'estudi de la biocompatibilitat del material i a avaluar la idoneïtat del seu disseny per la funció a complir. Disposar d'aquesta valuosa informació permetria als científics de materials optimitzar el disseny del material i investigar els efectes de les seves modificacions. Per tal d'aconseguir això, no obstant, es requereix un sistema biològic fàcil de mantenir dins el laboratori de síntesi química.

En general, els assajos biològics inicials es realitzen en cultius cel·lulars en laboratoris biològics dedicats que disposen d'una infraestructura complexa. En canvi, hi ha organismes model simples como el peix zebra, la mosca *Drosophila* o el nematode *Caenorhabditis elegans* (*C. elegans*) amb pocs requeriments de manteniment que es poden tenir en el laboratori sintètic. Entre ells, *C. elegans* ha estat àmpliament utilitzat en l'estudi del desenvolupament i del sistema nerviós, i es considera molt prometedor en toxicologia, per validar nous fàrmacs, estudiar rutes bioquímiques i fins i tot per modelitzar malalties metabòliques i neurodegeneratives humanes. Per tot això, *C. elegans* ofereix un gran potencial en molts àmbits. A més, *C. elegans* presenta considerables avantatges respecte els experiments en cultius cel·lular. Com organisme pluricel·lular, presenta una rellevància fisiològica superior y el seu cos ofereix un model biològic tridimensional on estudiar la interacció amb nanomaterials. En canvi, la majoria d'experiments amb cèl·lules es realitzen usant monocapes, és a dir, en 2D. L'anatomia diferenciada de *C. elegans*, formada per unes 1000 cèl·lules, facilita també l'estudi dels mecanismes de transport dels nanomaterials a través de barreres biològiques (ex. a través de l'intestí o la dermis). Aquestes possibilitats permeten investigar rutes d'administració de nanomedicaments diferents de l'administració intravenosa, en concret utilitzant l'intestí de *C. elegans* com un model per l'estudi de la via oral. Així mateix, *C. elegans* també resulta un sistema molt interessant per estudis de biologia molecular i permet estudiar si els mecanismes de toxicitat de nanopartícules reportats en cèl·lules es troben conservats en organismes sencers.

El 2013 vam implementar en el nostre laboratori químic a l'Institut de Ciència de Materials de Barcelona (ICMAB-CSIC) una instal·lació per mantenir i créixer *C. elegans*. Concretament, vam adquirir una cabina de flux laminar, un estereoscopi, un incubador i un agitador. Un comitè del CSIC va aprovar l'ús d'aquest organisme model a l'institut,

complint amb les normes d'eliminació de residus biològics. El nostre principal objectiu era utilitzar *C. elegans* com un sistema biològic per avaluar nanopartícules amb finalitats biomèdiques *in vivo* en un organisme senzill d'anatomia diferenciada. La majoria d'estudis previs realitzats en el camp de *C. elegans* i NPs havia estat realitzat per biòlegs i es centraven en l'avaluació toxicològica del nanomaterial, amb poc èmfasi en l'estat dels nanomaterials en contacte amb *C. elegans*. En canvi nosaltres, com a científiques de materials que som, estem molt interessades en caracteritzar l'estat de les nanopartícules dins el cos del cuc per intentar-lo correlacionar amb els efectes observats. Entre les preguntes que ens van sorgir inicialment, trobem: Entren les NPs al cos de *C. elegans*? Quina és la via d'entrada? On es localitzen dins del cuc? Són capaces de creuar barreres biològiques? Quantes nanopartícules ingereixen? Les NPs s'acumulen en el cos del cuc o són excretades? S'agreguen dins de *C. elegans*? Es mantenen les seves propietats inicials? Influeixen les propietats del material (ex. mida, composició, propietats de superfície) en els efectes *in vivo*? Durant el desenvolupament d'aquesta tesi hem intentat donar resposta a aquestes qüestions.

L'objectiu d'aquesta tesi és avaluar nanopartícules inorgàniques en l'organisme model *C. elegans* i caracteritzar la interacció nano-bio centrant-nos especialment en les propietats del material *in vivo* incloent el seu estat, la seva ingesta, la seva localització i els seus efectes i mecanismes biològics.

Els objectius específics d'aquesta tesi són els següents:

- 1- Revisar estudis previs de nanopartícules en *C. elegans* per definir el punt de partida de la tesi i proposar i adoptar noves tècniques per avançar en el camp de les interaccions nano-bio.
- 2- Sintetitzar i caracteritzar nanopartícules inorgàniques d'alta qualitat d'òxid de ferro amb diferents recobriments superficials (citrat i albúmina sèrica bovina) i nanopartícules d'or de dues mides diferents (11 i 150 nm) a través de reaccions sintètiques robustes i escalables.
- 3- Avaluar la ingesta, la localització, el metabolisme i els efectes biològics i mecanismes moleculars de les nanopartícules sintetitzades en *C. elegans*.
- 4- Estudiar la importància de les propietats inicials de les nanopartícules (mida, recobriment superficial i composició) en el seu comportament *in vivo* en *C. elegans*.

Aquesta tesi es divideix els següents apartats:

- El *Capítol 1* introdueix les aplicacions dels nanomaterials en medicina, i descriu els sistemes biològics més emprats per avaluar nous materials en les fases inicials de desenvolupament. Finalment, es presenta *C. elegans* com a organisme model per l'avaluació de nanopartícules.

- El *Capítol 2* revisa bibliografia rellevant d'investigació de nanopartícules en *C. elegans* i descriu el potencial de combinar la ciència de materials amb *aquest organisme* per l'estudi de la interacció nano-bio.
- El *Capítol 3* descriu les propietats i les aplicacions biomèdiques de les nanopartícules d'òxid de ferro i d'or, i presenta els procediments sintètics usats per la seva obtenció en el nostre laboratori, la seva caracterització i estudis d'estabilitat col·loïdal en medis per *C. elegans*.
- El *Capítol 4* presenta els protocols emprats en aquesta tesi per estudiar la interacció entre les nanopartícules i *C. elegans*.
- El *Capítol 5* conté un estudi detallat de la interacció de les nanopartícules d'òxid de ferro amb *C. elegans* combinant assajos de toxicitat, tècniques de ciència de materials i d'imatge, i anàlisis de l'expressió gènica. També s'investiga l'efecte del recobriment superficial (citrat *versus* albúmina sèrica bovina).
- El *Capítol 6* conté un estudi detallat de la interacció de les nanopartícules d'or amb *C. elegans* combinant assajos de toxicitat, tècniques de ciència de materials i d'imatge, i anàlisis de l'expressió gènica. També s'investiga l'efecte de la mida (11 nm *versus* 150 nm) i de la composició (or *versus* òxid de ferro).
- El *Capítol 7* resumeix les principals troballes d'aquesta tesi i proposa experiments futurs per complementar els resultats obtinguts.
- Les *Referències* llisten els articles de revistes, llibres, capítols de llibres i altres fonts d'informació utilitzades en aquesta tesi.
- L'*Apèndix 1* descriu els protocols usats per mantenir i créixer *C. elegans*.
- L'*Apèndix 2* presenta resultats preliminars fent servir tècniques experimentals de ciència de materials en *C. elegans*, no inclosos en capítols anteriors, i descriu el seu potencial.
- L'*Apèndix 3* conté els encebadores i les combinacions de sondes utilitzades en els experiments de qPCR.
- El *CV i Publicacions* inclou el currículum vital del autor i el llistat de publicacions resultants d'aquesta tesi.

Attributions

I would like to thank the people who contributed to this thesis:

- Dr. Elisa Carezza, Dr. Siming Yu and Víctor Fuentes (ICMAB-CSIC) provided me most of the nanoparticles used in this thesis and taught me how to synthesise them.
- Gökay Avcı (Sabancı University, Istanbul) collaborated in the experiments of gradient centrifugation during his short stay in our group as part of his MSc thesis.
- Dr. Judit Oró (ICMAB-CSIC) performed TEM visualization of the in-house fabricated nanoparticles.
- Dr. Belén Ballesteros and Pablo Garcia (ICN2) performed HAADF STEM observations and SAED and EELS analysis of *C. elegans* cross-sections.
- The Electron Microscopy Core Facility (EMBL), led by Dr. Schwab, performed the laser etching and sectioning of the *C. elegans* ultrathin sections for TEM visualization.
- Dr. Ignasi Villarroya (Servei d'Anàlisi Química, UAB) performed the chemical analysis for the determination of nanoparticle uptake.
- Dr. Bernat Bozzo (ICMAB-CSIC) carried out the magnetometry experiments.
- Dr. Sílvia Lope (Servei de Resonància Magnètica, UAB) performed the MRI experiments.
- Dr. Romain Quidant, Dr. Pascal Berto and Dr. Clara Vilches (ICFO) collaborated in the absorbance micro-spectroscopy analysis and in the two-photon luminescence microscopy study.
- The group of Dr. Stephen Stürzenbaum (KCL) collaborated in the transcriptomic analysis by qPCR and microarrays.
- The Genomics Center (KCL) performed the microarray experiments.
- The group of Dr. Conxita Solans (ICAQ-CSIC) collaborated in the CytoViva visualizations.
- The group of Dr. Jesús de la Fuente (INA-UNIZAR) performed the hyperthermia trials.

List of abbreviations

%(w/w)	%(weight/weight)
AEMPS	Agencia Española de Medicamentos y Productos Sanitarios
ASTM	American Society for Testing and Materials
ATPS	Aqueous Two-Phase Systems
Au	Gold
Au-NPs	Gold nanoparticles
BSA	Bovine serum albumin
CB	Citrate buffer at pH 4.6
cDNA	Complementary DNA
CGC	<i>Caenorhabditis</i> Genetics Center
CSIC	Consejo Superior de Investigación Científica
CT	Computed Tomography
NIR	Near Infrared
DLS	Dynamic Light Scattering
DMEM	Dulbecco's Modified Eagle's Medium
DNA	Deoxyribonucleic acid
EDX	Energy-Dispersive X-ray Spectroscopy
EELS	Electron Energy Loss Spectroscopy
EMA	European Medicine Agency
EMBL	European Molecular Biology Laboratory
ER	Endoplasmic Reticulum
FBS	Fetal bovine serum
FDA	Food and Drug Administration
Fe(acac) ₃	Iron acetylacetonate
Fe ₃ O ₄	Magnetite
HA	Humic Acid
HAADF STEM	High-Angle Annular Dark-Field Scanning TEM
HDFM	Hyperspectral Dark Field Microscopy
HPF	High Pressure Freezing
HTS	High Throughput Screening
ICH	International Council for Harmonisation of Drug Registration
ICMAB	Institut de Ciència de Materials de Barcelona
ICN2	Institut Català de Nanociència i Nanotecnologia
ICP-MS	Inductively Coupled Plasma Mass Spectrometry
ISO	International Organization for Standardization
KCL	King's College London
L1	First larval stage of <i>C. elegans</i>
L4	Last larval stage of <i>C. elegans</i>
LB	Luria-Bertani (LB) broth
LM	Light Microscopy
M(H)	Magnetic moment over applied field
M9	M9 buffer
MEM	Minimum Essential Medium Eagle
M _R	Remanence Magnetization
MRI	Magnetic Resonance Imaging
M _s	Saturation Magnetization
MW	Microwave
Na ₃ Cit	Trisodium citrate dihydrate
NGM	Nematode Growth Media agar
nm	Nanometer
NMs	Nanomaterials
NPs	Nanoparticles
OM	Optical Microscopy
PB	Prussian Blue staining
PBS	Phosphate Buffered Saline
PEG	Polyethyleneglycol
PFA	Paraformaldehyde

PQ	Paraquat (or Methyl viologen dichloride)
PS	Polystyrene
qPCR	Quantitative Polymerase Chain Reaction
R&D	Research and Development
r_1	Longitudinal relaxivity or spin-lattice relaxivity
r_2	Transversal relaxivity or spin-spin relaxivity
RNA	Ribonucleic acid
ROS	Reactive Oxygen Species
RPMI	Roswell Park Memorial Institute Medium
SAED	Selected Area Electron Diffraction
SEM	Scanning Electron Microscopy
SPIONs	Superparamagnetic iron oxide nanoparticles
SPR	Surface Plasmon Resonance
T_1	Longitudinal relaxation time
T_2	Transverse relaxation time
T_B	Blocking temperature
TEM	Transmission electron microscope
UAB	Universitat Autònoma de Barcelona
UV-Vis	Ultraviolet–visible spectroscopy
W	Watts
wt. %	Weight%
XANES	X-ray Absorption Near Edge Structure
ZFC-FC	Zero-Field-Cooled/Field-Cooled
ZP	Zeta Potential
γ - Fe_2O_3	Maghemite
τ_B	Brown relaxation time
τ_N	Neel relaxation time
μ -SRXRF	Synchrotron Radiation X-ray Fluorescence

Table of contents

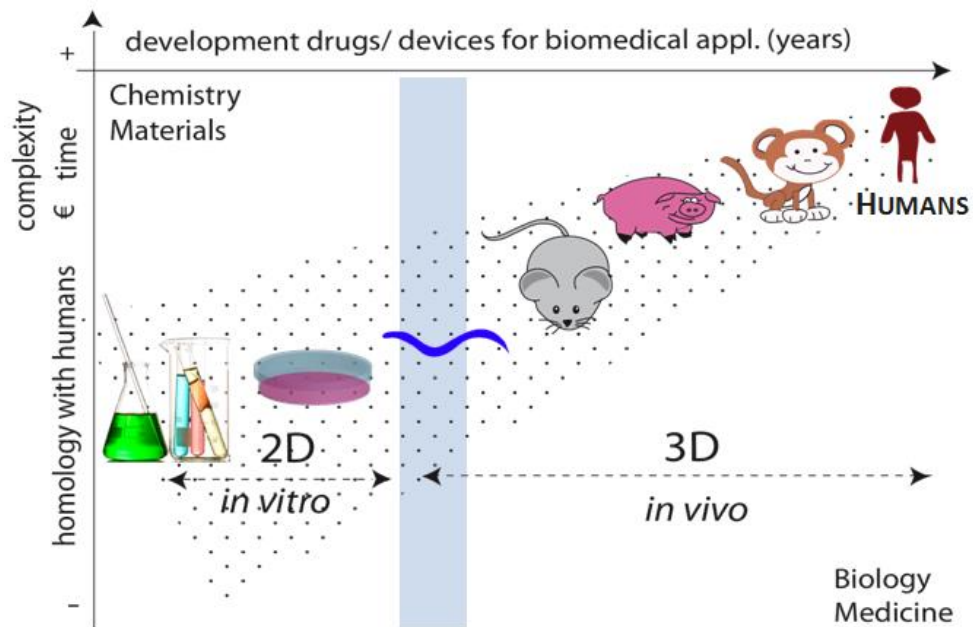
Acknowledgements	i
Foreword and aim of this thesis	iii
Presentación y objetivos de la tesis	vii
Presentació i objectius de la tesi	xi
Attributions	xv
List of abbreviations	xvii
Table of contents	xix
CHAPTER 1. Introduction to Nanomedicine and Nano-bio interactions	1
1.1 Nanotechnology and Nanomedicine	3
1.1.1 Nanotechnology: General concepts	3
1.1.2 Nanomaterials for medicine	3
1.2 Current status of nanomedicine	7
1.2.1 Timescale of nanomedicine research	7
1.2.2 Therapeutic area of nanomedicine products.....	8
1.2.3 Route of administration of nanomedicine products.....	8
1.2.4 Future perspectives.....	10
1.3 Synthesis and characterisation of nanomaterials for biomedicine	10
1.3.1 Considerations regarding material synthesis	10
1.3.2 Physicochemical characterisation	11
1.3.3 Biological evaluation of NPs.....	13
1.4 C. elegans as a model organism for NP assessment.....	20
1.4.1 Origin of the specie	21
1.4.2 Establishment as a model organism	21
1.4.3 Key experimental features of <i>C. elegans</i>	22
1.4.4 Anatomical features	24
1.4.5 Regulatory use of <i>C. elegans</i>	28
1.5 Thesis framework.....	28
CHAPTER 2. NP evaluation in C. elegans: State-of-the-art	31
2.1 NP evaluation in C. elegans: State-of-the-art	33
2.1.1 Biological role of metals in <i>C. elegans</i>	33
2.1.2 Classification of previous work.....	34
2.1.3 Importance of the exposure mode	36
2.1.4 Entrance route, biodistribution and uptake	41
2.1.5 Dermal effects	44
2.1.6 Reprotoxicity effects.....	45
2.1.7 Importance of NP size, surface properties and composition	45
2.1.8 Endocytosis and translocation pathways	48
2.1.9 Biological mechanisms triggered by NP exposure	48
2.2 Materials science techniques with potential to assess nano-bio interactions	55
2.3 Chapter conclusions.....	57

CHAPTER 3. Synthesis and characterisation of in-house fabricated SPIONs and Au-NPs.....	59
3.1 Overview.....	61
3.2 Introduction to the properties and applications of superparamagnetic iron oxide nanoparticles in nanomedicine	62
3.2.1 Applications of SPIONs	63
3.2.2 Current status of clinical applications	65
3.3 Synthesis and characterisation of superparamagnetic citrate and BSA-coated iron oxide nanoparticles.....	65
3.3.1 Synthesis by microwave-assisted thermal decomposition	65
3.3.2 BSA adsorption protocol.....	67
3.3.3 Scale-up of SPION synthesis	68
3.4 Introduction to the properties and applications of Au- NPs in nanomedicine	71
3.4.1 Applications of Gold Nanoparticles	71
3.4.2 Current status of clinical applications	74
3.5 Synthesis and characterisation of gold nanoparticles	75
3.5.1 Synthesis of 11-nm Au-NPs	75
3.5.2 Seeded growth to 150-nm Au-NPs	75
3.5.3 Characterisation	76
3.6 Comparison of as synthesised SPIONs and Au-NPs	77
3.7 Evaluation of <i>C. elegans</i> exposure conditions for in-house inorganic NPs	77
3.8 Chapter conclusions	80
CHAPTER 4. Protocols used to characterise the nano-bio interaction	81
4.1 Introduction.....	83
4.2 Worm exposure	83
4.3 Analysis of toxicity endpoints	84
4.4 Uptake of NPs in <i>C. elegans</i>.....	85
4.4.1 Sample preparation	85
4.4.2 Magnetometry	85
4.4.3 Chemical analysis by ICP-MS	86
4.4.4 Magnetic Resonance Imaging.....	86
4.5 Biodistribution of NPs	86
4.5.1 Optical microscopy	86
4.5.2 SEM-EDX analysis	88
4.5.3 TEM analysis of targeted cross-sections	89
4.6 NP status inside <i>C. elegans</i>	91
4.6.1 Magnetometry	91
4.6.2 Absorbance micro-spectroscopy.....	91
4.6.3 Recovery of ingested nanoparticles from treated worms	92
4.6.4 Induction of NP-excretion in treated worms	92
4.7 Biological mechanisms	92
4.7.1 Gene expression profiling analysis	92
4.8 Statistical analysis	96
4.9 Chapter conclusions	96

CHAPTER 5. Evaluation of SPIONs using the <i>in vivo</i> model <i>C. elegans</i>. The effect of NP coating.....	99
5.1 Overview	101
5.2 Analysis of toxicity endpoints	101
5.3 Uptake of NPs in <i>C. elegans</i>.....	104
5.3.1 Magnetometry	104
5.3.2 Chemical analysis	106
5.4 Biodistribution of SPIONs	107
5.4.1 Optical microscopy.....	107
5.4.2 Electron microscopy (EM).....	109
5.5 NP status inside <i>C. elegans</i>.....	114
5.5.1 Magnetic characterisation of treated worms	115
5.5.2 Nanoparticle size inside <i>C. elegans</i>	115
5.5.3 Evaluation of NP excretion.....	116
5.5.4 Comparison with in vitro experiments	117
5.6 Biological mechanisms	119
5.6.1 Effects of citrate and BSA	119
5.6.2 Effects of iron ions.....	120
5.6.3 Gene expression analysis.....	121
5.7 Chapter conclusions.....	136
CHAPTER 6. Evaluation of gold nanoparticles and <i>C. elegans</i>. The effect of NP size and composition.	139
6.1 Analysis of toxicity endpoints	141
6.2 Uptake of NPs in <i>C. elegans</i>.....	143
6.3 Biodistribution of Au-NPs	144
6.3.1 Optical microscopy.....	144
6.3.2 Electron microscopy.....	147
6.4 NP status inside <i>C. elegans</i>.....	150
6.4.1 Nanoparticle size inside <i>C. elegans</i>	150
6.4.2 Aggregation status and optical characterisation	151
6.4.3 Evaluation of NP excretion.....	153
6.4.4 Comparison with in vitro experiments	153
6.5 Biological mechanisms	154
6.5.1 Gene expression analysis of 11-nm Au-NP treated <i>C. elegans</i>	154
6.5.2 Comparison of the effects of 11-nm Au-NPs and 6-nm SPIONs	157
6.6 Chapter conclusions.....	158
6.6.1 Effects of composition	160
CHAPTER 7. Conclusions and future work	161
7.1 Conclusions.....	163
7.2 Conclusiones.....	167
7.3 Conclusiones.....	171
7.4 Future work.....	175
7.4.1 Future experiments	175
7.4.2 Challenges and Prospects	176
THESIS REFERENCES.....	179

APPENDIX 1. Working with <i>C. elegans</i> in the synthetic laboratory	193
1.1 Set-up of the <i>C. elegans</i> facility in a Materials Science laboratory.....	195
1.1.1 Equipment	195
1.1.2 Working under sterile conditions	195
1.2 Maintenance of <i>C. elegans</i>	196
1.2.1 Obtaining <i>C. elegans</i>	196
1.2.2 Preparation of Nematode Growth Media (NGM).....	196
1.2.3 Preparation of the bacterial food source	197
1.2.4 Transference of worms.....	198
1.2.5 Freezing bacteria stocks	198
1.2.6 Freezing worm stocks	199
1.2.7 Preparation of other Media (M9 Buffer, S Basal, K-medium).....	199
1.2.8 Bleaching for cleaning and synchronizing worms	199
1.2.9 Obtaining the desired worm population.....	200
APPENDIX 2. Open avenues between <i>C. elegans</i> and the nano-world	201
2.1 Introduction.....	203
2.2 Promising techniques for future work	203
2.2.1 Magnetic separation	203
2.2.2 Magnetic Resonance Imaging.....	203
2.2.3 Hyperthermia.....	204
2.2.4 Fluorescence microscopy.....	205
2.2.5 Gradient centrifugation to study stress responses	206
2.3 Chapter conclusions	207
APPENDIX 3. Primers and probe combinations of qPCR analysis	209
3.1 Primers (and probe combination) already available in the lab.....	211
3.2 Primers (and probe combination) designed during my stay	214
3.3 Primers (and probe combination) designed for the validation of the microarrays	221
CV and Publications.....	227
Curriculum vitae	228
Publications	231

CHAPTER 1. Introduction to Nanomedicine and Nano-bio interactions



CHAPTER SUMMARY

This chapter includes some basic concepts of nanotechnology and nanomedicine. It also presents the importance of the physicochemical characterisation of novel nanomaterials intended for biomedical uses and describes the approaches traditionally used for their initial biological evaluation. Finally, I present the model organism *Caenorhabditis elegans* as an alternative animal model to host in synthetic laboratories for NP assessment, describe its key experimental features and highlight its advantages over other models.

CHAPTER INDEX

1.1 Nanotechnology and Nanomedicine	3
1.1.1 Nanotechnology: General concepts	3
1.1.2 Nanomaterials for medicine.....	3
1.2 Current status of nanomedicine	7
1.2.1 Timescale of nanomedicine research	7
1.2.2 Therapeutic area of nanomedicine products.....	8
1.2.3 Route of administration of nanomedicine products.....	8
1.2.4 Future perspectives.....	10
1.3 Synthesis and characterisation of nanomaterials for biomedicine	10
1.3.1 Considerations regarding material synthesis	10
1.3.2 Physicochemical characterisation	11
1.3.3 Biological evaluation of NPs.....	13
1.4 <i>C. elegans</i> as a model organism for NP assessment	20
1.4.1 Origin of the specie	21
1.4.2 Establishment as a model organism	21
1.4.3 Key experimental features of <i>C. elegans</i>	22
1.4.4 Anatomical features.....	24
1.4.5 Regulatory use of <i>C. elegans</i>	28
1.5 Thesis framework	28

1.1 Nanotechnology and Nanomedicine

1.1.1 Nanotechnology: General concepts

Nanotechnology deals with the design, characterisation, production and applications of structures, devices and systems by controlling their shape and size at the nanometric scale.^[1] It is a multidisciplinary field where many basic and applied disciplines converge.^[1, 2] According to the Food and Drug Administration (FDA), a nanomaterial is an engineered material or end product that has at least one dimension in the nanoscale range (approximately 1 nm to 100 nm); or that exhibits properties or phenomena, including physical or chemical properties or biological effects, that are attributable to its dimensions, if these dimensions are up to one micrometer.^[2] Due to their small size, nanomaterials exhibit unique physicochemical properties compared to the bulk material. They can be classified into nanoparticles (three dimensions at the nanoscale), nanofibers (two dimensions at the nanoscale) or nanoplates (one dimension in at nanoscale).^[1, 3]

Among the most promising applications of nanomaterials: energy, environmental uses and biomedical applications stand out and attract great interest from academic and industrial research based on their unique properties.^[4, 5] Nowadays, nanomaterials are already present in a wide range of consumer goods (more than 1 600), particularly in healthcare products such as sunscreens, toothpastes and beauty creams.^[5] Wound dressings and other medical devices containing nanomaterials are already emerging. In the last decades, applications in drug delivery, imaging, early disease detection and cancer treatment have been actively explored.^[6, 7] Based on their properties, nanomaterials are extremely promising in medicine and offer prospects for new curing and diagnostic products, as well as theranostic agents which combine both diagnostic and therapeutic abilities.^[6, 8-10] A wide variety of nanomaterials have been investigated for such purposes, among them organic nanomaterials (such as vesicles or liposomes), inorganic particles (for example metals or oxides including silver, gold, iron oxide, silica or titania NPs), members of the carbon-family (like carbon nanotubes, graphene or nanodiamonds) and quantum dots.^[11, 12]

Because of the not yet predictable properties of nanomaterials *in vivo*, safety concerns regarding the use of nanomaterials arose as rapidly as their potential applications.^[13-16] Although the efforts done to date have shed some light on the potential impact of nanomaterials in human health and the environment, there is still an important knowledge gap to meet before specific regulations for NP-containing products can be established based on sound scientific evidence.^[13, 17-20]

1.1.2 Nanomaterials for medicine

Many biological systems operate at the nanoscale (**Figure 1**). For instance, human serum albumin, the most abundant plasma protein, has a size of ~8 nm. Other examples of natural-occurring nano-sized biomolecules include DNA, water molecules, viruses and red blood cells (RBC), among others.^[2] The ability of nanoparticles to imitate

and interact with biological systems at the same scale of their parts can have a great impact on the fields of medicine and biotechnology in the near future.^[7, 16, 17]

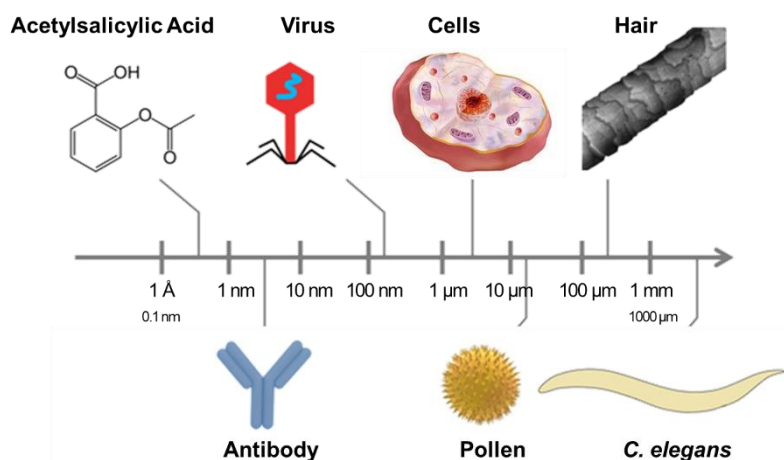


Figure 1. Illustration of biomolecules and living entities with sizes within the nanoscale.

The application of nanotechnology in medicine, coined as nanomedicine, includes a range of new devices, tools, clinical approaches and therapies and encompass the development of novel drugs, drug delivery systems, advanced diagnostic tools, theranostic agents, tissue engineering, development of bioactive surfaces, hyperthermia treatment, implant technology, and development of biosensors and biomarkers using materials at the nanoscale.^[4, 11, 21, 22] Doxil®, consisting in nano-liposomal doxorubicin, was the first nano-drug approved by the FDA in 1995.^[23] Inorganic nanoparticles such as gold nanorods and spheres, iron oxide nanoparticles and silica nanoparticles have been intensively investigated for disease detection, imaging and drug delivery purposes (**Table 1**) taking advantage of their unique properties and high biocompatibility.^[24, 25] Other promising nanomedicine products include polymeric nanoparticles, organic nanomaterials (i.e. liposomes, dendrimers) and core shell nanoparticles.^[11, 26]

In nanomedicine, novel materials are prospectively designed to interact with living organisms.^[21] Nanomaterials are small enough to be internalised by cell membranes by a variety of mechanisms, hence they may interact with the body in inaccessible ways for traditional drugs and biomedical devices.^[15, 27] Among the promising candidates in nanomedicine, superparamagnetic iron oxide nanoparticles (SPIONs) and gold nanoparticles (Au-NPs) constitute successful examples of inorganic nanoparticles for human use.^[24, 25, 28, 29] Formulations of SPIONs reached the market as magnetic resonance imaging (MRI) contrast agents in 1996 (Feridex®) and are currently approved for intravenous anaemia treatment in adult chronic kidney disease patients (Feraheme®, 2009).^[29] Au-NPs are currently under clinical investigation for cancer and atherosclerosis treatment by photothermal therapy.^[30, 31]

Table 1. Brief description of nanomaterials for biomedical applications: classification, properties and applications. Adapted from Nahar *et al.*^[11] and Ma *et al.*^[32]

Type of nanomaterial	Characteristics	Main applications
Carbon-based nanomaterials		
Carbon nanotubes	<ul style="list-style-type: none"> • Third allotropic crystalline form of carbon sheets either single layer (single walled nanotube) or multiple layer (multi-walled nanotube). • Size: 0.5–3 nm diameter, 20–1000 nm length • Remarkable strength. • Unique electrical properties. 	Delivery of nucleic acids and proteins. Imaging.
Fullerenes	<ul style="list-style-type: none"> • Ellipsoidal or spherical hollow carbon compounds. • Size: 0.5–1.2 nm 	
Metal-based nanomaterials		
Quantum dots, QD	<ul style="list-style-type: none"> • Semi conducting material synthesised with II–VI and III–V column elements. • Size between 1 and 10 nm. • Bright fluorescence, narrow emission wavelength. • Broad UV excitation wavelength. • High photostability. 	Contrast agent for MRI and PET.
Gold nanoparticles, Au-NPs	<ul style="list-style-type: none"> • Strong binding to peptides, antibodies, pathogens and oligonucleotides. • Small size (diameter <100 nm). • High surface area available for functionalization. 	Delivery of nucleic acids. Drug targeting. Imaging and diagnosis. Photothermal therapy.
Silver nanoparticles, Ag-NPs	<ul style="list-style-type: none"> • Antibacterial. • Small size (diameter <100 nm). • High surface area available for functionalization. 	Antibacterial.
Iron oxide nanoparticles, SPIONs	<ul style="list-style-type: none"> • Size: 4–5 nm diameter with a hydrodynamic size of 15–25 nm. • Superparamagnetic. 	Contrast agent for MRI. Magnetic hyperthermia. Drug targeting.
Silica nanomaterials		
Silica nanoparticles	<ul style="list-style-type: none"> • Size: 50–200 nm . • Stealth. • Biodegradable and biocompatible. 	Delivery of nucleic acids. Drug targeting. Diagnosis.
Polymeric nanomaterials		
Self-assembled (liposomes, polymeric micelles); Non-self-assembled (dendrimers, nanospheres)	<ul style="list-style-type: none"> • High drug-loading. • Stealth. • Biodegradable. • Surface modification for drug targeting. 	Drug targeting. Imaging. Diagnosis

In this PhD thesis, we have chosen SPIONs and Au-NPs as model nanoparticulate systems based on their promising prospects in nanomedicine. We describe their properties and applications in more detail in the Chapters 3.

1.1.2.1 The potential of nanomaterials in pharmaceutical R&D

The pharmaceutical industry is increasingly moving their research towards nanotechnology given its huge potential in diagnosis and therapeutics.^[33-35] Traditionally, the development of new medicinal products, consisting of small molecules, required an average of 12 years from patent submission to market authorization and cost approximately \$870M (**Figure 2**). Loss of patent protection in the middle term (20 years) causes huge revenue loss in the pharmaceutical industry, as new products (so-called ‘star

products') are the main source of profit of these companies during the patent protection period.^[36-40] Nanotechnology can help to increase the number of new products reducing the dependency of the industry revenue on very few 'star products'.

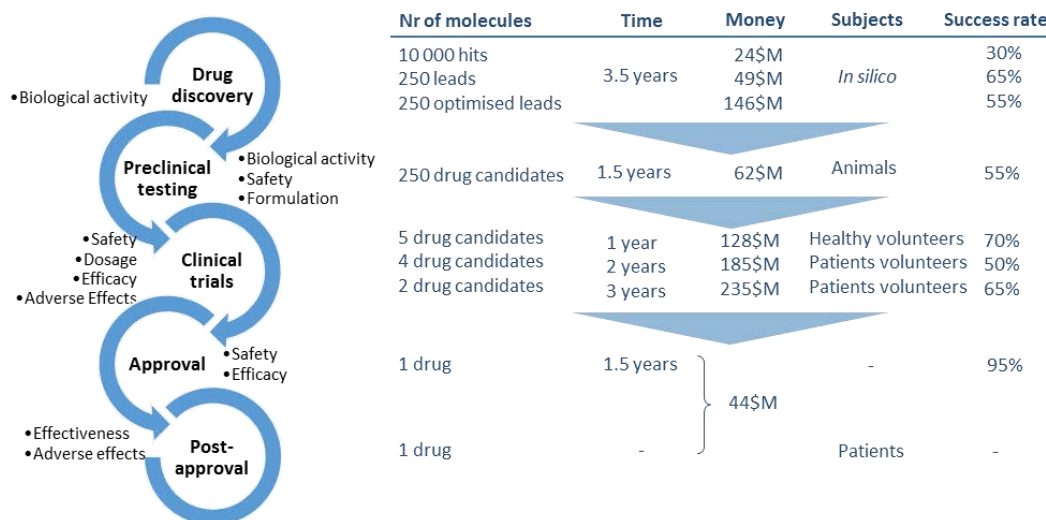


Figure 2. Pipeline of the development of new materials to be marketed as drugs according to the traditional pharmaceutical R&D, which requires about 12-year development and costs \$870M. Data extracted from Morgan *et al* and DiMasi *et al*.^[36, 39]

To this end, nanomaterials can help to reduce or overcome the most common problems that small molecules have when applied to diagnostics and therapeutics, including their toxicity, poor stability and bioavailability¹ and low therapeutic concentration at target.^[27, 41, 42] These drawbacks generally withdraw new candidates from the development pipeline, resulting in a very low success rate of the pharmaceutical R&D despite its high cost.^[37, 38] Size reduction of active principles to the nanoscale offer major advantages over bulk small molecules, among them: i) increased surface area, ii) enhanced solubility, iii) increased rate of dissolution, iv) increased oral bioavailability, v) more rapid onset of therapeutic action, and vi) less amount of dose required.^[8, 12] Moreover, nanomaterials also provide smart drug delivery systems as an alternative to conventional dosage forms, significantly improving the available options of drug carriers and vehicles for commercialized drugs and drug candidates.^[12, 43, 44] Therefore, industrial research is interested in nanomedicine and will exploit this field in the future years.^[33-35, 45]

1.1.2.2 The regulatory framework in the pharmaceutical industry

The pharmaceutical R&D can be divided into two phases: discovery and development. During the discovery of new medicines, experiments are not usually carried out following standards and usually rely on the criteria of the responsible laboratory. For instance, there are many approaches employed to find new drug candidates, i.e. searching into nature (either plants or marine products), performing 'rationale design'

¹ The word 'bioavailable' defines substances that can be absorbed by living organisms and used in their biochemistry.

based on biological structural information, applying high-throughput screening (HTS) methods in products from chemical libraries, or the strategy known as Drug Repurposing, Repositioning and Rescue (DRPx), among others.^[46-49] A more modern approach consists of applying nanotechnology to this purpose.^[6, 27]

After a candidate material has been proposed for biomedical purposes, its further development must comply with the requirements from the corresponding regulatory agency (i.e. the FDA in the USA and the EMA in Europe), the Organisation for Economic Co-operation and Development (OECD) and the International Council for Harmonisation of Technical Requirements for Pharmaceuticals for Human Use (ICH).^[50, 51] These regulations and guidelines aim to ensure maximum efficiency, quality and safety, however the fulfilment of such high standards delay the arrival of promising products to the market.^[51] Even after market authorization, medicine products are subjected to permanent vigilance, called pharmacovigilance, by the Regulatory Agencies.^[52]

Between the discovery and the regulatory stages in the pharmaceutical R&D there is a gap that is currently being covered by alternative methods that are of intermediate complexity but yet highly informative, and associated with low expenditure of cost and time.^[37] These approaches are less regulated but highly cost-efficient and involve minor ethical issues, hence they are in high demand.^[53]

1.2 Current status of nanomedicine

1.2.1 Timescale of nanomedicine research

Compared to the traditional pharmaceutical R&D, the discovery phase of nanomedicines has been longer due to the novelty of this type of materials and the potential safety issues related to their largely unknown *in vivo* properties and behaviour. Many of the revolutionary nano-drugs appeared in the literature 20 or more years before their approved clinical use.^[19, 20] Although it is difficult to predict in which forms medical nanomaterials may finally be implemented and their impact, they have and will have great impact on healthcare in the near future.^[54] A survey conducted with academic, government, and industry experts in 2006 revealed little expectation on the clinical use of nano-theranostic agents before 2025,^[55] however it has turned into reality much before.^[9, 54] According to Etheridge *et al*, in 2013 there were 247 nanomedicine products either approved or in clinical trials. Among the type of nanomaterials identified, different products consisting of free NPs, i.e. hard NPs, nanodispersions, polymeric and protein NPs, among other forms, were the most prevalent categories for both commercial and investigational status (**Table 2**).^[54]

Figures from a 2015 report revealed 40 marketed products and around 300 in development including a wide range of diagnostics, pharmaceuticals and devices. Currently, more than 200 clinical trials involving nanoparticles are being conducted.^[8]

Table 2. Type of nanostructures for confirmed and likely nanomedicine applications and products, by developmental status. Adapted from Etheridge *et al.*^[54]

Nanocomponent	Investigational			Commercial		
	Therapeutic	Device	Total	Therapeutic	Device	Total
Hard NP	3	12	15	0	28	28
Nanodispersion	5	0	5	1	1	2
Polymeric NP	23	0	23	9	0	9
Protein NP	4	0	4	2	0	2
Liposome	53	0	53	7	1	8
Emulsion	18	1	19	9	0	9
Micelle	8	0	8	3	1	4
Dendrimer/ Fleximer	2	2	4	0	3	3
Virosome	6	0	6	2	0	2
Nanocomposite	0	0	0	0	18	18
NP coating	0	2	2	0	6	6
Others	0	8	8	0	9	9
Total	122	25	147	33	67	100

1.2.2 Therapeutic area of nanomedicine products

Nanomedicine products can be classified into therapeutics and devices, according to their final purpose.^[54] Therapeutics include drugs, vaccines and biological products intended to directly mitigate a pathological condition. The therapeutic areas covered by commercial or investigational nanomaterials include cancer treatment, hepatitis and other infectious diseases, anaesthetics, multiple disorders such as cardiac/vascular, inflammatory/immune, endocrine/exocrine or degenerative, and others (**Figure 3A**). Although the number of approved products is similar for all the categories, two-thirds of the products under investigation focus on cancer treatment.^[54]

The applications and products other than therapeutics, named devices, can be categorized into: *in vitro* testing, *in vivo* imaging, *in vivo* device coatings, bone substitutes, dental, medical dressings/textiles, cancer treatment, surgical devices, drug delivery, tissue engineering, and others. *In vitro* testing and *in vivo* imaging are the most prevalent categories, followed by *in vivo* device coatings and bone substitutes (**Figure 3B**). Interestingly, there are many fewer investigational devices than investigational therapeutics, which may be attributed to the different approval procedures between drugs and devices.^[19, 20, 54]

1.2.3 Route of administration of nanomedicine products

The most usual route of administration for nanomedicine products is intravenous administration (73%) followed by topical application (10%). The remaining products are relatively evenly distributed between intramuscular, subcutaneous and interstitial injection and oral, aerosol, nasal, and ophthalmic ingestion (**Figure 4**).^[54]

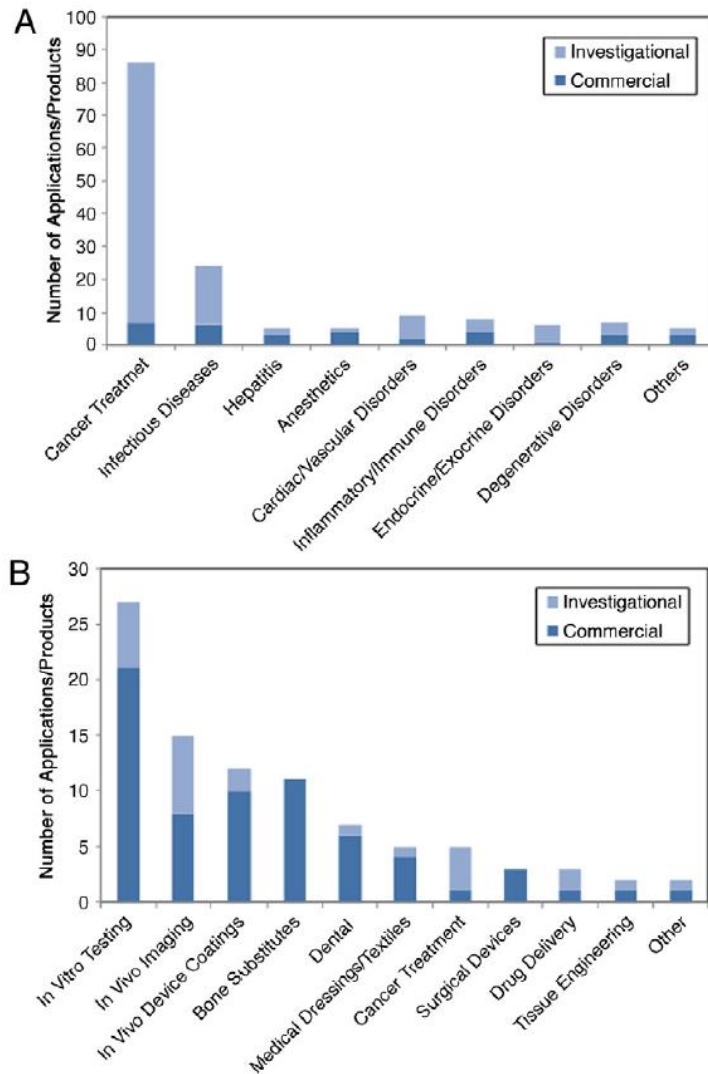


Figure 3. Medical uses for confirmed and likely nanomedicine A) therapeutics and B) devices. Adapted from Etheridge *et al.*^[54]

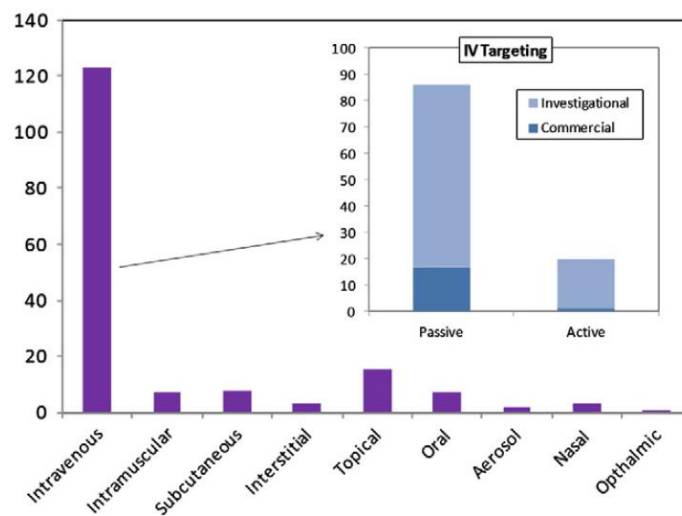


Figure 4. Route of administration for investigational and commercial nanomedicine products, with a description of passive *versus* active targeting for those intravenously administered. Adapted from Etheridge *et al.*^[54]

1.2.4 Future perspectives

Advances in nanomedicine have demonstrated great potential in the treatment of heart disease and cancer, which account for approximately half of all deaths annually in many developed countries.^[56] Meanwhile, the use of nanomedicine in public health, i.e. as rapid and portable diagnostics and more effective vaccinations, has the potential to revolutionize global health, improve the quality and extend the life expectancy at both individual and population levels.^[56, 57] However, the potential health and safety implications derived from exposure to engineered nanomaterials must be continuously investigated in order to fill the current knowledge gaps.^[8, 56] Overall, nanomedicine is entering and transforming medicine and public health in the 21st century, however this process must take place in parallel to a dynamic, proactive, and socially responsible research in the quest for new and safe applications.^[56, 57]

The market value of nanomedicine and nanodiagnostics clearly illustrates the expansion of nano-formulations in medicine, pushed by the lack of new patents for traditional drugs and the expiry of the patent of commercialized drugs (**Table 3**). The nanomedicine market reached US\$72.8 billion in 2011, and is expected to double by 2016.^[58]

Table 3. Examples of applications of nanomaterials in medicine and the relative market value of different areas. Adapted from Kendall *et al.*^[58]

Medical area	Nanomaterials used	Market value† (billion)
Nanomedicines		
Anticancer	Paclitaxel-loaded polymer micelle	US\$28
Central nervous system	Polymer–drug conjugates	US\$14
Anti-infective	Liposomal amphotericin B	US\$9.3
Anti-inflammatory	Polymer–protein conjugate	US\$7.3
Ocular ageing	PEG–anti-VEGF aptamer	-
Cardiovascular	SPIONs (clinical trials)	US\$4
Nanodiagnostics		
MRI contrast agent	Silicone-coated ferumoxsil SPIONs	US\$7.9
Circulating tumour cell detection	Antibodies bound to iron oxide NPs	
Lab on a chip	DNA-based tests	
Diagnostics: biomarkers	Functionalized gold NPs	

Legend: VEGF, vascular endothelial growth factor. †Values for 2011, predicted to double by 2016.

1.3 Synthesis and characterisation of nanomaterials for biomedicine

1.3.1 Considerations regarding material synthesis

In the last decades, material scientists have learned how to control and tune the properties of nanomaterials through their synthetic procedure.^[59, 60] Nanomaterials intended for clinical use not only must be biocompatible (safe) and efficient but also have to be high quality in respect of their physicochemical characteristics. One of the key aspects to achieve these properties and ensure repeatability among different batches is the robustness of the synthetic reaction.^[61, 62] This requirement is not always easy to meet, especially at the discovery stages when the reactions still require further optimization.

Moreover, large amounts of material will be required to meet the market needs when the product reaches commercialization. Hence, synthetic processes must be tested for scalability and be scaled-up at an early stage of product development. Scaling up a reaction might not be straight forward either, i.e. it may require changes on the equipment used or optimization of the reaction conditions, which involves money, time and effort. The scaled-up reaction has to be robust and fully controlled, and yield a material with identical or very close properties to the laboratory-scale product; it also has to ensure minimum variability between batched and maximum quality.^[63-65]

1.3.2 Physicochemical characterisation

Any material for biomedical use has to be very well-characterised regarding their physicochemical properties.^[26, 66, 67] A detailed characterisation of the material includes the parameters listed in **Table 4**, which are known to influence the toxicity and biodistribution² of nanomaterials. Remarkably, the parameters of the surface including composition, charge or roughness can greatly affect the nano-bio interactions as the interface between nanoparticles and biological systems occurs at the surface of nanoparticles.^[67, 68] Thus, surface engineering is suggested to be a highly favourable approach to increase the biocompatibility of engineered nanomaterials.^[15, 59, 69, 70]

Table 4. Overview of relevant NP characteristics which should be controlled to improve biocompatibility graded according to their relative importance.^[67, 68, 71, 72] +++ Essential; ++ Important

Parameter	Category	Comments
Particle size	+++	<5 nm: too small, higher probability of inducing cytotoxic effects. >40 nm: cellular uptake decreases with size.
Agglomeration	++	Higher uptake of NP aggregates than monodisperse NPs.
Particle shape	++	Spherical: highest uptake, highest toxicity. Rods: diminished uptake and reduced toxicity.
Chemical composition / Purity	+++	Metal or organic impurities within nanocores or in NP suspensions may induce cytotoxic effects and should preferably be avoided During storage, metal ions or coating molecules can leach from the NP surface which can induce toxic effects. These can be removed (dialysis) or avoided (i.e. providing a protective secondary coating).
Solubility	+++	Soluble NPs combine nano-specific effects with the effects of the soluble fraction, while the effects of insoluble can only be attributed to the nano-scale properties.
Surface properties (surface area, reactivity, adsorbed species, surface charge)	+++	For acid-degradable nanocores, the surface coating should preferably completely avoid degradation or result in a more gradual and slow degradation. Positively charged NPs have a greater tendency to interact with biological components and are generally defined as more cytotoxic. Surface functionalisation does not alter the intrinsic NP toxicity, but may reduce the extent of cell-NP interaction.
Physical properties (density, crystallinity, microstructure, optical and electrochemical properties)	++	<i>In vivo</i> behaviour depends on the physical properties of NPs: i.e. different biocompatibility and biological effects have been reported depending on the crystal structure.
Concentration	+++	Concentration-dependent uptake.

² The word 'biodistribution' refers to the accumulation and transfer of nanoparticles within an organism.

A combination of techniques is employed to thoroughly characterise different features at the nanoscale, as described below.^[26, 66, 67, 73]

Core size

Electron microscopy can determine many features at the nanoscale. Scanning electron microscopy (SEM) produces images down to length scales of 10 nm and provides valuable information regarding structural arrangement, spatial distribution as well as surface morphology. Transmission electron microscopy (TEM) has higher resolution and give more detailed information such as crystal structure, quality, and orientation of nanoparticles. It is the standard technique to determine the nominal core diameter and study particle size distribution. Cryo-TEM also provides useful information regarding the colloidal stability of NP dispersions. Others techniques such as Scanning Tunnelling Microscope (STM), Electrical Field Gradient Microscopy (EFM) or Atomic Force Microscopy (AFM) have been employed to study structural, electronic, magnetic, thermal and topographical properties of nanomaterials.^[26, 66, 67, 73]

Hydrodynamic size

Particles in solution are dynamic and solvated. The hydrodynamic size measured by Dynamic Light Scattering (DLS) is the size of a sphere that has the same translational diffusion coefficient as the particle being measured, assuming a hydration layer surrounding the particle. The hydrodynamic size, hence, is calculated from the diffusional properties of the particle and is indicative of the apparent size of the dynamic hydrated/solvated particle. Briefly, DLS measures Brownian motion and relates it to the size of the particle. Brownian motion is the random movement of particles suspended in a fluid resulting from their collision with the fast-moving solvent molecules that surround them. The larger the particle, the slower the Brownian motion will be. The velocity of the Brownian motion is defined by a property known as the translational diffusion coefficient. The size of a particle is calculated from the translational diffusion coefficient by using the Stokes Einstein equation.^[26, 66, 67]

DLS also provides a polydispersity index that describes the width of the assumed Gaussian distribution of the single particle sizes measured. The polydispersity index is an important aspect during the formulation of nanomaterials. The lowest polydispersity index is desired; a % polydispersity less than 20% indicates that the sample is highly monodisperse.^[73]

Surface status

Zeta Potential is used to determine the charge status at the particle surface. Most particles dispersed in an aqueous system will acquire a surface charge, principally by ionization of surface groups or adsorption of charged species. Zeta potential is a measure of the magnitude of the electrostatic or charge repulsion/attraction between particles, and is one of the fundamental parameters known to affect colloidal stability. A high zeta potential, either positive or negative, will confer stability. Briefly, zeta potential is measured by applying an electric field across the NP dispersion. Particles within the dispersion with

a zeta potential will migrate toward the electrode of opposite charge with a velocity proportional to the magnitude of the zeta potential. This velocity is measured using the technique of laser Doppler anemometry. The frequency shift or phase shift of an incident laser beam caused by these moving particles is measured as the particle mobility, and this mobility is then converted to the zeta potential.^[26, 66, 67, 73]

Crystallinity

Differential Scanning Calorimetry (DSC), X-Ray Diffraction (XRD) and other analytical methods such as Selected Area Electron Diffraction (SAED) are used to assess the crystalline structure of nanomaterials.^[26, 66, 67, 73]

Other techniques

Depending on the nature of NPs, other characterisation techniques can be applied: i.e. magnetic measurements in the case of magnetic nanoparticle; UV-Vis spectra of NPs with Surface-Plasmon Resonance (SPR) such as gold or silver NPs; or Fourier transform infrared spectroscopy to study core/coating modifications, etc.^[26, 66, 67, 73]

1.3.3 Biological evaluation of NPs

Nanomaterials elicit different biological responses compared to their bulk materials. The knowledge gathered to date regarding the influence of NP size, shape, composition and surface chemistry in their biological effects is still limited, thus it remains uncertain under which circumstances engineered nanomaterials can have a harmful impact.^[13, 15, 68, 74] Further studies on how living organisms respond to nanomaterials are required to advance in this field.^[13] Nanotoxicology emerged to address these questions, and currently attracts enormous interest.^[14, 42] Regulatory agencies are also adapting their rules and developing specific risk assessment methodologies for engineered nanomaterials in human health based on a benefit-risk criteria.^[8, 19, 27, 74]

The various interactions of nanoparticles with biofluids, cells and tissues, and their biological responses at each of these levels need to be adequately addressed before a novel material can be administered to humans. In living organisms, nanomaterials are immersed in biological fluids (i.e. blood, saliva, intestinal content, interstitial fluid), move through biological entities of different magnitude (organs, tissues, cells) by several transport mechanisms (i.e. endocytosis, paracellular transport); until they finally reach a desired or undesired subcellular localization (i.e. cytoplasm, lysosomes, mitochondria).^[15, 16, 75-77] Investigation of NP dynamics, kinetics and fate *in vivo* demands a multidisciplinary approach and is an essential step in the path towards the clinical use of nanomedicine products.^[17, 54, 78]

Biological evaluation of medicinal products typically occurs in two phases, initially *in vitro* and then *in vivo*, moving from lower to higher complexity (**Figure 5**). *In vitro* studies are performed in a controlled environment outside of a living organism, for instance, cell culture assays. Their main limitation is that they fail to replicate the precise conditions of an organism, hence they may lead to results that are directly extrapolable to whole

organisms. In contrast, *in vivo* studies use whole living organisms, hence they are better suited for observing the overall effects of a treatment. Still, *in vivo* studies are not infallible as many circumstances can lead to misleading conclusions, i.e. a therapy can offer a short-term benefit but a long-term harm. Therefore, the knowledge from biological evaluation must not be taken as conclusive, but only as informative about the nature of beneficial and harmful effects of a treatment.^[79-81]

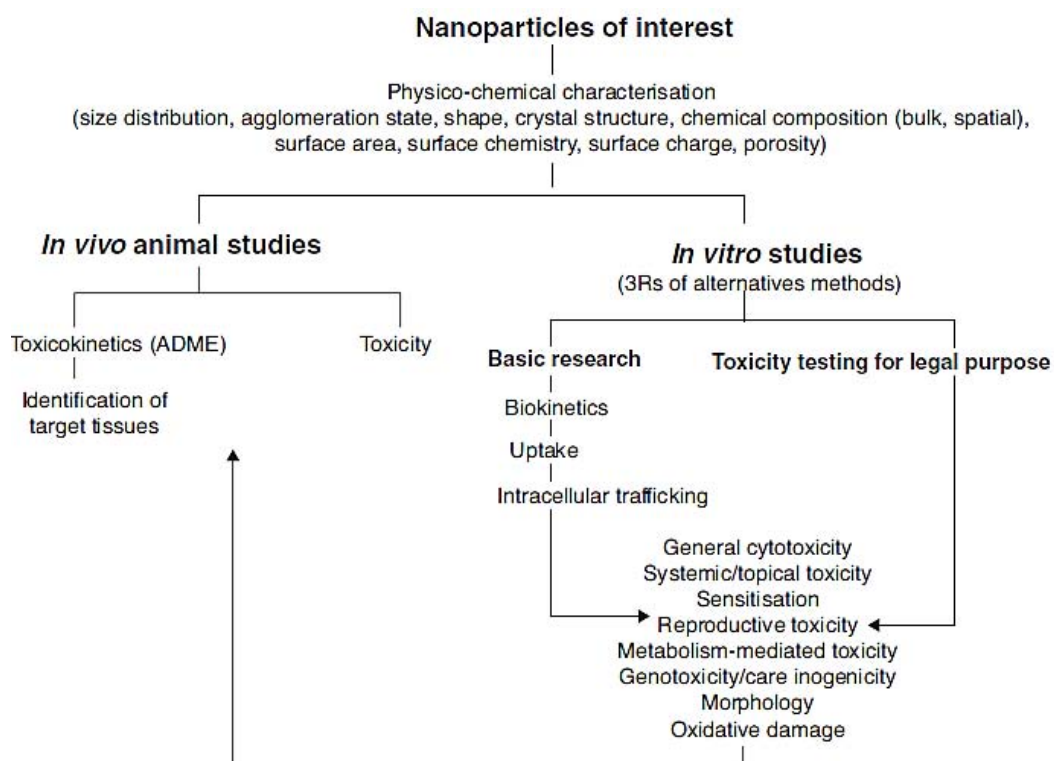


Figure 5. *In vivo* and *in vitro* studies for nanotoxicological research. Adapted from Yu *et al.*^[81]

1.3.3.1 *In vitro* evaluation

In vitro evaluations of nanoparticles are aimed to study their biocompatibility and their effects on cell viability, immune function and blood components.^[26, 68, 82]

Stability in Biological Media

Cells are grown and handled using chemically defined mediums, generally named biological media, in order to control the environment of the assays. The properties of different biological mediums can deeply influence the physicochemical properties of nanomedicines including their hydrodynamic diameter, aggregation status and surface properties, but also their optical, electrical or magnetic features. The changes in the material properties can modify the efficiency of the material but it can also affect its predicted toxicological profile. Therefore, the study of the new bio-identity acquired by nanomaterials when placed in biological environments is of vital importance.

Colloidal stability is routinely evaluated in different biological media before progressing to cell assays (**Table 5**). Other media commonly used in biological research

include Phosphate-Buffered Saline (PBS) for cell handling and Citrate Buffer (CB) at pH 4.6 to simulate lysosomal digestion.^[68, 82-84]

Table 5. Cell culture media used in the *in vitro* characterisation of nanomaterials for biomedical applications.

Name	Components	pH	Use
DMEM	Aa, vitamins, inorganic salts, trace elements, D-glucose, linoleic acid, phenol red, 10% CO ₂ .	7.4	Frequently used cell culture media.
RPMI	Aa, vitamins, inorganic salts, D-glucose, phenol red, 5% CO ₂ .	7.4	Frequently used cell culture media.
PBS	Inorganic salts (sodium phosphate dibasic and monobasic)	7.4	Osmolality. Buffering and pH control in cell handling.
Citrate buffer	Organic salts (citric acid, trisodium citrate)	4.6	Lysosomal environment mimicking.
FBS	Mainly proteins (growth factors, adhesion factors, antitrypsin, minerals, lipids, and hormones)	7.4	Protein supplement to Serum-Free Media.

DMEM–Dulbecco’s Modified Eagle’s Medium; RPMI–Roswell Park Memorial Institute Medium; PBS–Phosphate-Buffered Saline; FBS–Fetal bovine serum; MEM–Minimum Essential Medium Eagle; Aa–aminoacids.

In culture media, nanomaterials find a new environment with neutral pH, high ionic strength and the presence of biomolecules, especially proteins. It is well known that a high ionic strength can compromise the colloidal stability of nanomaterials, thus promoting aggregation. The resulting material may not be nano- but micro-sized and even precipitate, hence the identity of the material can suffer dramatic changes in such complex environments.^[71, 85] The presence of biomolecules can also strongly influence the identity of NPs and how cells ‘see’ them. When NPs are placed in a biological environment, they get surrounded by biomolecules which are non-specifically attached to or adsorbed onto the NP surface, forming the so-called protein corona, which provides new surface properties to the NPs. These post-synthesis modifications can notably affect how the NPs behave *in vivo* and their biological effects.^[86, 87] Several strategies have been investigated to increase the colloidal stability of nanomaterials and control the formation of the protein corona. A widespread approach is to cover the material with polyethylene glycol (PEG), process known as pegylation, or another biocompatible polymer.^[88] A more recent approach consists on coating the material with a layer of proteins to pre-form a hard protein corona around the NPs before they contact more biomolecules.^[85, 89, 90] These approaches are used also in order to ‘hide’ the NPs from the immune system and reduce unspecific cell uptake.

The use of other media, i.e. citrate buffer pH 4.6, complements the experiments with cell culture media and allows the study of the kinetics of degradation of NPs in the lysosomal compartment. When NPs are engulfed by cells through the endocytic pathway and end up inside lysosomes, they encounter a more acidic pH than in the cytosol, which could contribute to the digestion of acid-degradable NPs.^[91] *In vitro* studies mimicking these conditions revealed that the composition of the NP core is a determinant factor in lysosomal digestion.^[92] For instance, naked iron oxide nanoparticle are rapidly biodegraded at pH 4.6 (complete degradation within 10 days, most occurring in the first 4

days), while protein-coated iron oxide nanoparticles undergo a much slower degradation both in time and extend (up to 50% in 30 days).^[93] In contrast, gold nanoparticles are much more resistant to dissolution under these conditions.^[94, 95]

After characterisation in biological media, nanoparticles' design should be optimized to enhance their colloidal stability.

Cell assays

The next step in NP biological assessment is the study of the interaction between nanomaterials and the simplest biological entity, the cell. The choice of cell line, exposure parameters and the assays to be performed require careful planning in advance (**Figure 6**).^[96] These experiments are generally beyond the reach of materials scientists due to the lack of cell facilities in their laboratories, which are costly, and the complexity of the experiments.^[97, 98] Therefore, these assays are often carried out in collaboration with biologists

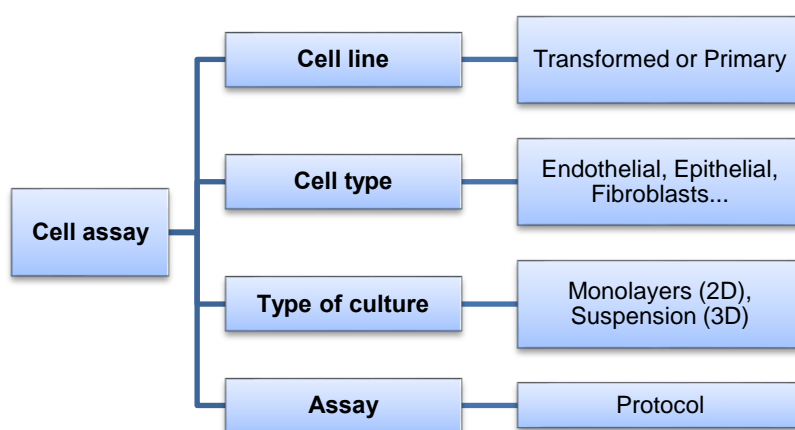


Figure 6. Aspects to consider while planning a cell culture experiment.

Cell growth for *in vitro* experiments requires a controlled environment (37 °C and 5% CO₂) and sterile handling.^[97, 98] The use of sterile disposable materials is also associated with high cost but results convenient for biological research (**Table 6**).^[99, 100] In addition, handling biological waste demands the use of specific containers that must be disposed according to the applicable regulations.^[99]

Table 6. Minimum infrastructure required for cell culture.^[101]

Requirement	Equipment	Material
Sterility	Laminar Flow Hood; Autoclave	Aseptic handing technique with sterile pipettes, etc.
Temperature of 37 °C	Incubator with controlled temperature, humidity and CO ₂ levels	Sterile plates or bottles.
95% Relative Humidity		
5% CO₂		

1.3.3.2 *In vivo* evaluation

The results of *in vitro* evaluations cannot be easily extrapolated *in vivo* due to the controlled environment in which they are performed, unlikely to occur in living organisms.

Indeed, there is a big leap from *in vitro* to *in vivo* experiments, which are far more complex, costly, time-consuming and require significant resources. Therefore, it is essential to obtain positive results in the early discovery of novel materials before advancing to *in vivo* experiments.^[17, 79]

Remarkably, *in vivo* experiments offer higher physiological relevance than *in vitro* assays as the metabolism of a living organism is preserved, including intact cell-to-cell communication, neuroendocrine signalling, and every aspect of the animal's metabolism necessary to survive and reproduce.^[79-81] Hence, *in vivo*, nanomaterials could be metabolized or altered in a way that their properties (such as size, shape and/or composition) changed, resulting in different biological effects than the initial material.^[79-81] The knowledge accumulated over decades about the biological responses to small molecules *in vivo* have provided well-established methods to predict *in silico*³ their *in vivo* behaviour, i.e. the Lipinski's rule of five or quantitative structure–activity relationship (QSAR) models.^[102-104] In contrast, nanomaterials still have a poorly understood and unpredictable behaviour *in vivo* due to their unique properties and further knowledge is needed to unravel the complex relationships between the properties of the material (size, composition, surface charge, surface properties, aggregation status...) and their *in vivo* effects. Gathering these evidences would allow *in silico* predictions of the biological responses to nanomaterials depending on their physicochemical. Although some efforts have already been done in this direction,^[105] the only way to determine the *in vivo* effects of nanomaterials is conducting animal studies.^[17, 79]

In the pharmaceutical R&D, *in vivo* evaluations of drug candidates have been traditionally conducted in the preclinical phase using mammalian models, mainly rodents (mice, mouse and/or rats) and also non-rodents (such as rabbits, dogs and pigs), in compliance with strict regulations and guidelines.^[50, 51] The low success rate associated with these experiments reveals a high risk of progressing to this stage (**Figure 2**) without a wise evaluation of the drug discovery/development interface.^[37] Therefore, often the resources and time spent up to this point doesn't pay off as the drug candidate is discarded due to negative *in vivo* output related either due to efficacy or safety.^[40] In recent years, an emerging trend in toxicology and drug assessment is the use of simple animal organisms to bridge *in vitro* and *in vivo* assays in the transition between chemistry and biology.^[106, 107] In particular, the use of alternative models has been proved to be a cost-efficient strategy in nanotoxicology, allowing information-rich experiments and encompassing the 3Rs ethical principles (Reduction of the use of higher animals, Refinement of current techniques, and Replacement of animals with alternative methods).^[14, 53, 79]

³*In silico* is an expression used to mean “performed on computer or via computer simulation”.

Simple organisms

The use of simple non-mammalian model organisms minimizes the cost associated with *in vivo* experiments at the early stages of discovery and yields highly informative results.^[107] Among them, the fruit fly *Drosophila melanogaster*, *Danio rerio* (also known as zebra fish) and the tiny worm *Caenorhabditis elegans* are the most widely employed animals, especially in biomedicine.^[108] However, for environmental purposes other aquatic organisms such as the trout, or terrestrial ones like the earthworm are also highly used. The use of these model organisms is in high demand, especially for chemists and materials scientists aimed to assess their candidate materials for biomedical applications within their laboratories.^[109, 110] The pharmaceutical industry also relies on these models to validate their *in silico* and *in vitro* results.^[108] These simple organisms are claimed to fill the gap between the *in vitro* experiments and the *in vivo* tests in mammalian models and offer worthy biological information in the initial stages of product development (**Figure 7**). Each of them has specific features that make them more suitable for one or another purpose (**Table 7**). For instance, *Drosophila* has been long used to study the effects of mutations by crossing and studying the subsequent generations. In contrast, zebra fish is highly used to study the heart and the vascular system, which is absent in *C. elegans*. Zebra fish embryos, as well as *C. elegans*, result very interesting to study development due to their small size and rapid life cycle.^[111, 112] These simple models have their own specific culture requirements, for instance *Drosophila* are kept in bottles, while zebra fish require aquariums, and *C. elegans* can be grown in temperature-controlled incubators.^[108, 113]

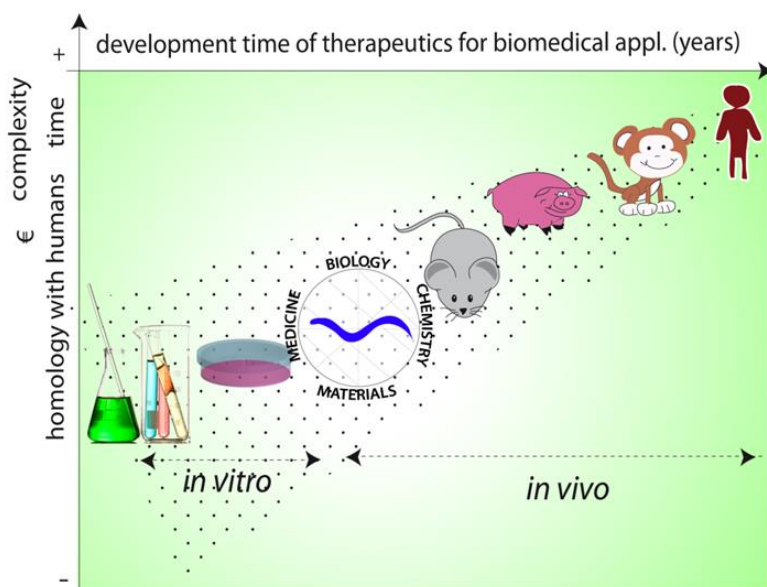







Figure 7. Simple animal models bridge the gap between *in vitro* and *in vivo* assays.

Based on their minimal maintenance and growth requirements, these animal models can be hosted in any synthetic laboratory after notification and authorisation by the corresponding authority. In contrast, the regulatory pre-clinical assays during

pharmaceutical R&D that involve the use of mammalian organisms are far more demanding and require a dedicated infrastructure. For instance, mice are kept in cages in a dedicated room and require daily maintenance by specialised technicians. Moreover, each assay to be performed requires the approval by an ethical committee, which is also tedious and costly.^[36, 40] Therefore, simple model organisms are an optimal solution to screen materials within synthetic laboratories in the progress towards superior model animals.

Table 7. Simple model organisms widely used in toxicological evaluations. Adapted from Gonzalez-Moragas *et al.*^[114]

	INVERTEBRATES			VERTEBRATES	
	<i>Caenorhabditis elegans</i>	<i>Hydra vulgaris</i>	<i>Drosophila melanogaster</i>	<i>Danio rerio</i>	<i>Mus musculus</i>
					
Common name	Worm	Hydra	Fruit fly	Zebrafish	Mouse
Habitat	Terrestrial (soil)	Aquatic (freshwater)	Terrestrial	Aquatic (freshwater)	Terrestrial
Cultivation	Inexpensive and easy	Inexpensive and easy	Inexpensive and easy	Inexpensive and easy	Expensive
Space	Hundreds of animals in a 10-cm Petri dishes in an incubator in the laboratory	20-L aerated aquaria	Bottles in a dedicated room.	45-L aerated aquaria in a dedicated room	Cages in a dedicated room.
Food	Bacteria	Shrimp larvae	Fly food (water, agar, sugar, corn meal, yeast...)	Adult shrimp	Pelleted mouse feed
Environmental conditions	16 – 25° C	18 – 21° C	18 – 29° C	25 – 31 °C	18 – 23 °C; 40-60% humidity
Adult Size (length x width)	~1 mm x 70-90 µm	Column: 2-10 x 0.3-1.8 mm; Tentacles(6-9): ~¾column	~3 mm x ~2 mm	~4.5 cm x ~1 cm	~17 cm (9-cm tail)
Adult Weight	~4 µg	~400 µg	200-250 µg	150-250 mg	17-25 g
Gender	Hermaphrodite and ♂ ~0.1%)	Hermaphrodite	♀ and ♂	♀ and ♂	♀ and ♂
Lifecycle	Short (2-3 days)	They do not undergo senescence and can regenerate.	Short (10 days)	Long (2-4 months)	Long (2-3 months)
Embryogenesis	18 hours at 20 °C	Budding predominates over sexual reproduction.	24 hours at 25 °C	48-72 hours at 28.5 °C	19-21 days
Lifespan	2-3 weeks; up to months as dauer larva	'biologically immortal'	~30 days	2-3 years	2-3 years
Number of offspring (per animal)	~300	~112/year, mainly clonal offspring	~400	100-200 eggs/clutch	40-100
Year Genome sequenced	1998	ongoing	2000	2013	2002
%Homology with humans	60-80%	Some functional conservation has been reported.	50-80%	70%	Up to 99%
Automated high throughput assays	Possible at all stages.	Possible at all stages.	Only possible with larvae.	Only possible with embryos	Not possible.
Other features	Transparency; Storage by freezing. Many mutants available.	Biological indicator of water pollution.	Difficulty of conservation of mutants	Transparent and small embryo	Strong bioethical issues

In our research group, this rationale gave birth to a new research line consisting of the use of *C. elegans* to screen NPs for biomedical applications at the early stages of discovery and to study the largely unexplored nano-bio interactions in a complex biological system. Based on the increase in the number of articles related to nanoparticle assessment in *C. elegans* (**Figure 8**), it is clear that the scientific community is working in the same direction and is devoting efforts to exploit the potential of this small animal.^[114-116] Even though, it is noteworthy that the use of alternative systems initially results less straight forward given the absence of standardized protocols and techniques compared to cells or mice.^[53, 117] The work done in the framework of this thesis has contributed to advance the present state of the art by combining an array of techniques from different disciplines including chemistry, physics and biology to get an overall picture of the interaction between inorganic nanoparticles for biomedical uses and the model organism *C. elegans*.

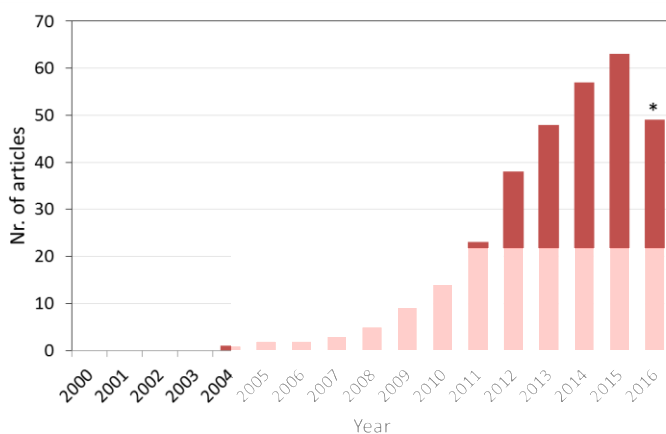


Figure 8. Number of articles indexed by Web of Science with the words “*Caenorhabditis elegans*” and “nanoparticles” in the topic. * indicates the number of articles published until Sep 13, 2016.

1.4 *C. elegans* as a model organism for NP assessment

Caenorhabditis elegans is a free-living soil nematode about 1 mm long fed primarily on bacteria that is found commonly in many parts of the world (**Figure 9**). Its name is a blend of Greek and Latin: *Caeno*, recent; *rhabditis*, rod; *elegans*, nice. They have a rapid life cycle, about 3 days, and a life span of 2-3 weeks. Adult *C. elegans* are predominantly hermaphroditic, and males arise spontaneously at low frequency. *C. elegans* is a simple organism, both anatomically and genetically, however it shows a high level of conservation to vertebrates and humans in regard to genes and biochemical mechanisms (60–80% of homology).^[118-121]

C. elegans was first chosen as a promising model animal by Sydney Brenner in 1963 to study development and the nervous system.^[118] In 1998, *C. elegans* became the first multicellular organism for which the genome was sequenced.^[122] Since its establishment as a model organism, the work with *C. elegans* has led to important discoveries in neuroscience, biological development, signal transduction, cell death,

aging, and RNA interference.^[118, 123-126] The success of *C. elegans* as a model has attracted increased attention in the fields of biomedicine and environmental toxicology. ^[106, 127]



Figure 9. Light microscopy image of an adult *C. elegans* in NGM agar.

1.4.1 Origin of the specie

Caenorhabditis elegans was initially described and named *Rhabditis elegans* by Maupas in 1900. It was subsequently placed in the subgenus *Caenorhabditis* by Osche in 1952 and then raised to generic status by Dougherty in 1955 (**Table 8**). Two strains have historical importance: Bergerac (Nigon, 1949) and Cristal (Nicholas *et al*, 1959). The Bergerac strain was collected from the soil in France by Nigon of the Université de Lyon. The Bristol strain was isolated by Staniland (National Agricultural Advisory Service, London) from mushroom compost near Bristol. Other wild-type strains of *C. elegans* have been isolated from numerous sites around the world. *C. elegans* Bristol N2 strain was defined in 1965 as the wild-type reference. It is a laboratory strain that was derived by Sydney Brenner from the Bristol culture he obtained from Dougherty in the spring of 1964. We will use this strain in this work.^[118]

Table 8. Taxonomy of *C. elegans* sp.

KINGDOM	Animalia
PHYLUM/DIVISION	Nemata
CLASS	Secernentea
ORDER	Rhabditida
FAMILY	Rhabditidae
GENUS	<i>Caenorhabditis</i>
SPECIES	<i>elegans</i>

1.4.2 Establishment as a model organism

The establishment of *C. elegans* as a model system for biological research began with the molecular biologist Sydney Brenner in 1963. At that time, Brenner was working at the Medical Research Council (MRC) Laboratory of Molecular Biology in Cambridge, and he was focused on the study of biological processes in bacteria using the techniques of genetic analysis. Brenner foresaw that nearly all the ‘classical’ problems of molecular biology had been solved or would be in the near future based on the recent discoveries in molecular biology: the double helical structure of DNA by Watson and Crick in 1953, the mechanisms of genetic replication and transcription, and the elucidation of the genetic

code in 1961. With these discoveries, in the late 1960s the connection between gene structure and gene function was already clear. Therefore, Brenner was convinced that the future of molecular biology was in the study of development and the nervous system. In his effort to extend his research activity to higher organisms, in 1963 he submitted a formal proposal to study the genetics of differentiation in the nematode *Caenorhabditis elegans*. To start with, Brenner proposed to identify every cell of the worm and trace lineages; to investigate the constancy of development; and to study its genetic control using mutants.^[118, 120] The accomplishment of such an ambitious plan required major technical advances (i.e. reverse genetics, laser microsurgery...) that were not available at the time of his proposal, and the work of a large community of scientists.^[128, 129]

In 2002, the Nobel Prize in Physiology or Medicine 2002 was awarded jointly to Sydney Brenner, H. Robert Horvitz and John E. Sulston for their discovery of genes in *C. elegans* that regulate organ development and programmed cell death. However, the impact of *C. elegans* has extended further beyond developmental biology towards other disciplines including chemistry and material sciences, and *C. elegans* is now widely employed in fields such as drug discovery and toxicology.^[106, 130]

1.4.3 Key experimental features of *C. elegans*

The small size of *C. elegans*, together with its transparency, short and prolific life cycle, constant cell number, sequenced genome, anatomical features and easy genetic manipulation, are the top-listed and most appreciated attributes of *C. elegans* that make it a successful experimental animal in research laboratories.^[118, 119]

Small size and transparency

The combination of the small size and transparency of *C. elegans* allows its study under the optical microscopy down to single-cell level, i.e. by Nomarski Microscopy. Its transparency allows the simultaneous visualization of the different anatomical structures without need of dissection, and allows the tracking of coloured substances throughout their body without staining.^[131, 132] Due to the small size, hundreds of animals can be kept in a single Petri dish, which allows their use in high-throughput assays.^[133] Their micrometric size from embryo to adults^[119] is also advantageous for their use in microfluidic platforms, a field in which *C. elegans* is widely employed. Microfluidics allows the monitorisation of the health, behaviour and ageing of *C. elegans* to shed light on the toxicological profile of the test material in an automated manner and at high-throughput level.^[109, 129]

Life cycle and development

C. elegans can be maintained between 16 °C and 25 °C, most typically at 20 °C. It has rapid life cycle: at 20 °C, embryogenesis lasts 23 h, and postembryonic development to adult lasts 58 h. Its growth rate is temperature-dependent: it is 2.1 times faster at 25 °C than at 16 °C, and 1.3 times faster at 20 °C than at 16 °C. The postembryonic development progresses through four larval stages known as L1, L2, L3 and L4 before

becoming a fully-developed, sexually mature adult (**Figure 10**).^[119, 133] Under continued exposure to harsh environmental conditions such as overcrowding, high temperatures or a scarce food supply during L1 or L2, *C. elegans* forms an alternative third larval stage called dauer. Dauers are motile, but do not eat, and have structural, metabolic and behavioural adaptations, including the development of a thick cuticle. This state increases life span up to ten times, so that dauers can live for several months without food. Worms remain in the dauer state until conditions improve, whereupon they exit the dauer state, resume their lifecycle as L4 animals and continue their regular development to the adult stage.^[119, 134]

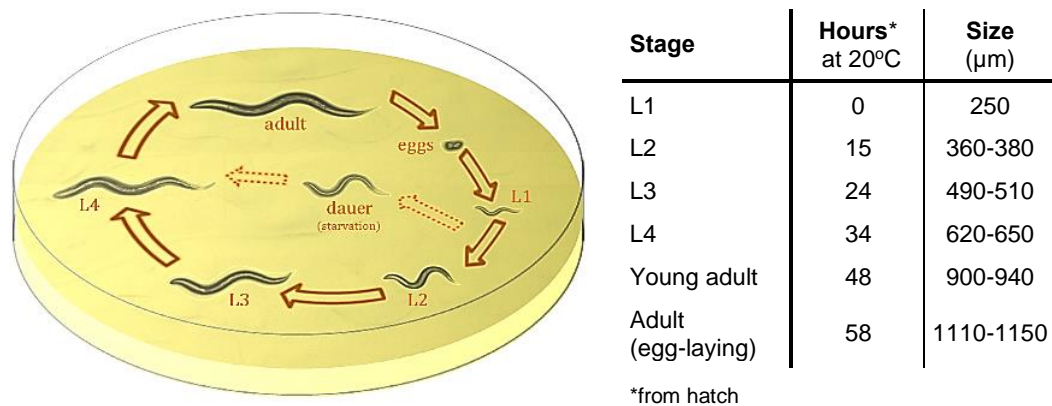


Figure 10. *C. elegans* life cycle. Schematic drawing of life cycle progression through four larval stages to adulthood (left panel). The table indicates the growth rate at 20°C and the size of each developmental stage (right panel).^[119, 133]

Adult animals are predominantly hermaphroditic, with males arising spontaneously at low frequency (approximately 0.1%).^[119, 135] The hermaphrodite can reproduce by selfing: in the late L4 stage they produce sperm, turning to the production of oocytes as adults. The adult hermaphrodite is structurally a female, with its previously produced sperm stored in its spermathecae. Unmated hermaphrodite can produce about 300 offspring by selfing. Mating stimulates oocyte production, so that a single hermaphrodite can produce more than thousand progeny when mated.^[119, 133, 136]

Constant cell number

The adult hermaphrodite has 959 somatic cells, and the adult male 1031. The invariance of cell number (or eutely) and cell fate within the somatic tissues of *C. elegans* have enabled the identification of every cell in the animal and assigned a unique label. This information has been related to the cell lineages, providing a comprehensive description of the ontogeny and ultimate differentiated state of all the various cells that comprise *C. elegans*.^[118]

Sequenced genome

C. elegans was the first multicellular organism for which the genome was sequenced in 1998. Its genome sequencing project formed the cornerstone of efforts ultimately aimed at decoding the human genome.^[122] The genome size of *C. elegans* is about 100 million base pairs long. Although it is substantially smaller than the human

genome, which is about 3.2 billion base pairs long, both genomes have nearly as many genes (worms have about 20 000 genes; humans have about 23 000).^[137] It shows a high level of conservation with the vertebrate genome with respect to gene function and metabolic pathways (bioinformatic analyses suggest that 60–80% of the genes of the worm are homologous to human genes).^[121] These features make *C. elegans* an ideal model organism for functional genomics studies aimed to understand the complex relationship between genotype and phenotype on a global (genome-wide) scale. With this information, complex biological processes can be identified and compared to human disease genes homologs of *C. elegans*.^[122, 138-140] At least 83% of *C. elegans* proteome has human homologous genes, with 7 954 records of *C. elegans* proteins matching known human gene transcripts.^[141]

1.4.4 Anatomical features

The body of the worm is essentially a tube, the alimentary tract, inside of another tube formed by the hypodermis and the cuticle (**Figure 11**). Between the two tubes there is a fluid-filled body cavity, the pseudocoelom. The anatomy of *C. elegans* includes the following systems: an alimentary system (mouth, pharynx, intestine, rectum, anus),^[142] a reproductive system (gonad, uterus, spermatheca, vulva in the hermaphrodite;^[143] gonad, seminal vesicle, vas deferens, cloaca in the male^[135]), a nervous system (302 neurons in the hermaphrodite, with a cluster of synapses forming the 'nerve ring', which is located in the head)^[144], and an excretory system (formed by a group of four cells believed to control osmolarity and the elimination of waste). Worms have muscle (striated and non-striated), hypodermis, a protective cuticle covering the body (secreted by the hypodermis), as well as connective tissues and basement membrane.^[119, 145] The cuticle is a 0.5- μm thick coating on the external surface of the worm. It comprises five layers (from innermost to outermost): the basal layer, that consists in collagen fibrils; the medial layer, which is a fluid-filled layer with "struts" of collagen; the cortical layer, that consists in collagens and cuticle-specific proteins; the epicuticle, which is a layer of lipids; and a surface coat of glycoproteins.^[146] *C. elegans* does not have a circulatory system and relies on passive diffusion in the pseudocoelomic fluid for the transport of O_2 , CO_2 and nutrients. It is also possible that the locomotory movement of the body of the worm mixes the contents of its interior fluid. Gas exchange with the environment occurs by diffusion through the cuticle or the surface of the gut.^[119]

Males and hermaphrodite are similar in length but differ in appearance as adults. The major male mating structures consist of the blunt tail with fan and rays, the hook, the spicules and proctodeum, and the thin body.^[119, 135]

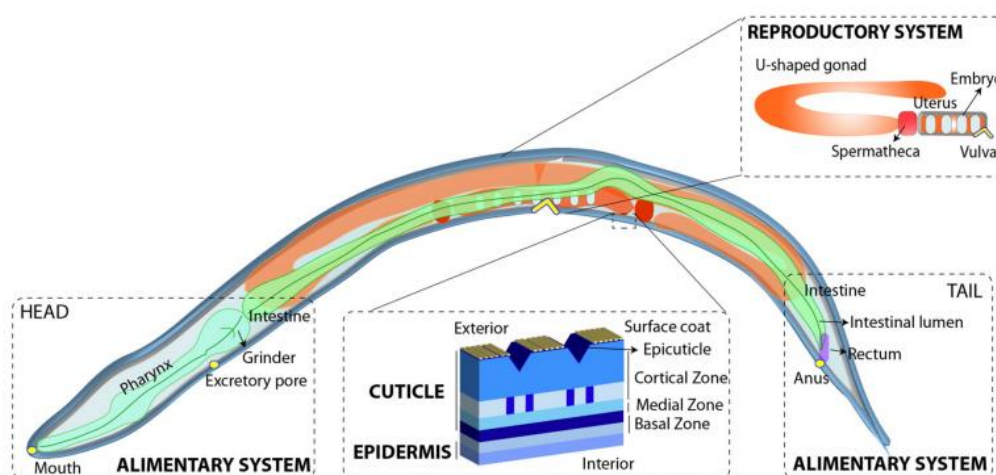


Figure 11. Scheme of the *C. elegans* anatomy showing the parts of interest for NPs assessment: cuticle and epidermis (blue), alimentary (green) and reproductive (orange) systems, pseudocoelom (light blue). Portals of entry (mouth) and exit (excretory pore, vulva, anus) are indicated in yellow.

The cuticle

The cuticle is the tough extracellular surface of the worm, which protects the animal from the environment, maintains the morphology and integrity of the body, and has a critical role in locomotion by acting as an external skeleton. The adult cuticle is $\approx 0.5 \mu\text{m}$ thick and comprises five layers based mostly on collagen, lipids, and some glycoproteins. The combination of structural proteins and lipids is present in both human skin and *C. elegans* cuticle, whereas other components lead to different properties.^[119, 146] The cuticle prevents leakage of internal solutes into the environment and blocks the entry of some molecules from the environment, although it allows some specific diffusion. At each larval stage, an entirely new cuticle is generated and the old cuticle is shed, which permits growth. Cuticles at different stages differ significantly in their surface protein expression, layer number, relative thickness and composition. In humans, the skin is composed of three primary layers; epidermis, dermis, and hypodermis. It functions as a protective barrier to the environment similar to the cuticle of *C. elegans*. The epidermis of invertebrates is, in its structure and function, the primitive forerunner of human skin and of all other vertebrate animals. Thus, the cuticle and epithelial system of *C. elegans* can be used as a simplified skin (epidermis) model for NP assessment to study possible adverse effects (i.e. abrasion) and to assess NP adsorption or absorption mechanisms.^[147, 148]

The alimentary system

In *C. elegans* the alimentary system carries out multiple functions performed by distinct organs in higher organisms, including food ingestion and digestion, nutrient absorption, synthesis and storage of macromolecules, initiation of innate immune responses, and yolk production to nurture the germ cells.^[119, 142] The intestine consist of 20 large epithelial cells, the enterocytes, that position as pairs in the form of intestinal rings to delimit a long tube around a lumen. There are nine intestinal rings, each of them formed

by a cell pair (II-IX intestinal rings) except the anteriormost, which consists of four cells (intestinal ring I) (**Figure 12**). The enterocytes attach to each other by apical junctions.

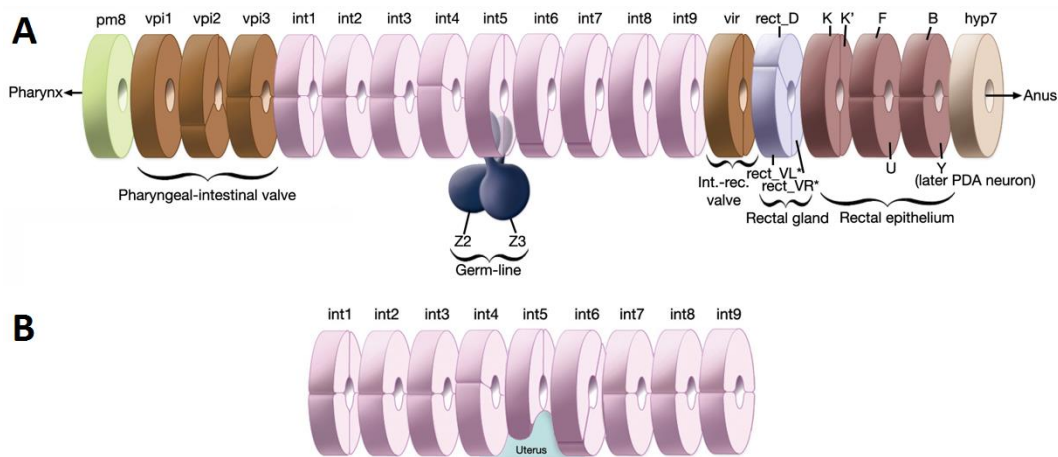


Figure 12. A) 430-minute embryo. Germ cell precursors extend lobes into the int5 cells. B) Newly hatched larva. The arrangement of intestinal cells reflect the second 90° turn that takes place around the longitudinal axis in the posterior. Adapted from WormAtlas.^[149]

C. elegans is a filter feeder: it draws bacteria suspended in liquid into its pharynx, traps the bacteria, and ejects the liquid.^[150] The alimentary system promotes intake and efflux of fluids and nutrients through the mouth and anus, respectively. Two motions are involved in the feeding behaviour of *C. elegans*: pharyngeal pumping and isthmus peristalsis. Pumping is a contraction–relaxation cycle in which particles and liquid are sucked in. During relaxation, liquid is ejected to the exterior and bacteria are retained in the pharynx and transported into the intestine.^[119, 150, 151] Bacteria reside in the intestine of *C. elegans* for less than 2 min. Although digestion is not completely understood in *C. elegans*, it seems to start with passage of bacteria through the grinder, which damages the bacterial cells. The processes of food ingestion during pharyngeal pumping and maceration in the grinder in *C. elegans* is equivalent to the chewing and swallowing actions in human feeding. Next, the bacterial cell wall and the plasma membrane are degraded by secreted lysozymes and saposins/amoebapores in the *C. elegans* intestine, and the contents of the bacteria pass to the intestinal lumen. Hydrolysis of the macromolecules is performed by secreted peptidases and lipases in the anterior gut. Most of these types of enzymes are also present in the human gut. Finally, nutrient absorption occurs in the apical domain of the intestinal cells in the microvillar brush border (**Figure 13**), which increases the surface area for absorption, and also contains digestive enzymes and transporters involved in absorption.^[119, 142] The primary surface for nutrient absorption in humans is also the microvilli in the apical domain of the enterocytes, which share significant structural similarities with those of the worm.^[119, 142] Interestingly, the pH of intestinal lumen of *C. elegans* has been recently investigated^[152] and found to range from ≈6 in the anterior pharynx to 3.6 in the posterior intestine, where digestive enzymes are released.^[142]

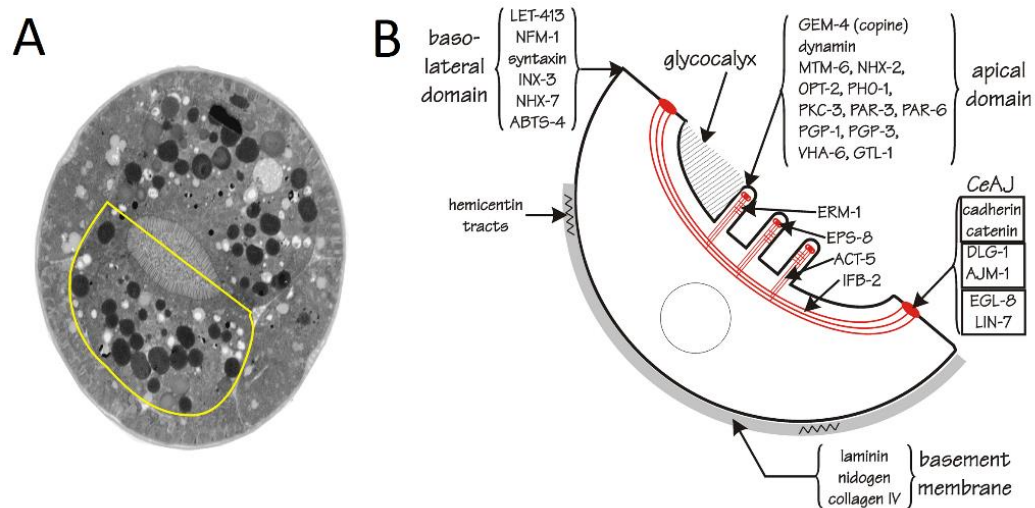


Figure 13. Structure of the *C. elegans* enterocyte. A) Transmission electron micrograph of a cross-section of a newly-hatched L1 larva. A single enterocyte, corresponding to half of an intestinal ring, is outlined in yellow. B) Schematic view of the enterocyte. Gene products and other markers that show differential localization to the apical or the basolateral domain are indicated. Adapted from Wormbook.^[142]

Finally, food digestion finishes with *C. elegans* defecation, consisting of the removal of undigested materials from the alimentary system through the anus in 50-second cycles. In each cycle, 47% of the total intestinal volume is expelled to the exterior. Defecation is under the control of the nervous system, and is achieved through rhythmic activation of a cycle of muscle contractions. When the intestinal contents press near the posterior end of the intestine, the enteric muscles contract promoting defecation, in a similar way that in vertebrates. *C. elegans* defecation is temperature independent, but it is slow when food is scarce (the cycle increases to 80 s), and can be inhibited as feeding ceases, being only resumed when food is available.^[119, 153]

The reproductive system

The reproductive system produces mature gametes (gametogenesis) and provides the structure and environment for fertilization and egg-laying. Spermatogenesis begins during the L4 larval stage and it is completed in the young adult shortly after molting. When sperm production stops, sperm stored in the spermatheca fertilizes the oocytes.^[119] Hermaphrodites produce ≈ 300 embryos by self-fertilization. Fertilized eggs move into the uterus and are laid outside through the vulva.^[133] Egg-laying is facilitated by contraction of the sex muscles, which are regulated by the nervous system. Several parameters can be studied in *C. elegans* including the number of eggs or progeny (also referred as brood size), the effects on the development of the progeny, or the effects on the reproduction of different filial generations.^[119] Thus, *C. elegans* facilitates experimentation and enables rapid initial results in the field of reprotoxicity.

Interestingly, a number of mechanisms and factors to establish germline and gametogenesis are conserved between *C. elegans* and humans. For instance, the *C. elegans* protein DSS-1, required for embryogenesis, larval growth and oogenesis, is

71% similar and 46% identical to the human DSS1 gene product, and is functionally conserved.^[154] *Foxo* genes constitute another good example. Mammals have four *Foxo* genes that are highly conserved but redundant in some contexts, which control multiple aspects of development, metabolism, reproduction, and tissue stem-cell function. In contrast, *C. elegans* has a single ancestral *Foxo* homolog that is required for maintenance of the germline, demonstrating that *Foxo* functions are quite ancient and functionally conserved.^[126] Therefore, *C. elegans* can be useful to study the effects of NP exposure on oogenesis and its molecular mechanisms.^[139]

1.4.5 Regulatory use of *C. elegans*

Although *C. elegans* is not considered a regulatory model organism in the regulations for the assessment of chemicals and drugs (p.e. in the guidelines of OECD, FDA or EMA), standards such as ISO and ASTM include invertebrates, among them *C. elegans*, as test organisms to assess water quality and soil toxicity (**Table 9**).

Table 9. Standard guides that include the use of *C. elegans* for environmental tests.

Standard guides that include the use of <i>C. elegans</i>	
ISO 10872:2010	Water quality -- Determination of the toxic effect of sediment and soil samples on growth, fertility and reproduction of <i>Caenorhabditis elegans</i> (Nematoda)
ISO 10872:2010 specifies a method for determining the toxicity of environmental samples on growth, fertility and reproduction of <i>Caenorhabditis elegans</i> . The method applies to contaminated whole fresh-water sediment (maximum salinity, 5 ‰), soil and waste, as well as to pore water, elutriates and aqueous extracts that were obtained from contaminated sediment, soil and waste.	
ASTM E2172-01(2014)	Standard Guide for Conducting Laboratory Soil Toxicity Tests with the Nematode <i>Caenorhabditis elegans</i>
Soil toxicity tests provide information concerning the toxicity and bioavailability of chemicals associated with soils to terrestrial organisms. As important members of the soil fauna, nematodes have a number of characteristics that make them appropriate organisms for use in the assessment of potentially hazardous soils.	

ISO: International Organization for Standardization;
ASTM: American Society for Testing and Materials

1.5 Thesis framework

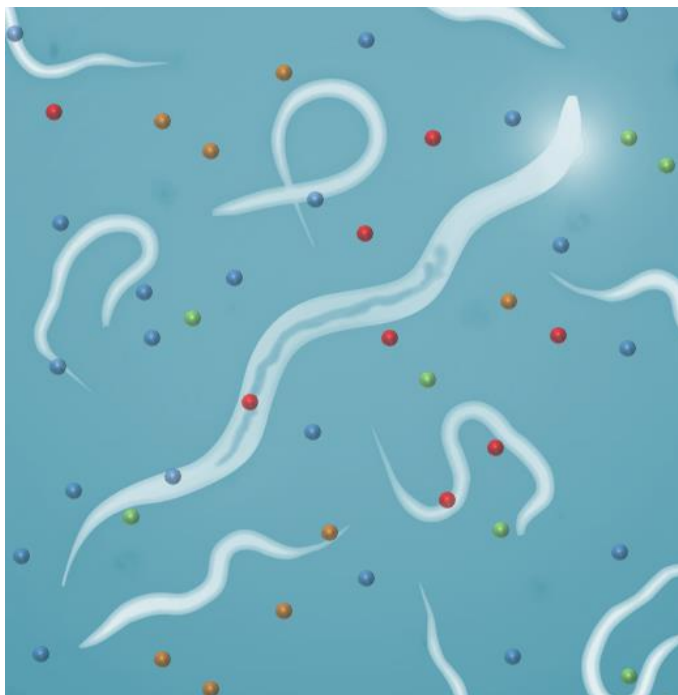
The great potential of nanomaterials in the medical field has still to be exploited.^[8] One of the main concerns about the clinical use of nanomaterials is whether they can induce harmful responses due to their small size and unique properties. This issue requires a deep understanding of the behaviour of nanomaterials in biological environments and progressing from *in vitro* to *in vivo* assays.^[15, 155] Given the large diversity of investigational materials, it is not feasible to evaluate them all in mammalian models such as mice or rats in the early stages of development, hence more simple approaches are in high demand to gather valuable evidence of nano-bio interactions.^[156] The analysis of vast amounts of nanotoxicological information (i.e. by applying big data or conducting meta-analysis^[157]) would allow building predictive models of the biological responses based on structure-activity relationships, in a similar way as it occurred for small molecules few decades ago.^[35, 105] In this direction, the use of simple model

organisms can help to greatly advance in the screening of nanomaterials for biomedicine within the synthetic lab, providing feedback for rationale optimization of NP design to increase biocompatibility.^[111, 112, 131] This approach could help to increase the success rate of novel nanomedicines during product development, significantly cutting off the translation time and cost.^[33, 36, 40]

Among simple *in vivo* models, the experimental features of *C. elegans* make it a highly promising animal for NP screening. Based on their few requirements of maintenance, it is easy to accommodate them in a materials science laboratory. The existing knowledge about their biological traits and genetics, together with its small size and transparency, offer great potential to study the behaviour of nanoparticles in a living organism by combining physical, chemical and biological techniques.

The evaluation of nano-bio interactions in *C. elegans* allows an in-depth study of many parameters, among them: i) NP localization at different biological scales (organ, tissue, cells, cell organelles); ii) NP status, properties and colloidal stability inside the animal body; iii) transport mechanisms across biological barriers; iv) molecular mechanisms triggered by NP exposure.^[114-116] These parameters have been thoroughly investigated in this thesis for iron oxide nanoparticles and gold nanoparticles to shed light on the size-, coating- and composition-dependence of NP effects *in vivo*.

CHAPTER 2. NP evaluation in *C. elegans*: State-of-the-art



CHAPTER SUMMARY:

This chapter describes how *Caenorhabditis elegans* can be exploited as a biological platform to evaluate nanomaterials within synthetic labs. First, we critically review relevant literature to detect common findings and to identify some shortcomings of the techniques employed. Next, we propose to extend the use of a range of techniques commonly employed in materials science to characterise nano-bio interactions in *C. elegans*.

CHAPTER INDEX

2.1 NP evaluation in <i>C. elegans</i>: State-of-the-art	33
2.1.1 Biological role of metals in <i>C. elegans</i>	33
2.1.2 Classification of previous work	34
2.1.3 Importance of the exposure mode	36
2.1.4 Entrance route, biodistribution and uptake.....	41
2.1.5 Dermal effects	44
2.1.6 Reprotoxicity effects	45
2.1.7 Importance of NP size, surface properties and composition.....	45
2.1.8 Endocytosis and translocation pathways	48
2.1.9 Biological mechanisms triggered by NP exposure.....	48
2.2 Materials science techniques with potential to assess nano-bio interactions	55
2.3 Chapter conclusions	57

2.1 NP evaluation in *C. elegans*: State-of-the-art

Currently, there is little conclusive evidence relating nanomaterials' properties and its behaviour in biological systems despite the huge number of papers studying nano-bio interactions (more than 10 000 in the last 15 years)^[158] and the intensive resources devoted to this aim. The heterogeneity of the experimental procedures (mode of exposure, endpoints...) has led to results that are generally not comparable and to conclusions that are sometimes even contradictory. Therefore, the use of standardised procedures could accelerate advances in the field and facilitate major discoveries. Moreover, it would facilitate a meta-analysis of piles of research studies and offer more conclusive results, albeit great disparity in experimental protocols is common at the early stages of discovery.^[158] Even though, the work published to date has provided valuable knowledge and illustrated the potential of several methodologies and techniques that can be of great value to screen the interaction between nanomaterials and living organisms. In this section, we will present relevant work concerning the effects of nanomaterials with different sizes, shapes, coating and composition, and their mechanisms of action in the *C. elegans* model. In particular, we will extensively review literature of metal and metal oxide NPs. We will also propose potential applicable materials science techniques to shed light on the interaction between inorganic NPs and *C. elegans*. Finally, we will present the protocols used in the experimental sections of this thesis.

2.1.1 Biological role of metals in *C. elegans*

Before reviewing previous work of nanoparticles (NPs) in *C. elegans*, it is important to note that some metals have a biological role in this model organism. Indeed, *C. elegans* has been used as a model organism in the study of metals in biology, thus its use in the evaluation of metal and metal oxide NPs is only a new branch in a field with decades of validated research.^[159, 160] In this sense, it is also important to note that the biological responses triggered by NP exposure can be nano-specific, but NPs can also partially dissolve as cations in the exposure media or inside the organism, leading to a more general element-related toxicity (**Figure 14**). Previous research using bulk metals has shown that accumulation of metals depends on the physicochemical properties of metals, the physiology of organisms and the nature of the metal (essential or not).^[161-163] In both humans and *C. elegans*, zinc, copper, manganese and iron are essential metals and play an important role in diverse biological processes (**Table 10**). Metal homeostasis and transport involve sophisticated mechanisms in regulation of its uptake and distribution within an organism because an imbalance caused by either deficiency or overload can cause severe dysfunctions.^[161, 162]

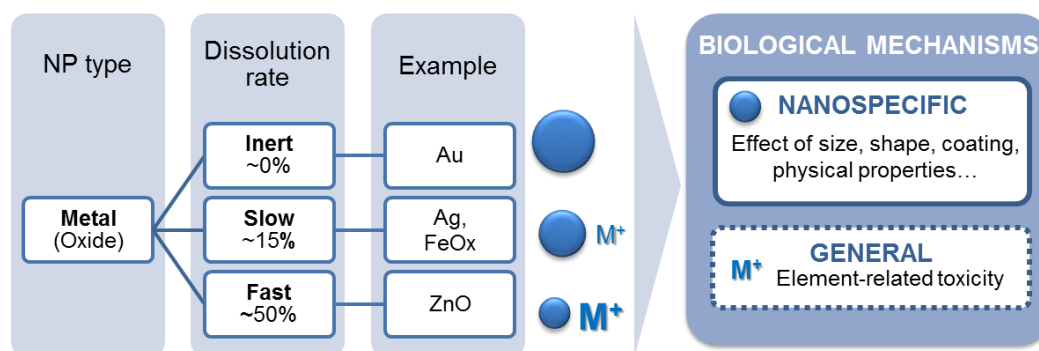


Figure 14. Mechanism of action of nanoparticles.

Table 10. Biology of metals in *C. elegans*. Data extracted from Chen *et al.*^[162]

	Copper	Iron	Manganese	Zinc
Functions	<ul style="list-style-type: none"> - Iron homeostasis - Neurotransmitter biosynthesis - Oxidative phosphorylation, - Oxidative stress protection 	<ul style="list-style-type: none"> - DNA synthesis - Mitochondrial respiration - Oxygen transport - Neurotransmitter synthesis. 	<ul style="list-style-type: none"> - Fat and carbohydrate metabolism - Oxidative stress protection (SOD) - Neurotransmitter synthesis and metabolism. 	<ul style="list-style-type: none"> - Cofactor in several cellular processes and cellular signalling pathways.
Deleterious Effects	<p>Deficiency Decreased SOD, reducing defenses against oxidative stress.</p> <p>Excess Detrimental effects on brood size and life span, an increase in generation time and impaired development.</p>	<p>Deficiency HIF-1 inhibits <i>ftn-1</i> and <i>ftn-2</i> transcription. The activation of <i>smf-3</i> provides a mechanism to maintain sufficient Fe stock for growth and survival.</p> <p>Excess Phenotypic and behavioural defects like reduced lifespan, brood size, locomotion, and alters the resistance to oxidative stress</p>	<p>Excess Accelerated development, increase in fertility, reduced body and brood size and life span. Increased ROS formation and glutathione production, head mitochondria membrane potential and DA neuronal death.</p>	<p>Excess Multiple biological defects affecting life span, reproduction, locomotion behaviour and chemotaxis plasticity.</p>
Genes	Highly conserved: Cu/Zn superoxide dismutase (SOD), Divalent metal transporters (SMF-1, SMF-2, SMF-3), Ca ²⁺ /Mn ²⁺ ATPases (PMR1), Homolog of mammalian Nrf2 (SKN-1), Cation diffusion facilitators (CDFs), Zrt- and Irt-like proteins (ZIPs), Ferritin (<i>ftn-1</i> , <i>ftn-2</i>), Fe sulfuric cluster assembly proteins, Metallothioneins (MTs).			

2.1.2 Classification of previous work

In recent years, some efforts have been made to screen an extensive range of nanomaterials in the *C. elegans* model, including metal and metal oxide nanoparticles, carbon nanomaterials, and others like quantum dots or up-converting nanophosphors.^[164-173] Given the broad spectrum of the study of nano-bio interactions and the versatility of *C. elegans*, multiple disciplines such as environmental sciences or biomedical research have converged but maintaining divergent perspectives (Figure 15). For instance, in environmental toxicology *C. elegans* is used as terrestrial animal model and treated with concentrations environmentally relevant, typically ppm. Hence, doses are much lower than those relevant for clinical settings in humans (at least 3 orders of magnitude below). Moreover, those studies tend to focus on toxicity endpoints mainly. In contrast, in nanomedicine *C. elegans* is used as a simple model organism to gather preliminary data on the biocompatibility of novel materials. Biomedical studies assess a broad range of

doses and generally perform an integral evaluation of uptake, biodistribution, translocation pathways, as well as molecular mechanisms affected by NP exposure. Furthermore, *C. elegans* has also been used as an *in vivo* platform to validate the efficiency of nanomaterials for a given application such as imaging,^[152, 165, 170] drug delivery^[174, 175] or targeted agents^[176-178] without further study of the biological consequences of NP exposure in a wider time window or dose scale.

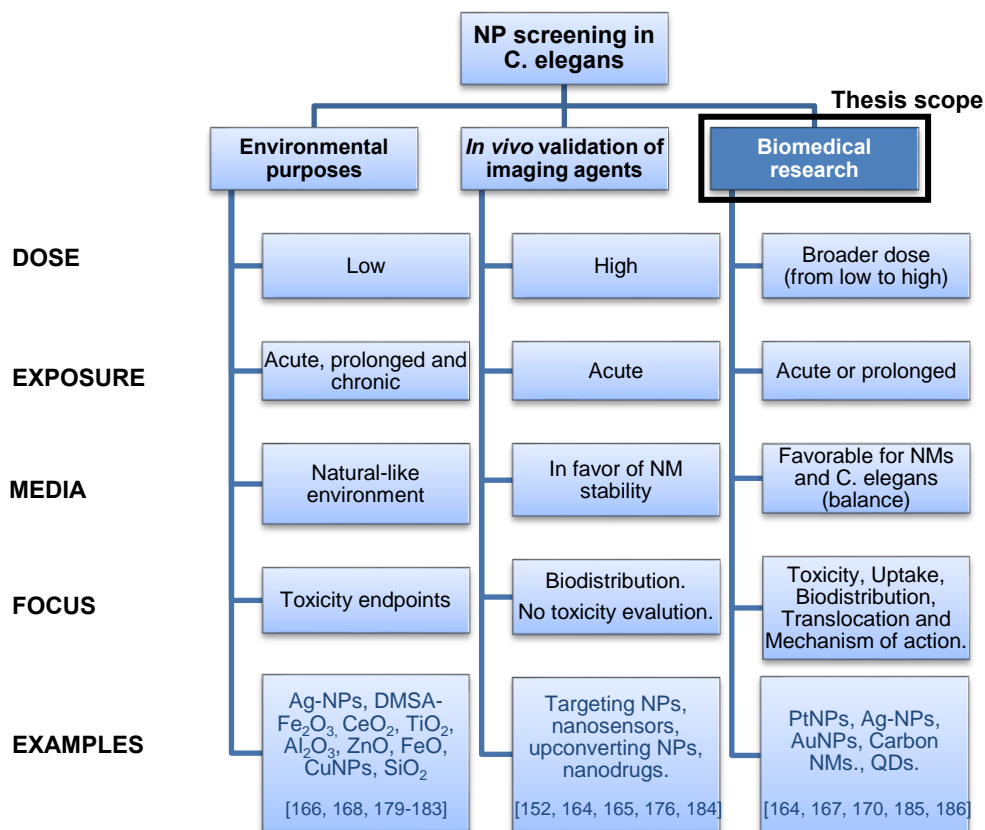


Figure 15. Purpose and main experimental features of previous work screening nanomaterials in *C. elegans*. NMs: nanomaterials.

A solid approach to screen nanomaterials in *C. elegans* consists on the development of high-throughput systems able to study multiple endpoints at both population and organism level in an automated way, taking advantage of the micro-metric size of *C. elegans* and their physiological traits. This strategy allows scientists to perform a fast study of different nanomaterials at different concentrations, however few authors have explored this possibility.^[187] The study of nanomaterials' effects using different bioassays on a diversity of organisms representing distinct trophic levels using a collaborative approach between a consortium of laboratories could also evaluate the risk posed by nanomaterials in the environment and humans with superior robustness, as it has been previously done for chemicals.^[188]

The majority of the work on metal NPs in *C. elegans* have been performed by the group of Dr. Joel Meyer at the Duke University^[115, 167, 189-192] and Dr. Olga Tsyusko^[115, 182, 186, 193, 194] at the University of Kentucky, and investigated predominantly silver

nanoparticles. Fewer efforts have been devoted to other metals such as gold,^[186, 195] platinum^[185, 196] and copper.^[181] In contrast, the evaluation of metal oxide NPs in *C. elegans* have studied diverse compositions to a similar extent, including titania, ceria, aluminium oxide, and zinc oxide nanoparticles, among others. However, most assays have been performed considering those concentrations that could end up in soils due to waste disposal of NP-containing materials, hence were investigated from an environmental point of view. For instance, ZnO-NPs are used in large quantities by the cosmetic, food and textile industries, while TiO₂-NPs are used in paints, plastics, inks, paper, creams, cosmetics, drugs, and foods. The groups of Dr. Mikecz^[197, 198] at Heinrich Heine Universität Düsseldorf, Dr. Stürzenbaum^[199] at King's College London, Dr. Wang^[168, 172, 179, 200, 201] at Medical School of Southeast University, Nanjing, and Dr. Marie-Helen Delville^[202] at Institut de Chimie de la Matière Condensée de Bordeaux CNRS have been actively working with metal oxide NPs in the last years. Currently, the evaluation of nanomaterials in *C. elegans* is an active field of research as a model organism in both ecology and biomedicine fields.^[127]

2.1.3 Importance of the exposure mode

C. elegans is typically grown in NGM agar plates with *E. coli* OP50 as food source. If NGM agar is mixed with nanoparticles during its preparation, it is difficult to ensure that NPs get evenly distributed in the media once solid. Moreover, the high ionic strength of NGM can compromise the colloidal stability of NPs leading to aggregation or precipitation, hence resulting in a non-homogenous NP exposure of *C. elegans*. In addition, the presence of living bacteria adds biological surface and active metabolism that can lead to uncontrollable and unpredictable effects on NP status before and during *C. elegans* exposure (i.e. adsorption of NPs onto the bacterial surface, biotransformation of NPs into subproducts...). Other exposure conditions have also been proposed to overcome these difficulties, p.e. short exposures in liquid media (either MHRW or K-medium) in the absence of food,^[186, 203] or prolonged exposures in liquid media (K-medium or S basal) with food supplementation.^[167, 185] Some authors have also studied the effect of food presence in NP toxicity.^[182, 189, 193, 204] Given the environmental focus of most investigations using metal oxide NPs, authors have further investigated the influence of several parameters related to the exposure media to better understand more realistic environments that could occur in the soil, p.e. the presence of natural organic matter, different ionic strength of the media, or the presence of specific salts.

In this section, we review the exposure conditions used by the different groups (i.e. exposure media, developmental stage, duration...) (**Table 11**).

Table 11. Summary of the experimental conditions of the literature reviewed.

NP core	NP Size	NP Coating	Exposure Concentration	Stage	Exposure Media	Exposure Duration	Ref
Metal NPs							
Ag	60	Bare, Sulfidized	0.35, 1.50 mg/L	L1	K-medium, MHRW ± food	24, 48, 72 h	[194]
	25	Citrate, PVP, gum arabic	0.1-1.5 mg/L	YA	MHRW, no food	24 h	[191]
	60	Bare, Sulfidized	0.5-3, 3-9 mg/L	L3 / L4	MHRW ± food	24 h	[193]
	8-38	Bare, Citrate, PVP	0.15-5 mg/L	YA	MHRW, no food	24 h	[189]
	2, 5, 10	mPEG-SH	1-100 mg/L	L1	NGM, food	24 h	[205]
	8-38	PVP, bare	0-6.5 mg/L	YA	K-medium, no food	24 h	[192]
	1-75	Citrate, PVP, Gum Arabic,	0-15 mg/L	L1	MHRW, food	72 d	[190]
	14~20	N.S.	0.1, 1 mg/L	3d A	K-medium, no food	48 h	[206]
	20-30	N.S.	0.1-1 mg/L	3d A	K-medium, no food	4, 24 h	[203]
	10-30	Citrate	0-1000 mg/L	L3	NGM agar	24, 48 h	[207]
	1, 28	Bare, PVP	0-10, 0-3 mg/L	L2	K-medium ± food	24, 48, 72 h	[204]
	10-75	Citrate, PVP	0-104 mg/L	L1	K-medium, food	24, 72 h	[167]
	14~20	N.S.	0.05-5 mg/L	3d A	K-medium, no food	24 h	[180]
Au	10	N.S.	0-5.10 ¹¹ NPs/ml	L1	NGM agar, food	48 h	[195]
	4	Citrate	0-30 mg/L	L3	50% K-medium, no food	12h	[186]
Pt	2.4	Bare, TAT	500, 5 µM	L4	S medium, food	48 h / 10 d	[196]
	2.4	Bare	500 µM	L4	S medium, food	48 h	[185]
Cu	23.5	N.S.	1.0.10 ⁻⁴ mol/L	L1	NGM agar, food	36 h	[181]
Metal Oxide NPs							
TiO ₂	25-35	Native, TRITC	2 g/cm ²	YA	NGM agar, food	4 h	[202]
	10	N.S.	100 mg/L	YA / L1	NGM agar, food	YA: 24 h L1: To A	[201]
	30	N.S.	0-0.050 mg/L	L1	K-medium, food	To A	[173]
	10	N.S.	0.020, 25 mg/L	YA	K-medium, food	24 h	[168]
	50	N.S.	0-240 mg/L	L1	Ultrapure water, food	24 h / 5 d	[169]
	7,20	N.S.	1 mg/L	3 d A	K-medium, no food	24 h	[208]
ZnO	10, 50, 100	Fluorescent polymer	100, 2000 mg/L	3 d A	Buffered K-medium, no food	24 h	[209]
	30	Bare	0-50mg/L	L1	NGM agar, food	48 h	[199]
	30	N.S.	0-0.050 mg/L	L1	K-medium, food	To A	[173]
	20	N.S.	0-8.1 mg/L	L1	Ultrapure water, food	24 h / 5 d	[169]
	1.5	N.S.	325, 1625 mg/L	4 d A	Buffered K-medium, no food	24 h	[166]
CeO ₂	4	Dextran (+), (-), neutral	0-100 mg/L (L1) 0-1000 mg/L (L3)	L1, L3	MHRW, food ± HA	48 h	[182]
	50	N.S.	0-94 mg/L	L1	MHRW, food	3 d	[210]
	15, 45	N.S.	1 mg/L	3 d A	K-medium, no food	24 h	[208]
SiO ₂	30	N.S.	0-0.050 mg/L	L1	K-medium, food	To A	[173]
	50	Unlabeled, rhodamine, FITC	2500 mg/L	1 d A	NGM agar, food	24 h	[198]
	50	Fluorescently labelled	250-5000 mg/mL	L4	NGM agar, food	16 h	[197]
Al ₂ O ₃	60	N.S.	0-23 mg/L	YA	Modified K-medium, food	6, 48 h, 10 d	[200]
	60	N.S.	0-408 mg/L	L1	Ultrapure water, food	24 h, 5 d	[169]
FeO _x	9	DMSA-Fe ₂ O ₃	0-1000 mg/L	L4 L1	K-medium, food	L4: 24 h L1: to A / 8 d	[211]
	Variable	Soil-derived, variable	0-447 mg/L	L3 + L4	K-medium, food	6 h	[183]

NP: nanoparticle; Stage: developmental stage of *C. elegans*; N.S.: Not specified; PVP: polyvinylpyrrolidone; PEG: polyethylene glycol; FITC: Fluorescein isothiocyanate; DMSA: dimercaptosuccinic acid; A: adult; L: larva; YA: young adult; MHRW: moderately hard reconstituted water; HA: humic acid; NGM: nematode growth media; d: day(s); h: hours.

Exposure in liquid media

Meyer *et al* reported formation of Ag-NP aggregates with diameters of 1~2 μm in K-medium that rapidly settled from suspension leading to an elevated effective local “dose” in the bottom of the wells, where *C. elegans* also settle out in unshaken conditions.^[167] Ellegaard-Jensen *et al* also observed a rapid formation of micrometric agglomerates of Ag-NPs in K-medium.^[204] These events can hinder NP evaluation based on the no longer nano-scale but micrometric size of the test materials, and determine NP toxicity. For instance, Yang *et al* attributed the reduced toxicity of citrate Ag-NPs compared to the other surface coatings (gum arabic and PVP-coated) to the formation of aggregates and subsequent decrease of available surface area for dissolution.^[190] In order to reduce aggregation in liquid media, several strategies have been employed. Ma *et al* observed aggregation when ZnO-NPs were diluted in unbuffered K-medium, but not in acetic acid/acetate-buffered K-medium, hence they used the latter in their experiments.^[166] Gupta *et al* followed the same approach.^[209] Roh *et al* reported aggregation and precipitation of CeO₂ and TiO₂-NPs in K-medium at high doses, thus selected exposure to low doses (1 mg/L) without food for 24 h to ensure the stability and uniformity of the NP suspensions during the testing period.^[208] Arnold *et al* used higher doses of CeO₂-NPs (2.5-93.75 mg/L) in MHRW for 3 days, however they renewed the dosing solutions daily to minimize aggregation effects.^[210] Despite the recurrent efforts to maintain the nano-scale size of the nanomaterials under study, it is controversial whether the study of non-dispersed material would be more relevant as it is the status that will likely occur in real environments, either in the environment or the human body. However, the efforts of preserving NP stability and uniformity across the exposure media is of vital importance to ensure repeatability of the experiments and to discern effects arising solely from the nano-scale properties of the test materials.

Effect of ionic strength and natural organic matter

Yang *et al* investigated the effect of the ionic strength of the exposure media in Ag-NP toxicity and found that lower ionic strength resulted in greater toxicity: effect and lethal doses were 1.5–12 times higher in MHRW than in K-medium.^[190] Similarly, Wang *et al* exposed nematodes to ZnO-NPs in ultrapure water and K-medium, and observed lower toxicity in the presence of salts.^[169] The reduced toxicity of several metals in the presence of potassium and sodium salts was also reported by Donkin and Williams.^[212] Yang *et al* also studied the effect of natural organic matter (NOM) in Ag-NP toxicity and reported that the presence of NOM resulted in the formation of NOM/Ag-NP composites both that rescued Ag-NP-induced cellular damage, likely by decreasing intracellular uptake.^[189] Collin *et al* exposed nematodes to CeO₂-NPs with and without humic acid (HA) as a source of NOM, and observed that HA significantly decreased the toxicity when of CeO₂-NPs. The authors proposed that the adsorption of HA at the surface of the NPs could form a physical barrier to NP interaction with the cell membrane, reduce binding of NPs to important proteins and biomolecules, and also act as an antioxidant by reacting with ROS

mitigating the oxidative stress induced by CeO₂-NP exposure. Moreover, the presence of HA highly influenced Ce bioaccumulation depending on the NP/HA ratio: a high ratio increased Ce accumulation, while a low ratio decreased it, likely due to the negative surface charge of the HA/NP composites.^[182]

Effect of food presence

We found contradictory results concerning the effect of food presence during NP exposure in liquid. According to Ellegaard-Jensen, including *E. coli* in the test medium (K-medium) as a food source increased the toxicity of 1-nm Ag-NPs towards nematodes, likely by increasing Ag-NPs bioavailability.^[204] In contrast, Starnes *et al* observed decreased mortality after exposure to 60-nm Ag-NPs in MHRW in the presence of food. The concentrations at which *C. elegans* exhibited equivalent mortality were 4–30 fold higher in the experiment with feeding than without feeding.^[193] Yang *et al* also reported strongly mitigated toxicity of 8-nm PVP-coated Ag-NP in MHRW with NOM when food was included.^[189] Collin *et al* observed that the effects of food in NP bioavailability depended on the presence of HA in the exposure media: upon addition of *E. coli*, the accumulation of CeO₂-NPs in *C. elegans* did not significantly change in the absence of HA, but it decreased in the presence of HA. They also investigated the Ce oxidation state and found no significant changes due to HA or food addition. However, the authors did not study whether the changes in Ce bioavailability related to food presence also resulted in changes in NP toxicity.^[182]

Controlled exposure in standard culture conditions

Other authors have chosen exposure in standard culture conditions consisting of Nematode Growth Media agar plates with food. In order to perform controlled and reproducible exposures, Pluskota *et al* applied NP suspensions to the bacterial lawn and monitored the area and the resulting particle-load per area. They studied the dispersity of NPs in suspension by fluorescence correlation spectroscopy (FCS), which showed that single, monodisperse 50-nm silica and polystyrene NPs (PS-NPs) constituted the major mobile fraction. However, they also reported the occurrence of differently sized NP agglomerates in low frequency.^[197] Polak *et al* carefully characterised the physicochemical properties of ZnO-NP suspensions in bacteria/LB mixtures, before pouring them into NGM plates for *C. elegans* exposure (**Figure 16**). In LB broth, 30-nm ZnO-NPs assembled into 1- μ m clusters without time-dependent changes in agglomerate levels, suggesting stability of the agglomerates in the test medium. TEM studies showed that the majority of ZnO-NPs formed acicular clusters of few hundred nanometers, resulting in reduced surface charge and thus weaker electrostatic repulsive forces. ZnO-NPs agglomerates did not induce morphological changes or entered the bacteria, but caused the bacteria to secrete extracellular polymeric substances which coated the nanoparticles within 24 h and could affect the bioavailability of ZnO-NPs. The authors also reported a significant dissolution of the nanoparticles in the exposure media: dissolved ZnO constituted over 50% of total Zn within a two day exposure. Therefore, exposure to pure ZnO-NPs *in vivo* represented a

mixture exposure of Zn²⁺ and nanoparticles. However, the authors could not conclude to what extent the observed biological effects were driven by the bioavailable fraction of ZnO-NPs or indeed the derived ionic Zn.^[199]

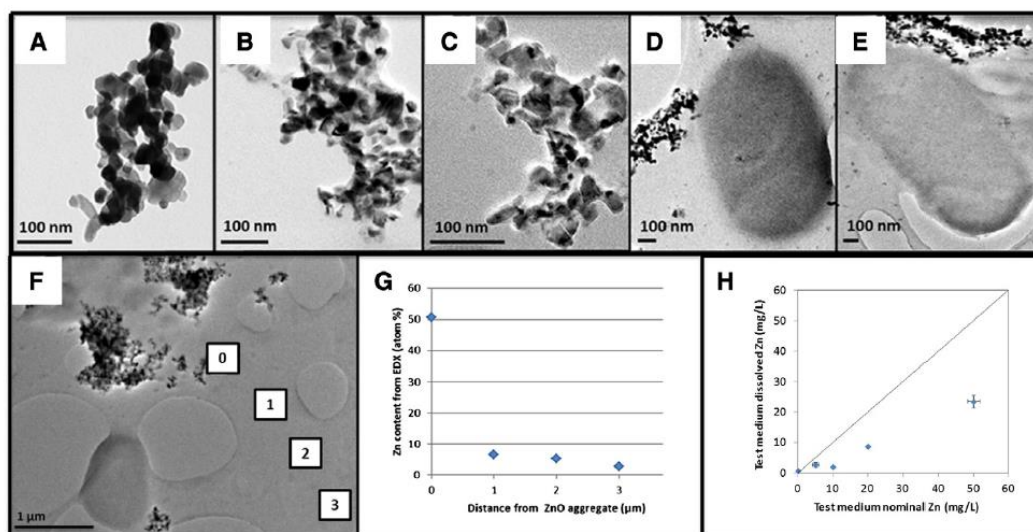


Figure 16. Transmission Electron Microscopy (TEM) of ZnO nanoparticles. Images of ZnO-NPs in: A) HPLC water, B) LB-broth at 0 h, C) LB-broth at 24 h, D) LB-broth with bacteria (OP50) at 0 h, E) LB-broth with bacteria (OP50) at 24 h. F) Energy-dispersive X-ray spectroscopy (EDX) analyses and chemical mapping on four micron-sized windows were performed to determine: G) the percentage of Zn content, H) the relative dissolution rate quantified (H). Adapted from Polak *et al.*^[199]

Effects of C. elegans stage and duration of the exposure

Different studies showed that the extent of NP toxicity depended on the developmental stage of the nematodes at which NP exposure began, and also on the duration of the exposure. For instance, Collin *et al* found that L3-larvae were more resistant than L1-larvae to 4-nm CeO₂ exposure.^[182] Zhao *et al* also reported that L1 worms were more sensitive than L4 individuals or adult nematodes to 10-nm TiO₂-NP toxicity.^[201] Interestingly, Wu *et al* evaluated the effects of DMSA coated 9-nm Fe₂O₃-NPs in K-medium using three different assay systems: a) 24 h exposure of L4 nematodes; b) prolonged exposure from L1 to adults (~3 days); c) chronic exposure from L1 to 8-day adult. Adverse effects were observed at concentrations higher than 50 mg/L, 0.5 mg/L and 0.1 mg/L, respectively, indicating higher toxicity with increasing treatment duration.^[211] Zhao *et al* also found differences on the recovery response after acute exposure (24 h; young adults) and chronic (from L1 to adult) to nano-TiO₂. Chronically-treated nematodes had uptaken more NPs than acutely-treated animals and had reduced capacity of NP excretion. Moreover, animals could not recover and endpoints such as length, locomotion or pharyngeal pumping remained altered even after 48 h under normal conditions, while acutely-treated nematodes fully recovered.^[213]

The evidence presented in this section highlights the importance of the selection of test media and exposure conditions as determinant factors in the NP toxicity. Moreover, the heterogeneous exposure conditions used by the different authors clearly illustrates the importance of standardization to gather comparable experimental data and lead to more solid conclusions.

2.1.4 Entrance route, biodistribution and uptake

Entrance of metal and metal oxide NPs have been reported to occur mainly through the alimentary system, both in the presence and absence of food and either in liquid or solid media, consistent with the fact that *C. elegans* do not discern between entities up to 5 μm when feeding.^[214] The most prevalent techniques to study NP fate and uptake have included fluorescent microscopy,^[196-198] hyperspectral dark-field microscopy,^[167, 192] and to a much lesser extent, transmission electron microscopy^[207], synchrotron-based techniques and chemical techniques. When using fluorescence microscopy to track NPs, it is important to note that this technique is limited to a theoretical resolution of 200 nm, hence it cannot be excluded that single NPs penetrate further into *C. elegans* tissue or are taken up intracellularly without the use of complementary techniques such as electron microscopy. Transmission electron microscopy has sufficiently low spatial resolution to allow single-NP detection enabling the study of NP localization at the subcellular scale. Among the synchrotron microbeam techniques, synchrotron radiation X-ray fluorescence ($\mu\text{-SRXRF}$) have been used to map the metal distribution in *C. elegans*, while synchrotron X-ray absorption near-edge spectroscopy ($\mu\text{-XANES}$) have provided information regarding the oxidation state and coordination environment of metals.^[181, 202] The combination of $\mu\text{-SRXRF}$ and $\mu\text{-XANES}$ is a powerful tool to study the subcellular distribution and chemical species of metals of interest.

Based on the small size of the materials under study, scientists must select techniques with nanometric spatial resolution to discern and identify particles with certainty at multiple biological scales, from the organ level to subcellular compartments, in order to shed light on single-NP localization, translocation mechanisms and NP status *in vivo*. The correlation of the physicochemical properties of the nanoparticles with their *in vivo* status and toxicity would provide feedback to further optimize NPs within the synthetic laboratory to ensure maximum quality, efficiency and safety 'by design', a growing trend in the pharmaceutical industry at the early stages of discovery.^[215]

Fluorescence microscopy

Using epifluorescence microscopy, Pluskota *et al* showed that fluorescently labelled 50-nm nanoparticles (polystyrene and SiO_2) were efficiently taken up by the worms during feeding, and translocated to primary organs such as epithelial cells of the intestine, as well as to secondary organs belonging to the reproductive tract. Within the intestine, NPs followed an uptake-gradient with decreasing concentrations from the

anterior to the posterior regions of the intestine. Cytoplasmic uptake of 50-nm polystyrene NPs was observed in early embryos.^[197] Scharf *et al* identified two entry portals of silica and PS-NPs: via the pharynx to the intestinal system, and via the vulva to the reproductive system. Using light sheet microscopy, they identified NPs throughout the cytoplasm and the cell nucleus in single intestinal and vulval cells (**Figure 17**).^[198] Gupta *et al* investigated the biodistribution of 10, 50, 100 nm ZnO-NPs conjugated with a fluorescent polymer, and reported that the smaller nanoparticles showed a uniform distribution of fluorescence in a wide range of cells and tissues including a large number of eggs, whereas 50 and 100 nm ZnO-NPs were only recorded at particular points either in anterior or posterior intestinal regions.^[209]

Hyperspectral microscopy

Meyer *et al* studied the biodistribution of citrate and PVP-coated Ag-NPs (10-75 nm) using hyperspectral microscopy and observed that all the NPs tested were internalised by the intestinal cells, but only the citrate ones transferred to the germ line (**Figure 17**).^[167] Yang *et al* reported that the majority of Ag-NPs (8-38 nm) located in the digestive tract, and detected limited tissue uptake by hyperspectral microscopy but not by transmission electron microscopy.^[189] Arnold *et al* also applied hyperspectral imaging to study the localization of 50-nm CeO₂-NPs and detected NPs both in the intestinal tract and on the surface of the worm, but not inside the intestinal cells.^[210]

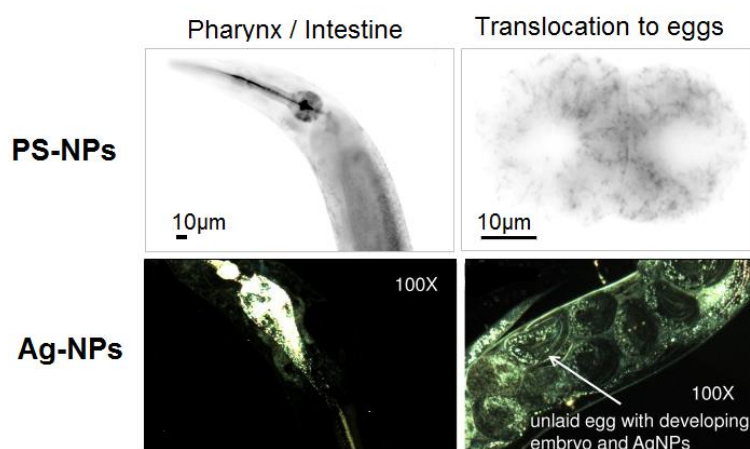


Figure 17. Worms fed on a bacterial together with PS-NPs and Ag-NPs. Upper panels show epifluorescence images showing carboxy 50-nm PS-NPs in the intestine (left) and cytoplasm of early embryos (right). Adapted from Scharf *et al* and.^[198] Lower panels present hyperspectral images showing 10-nm citrate Ag-NPs in the intestine (left) and transference to the offspring (right). Ag-NP identity was confirmed by hyperspectral analysis. Adapted from Meyer *et al*.^[167]

Synchrotron techniques

Using μ -SRXRF, Gao *et al* showed that 24-nm Cu-NP exposure resulted in elevation of Cu and K levels in the *C. elegans* body, and also in changes in the Cu, Fe and Zn bio-distribution (**Figure 18**). However, Cu²⁺ exposure resulted in a much higher absorption and accumulation.^[181] Le Trequesser combined μ -SRXRF and μ -XANES to

detect and quantify 30-nm TiO₂-NPs in *C. elegans*. After 4 h exposure, NPs were visible only in the lumen of the alimentary system extending from the pharynx to the anal region, and continued retained there even 24 h after feeding.^[202] Given that alterations in the distribution of trace metal such as Fe, Cu, Zn or Mn are sometimes related to certain pathological states, the use of these techniques is of relevance in the study of alterations in metal homeostasis.

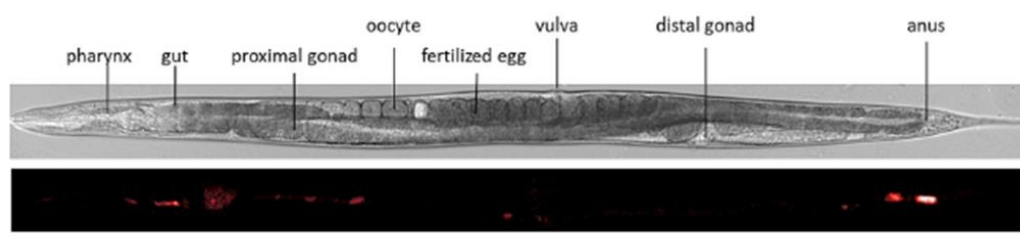


Figure 18. In situ chemical imaging of a lyophilized *C. elegans*. Above, synchronized worm observed by conventional microscopy. The different organs of the worm are depicted. Below, I-PIXE maps of titanium in *C. elegans* body. Scale bar, 150 μ m. Adapted from Le Trequesser *et al.*^[202]

Chemical techniques

Chemical approaches to study NPs in *C. elegans* include the use of microspectroscopic techniques to characterise NP status and quantitation of NP uptake by chemical assays. Interestingly, Polak *et al* used Raman microspectroscopy to identify differences in biomolecular composition and quantify changes in internal Zn load within individual nematodes (**Figure 19A**). A significant separation of the spectra was observed in the head and tail region of the *mtl-1;mtl-2;pcs-1* mutant upon exposure to ZnO-NPs compared to wild-type nematodes, confirming that the phenotype of the metallochaperone mutant is more affected by ZnO-NP exposure. Exposure to ZnO-NPs in *mtl-1;mtl-2;pcs-1* nematodes caused reductions in peak intensities of proteins, amino acids (cytochrome c, amide I, phenylalanine) and nucleic acids, highlighting a broad effect on the nematode phenotype.^[199] Höss *et al* investigated the accumulation of soil-derived ferrihydrites associated with citrate, predominantly <50 nm, after 6 h exposure using the ferrozine assay for iron determination. Immediately after exposure, relatively high Fe concentrations were measured (2 μ g/mg worm). However, after 2 h under normal condition, defecation of the NPs contained in the intestinal lumen led to the disposal of 50% Fe. Disposal of the surface-attached Fe during molting caused an additional 80% reduction of nematode-associated Fe. The Fe concentration in *C. elegans* tissue was 4.5 times higher in exposed *C. elegans* than in control organism. According to the authors, accumulated Fe is the fraction responsible for toxicity, however they could not prove whether it still represented intact ferrihydrites colloids. Under the mildly acidic conditions of the gut, FeO_x can partly be dissolved allowing a minor transfer of ionic Fe³⁺ from the gut to the tissue. However, the very short residence time of FeO_x in the intestine when food is present in the exposure media (<2 min)^[150] makes a quantitative dissolution of FeO_x unlikely from a kinetic point of view.^[183] Interestingly, the authors also performed uptake experiments with ionic Fe³⁺ and

observed only slightly, not significantly elevation of Fe accumulation in *C. elegans*, suggesting that the higher internalisation of colloidal FeO_x was due to its particulate nature (Figure 19B).

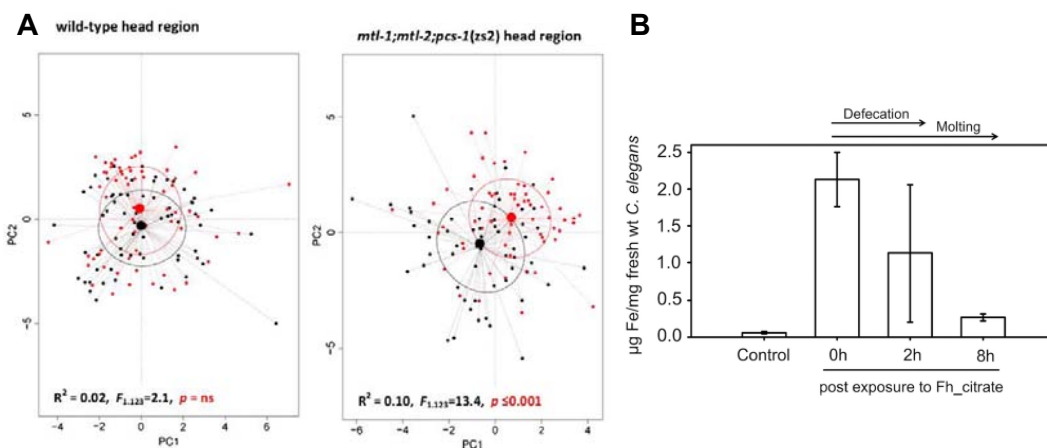


Figure 19. A) Principal component analysis showing the relationship between the Raman phenotype of ZnO-NP exposed and control treatments in wild-type (left panel) and *mtl-1;mtl-2;pcs-1* mutant (right panel) nematodes in the head regions. Black points represent spectra from control nematodes, red points represent spectra from ZnO-NP exposed nematodes. Black and red ellipses represent standard deviations of point scores for the control and treatment groups, respectively. Adapted from Polak *et al.*^[199] B) Fe concentrations measured in *C. elegans* after 6 h exposure to K-medium (control) and ferrihydrite colloids associated with citrate (Fh_citrate) (28 mg Fe/L); 0 h post exposure: comprises bioaccumulated, attached and ingested Fe; 2 h post exposure: comprises bioaccumulated and attached Fe; 8 h post exposure: comprises bioaccumulated Fe; bars: arithmetic mean, error bars: standard deviation (n = 3). Adapted from Höss *et al.*^[183]

2.1.5 Dermal effects

The dermal route has not been usually explored in the evaluation of NPs in the *C. elegans*. Kim *et al* addressed the issue with a combination of scanning electron microscopy (SEM), transmission electron microscopy (TEM) and high resolution microscopy (HRM).^[207] After 24-h treatment to citrate coated 10-nm Ag-NPs in NGM agar, severe epidemic edema and burst occurred in the biological surfaces of *C. elegans* without evidence of NP intake (Figure 20). This study suggests that metal toxicity and adverse physical effects can be induced via the dermal route. Given that previous studies in liquid^[167] attributed nanotoxicity to NP feeding, Kim *et al* proposed that the epidermal effects could be caused by the movement of *C. elegans* in the agar plates where the Ag-NPs were distributed. Indeed, the main uptake route for metals into the tissue of *C. elegans* is considered to be the gut, rather than via the cuticle.^[216, 217] However, adhesion of metal or metal oxide NPs onto the surface of the worm has been reported for some metal and metal oxide NPs.^[167, 182, 210] Using Hyperspectral Microscopy, Meyer *et al* concluded that the extend of the Ag-NP adsorption was size- and coating-dependent: greater adsorption occurred for 10-nm citrate Ag-NPs and 21-nm PVP-Ag-NPs than for 75-nm PVP-Ag-NPs. Arnold *et al* also detected 50-nm CeO₂-NPs on the surface of treated animals, however using hyperspectral imaging the authors could not determine whether the NPs were translocated into the epithelial cells or just adsorbed onto the surface of cuticle cells.^[210] By synchrotron X-ray analysis, Collin *et al* observed adhesion of 4-nm

positively charged CeO₂-NPs in the cuticle of the worm and attributed it to electrostatic attraction between the cuticle and the NPs.^[182] Recently, transcriptomic studies of nematodes exposed to pristine and sulfidized 60-nm Ag-NPs revealed severe effects of NP treatment to molting and cuticle in the case of the sulfidized Ag-NPs but not in the case of pristine Ag-NPs, suggesting distinct responses depending on the NP coating.^[194]

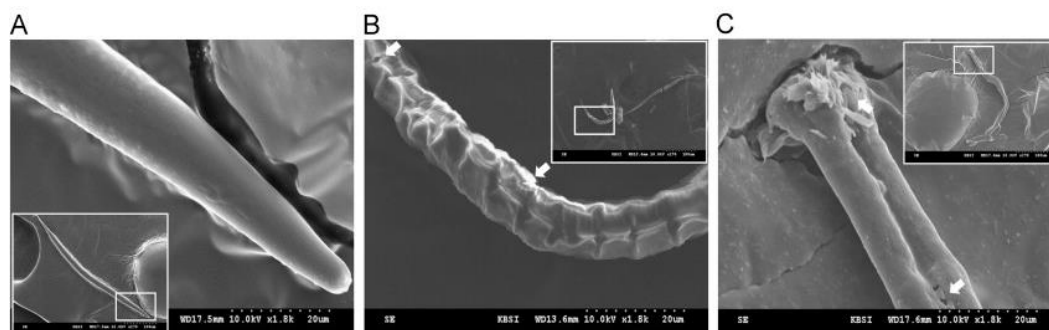


Figure 20. Scanning electron micrograph of *C. elegans* exposed to citrate Ag-NPs: A) control, B) 10 mg/L, and C) 100 mg/L. The white arrows indicate epidermal divisions and necrosis. Adapted from Kim *et al.*^[207]

2.1.6 Reprotoxicity effects

Adverse effects on the reproduction of *C. elegans* treated with NPs have been extensively reported,^[195, 208, 211] whereas germ line and transgenerational transfer have been much less observed.^[167, 198] Meyer *et al* described internal retention of developing eggs, called bag-of-worm (BOW) phenotype, and NP transference to the fertilized eggs after treatment with 10-nm citrate Ag-NPs but not in the case of PVP-coated Ag-NPs of 21 and 75 nm.^[167] Lim *et al* attributed to oxidative stress a major role in reproduction toxicity of Ag-NPs given that the decreased reproductive potential was rescued in *pmk-1* mutants.^[203] Decrease in fertility have also been prominently reported after metal oxide NP exposure, including CeO₂, TiO₂, ZnO, or Fe₂O₃ NPs.^[208, 211] Pluskota *et al* observed a reduction of progeny production in silica-nanoparticle exposed worms, accompanied by a significant increase in the BOW phenotype. The authors found evidence that SiO₂-NPs impaired neural innervation of vulval muscle cells, which led to defective egg-laying.^[197] Interestingly, Kim *et al* performed a multigenerational study (F0-F4 generations) using 10-nm Au-NPs, and observed that the reproduction rate was clearly affected in the F2 generation and then gradually recovered in the F3 and F4 generations. The abnormalities of the reproductive system showed a close relationship with reproduction rates, hence the authors proposed that the germ line may be affected due to maternal exposure, causing transgenerational effects on future generations.^[195]

2.1.7 Importance of NP size, surface properties and composition

Effect of size

Most studies agree on the higher toxicity of small NPs. Meyer *et al* reported more intracellular uptake of small Ag-NPs (10 and 21 nm) than larger particles (75 nm) in K-medium. Among their biological effects, growth inhibition was reported for all the tested

NPs but bagging and transgenerational transfer was solely observed for 10-nm citrate Ag-NP, suggesting that Ag-NP uptake and reprotoxicity are size and coating dependent.^[167] Contreras *et al* compared the uptake of 2, 5 and 10-nm PEG-coated Ag-NPs and found that a lesser amount of Ag was internalised in *C. elegans* exposed to small Ag particles compared with larger particles, probably due to the increased mobility of the smaller NPs out of the body. They also reported size-dependent effect on lifespan and fertility after exposure for multiple generations but no size-dependence of body length and motility.^[205] Besides, Ellegaard-Jensen *et al* observed higher lethality of 28-nm PVP Ag-NPs than 1-nm bare Ag-NPs and attributed it to a combination of effects of coating, Ag-solubility and higher uptake rates. They proposed that larger particle size may enable faster uptake rates by oral ingestion and thus higher mass doses than exposure to smaller stable particle sizes.^[204] Ahn *et al* also observed reduced toxicity of PVP-Ag-NPs compared to bare Ag-NPs, and higher toxicity for the smaller NPs.^[192] Yang *et al* evaluated Ag-NPs of 1-75 nm and observed no relationship between the growth inhibition and the diameter of Ag-NP, but a linear correlation between Ag-NP toxicity and dissolved silver.^[190] Taken together, these studies suggest size-dependent uptake, reprotoxicity and lifespan of Ag-NPs, but no effect of size in locomotion behaviour and body length.

In the study of metal oxide NPs, Roh *et al* reported differences in toxicity endpoints (growth, fertility and survival) depending on the size of CeO₂-NPs and TiO₂-NPs: the toxicity exhibited by the smaller sized NPs (7, 15 nm) was higher than that observed for the larger sized ones (20, 45 nm).^[208] Gupta *et al* also observed higher toxicity for small ZnO-NPs (10 nm) than larger-sized particles (50 and 100 nm), especially at high doses.^[209]

Effects of surface properties

The surface coating can significantly affect NP toxicity by modulating NP uptake, bioavailability and reactivity, hence its engineering can be used as a strategy to gain control over the nano-bio interactions and prevent undesired post-synthesis modifications either in the environment or in the human body. Yang *et al* studied citrate, PVP and gum arabic as surface coatings of small Ag-NPs (<10 nm) and found coating-dependent effects: gum arabic was ~9-fold more toxic than PVP, which in turn was ~3-fold more toxic than citrate. The authors found that the most toxic Ag-NPs were also the most soluble. Starnes *et al* investigated the effect of Ag-NP sulfidation, a major transformation occurring in the wastewater treatment process, and reported reduced bioavailability, lower toxicity and distinct toxicity mechanisms of sulfidized Ag-NPs compared to bare particles.^[193, 194] Surface engineering can also result in enhanced bioavailability, e.g. Kim *et al* conjugated nano-Pt with HIV-1 TAT fusion protein, a cell-penetrating peptide, resulting in an antioxidant activity 100 times higher than unconjugated PtNPs.^[196]

Collin *et al* studied the effect of surface charge using 4-nm dextran-coated CeO₂-NPs and concluded that NP toxicity and accumulation in tissues and organs depended on NP surface properties. Positively charged CeO₂-NPs were significantly more toxic to

C. elegans and bioaccumulated to a greater extent than neutral and negatively charged NPs. The latter NPs mainly accumulated in the gut, while positively charged ceria nanoparticles were also detected throughout the *C. elegans* body. The authors related the higher cytotoxicity of the positively charged NPs to higher cellular uptake, and also due to the direct interaction of cationic NPs with cells which could disrupt the cell membrane's lipid bilayer.^[182] Surface charge also affected the oxidation state of Ce in the *C. elegans* tissues after uptake: greater reduction of Ce from Ce (IV) to Ce (III) was found in *C. elegans* when exposed to the neutral and negatively charged relative to positively charged CeO₂-NPs. The Ce reduction suggests oxidative damage of macromolecules or generation of ROS. Interestingly, the authors also showed that coating CeO₂-NPs with NOM at environmentally realistic ratios of HA to CeO₂ reduced the effects of initial surface status, and rendered positively charged CeO₂-NPs significantly less toxic.^[182]

Höss *et al* investigated the toxicity of soil-derived colloidal iron oxides (FeO_x) with variable aggregate size and variable association with NOM, and found that the toxicity was dependent on aggregate size and specific surface area (**Figure 21**) with differences up to 7-fold in their toxic concentrations. FeO_x associated with HA or citrate were less toxic than NOM-free colloids. In contrast, ferrihydrite containing proteins and polysaccharides from mobile NOM was even more toxic than NOM-free ferrihydrite of similar aggregate size.^[183] This study reinforces the importance of NOM as determinant of the ecological risks posed by nanomaterials.

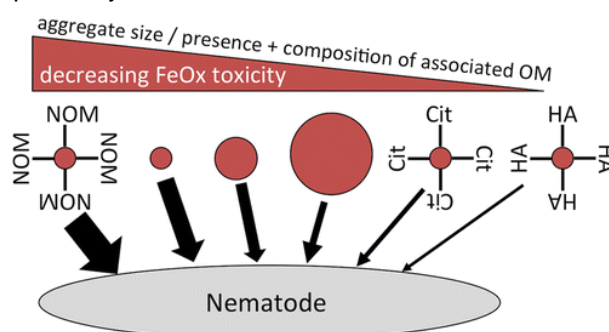


Figure 21. Scheme of the effect of aggregate size and presence of NOM in the toxicity of soil-derived colloidal iron oxide in *C. elegans*. Adapted from Höss *et al.*^[183]

Effects of composition

Pluskota *et al* assessed fluorescently labelled 50-nm SiO₂ and PS-NPs in *C. elegans* and concluded that their translocation was dependent on the composition (**Table 12**): SiO₂-NPs were exclusively found in primary organs of entry, e.g. the lumen of the digestive tract, while carboxy PS-NPs translocated to secondary organs and also to the cytoplasm of early embryos.^[197] Wu *et al* also compared the toxicity of TiO₂, ZnO and SiO₂ NPs with the same nano-size (30 nm), and reported differences in their toxicity solely due to the different composition. The toxicity order was: ZnO-NPs>TiO₂-NPs>SiO₂-NPs, using growth, locomotion behaviour, reproduction, and ROS production as endpoints.^[173]

Table 12. Translocation of nanoparticles in *C. elegans* is dependent on their composition. Adapted from Pluskota *et al.*^[197]

organ/tissue	silica-NPs	polystyrene-NPs	carboxy polystyrene-NPs
pharynx - lumen	+	+	+
intestine - lumen	+	+	+
intestine - tissue	–	+	+
proximal gonad	–	+	+
spermatheca	–	–	+
early embryo/cytoplasm	–	–	+

+ presence, – absence

2.1.8 Endocytosis and translocation pathways

Given the technical difficulty of studying nanoparticle fate with nanometric resolution inside living organisms at present, there is limited evidence of the internalisation and translocation mechanisms of NPs in *C. elegans*. *In vitro* assays have shown that upon internalisation, the surface functionality of NPs dictates their behaviour and subcellular location.^[218] It is worth noting that different cellular compartments have different characteristics (i.e. the cytoplasm and lysosomes have different redox status and pH), hence the local environment of NPs may influence their reactivity and oxidation status. Moreover, the negative membrane potential of most cells interacts differently with particles with a positive or negative surface charge. The electrostatic interaction of NPs with the negatively charged bilayer of a membrane mediates their binding and their toxicity. Therefore, many aspects at the cellular scale deserve to be further addressed *in vivo* to better understand the complex nano-bio interactions occurring inside living organisms.

In 2010, Meyer *et al* reported the first direct evidence of intracellular uptake and intergenerational transfer of 10-nm citrate Ag-NP in *C. elegans* using hyperspectral microscopy, however they did not perform mechanistic studies. Using fluorescence microscopy, Scharf *et al* also observed intracellular uptake of 50-nm SiO₂-NP in the intestinal and vulval cells.^[198] Employing genetic analysis tools, Tsyusko *et al* reported elevation of *chc-1* expression and significant responses of endocytosis mutants (*chc-1* and *rme-2*) to Au-NPs, suggesting that cell uptake of Au-NPs occurs via clathrin-mediated endocytosis.^[186] Recently, Maurer *et al* showed that early endosome formation is necessary for Ag-NP-induced toxicity *in vivo* using endocytosis-deficient mutants (*rme-1*, *rme-6* and *rme-8*) and lysosomal function deficient mutants (*cup-5* and *glo-1*), as well as a clathrin-mediated endocytosis inhibitor.^[191]

2.1.9 Biological mechanisms triggered by NP exposure

Different strategies have been applied to discern the molecular mechanisms triggered by NP exposure in *C. elegans*, among them biochemical assays to detect ROS formation, imaging protocols to quantify lipofuscin accumulation or pharmacological evaluations such as antioxidant treatment. The role of specific genes in NP

sensitivity/defence have also been investigated using mutant and transgenic strains, RNAi, together with genomic studies, helping to dissect the importance and regulation of different molecular pathways upon NP exposure. **Table 13** summarises frequently investigated genes and pathways in NP toxicity.

Table 13. Frequently investigated genes and pathways in NP toxicity.

Pathway	<i>C. elegans</i> gene
General stress	<i>hsp-16.2, hsp-16.41, hsp-16.48, daf-2, daf-12, daf-16, daf-21, sgk-1, akt-1, akt-2.</i>
Metal stress	<i>mtl-2, pcs-1, mtl-1, mtl-2, cdr-1, pcs-1</i>
Oxidative stress	<i>sod-1, sod-2, sod-3, sod-4, sod-5, ctl-1, ctl-2, ctl-3, mev-1, nth-1</i>
DNA damage	<i>cep-1, ced-3, ced-4, xpa-1, nth-1, ape-1</i>
Metabolic stress	<i>ire-1, sir-2, aak-2</i>
Mitochondrial function	<i>gas-1, coq-7</i>
Collagen	<i>col-158, col-131, col-101</i>
Endocytosis	<i>rme-1, rme-6, rme-8, dyn-1, chc-1, rme-2</i>
Lysosomal function	<i>cup-5, glo-1</i>
Non-canonical UPR	<i>abu-11, pqn-5, hsp-16.1, hsp-70, hsp-3, hsp-4</i>
ER stress	<i>hsp-4</i>
Metabolism	<i>gst-1, gst-4, gst-5, gst-8, gst-24, and gst-42, age-1, gas-1, cyp35a2</i>
Yolk proteins	<i>vit-2, vit-6</i>
MAPK signalling pathway	<i>jnk-1, mpk-2, nsy-1, sek-1, pmk-1, jkk-1</i>

2.1.9.1 Metal nanoparticles

Gold NPs as a model system

In the attempt to study particle-specific effects of manufactured nanomaterials, Tsyusko *et al* chose gold nanoparticles as a model since they are resistant to oxidative dissolution. As part of a larger-scale experiment investigating interactions between metals and nanoparticles, Tsyusko *et al* investigated the transcriptomic effect of 4-nm citrate Au-NPs after 12 h exposure of L3 nematodes.^[186] The authors proposed that Au-NPs are taken inside the cell through clathrin-mediated endocytosis and once inside the cell, they cause endoplasmic reticulum (ER) stress, resulting in increased amounts of misfolded or unfolded proteins and activation of canonical (molecular chaperones) and non-canonical UPR pathways. In case of excess accumulation of misfolded proteins, activation of UPR leads to cell death. Furthermore, Au-NPs also seemed to activate Ca signalling and amyloid processing pathways, which would lead to intracellular Ca²⁺ increase and trigger calpain–cathepsin-mediated events leading to cell necrosis and ultimately to mortality. The results from this study provided evidence that 4-nm citrate Au-NPs can be internalised by the *C. elegans* cells and trigger different biological responses capable of causing adverse effects on whole organisms.

Toxicity mechanism of Ag-NPs

Ellegaard-Jensen *et al* hypothesised that *C. elegans* resistance to nano-silver would increase via physiological adaptation after pre-exposure to low concentrations. In

contrast, they found that pre-exposed nematodes were slightly more sensitive to further exposure compared to non-pre-exposed animals.^[204] In good agreement, Contreras *et al* showed that Ag-NP pre-exposed nematodes suffered cumulative damage.^[205] These results suggest that *C. elegans* has no efficient physiological ability to counteract nano-silver toxicity by acclimation.

Roh *et al* reported increased expression of the superoxide dismutases-3 (*sod-3*) and metallothionein-2 (*mtl-2*) occurring in a concentration dependent manner and concurrently with significant decreases in fertility. Hence, the authors concluded that oxidative stress played an important mechanism in Ag-NPs toxicity. Meyer *et al* also studied the expression levels of oxidative stress and metal genes, and reported greater Ag-NP sensitivity of a *mtl-2* deficient mutant, but did not find evidence for a role for oxidative stress in Ag-NP toxicity. The authors attributed at least part of the toxicity observed to dissolved silver.^[167] In contrast, Ellegaard-Jensen evaluated Ag-NPs of different size (1 and 28 nm) and coating (bare or PVP) and found that toxicity was dependent on the type of Ag-NP but not on the soluble fraction alone. In a posterior study, Roh *et al* reported the formation of reactive oxygen species (ROS) and analysed the expression of genes in MAPK signalling pathways. They found an increase in gene expression of less than 2-fold compared to control worms, but a dramatic increase in *sod-3* mutants after exposure, suggesting a PMK-1 p38 MAPK-dependent activation. The authors proposed that MAPK-based integrated stress signalling network could be involved in defence to Ag-NPs exposure in *C. elegans*.^[206] Studies of the same group confirmed increased ROS formation after Ag-NP exposure, as well as increased expression of PMK-1 p38 MAPK and hypoxia-inducible factor (HIF-1), GST enzyme activity, and decreased reproductive potential in *C. elegans*. The authors found evidence that oxidative stress was an important mechanism of Ag-NP-induced reproduction toxicity in *C. elegans*, and that PMK-1 p38 MAPK played an important role in it.^[203]

Yang *et al* observed a linear correlation between Ag-NP toxicity and dissolved silver, and concluded that Ag-NP toxicity was driven at least in part by release of dissolved silver, in agreement with Meyer *et al*, even though oxidative dissolution was limited (max. 15%). Given that the bioavailability of ionic silver can be reduced by binding to glutathione (GSH) or thiol-containing proteins such as metallothionein, the authors showed that growth inhibition could be rescued by complexation of dissolved silver with thiol groups, while partial or no rescue was observed with antioxidants. This study highlighted a critical role for dissolved silver in the toxicity of all tested Ag-NPs, and also proposed an specific nano-Ag effect via oxidative stress typically for the less soluble Ag-NPs, hence encompassing the two most prevalent Ag-NPs toxicity mechanisms reported previously.^[190] Starnes *et al* reported that the mechanism of Ag-NP toxicity was dependent on the concentration: at low concentration, a greater proportion of the toxicity could be explained by dissolved Ag, whereas at high concentration, the toxicity appeared to be dominated by particle specific effects.^[193] Recently, Ahn *et al* combined qPCR studies, the

use of mutants and biochemical assays to study the role of different genes related to general stress, immune response, metal stress, oxidative stress, metabolic stress and DNA damage in nematodes treated with Ag-NPs, and concluded that oxidative stress-related mitochondrial and DNA damage could be a potential mechanism of toxicity, in particular for the smaller Ag-NPs irrespective of their coating.^[192]

Differences in the Ag-NP toxicity mechanisms and their relative importance reported in literature could arise from differences in the experimental design such as developmental stage or strain of *C. elegans*; exposure conditions including exposure media, food source, temperature, or exposure duration; but also from differences on the nanomaterial concentration, properties (size, coating) and colloidal stability.

Antioxidant properties of Nano-Pt

Kim *et al* investigated the anti-ageing properties of Pt-NPs, which have superoxide dismutase (SOD)/catalase activity. Treatment of *C. elegans* with Pt-NPs significantly reduced the accumulation of lipofuscin and ROS induced by paraquat, conferring resistance against oxidative stress and prolonging lifespan by 25%.^[185] The authors proposed that in normal culture conditions, *C. elegans* maintain an excessive ROS level, hence the scavenging of endogenous ROS by nano-Pt attenuates intracellular damage and induces extension in lifespan.^[196]

2.1.9.2 Metal oxide NPs

The role of dissolution

Ma *et al* investigated the toxicity of ZnO-NPs and did not find differences from Zn²⁺. The two treatments induced expression of *mtl-2* in a similar manner. These findings suggest biotransformation of the nanoparticles to Zn²⁺ to enact toxicity.^[166] Wang *et al* also reported similar lethal doses 50 (LC₅₀) of ZnO-NPs and bulk ZnO, while Al₂O₃-NPs and TiO₂-NPs resulted twice more toxic than their bulk counterparts, hence their toxicity could not be adequately explained by dissolution of the particles alone.^[169]

Oxidative stress

Wu *et al* observed a correlation between ROS production toxicity in nematodes chronically exposed to environmental relevant concentrations of TiO₂-NPs, ZnO-NPs and SiO₂-NPs, and showed that antioxidant treatment effectively retrieved NP adverse effects.^[173] Rui *et al* investigated the effects TiO₂-NPs in mutants associated with oxidative stress and stress response (among them, some metallothioneins, superoxide dismutase, glutathione-transferase and heat shock proteins mutants) and found that they were more susceptible when exposed to high dose for 24 h, but not at lower dose and for shorter periods.^[168] Roh *et al* exposed *C. elegans* to CeO₂-NPs (15 and 45 nm) and TiO₂ (7 and 20 nm) and studied the expression levels of stress-responsive genes including metal response proteins, xenobiotic metabolism enzymes, antioxidant enzymes, apoptosis markers, and yolk proteins. Whereas the expression of most of the tested genes did not change significantly, likely due to the low dose used (1 mg/L), the expression of *cyp35a2*

significantly increased after treatment, hence suggesting a possible role in nanoparticles metabolism and/or toxicity in *C. elegans*.^[208]

Li *et al* studied chronic exposure of *C. elegans* to 60-nm Al₂O₃-NPs in the dose range 0.01-23.1 mg/L and reported a severe stress response and oxidative stress. These effects were much subtle in bulk Al₂O₃, and not observed in acute exposure regimes. Oxidative stress was caused by both increase in ROS production and suppression of ROS defence mechanisms. Treatment with antioxidants and SOD-3 overexpression suppressed oxidative stress and prevented NP adverse effects, while *sod-2* and *sod-3* mutants were more susceptible than the wild-type to NP treatment.^[200] Exposure of *C. elegans* to DMSA-coated Fe₂O₃-NPs (9 nm) also resulted in a pronounced induction of ROS production linearly correlated to adverse effects, irrespective of the duration of the exposure (24 h, 3 days or 8 days). Again, *sod-2* and *sod-3* mutants resulted more susceptible properties than wild-type, with safety concentrations at least 10 times lower.^[211]

Metal toxicity

Polak *et al* evidenced the protective role of metalloproteins and phytochelatin synthase against to 30-nm ZnO-NP. The authors found that NP adverse effects were significantly amplified in a metal sensitive triple knockout mutant (*mtl-1;mtl-2;pcs-1*). They reported transcriptional activation of metallothioneins (*mtl-1* and *mtl-2*), phytochelatin synthase (*pcs-1*), and an apoptotic marker (*cep-1*) upon ZnO-NPs exposure. They demonstrated the oxidative potential of ZnO-NPs in the metal sensitive mutant, and observed significant changes in their biomolecular phenotype upon ZnO-NPs treatment, suggesting that metalloproteins and phytochelatin synthase are instrumental in the protection against ZnO-NPs induced cytotoxic damage.^[199]

Controversy on the role of oxidative and metal stress

Not all the studies support the role of oxidative stress or metal response as mediators of the toxicity of metal oxide NPs. For instance, Arnold *et al* could not attribute CeO₂NP-induced growth inhibition to oxidative or metal stress, but they proposed a non-specific inhibition of feeding caused by NPs aggregating in the test media and/or inside the gut tract. The authors observed little or no increased sensitivity to CeO₂-NP exposure in metal (*pcs-1*, *mtl-2*) and oxidative stress (*sod-3*) mutants, hence they argued that there may be only a minor effect of metal or oxidative stress.^[210] Höss *et al* also concluded that oxidative stress was not the predominant mechanism of toxicity of soil-derived iron oxide colloids, although *sod-2* mutants resulted more sensitive to some FeO_x and Fe³⁺ ions.^[183] Interestingly, Gupta *et al* found that expression of *mtl-1* and *sod-1* was significantly increased with application of high concentrations of 10 nm ZnO-NPs, but significantly unaffected at lower doses or with 50 and 100 nm.^[209]

Other scenarios: recovery response, ageing...

Other mechanistic studies of NP behaviour in *C. elegans* have included the study of the recovery response of *C. elegans* after NP exposure, and the effect of NPs in the

ageing processes of *C. elegans*. Zhao *et al* investigated the recovery responses of TiO₂-NPs in acutely and chronically-treated nematodes. Adverse effects could only be retrieved to control levels within a recovery period of 48 h in acutely-treated worms, while prolonged exposure induced lasting defects including severe deficits in development of intestinal barrier and neurons controlling defecation (**Figure 22**).^[201] This study highlights the importance of defecation and the integrity of primary biological barrier in NP toxicity, hence new safe NPs should be designed to prevent these effects. Differently, Scharf *et al* investigated the effect of 50-nm SiO₂-NPs on aging at the molecule, cell, and whole organism level in *C. elegans*. Treated animals significantly accumulated insoluble, ubiquitinated proteins in comparison to controls (2- to 3-fold), in a way that resembled the increase of insoluble, endogenous proteins in old worms. The authors also studied bulk silica, PS-NPs and Ag-NPs, and did not observe induction of protein insolubility, suggesting that it is a specific effect of silica NPs. They also observed formation of amyloid-like structures in the cell nucleoli of intestinal cells in SiO₂-NP treated worms, but not in untreated worms, and reported that SiO₂-NPs directly interfered with pharyngeal function by premature initiation of an age-related reduction of pharyngeal pumping.^[198]

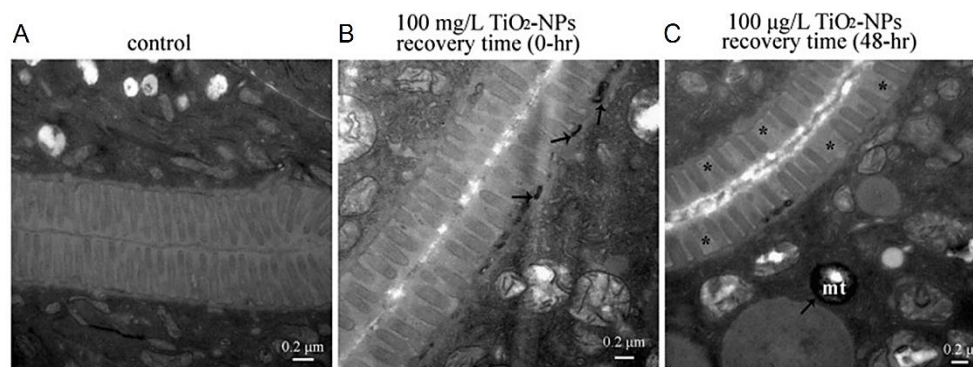


Figure 22. Ultrastructural changes of intestine and uptake in TiO₂-NPs exposed nematodes after transfer to the normal condition. A) Unexposed nematodes. B) Nematodes exposed to 100 mg/L TiO₂-NPs immediately upon transfer to normal conditions. C) Nematodes exposed to 100 µg/L TiO₂-NPs after 48 h in normal conditions. Asterisks indicate the position without microvilli. Arrowheads indicate the location of TiO₂-NPs. Mitochondria, mt. Adapted from Zhao *et al*.^[201]

The effects and responses observed in the screening of metal and metal oxide NPs in *C. elegans* are summarised in **Figure 23**.

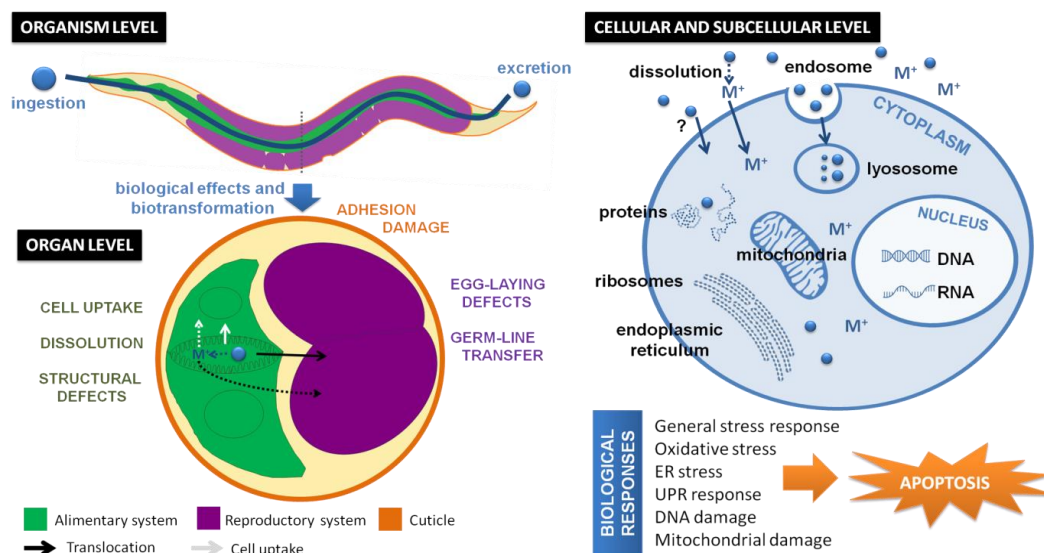


Figure 23. Effects and mechanisms observed in the screening of metal and metal oxide NPs in *C. elegans* at the organism, organ, cellular and subcellular levels.

Table 14 presents different biological mechanisms reported to be triggered by NP exposure, illustrating the controversy among the conclusions of different studies. For instance, some studies using silver nanoparticles concluded that oxidative was an important factor determining Ag-NP toxicity,^[192, 203, 207] whereas other authors were not able to find a link between Ag-NP toxicity and oxidative stress,^[167] and others proposed that it was restricted to the less soluble due to size or coating.^[190] Similarly, we have found controversial results concerning iron oxide nanoparticles: some studies reported a correlation between oxidative stress and NP toxicity (either major^[211] or minor^[183]) and also proposed that dissolution inside *C. elegans* and ion release could occur, contributing to the biological effects on *vivo*.^[183] Therefore, to date there is no clear evidence of general biological mechanisms triggered by NP exposure nor specific mechanisms depending on the NP properties such as composition, size or coating. With this thesis, we aim to contribute to better understanding the *in vivo* response of *C. elegans* to gold and iron oxide nanoparticles.

Table 14. Biological mechanisms triggered by NP exposure reported in the selected literature.

NP core	Oxidative Stress	Metal stress	Dissolution	NP-specific effects	Other mechanisms
Metal NPs					
Ag	● ^[192, 203, 207] ○ ^[190] X ^[167]	● ^[180, 207]	● ^[190, 193]	● ^[193]	<ul style="list-style-type: none"> - Alteration of metabolic processes.^[193] - Dermal effects.^[193, 207] - Early endosome formation is necessary for Ag-NP-induced toxicity <i>in vivo</i>.^[191] - NP-induced cellular damage after intracellular uptake of Ag-NPs.^[192] - Oxidative stress-related mitochondrial and DNA damage.^[192] - MAPK-based integrated stress signalling network as a defence to Ag-NP exposure.^[203, 206] - Pre-exposed nematodes suffered cumulative damage.^[204]
Au	X ^[219]	-	-	-	Cell uptake by clathrin-mediated endocytosis causes ER stress, and activates UPR pathways that can lead to cell death. Cell uptake also activates Ca signalling and amyloid processing pathways, which can lead to intracellular Ca ²⁺ increase and trigger calpain–cathepsin-mediated events causing cell necrosis and ultimately mortality. ^[186]
Pt	● ^[185, 196]	-	-	-	Nano-Pt scavenges endogenous ROS, attenuating intracellular damage. ^[185, 196]
Metal Oxide NPs					
ZnO	● ^[173, 199] ○ ^[209]	● ^[166, 199]	● ^[166, 169] ○ ^[209]	● ^[169]	-
TiO ₂	● ^[168, 173] ○ ^[213] X ^[208]	● ^[168]	● ^[169]	● ^[208]	<ul style="list-style-type: none"> - Deficit in development of intestinal barrier and neurons controlling defecation unabling recovery after chronic exposure.^[201] - Increase in the expression of cyp35a2.^[208]
SiO ₂	● ^[173]	-	-	-	- Aging phenotype. ^[197, 198]
CeO ₂	○ ^[210] X ^[208]	○ ^[210]	-	-	<ul style="list-style-type: none"> - Growth defects by inhibition of feeding caused by NP aggregates.^[210] - Defence and/or compensatory mechanism mediated by cyp35a2.^[208]
FeO _x	● ^[211] ○ ^[183]	-	? ^[183]	-	-
Al ₂ O ₃	● ^[200]	-	● ^[169]	● ^[169]	-
● major role, ○ minor role, X lack of evidence, ? hypothesis					

2.2 Materials science techniques with potential to assess nano-bio interactions

Based on extensive literature review, it is clear that authors tend to focus on the evaluation of the NP effects on *C. elegans*, and generally did not give enough importance to the characterisation of NP status inside *C. elegans* (size, aggregation, and *in vivo* properties). Therefore, there is very little evidence about the effect of the *C. elegans* in the identity of NPs *in vivo* (i.e. formation of protein corona, digestion in the gut...). Based on the experimental features of *C. elegans*, we advocate for the empowerment of materials science techniques in combination with biological evaluations to thoroughly characterise the interaction between inorganic nanoparticles (in our case, iron oxide and gold NPs) and *C. elegans*. In particular, we propose the experimental scheme presented in Figure 24.

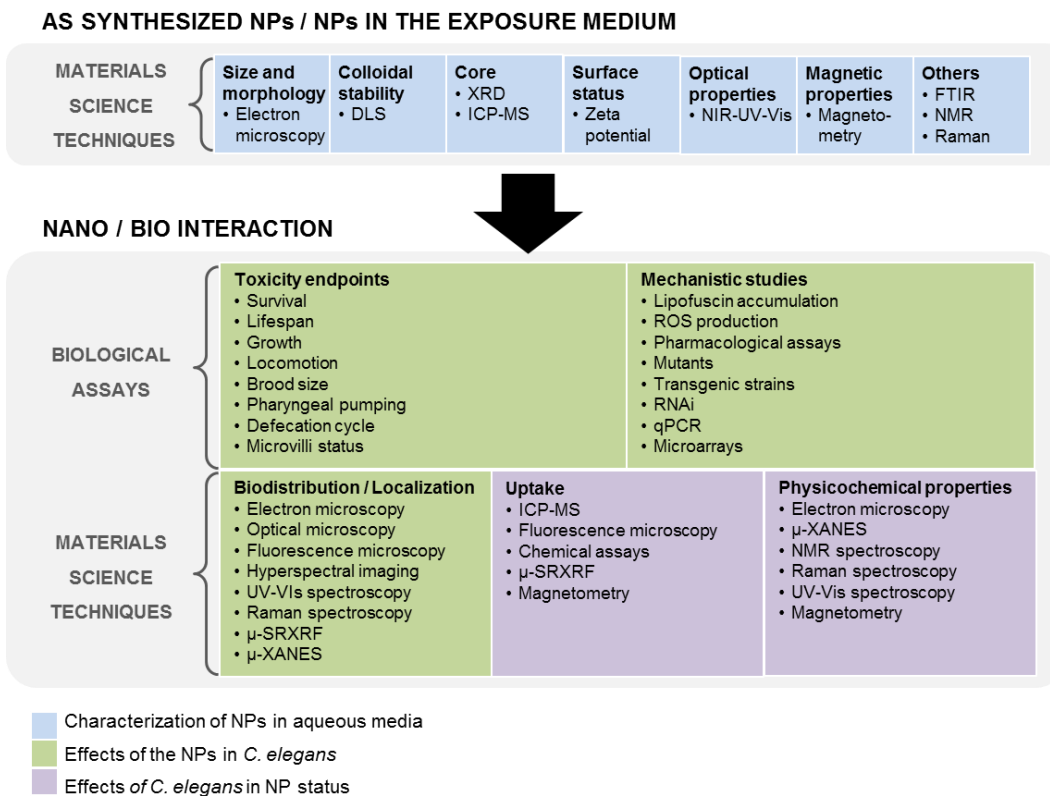


Figure 24. Summary of the proposed techniques to study the interaction between nanoparticles and *C. elegans*

Pre-exposure considerations

Firstly, nanoparticles have to be very well-characterised after their synthesis or their purchase. Then, the suitability of different exposure conditions should be investigated based on the colloidal stability of the test material, the goal of the investigation (i.e. acute or chronic exposures), and the tolerance of the *C. elegans* (i.e. to pH, salinity...). At this step, both biological and materials science evaluations must be performed: the former, to study the influence of the media in the *C. elegans*, and the latter to characterise the NP status in the test media. Based on the results, the optimum assay system will be selected and applied to further experiments. The experimental design must include NP concentration range, the developmental stage of *C. elegans*, and also the time-points of study.

Study of the NP–*C. elegans* interaction

Thereinafter, the evaluation of the interaction between *C. elegans* and the nanoparticles will combine the two disciplines, biology and materials science, taking advantage of the experimental features of this model organism. For instance, the transparency and small size of the worm facilitates visualization of NPs under optical microscopy, enabling the study of its internal organs without need of dissection. More advanced imaging techniques including TEM, SEM, MRI, hyperspectral dark field microscopy (HDFM) or μ -SRXRF can help identify, locate and characterise individual NPs in specific locations of the body, and unravel the mechanisms by which NP cross

biological barriers in complex organisms. Together with micro-spectroscopy, they provide insights on the *in vivo* fate, aggregation and degradation of NPs, and address questions of bio-accumulation and bio-persistence. Elemental analysis such as energy-dispersive X-ray spectroscopy (EDX) and μ -XANES are valuable to confirm the identity of materials and determine their oxidation status, and can be applied to study the intracellular uptake of NPs when images are not conclusive, or to determine if oxidative dissolution is occurring inside the nematode. Quantitative techniques like inductively coupled plasma mass spectrometry (ICP-MS) allow the quantification of NPs inside the worm to investigate dose- and time-dependence accumulation, NP metabolism... Interestingly, some techniques such as chemical imaging, magnetometry, or microprobe techniques allow the simultaneous characterisation and quantitation of NPs inside treated animals. However, protocols for sample preparation must be specifically adapted to study nanoparticle-treated *C. elegans* using materials science techniques, i.e. targeted ultramicrotomy protocol for TEM specimens.

2.3 Chapter conclusions

Although some efforts have been done in the evaluation of nanoparticles in *C. elegans*, the amount of data is still limited and most of the work was performed from a toxicological perspective. Hence, very few knowledge is available on the NP status inside the *C. elegans*, and there is plenty of room for materials scientists to complement biological assays. **The combination of the two disciplines to address the study the interaction between inorganic nanoparticles and *C. elegans* can yield more comprehensive results and help to unravel the big picture from both sides, “nano” and “bio”. In this direction**, we implemented a *C. elegans* facility in our chemical laboratory to systematically apply materials science techniques to characterise NP-treated worms (**Figure 25**), complementing the classical toxicological evaluations.^[220]

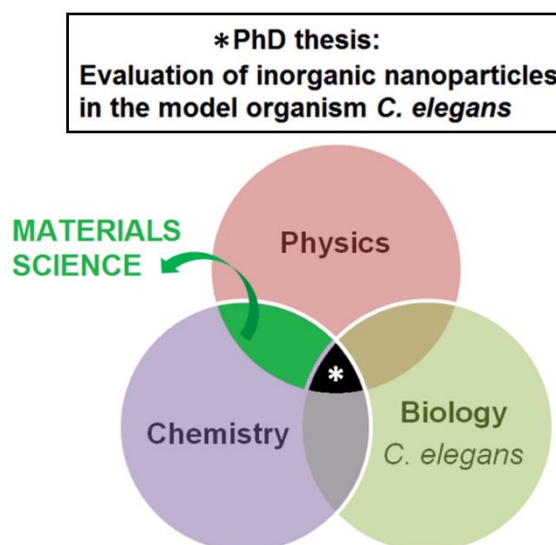


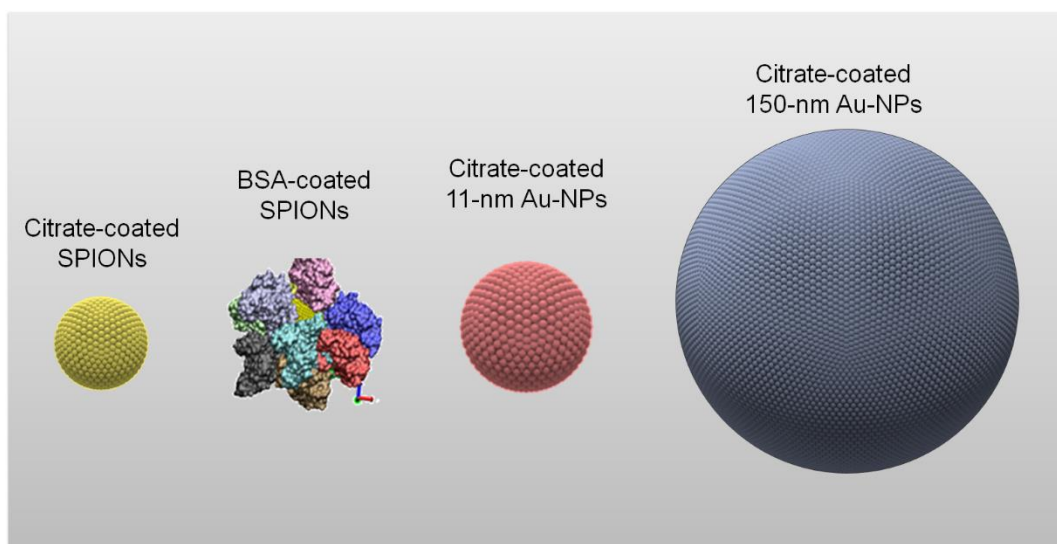
Figure 25. Framework of this thesis.

In particular, we propose to use magnetometry to study SPION-treated worms and absorbance spectroscopy to characterise Au-NP status inside *C. elegans*. We also plan to apply a range of imaging techniques such as:

- Light Microscopy
- Two-Photon Light Microscopy
- Hyperspectral Dark Field Microscopy
- Electron Microscopy.

We propose to exploit the potential of Scanning Electron Microscopy to study the interaction of NPs with the external surface of the worm, and Transmission Electron Microscopy to achieve single-particle localization in *C. elegans* cross-sections. Combination of TEM with elemental analysis techniques like EDX or EELS can be used to confirm NP internalisation. From the biological perspective, we plan to study lethal and sub-lethal toxicity endpoints, e.g. survival and brood size respectively. Gene expression profiling can shed light on the biological mechanisms triggered by NPs in *C. elegans*. The application of such range of techniques, however, requires the optimization of protocols to specifically evaluate NP-treated *C. elegans* specimens.

CHAPTER 3. Synthesis and characterisation of in-house fabricated SPIONs and Au-NPs



CHAPTER SUMMARY:

This chapter presents the properties and applications of iron oxide and gold nanoparticles and describes the synthetic routes used to produce in-house high quality inorganic nanoparticles for their evaluation in the model organism *C. elegans*. Then, the properties of the as synthesised materials are compared, and their behaviour is evaluated in different biological media to optimize the conditions for *C. elegans* exposure.

CHAPTER INDEX

3.1 Overview.....	61
3.2 Introduction to the properties and applications of superparamagnetic iron oxide nanoparticles in nanomedicine	62
3.2.1 Applications of SPIONs	63
3.2.2 Current status of clinical applications	64
3.3 Synthesis and characterisation of superparamagnetic citrate and BSA-coated iron oxide nanoparticles.....	65
3.3.1 Synthesis by microwave-assisted thermal decomposition.....	65
3.3.2 BSA adsorption protocol.....	67
3.3.3 Scale-up of SPION synthesis	68
3.4 Introduction to the properties and applications of Au- NPs in nanomedicine	71
3.4.1 Applications of Gold Nanoparticles	71
3.4.2 Current status of clinical applications	74
3.5 Synthesis and characterisation of gold nanoparticles	75
3.5.1 Synthesis of 11-nm Au-NPs	75
3.5.2 Seeded growth to 150-nm Au-NPs	75
3.5.3 Characterisation	76
3.6 Comparison of as synthesised SPIONs and Au-NPs.	77
3.7 Evaluation of <i>C. elegans</i> exposure conditions for in-house inorganic NPs	77
3.8 Chapter conclusions	80

3.1 Overview

From the plethora of inorganic NPs available, superparamagnetic iron oxide and gold nanoparticles show interesting properties that make them promising candidates for clinical use. **Table 15** summarises the properties that make these NPs ideal as diagnostic, therapeutic and combined (theranostic) agents which will be analysed into more detail in the following sections.

Table 15. Properties of SPIONs and Au-NPs that are currently exploited for biomedical applications.

Biomedical application	Superparamagnetic iron oxide NPs		Gold NPs	
	Modality	Properties of interest	Modality	Properties of interest
Diagnostics				
Contrast agent	MRI	Superparamagnetism; High r_2	X-ray CT	High absorption of X-rays
Therapeutics				
Drug delivery	Nano-carrier	Easy functionalization; Tunable surface properties; Biodegradability	Nano-carrier	Easy functionalization; Tunable surface properties; Chemical inertness
Hyperthermia	Magnetic hyperthermia	Superparamagnetism	Photothermal hyperthermia	NIR absorption
Cell tracking	MRI (cell guiding and imaging)	High r_2	X-ray CT; Photoacoustic imaging	Bioluminescence

CT: computed tomography; MRI: magnetic resonance imaging, NIR: near infrared; r_2 : transversal relaxivity.

Our group has years of experience in the synthesis of SPIONs and recently developed a scalable microwave-assisted synthetic route of monodisperse water-soluble SPIONs where no ligand exchange is required.^[221] We chose SPIONs as model nanoparticles to evaluate in *C. elegans* based on their promising properties for biomedical applications, among them their biodegradability, and our expertise on their synthesis. In particular, we aimed to evaluate two 6-nm SPION systems with different surface properties: i) citrate SPIONs (C-SPIONs), stabilized with the anionic stabilizer citrate; and ii) SPIONs coated with Bovine Serum Albumin (BSA-SPIONs) mimicking a pre-formed hard protein corona. SPIONs are an example of NPs containing metals that are essential for *C. elegans*, which has specific metabolic routes that are highly conserved in mammals to maintain constant iron levels. In contrast, we selected gold nanoparticles (Au-NPs) as an example of a nanoparticulate material consisting of a non-essential noble metallic core stabilized by citrate. We selected two different sizes, 11 nm and 150 nm, based on the expertise of the group to synthesise them and the great potential of Au-NPs in multiple biological and medical applications. Moreover, based on the selection of materials we aimed to study of the effects of nanoparticle composition, size and surface coating in *C. elegans*.

3.2 Introduction to the properties and applications of superparamagnetic iron oxide nanoparticles in nanomedicine

Superparamagnetic iron oxide nanoparticles (SPIONs) hold unique physical and chemical properties that lend them high biocompatibility and biodegradability, and interesting magnetic properties. In particular, SPIONs show superparamagnetism at room temperature, which permits their detection by magnetic resonance imaging (MRI). Additionally, they have high surface area to volume ratio allowing analyte detection at extremely low amount of sample. Furthermore, iron oxide nanoparticles allow the use of magnetic hysteresis for hyperthermia of cancer cells. The low cost and facile chemistry of SPIONs are also very advantageous for the application of SPIONs in medicine.^[222]

Nanoparticles of magnetite (Fe_3O_4) and maghemite ($\gamma\text{-Fe}_2\text{O}_3$) phases have been the most extensively studied, primarily due to their useful property of room-temperature superparamagnetism, that is, the ability of nanocrystals to lose a net magnetization except on application of an external magnetic field. Superparamagnetism arise from the small size of SPIONs, which only contain one domain whose spin reverses under an external perturbation field. Superparamagnetism is lost above ~ 30 nm, where upon the particle have more than one of domain and display conventional ferromagnetism.^[223]

Owing to their nanosized dependent attributes, SPIONs have become a powerful platform in many diverse aspects of biomedicine, including magnetic resonance imaging, drug and gene delivery, biological sensing, and hyperthermia (**Figure 26**).^[222]

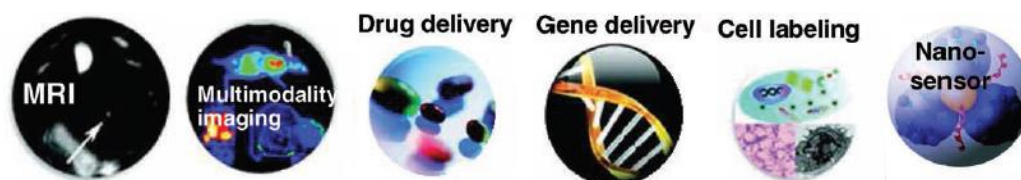


Figure 26. Biomedical applications of SPIONs. Adapted from Liu *et al.*^[222]

Careful optimization of the SPION physicochemical properties can help to enhance the biocompatibility of SPIONs. It is known that parameters such as surface coating, charge, and morphology, influence the biological interaction of nanoparticles, as interactions with biological organisms typically occur at the surface of particles. Proper surface coatings can stabilize SPIONs and avoid agglomeration, and can also prevent dissolution and release of ions. Surface charge also plays a role in nanotoxicity, as it influences the adsorption of molecules and ions that may change the biological responses toward nanoparticles. Surface charge is also a major determinant of nanoparticle colloidal stability, which influences the organism response by changing the shape and size of nanoparticle through aggregation/agglomeration.^[222]

3.2.1 Applications of SPIONs

Magnetic Resonance Imaging

SPIONs have been used for many years in clinical practice to obtain contrast enhancement and signal amplification in Magnetic Resonance Imaging of the liver.^[222] When administered intravenously, SPIONs localize in normal liver causing a loss of signal on MRI. However, abnormal liver tissue has reduced reticuloendothelial system function and retains its native signal intensity, showing areas of higher signal intensity compared to normal liver tissue.

The high magnetic moments of iron oxide nanoparticles make them effective in reducing T_2 relaxation time and thus MRI is usually performed using T_2/T_2^* -weighted sequences in which the tissue signal loss is due to the susceptibility effects of the iron oxide core (**Figure 27**). However, the drawbacks of SPIONs as T_2 contrast agents are magnetic susceptibility artifacts and negative contrast effects.^[222]

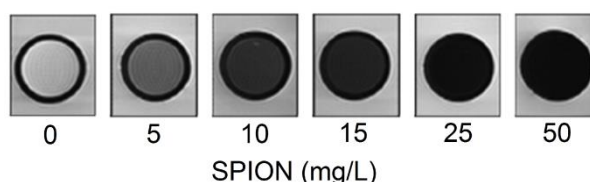


Figure 27. T_2 -weighted MR phantom images of increasing concentrations of SPIONs. Adapted from Carenza *et al.*^[224]

Recent works have also reports that ultras-small SPIONs (<5 nm) can be also used as T_1 contrast agents, which may broaden the applications of SPIONs in molecular imaging. Furthermore, SPIONs can also be easily adapted to other imaging modalities for multimodality molecular imaging by incorporating a nuclear or optical imaging moiety that enable to obtain anatomical, functional and molecular information.^[225, 226]

Drug delivery

SPIONs have been intensively studied as drug delivery vehicles. Generally, SPIONs are loaded along with therapeutics into polymer-based matrices by co-capsulation. Therapeutics can also be loaded into iron oxide nanoparticles by direct covalent coupling (conjugation) with the nanoparticle surface after proper chemical modification (**Figure 28**).

Coating SPIONs with protein molecules also provides a matrix for drug loading. Finally, therapeutics can also be loaded into hollow SPIONs also via physical absorption. These nanoplatforms combine the diagnostic (MRI imaging probe) and therapeutic elements, hence they are theranostic agents.^[227, 228]

Gene delivery

Gene therapy has great potential in the treatment of various diseases, however its success depends on the efficiency of gene transfer into target cells to replace or silence defective genes associated with diseases. Genes have difficulty in passing through cell

membrane by themselves given their negative charge. Many efforts have been done to use SPIONs as vehicles for gene delivery with successful results and therapeutic efficacy, yielding functional nanocomposites for gene delivery with non-invasive imaging monitoring capability.^[229]

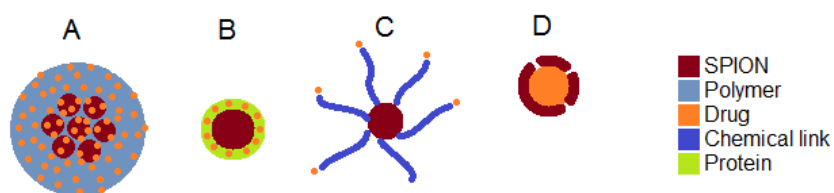


Figure 28. Schematic representation of SPION-based drug delivery systems. A) Co-capsulation of SPIONs and drugs in a polymeric matrix. B) Drug loading into protein-coated SPIONs. C) Conjugation of drugs with the surface of chemically-modified SPIONs. D) Physical absorption of drugs into porous hollow SPIONs.

Cell labelling

SPIONs are used in regenerative cellular therapy to track the fate of transplanted cells by non-invasive and dynamic imaging; i.e. stem cells, T cells, or dendritic cells are labelled with SPIONs before transplanted back to the body. Different strategies have been applied to improve intracellular SPION uptake for cell labelling, i.e. increased concentration of SPIONs, conjugation with penetrating peptides, or co-administration with positively charged substances. Still, the main disadvantage of cell MRI labelling is the dilutions of SPIONs with cell divisions: after a few cycles of division, the remaining intracellular SPIONs may not be strong enough to generate detectable signals. Moreover, when cells die SPIONs can leak out and be uptaken by neighbour cells or end up in the extracellular matrix. Hence, a comprehensive understanding of the clearance pathways and timelines of SPIONs can help to design cell labelling strategies with high tracking accuracy.^[222]

Nanosensors

SPIONs show desirable properties for biomarker detection. In general, the controlled clustering or aggregation of a few SPIONs can greatly shorten T_2 relaxation time compared to single nanoparticle at the same iron concentration. Thus, when magnetic nanosensors aggregate through affinity ligands to the biomarkers, a decrease in the T_2 relaxation time is observed, allowing the sensitive and accurate detection of biomarkers with excellent temporal and spatial resolution.^[222]

Hyperthermia

Cancer treatment by magnetic hyperthermia has been explored extensively with SPIONs. In magnetic hyperthermia, SPIONs are injected into the tumor and then heated by external alternating magnetic field, resulting in hyperthermia of cancer tissue. The underlying mechanisms is that SPIONs act as an antenna to convert electromagnetic energy into heat. This strategy hold great promise in cancer therapy as cancer cells are more susceptible to elevated temperature than normal cells.^[230]

3.2.2 Current status of clinical applications

Different types of SPIONs have been clinically evaluated as magnetic resonance contrast agents, including Ferumoxides (e.g. Feridex®), Ferucarbotran (Resovist®) and Ferumoxtran-10 (Combidex®, Sinerem®), among others. At present, only Resovist® is commercialized in a few countries while the other agents have been stopped for further development or withdrawn from the market mostly due to commercial issues. Another SPION agent called Ferumoxytol (Feraheme®) is approved for the treatment of iron deficiency in adult chronic kidney disease patients. Ferumoxytol is comprised of iron oxide nanoparticles surrounded by a carbohydrate coat and is being explored as a potential imaging agent to evaluate lymph nodes and certain liver tumors.^[231]

3.3 Synthesis and characterisation of superparamagnetic citrate and BSA-coated iron oxide nanoparticles.

3.3.1 Synthesis by microwave-assisted thermal decomposition

Different methods have been established for the synthesis of SPIONs through years, including co-precipitation, microemulsion, hydrothermal synthesis, thermal decomposition, and microwave-assisted synthesis.^[232] Each of those methods displays advantages as well as some drawbacks detailed in **Table 16**.

Table 16. Advantages and drawbacks of the main synthetic routes for SPIONs. Adapted from Gonzalez-Moragas *et al.*^[232]

	Advantages	Drawbacks
Co-precipitation	<ul style="list-style-type: none"> + Simple + Aqueous media + Large amounts of NPs can be obtained (grams) + Size and morphology control + Generally performed at RT + Easy surface functionalization 	<ul style="list-style-type: none"> - Broad size distribution - Poor crystallinity - Basic pH is required - Long reaction times hours
Microemulsion	<ul style="list-style-type: none"> + Narrow size range + High crystallinity + Uniform physical properties + Size and morphology control 	<ul style="list-style-type: none"> - Low yield $\leq 3\%$ per mass of microemulsion - Uses large amounts of organic solvents
Hydrothermal synthesis	<ul style="list-style-type: none"> + Aqueous media + Size control 	<ul style="list-style-type: none"> - High temperature ≥ 200 °C - High pressure ≥ 2000 psi - Special reactors / autoclaves are required
Thermal decomposition	<ul style="list-style-type: none"> + Narrow size distribution, high monodispersity + High crystallinity + High yield $\sim 80\%$ + Size and morphology control 	<ul style="list-style-type: none"> - High temperature ~ 300 °C - Long reaction times hours - Requires organic solvents - Hydrophobic particles; ligand-exchange is required to make them into hydrophilic but aggregation may occur. - Safety issues
Microwave-assisted synthesis	<ul style="list-style-type: none"> + Narrow size distribution, high monodispersity + High crystallinity + High yield $\sim 80\%$ + Water dispersible + Short reaction times minutes + Moderate temperature $160\text{--}210$ °C + Efficient heating, resulting in low energy consumption + Easy post-synthesis surface functionalization 	<ul style="list-style-type: none"> - Requires organic solvents - Limited penetration depth of the microwave.

In the last years, microwave-assisted synthesis of SPIONs has attracted considerable interest since it is a facile and fast synthetic route to produce monodisperse nanoparticles with good magnetic properties under moderate temperature.^[71, 221] Moreover, microwave synthesis reduces the energy consumption and the overall fabrication cost compared to the high temperature thermal decomposition approach.^[221]

A microwave-assisted route previously developed in our group was used to synthesise citrate SPIONs in a single-mode CEM Discover unit (Explorer 12-Hybrid) at a frequency of 2.45 GHz and 300 W (**Figure 29**).^[71] Briefly, 0.35 mmol iron acetylacetonate, $\text{Fe}(\text{acac})_3$, were dissolved in 4.5 mL benzyl alcohol in a microwave glass tube and vortexed for 30 seconds. Reaction tubes were transferred to the microwave reactor and the following heating ramp was applied: 1) 5 min at 60 °C, 2) 10 min reaction at 180 °C, 3) cooling down to 50°C in 3 min using compressed nitrogen. After the reaction, 150 μL of 10 wt.% trisodium citrate, Na_3Cit , was added to each tube and sonicated for 1 min. Then, SPIONs were transferred to 50 ml centrifugal tubes, filled up to 50 ml with acetone, and centrifuged at 6000 rpm for 30 min to precipitate SPIONs. The supernatant was removed and the tube was re-filled with acetone together with 150 μL of 10 wt.% Na_3Cit . The tube was sonicated for 1 min and centrifuged again under the same conditions. These washing steps facilitated SPION purification before dispersing them in water. After removal of the supernatant, the SPIONs pellet was completely dried at 60°C overnight, and redispersed in 2 ml Milli-Q H_2O .

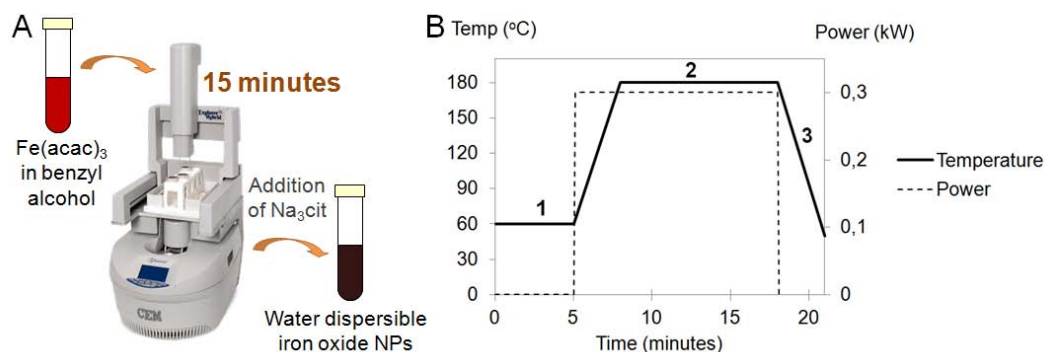


Figure 29. Microwave assisted reaction of C-SPIONs. A) Scheme of the reaction. B) Temperature and power ramp indicating the three steps described: 1) 5 min at 60 °C, 2) 10 min reaction at 180 °C, 3) cooling down to 50 °C in 3 min.

The mechanism of formation of SPIONs in benzyl alcohol by microwave heating was proposed by Niederberger and Garnweitner (**Figure 30**).^[233] Benzyl alcohol nucleophilically attacks one carbonyl group of the acetylacetonate ligand, and alcoholysis leads to benzyl acetate and an enolate ligand. Then, benzyl alcohol coordinates to the Fe center, releasing benzyl acetate in a ligand exchange reaction, and the enolate attacks the coordinated benzyl alkoxide releasing 4-phenyl-2-butanone. The Fe-bound hydroxyl group binds to another Fe center, representing the starting point of nanoparticle formation.

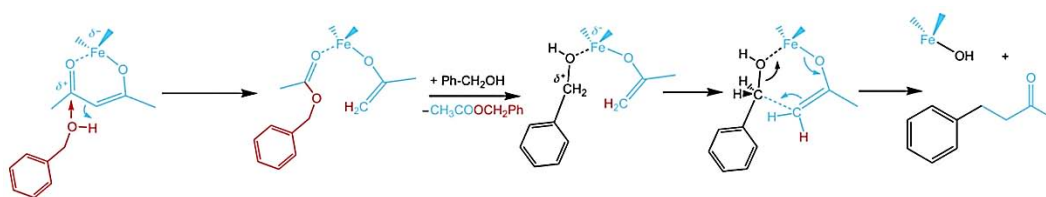


Figure 30. Main reaction occurring upon solvothermal treatment of $\text{Fe}(\text{acac})_3$ in benzyl alcohol involving solvolysis of the acetylacetonate, followed by condensation reactions. Adapted from Niederberger and Garnweitner.^[233]

C-SPIONs produced by microwave-assisted thermal decomposition were characterised by TEM, DLS, and zeta potential. C-SPIONs had a TEM diameter of 5.6 ± 0.8 nm, a hydrodynamic mean diameter of 17 nm and a zeta potential of -41 mV. They were superparamagnetic above 39 K and showed high saturation magnetization (76 $\text{emu/g Fe}_2\text{O}_3$ at 5 K). The characterisation of C-SPIONs is presented in **Figure 31**.

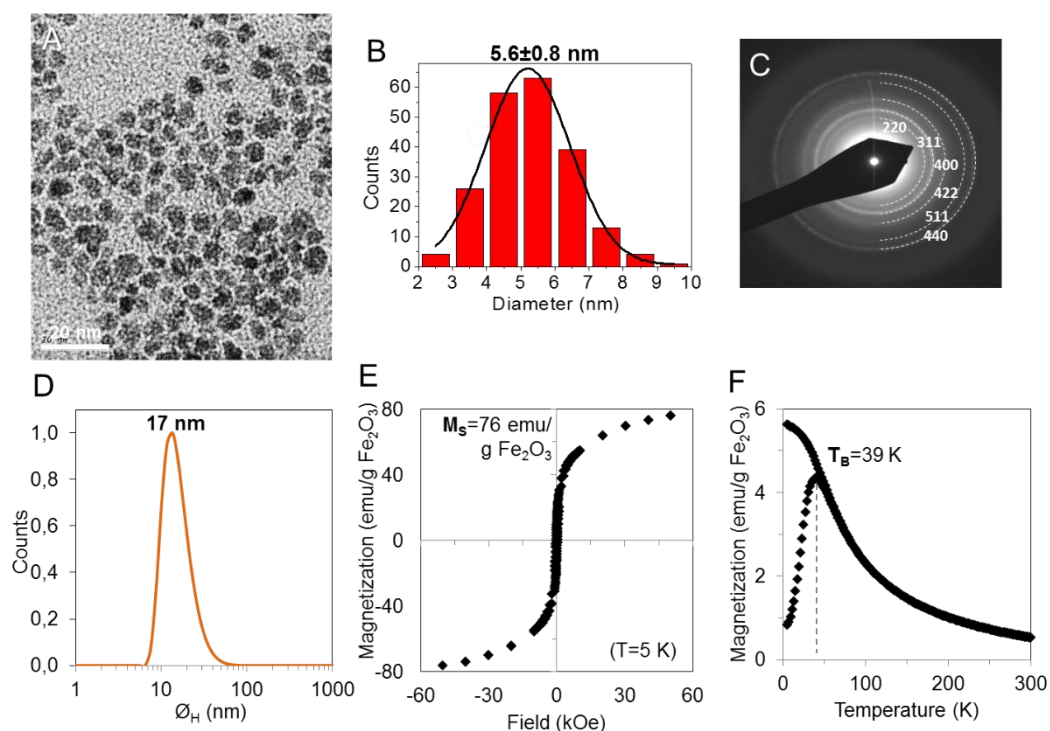


Figure 31. Characterisation of C-SPIONs: A) TEM image. B) TEM size distribution. C) Selected Area Electron Diffraction (SAED) measurement. D) DLS measurement. E) $M(H)$ measurement at 300 K up to 6 Tesla. F) ZFC-FC measurement from 4 to 300 K at 50 Oe.

3.3.2 BSA adsorption protocol

We chose to fabricate BSA-SPIONs since it is well-known that albumin can form a hard protein corona around NPs that improves their colloidal stability, increases their stealth behaviour and extends their circulation time *in vivo*.^[85, 93, 234] We used a BSA adsorption protocol developed previously in our group by Dr. Siming Yu.^[85] Briefly, 1.575 ml of a dispersion containing 1 mg/mL C-SPIONs was prepared using Milli-Q H_2O . The pH of the dispersion was adjusted to 11 by adding 100 μl of 0.1 M NaOH. Then 200 μl of 25 mg/mL BSA solution (freshly prepared) was added drop by drop and the mixture was

vortexed for 5 min. After 1 hour, the pH was adjusted to 7.4 by adding 125 μl of 0.06 M HNO_3 . In order to remove excess of BSA, the dispersion was centrifuged using filter units of 100 000 molecular weight for 15 min at 3000 rpm three times. Finally, BSA-SPIONs were resuspended to 2 ml using Milli-Q water. The formation of the BSA coating was studied by negative staining TEM, which stain protein as white, and the stability of the BSA-SPIONs was evaluated by dynamic light scattering (DLS).

We obtained BSA-SPIONs with a hydrodynamic mean diameter of 25 nm and a zeta potential of -26 mV. TEM observations performed with negative staining also gave a 7-nm increase in diameter indicating that a single monolayer of BSA was coating the SPION surface.^[235] The characterisation of BSA-SPIONs is summarized in **Figure 32**. Yu *et al* demonstrated enhanced colloidal stability of BSA-SPIONs in different biological media compared to C-SPIONs.^[85] The authors also determined by both molecular simulations and experimentally that ten molecules of BSA formed a monolayer around the outside of the SPIONs with high binding strength, ten times higher than the adsorption of other proteins frequently present in biological media such as fetal bovine serum (FBS).^[235]

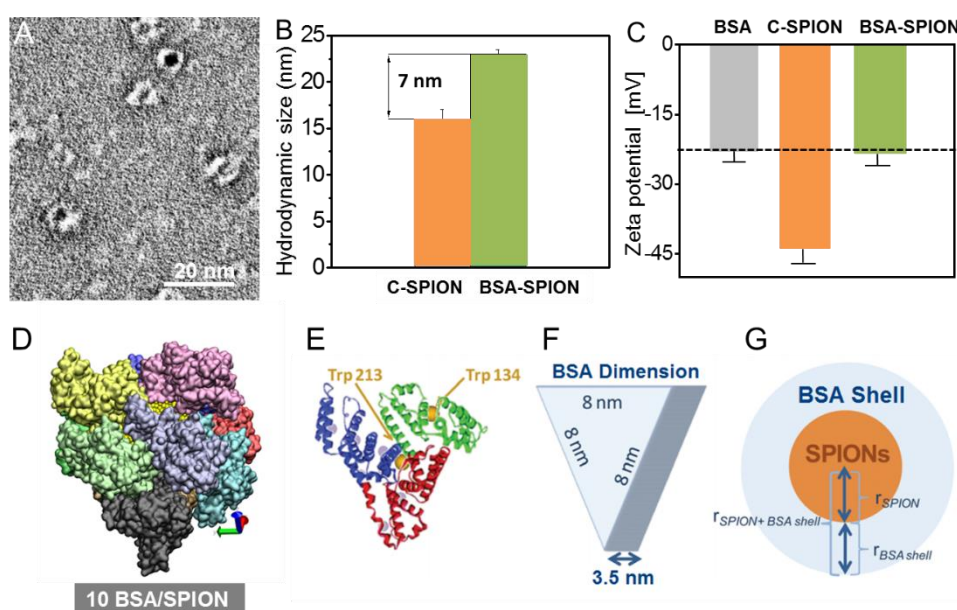


Figure 32. Characterisation of BSA-SPIONs: A) Uranyl-stained TEM images; the inorganic SPIONs appear dark and the BSA hard protein corona appear white. B) Hydrodynamic diameter of the C-SPIONs and BSA-SPIONs. C) Zeta potential values of BSA, C-SPIONs, and BSA-SPIONs. D) Representation of a pre-formed protein corona coated nanoparticle BSA-SPION resulting from molecular dynamic modelling analysis, each protein is displayed with a different colour. E) Crystal structure of BSA. F) Scheme of the dimensions of the BSA as an equilateral triangular prism. G) Schematic of the BSA-SPION complex. Adapted from Yu *et al.*^[93, 235]

3.3.3 Scale-up of SPION synthesis

As the number of applications of SPIONs for nanomedicine increases, larger amounts of SPIONs at reasonable cost are in high demand. Microwave-assisted synthesis results in high quality SPIONs, however the typical laboratory reaction yields up to 20 mg of SPIONs per vessel. Attempts of large-scale synthesis of SPIONs have already been

done by co-precipitation achieving relatively low yield and resulting in highly polydisperse NPs.^[236] Ibarra-Sánchez *et al* evaluated the high temperature decomposition in a large scale, which yields hydrophobic SPIONs, hence a ligand exchange is required before they can be used for *in vivo* use.^[237] Based on the biomedical applications of SPIONs, a promising synthetic method to scale-up should be simple, safe, energy and cost efficient, and yield water dispersible, biocompatible SPIONs with high saturation magnetization. All these requirements can be met using a microwave-assisted reaction, however many experimental factors hinder the scale-up process including increased heat loss, changes in absorption, limited penetration depth of the radiation into the reaction medium and the additional reflection of the microwaves.

There are two main types of scientific microwave equipment: single-mode and multi-mode.^[238] Single-mode reactors generate a single, highly homogeneous energy field of high power density. These systems couple efficiently with small samples, provide high quality products and are affordable, hence they are widely employed in laboratory-scale reactions. Multi-mode units have a larger microwave cavity, allowing the use of larger reaction vessels or the use of multivessel rotors that can be simultaneously irradiated. Based on their benchtop dimensions and standard electrical requirements, they can be used in any laboratory, however they are more costly than single-mode systems. In multimode units, the microwaves that enter the cavity are reflected homogeneously by a diffusor, the walls and the load over the large cavity. Indeed, field homogeneity is a key parameter determining the final properties of the as-synthesised material in multi-mode systems.^[238, 239]

When a microwave-assisted synthesis developed at the lab-scale is used as a starting point, scale-up typically begins with processing a 50 mL reaction mixture, corresponding to a ten- to 100-fold scale-up of the lab-scale reaction. However, re-optimization of the reaction parameters (e.g. precursor concentration, temperature, reaction time and microwave frequency) is typically required.^[240, 241] We used a multi-mode Milestone ETHOS One unit to scale up our laboratory-scale reaction. **Table 17** summarises the main features of this equipment in comparison to the single-mode CEM Discover reactor used in the synthesis of the lab-scale product.

Table 17. Main features of the microwave equipment used: the single-mode CEM Discover unit and the multi-mode Milestone ETHOS One.

	CEM Discover	Milestone ETHOS ONE
Cavity	Focused single mode cavity.	Large microwave cavity (43 L).
Magnetron	2.45 GHz magnetron.	Dual magnetron system (2.45 GHz) with pyramid-shaped diffuser.
Power	Up to 300 W. Automated power control based on temperature feedback.	Up to 1600 W. Automated power control based on temperature feedback. (PID Algorithm)
Temperature	Up to 300 °C.	Up to 300 °C.
Pressure	Up to 30 bar.	Up to 100 bar.
Weight	17 Kg.	90 Kg.
External size	36 x 43 x 28 cm.	55 x 55 x 65 cm.
Electrical requirements	220/240 V, 50 Hz.	230 V, 50-60Hz.

We evaluated the impact of different microwave-specific factors (equipment, reaction time, temperature, power) on the reaction product, and focused on the reproducibility between the lab-scale synthesis and the scaled-up synthesis.^[242] After re-optimization of reaction temperature and time in the multi-mode unit (**Figure 33**), we achieved a 10-fold scale-up our synthesis yielding >200 mg of material with very similar properties and quality than our lab-scale SPIONs in terms of their size, colloidal stability and magnetic properties (**Table 18**). Remarkably, the experimental set-up used allows up to 100-fold straightforward scale-up by parallel synthesis, yielding up to 3 grams of high quality material.

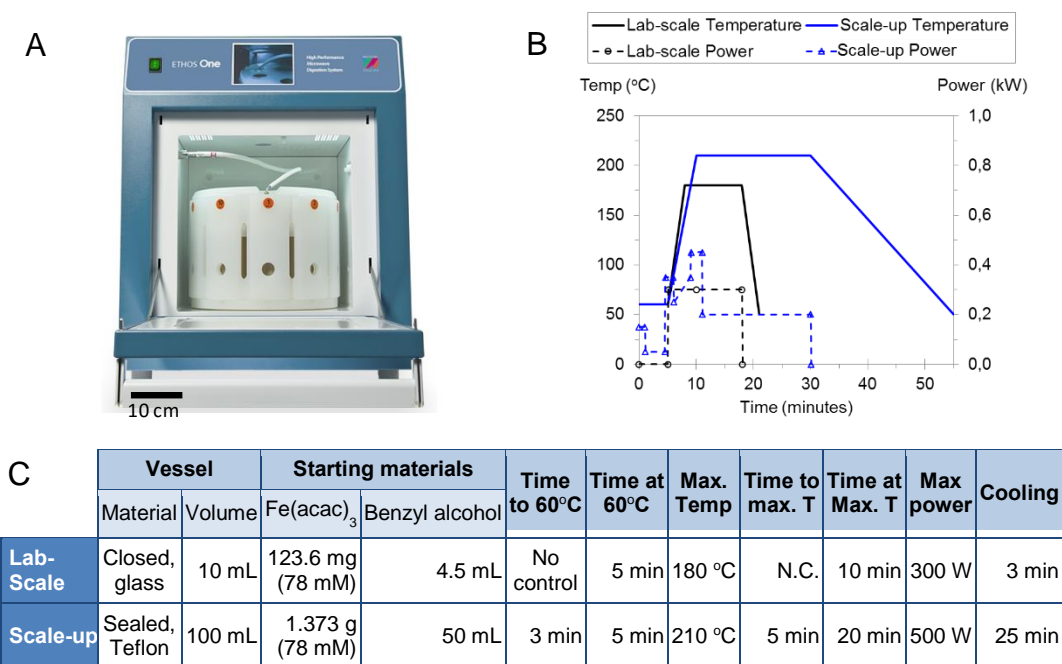


Figure 33. A) Image of the ETHOS One multimodal unit. B) Temperature and Power ramp of lab-scale (black) and scale-up (blue) synthesis. C) Comparison of the reaction conditions of the laboratory-scale and scale-up synthesis.

Table 18. Physicochemical characterisation of the laboratory-scale and the scale-up batches.

		Lab-Scale	Scale-up
TEM size	nm	5.7 ± 0.9	5.9 ± 1.4
Hydrodynamic size	nm	17	16
Saturation magnetisation at 300 K	emu/	62	53
Blocking temperature at 50 Oe	K	49	103
Yield	% Fe	79%	84%
Mass of NPs per vessel	mg Fe ₂ O ₃	22	261
Time ^a	hours	136	2
Energy consumption	KWh	40.9	1.1
Energy cost ^b	€	3.75	0.10
Reagents price ^c	€	86.36	80.61

^aCalculated considering the necessary time used in one batch and adding the required batches to yield 10 g of material.

^bCalculated considering 0.0917 €/KWh energy price, according to Eurostat 2014 (<http://ec.europa.eu/eurostat>, 2014).

^cFor the reagents, supplier prices from 2014 were used.

The high quality of the material is key for the biological evaluations that will be performed in the next Sections. In addition, a thorough characterisation of the material under study is also essential to analyse the interaction between nanoparticles and living animals in a comprehensive way and to correlate the biological effects with the properties of the test material. Therefore, our biological evaluations began with the synthesis of the material, its characterisation in the test media, and progressed to a detailed analysis in *C. elegans*. Using this methodology, we aimed to ensure a systematic evaluation of the nano-bio interactions from both perspectives, material sciences and biology, and achieve robust conclusions.

3.4 Introduction to the properties and applications of Au- NPs in nanomedicine

Gold nanoparticles have unique features that make them excellent nanomaterials for targeting, imaging and therapeutics in a single theranostic platform (**Figure 34**). The most promising features of Au-NPs in nanomedicine include their intense surface plasmon resonance (SPR), their easy tuning of size and shape, and their easy functionalization with almost any kind of molecule. In particular, their intense SPR resulting from photon confinement due to the small particle size results in intense light absorption and scattering, and a high photothermal conversion rate. SPR is also exhibited by other noble metal nanoparticles such as Ag-NPs, and have found a multitude of biological and medical applications.^[243]

Au-NPs can be synthesised with diameters from 2–5 nm up to 100 nm, in different shapes such as spheres, hollow, rods, diamonds, prisms, cages, either single solid bodies or in a core shell format. Each combination of size and shape shows slightly different properties that may be explored for specific purposes. For instance, shapes like nanostars or nanorods present a high absorption peak in the NIR range, which have been applied in phototherapy approaches. However, the majority of the described nanomedicine systems using Au-NPs have focused on spherical NPs.^[243]

Compared to other types of nanoparticles, Au-NPs have been considered to exhibit low toxicity and high chemical stability. Indeed, spherical Au-NPs between 10 and 60 nm in diameter are generally considered as non-toxic, while sharp-edged nanoparticles tend to have higher cytotoxicity but are more prone to endosomal escape favoring drug delivery.^[243]

3.4.1 Applications of Gold Nanoparticles

Targeting agents

Targeting has been crucial for the development of vectorization systems capable of site specific accumulation/retention enabling nanoparticles to deliver their cargo on site for improved therapeutic effect. Au-NPs typically reach target cells through ligand-receptor interactions that induce receptor-mediated endocytosis and release of the drug payload inside the cell.^[243]

Au-NPs can be functionalized with molecules for targeting that also enhance stability and biocompatibility *in vivo*. Indeed, a wide range of stabilizers available may also act as therapeutic agents (e.g., miRNA, siRNA, DNA, peptides and antibodies) or reduce NPs' immunogenicity (e.g., PEG).^[243] In particular, bi-functional PEGs (with a thiol group in one extremity and another group at the other end—amine, carboxylic, biotin, azide) have been widely used for direct coupling to another molecule of interest via straight forward chemistry with high yield.^[244, 245] Peptide conjugation allows active and specific targeting, enhancing targeted delivery. Successful targeting has also been achieved via functionalizing Au-NPs with antibodies that target specific receptors involved in cancer or infectious diseases. Au-NPs can be further engineered to avoid removal from circulation (e.g. becoming trapped in the liver, kidneys, spleen) or to cross biological barriers (e.g., blood-brain barrier), in order to increase therapeutic efficacy and allow systemic tracking.^[243]

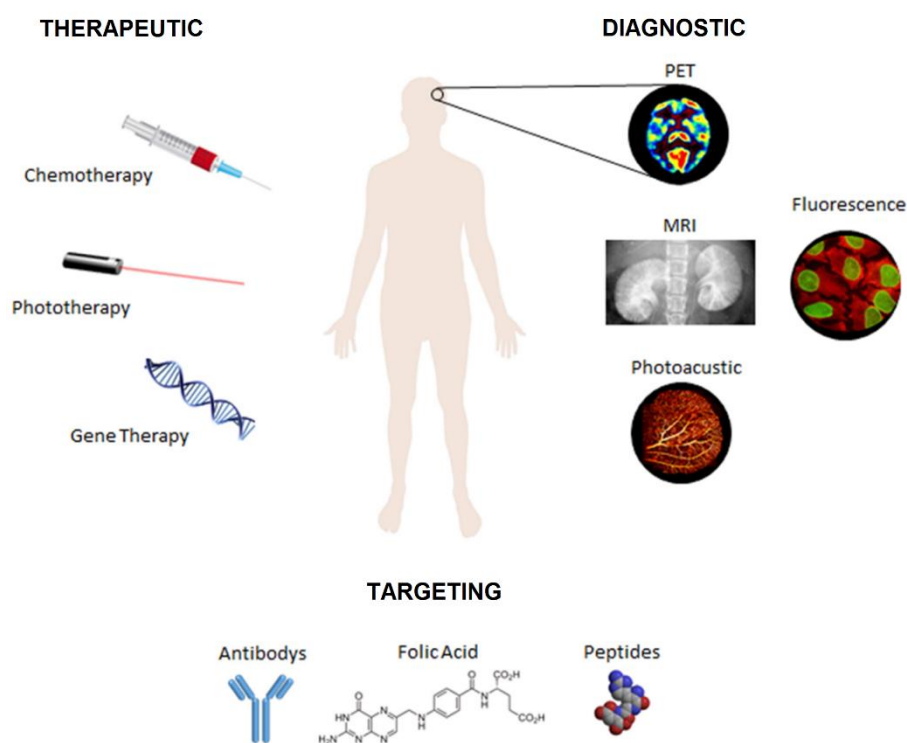


Figure 34. Different types of nanoparticles and their applications in theranostic. Schematic overview of the possible functionalization and application of Au-NPs as nano-carriers for theranostics. Adapted from Pedrosa *et al.*^[243]

Therapeutic agents

Several therapeutic agents can be packed in Au-NPs-based targeted delivery systems, including small drugs, a peptide/antibody, a ribozyme, a siRNA or an antisense oligonucleotide. Doxil®, consisting of doxorubicin encapsulated into PEGylated liposomes, was the first nano-drug approved by the FDA in 1995 based on their improved efficacy.^[23] Au-NPs doxorubicin nano-formulations attempted to mimic their liposome counterpart and showed promising advantages, such as increased targeting and functionalization as well

as the possibility to couple with phototherapy and to act as imaging/contrast agents.^[246, 247] Au-NPs have been also applied in theranostic approaches with other anti-tumour drugs allowing simultaneous chemo-phototherapy and imaging.^[243]

Gene therapy

Gene therapy has been receiving increasing attention in many diseases including cancer. In particular, small interfering RNA (siRNA) has shown potential to downregulate specific oncogens in cancer cells, however naked siRNAs show extremely short half-lives. Hence, the development of efficient delivery vehicles for *in vivo* applications is a major challenge to translating siRNA into effective therapeutics. Au-NPs with different shapes and sized have been used to vectorize gene silencing elements into cancer cells. For instance, gold spheres were described for siRNA targeting and delivery using models of increasing complexity (cells, hydra and mice), achieving effective a ~65% reduction in c-MYC gene expression.^[248]

Phototherapy

Photothermal therapy (PTT) is based on the selective sensitization of cells to thermal damage, or hyperthermia, near 45 °C. Au-NPs can improve traditional PTT thanks to their ability to convert absorbed photons into thermal energy, and also allow selective targeting and vectorization of additional cargo. By modulating the Au-NPs' shape and/or shell thickness, it is possible to shift the SPR peak of Au-NPs toward the near-infrared (NIR), allowing deeper light penetration into tissues. Moreover, the laser energy required to achieve this transformation is far below that stipulated in medical safety standards. AuNP-mediated PTT is predominantly associated with nanorods, nanoshells and nanocages, and is showing promising results in clinics.

Multimodal Imaging

Au-NPs show potential in imaging modalities such as computed tomography (CT), photoacoustic tomography (PAT) and fluorescence imaging. Computed tomography provides image contrast to visualize tissue density differences and may be tuned to distinguish between normal and cancerous tissue. However, the iodinated molecules that are typically used as CT contrast enhancers tend to undergo a rapid renal clearance and nonspecific vascular permeation causing a decrease in the technique sensitivity. Au-NPs are optimal contrast agents for CT due to the relatively high X-ray attenuation of gold and the stability of gold colloids. Since gold has higher absorption than iodine, Au-NPs can achieve better contrast with lower X-ray dose. Photoacoustic tomography takes advantage of the photoacoustic phenomenon of Au-NPs to improve spatial resolution and image contrast. Furthermore, in fluorescence-based imaging, using the NIR part of the spectrum of Au-NPs improves spatial resolution and significantly reduces autofluorescence. The use of Au-NPs in diagnosis to combine two or more techniques can provide more accurate data on the clinical condition *in vivo*.

3.4.2 Current status of clinical applications

Despite the wide range of Au-NPs applications in nanomedicine, only Au-NPs used for local heat generation in the plasmonic photothermal therapy of atherosclerosis and cancers (i.e. lung and neck) have reached clinical stage (**Table 19**). Although some clinical trials are already completed, the results are either not disclosed yet or not conclusive due to the small number of participants. Therefore, given the enormous potential in nanomedicine, much remains to be done to effectively translate gold nanoformulations into the clinics.

Additionally, Au-NPs are present in our daily products as anti-ageing creams and masks, toothpastes and even marketed as food supplements according to the Consumer Products Inventory, compiled by the Project on Emerging Nanotechnologies.^[5]

Table 19. Clinical trials of gold nanoparticulate platforms.

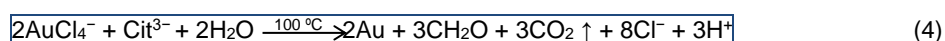
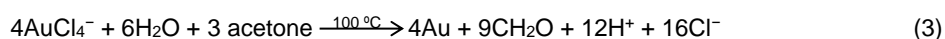
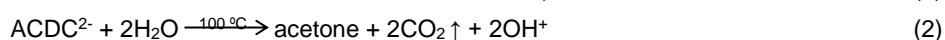
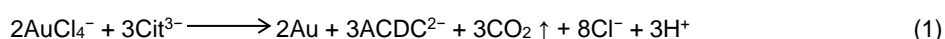
Name	Acronym	Register	Identifier	Start date	Last update	Status
Plasmonic Photothermal and Stem Cell Therapy of Atherosclerosis Versus Stenting	NANOM PCI	US	NCT01436123	09/2011	05/2015	Terminated
Plasmonic Nanophotothermic Therapy of Atherosclerosis	NANOM-FIM	US	NCT01270139	02/2016	05/2016	Completed
Exhaled Breath Olfactory Signature of Pulmonary Arterial Hypertension	SNOOPY2	US	NCT02782026	12/2010	10/2015	Recruiting
Pilot Study of AuroLase(tm) Therapy in Refractory and/or Recurrent Tumors of the Head and Neck	-	US	NCT00848042	02/2009	10/2015	Completed
Efficacy Study of AuroLase Therapy in Subjects With Primary and/or Metastatic Lung Tumors	-	US	NCT01679470	08/2012	10/2015	Active
MRI/US Fusion Imaging and Biopsy in Combination With Nanoparticle Directed Focal Therapy for Ablation of Prostate Tissue	-	US	NCT02680535	02/2016	02/2016	Recruiting
Diagnosis of Gastric Lesions With Na-nose	-	US	NCT01420588	08/2011	06/2013	Unknown
A Phase I SAD and MAD Clinical Trial of CNM-Au8 in Healthy Male and Female Volunteers	-	US	NCT02755870	04/2016	04/2016	Recruiting
Enhanced Epidermal Antigen Specific Immunotherapy trial - 1: A Phase 1a study of gold nanoparticles administered intradermally by microneedles to deliver immunotherapy with a proinsulin derived peptide in Type 1 diabetes.	EE-ASI-1	EU	2015-003934-28	03/2016	-	Ongoing

US: ClinicalTrials.gov ; EU: ClinicalTrials Register.eu

3.5 Synthesis and characterisation of gold nanoparticles

The most widely applied method to produce Au-NPs consists in the citrate reduction of chloroauric acid (HAuCl₄) in water, first reported by Turkevich in 1951. In the Turkevich method, colloidal gold forms because citrate ions act both as reducing agent and capping agent, and yields Au-NPs of 10-20 nm in diameters.^[249]

During Au-NP synthesis, Cit³⁻ is oxidized to acetone dicarboxylate (ACDC²⁻), a ligand that complexes Au³⁺, thus facilitating nanoparticle growth (eq.1). Following nanoparticle nucleation, ACDC²⁻ is thought to be rapidly degraded to acetate at the synthesis temperature of ≈100 °C (eq.2). Acetone or other carboxylate by-products formed by the degradation of ACDC²⁻ reduce auric chloride and lead to its complete conversion to Au⁰ (eq.3). In summary, the global synthetic reaction is presented in eq.4.



The Turkevich reaction was improved by Frens in the 1970s to tune the size of Au nanoparticles up to 150 nm by changing the ratio between trisodium citrate and gold precursor: to produce larger particles, less sodium citrate should be added in order to promote the aggregation of the small particles into bigger ones, based on the reduced amount of stabilizing agent.^[250] Recently, Punter's group refined the existing method by kinetic controlled seed growth allowing the synthesis of Au-NPs up to ~200 nm.^[251] We applied these last two methodologies to produce Au-NPs up to 150 nm starting from 11-nm seeds synthesised using the Frens-Turkevich method.

3.5.1 Synthesis of 11-nm Au-NPs

A solution of 2.2 mM sodium citrate in Milli-Q water (150 mL) was heated with a heating mantle in a 250 mL three-necked round-bottomed flask for 15 min under vigorous stirring. A condenser was utilized to prevent the evaporation of the solvent. After boiling had commenced, 1 mL of HAuCl₄ (25 mM) was injected. The colour of the solution changed from yellow to bluish gray and then to soft pink in 10 min. The resulting particles (~10 nm, ~3 × 10¹² NPs/mL) were coated with negatively charged citrate ions and hence were well suspended in H₂O.

3.5.2 Seeded growth to 150-nm Au-NPs

3.5.2.1 Seeded growth of Au NPs up to 32 nm in diameter

Immediately after the synthesis of the Au seeds and in the same vessel, the reaction was cooled until the temperature of the solution reached 90 °C. Then, 1 mL of sodium citrate (60 mM) and 1 mL of a HAuCl₄ solution (25 mM) were sequentially injected (time delay ~2 min).

3.5.2.2 Seeded growth of Au NPs up to 150 nm in diameter

Immediately after the synthesis of the Au seeds and in the same reaction vessel, the reaction was cooled until the temperature of the solution reached 90 °C. Then, 1 mL of a HAuCl₄ solution (25 mM) was injected. After 30 min, the reaction was finished. This process was repeated twice. After that, the sample was diluted by extracting 55 mL of sample and adding 53 mL of MQ water and 2 mL of 60 mM sodium. This solution was then used as a seed solution, and the process was repeated again.

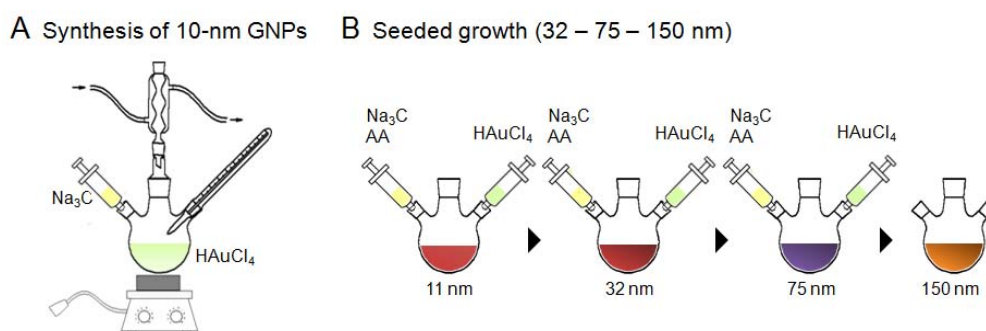


Figure 35. Synthesis of Au-NPs. A) Synthesis of 11-nm Au-NPs by the Frens-Turkevich method. B) Synthesis of 150-nm Au-NPs by seeded growth through two intermediate steps, 32 and 75 nm.

3.5.3 Characterisation

The 11-nm citrate-coated gold nanoparticles showed a nominal size of 11 ± 1 nm; a hydrodynamic mean diameter of 16 ± 3 nm; a zeta potential of -26.4 mV; and a maximum resonance plasmonic absorption band at 525 nm (**Figure 36**). The seeded growth protocol progressed through two intermediate steps of 32 and 75 nm diameter by TEM. Finally, the reaction yielded nanoparticles with a nominal size 150 ± 17 nm; a hydrodynamic mean diameter of 221 ± 49 nm; a zeta potential of -21.2 mV; and a maximum resonance plasmonic absorption band at 598 nm.

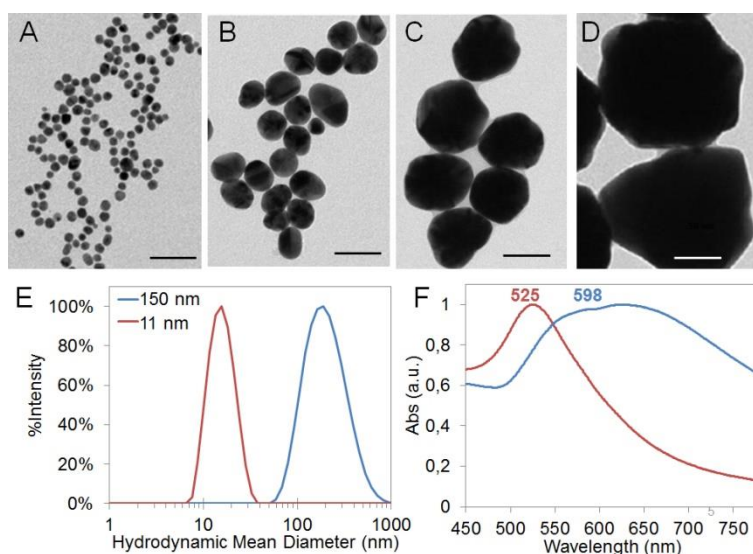


Figure 36. Characterisation of Au-NPs by TEM, DLS and UV-Vis. TEM images of A) 11-nm, B) 32-nm, C) 75-nm, D) 150-nm Au-NPs. Scale bar represents 50 nm. E) DLS of 11-nm (red) and 150-nm (blue) Au-NPs. F) UV-Vis spectra of 11-nm (red) and 150-nm (blue) Au-NPs.

3.6 Comparison of as synthesised SPIONs and Au-NPs

Gold is a noble metal with an atomic mass of 196.97 and a density of 19.3 g/cm³. It is one of the least reactive chemical elements. Gold nanoparticles are composed of metallic gold, gold (0). In contrast, iron oxide nanoparticles are composed of maghemite (γ -Fe₂O₃), which has a molecular weight of 159.69 (111.69 corresponds to iron) and a density of 4.9 g/cm³. Iron is an essential element in organisms: it is present in proteins involved in key metabolic processes such as DNA synthesis, mitochondrial respiration and oxygen transport.^[252] The physicochemical properties of gold and maghemite are compared in **Table 20**.

Table 20. Physicochemical properties of Gold and Maghemite.

	Gold	Maghemite
Atomic Number	79	26 (Fe) 8 (O)
Molecular Weight (g/mol)	196.97	159.69
Density (g/cm ³)	19.3	4.9
Melting Point (°C)	1 063	1 597
Crystallography	Cubic structure, face centered	Cubic, inverse spinel
Refractive index	0.27	2.42

Based on the nominal size of nanoparticles and their density, it is possible to calculate the surface area per NP and the ratio surface area to volume, as shown in **Table 21**. These parameters will be used to express NP uptake in *C. elegans* as number of nanoparticles and surface area of ingested nanoparticles, which may be better correlated with the *in vivo* effects of the nanoparticles than the absolute metal quantity alone based on the unique properties at the nanoscale.

Table 21. Comparison of size and surface area of SPIONs and Au-NPs.

	6-nm SPIONs	11-nm Au-NPs	150-nm Au-NPs
Diameter (nm)	6	10	75
V (nm ³ /NP)	113	524	1767146
Surface Area (nm ² /NP)	113	314	70686
Surface Area / Volume	1.00	0.60	0.04

Maghemite particles are biodegradable: they can be dissolved intracellularly to iron ions (eg. in the lysosomes) and degraded.^[93] In contrast, gold nanoparticles are resistant to corrosion and oxidation, however it has been reported that surface atoms can be gradually dissolved *in vitro* into Au¹⁺ ions that can be also intracellularly oxidized to Au³⁺ and act as oxidative agent.^[253, 254] These properties can determine at least in part the *in vivo* effects and biocompatibility of the nanoparticles.

3.7 Evaluation of *C. elegans* exposure conditions for in-house inorganic NPs

We evaluated the stability of our in-house fabricated iron oxide nanoparticles and gold nanoparticles in different liquid media, which allows a more even distribution of NPs than solid media and facilitates a homogenous contact between the NPs and the worms. Moreover, liquid media is more convenient to monitor NP status and is, indeed, the natural

habitat of *C. elegans*, as they live in the interstitial water of soil. We did not include food to avoid the presence of additional biological surface and active metabolism from bacteria. We assessed different media of increasing ionic strength: Milli-Q water, Moderately Hard Reconstituted Water (hereinafter, EPA), EPA supplemented with 10 ppm Humic Acid, HA (labelled EPA2) and 100 ppm HA (labelled EPA3), and M9 buffer. We used HA to mimic the presence of organic matter in the exposure media in concentrations similar to those found in surface water. We tested the stability of SPIONs and Au-NPs in Milli-Q water, M9 buffer, EPA, EPA2 and EPA3 mediums by DLS and ZP measurements (**Figure 37**). These investigations were performed using 6-nm citrate-coated SPIONs (C-SPIONs) and 11-nm citrate-coated Au-NPs. In the media with the highest ionic strength, M9 buffer, both C-SPIONs and 11-nm Au-NPs underwent severe aggregation resulting in the precipitation of micrometric aggregates. In contrast, all EPA mediums maintained the nano-scale size of C-SPIONs (~30 nm) and 11-nm Au-NPs (~200 nm), however only dilution in Milli-Q water fully maintained their initial size. The ZP measurements were in good agreement with the DLS findings: M9 compromised more pronouncedly the colloidal stability of both materials, while NP suspensions in Milli-Q water were the most stable.

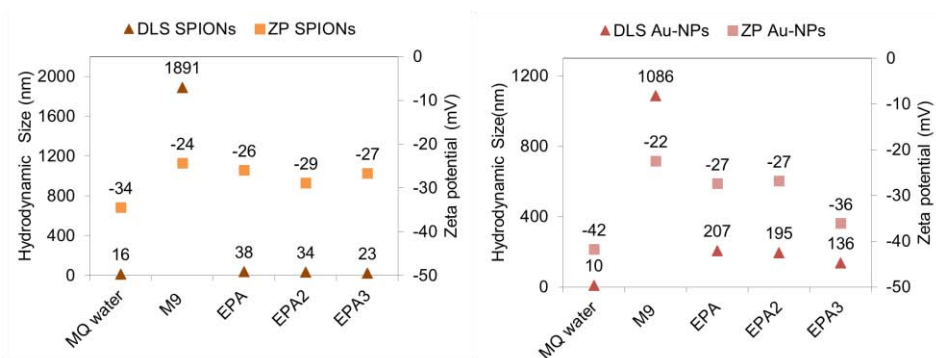


Figure 37. Hydrodynamic Size and Zeta Potential variations after 20 min incubation of C-SPIONs (left) and 11-nm Au-NPs (right) in MQ water, M9, EPA, EPA2 and EPA3.

To compare the NP status that *C. elegans* would find in solid exposure, we also characterised the NP dispersions in LB/bacteria at the exposure concentration by DLS and reported an hydrodynamic mean diameter of 27 ± 8 nm for SPIONs and 142 ± 24 nm for 10-nm Au-NPs, while bacteria appeared as a peak at $1 \sim 2 \mu\text{m}$ consistent with the size of *E. coli*. Based on these results, we decided to perform the exposure in the absence of food to favour NP stability and chose the latter juvenile stage of *C. elegans*, named L4. We limited the incubation time to 24 h at 20°C due to the lack of food and evaluated the biological effects of NP treatment after the testing period comparing treated versus untreated worms. We evaluated the tolerance of *C. elegans* to the various liquid media assessed and found no lethality neither significant differences in the locomotion behaviour of *C. elegans* in the different media. Given the high NP stability in Milli-Q and its non-harmful effects on *C. elegans* behaviour under our exposure conditions, we chose Milli-Q water as test media to ensure that nanoparticles maintained intact their initial properties and status before the exposure. For material scientists, it is very important to control NP

status in order to correlate NP initial properties with the biological effects observed *in vivo*. Because the unique properties of engineered nanomaterials are primarily attributed to their nanoscale structure, size, and shape, any modification occurred prior to application or acquired in the test media can significantly alter properties such as size and surface properties, which in turn can influence the biodistribution and interaction of nanoparticles with the biological environment.^[110] For instance, the uncontrolled formation of aggregates and the subsequent decrease of available surface area would result in a modified toxicity in *C. elegans* compared to a monodisperse suspension consisting of the same nanoparticles. Furthermore, it is difficult to formally correlate the aggregation state with toxicity.^[190] We monitored the stability of our test NPs (6-nm citrate-coated SPIONs, 6-nm BSA-coated SPIONs, 11-nm citrate-coated Au-NPs and 150-nm citrate-coated Au-NPs) in the media before and after *C. elegans* exposure by DLS (24 h) and found no significant changes related to incubation with *C. elegans*, confirming that Milli-Q water is an excellent media to retain monodisperse NP dispersions (**Figure 38**). However, during the progress of this thesis, we realized that *C. elegans* suffered some osmotic stress due to the absence of salts in the media. Particularly, in our initial TEM analysis the excretory pore of both treated and untreated worms was more open compared to animals grown in NGM plates. These findings suggested that Milli-Q water could increase the baseline of stress of nematodes in our assay system, hence for mechanistic studies we used 50% M9 buffer to minimize the stress, similarly to Tsyusko *et al.*^[186] We monitored the status of SPIONs and Au-NPs in 50% M9 buffer by DLS and found that they remained nano-size although gold nanoparticles suffered some aggregation (19 ± 4 nm SPIONs and 159 ± 48 nm Au-NPs).

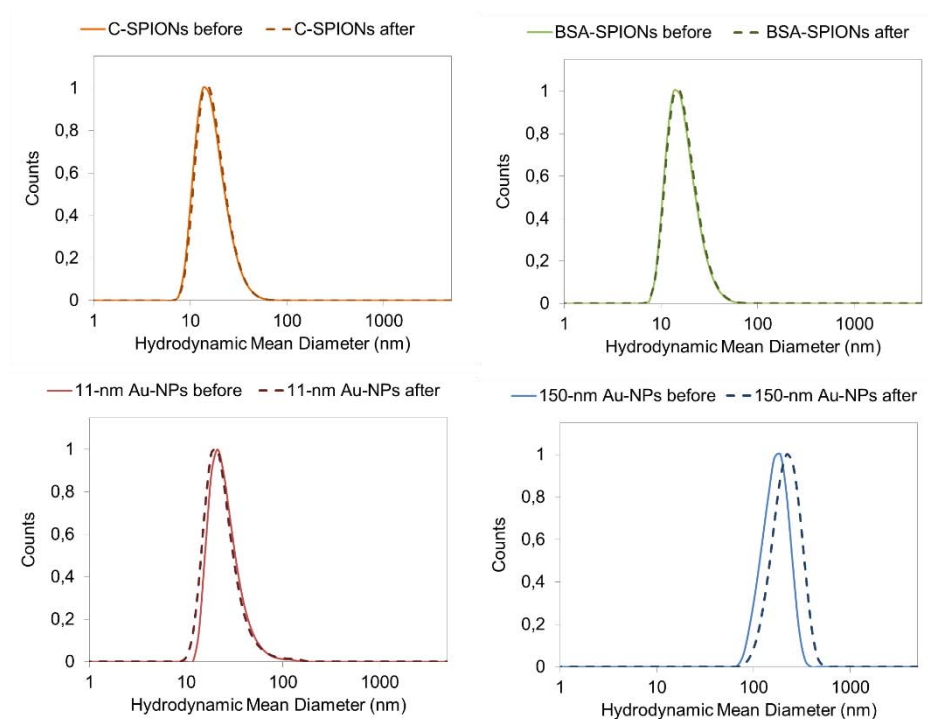


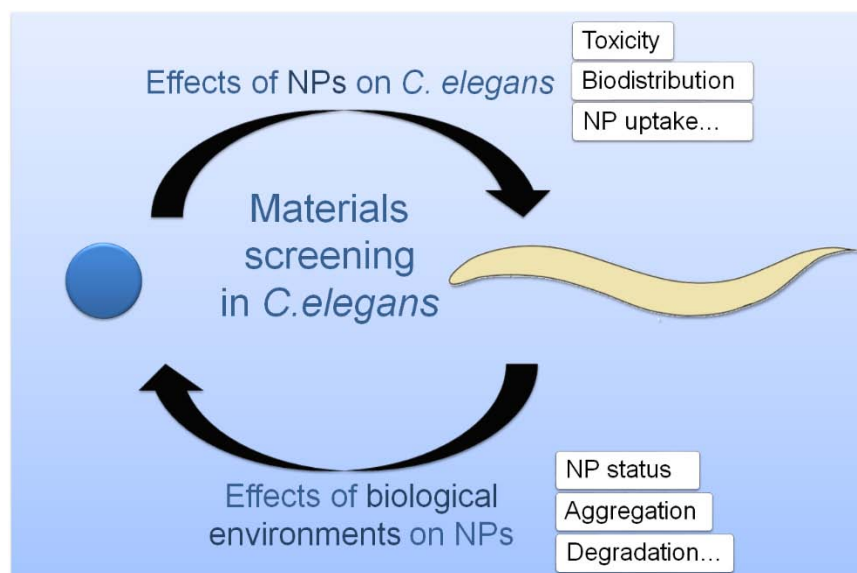
Figure 38. DLS measurements of NPs upon incubation with *C. elegans*: C-SPIONs (orange), BSA-SPIONs (green), 11-nm Au-NPs (red) and 150-nm Au-NPs (blue)

Overall, we believe that short-term exposure using liquid media in the absence of food is a good experimental system to study nano-specific effects and mechanisms even though evaluations are not performed using physiological conditions for *C. elegans*. For more prolonged regimes, growth assays, or ageing studies, we propose the dispersion of NPs in an LB/bacteria mixture with proper monitorization of NP status by DLS.

3.8 Chapter conclusions

We have described the current applications of SPIONs and gold nanoparticles in nanomedicine based on their physicochemical and nanospecific properties, illustrating their potential uses and their clinical status. We have presented robust synthetic routes that yield high quality water dispersible nanoparticles that are ready for *in vivo* use. Moreover, we have demonstrated the scalability of the microwave-assisted thermal decomposition reaction for the synthesis of SPIONs and presented a BSA-adsorption protocol to form a protein corona around the maghemite core. We have thoroughly characterised the as synthesised materials by TEM, DLS, Zeta Potential, magnetometry and UV-Vis spectroscopy, and assessed their colloidal stability in biological media for *C. elegans* exposure. We found that SPIONs are more stable in media with high ionic strength than Au-NPs, which aggregated more easily. Finally, we have defined the exposure conditions for the evaluation of the interaction between inorganic nanoparticles and *C. elegans* based on the stability of the NPs in the different media and the tolerance of *C. elegans*: acute (24 h) treatment in liquid media without food.

CHAPTER 4. Protocols used to characterise the nano-bio interaction



CHAPTER SUMMARY

This chapter sets up the methodology and experimental framework of this thesis. It details the protocols we have adopted to evaluate NP-treated worms, including biological evaluations such as survival and brood size; sample preparation for chemical analysis, magnetometry, and light and electron microscopy; and genomic assays.

CHAPTER INDEX

4.1	Introduction.....	83
4.2	Worm exposure	83
4.3	Analysis of toxicity endpoints	84
4.4	Uptake of NPs in <i>C. elegans</i>.....	85
4.4.1	Sample preparation	85
4.4.2	Magnetometry	85
4.4.3	Chemical analysis by ICP-MS.....	86
4.4.4	Magnetic Resonance Imaging.....	86
4.5	Biodistribution of NPs	86
4.5.1	Optical microscopy	86
4.5.2	SEM-EDX analysis	88
4.5.3	TEM analysis of targeted cross-sections	89
4.6	NP status inside <i>C. elegans</i>	91
4.6.1	Magnetometry	91
4.6.2	Absorbance micro-spectroscopy.....	91
4.6.3	Recovery of ingested nanoparticles from treated worms	92
4.6.4	Induction of NP-excretion in treated worms	92
4.7	Biological mechanisms	92
4.7.1	Gene expression profiling analysis	92
4.8	Statistical analysis	96
4.9	Chapter conclusions	96

4.1 Introduction

The following sections describe with extensive detail the protocols we adopted to characterise the interaction between inorganic nanoparticles and *C. elegans* combining a range of techniques from biology and materials science (**Figure 39**). The protocols presented below have been applied to study SPIONs and Au-NPs *C. elegans*, but they can be readily extended to other types of nanomaterials. The protocols to grow and maintain *C. elegans* are described in Appendix 1. Other techniques that have been preliminarily investigated during this thesis are described in Appendix 2.

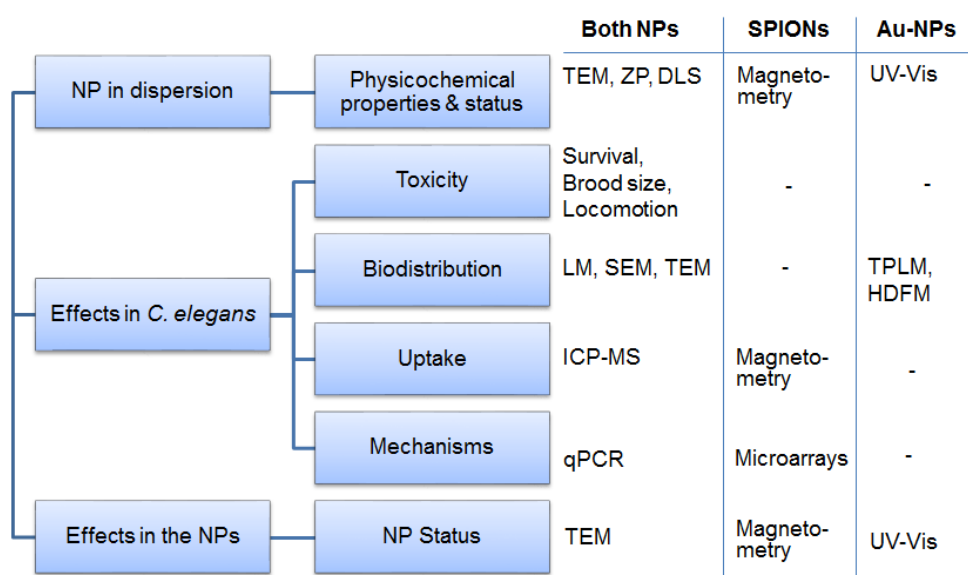


Figure 39. Techniques used in the characterisation of the interaction between *C. elegans* and NPs.

The following sections provide extensive details of the experimental procedures applied given that this is the first *C. elegans* thesis in the group, and they cover also the optimization of common protocols for the *C. elegans* specimens.

4.2 Worm exposure

C. elegans were grown following standard practices to obtain the desired population. The desired worm population was rinsed from NGM plates with Milli-Q water, and washed three times with Milli-Q water (10 min each) using gentle centrifugation (1 min 1400 xg). The supernatant was removed, and a worm pellet containing the desired number of worms at the desired developmental stage was then used for NP exposure. Depending on the type of evaluation, worms were treated with nanoparticles in liquid media in 24-well plates (for large population exposure, i.e. genomic analysis, uptake quantitation, biodistribution) or 96-well plates (i.e. for survival and brood size analysis). The volume of liquid of each well was 0.5-1 ml for the 24-well plates and 0.1 ml in the case of the 96-well plates (**Figure 40**).

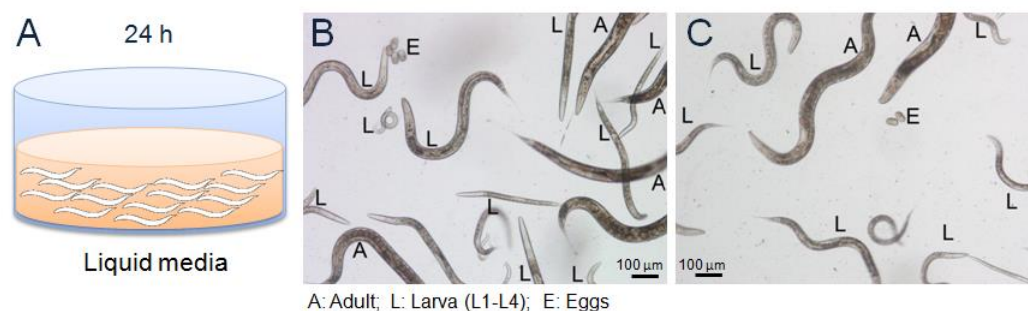


Figure 40. A) Illustration of our exposure system in liquid media. *C. elegans* was incubated in a NP dispersion in 24- or 96-well plates. B,C) Light micrographs of a mixed-stage culture illustrating the different developmental stages of the *C. elegans* lifecycle, from egg to adult.

The concentration range was selected based on previous *in vitro* data from the group and previous *C. elegans* published work.^[71, 186, 211] The concentrations assessed, expressed as $\mu\text{g/mL}$ of metal (or mg/L), were: 15, 50, 100, 200, 300, 400, 500 for SPIONs; and 15, 50, 100, 300, (500) for Au-NPs. These doses were expected to yield informative results from the biomedical perspective and be illustrative of relevant effects/mechanisms at low, medium and high doses.

4.3 Analysis of toxicity endpoints

Survival and brood size assays

We assessed survival as lethal endpoint and brood size as sub-lethal endpoint. In the survival assay, animals were treated in a final volume of 100 μL in 96-well plates for 24 h. The assay was performed in triplicate. The plates were tapped and the worms that moved were counted as alive. Each well contained 9 ± 3 young adult worms. To study the brood size, treated and untreated worms were transferred to a NGM plate seeded with an OP50 lawn at 20 °C. The number of progeny was scored after 72 h of food resumption. Results are expressed as percentage of brood size in respect to the untreated (control) worms. The reprotoxicity assay was performed in triplicate.

Locomotion behaviour

We used the automated platform Microtracker in the *C. elegans* facility at IDIBELL to monitor the locomotion behaviour, measured as bins, for 48 hours in 96-well plates. Staged animals (10-15 individuals) were treated in a final volume of 100 μL per well. We performed 6 replicates per condition.

Growth

Treated and untreated worms were transferred to an NGM plate seeded with an OP50 lawn at 20 °C. The body length was measured after 72 h of food resumption by light microscopy using ImageJ software. We measured 6 animals per condition.

4.4 Uptake of NPs in *C. elegans*

4.4.1 Sample preparation

Few thousand worms (adults: 2 000–6 000, larvae: ~10 times more than adults) were treated in 24-wells in 1 ml of liquid for 24 h. After exposure, worms were thoroughly washed, pelleted by centrifugation and transferred to a polycarbonate capsule. The capsule was dried at 60 °C overnight, and subsequently analysed by magnetometry and/or by ICP-MS.

4.4.2 Magnetometry

The as prepared sample was inserted in the SQUID magnetometer sample holder. A magnetometer from Quantum Design MPMS5XL was used to perform magnetization measurements. Magnetization versus applied field was measured at 5 K up to 5 Tesla. Given the low magnetic signal of our samples, we followed careful procedures in the preparation and handling of the samples to avoid contamination that could originate small magnetic signals such as the presence of dust, manipulation with metallic tweezers, or the use of commercial cotton. We prepared the samples inside a laminar flow cabinet, which prevents the presence of particles in the air; we manipulated the capsule with plastic tweezers during both sample preparation and analysis; and we avoided the use of cotton, as the sample dried inside the capsule and stuck firmly inside.

The diamagnetic signal from the polycarbonate capsule was subtracted from the raw data (**Figure 41A**) to obtain the magnetic curve of the worms (**Figure 41B**). SPIONs uptake was evaluated by measuring the remanence magnetization value of treated worms (M_{Rworms}) at 5 K. At temperatures lower than the blocking temperature, T_B , superparamagnetic particles display remnant magnetization at zero applied magnetic field, while the diamagnetic curve intersects zero and does not account for the magnetic moment detected. The M_{Rworms} of the treated worms (emu) was divided by the number of worms giving the magnetization per worm (emu/worm). To know the amount of iron per worm, the magnetization per worm was divided by the remanence magnetization value of the SPIONs ($M_{RSPIONs}$) (emu/g Fe) (**Figure 41C**).

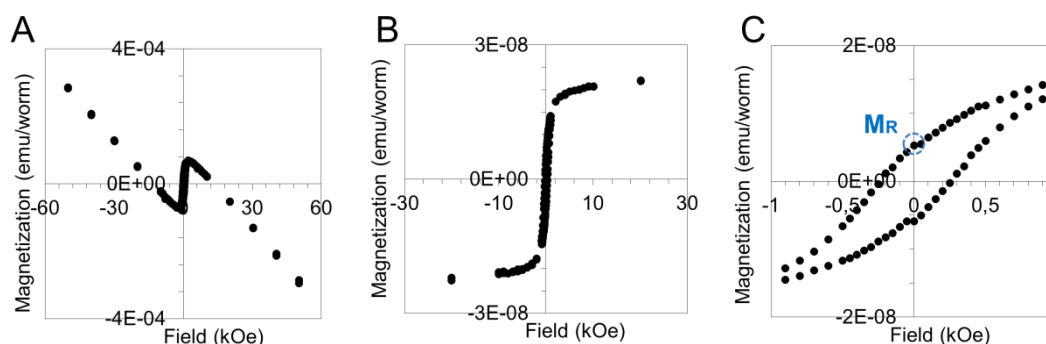


Figure 41. M(H) measurements of SPION-treated *C. elegans*. A) Raw data. B) Hysteresis curve after the diamagnetic component is subtracted. C) Blow-up of magnetization at low fields to determine M_R values of treated worms.

4.4.3 Chemical analysis by ICP-MS

After magnetometry measurements, the sample was diluted with HCl (1%), and the metal content of the resulting solution was determined in duplicate by using inductively coupled mass plasma spectrometry with an Agilent 7500ce spectrometer. The results were expressed as %(w/w). Metal uptake per worm was calculated by considering the weight of the sample, and dividing the result by the total number of worms.

4.4.4 Magnetic Resonance Imaging

Magnetic Resonance Imaging (MRI) of control and SPION-treated *C. elegans* (500 µg/ml C-SPIONs, 24 h) was performed using a Bruker 7T MRI BioSpec 70/30 USR. The samples were prepared in 0.5-ml eppendorf. First, 100 µl of 0.5% agar (60 °C) was poured. Once dry, 10-1500 worms were transferred, and an additional layer of 100 µl of 0.5% agar (60 °C) was poured (**Figure 42**). When solid, MRI T_{2w^*} images were acquired and T_2 values were measured.

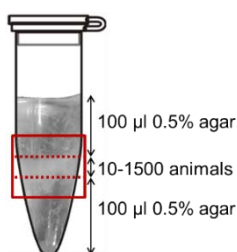


Figure 42. Preparation of MRI samples

4.5 Biodistribution of NPs

The presence of NPs was evaluated in the different anatomical structures of the worm. In particular, we focused on the alimentary system of the worm as the main NP entry portal; the cuticle, as an alternative potential NP entry portal; and the reproductive system as a potential secondary organ. The cuticular interaction was studied by SEM-EDX. The alimentary and reproductive systems were evaluated by optical microscopy (spatial resolution up to 200 nm) and transmission electron microscopy (spatial resolution up to 1 nm).

4.5.1 Optical microscopy

Light microscopy

After exposure, worms were fixed with 4% paraformaldehyde (PFA) for 2 hours in Milli-Q water, washed three times with Milli-Q water and centrifuged. A large number of worms (>100) was transferred using a glass Pasteur pipette onto a clean glass slide, and the excess of water was removed. We added a drop of Fluoromont aqueous mounting media (Sigma Aldrich), placed a coverslip and sealed it off with nail polish (**Figure 43**). The preparation was then observed either by light or by fluorescence microscopy.



Figure 43. Optical microscopy specimen preparation.

Perl's Prussian Blue staining (iron staining)

A Perl's stock solution consisting of 10% (w/v) Potassium ferrocyanide in Milli-Q water was prepared and stored in the dark. Before each use, 2% Perl's solution and 2% HCl were mixed 1:1. Fixed worms were incubated with the mixture for 1 h in the dark, then washed three times with Milli-Q water, and mounted for microscopy visualization.

Biodistribution map

In order to semi-quantify NP biodistribution in treated *C. elegans*, we divided the alimentary system into five parts according to their different biological features and pH (**Figure 44**): Grinder (G), Anterior Gut (AG), Mid-gut or Central Gut (MG), Posterior Gut (PG), and Rectum (R). We counted the number of worms that exhibited NPs in the different sections of the alimentary system (Grinder, Anterior gut, Mid-gut, Posterior Gut, and Rectum) in at least 30 animals per condition, and calculated the frequency of NP visualisation in each of the sections. A colour map was built based on this information.

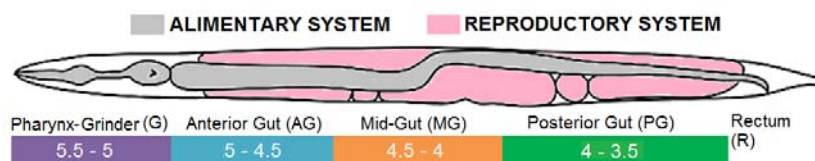


Figure 44. Anatomical areas evaluated in the study of NP biodistribution. The colour legend illustrates the different pH of each region according to Chauhan *et al.*^[152]

Advanced Optical Microscopy

Slides consisting of Au-NPs treated-nematodes and untreated worms (adults and larvae) were prepared as described for Light Microscopy, and visualized using a CytoViva microscope (Hyperspectral Dark-Field Microscopy).

Two-Photon Luminescence Microscopy

We used large cover slips and adhesive wells in-between (Sigma) to delimit a small chamber, as shown in **Figure 45**, where around 50 fixed worms were transferred (~10 μ l), together with 5 μ l of aqueous media.



Figure 45. Specimen preparation for TPLM studies.

A Two-Photon Luminescence Microscope based on a commercial Leica TCS SP5 confocal system, coupled to a MIRA 900F Ti:Sa laser source (Coherent), was used to acquire the two-photon luminescence of Au-NPs inside *C. elegans*. The femtosecond laser beam was tuned in the near infrared ($\lambda=800$ nm) and focused onto the sample by means of a microscope objective (HCX PL APO 10x/0.40 CS). The epi-collected luminescence signal was acquired in the 400–700 nm range with a hybrid detector (HyDs, Leica). Each image was taken in a 1024×1024 pixel format, and a scanning speed of 200 Hz. Z-stacks were collected in 6.5 μm step size and processed using Image J software. Average power in the sample plane was measured to be 12 mW. No endogenous autofluorescence of the worms was detected. Experiments were repeated with six worms per condition.

4.5.2 SEM-EDX analysis

The interaction between the external part of *C. elegans* and NPs was investigated by SEM-EDX. EDX was used to evaluate of the presence of the nanoparticles by elemental analysis. Even though SEM lacks spatial resolution to visualize individual NPs, we applied different protocols to study the *C. elegans* cuticle (**Figure 46**): i) Alive treated worms (around 50 worms in 10 μl) were washed three times after NP exposure, transferred to the SEM stub and let them air-dry overnight; ii) Worms fixed with 4% PFA for 2 h (around 50 worms in 10 μl) were transferred to the SEM stub and let them air-dry overnight; iii) *C. elegans* were fixed in 4% PFA at RT for a few hours, then overnight in the fridge, washed 3x 10 min with PBS, washed 2x 5 min with Milli-Q water, dehydrated with ethanol at room temperature (30% 20-30 min, 50% 20-30 min, 70% overnight at 4 °C, 90% 20-30 min, 95% 20-30 min, then 3x each 100% ethanol 30 min). The ethanol was removed from the eppendorf tube and quickly replaced with pure Hexamethyldisilazane (HMDS). The excess of HMDS was removed after 2-3 min and the samples were allowed to dry. Individual worms were picked up and transferred to the carbon adhesive on the SEM stub.

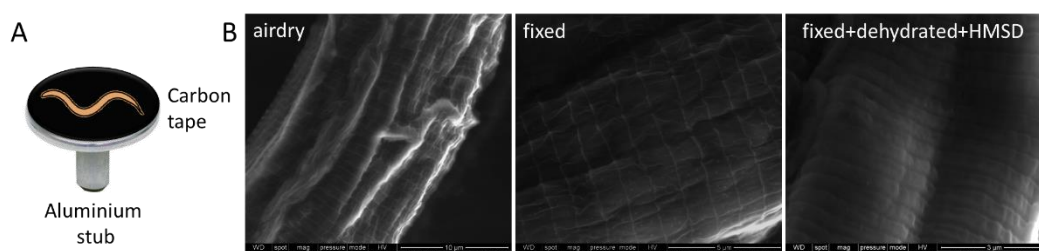


Figure 46. A) SEM stub B) SEM images of samples prepared following different protocols: left panel corresponds to protocol i); central panel corresponds to protocol ii); right panel corresponds to protocol iii).

Procedures i) and ii) resulted informative to evaluate the presence of NP in the cuticle, however the preservation of the *C. elegans* structure was very poor, especially in protocol i). Procedure iii) allowed us to obtain nicer images, however the use of organic

solvents could remove NP attached on the *C. elegans* cuticle, hence it was not suitable for the evaluation of the interaction between NPs and *C. elegans* cuticle. Freeze-drying of alive treated *C. elegans* was also tried, but did not yield successful results regarding structure preservation.

4.5.3 TEM analysis of targeted cross-sections

These experiments were performed at the Electron Microscopy Core Facility at the European Molecular Biology Laboratories (EMBL, Germany) in collaboration with Dr. Schwab. The samples were prepared according to a protocol for targeted ultramicrotomy developed by Dr. Schwab. Briefly, it consisted on high pressure freezing treated worms, freeze-substitute them, flat-embed, laser-etch the targeted regions, and section the sample (**Figure 47**).

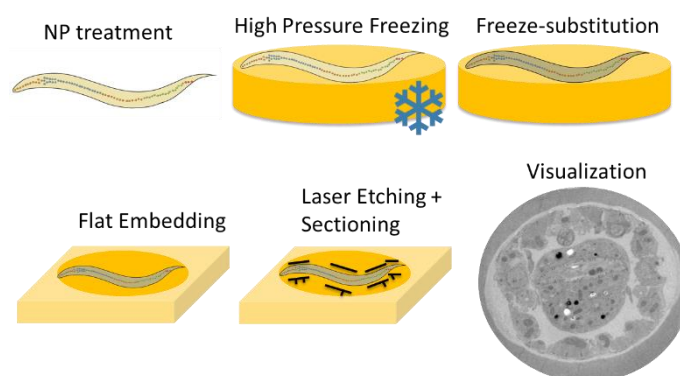


Figure 47. Targeted ultramicrotomy protocol

Prior to the freezing, the carriers were pretreated with 0.5% phosphatidylcholine (diluted in chloroform) to improve the success rate of sample removal from the carriers during the freeze-substitution and infiltration steps. An empty high-pressure freezing (HPF) carrier was placed onto a filter paper with hexadecene, an external cryo-protectant commonly used in HPF to facilitate the separation of the carrier under liquid nitrogen (LN) temperatures (**Figure 48A**). One of the carriers was placed into the holder under the LM for loading. The treated worms were allowed to settle down for 10-30 minutes. The NP supernatant was replaced with 20% BSA in M9 twice. 2 μ L of sample were pipetted and then fitted inside the carrier. The carrier was capped, and quickly frozen. The samples were then transferred to eppendorfs and stored in liquid nitrogen. For the freeze-substitutions (FS), we prefilled tubes containing 0.5 ml of FS mix and cooled them to liquid nitrogen temperature. The FS mix contains 1% osmium tetroxide, 0.1% uranyl acetate in acetone. As described previously,^[255] a small percentage of water (5%) is added to enhance the contrast of membranes. The HPF samples were then transferred to the frozen mix and placed in the chamber of the FS unit that was precooled to -90°C . The temperature was increased at $5^{\circ}\text{C}/\text{h}$ until it reached -30°C . The samples stayed at -30°C for 3 hours and the temperature was then raised $5^{\circ}\text{C}/\text{h}$ until the samples reached 0°C . They were then taken out and rinsed 5 times with dried acetone at room temperature.

Infiltration was performed using glycid ether 100 (EPON 812) 25% (4 h), 50% (2 h) 75% (o/n), and 100% (30 min per triplicate) in acetone. At this step, the samples were removed from the HPF carriers in the cavity of a pyrex plate under a dissecting microscope (**Figure 48B**). The carriers were manipulated with a pair of fine forceps, and the sample was pushed out by applying a slight pressure or rotary motion on its side. Samples were then placed between two sheets of Aclar separated by a spacer also made of Aclar. All these sheets were 200 μm thick. The resins were polymerized by heat (60°C) for 48 h (**Figure 48C**).

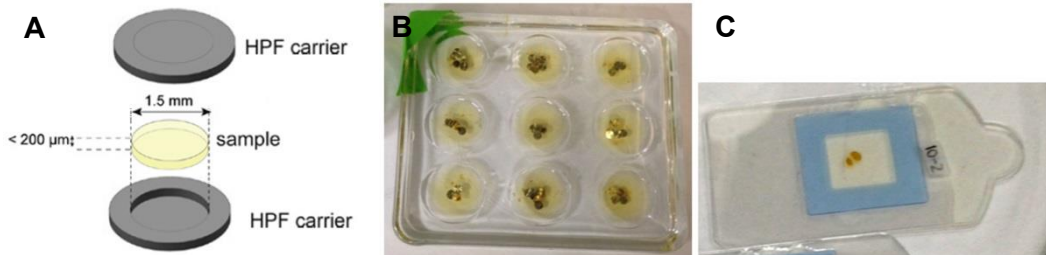


Figure 48. A) HPF carrier scheme. B) Removal of the samples from the HPF carriers. C) Flat embedding of the samples.

The flat blocks were removed from their molds and placed on a glass slide. To perform the targeting of the region of interest, a Cell Cut from Olympus consisting of an inverted widefield microscope equipped with a pulsed 355-nm laser device, was used to etch landmarks on the block surface (**Figure 49A**). It is important at this step to align the marks to be etched with the axis of the worm, which will later be used as a guide to set the alignment of the diamond knife. Serial sections of 60-150 nm thickness were cut from each targeted area using a ultramicrotome Leica EM UC. Slot grids covered by a support film of either pioloform or Formvar were used to collect the thin sections (**Figure 49B**)

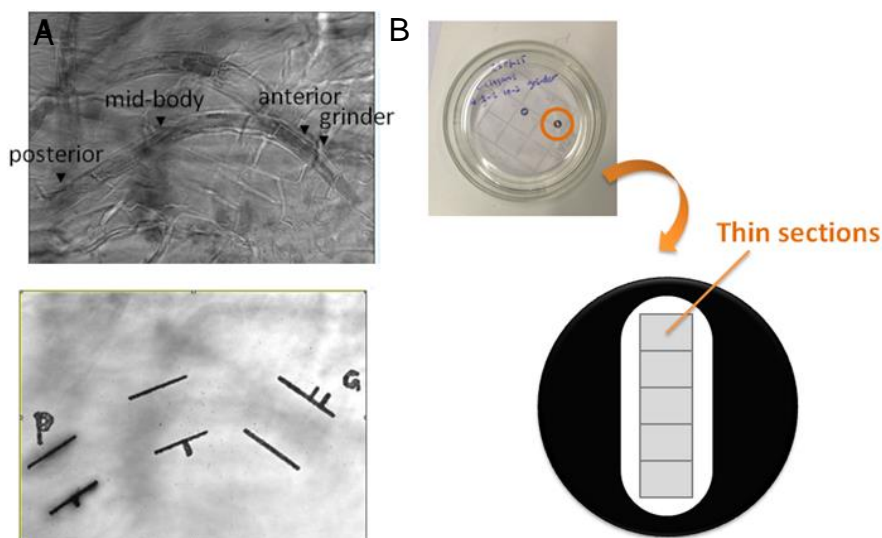


Figure 49. A) ROI targeting by Laser Etching. B) Sectioning and collection of thin section in slot grids.

The as prepared thin sections were visualized using a Philips CM120 Transmission Electron Microscope at the European Molecular Biology Laboratories

(Heidelberg, Germany). Further TEM and SAED analysis were performed at ICMA B using a 120 kV JEOL 1210. Finally, STEM HAADF visualization of these samples, as well as their EELS analysis, were performed at the Catalan Institute of Nanoscience and Nanotechnology (ICN2) using in a FEI Tecnai G2 F20 S-TWIN HR(S)TEM 200 kV. Nanoparticle status (size, confinement) and localization at the organ, cellular and subcellular levels were investigated, with particular interest in understanding the transport mechanisms of NPs within living organisms.

4.6 NP status inside *C. elegans*

4.6.1 Magnetometry

We measured the zero-field-cooled/field-cooled magnetization (ZFC-FC) with a 50 Oe applied field in the range of 4–300 K using the samples described in Section 2.4.3.1 in a Quantum Design MPMS5XL magnetometer. We obtained the blocking temperature of treated worms (T_B) and estimated NP size inside *C. elegans* from the variation of the blocking temperature of the NPs internalised inside the worms, according to the Néel–Arrhenius equation (**Figure 50**).

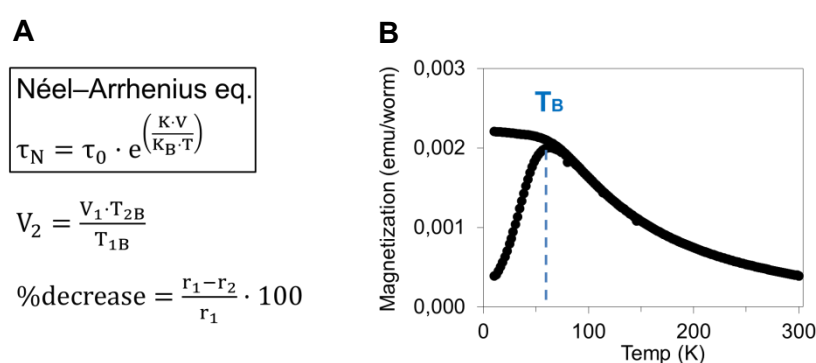


Figure 50. A) Néel-Arrhenius equation used to infer NP size inside treated nematodes. τ_N is the Néel relaxation time; τ_0 is the attempt time; K is the magnetic anisotropy energy density; V is the NP volume; k_B is the Boltzmann constant; T is the temperature; T_B is the blocking temperature; r is the NP radius; 1 refers to as-obtained NPs; and 2 refers to the internalised NPs. B) ZFC-FC measurement of SPION-treated worms at 4–300 K.

4.6.2 Absorbance micro-spectroscopy

Absorbance micro-spectroscopy was used to acquire the UV-Vis spectra of Au-NP treated worms at specific locations within the body: pharynx, anterior gut, mid-gut, posterior gut, rectum and eggs. The samples were prepared as described for TPLM (**Figure 45**) and visualised using an Olympus BX51 microscope. Spatially resolved absorbance spectroscopy was performed by fiber-coupling the signal to a spectrometer (Shamrock SR-303i-B with Andor Solis camera: iDus DV401A-BV). The sample, illuminated in bright field geometry, was imaged at the entrance of the optical fiber to reduce the collection area to a 10- μm spot size. Spectra were background subtracted

against and normalized with a reference spectrum (the glass slide). The spectra of ten worms per condition were acquired using 1000 s accumulation per triplicate. The spectra was fitted to a Lorentz function. The position of the maximum absorption peak and the FWHM (Full width at half maximum) were determined for the NPs and treated-nematodes, and their values were compared. Peak shift and peak broadening were used to quantify NP aggregation and confinement in *C. elegans*.

4.6.3 Recovery of ingested nanoparticles from treated worms

Treated worms were washed three times with Milli-Q water and dissolved with a mixture of sodium hypochlorite and sodium hydroxide following standard procedure (Appendix 1). The same procedure was applied to the NP dispersion (control nanoparticles). The solutions were centrifuged at 14 rpm until an observable pellet was obtained (~90 min). The supernatant was discarded and the NPs were redispersed in Milli-Q water (5-min sonication). Hydrodynamic mean size control and ingested nanoparticles was monitored of by DLS, and particle size distribution was analysed by TEM.

4.6.4 Induction of NP-excretion in treated worms

When *C. elegans* are exposed to NPs in the absence of food, defecation ceases and the NP concentrate in the gut. Upon food resumption, treated worms start to excrete.^[170, 202] To induce NP excretion, treated worms were washed three times with Milli-Q water after exposure to remove excess of NP from the exposure media, and then transferred to an NGM plate seeded with food. Excretion was monitored by light microscopy up to 24 h after feeding.

4.7 Biological mechanisms

4.7.1 Gene expression profiling analysis

These experiments were performed at King's College London in the Toxicogenomics group under the supervision of Dr. Stephen Stürzenbaum. We evaluated gene expression in treated worms using qPCR and microarrays to shed light on the mechanisms of nanotoxicity. While qPCR allows the analysis of specific genes, microarrays allow a genome-wide evaluation of the transcriptome but are much more costly.

4.7.1.1 RNA extraction

The starting material of transcriptomic analysis is RNA extracted from control and treated worms. We performed RNA extraction of a total of 9 samples per triplicate, using two different exposure systems. In the acute liquid exposure system (treatment in 50% M9 at L4 stage for 24 h), the RNA of 6 samples was extracted: control worms, worms treated with 100 µg/ml C-SPIONs, BSA-SPIONs and 10-nm Au-NPs, and worms treated with 500

$\mu\text{g/ml}$ C-SPIONs, BSA-SPIONs. In the prolonged solid exposure system (treatment in NGM plates with food for 48 h from L1 to L4), the RNA of control worms, worms treated with 100 $\mu\text{g/ml}$ Au-NPs, and worms treated with 500 $\mu\text{g/ml}$ C-SPIONs and BSA-SPIONs was extracted. A minimum of 2 000 staged L4 wild-type were exposed to the NPs per each sample. Total RNA was extracted using Tri-reagent (Biomatik) as recommended by the manufacturer, however including an additional initial vortexing step (3 min) with equal quantity of acid-washed glass beads (Sigma). The total concentration of RNA was quantified using a Nanodrop ND1000 spectrometer (Thermo Scientific) and the quality of the RNA was analysed by 0.8% agarose gel electrophoresis to determine RNA integrity and the genomic DNA carry over (**Figure 51**). Nanodrop also can assess the purity of RNA based on the ratio 260/280; a value of ~ 2 indicates high purity RNA with very low protein contamination.

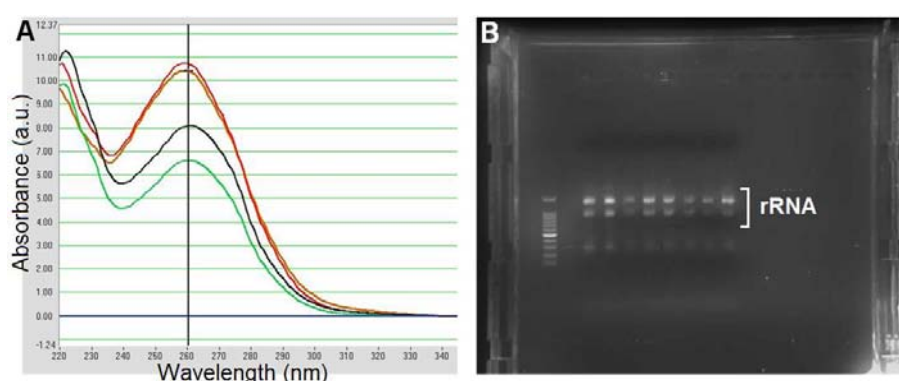


Figure 51. A) RNA quantification and purity assessment performed by Nanodrop measurements. B) RNA quality assessment by gel electrophoresis confirming the integrity of the sample and negligible DNA carry over.

4.7.1.2 Quantitative Polymerase Chain Reaction (qPCR)

PCR relies on the use of specific primers (forward, FOR and reverse, REV) to amplify a gene of interest. In order to be quantitative, an oligonucleotide specific to the target, called probe, is included in the reaction. Probes are labelled with a fluorescent dye and quencher; they have no significant fluorescence by themselves, but fluoresce either when annealed to the template or when the dye is clipped from the oligo during extension (**Figure 52A**). When the DNA is in the log linear phase of amplification, the amount of fluorescence increases above the background. The point at which the fluorescence becomes measurable is called the Threshold cycle (C_T) or crossing point (**Figure 52B**).

We assessed the transcriptional responsiveness of target genes involved in the following pathways: i) oxidative stress response: superoxide dismutases (*sod-2*, *sod-3*); ii) metal detoxication: metallothioneins (*mtl-1*, *mtl-2*), phytochelatin synthase (*pcs-1*), iii) endocytosis and microvilli structure: clathrin heavy chain (*chc-1*), dynamin (*dyn-1*), actin (*act-5*), Erythroid-Like Transcription factor family (*elt-2*), and iv) iron homeostasis: ferritin (*ftn-1*, *ftn-2*), divalent cation transporter (*smf-3*). Their functions are summarised in **Table 22**. cDNA was synthesised with 1000 ng of RNA by means of an oligo-dT primer. The cDNA purity and concentration was checked using Nanodrop. A ratio 260/280 of ~ 1.8

indicates high purity of ssDNA. cDNA was stored at -20 °C until analysed. qPCR was carried out using the ABI Prism 7500 FAST platform (Applied BioSystems, Warrington, UK). All probes were sourced from the Universal ProbeLibrary (Roche Applied Science, UK) and primers designed to be intron-spanning (**Table 23**). The combination of primers and probes are detailed in Appendix 3. For each qPCR well a mastermix was prepared containing 5 µL ROX (Roche), 0.1 µL of probe (10 µM), 0.4 µL of each primer (10 pM) and made up to a final volume of 8.8 µL. Using standard ABI Prism cycling conditions (2 min at 50 °C, followed by 10 min at 95 °C, and 40 cycles of 15 s at 95 °C and 1 min at 60 °C), C_T (threshold cycle) values were determined. Subsequent data analysis was performed using the ABI 7000 system software, and the $\Delta\Delta C_T$ method was used to calculate the fold change in gene expression. Gene expression was normalized to the house-keeping gene *rla-1* (encoding for an acidic ribosomal subunit protein P1) previously shown to be invariant within a metal exposure setting.^[256, 257] The qRT-PCR quantifications were performed on samples derived from three independent experiments (each sample consisting of a pool of 2250 worms), and four technical replicates were analysed for each.

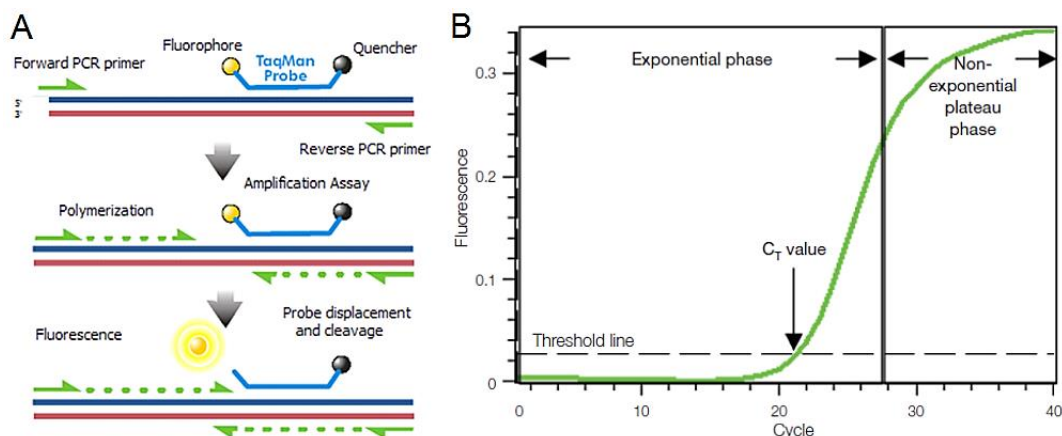


Figure 52. A) Working principle of probe. B) Amplification plot showing the different phases of DNA amplification and C_T calculation.

4.7.1.3 Microarray

Genome-wide transcriptomic analysis was performed using Affimetric *C. elegans* microarrays in triplicate for the control worms and worms treated with 500 µg/ml C-SPIONs and BSA-SPIONs for 24 h in 50% M9. The expression levels of treated and untreated worms were compared and their relative fold change was determined. The genes *vit-1*, *col-179*, *skr-7*, *F59A6.10*, *R12B2.8*, *F32A7.8*, *nlp-37*, *scl-22*, *cul-3*, *hrp-2*, *F55G11.8*, and *cld-9*, which were among the 25 most responsive genes by C-SPION treatment, were quantitatively assessed by qPCR to validate the microarray experiments using the primers and probed indicated in **Table 23**. The combination of primers and probes used are detailed in Appendix 3.

The analysis of the results was performed using Functional Annotation Tools: DAVID was used to identify molecular pathways affected by NP exposure studying the most responsive genes, and PANTHER was used to classify the most responsive genes

according to their biological function and the molecular process in which they were involved.

Table 22. Stress- and intestine-related genes analysed by qPCR. Data adapted from WormBase.

Gene, Protein and Function	Expression
<p>Genes: <i>ftn-1</i>, <i>ftn-2</i> Protein: Ferritin Function: Iron homeostasis</p>	<p><i>ftn-1</i>: The intestine at all stages of development. Its expression increases under iron stress conditions. <i>ftn-2</i>: Diverse tissues, including the pharynx, intestine, and hypodermis. Its expression does not appear to change significantly under iron stress conditions.</p>
<p>Gene: <i>smf-3</i> Protein: Divalent metal ion transporter Function: Manganese uptake transporter</p>	<p>Broadly expressed from late embryogenesis through adulthood. Strongest expression in the medial intestine. It is regulated in response to manganese, and SMF-3 is subject to post-translational downregulation in response to manganese</p>
<p>Genes: <i>mlt-1</i>, <i>mlt-2</i> Protein: Metallothionein Function: Metal detoxification and homeostasis; stress adaptation</p>	<p><i>mlt-1</i>: Constitutively expressed in the terminal bulb of the pharynx. It is induced in larval intestinal cells following exposure to cadmium, heat shock, while its expression is repressed in response to <i>P. aeruginosa</i> infection. Its intestinal expression is dependent upon ELT-2. <i>mlt-2</i>: It is induced in larval and adult intestinal cells following exposure to cadmium or heat shock. It is induced in larval and adult intestinal cells following exposure to cadmium or heat shock. Its intestinal expression is dependent upon ELT-2.</p>
<p>Genes: <i>sod-2</i>, <i>sod-3</i> Protein: Superoxide dismutase Function: Defence against oxidative stress</p>	<p>Induced by oxidative stress</p>
<p>Gene: <i>pcs-1</i> Protein: Phytochelatin synthase Function: Detoxification of heavy metals.</p>	<p>Induced by heavy metal exposure</p>
<p>Gene: <i>chc-1</i> Protein: Clathrin heavy chain Function: Clathrin-mediated endocytosis.</p>	<p>Expressed in cells with high membrane traffic by clathrin-mediated endocytosis, especially the germline, early embryo, coelomocytes and intestine.</p>
<p>Gene: <i>dyn-1</i> Protein: Dynamin Function: Endocytosis, synaptic vesicle recycling, cytokinesis and degradation of apoptotic cells</p>	<p>Expressed in motor neurons, intestinal cells, and pharyngeal muscle.</p>
<p>Gene: <i>act-5</i> Protein: Actin Function: Formation of the terminal web and microvilli on the apical surface of intestinal cells</p>	<p>Expressed only in intestinal cells and in the excretory cell.</p>
<p>Gene: <i>eps-8</i> Protein: Cell signaling adaptor protein Function: Epidermal and intestinal cells morphogenesis</p>	<p>Expressed throughout development and localizes to sites of cell-matrix attachment and to the apical side of polarized cells.</p>
<p>Gene: <i>elt-2</i> Protein: GATA-type transcription factor Function: Differentiation of the intestine Regulation of the intestinal innate immune response.</p>	<p>Expression solely in the intestine throughout the life of the animal. Responsible for initiating and maintaining terminal differentiation of the intestine and for regulating the intestinal innate immune response. It regulates transcription of a number of intestine-specific terminal differentiation genes to ensure maintenance of intestinal differentiation.</p>
<p>Gene: <i>rla-1</i> Protein: Acidic ribosomal subunit protein P1 Function: Ribosome structure.</p>	<p>Invariant expression.</p>

Table 23. Primers and Probes used in the qPCR experiments.

Gene	Primer F	Primer R	UPL Probe	Amplicon Size (kb)
Primers and Probes used in qPCR to study molecular pathways of interest.				
<i>rla-1</i>	ACGTCGAGTTCGAGCCATA	CCGGAAGAGACAGAAGTGATG	#162	91
<i>mtl-1</i>	CATGGCTTGCAAGTGTGACT	CACAGCAGTACTTCTCACAAC	#86	94
<i>mtl-2</i>	AAAAATGGTCTGCAAGTGTGA	GGCAGTTGGGCAGCAGTA	#100	111
<i>pcs-1</i>	AAGCGCCGTGGAGATTCTA	GTTGTAGATTGATTCCACTT	#159	87
<i>sod-2</i>	TTGTTCAACCGATCACAGGA	GTAATCTGGCAGCGAGTGC	#150	60
<i>sod-3</i>	CACTGCTTCAAAGCTTGTTC	ATGGGAGATCTGGGAGAGTG	#152	77
<i>ftn-1</i>	GACGCGCACTTGACAAATTA	CATTGATCGAATGTACCTGCTC	#2	64
<i>ftn-2</i>	CGTGCTTCAGGACATCCA	CGGCTTCAAAGCCTTCA	#106	68
<i>smf-3</i>	GCTATGGAGGGCTTTATCCA	GCCAAAGATCGGGTGATAAG	#60	68
<i>chc-1</i>	CAATGAGAGCCGATAGAACTC	TTGAGTTCACATCGAATTTCTTG	#50	144
<i>dyn-1</i>	GCTCCCATTGGATGGTGT	GCTGCTTGTAACTTGTAGATGTT	#161	116
<i>act-5</i>	CCAATCTATGAAGGATATGCC	CATCATGTAGTCGGTCAAGTC	#158	80
<i>elt-2</i>	AGTAAACGGAGGAATGATGTG	GGTTGTCCCAAAGAAGTGCTA	#25	90
<i>eps-8</i>	ATATCAGAGTCGCCATCC	GACTGTGTGAGGGTGATGGA	#131	86
Primers and Probes used in qPCR to validate the microarray results				
<i>vit-1</i>	TCAATGGAGAGAAGGAAAGCA	GGCGAACTCAGCCTTATCTC	#103	92
<i>col-179</i>	CGAACAACCTTCTGTTACTCGTG	GCAAGTTTGTGGAGTTTGACG	#11	61
<i>skr-7</i>	CGAGAAGGCTGCAAAGGA	GCTGCGTCCTTCTCTGTGAT	#41	63
<i>F59A6.10</i>	GATGCAGACACCTGCATTGA	ATGGACCTGGCCTTTCATC	#95	67
<i>R12B2.8</i>	GACAGAAACATGTTATCCAGACACA	TCACAACATGTTCCAAATGAGA	#130	75
<i>F32A7.8</i>	CCGCTGTATCTCGTTCTCT	GGTCATGTTCCGATTGTGC	#9	71
<i>nlp-37</i>	ATGATGCGTTACGGCAACT	TGTAACAAACGGTATAAGACATGTGG	#11	61
<i>scl-22</i>	TACATACGGCCGTCGAGAA	CGTTATCAATTGGAGTACCGAAC	#87	63
<i>cul-3</i>	CGAAAGAAGTTGAATCACAATAATCT	GATTGGTGACGGCATGAAG	#53	78
<i>hrp-2</i>	CAGTGGGGTGGAAATGCT	GCATGTCGTAGCCATTGTTG	#79	67
<i>F55G11.8</i>	CGAAGGATTTGCTACACTTGG	CCAACGCCATAGTTGGTATTC	#144	75
<i>cld-9</i>	GAAGCAACATCAGGATACAATCA	TTAAATCCTGGTAGTCCAACCTGA	#19	131

4.8 Statistical analysis

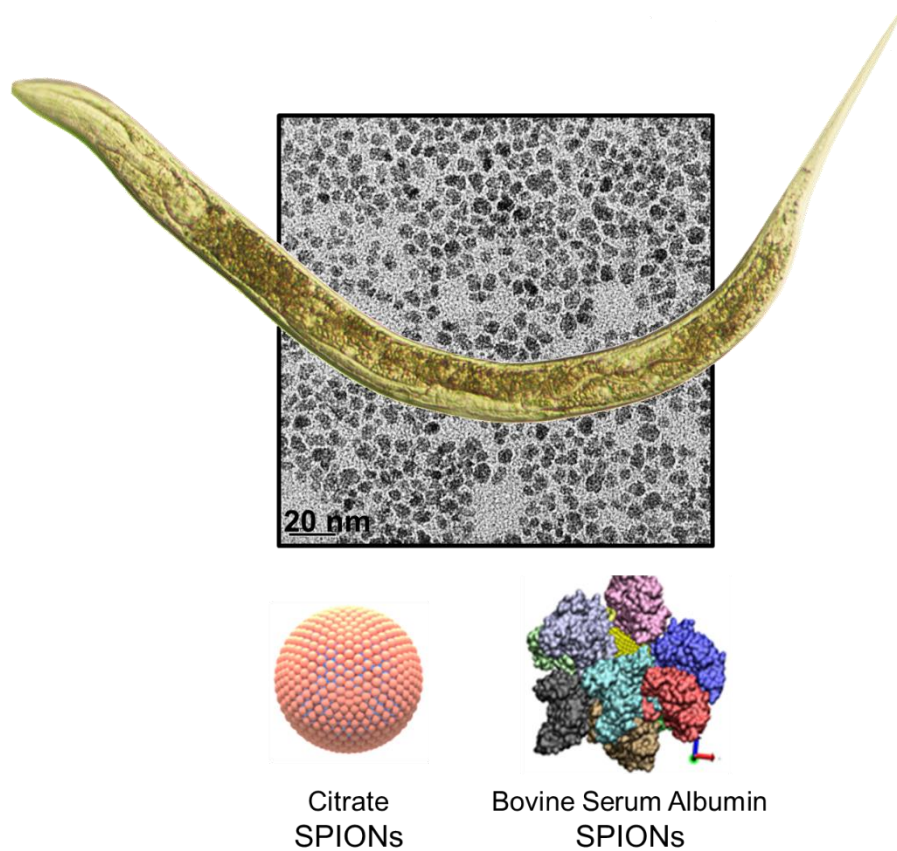
Past 3.03 was used for all statistical analyses. Statistical significance between two groups was assessed by T test. Statistical significance between more than two groups was assessed using ANOVA followed by the Tukey's post-hoc test. Two-way ANOVA was applied to evaluate the significance of two factors and their interaction. Three levels of statistical significance were considered in all cases: * $p < 0.05$; ** $p < 0.01$; *** $p < 0.005$.

4.9 Chapter conclusions

We have successfully adopted material science techniques including magnetometry and absorbance spectroscopy to characterise NP status inside *C. elegans*. We also have employed a range of imaging techniques, from light microscopy, two-photon light microscopy, hyperspectral dark field microscopy to electron microscopy. In particular, we have exploited the potential of scanning electron microscopy to study the interaction of NPs with the external surface of the worm, and transmission electron microscopy to achieve single-particle localization in *C. elegans* cross-sections. We have combination TEM with elemental analysis (EDX, EELS) to confirm NP endocytosis. From the biological perspective, lethal and sub-lethal toxicity endpoints were studied (survival and brood size, respectively) and gene expression profiling was applied to shed some light on the

mechanism of action of NPs in the molecular pathways. The application of such range of techniques has required the setting of a *C. elegans* facility within the synthetic lab and the optimization of protocol specifically adapted to evaluate NP-treated *C. elegans* specimens as described in this Chapter.

CHAPTER 5. Evaluation of SPIONs using the *in vivo* model *C. elegans*. The effect of NP coating.



CHAPTER SUMMARY

Chapter 3 focuses on the study of iron oxide nanoparticles in *C. elegans*. Two different systems are used: citrate-capped and protein-coated iron oxide NPs. The choice of these two nanoparticle systems that bear the same size is based on their different surface properties: citrate, an anionic stabilizer; *versus* a pre-formed protein corona consisting of a monolayer of bovine serum albumin (BSA). The interaction between these NPs and *C. elegans* is thoroughly assessed employing a combination of toxicity assays (survival, brood size and growth), materials science techniques (magnetometry and ICP-MS), imaging (light and electron microscopy) and gene expression analysis (qPCR and microarrays) which have enabled us to study NP effects, uptake, fate and mechanisms of action on the worm.

CHAPTER INDEX

5.1 Overview	101
5.2 Analysis of toxicity endpoints	101
5.3 Uptake of NPs in <i>C. elegans</i>	104
5.3.1 Magnetometry	104
5.3.2 Chemical analysis	106
5.4 Biodistribution of SPIONs	107
5.4.1 Optical microscopy	107
5.4.2 Electron microscopy (EM)	109
5.5 NP status inside <i>C. elegans</i>	114
5.5.1 Magnetic characterisation of treated worms	115
5.5.2 Nanoparticle size inside <i>C. elegans</i>	115
5.5.3 Evaluation of NP excretion	116
5.5.4 Comparison with <i>in vitro</i> experiments	117
5.6 Biological mechanisms	119
5.6.1 Effects of citrate and BSA	119
5.6.2 Effects of iron ions	120
5.6.3 Gene expression analysis	121
5.7 Chapter conclusions	136

5.1 Overview

The interaction between SPIONs and *C. elegans* have been investigated from the organism level down to the subcellular level (**Figure 53**), with particular focus on the study of toxicity, uptake, biodistribution, transport mechanisms, NP status. Genetic studies have also been performed to shed light on the biological pathways triggered by NP exposure.

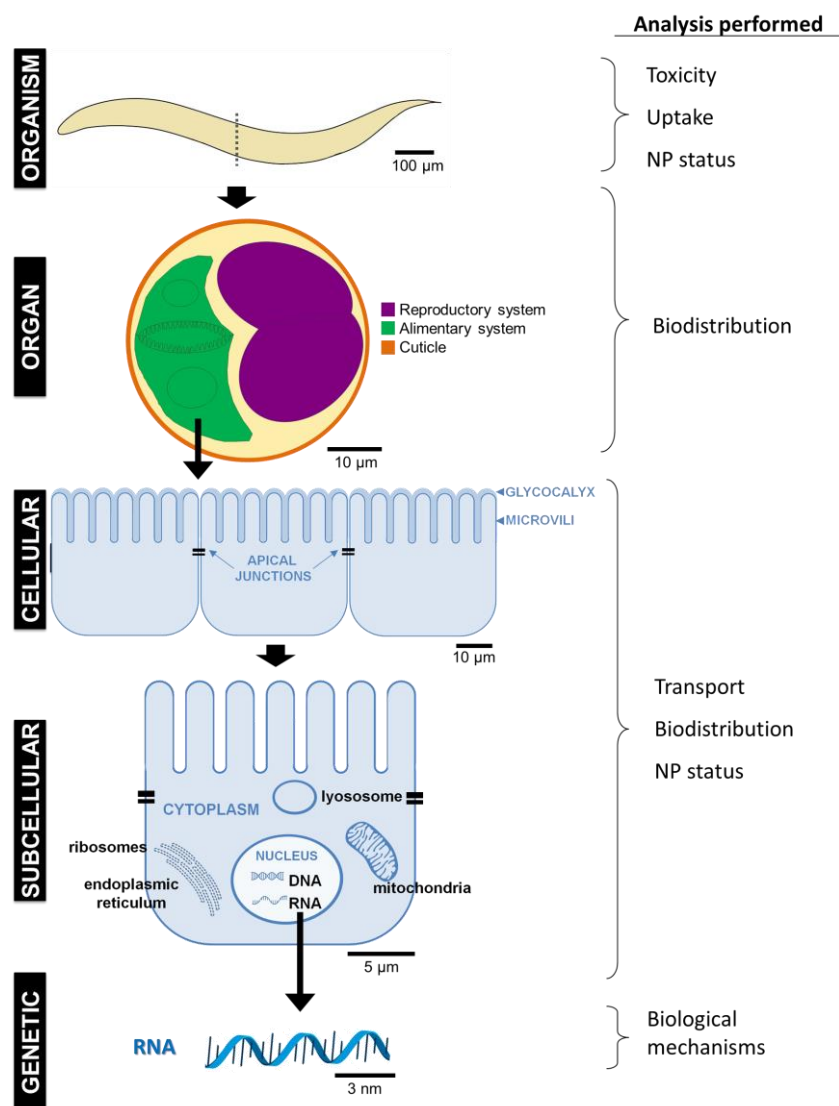


Figure 53. Schematic summary of Chapter 5 contents.

5.2 Analysis of toxicity endpoints

We assessed several toxicity endpoints in *C. elegans*, namely: survival, reproduction and body length, after their treatment with different concentrations of SPIONs up to 500 μg/ml.

Survival

Survival was measured by counting the number of alive worms after SPION exposure.^[220] These studies were performed separately for adult and larval populations, obtained by size-separation from a mixed-stage culture. We found a dose-response relationship for both SPIONs at both developmental stages (**Figure 54**), however the

slope of the linear-fitted curves was steeper for C-SPIONs than BSA-SPIONs, indicating their higher toxicity. The protective effect of the BSA coating in the *C. elegans* survival was enhanced in larvae, which at the same time showed higher sensitivity to C-SPIONs than adults with significant effects starting at doses ≥ 200 $\mu\text{g/ml}$.

Lethal Dose 50% (LD_{50}) values were calculated from the fitted curves. LD_{50} represents the amount of a material, given all at once, which causes the death of 50% of test animals and is frequently used to measure the short-term poisoning potential (acute toxicity) of a material. These values evidenced that C-SPIONs resulted more toxic in larvae than in adults and that the surface coating determined to a great extent the toxicity of the material. The lower LD_{50} of C-SPIONs compared to BSA-SPIONs is especially notable in the larval population, which may be inherently more sensitive to any toxicant including NPs due to their immature developmental state.^[182, 201, 211]

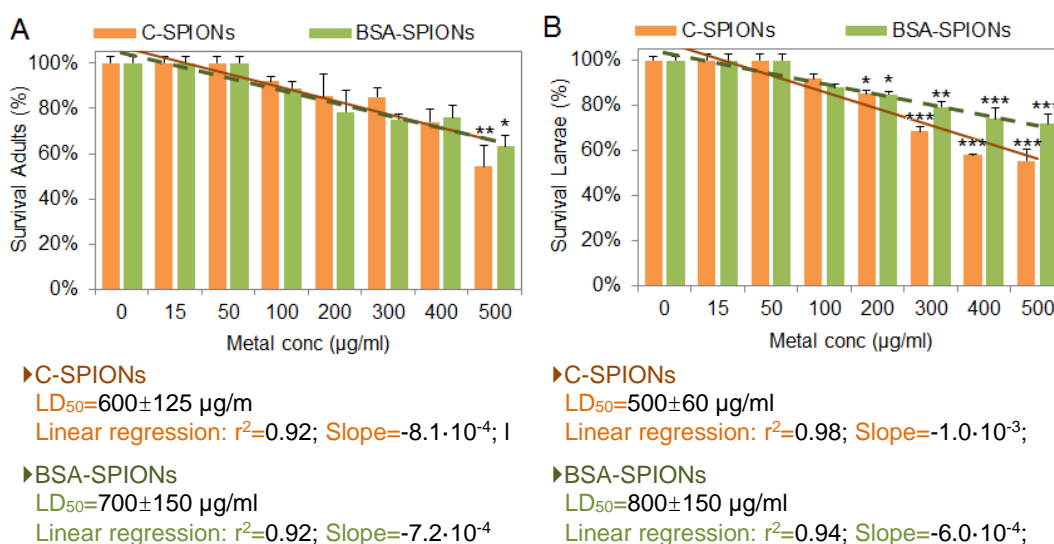


Figure 54. Effect of C-SPIONs (in orange, solid line) and BSA-SPIONs (in green, dotted line) in the survival of *C. elegans* ($n=3$). A) Adults and B) Larvae. Error bars indicate standard error. * $p < 0.05$; ** $p < 0.01$; *** $p < 0.005$.

Reproduction

Reproduction was assessed by counting the number of offspring laid by 24-h treated animals after three days in normal conditions (**Figure 55**).^[160, 220] We found a dose-dependent decrease in brood size, however fertility was only significantly reduced (~20% decrease) at the highest dose for both C- and BSA-SPIONs, without differences attributable to the NP surface coating. Moreover, we did not find a delay in the the egg-laying onset in SPION-treated worms.

According to our results, SPIONs do not pose a severe hazard in the reproduction capabilities of treated *C. elegans* compared to untreated animals. The fact a sub-lethal endpoint such as reproduction is not significantly affected up to high doses emphasize the high biocompatibility of SPIONs *in vivo*. Furthermore, because the number of progeny is scored in the fraction of survivor animals, these results suggest that if SPIONs do not compromise the viability of the *C. elegans*, treated animals can recover upon normal

culture conditions and exhibit a reproductive ability close to that of untreated worms after 72 h.

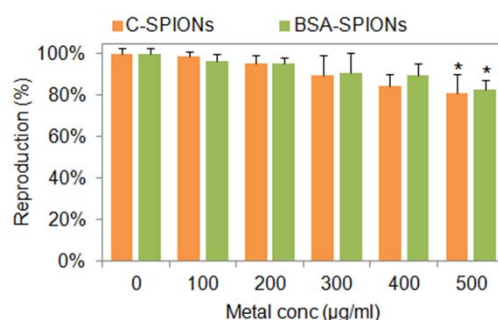


Figure 55. Effect of C-SPIONs (in orange) and BSA-SPIONs (in green) in the reproduction of *C. elegans* (n=6). Error bars indicate standard error. * $p < 0.05$; ** $p < 0.01$; *** $p < 0.005$.

Body length

Growth was assessed measuring the length of exposed nematodes after 3 days in normal condition using ImageJ software. We did not find significant differences in the length of untreated and SPION-treated worms. Furthermore, all nematodes showed normal phenotype: no dumpy, no blister, no BOW (**Figure 56**). These results suggest that the feeding processes and the nutrition status of acutely treated worms were not impaired by SPION treatment, or at least that such effects were recovered to control levels within three days in standard culture conditions.



Figure 56. Light micrographs of control worms (left panel) and treated worms (right panel) showing a normal appearance and no size change associated NP exposure after 72 h in normal conditions. Scale bar indicates 100 µm.

In summary, we exposed *C. elegans* to a range of SPION concentrations (0-500 µg/ml) to determine the effects of treatment on survival, reproduction and growth, and did not observe severe effects up to doses associated with 40~50% lethality. These findings suggest that acute exposure to SPIONs is safe up to high doses and does not pose severe irreversible effects on the biological functions and status of the surviving animals. The assays also showed that larvae were more sensitive to SPION toxicity than adults, in agreement with previous work,^[182, 201] and that BSA has a protective effect on *C. elegans* against SPION toxicity.^[258]

5.3 Uptake of NPs in *C. elegans*

Several techniques have been applied to investigate the iron content of treated cells. Inductively coupled plasma (ICP) spectroscopy techniques such as mass spectrometry (ICP-MS), optical emission spectroscopy (ICP-OES), and atomic emission spectroscopy (ICP-AES) have been widely used. More recently developed techniques are quantitative flow cytometry, superconducting quantum interference device, magnetic resonance imaging, relaxometry, and UV–Vis spectrometry. **Table 24** summarizes the requirements and main features of these techniques. In this thesis, we have employed SQUID magnetometry to quantify SPION uptake in *C. elegans* and validated the results with chemical analysis by ICP-MS.

Table 24. Advantages and drawbacks of the main techniques used to quantify iron uptake in SPION-treated cells.

	MAGNETOMETRY	UV-VIS SPECTROSCOPY	ICP SPECTROSCOPY	FLOW CYTOMETRY
ADVANTAGES	<ul style="list-style-type: none"> • Easy simple preparation • Calibration not required • Rapid 	<ul style="list-style-type: none"> • Widely available • Rapid • Different colorimetric reactions can be exploited 	<ul style="list-style-type: none"> • Rapid • Accurate 	<ul style="list-style-type: none"> • Universal: it detects changes in the cellular complexity • Easy sample preparation • Rapid • Widely available • Can differentiate adsorbed v.s. internalised NPs
DRAWBACKS	<ul style="list-style-type: none"> • Limited to magnetic materials • Two samples must be measured: NPs and labelled cells • Not widely available • Care to avoid contamination 	<ul style="list-style-type: none"> • Calibration required • Digestion required • Limited sensitivity • Significant differences between protocols 	<ul style="list-style-type: none"> • Not widely available • Calibration required • Digestion required • Limited to some elemental species 	<ul style="list-style-type: none"> • Calibration required

5.3.1 Magnetometry

We quantified SPION uptake and characterised their properties inside *C. elegans* using Superconducting Quantum Interference Devices (SQUID) magnetometry. SQUID are the most sensitive magnetic flux detectors, allowing the measurement of magnetic properties of materials exhibiting a very low magnetic moment. Due to the high sensitivity, SQUID can be used to measure biomagnetism, whether it has a physiological origin or arises from magnetic markers. The changes of magnetization over magnetic field, $M(H)$, can be used to determine the loading of magnetic material in a biological system, while the changes of magnetization over temperature, known as Zero Field Cooled Field Cooled (ZFC-FC), reveal different aspects of NP status including their magnetic behaviour, aggregation status and size.

Exposure to 200 $\mu\text{g/ml}$ SPIONs of $\approx 1 \times 10^4$ animals did not allow us to quantify SPION uptake, hence a higher treatment dose (500 $\mu\text{g/ml}$) was used to ensure that the magnetic signal from treated worms was above the quantification limit of SQUID. Therefore, to quantify the uptake of low dose exposures, techniques with higher sensitivity

would be required. We measured the remanence magnetization (M_R) of worms at 5 K after exposure to 500 $\mu\text{g/ml}$ SPIONs for 24 h and compared these values to the remanence magnetization of SPIONs at the same temperature (**Table 25**). We found that the amount of iron uptake per worm depended on the stage of the worms for both types of SPIONs and was 4–6 times higher in adults than in larvae. Differences between the uptake of the two types of SPIONs in adults were not significant, however larvae showed significant higher uptake of BSA-SPIONs than C-SPIONs. In order to compare adult and larval uptakes, we normalized NP uptake relative to their body volume and found that the uptake of adults was significantly different than larvae ($p < 0.05$) (**Table 25**), suggesting an interaction between developmental stage and NP type in SPION uptake which was confirmed applying a Two-Way ANOVA ($p < 0.01$). Interestingly, ZFC-FC measurements showed that at room temperature SPIONs kept their superparamagnetism inside *C. elegans*, which indicates that SPIONs do not suffer strong aggregation inside the animal but remain as individual NPs. If SPIONs aggregated inside the animal, the blocking temperature would increase considerably. ZFC-FC analysis are described into more detail in Section 5.5.1.

Table 25. Iron content of *C. elegans* treated with 500 $\mu\text{g/ml}$ for 24 h ($n=3$), indicated as (mean \pm standard deviation).

		Per worm ($\mu\text{g Fe/worm}$)	Per body volume ($\mu\text{g Fe/nl worm}$)
C-SPIONs	Adults	131 \pm 8	89 \pm 5
	Larvae	23 \pm 2	70 \pm 6
BSA-SPIONs	Adults	136 \pm 17	93 \pm 11
	Larvae	39 \pm 3	118 \pm 8

The significant influence of SPION type in NP uptake ($p < 0.001$ in the Two-Way ANOVA) reinforce that NP coating is a determinant factor for NP uptake in *C. elegans*. We attribute the effect of BSA in NP uptake to a combination of the less negative surface charge of the BSA-SPIONs, which diminishes the electrostatic repulsion between the biological surfaces of *C. elegans* and the nanoparticles, and the protein surface coating of the BSA-SPIONs, which presents the nanoparticles to *C. elegans* as a compact monolayer of biomolecules and prevents the direct contact of the SPION core with the cells of *C. elegans*.

SPION uptake in *C. elegans* can be compared to human doses after normalization of NP uptake per body mass. For instance, Feraheme® is a SPION formulation marketed for intravenous injection to treat anaemia in adults at 7 mg/kg. According to our results, *C. elegans* ingests ~ 110 mg/kg SPIONs, which corresponds to metal doses 16 times higher than human doses. Remarkably, the evaluation of NPs in *C. elegans* allows the study of NP behaviour under harsh conditions (i.e. very high dose), which would not be ethically permitted in superior model organisms. However, these studies are relevant from a toxicological perspective. Thus, the use of simple organisms aside from ethical issues greatly contributes to understand the potential threats derived from undesired scenarios

which otherwise would not be evaluated. It also reveals that doses similar to those used in humans would cause almost no adverse effects on *C. elegans* as shown in the study of toxicity endpoints, highlighting the high biocompatibility of SPIONs *in vivo* at clinical doses.

Considering the relevance of *C. elegans* as a terrestrial model organism from an environmental perspective, these results also indicate that exposure to environmentally relevant concentrations, which are at least 2-3 orders of magnitude below clinical doses, would be safe for this soil invertebrate.

5.3.2 Chemical analysis

We validated the uptake values obtained by magnetometry using chemical analysis by ICP-MS in the same samples taking advantage of the non-destructive nature of magnetometry. We found a good correlation between the results of both techniques (**Table 26**), emphasizing the potential of magnetometry to quantify and characterise SPION-treated *C. elegans*.

Table 26. Comparison of the SQUID and ICP-MS results. The relative error is indicated.

NP type	Stage	Magnetometry (pg/worm)	ICP-MS (pg/worm)	Error (%)
C-SPIONs,	Adult	131	140	5%
	Larva	23	22	3%
BSA-SPIONs	Adult	136	146	5%
	Larva	39	48	15%

Based on the volume of the NP, it is possible to calculate the number of NPs ingested by the animal and also the amount of surface area in contact with biological environments (**Table 27**). These parameters might be relevant for the *in vivo* effects of NPs and even correlate with them.

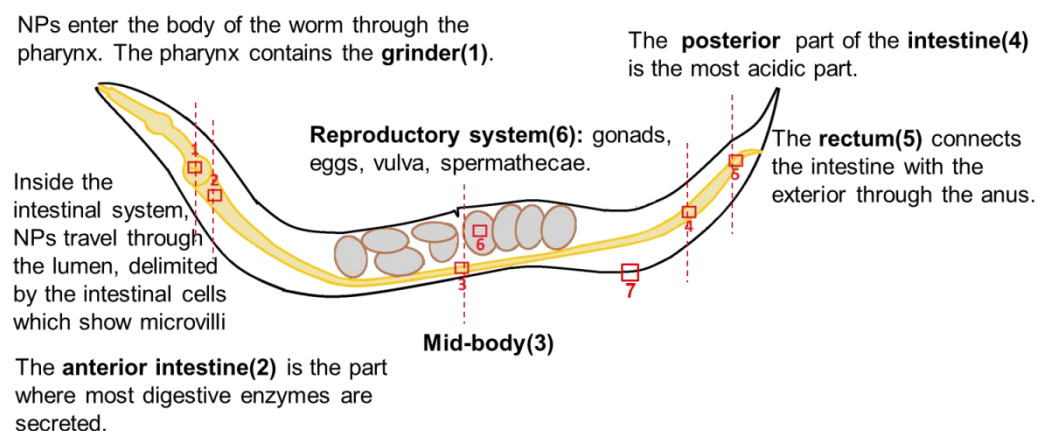
Table 27. NP uptake expressed as number of ingested NPs and surface area in contact with the worm.

NP type	Stage	Millions of NPs	Surface area (10^{10} nm ²)
C-SPIONs	Adults	316	3.57
	Larvae	55	0.62
BSA-SPIONs	Adults	328	3.71
	Larvae	94	1.06

We checked if the concentration in the media could be a limiting factor for *C. elegans* NP uptake, and found that ingested NPs corresponded to a tiny amount (0,00004%) of the NP present in the exposure media. However, it is plausible that higher concentrations in the exposure media might lead to higher NP ingestion by *C. elegans* due to the higher number of particles able to enter the *C. elegans* body at every pharyngeal pumping during feeding.

5.4 Biodistribution of SPIONs

Figure 57 highlights the areas under study in the *C. elegans* anatomy and summarises our hypothesis regarding the effects of *C. elegans* in NP status in each area.



Part of interest	Anatomical/ Physiological features	Hypothetical effects
Pharynx (grinder, 1)	pH 5-5.5 Highly constrained space	<ul style="list-style-type: none"> • Low inter-particle distances • NP aggregation • NP adhesion to the inner cuticle
Microvilli (2,3,4)	High cell surface	<ul style="list-style-type: none"> • Damage of the microvilli • NP translocation
Anterior gut (2)	pH 4-4.5 Presence of enzymes	<ul style="list-style-type: none"> • Formation of a protein corona around the NP core • NP degradation
Mid-body (3) Posterior gut (4)	Acidic pH (pH 3.5-4)	<ul style="list-style-type: none"> • Ion release • Decrease of NP size
Rectum (5)	Highly constrained space	<ul style="list-style-type: none"> • High accumulation of NPs • NP aggregation
Reproductive System (6)	U-shaped gonads, Spermathecae, Vulva	<ul style="list-style-type: none"> • NP translocation • Presence of NPs in the eggs
Cuticle (7)	Negatively charged tough structure	<ul style="list-style-type: none"> • NP adhesion • Damage of the cuticle

Figure 57. Areas of interest to evaluate NP presence and status.

5.4.1 Optical microscopy

Taking advantage of the transparency of *C. elegans*, we could observe SPION treated worms using light microscopy and identify the nanoparticles inside the animal in brown according to the colour of SPIONs in dispersion (**Figure 58**). SPIONs were predominantly located in the alimentary tract, indicating that the major route of particle entrance into the *C. elegans* body is oral ingestion during feeding. To further confirm SPION accumulation, we used the iron staining technique called Perl's Prussian Blue. Perl's Prussian Blue is a qualitative staining technique used to detect and identify iron in histological tissue preparations. Treatment of samples with dilute hydrochloric acid releases ferric ions, which react with potassium ferrocyanide to produce ferric ferrocyanide (known as Prussian Blue) which forms a blue precipitate. After staining of SPION treated

worms, the characteristic brown colour of SPIONs turned into blue inside the *C. elegans* and we confirmed the predominant accumulation of SPIONs in the alimentary system. We could not detect NPs in other anatomical areas such as the reproductive system within 24 h, however given the limited resolution of light microscopy (~200 nm), complementary techniques such as EM are required to achieve single particle tracking at the organ, cellular and subcellular scales.

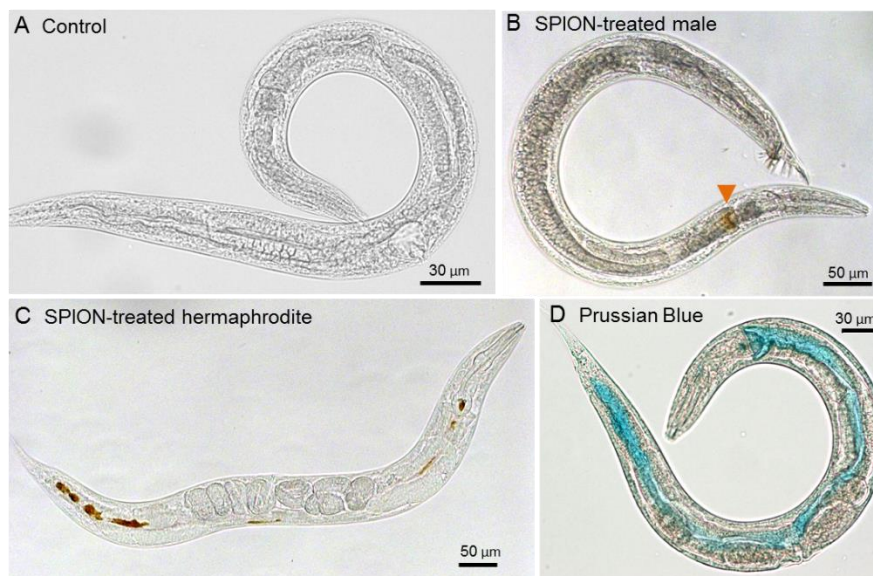


Figure 58. Light microscopy images of SPION-treated *C. elegans*. A) Control worm. B) SPION-treated male (occasional observation, according to the very low predominance of male across hermaphrodite populations). The orange arrowhead indicate SPION presence. C) Direct observation of C-SPIONs, in brown, inside a hermaphrodite *C. elegans*. (B) Prussian blue stained worm where BSA-SPIONs appear blue along the digestive *C. elegans* tract.

Biodistribution map

We analysed the predominance of SPIONs in different regions of the *C. elegans* alimentary system (pharynx, anterior gut, central gut, posterior gut) in Prussian blue stained worms by analysing more than 30 individuals at both adult and larval stages. The colour map shown in **Figure 59** depicts the frequency of SPION presence in the different areas. SPIONs were more frequently visualized in the pharynx of adults than in larvae, which may be due to their wider pharyngeal lumen facilitating NP accumulation and visualization. In adults, BSA-SPIONs appeared distributed from the pharynx to the posterior gut without high specific retention in any of the regions, which suggests a weak interaction between BSA-SPIONs and the intestinal cells, and little effect of the surrounding biological matrix in the NP stability. In larvae, BSA-SPION distribution clearly followed a gradient being more frequently observed in the posterior regions of the intestine than in the more anterior ones, thus suggesting a more facile transport of BSA-SPIONs through the intestine. In contrast, C-SPIONs tended to remain closer to the entry portal. These observations suggest that BSA acts as a biomolecular shield between the *C. elegans* cells and the SPION core and enhances NP stability in biological environments. In particular, we propose that the enhanced monodispersity of BSA-

SPIONs in biological environments^[85] facilitates the progress of the NPs through the *C. elegans* intestine during the muscle contractions of *C. elegans* either resulting in homogenous accumulation throughout the intestine in adults or larger accumulation in the posterior gut of larvae following a gradient.

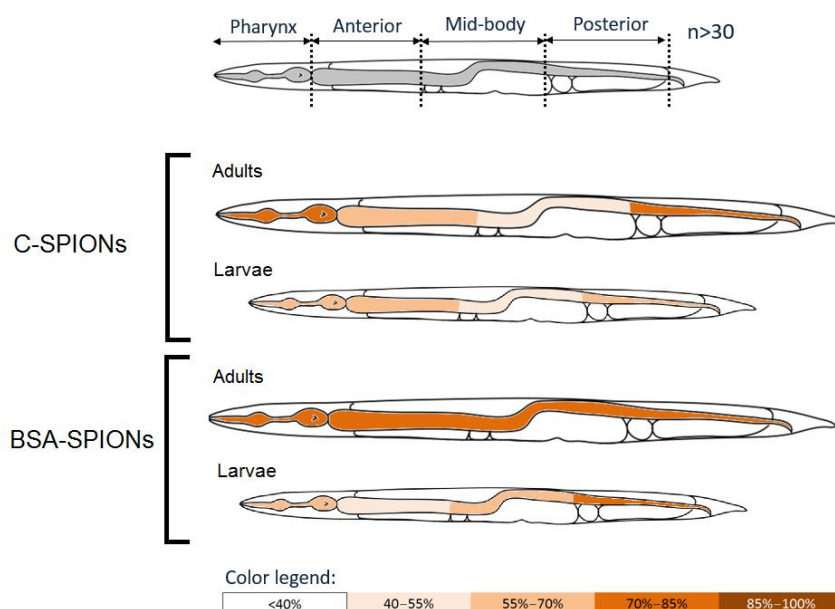


Figure 59. Biodistribution of SPIONs in adult and larval *C. elegans* after 24 h exposure to 500 $\mu\text{g}/\text{ml}$. The upper panel show the division of the alimentary system into four regions: pharynx, anterior gut, central gut and posterior gut. The lower panels show a colour map representing the frequency of observation of each NP type in the specific areas within treated animals. The percentage of worms with visible NPs in a specific region is represented according to the colour legend.

Reported *in vitro* experiments using Caco-2 cells, human epithelial colorectal adenocarcinoma cells, concluded that pretreatment of NPs with BSA reduced the adherence of the NPs to the cells by enhancing their colloidal stability and reducing adherence.^[93, 259] Moreover, it has been shown that albumin facilitates the transport of drugs in biological environments, facilitating the accumulation of the active principle in the therapeutic target compared to the active principle alone.^[260] Therefore, BSA-coated NPs seem to interact less with biological systems than non-coated NPs, resulting in a convenient coating for drug nanocarriers: BSA-coated systems could travel within an organism to reach specific tissues with higher efficiency and with fewer side effects than non-protected particles. The FDA-approved drug Abraxane®, consisting of the antitumoral active principle (paclitaxel) bound to human albumin, illustrates the potential of albumin in drug delivery systems: enhanced accumulation in the tumor is obtained due to the albumin-facilitated transport of paclitaxel through the endothelial cells compared to paclitaxel alone.^[260]

5.4.2 Electron microscopy (EM)

To study NP distribution with nanometric resolution, we used EM and focused specifically in three anatomical parts: the alimentary system as primary organ of entrance,

the reproductive system as the main secondary organ, and the cuticle as the principal barrier epithelia. **Figure 60** illustrates a *C. elegans* cross-section and presents the anatomical structure of the cuticle and the intestine.

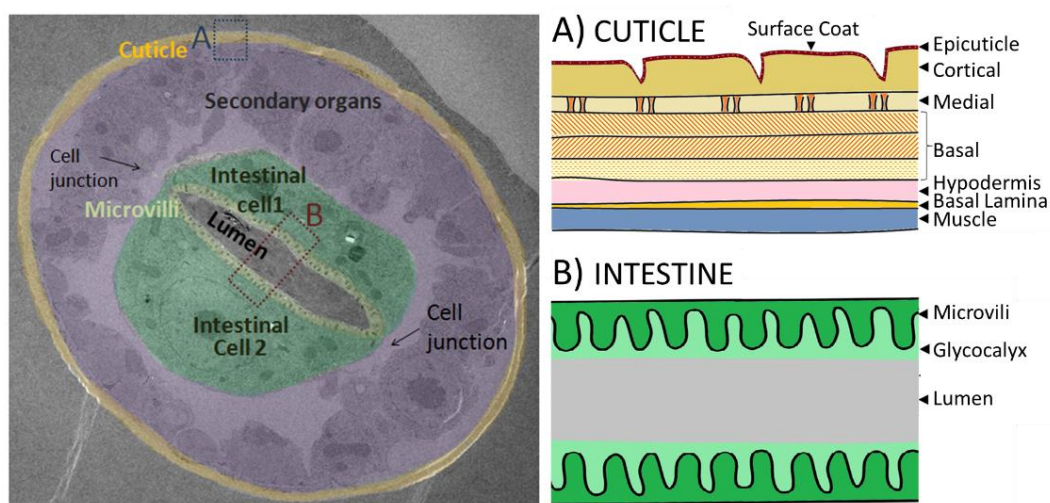


Figure 60. TEM micrograph of a *C. elegans* cross-section with the areas under study highlighted in colour: cuticle (yellow), secondary organs (purple) and intestine (green). The intestine can be subdivided into the intestinal cells (dark green), the microvilli (light green); cell junctions (arrowhead) and lumen (grey). A) Anatomical structure of the cuticle. B) Anatomical structure of the intestine.

Samples preparation and visualization was performed in the Electron Microscopy Core Facility at EMBL in collaboration with Dr. Yannick Schwab based on his expertise in targeted ultramicrotomy of *C. elegans* for TEM.^[261]

5.4.2.1 Interaction between the *C. elegans* cuticle and SPIONs

C. elegans interfaces with SPIONs in the exposure media through its external surface, the cuticle, during the 24 h exposure, hence NPs could get adsorbed onto this epithelial barrier and even enter *C. elegans* body through the dermal route. Because the epidermis of invertebrates is considered a primitive predecessor to the skin of vertebrates, we used *C. elegans* cuticle as a simplified skin model for NP assessment *in vivo* and evaluated its interaction with SPIONs by SEM-EDX. Using SEM, we did not observe the presence of SPION aggregates adhered onto the surface of *C. elegans*, however SEM resolution is not sufficient to observe individual 6-nm NPs. We used EDX to study the presence of iron in the *C. elegans* cuticle and did not detect iron (**Figure 61**), indicating that SPIONs do not interact strongly with this biological barrier. Given that the outermost layer of the *C. elegans* cuticle is a glycoprotein-rich negatively charged surface coat, we believe that electrostatic repulsion between the negatively charged SPIONs and the *C. elegans* surface can explain the lack of affinity between them and exclude the dermal route as a NP entry portal. These results confirm that the alimentary system of *C. elegans* is the unique entrance route of NP into its body. Using zeta potential, we confirmed a negative surface charge (-20.1 mV in Milli-Q water) corresponding to the cuticle of *C. elegans*.

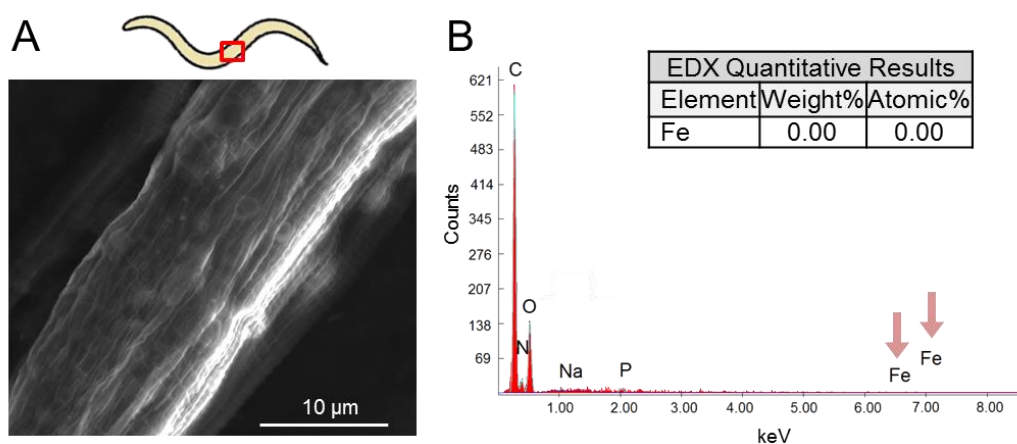


Figure 61. SEM-EDX analysis of treated *C. elegans*. A) SEM image of treated *C. elegans*. SPION aggregates are not observed in the cuticle. B) Representative EDX measurement showing the absence of iron in the cuticle of treated *C. elegans*. Adapted from Gonzalez-Moragas *et al.*^[258]

The *C. elegans* cuticle also covers the anus, the excretory pore, the vulva and the pharynx, which are the four major openings of the *C. elegans* body to the exterior. We specifically studied the interaction between the inner cuticle of the pharynx and SPIONs by TEM (**Figure 62**) and did not observe a strong interaction between them: SPIONs were distributed inside the pharyngeal lumen and not attached onto the cuticle surfaces. SPIONs remained monodisperse in the pharynx and could be visualized individually at high magnification.

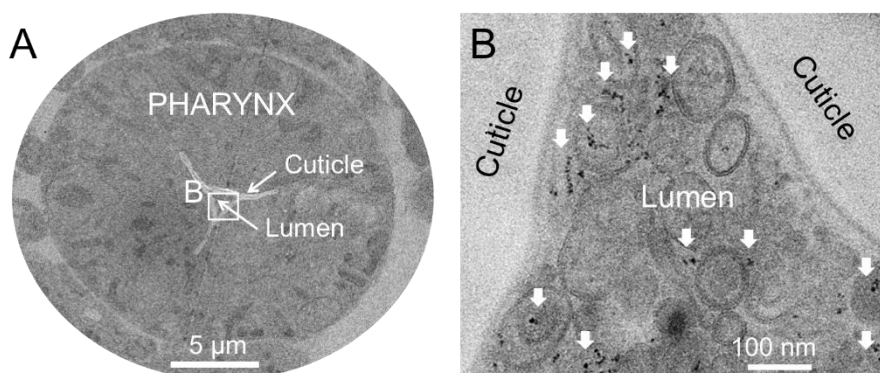


Figure 62. Interaction between SPIONs and the pharyngeal cuticle. A) *C. elegans* pharynx. B) SPION visualization inside the pharyngeal lumen of SPION-treated *C. elegans*. SPIONs are indicated with white arrowheads.

5.4.2.2 Study of *C. elegans* cross-sections with single particle resolution

We prepared cross-sections of three different regions of the *C. elegans* body, considering the alimentary system as the main entry portal of SPIONs into the animal: i) the pharynx, ii) an anterior area of the intestine (within the two first intestinal rings), and iii) a more posterior area of the intestine closer to the anus. Animals were treated with 100 $\mu\text{g}/\text{ml}$ SPIONs for 24 h in liquid media. This dose is more clinically relevant than higher (more toxic) doses where NP exposure could cause the malfunction of several biological systems or compromise the integrity of biological barriers. In the cross-section,

we specifically focused on the evaluation of NP status, NP localization and transport mechanisms.

With this aim, we evaluated the presence and identity of SPIONs in the following biological compartments at both anterior and posterior areas of the intestine: i) intestinal lumen, ii) the surface structures of the intestinal cells (glycocalyx and microvilli), iii) subcellular compartments of the intestinal cells, and iv) apical junctions. We found that most SPIONs were located inside the intestinal lumen and only a very small fraction of individual particles was detected close to the apical surface of the enterocytes, the microvilli, which is protected by the glycocalyx. All along the intestine SPIONs remained separated from the microvillar surface by the glycocalyx (**Figure 63A**), which prevents direct contact between the microvilli and foreign bodies protecting the intestinal cells from potential cytotoxicity.^[119] SPIONs were not observed in the apical junctions that adhere to neighbouring intestinal cells (**Figure 63BC**), hence paracellular transport of individual SPIONs or small aggregates is excluded. However, individual NP cell entrance by transcellular transport cannot be discarded due to the small size of SPIONs.

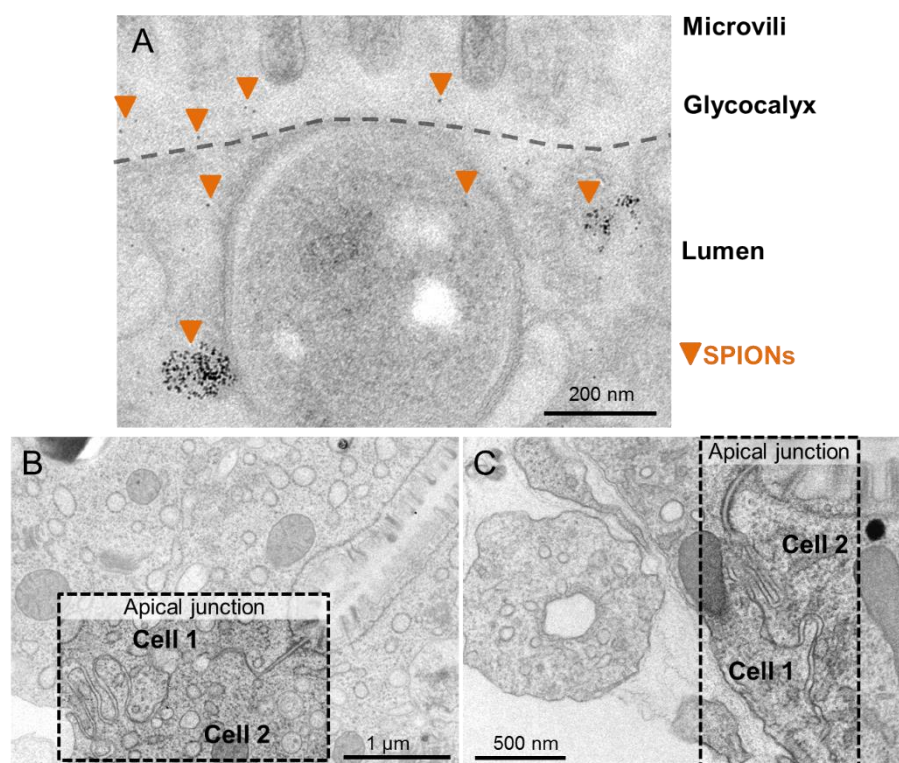


Figure 63. TEM image showing A) SPIONs (indicated with arrowheads) in the intestinal lumen and glycocalyx. The dotted line delimits the glycocalyx. B, C) High magnification of the apical junctions between the two intestinal cells showing the absence of SPIONs in this subcellular compartment.

All the intestinal cells observed had a normal appearance (viable cells, no apoptosis) and the size and morphology of the microvilli was not affected by SPION treatment, suggesting that SPIONs do not affect adversely the structure of the *C. elegans* intestine and are not cytotoxic at 100 µg/ml. In the anterior area of the gut, both C-SPIONs and BSA-SPIONs remained monodisperse and sometimes formed big agglomerates

(**Figure 64**) irrespective of their coating, probably due to the high SPION loading because of the proximity to the entry portal. In posterior regions of the intestine, smaller clumps (<200 nm) of individual SPIONs were observed.

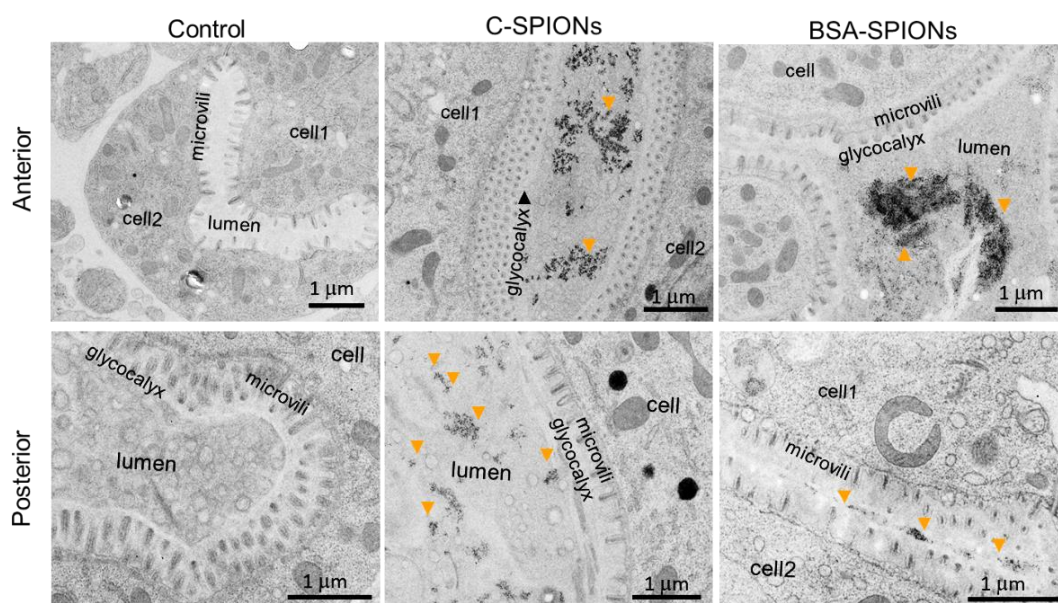


Figure 64. Cross-sections of control, C-SPION treated and BSA-SPION treated *C. elegans* at two body locations (anterior and posterior). SPIONs are indicated with orange arrowheads. Adapted from Yu *et al.*^[93]

Very interestingly, we observed endosomes with NP-like content inside the intestinal cells at both anterior and posterior regions in nematodes treated with both C- and BSA-SPIONs. Moreover, on a few occasions untreated animals also exhibited endosomes with nanoparticles-like features. We further characterised the endosomes of control and treated worms by EDX and EELS (**Figure 65**). Both techniques confirmed the presence of iron in the endosomes of treated worms but could not detect iron in the endosomes of unexposed worms. *C. elegans* cross-sections were also visualized by High Angle Annular Dark Field Scanning Transmission Electron Microscopy (HAADF STEM), a type of microscopy where the intensity of the materials is approximately proportional to the square of the atomic number, Z^2 . In **Figure 65**, the high intensity of the SPIONs both inside the lumen and inside the endosomes can be attributed to Fe ($Z=26$) whereas C ($Z=6$) has lower intensity. Thus, SPIONs are observed as bright spots which are not observed in the control worms. As far as we know, it is the first time that SPION internalisation in endosomes is unambiguously visualized and confirmed in *C. elegans*.

To compare C-SPIONs and BSA-SPIONs endosomes, we evaluated their size and colour intensity (measured as the mean gray intensity) using ImageJ but could not detect significant differences in any of the parameters studied (**Table 28**). These results suggest that the endocytosis pathway is activated to a similar extent independent of the type of SPIONs, which could be an effect arising from SPION confinement in the intestine in the absence of food.

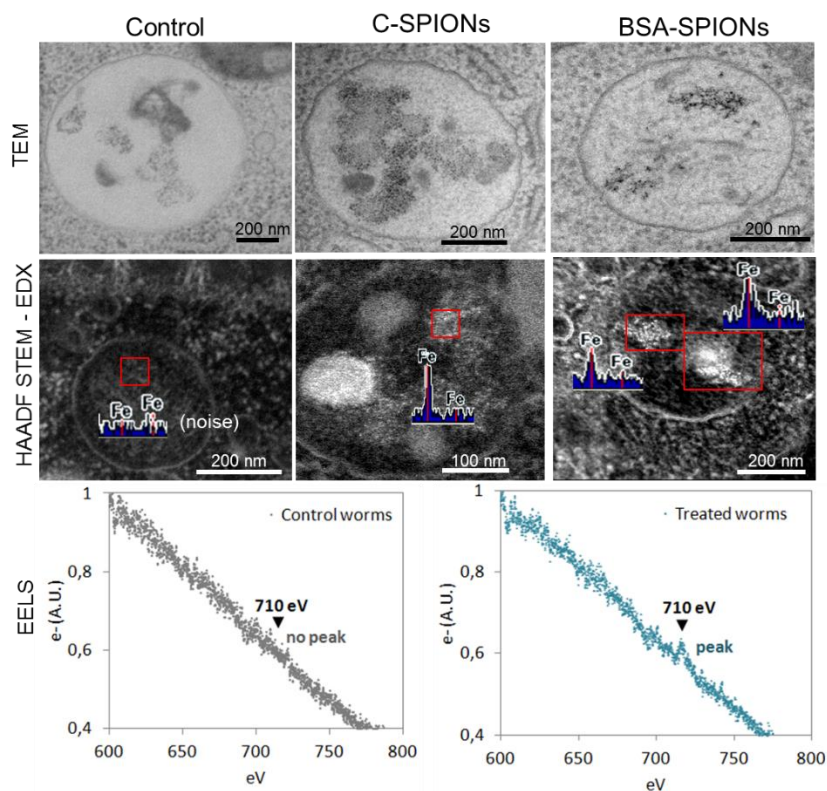


Figure 65. Endosome characterisation by TEM (upper panel), HAADF STEM – EDX (central panel) and EELS (lower panel), confirming the presence of iron in the endosomes of C-SPION and BSA-SPION treated worms, but not in unexposed animals. Adapted from Yu *et al.*^[93]

Table 28. Characterisation of C-SPION and BSA-SPION endosomes.

	C-SPIONs (n=17)		BSA-SPIONs (n=19)	
	Mean	SD	Mean	SD
Endosome size	463 nm	209 nm	615 nm	299 nm
Colour intensity v.s. cell ¹	↑13%	17%	↑13%	22%
Colour intensity v.s. endosome ²	↑21%	8%	↑20%	10%
Ratio NP/Endosome ³	27%	13%	31%	18%

¹ Increase in colour intensity of the NP-like content of the endosome compared to the cytoplasm.

² Increase in colour intensity of the NP-like content of the endosome compared to the endosome background.

³ Ratio between the surface occupied by NPs and the surface of the whole endosome.

5.5 NP status inside *C. elegans*

Nanoparticle digestion have been generally studied *in vitro* using simulated lysosomal conditions (p.e. citrate buffer at pH 4.6)^[93, 254, 262] and to a much lesser extent in cell experiments.^[263, 264] To our knowledge, this topic has never been thoroughly addressed in *C. elegans* and only a few studies have reported evidences of NP digestion.^[164, 166, 178, 190] To investigate whether any modifications occurred to the SPIONs that had been internalised by *C. elegans* after 24 h, and the effects of a surface coating, we combined magnetometry measurements, TEM analysis and the evaluation of excreted NPs.

5.5.1 Magnetic characterisation of treated worms

From the ZFC-FC plots (**Figure 66AB**), we identified the blocking temperatures (T_B) values of SPIONs and SPION-treated animals, which correspond to the maximum value of the ZFC curve. The variation of T_B was used to estimate the size of SPIONs inside *C. elegans* by applying the Néel–Arrhenius equation, as described in the Methods. We estimated a 14% decrease in the diameter of C-SPIONs and a 6% decrease of BSA-SPIONs core after 24 h in *C. elegans*. (**Table 29**). In both cases, the size reduction was higher in adults than larvae. The sharp increase of the FC curve at low temperatures of treated *C. elegans* compared to SPIONs indicates the presence of a paramagnetic component in the system, which may arise from the release of Fe^{3+} ions inside *C. elegans*, especially in the case of C-SPIONs.

Table 29. Blocking temperatures of C- and BSA-SPIONs as synthesised and inside the *C. elegans* adults and larvae.

		TEM size (nm)	T_B (K)	Size decrease*
C-SPIONs	As synthesised	6.2	62	-
	Inside Adults	5.3	39	15%
	Inside Larvae	5.9	43	12%
BSA-SPIONs	As synthesised	5.6	35	-
	Inside Adults	5.2	31	7%
	Inside Larvae	5.3	33	5%

*Calculated applying the Néel–Arrhenius equation.

The decrease in SPION size indicates partial digestion of SPIONs inside *C. elegans*. We believe that this transformation occurs during the residence time of SPIONs inside the *C. elegans* gut, which has mildly acidic pH and digestive enzymes that can contribute to the oxidative dissolution of SPIONs observed.

5.5.2 Nanoparticle size inside *C. elegans*

Analysis of TEM cross-sections of treated *C. elegans* allowed us to accurately study NP size at anterior and posterior locations of the intestine of the worm. In the anterior intestine, nanoparticle size distribution showed a 10% size decrease in the case of C-SPIONs, while BSA-SPIONs remained unchanged (**Figure 66CD**). In posterior regions of the intestine, C-SPIONs were slightly smaller than in the anterior area, corresponding to a 15% size decrease compared to their initial size, while BSA-SPIONs size again did not change. These observations are in good agreement with our magnetometry findings, supporting that C-SPIONs can be partially digested in the intestinal conditions of *C. elegans*.

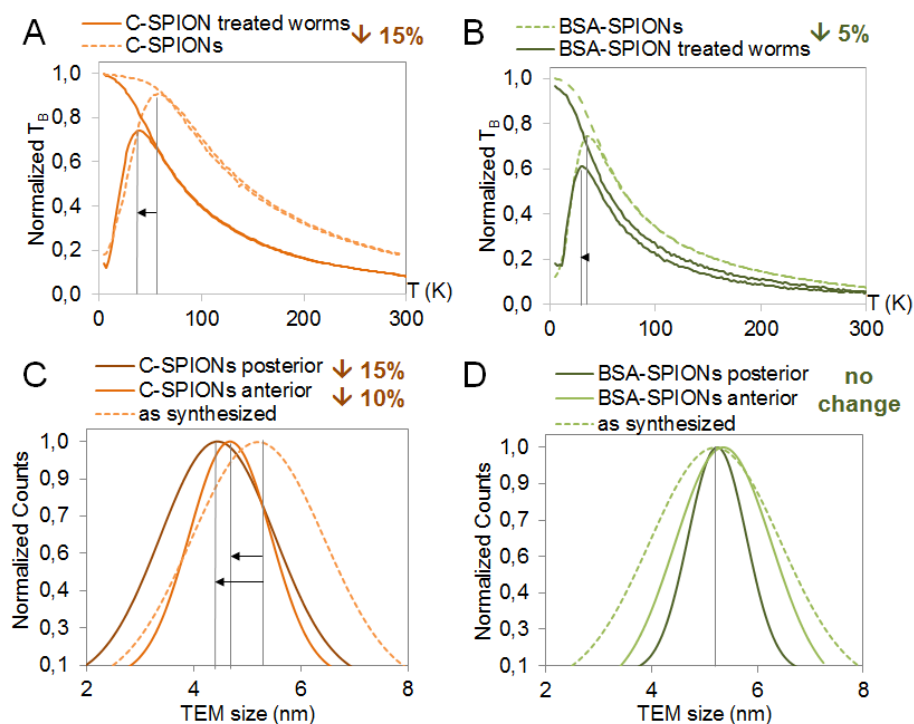


Figure 66. Characterisation of the SPIONs internalised by *C. elegans* using magnetometry and TEM. A,B) ZFC-FC plots of the as synthesized SPIONs (dotted lines) and SPIONs inside *C. elegans* (solid lines) showing T_B values: A) C-SPIONs, B) BSA-SPIONs. C,D) TEM size distribution of the as synthesized SPIONs (dotted lines) and SPIONs inside two areas of the *C. elegans* intestine, anterior and posterior (solid lines): C) C-SPIONs, D) BSA-SPIONs. The calculated size decreases are indicated.

5.5.3 Evaluation of NP excretion

To further confirm the TEM results from the *C. elegans* cross-sections, we managed to recover the NPs internalised by *C. elegans* and directly visualize them by TEM. It is known that when food is not provided, defecation ceases in *C. elegans*,^[119, 150] which greatly contributes to the accumulation of NPs inside *C. elegans* in our exposure system. Recent studies showed that NP-treated *C. elegans* excreted the nanoparticles accumulated in their intestine when fed, while in the absence of food NPs are long retained in the animal (up to 24 h).^[170, 202] In order to recover SPIONs from inside treated nematodes, after NP exposure we transferred the animals onto Nematode Growth Medium (NGM) agar plates with food. Upon food resumption, worms began to excrete NPs through the anus in the form of micrometric brown agglomerates within the first few minutes (**Figure 67**). After 2 h, SPIONs were no longer visible inside *C. elegans*, suggesting complete excretion of the material contained in the lumen. Prussian Blue staining after NP excretion in worms did not evidence SPION content either. In contrast, when treated worms were transferred to NGM plates without food they still exhibit significant SPIONs content in their intestinal lumen after 12 h.

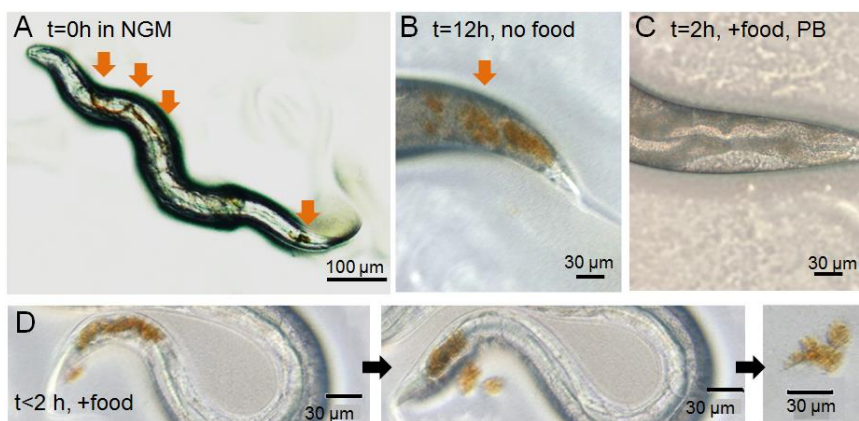


Figure 67. Excretion of SPIONs. A) Treated animal immediately transferred to NGM with food. SPIONs are visible inside the animal in brown. B) Treated animal transferred to NGM without food for 12 h. SPIONs are still visible inside it. C) Treated animal stained with Prussian Blue after 2 h of food resumption. SPIONs are no longer visible inside the worm. D) Excretion of SPIONs, in the form of micrometric brown agglomerates, when treated animals are transferred to NGM with food.

We adapted a standard bleaching procedure to dissolve the worm tissue and recover the ingested SPIONs. We first confirmed that the procedure did not affect the initial size or colloidal stability of SPIONs by TEM and DLS (**Figure 68**), thus we could attribute any change in SPION status to their interaction with *C. elegans* intestine. We dissolved a mixed-stage population of worms treated with C-SPIONs and BSA-SPIONs, and found 12% size reduction in the case of C-SPIONs released by treated worms compared to their initial size, whereas the diameter of the released BSA-SPIONs remained unchanged.

5.5.4 Comparison with *in vitro* experiments

To complete the *in vivo* observations the digestion process of both C- and BSA-SPIONs was followed in two simulated lysosomal environments, from less to more complex (and realistic): i) citrate buffer (CB) at pH 4.6, and ii) CB supplemented with 10% FBS. These experiments were performed by the former PhD student Siming Yu. Particle digestion was monitored by analysing the colour intensity of the solutions at fixed times (**Figure 69**). C-SPIONs incubated with CB were digested quickly during the first 4 days, and completely after 7 days. The addition of FBS lowered the degradation rate suggesting that FBS proteins adsorb weakly onto the C-SPIONs surface and slightly protect SPIONs from degradation. However, a complete dissolution was still found on day 15. In contrast, BSA-SPIONs were only slightly digested during the first 7 days and 50% of the BSA-SPIONs remained after 30 days incubation. Remarkably, in the presence of FBS, only negligible degradation of BSA-SPIONs was observed even at day 30, suggesting that both the hard corona of the preformed BSA monolayer and the additional adsorbed soft FBS protein corona act synergistically to protect SPIONs from being degraded. NP size was monitored by DLS and TEM. The hydrodynamic diameter of C-SPIONs incubated in CB displayed a gradual decrease upon time, from the initial 17 nm to less than 3 nm at day 6,

while no differences were detectable for BSA-SPIONs over time. TEM analysis showed consistency with these findings.

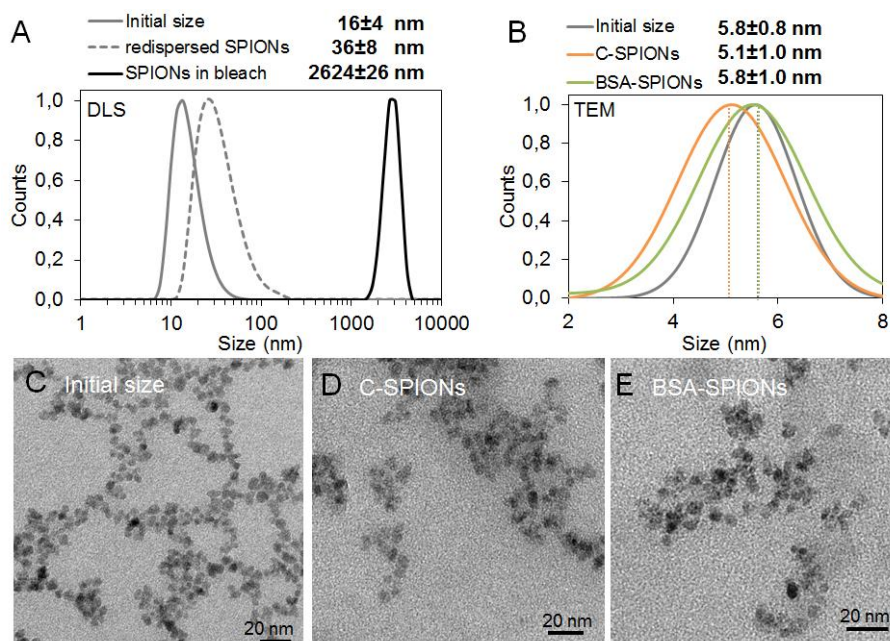


Figure 68. Recovery and characterisation of internalised SPIONs. A) DLS of C-SPIONs before bleaching (solid grey line), after bleaching (black line), and after proper washing and redispersion of SPIONs in Milli-Q water (dotted grey line) confirming that the process of SPION recovery does not affect NP stability. B) Gaussian distribution of TEM size of control C-SPIONs (in grey), C-SPIONs recovered from *C. elegans* (in orange) and BSA-SPIONs recovered from *C. elegans* (in green). C) TEM image of C-SPIONs after the recovery process, showing no size alteration. D) TEM image of C-SPIONs recovered from *C. elegans*. D) TEM image of BSA-SPIONs recovered from *C. elegans*.

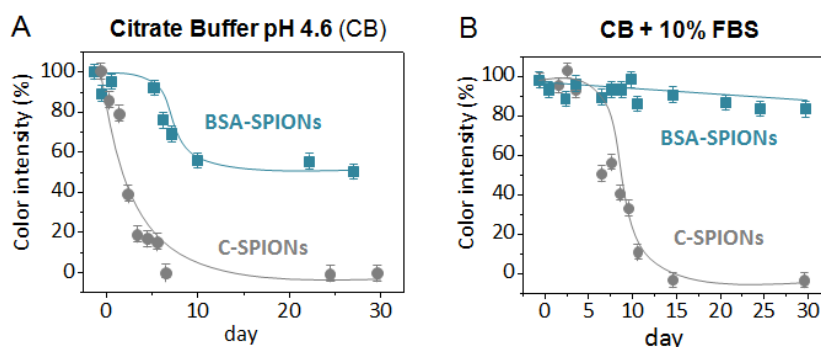


Figure 69. Degradation kinetics of C- and BSA-SPIONs in A) Citrate Buffer pH=4.6 (CB) and B) CB supplemented with 10% Fetal Bovine Serum (FBS). Adapted from Yu *et al.*^[93]

All in all, these results are in good agreement with the biodegradability of the material observed inside the *C. elegans* intestine. We also performed magnetometry measurements of C-SPIONs after 24 h at pH 4 and observed a decrease in the blocking temperature corresponding to a 17% size reduction, close to the value reported in our *in vivo* observations for C-SPIONs. Interestingly, inside the *C. elegans* gut SPIONs could interact with a variety of biomolecules, resulting in the formation of a protein corona inside

the intestinal lumen. This corona could reduce NP digestion and protect SPIONs, however to a lesser extent than the hard BSA pre-formed protein corona in the case of the BSA-SPIONs.^[93] The study of protein corona formation is out of the scope of this thesis, but is of high relevance in the field.

In conclusion, all the evidence presented supports that SPIONs can be partially digested during their residence time in the intestinal microenvironment of *C. elegans*. The acidic conditions of the gut could partially dissolve the C-SPIONs resulting in the release of Fe³⁺ ions. In contrast, the presence of BSA would protect the acid-degradable SPION core and require enzymatic digestion of the protein surface coating before the occurrence of oxidative dissolution of the nanoparticles.

The size decrease observed for 6-nm C-SPIONs involves the release of 39% of the total ferric ions of the NPs, corresponding to the local release of 71 billion ferric ions (0.11 picomoles Fe). In contrast, according to our results, the BSA coating reduces by at least two thirds the amount of ions released, which may reduce the biological effects triggered by the NPs. In the case of BSA-SPIONs, digestion of the protein layer is required before the iron oxide core is accessible to the environmental conditions and contacts with the intestinal cells.^[265] Therefore, albumin might act preventing the direct interaction between SPIONs and the biological environment, thus decreasing the potential biological effects of SPIONs. *In vitro* experiments in simulated digestive fluid showed that although the BSA coating of nanoparticles could be digested by proteinases, it still delayed the contact between the core of the NP and the intestinal microenvironment. It also provided an additional barrier for diffusion and decreased the accessibility or digestibility of NPs by digestive enzymes.^[266] Similarly, our findings indicate that the BSA coating improves the stability of SPIONs in the gastrointestinal tract of *C. elegans* and reduces NP digestion compared to uncoated particles.^[93]

However, at present it is not clear whether BSA is preserved during the endocytic entrance of SPIONs to the intestinal cells of *C. elegans*, which could determine the intracellular behaviour of C-SPIONs and BSA-SPIONs to a great extent (i.e. the different coating could modulate the kinetics of SPION dissolution into ferric ions in the lysosomal compartment, resulting in different amounts of intracellular iron available for a range of molecular pathways).^[267] We plan to address this topic performing immunogold experiments in control and treated worms, as explained in Chapter 7.

5.6 Biological mechanisms

5.6.1 Effects of citrate and BSA

We evaluated the survival of *C. elegans* after 24 h exposure to concentrations of citrate and BSA similar to those found in the nano-dispersions of C-SPIONs (2 mg/ml sodium citrate) and BSA-SPIONs (2.5 mg/ml BSA) for 1 mg/mL concentration of SPIONs and found no lethality associated with the treatments. Therefore, we assume that the

biological effects observed can be attributed to the nanoparticles whereas the chemical composition of the surface coating by itself is non-toxic.

5.6.2 Effects of iron ions

We treated adult and larvae with Fe^{3+} , using $\text{Fe}(\text{NO}_3)_3$, as the iron source in the same concentration range as SPIONs (0-500 $\mu\text{g}/\text{ml}$) to investigate the influence of dissolved iron in the toxicity of SPIONs and evaluated *C. elegans* survival after 24 h (**Figure 70A**). *C. elegans* has specialized mechanisms to tightly regulate iron uptake, storage and efflux, known as iron homeostasis, which are responsible for maintaining cellular iron content within a narrow range to avoid the adverse consequences of iron depletion or excess.^[268] After $\text{Fe}(\text{NO}_3)_3$ treatment, we did not observe significant differences between the survival of control and treated worms, highlighting the tolerance of *C. elegans* to high concentrations of iron ions. Very similar results were obtained when *C. elegans* was exposed to FeCl_3 in the exposure conditions, without significant lethality associated.

We also investigated the biodistribution of iron using Prussian blue staining and observed iron in the alimentary tract from the mouth to the posterior gut but in notably lower amounts than SPION-treated worms (**Figure 70B**). These results suggest that SPION treatment enhances intestinal retention of iron compared to other sources of iron ions, resulting in an increased bioavailability of iron for biological processes and higher biological effects including higher lethality. Iron uptake could be quantified by ICP-MS to confirm the lower uptake after Fe^{3+} treatment compared to SPIONs. We have confirmed by TEM that both C- and BSA-SPIONs effectively entered enterocytes by endocytosis which may be attributed to the particulate nature of SPIONs as endocytosis is not the predominant route of nutrient absorption and might be triggered by Fe^{3+} exposure. Therefore, we hypothesise that the more rapid passage of iron after Fe^{3+} administration can largely explain the different *in vivo* effects of this source of iron ions.

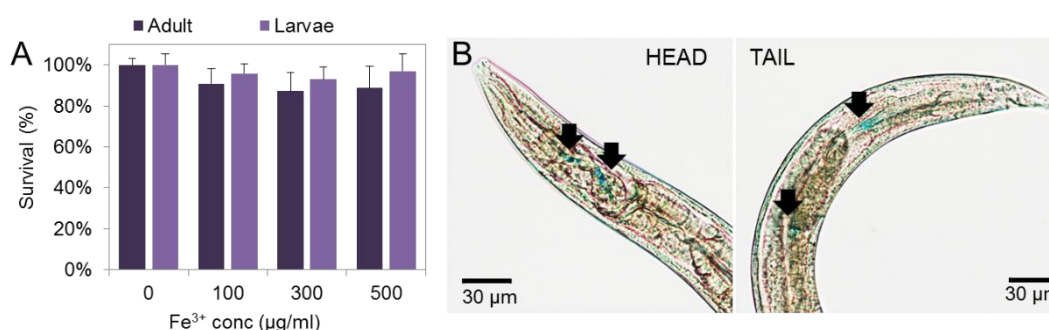


Figure 70. Study of $\text{Fe}(\text{NO}_3)_3$ treated worms. (A) Survival of $\text{Fe}(\text{NO}_3)_3$ treated worms in the concentration range 0–500 $\mu\text{g}/\text{ml}$. (B) Biodistribution of iron in $\text{Fe}(\text{NO}_3)_3$ treated worms at 500 $\mu\text{g}/\text{ml}$ and stained with Prussian blue.

The enhanced bioavailability of iron from SPIONs may be of interest in the investigation of SPIONs as an oral iron supplement for anaemia treatment, thus *C. elegans* could serve as a promising model organism to extend oral administration to products that had been only applied intravenously to date and get preliminary results.

Once in the lysosomal compartment, the digestion of SPIONs could lead to a coating-dependent local release of iron ions into the cytoplasm. If iron levels reached toxic doses exceeding the detoxifying molecular mechanisms of *C. elegans* iron homeostasis, free iron ions could impair several biochemical pathways and result in toxicity. For instance it is known that, in excess, iron can catalyse the formation of free radicals that damage macromolecules through Fenton reactions.^[252] In contrast, the difficult access of Fe³⁺ from Fe(NO₃)₃ into the cell would result in fewer biological effects due to its poorer bioavailability.

The higher biocompatibility of Fe(NO₃)₃ compared to SPIONs suggests that the release of metal ions could contribute to SPION toxicity, but we believe it is not the unique toxicity mechanism that operates given the *C. elegans* iron homeostasis. It is still to be investigated whether the intracellular identity of C-SPIONs and BSA-SPIONs is distinct or if the BSA coating has been fully digested due to the acidic conditions and the presence of enzymes in the intestinal lumen and/or the lysosomes. All in all, we propose that the effects of SPIONs, especially at high doses, are largely mediated by a nano-specific mechanism that involves a variety of factors including the small size of the NPs, their high surface-area-to-volume ratio, and their high reactivity, in which localized iron release could also play a role.

5.6.3 Gene expression analysis

The effects of NP treatment in the gene expression of treated worms was investigated by quantitative Polymerase Chain Reaction (qPCR) to determine the levels of transcript (mRNA) of specific genes that had been previously identified in nano-mechanistic studies in *C. elegans*.^[186, 199] We also performed microarray experiments to study the effects of SPIONs in gene expression at the whole-genome level and identify molecular pathways affected to C-SPION treatment. Finally, the microarray analysis also allowed us to identify the most responsive genes by C-SPION exposure and compare their response in nematodes treated to BSA-SPION and 11-nm Au-NP.

5.6.3.1 Study of selected pathways

We used two different exposure conditions: i) acute exposure (24 h) of young adults to 100 and 500 µg/ml in liquid exposure (final volume: 2 ml); and ii) prolonged (48 h) exposure of L1 worms in NGM agar plates with food. We aimed to study the effects of NP coating and dose, and also to compare acute treatment *versus* prolonged treatment under more physiological conditions. We selected and studied genes involved in different pathways (**Table 30**): i) metal detoxification (*mtl-1*, *mtl-2*, *pcs-1*), ii) oxidative stress (*sod-2*, *sod-3*), iii) iron homeostasis (*ftn-1*, *ftn-2*, *smf-3*), iv) intestinal morphogenesis (*act-5*, *eps-8*, *elt-2*) and v) endocytosis (*chc-1*, *dyn-1*, *eps-8*).

It is important to note that we studied significant changes in gene expression levels, without differentiating between up-regulation and down-regulation in the interpretation of the results. Given the dynamic responses of gene expression, the down-

regulation of a specific gene could be a negative feedback loop resulting from up-regulation of other genes within the same molecular pathway. Hence, we assume that significant differences in gene expression between two exposure conditions identify molecular mechanisms affected by NP exposure.

Table 30. Genes involved in metal detoxification, oxidative stress, iron homeostasis, intestine structure and endocytosis evaluated by qPCR.

Gene	Protein	Function
Metal detoxification		
<i>mtl-1, mtl-2</i>	Metallothioneins	Metal detoxification and homeostasis. Stress adaptation.
<i>pcs-1</i>	Phytochelatin synthase	Detoxification of heavy metals.
Oxidative stress		
<i>sod-2, sod-3</i>	Superoxide dismutase	Defence against oxidative stress.
Iron homeostasis		
<i>ftn-1, ftn-2</i>	Ferritins	Iron storage.
<i>smf-3</i>	Divalent metal ion transporter	Divalent metal ion transporter.
Intestinal structure / Endocytosis		
<i>chc-1</i>	Clathrin heavy chain	Clathrin-mediated endocytosis.
<i>dyn-1</i>	Dynammin	Endocytosis, synaptic vesicle recycling, cytokinesis and degradation of apoptotic cells.
<i>act-5</i>	Actin	Formation of the terminal web and microvilli on the apical surface of intestinal cells.
<i>eps-8</i>	Cell signaling adaptor protein	Epidermal and intestinal cells morphogenesis. Endocytosis.
<i>elt-2</i>	GATA-type transcription factor	Terminal differentiation of the intestine. Regulation of the intestinal innate immune response.

Gene expression after acute exposure: Effects versus unexposed worms

Figure 71 shows the gene expression levels after 24 h exposure to a low dose (100 µg/ml) and a high dose (500 µg/ml) of C- and BSA-SPIONs in 50% M9 buffer. SPION exposure at both doses affected significantly the expression of iron homeostasis genes (*ftn-1, ftn-2, smf-3*) compared to untreated worms in a similar extent irrespective of the coating, suggesting release of iron ions inside *C. elegans*. Metal detoxification (*mtl-1, mtl-2, pcs-1*) and antioxidant pathways (*sod-2, sod-3*) were significantly disrupted, especially in the case of C-SPION exposure. The affectation of *chc-1* and *dyn-1* evidenced the effects of SPIONs in the clathrin-mediated endocytic pathway and identified it as an intracellular uptake of both NP types. We also found significant effects on the expression of *act-5, eps-8* and *elt-2*, which are involved in the microvilli structure and the integrity of the intestinal barrier. However, based on the absence of cytotoxicity and microvilli damage found in the TEM analysis, we believe that these effects are due to their proximity of the luminal NPs to the microvilli.

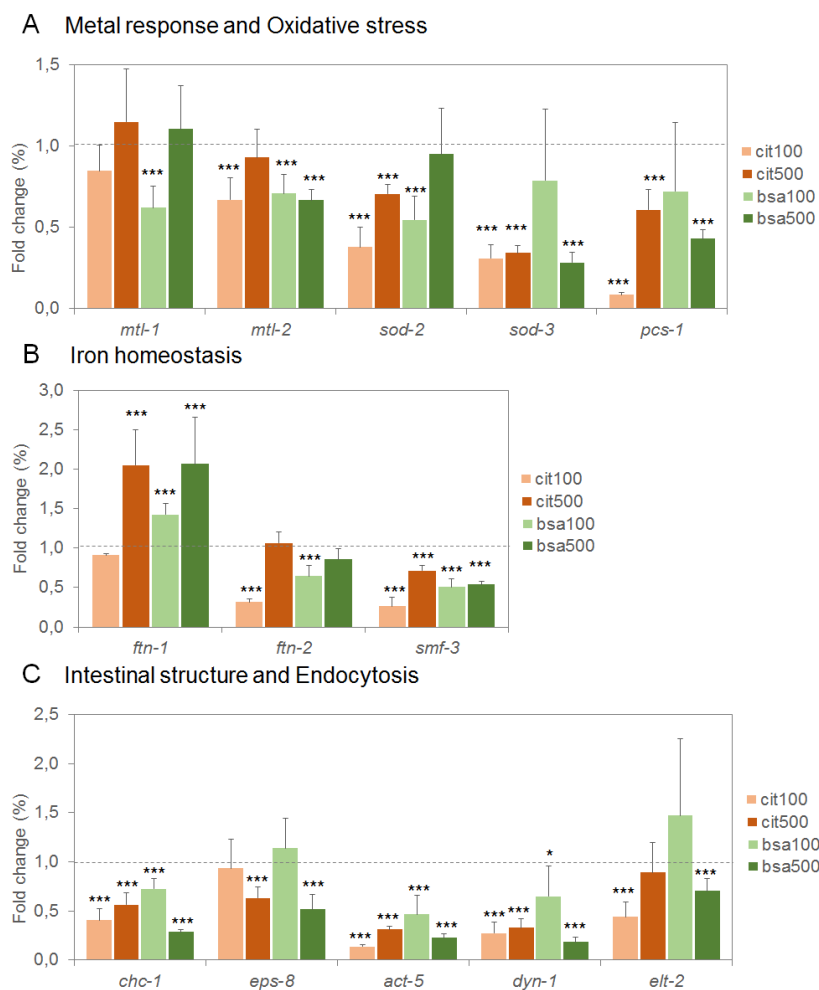


Figure 71. Gene expression levels of acutely treated animals to C- and BSA-SPIONs at 100 and 500 $\mu\text{g/ml}$. * $p < 0.05$; ** $p < 0.01$; *** $p < 0.005$.

Gene expression after prolonged exposure: Effects compared to unexposed worms

Figure 72 shows the gene expression levels after 48 h exposure of L1 larvae to 200 $\mu\text{g/plate}$ C- and BSA-SPIONs in NGM agar with food. This dose of exposure in plates corresponds to the same dose of the 100 $\mu\text{g/ml}$ acutely treated worms given that in liquid the total volume was 2 ml. We did not find a significant increase in the lethality of treated *C. elegans* compared to untreated worms after 48 h treatment in the presence of food, emphasizing the influence of the exposure conditions in the toxicological profile of the material under study.

After prolonged treatment, C-SPIONs affected the different pathways studied to a much greater extent than BSA-SPIONs: they disrupted metal detoxification (*mtl-1*, *pcs-1*) and affected the expression of the antioxidant mechanism (*sod-3*), iron homeostasis genes (*ftn-1*, *smf-3*), endocytosis (*chc-1*, *dyn-1*) and structural intestine genes (*act-5*, *elt-2*), potentially compromising the integrity of this biological barrier. In contrast, neither the intestinal-related genes nor the iron homeostasis genes were affected after BSA-SPION prolonged treatment except for a slight increase in *ftn-1* expression, suggesting little or no endocytosis, absence of effects on the intestinal barrier, and little or no oxidative

dissolution of SPIONs inside the *C. elegans*. Furthermore, the expression of the antioxidant genes *sod-2* and *sod-3* and the metal-responsive gene *pcs-1* was not affected, and only metallothioneins (*mtl-1* and *mtl-2*) were significantly downregulated, suggesting an involvement of the metal detoxification pathways after BSA-SPION exposure. These results highlight that BSA minimizes the undesired *in vivo* effects of C-SPIONs and contributes to increase their biocompatibility. Hence, we propose that BSA-coated nanoparticles can be applied for sustained release of therapeutics with enhanced kinetics control, i.e. BSA-SPIONs can be used as a source of iron slowly releasing iron ions from the SPION core for anaemia treatment; alternatively, drugs can be loaded in the BSA layer or NPs can be functionalized with drugs, among other therapeutic strategies. The effects on gene expression observed after BSA-SPION prolonged treatment, including the absence of endocytosis, suggests a different route of activation of the biological responses compared to C-SPIONs, associated with fewer biological adverse effects. For instance, interaction of NPs with cell surface receptors could trigger biochemical cascades ultimately affecting gene expression in a coating-specific manner.

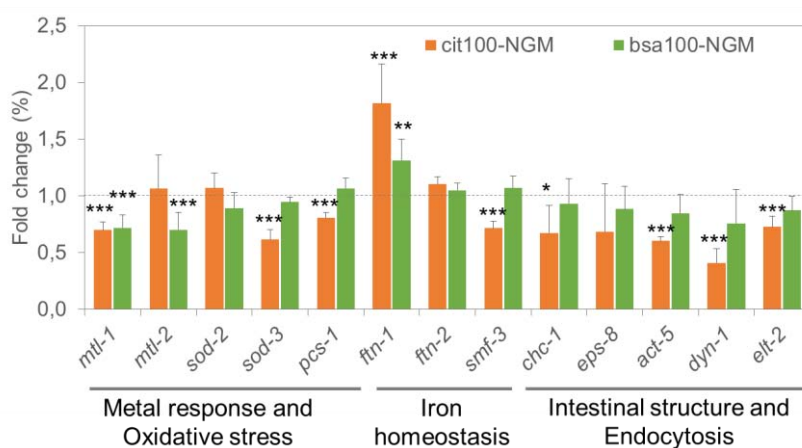


Figure 72. Gene expression levels after prolonged exposure to 200 µg/plate. * p < 0.05 ; ** p < 0.01 ; *** p < 0.005..

Effects of coating

After acute exposure to 100 µg/ml, BSA-SPION treated worms showed gene expression levels much closer to those of unexposed worms than C-SPION treated animals in all the pathways studied (**Figure 73**), indicating that at low dose BSA-SPIONs is lesser biologically active than C-SPIONs. In contrast, after acute exposure to 500 µg/ml the responses of both SPION types were much more similar, thus at high dose the coating-dependence of the biological effects was attenuated. After prolonged exposure, BSA-SPION treated worms still showed gene expression levels closer to those of unexposed worms than C-SPION treated animals. In particular, after 48 h differences were more prominent in the case of *sod-3*, *pcs-1* and *ftn-1*, suggesting that C-SPIONs are more disruptive for the metal detoxifying and antioxidant pathways than BSA-SPIONs, and that their release of iron is more pronounced. These effects can be attributed to the

absence of BSA coating, which prevents the direct contact with the biological surfaces of *C. elegans* and reduces the SPION dissolution rate, as confirmed in vitro.^[266] It is worth noting that the differences in the expression of intestinal-related genes between C- and BSA-SPIONs were not significant except for *act-5*, suggesting that even though C-SPIONs may affect the intestinal barrier and trigger endocytosis to a greater extent than BSA-SPIONs, the changes in gene expression required for those effects are not drastic. Despite the coating-dependent effects observed upon prolonged exposure, the significance of this dependence was lower than in the case of the acutely treated worms.

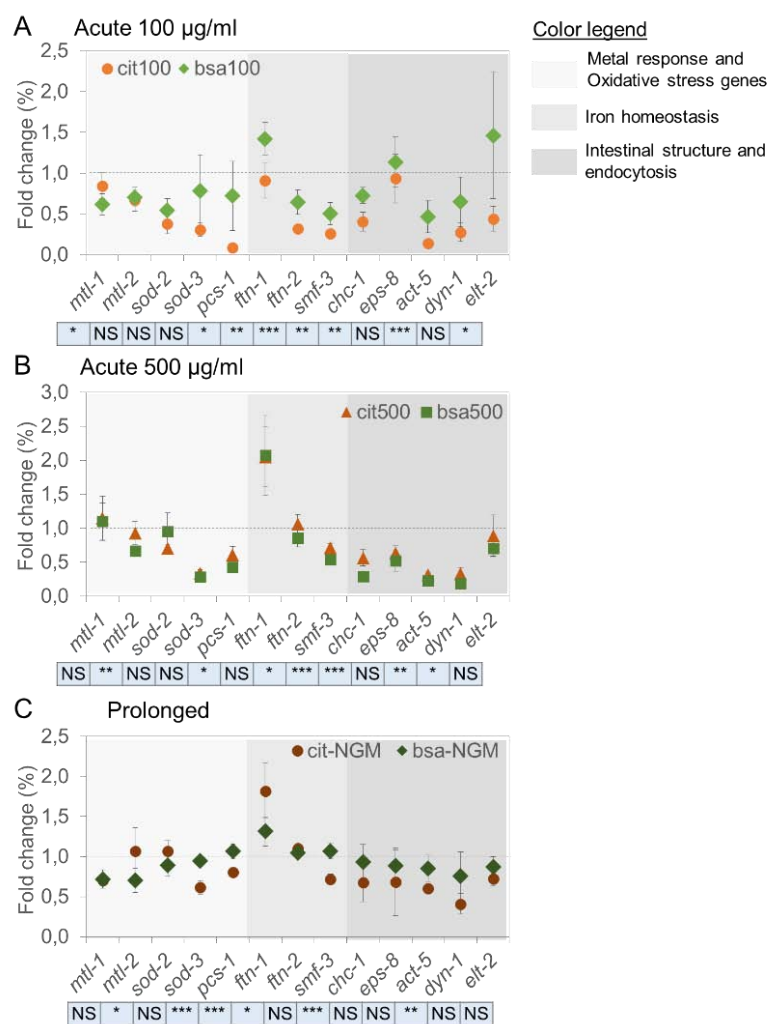


Figure 73. Effects of coating (citrate versus BSA) in gene expression
 A) Acute treatment to 100 µg/ml, B) Acute treatment to 500 µg/ml,
 C) Prolonged treatment to 200 µg. * $p < 0.05$; ** $p < 0.01$; *** $p < 0.005$.

In summary, the significance of the coating-dependent effects of SPIONs follows the order: 100 µg/ml Acute > 500 µg/ml Acute > Prolonged, hence the effect is diluted with increasing dose and/or exposure duration, which may occur in parallel with increased ingestion and accumulation of nanoparticles leading to more general toxic effects.

Effects of dose

Gene expression levels were notably dependent on the dose of exposure for both types of SPIONs (**Figure 74**). C-SPIONs showed greater dose-dependency in the expression of metal-, oxidative stress- and iron-responsive genes than BSA-SPIONs. However, the expression of genes involved in endocytosis and intestinal architecture was very similar at both doses after C-SPION treatment, without significant differences. In contrast, BSA-SPIONs exhibited dose-dependent expression of the intestinal genes: the low dose affected the expression to a lesser extent than the high dose. Overall, according to the statistical analysis, BSA-SPIONs showed a stronger dose-dependency than C-SPIONs suggesting that BSA-SPIONs effects increase with dose, while C-SPIONs induce more pronounced biological effects starting at lower doses.

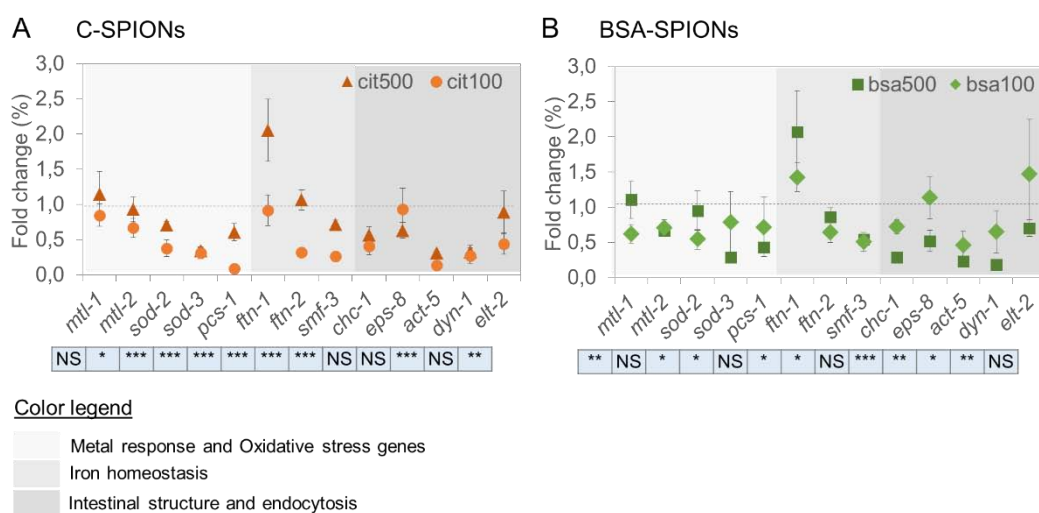


Figure 74. Effects of dose (100 versus 500 µg/ml) in the expression of selected genes after C-SPION and BSA-SPIONs *C. elegans* acute treatment. * p < 0.05 ; ** p < 0.01 ; *** p < 0.005.

Effects of exposure system

The effects of prolonged exposure in gene expression were compared to the effects of acute exposure at both low and high SPION doses (**Figure 75**). The low dose of BSA-SPIONs and the prolonged exposure regime induced very similar responses in gene expression, with levels very close to unexposed worms. In contrast, the high dose of BSA-SPIONs activated the response of the pathways under study to a greater extent compared to the 48 h regime with food, in particular iron homeostasis and endocytosis. The fact that low doses and chronic exposure to BSA-SPIONs result in similar effects suggest very low acute toxicity for the test material up to very high doses.

Prolonged treatment to C-SPIONs exhibited a behaviour that was similar to the high dose acute treatment with significant effects on all the pathways studied, confirming the impact and bioavailability of C-SPIONs in the two exposure systems.

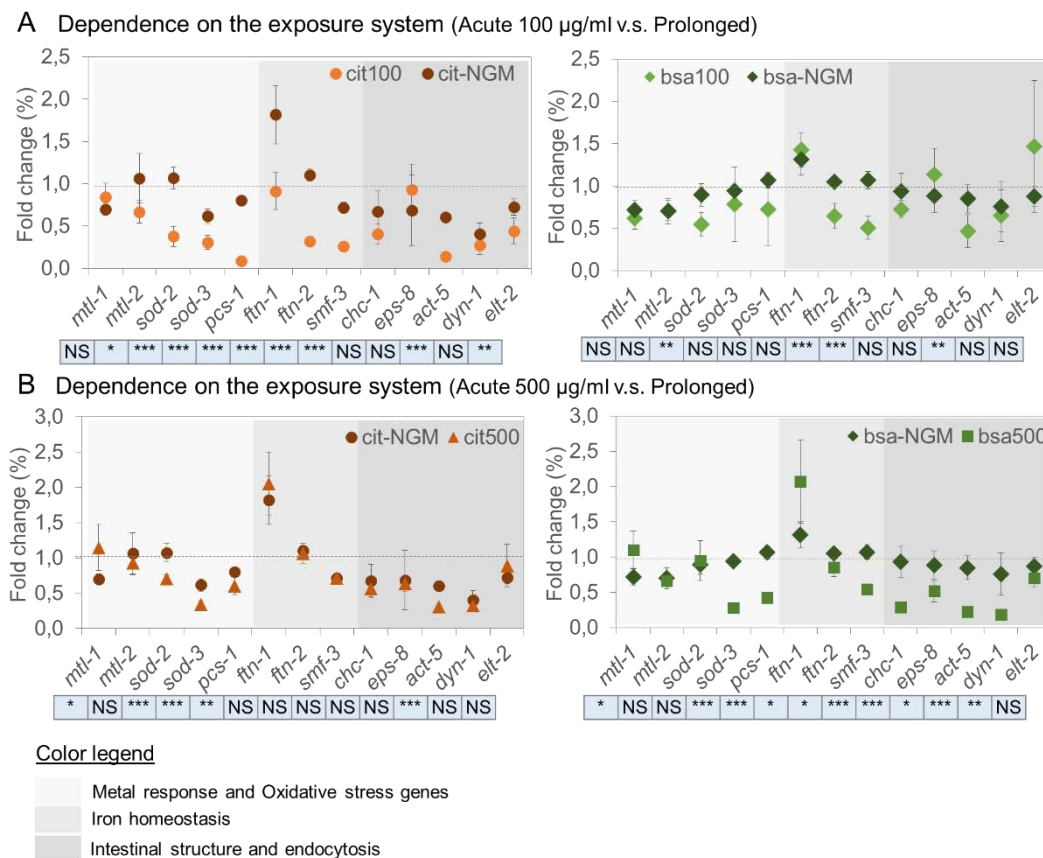


Figure 75. Effects of the exposure system in gene expression. A) Acute (100 µg/ml) versus Prolonged. B) Acute (500 µg/ml) versus Prolonged. * $p < 0.05$; ** $p < 0.01$; *** $p < 0.005$.

Analysing the significant differences of all the genes in a global level, we observed that the effects of BSA-SPIONs after acute treatment at low dose were similar to those triggered by the prolonged exposure. In contrast, the effects of C-SPIONs were similar to the prolonged regime after the high-dose acute treatment, confirming differences in the *in vivo* behaviour of SPIONs depending on their coating. We attribute the different bio-identity of C- and BSA-SPIONs to their distinctive bioavailability and bioactivity⁴, arising from their different surface properties.

When comparing our two exposure systems, it is worth considering that in the acute treatment, the only interaction occurring is between the nanoparticles and *C. elegans*. Moreover, the absence of food induces particular behaviours in *C. elegans* (i.e. defecation ceases, slow locomotion)^[119, 150] that may determine the accumulation and biodistribution of NPs and trigger specific molecular pathways. In contrast, in the prolonged regime the presence of bacteria adds another source of biological surface and active metabolism that can modify and modulate the interactions between the NPs and *C. elegans* (i.e. NPs may be incorporated to the food chain through the bacteria).^[189, 193, 204, 269] Due to the dispersion of SPIONs in the bacterial culture, the status of NPs may also be different by the time they are ingested by *C. elegans*: NPs can aggregate or

⁴ 'Bioactive' means that a compound has a biological effect on a living organism.

precipitate, undergo bacterial digestion, among other transformations. Under those conditions, NP status is not easy to characterise and monitor, hence it hinders the correlation between the effects observed and the NP properties.^[199, 204] Moreover, the presence of food maintains defecation and locomotion,^[119, 142] thus NP ingestion and excretion together with food is more dynamic and the residence time of NPs inside the *C. elegans* intestine may be much shorter (<2 min)^[150] despite longer total exposure time. Therefore, the affectation of biological pathways by NP exposure may also be different in such a dynamic system. For instance, if NP loading is much more transient (less persistent) inside *C. elegans* due to the presence of food, the activation might be determined by the strength of the interaction between NPs and the biological surfaces of *C. elegans*, hence largely dependent on the NP surface properties. These circumstances could explain, for instance, the coating-dependent effects on endocytosis observed after prolonged exposure: due to the biomimeticism of BSA-SPIONs attributed to their protein coating and their weaker interaction with biological surfaces compared to C-SPIONs,^[93] they would not activate clathrin-dependent endocytosis in the prolonged regime. In contrast, the poorer colloidal stability of C-SPIONs in biological environments^[85] could result in a more persistent accumulation in the *C. elegans* intestine and interact more strongly with the surface of the intestinal cells due to their non-protected surface, leading to biological effects –metal and antioxidant responses and endocytosis– similar to those of acute treatment at high dose in the absence of food.

Interaction between factors

The two-way ANOVA shown in **Table 31** summarises the significance of the effects of SPION treatment in gene expression discussed above depending on the NP coating, the exposure dose, the exposure system and the gene under study. As expected, the changes in gene expression significantly depended on the specific gene studied, indicating that the changes of the expression levels of the genes studied did not follow a general trend (i.e. up-regulation or down-regulation). Furthermore, we can conclude that the effects on gene expression depend on the interaction between two factors: i) the particular gene under study, and ii) the coating, dose or exposure regime, except for the acute treatment to 500 µg/ml. It is noteworthy that the exposure system does not have a significant influence on the gene expression levels in C-SPION treated worms at 500 µg/ml, hence their biological response is similar both after acute and prolonged exposure, and much greater than the 48 h BSA-SPION treated worms with food. These findings highlight the protective effects of BSA especially under more physiological conditions.

Table 31. Two-way ANOVA. * p < 0.05 ; ** p < 0.01 ; *** p < 0.005.

Factor 1	Conditions	Effects of Factor 1	Effect of Gene	Interaction
Coating	Acute 100 µg/ml	***	***	***
	Acute 500 µg/ml	**	***	N.S
	Prolonged	*	***	***
Dose	C-SPIONs	*	***	***
	BSA-SPIONs	***	***	***
Exposure system (Acute 100 µg/ml and Prolonged)	C-SPIONs	***	***	***
	BSA-SPIONs	*	***	***
Exposure system (Acute 500 µg/ml and Prolonged)	C-SPIONs	N.S.	***	**
	BSA-SPIONs	***	***	***

5.6.3.2 Genome-wide study by microarray experiments

A genome-wide transcriptomic analysis was performed using Affimetric *C. elegans* microarrays in triplicate for: i) control worms, ii) worms treated with 500 µg/ml C-SPIONs, and iii) worms treated with 500 µg/ml BSA-SPIONs, for 24 h in 50% M9. The expression levels of treated worms were compared to that of untreated worms and their relative fold change was determined.

Validation of the microarrays by qPCR

Microarray experiments analyse the expression of the whole genome of *C. elegans*, ~20 000 genes, at once. Therefore, it is necessary to confirm the gene expression results using qPCR in order to validate the microarray analysis. We evaluated the expression of the genes *vit-1*, *col-179*, *skr-7*, *F59A6.10*, *R12B2.8*, *F32A7.8*, *nlp-37*, *scl-22*, *cul-3*, *hrp-2*, *F55G11.8* and *cld-9* by qPCR (**Table 32**), which were among the 25 most responsive genes upon C-SPION treatment.

Table 32. Validation of the microarray experiments by qPCR. The genes highlighted in green will be studied in Section 5.6.3.3. FC: Fold change; FDR: q-value. † Genes of unknown function. * p < 0.05 ; ** p < 0.01 ; *** p < 0.005.

Gene	C-SPIONs					BSA-SPIONs				
	Microarray		qPCR		Agree	Microarray		qPCR		Agree
	FC	q-value	FC	p-value		FC	q-value	FC	p-value	
<i>vit-1</i>	↑3,19	0,33	↓0,43	***	No	↑4,48	0,09	↓0,26	***	No
<i>col-179</i>	↑3,01	0,35	↑1,53	***	Yes	↑3,59	0,15	↑1,32	***	Yes
<i>skr-7</i>	↑2,72	0,29	↑2,13	***	Yes	↑2,23	0,30	↑2,24	***	Yes
<i>F59A6.10</i> †	↓0,17	0,35	↓0,23	***	Yes	↓0,13	0,13	↓0,16	***	Yes
<i>R12B2.8</i> †	↓0,19	0,33	↓0,25	***	Yes	↓0,33	0,20	↓0,17	***	Yes
<i>F32A7.8</i> †	↓0,21	0,33	↓0,49	***	Yes	↓0,12	0,14	↓0,45	***	Yes
<i>nlp-37</i>	↓0,25	0,16	↓0,52	***	Yes	↓0,28	0,14	↓0,50	***	Yes
<i>vap-2</i>	↑2,64	0,26	1,10	NS	?	↑2,89	0,12	0,90	NS	No
<i>cul-3</i>	↑1,84	0,29	↑1,49	***	Yes	↑1,49	0,48	0,92	NS	?
<i>hrp-2</i>	↑1,84	0,34	↓0,83	***	No	↑1,78	0,21	↓0,51	***	No
<i>F55G11.8</i>	↓0,26	0,35	↓0,26	***	Yes	↓0,24	0,19	↓0,18	***	Yes
<i>cld-9</i>	↓0,28	0,26	↓0,54	***	Yes	↓0,29	0,17	↓0,34	***	Yes
<i>cyp-13A5</i>	↓0,28	0,28	↓0,16	***	Yes	↓0,33	0,10	↓0,10	***	Yes
<i>F49F1.5</i>	↓0,29	0,18	↓0,28	***	Yes	↓0,33	0,13	↓0,26	***	Yes
%Agreement	79%					71%				

We found good correlation between the results of qPCR and microarray (79% for C-SPIONs and 71% for BSA-SPIONs), confirming the validity of the microarray experiments. It should be considered that the lesser agreement with the BSA-SPION microarrays might be due to the fact that the genes selected were the most responsive after C-SPION treatment, therefore higher agreement would be expected in the study of the most responsive genes after BSA-SPION treatment.

Comparison of the 100 most responsive genes

We studied the 100 most significantly affected genes and identified only 4.5% common genes between the two treatments (**Figure 76**), indicating that the biological responses triggered by C- and BSA-SPIONs in *C. elegans* are very different.

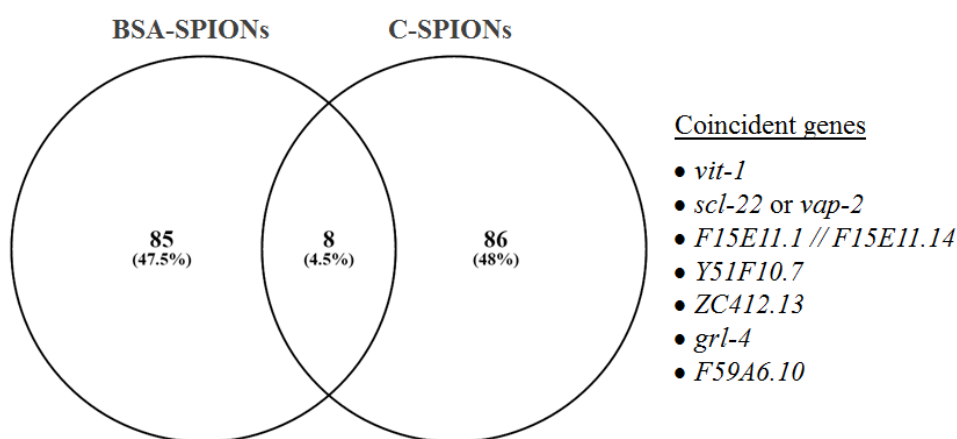


Figure 76. Venn diagram comparing the ~100 most responsive genes of *C. elegans* after SPION treatment, of a total of ~20 000 genes. The genes affected by both treatments are listed.

We evaluated the molecular functions of these genes and the biological processes in which they were involved using PANTHER bioinformatics tool, and confirmed the distinct responses depending on the NP coating (**Figure 77**). The molecular functions most affected by C-SPIONs treatment were binding and catalytic activity, while BSA-SPIONs also affected notably the activity of structural molecules. Other molecular functions affected in both cases, although to a much lesser extent than the functions already mentioned, were the activity of receptors and transporters. In the analysis of the biological processes, we found that both nanoparticles affected the metabolic processes to a similar extent. However, C-SPIONs affected more than BSA-SPIONs the organismal processes and development, while the effects of BSA-SPIONs tended to be restricted to the cellular level, suggesting less bioactivity of the protein-coated particles in *C. elegans*.

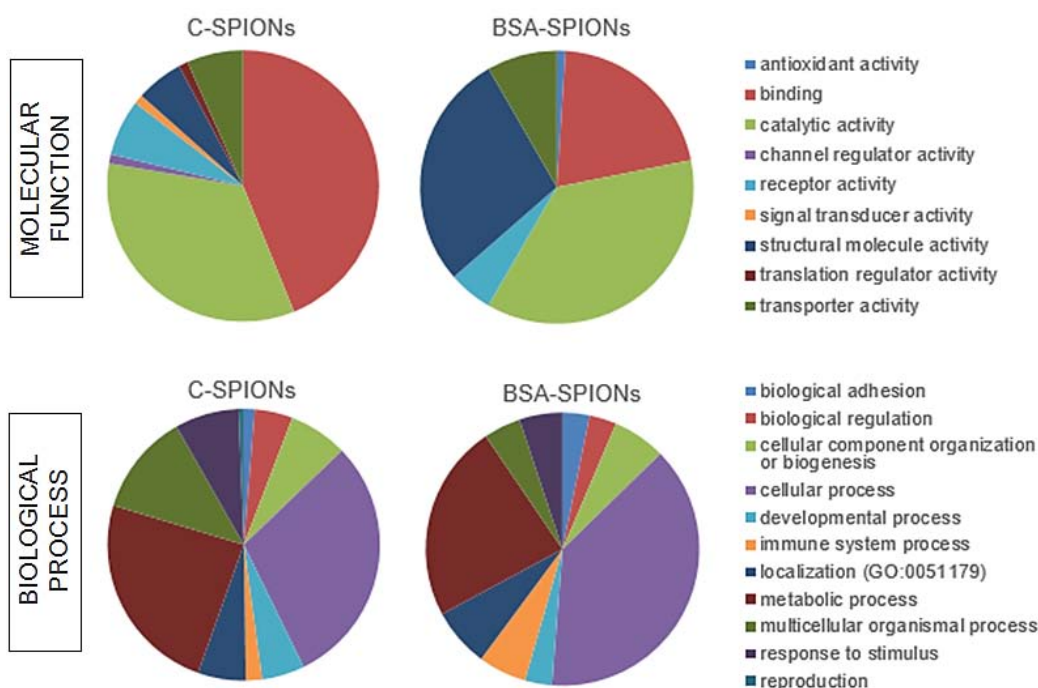


Figure 77. Molecular functions and biological processes of the 100 most responsive transcripts to SPION treatment. PANTHER bioinformation tool was used to identify such functions and processes.

Study of the 500 most affected genes

We studied the 500 most significantly affected genes and identified only 6% common genes between the two treatments (**Figure 78**), suggesting again that the biological responses of treated *C. elegans* are coating-dependent.

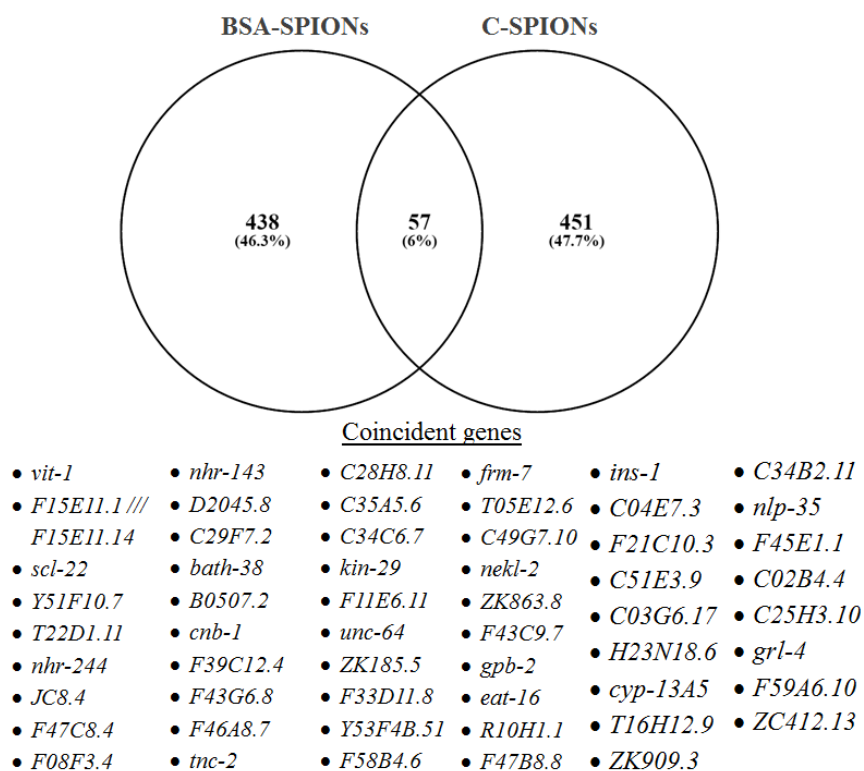


Figure 78. Venn diagram comparing the ~500 most responsive genes to SPIONs. The genes affected by both SPIONs are listed.

Analysis of pathways

Using DAVID 6.8 bioinformatic tool, we studied the different molecular pathways affected by SPION treatment and found that C-SPIONs affected the processing of environmental information (mediated by the TGF-beta, Wnt and MAPK pathways) and genetic information (RNA and protein processing) to a greater extent, while BSA-SPIONs predominantly affected metabolic mechanisms (glycosylation) (**Table 33** and **Figure 79**). Interestingly, the lysosomal pathway was triggered by both NPs in a similar magnitude, which could be attributed to the “dustbin” function of this cellular organelle, part of the NP detoxifying cellular mechanism independent of the coating.

Table 33. Pathways affected by C-SPION and BSA-SPION treatment (n=500 genes). † Information extracted from KEGG database. Fold change calculated using DAVID tool.

Signalling pathway	Function†	Fold change
C-SPIONs 500 µg/ml 24 h		
TGF-beta	Environmental Information Processing; Signal transduction	7.2
Insulin resistance	Metabolism; Longevity.	7.0
Wnt	Environmental Information Processing; Signal transduction	5.2
MAPK	Environmental Information Processing; Signal transduction	4.0
Lysosome	Genetic Information Processing; Translation	3.8
RNA transport	Cellular Processes; Transport and catabolism	3.3
Protein processing in endoplasmic reticulum	Genetic Information Processing; Folding, sorting and degradation	2.9
BSA-SPIONs 500 µg/ml 24 h		
Other glycan degradation	Metabolism; Glycan biosynthesis and metabolism	12.6
N-Glycan biosynthesis	Metabolism; Glycan biosynthesis and metabolism	6.5
Lysosomes	Cellular Processes; Transport and catabolism	4.3

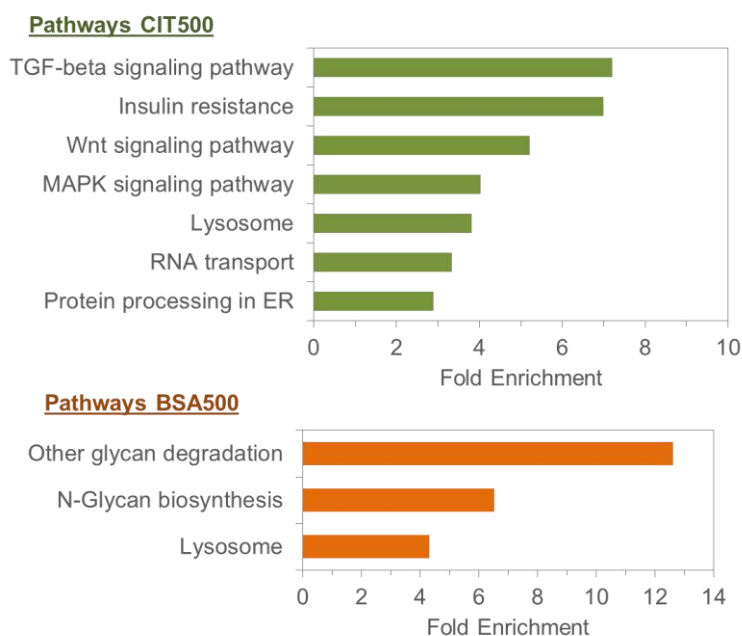


Figure 79. KEGG pathway enrichment analysis. Significantly enriched KEGG pathways ($p < 0.05$) are presented. For each pathway, the bar shows the fold-enrichment of the pathway. n=500 genes. ER: endoplasmic reticulum.

Therefore, this analysis revealed that C-SPION treatment caused higher affectation of signalling pathways than BSA-SPIONs. Among them, endoplasmic reticulum (ER) stress suggested some possible oxidative stress link. In contrast, the effects of BSA-SPIONs in glycosylation routes is indicative of activation of innate defence,^[270-272] which could be sufficient to deal with the less harmful toxicological profile of this material *in vivo* without triggering adverse effects on key biological functions.

Analysis of albumin receptors

It is known that several receptors of mammalian cells are able to bind specifically to albumin and mediate the entrance of albumin-coated nanoparticles by active transport through the formation of caveols.^[273] *C. elegans* have ortholog genes for some of these receptors, for instance the *C. elegans ost-1* gene encode SPARC, *crt-1* encode calreticulin and *ZC116.3* hypothetically encode cubilin. However, by microarray analysis we were not able to find significant differences between the expression of these genes in C- and BSA-SPION treated nematodes. Still, these receptors could potentially influence the translocation of SPION at low doses or after more prolonged exposures.

5.6.3.3 Quantitative study of most responsive transcripts

We analysed the expression levels of eight of the genes used to validate the microarrays, which belong to the 25 most up-regulated and down-regulated genes identified by microarrays in C-SPION treated worms. The genes selected were those that showed good agreement between the microarray and qPCR results, and whose biological function was known (**Table 34**).

Table 34. Description of the genes identified by microarrays as very responsive to C-SPION treatment. Information extracted from Wormbase.

	Protein	Function
Up-regulated genes		
<i>col-179</i>	Collagen	Involved in defence response to Gram-negative bacterium, innate immune response and lipid storage. Structural constituent of cuticle
<i>skr-7</i>	SKp1 Related (ubiquitin ligase complex component)	Required for posterior body morphogenesis, embryonic and larval development, and cell proliferation.
<i>cul-3</i>	Cullin	Ubiquitination and degradation of target proteins. Expressed in many somatic tissues, including the pharynx, intestine, hypodermis, and several different muscle types.
Down-regulated genes		
<i>nlp-37</i>	Neuropeptide-Like Protein	Expressed in the <i>virR</i> , <i>virL</i> , <i>rect_VR</i> , <i>rect_VL</i> , <i>rect_D</i> , certain interneurons, certain sensory neurons, arcade cell, and certain head motor neurons.
<i>F55G11.8</i>	Ortholog of human EPHX1 (epoxide hydrolase 1, microsomal (xenobiotic))	Involved in innate immune response.
<i>F35E12.8</i> (or <i>clt-9</i>)	Cub (CUB) Like Domain containing protein	Involved in innate immune response.
<i>cyp-13A5</i>	Putative Cytochrome P450 CYP13A5	Membrane-associated, heme-containing NADPH-dependent monooxygenases that catalyze the oxidative metabolism of a variety of exogenous compounds and endogenous substrates.
<i>F49F1.5</i>	Hypothetical protein	Engulfment of apoptotic cells.

They were involved in: i) innate immune response (*col-179*, *F44G11.8*, *F35E12.8*) and oxidative metabolism (*cyp-13A5*), which may be activated as response to xenobiotics; ii) apoptosis (*F49F1.5*), iii) ubiquitination (*cul-3*), involved in protein degradation; iv) genes involved in the neurosignalling (*nlp-37*) and body morphogenesis (*skr-7*). We aimed to study the effects of coating and dose in the expression of these genes in acutely treated worms. Gene expression levels and the comparison of coating- and dose-dependent effects are shown in **Figure 80**. The effect of exposure system was not explored.

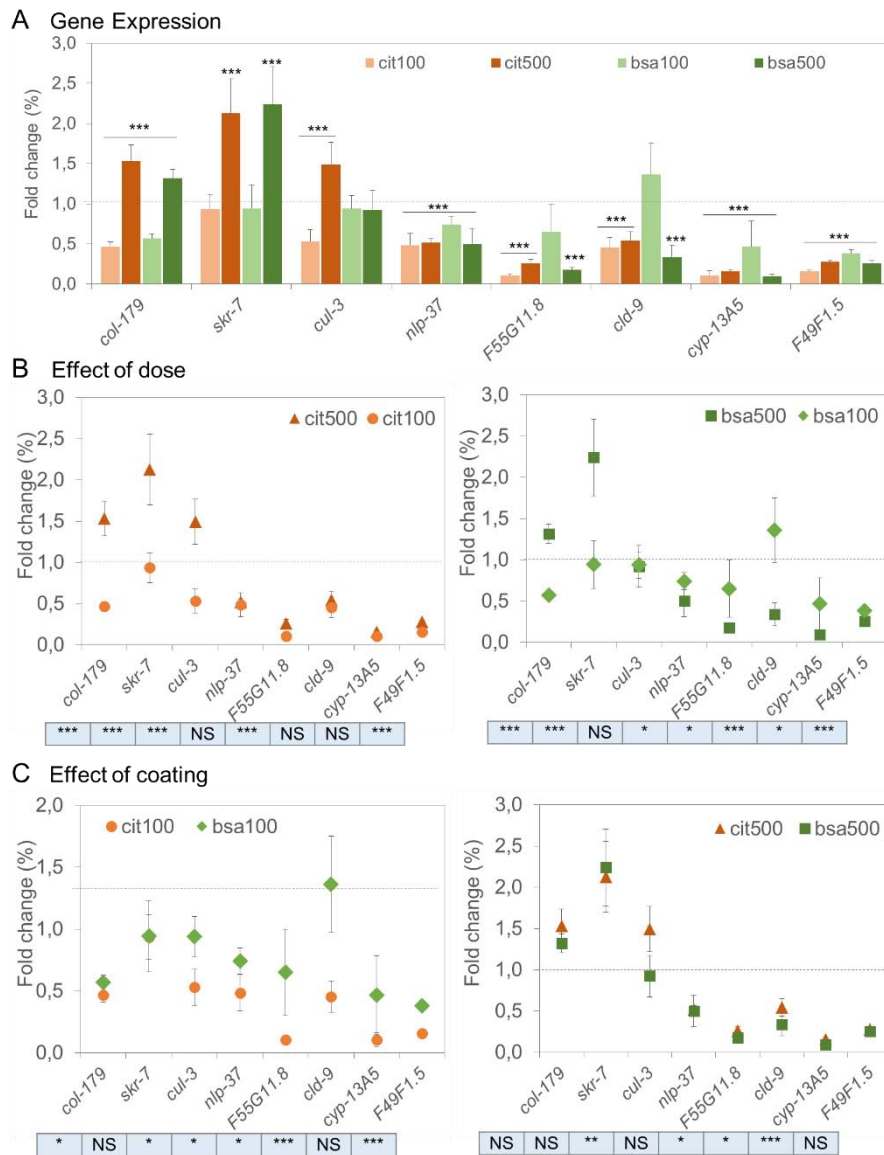


Figure 80. A) Gene expression of very responsive genes to C-SPION treatment. B) Effects of dose and C) coating. * $p < 0.05$; ** $p < 0.01$; *** $p < 0.005$.

Effects of treatment compared to unexposed worms

At both doses of exposure, the effects of C-SPIONs in gene expression compared to control worms were higher than those triggered by BSA-SPIONs, indicated by the higher significance of the fold change values. At the low dose, C-SPIONs activated the innate immune system to a greater extent than BSA-SPIONs, but none of them affected *skr-7* expression, involved in development. The response to 500 $\mu\text{g/ml}$ of BSA-SPIONs

was very similar to that of C-SPIONs except for *cul-3* gene, involved in ubiquitination. This topic might deserve further investigation. Despite the significant effect on *skr-7* expression at high dose, we did not observe effects on *C. elegans* growth or phenotype comparing treated and control animals. Similarly, we found a significant effect on *F49F1.5*, putatively involved in apoptosis, however we did not observe apoptotic cells in the TEM analysis. Remarkably, the response of *cyp-13A5* suggested a possible role of this enzyme in the nanoparticles metabolism/detoxification. Interestingly, iRNA screens showed that loss of *cyp-13A5* activity results in cadmium hypersensitivity,^[274] suggesting that *cyp-13A5* could be involved in a general mechanism for xenobiotic detoxification in *C. elegans*, rather than NP-specific.

Effect of dose

The analysis of these genes reinforced our previous findings: higher dose of BSA-SPIONs is needed to trigger effects to the same extent as C-SPIONs, especially in the case of the activation of the innate immune response and oxidative metabolism, which suggests that C-SPIONs are recognized as foreign substances at lower doses than BSA-SPIONs.

Effect of coating

The influence of NP coating in the biological effects was more prominent at the low dose: the effects on the innate immune response, ubiquitination, apoptosis and neurosignalling were coating dependent. In contrast, at the high dose we found that coating had a significant effect on the oxidative metabolism response and to a lesser extent in the innate immune system. The fact that the mechanisms triggered by high doses are less coating-dependent than the response observed at low doses suggests that at high doses general mechanisms triggered by toxicants prevail, whereas at low doses the mechanisms involved might be more specific to the NP properties.

Interaction between factors

The two-way ANOVA shown in **Table 35** summarises the influence of NP coating and dose in the gene expression of SPION-treated worms, highlighting the strong significance of these factors in gene expression. It is worth noting that the interaction between the coating and the gene is the less significant at 500 µg/ml than at 100 µg/ml, suggesting that the high dose might be a determinant factor of the biological responses by itself.

Table 35. Two-Way ANOVA considering Gene and Coating or Dose as Factors in the gene expression analysis of the most responsive gene. * p < 0.05 ; ** p < 0.01 ; *** p < 0.005.

Factor 1	Conditions	Effects of Factor 1	Effect of Gene	Interaction
Coating	Acute 100 µg/ml	***	***	***
	Acute 500 µg/ml	***	***	*
Dose	C-SPIONs	***	***	***
	BSA-SPIONs	***	***	***

5.6.3.4 Remarks

Interestingly, in the study of the most responsive genes we reported similar dose and coating effects than in the study of selected genes, hence the influence of coating and dose might apply to the whole transcriptome. In all cases, BSA-SPIONs showed greater dose dependency than C-SPIONs, while the effects of coating predominated at low dose and dissipated at higher doses or after longer exposures. In the prolonged regime, BSA-SPIONs had similar effects to the low dose acute treatment while C-SPIONs showed very similar effects to the high acute dose, emphasizing differences in the biological effects and bioavailability of the NPs depending on their coating.

Using qPCR, we identified clathrin-mediated endocytosis as an uptake mechanism of SPIONs by the intestinal cells, hence we confirmed that SPIONs can cross the intestinal barrier in *C. elegans* through a different route than nutrients, whose transport is predominantly mediated by specific transporters.^[119, 142] Microarray experiments confirmed that the lysosomal pathway was activated by both SPION types in a similar manner, consistent with our previous TEM observations. The microarray results also indicated that SPIONs activated innate immune response leading to a wide range of biological cascades of defence against xenobiotics that could include metal detoxification pathways and oxidative stress, which may be also related to the oxidative dissolution of SPIONs inside the treated animals. The deregulation of the defence pathways could disrupt key biological functions and lead to lethality. Such adverse effects, however, were mitigated in BSA-SPION treated nematodes compared to C-SPIONs.

Using the bioinformatics tool DAVID, we found that the most affected molecular pathways were specific for each NP type, suggesting different bio-identity of C-SPIONs and BSA-SPIONs inside the *C. elegans* cells with the consequently different biological responses observed. We found that C-SPIONs affected to a greater extent the processing of environmental and genetic information, while BSA-SPIONs predominantly affected cell metabolism, in particular glycan biosynthesis.

All in all, we propose that BSA protects SPIONs from dissolution inside the lumen and maybe inside the lysosomes, preventing or reducing the release of Fe³⁺ ions, and shield SPIONs from *C. elegans* making them more biomimetic and reducing the force of their interaction with the intestinal cells.

5.7 Chapter conclusions

We emphasize the imperative need of controlling the nanomaterial under study from the synthesis stage in order to ensure systematic biological studies and solid *in vivo* conclusions. To this end, we synthesised and characterised monodisperse water soluble SPIONs with two different coatings, citrate and bovine serum albumin, and exposed *C. elegans* up to 500 µg/ml. First, we studied the effects of NP treatment in the survival, reproduction and growth of *C. elegans* and did not find severe effects on the sub-lethal endpoints but reported certain lethality (40–45%) at the highest dose. These findings

suggest that acute exposure to SPIONs is safe up to high doses and does not impair irreversible effects on the biological functions and physiological status of the surviving animals. The effects on survival were coating dependent, being BSA-SPIONs more biocompatible than the citrate coated particles. Moreover, larvae resulted more sensitive to SPION toxicity than adults.

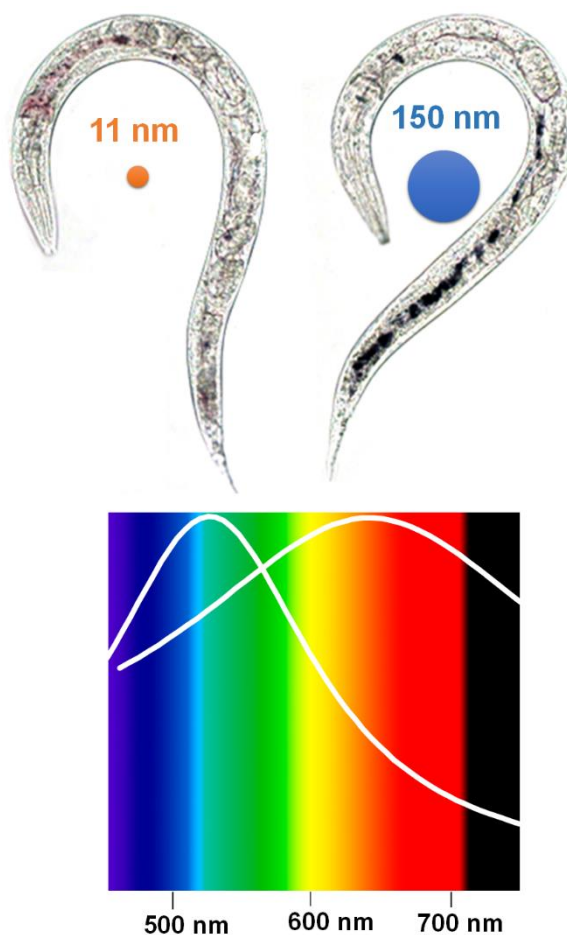
Despite the protective effect of the BSA coating against SPION toxicity in *C. elegans*, the uptake of C-SPIONs and BSA-SPIONs was within the same order of magnitude in both adults and larvae after 24 h oral feeding, suggesting that their different *in vivo* effects can be attributed to differences in their bio-identity inside *C. elegans*.

In the biodistribution studies by optical and electron microscopy, we found that both SPION types were mostly retained inside the intestinal lumen of *C. elegans*, with only a small fraction being internalised by endocytosis. We could not conclude differences in the endosome properties or number depending on the coating. Both materials remained monodisperse under the intestinal microenvironment of the *C. elegans* and kept their superparamagnetism, however we found that C-SPIONs were partially degraded while BSA-SPIONs resulted more resistant to digestion. We did not find evidence of NP entrance through the dermal route (that is, across the cuticle) or other body openings, either translocation to secondary organs such as the reproductive system.

In the mechanistic studies, we confirmed that despite both NP systems affected similarly the cell internalisation mechanism by clathrin-mediated endocytosis after acute treatment, C-SPIONs were more reactive than BSA-SPIONs *in vivo*: in general, higher doses of BSA-SPIONs were required to affect a given molecular pathways (e.g. oxidative stress, metal detoxification, innate immune response...) to a similar extent to the citrate-coated particles, suggesting lower bioavailability and/or bioactivity of BSA-SPIONs. However, after acute treatment to 500 µg/ml, the two kinds of SPIONs showed similar responses in the molecular pathways studied, suggesting that at such high doses more general mechanisms prevail. We have also characterised the whole genome expression and detected different profiles in the response of *C. elegans* to SPIONs depending on the coating: whereas the molecular function most affected by C-SPIONs was binding, BSA-SPIONs affected catalytic activity to a greater extent. In addition, the biological processes affected by BSA-SPIONs appeared restricted to the cellular level, while C-SPIONs also affected organismal processes, reinforcing the hypothesis of higher bioactivity and bioavailability of C-SPIONs compared to their protein-coated counterparts.

Overall, we attribute the different bio-identity of C- and BSA-SPIONs to their distinctive bioavailability and bioactivity arising from their surface properties. We hypothesise that the BSA coating has a double protective effect: i) it protects SPION core from acid degradation, reducing the release of iron ions in the intestinal microenvironment and avoiding the formation of toxic radicals; ii) it reduces the interaction with the membrane of the intestinal cells of the *C. elegans*, minimizing the activation of biochemical cascades with their subsequent biological effects.

CHAPTER 6. Evaluation of gold nanoparticles and *C. elegans*. The effect of NP size and composition.



CHAPTER SUMMARY

Chapter 6 describes the interaction between citrate-coated gold nanoparticles of two different sizes, 11 and 150 nm, and the model organism *C. elegans*. Nano-bio interactions are comprehensively evaluated combining the study of toxicity endpoints (survival, brood size, locomotion and growth), the use of materials science techniques (absorbance microspectroscopy and ICP-MS), imaging characterisation tools (by advanced optical and electron microscopy) and gene expression analysis to discern the effect of size. This chapter also compares the bio-identity of 6-nm citrate-coated SPIONs and 11-nm citrate-coated Au-NPs as nanoparticulate systems of different composition but comparable sizes and surface properties.

CHAPTER INDEX

6.1	Analysis of toxicity endpoints	141
6.2	Uptake of NPs in <i>C. elegans</i>	143
	Biodistribution of Au-NPs	144
6.3.1	Optical microscopy	144
6.3.2	Electron microscopy	147
6.4	NP status inside <i>C. elegans</i>	150
6.4.1	Nanoparticle size inside <i>C. elegans</i>	150
6.4.2	Aggregation status and optical characterisation	151
6.4.3	Evaluation of NP excretion	153
6.4.4	Comparison with in vitro experiments	153
6.5	Biological mechanisms	154
6.5.1	Gene expression analysis of 11-nm Au-NP treated <i>C. elegans</i>	154
6.5.2	Comparison of the effects of 11-nm Au-NPs and 6-nm SPIONs	156
6.6	Chapter conclusions	158
6.6.1	Effects of composition	160

We have performed an analogue study of the interaction between Au-NPs and *C. elegans* than the one presented in Chapter 5 for SPIONs, analysing different aspects (toxicity, uptake, biodistribution, transport mechanisms and NP status) from the organism level down to the subcellular level. We have also performed genetic studies to better understand the biological pathways triggered by NP exposure.

6.1 Analysis of toxicity endpoints

We assessed the same toxicity endpoints in *C. elegans* after Au-NP treatment (survival, reproduction, locomotion and body length) as those used for SPIONs. Exposure was performed also in the same conditions: 24 hours in liquid.

Survival

The survival studies were performed using a population of synchronized young adults. We used 11-nm Au-NPs to study the survival at doses up to 500 $\mu\text{g/ml}$ in order to assess the same metal concentration range as for SPIONs. We found a dose-response relationship that could be fitted by linear regression (**Figure 81A**). Significant differences between treated and untreated animals started at 100 $\mu\text{g/ml}$, hence we chose this dose as our working concentration for further studies in comparison with 150-nm Au-NPs and C-SPIONs. The bigger Au-NPs, however, did not significantly affect *C. elegans* survival (**Figure 81C**), showing lower lethality than 11-nm Au-NPs. Compared to SPIONs, 11-nm Au-NPs exhibit higher toxicity: the LD_{50} of SPIONs ($\sim 600 \mu\text{g/ml}$) is almost half than the value of 11-nm Au-NPs ($\sim 350 \mu\text{g/ml}$).

Reproduction

The results of number of progeny after treatment with 100 $\mu\text{g/ml}$ correlate well with those from the lethality test (**Figure 81D**): 11-nm Au-NPs have a more prominent effect on the reproduction of *C. elegans* (40% decrease) than the bigger nanoparticles (not significant reduction), indicating higher reprotoxicity of 11-nm Au-NPs. The effects of 11-nm Au-NPs in fertility occur at lower doses than for C-SPIONs (100 versus 500 $\mu\text{g/ml}$) and more acutely (40% compared to 20% reduction in the number of progeny). The adverse effects on reproduction of 11-nm Au-NPs may arise from direct reprotoxicity of the nanoparticles during treatment,^[186] potentially by oxidative damage or neuronal impairment,^[203, 275] or from the incapacity of recovery of treated worms upon normal culture conditions, leading to reduced brood size.^[200]

Locomotion

The behaviour of a mixed-stage population of *C. elegans* (adults and larvae) exposed to 11-nm Au-NPs at 0, 100, 300 and 500 $\mu\text{g/ml}$ was monitored for 24 h using Microtracker® platform (**Figure 81B**). Locomotion is used as a sub-lethal endpoints, together with reproduction, to assess the effects of toxicants in *C. elegans*.^[160] We found a dose-response decrease in the movement of *C. elegans* leading to significant effects at doses higher than 300 $\mu\text{g/ml}$, suggesting neuromuscular affectation.^[276]

Body length

We did not find significant differences between the length of untreated and Au-NP treated worms (**Figure 81E**), and all nematodes showed a normal appearance. These results indicate that the feeding processes, governed by multiple factors from neuronal structure to external stimuli, and the nutrition status of acutely treated worms are not impaired by NP treatment or at least are recovered upon standard culture conditions for three days.^[119, 150]

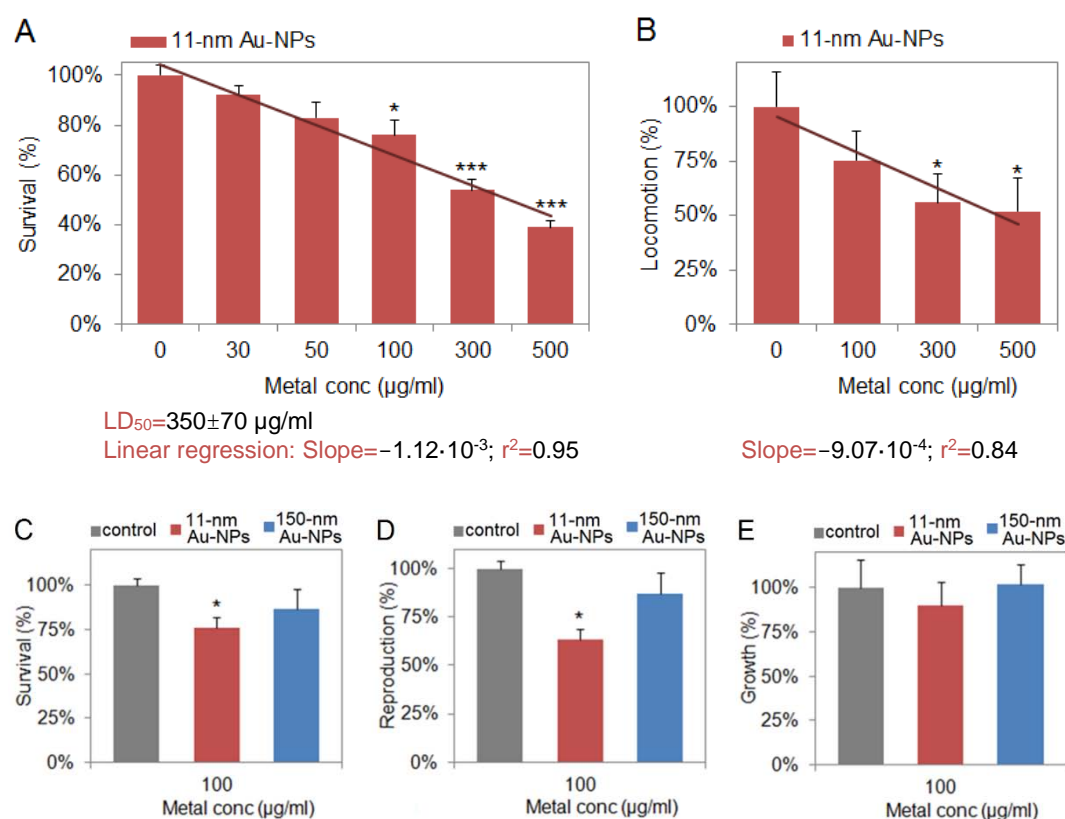


Figure 81. A-C) Effect of 11-nm Au-NPs in the A) survival (n=3) and B) locomotion (n=6) of *C. elegans*. Linear regression of the survival rates and the calculated LD₅₀ value are also shown. D-E) Comparison of the effect of 100 µg/ml exposure to 11 nm and 150 nm Au-NPs in the C) survival (n=3), D) reproduction (n=6) and E) growth (n=6) of *C. elegans*. Error bars indicate standard error. * p < 0.05 ; ** p < 0.01 ; *** p < 0.005.

In summary, we exposed *C. elegans* to two sizes of Au-NPs and studied their effects on survival, reproduction and locomotion. We observed a significant decrease on brood size and lethality at 100 µg/ml in the case of the smaller Au-NPs, but not in the case of 150-nm Au-NPs, indicating higher toxicity of the small particles. The final length of treated animals was not affected by Au-NP treatment. The locomotion behaviour was only slightly affected at 100 µg/ml (25% decrease), and higher doses (300 µg/ml) were required to significantly decrease *C. elegans* motility. These results suggest that acute exposure to Au-NPs at concentrations up to 100 µg/ml can be considered safe as the physiological status of the survivors is not significantly compromised.

6.2 Uptake of NPs in *C. elegans*

We performed chemical analysis using ICP-MS to determine Au-NPs uptake in *C. elegans* (Table 36) and found that treated worms ingested 500 times more 11-nm Au-NP than 150-nm particles. However, the gold mass contained in the worm's body was nearly seven times higher in the case of the bigger NPs due to their larger volume. Considering that the surface atoms are the most reactive ones, worms treated with the 11-nm Au-NP were exposed to double surface area of ingested NPs than the animals treated with 150-nm Au-NP, which could account for the higher nanotoxicity of the smaller NPs. Studies using other inorganic nanoparticles including silver, titania and zinc oxide suggested that small particles can trigger oxidative stress to a greater extent than their bigger counterparts due to their larger surface area.^[179, 192, 209] For both 11-nm and 150-nm Au-NPs, the concentration of particles in the media was not a limiting factor for NP uptake by *C. elegans* as their ingestion corresponded to 0,00074% and 0,00485% the total amount of NPs available, respectively.

Table 36. Au-NP uptake after 24-h exposure by chemical analysis. Results are indicated as number of nanoparticles per worm, surface area of ingested NPs, and gold mass.

NP type	Metal mass (pg/worm)	Millions of NPs	Surface area (10 ¹⁰ nm ²)
11-nm Au-NPs	738	73	2.29
150-nm Au-NPs	4850	0.14	1.01
Ratio	0.15	500	2

In terms of NP uptake per body mass, *C. elegans* ingested 600 mg/kg 11-nm Au-NPs and 4200 mg/kg 150-nm Au-NPs, which corresponds to metal doses 5–6 orders of magnitude above human doses. For instance, MesoGold® is a 20-ppm dispersion consisting on 3.2-nm Au-NPs marketed by Purest Colloids, Inc. (USA) as a mineral supplement to enhance the body's immune system. The recommended adult daily dosage is 4–17 µg/kg. Therefore, even when the worm is treated with metal doses much higher than expected human doses, the Au-NPs still show high biocompatibility. Based on these results, we expect that the use of clinical doses of Au-NPs in humans would be safe. Similarly, the concentration of Au-NPs in the environment is not expected to reach doses able to significantly harm *C. elegans*.

Comparing C-SPION and 11-nm Au-NP uptake at the doses with similar effects (500 µg/ml and 100 µg/m, respectively), *C. elegans* ingest 5 times more amount of metal in the case of gold nanoparticles. However, due to the smaller size of SPIONs, SPION uptake corresponds to 4 times more NPs than 11-nm Au-NPs (316 millions compared to 73 millions). In addition, the surface area of SPIONs inside *C. elegans* is 1.5-fold higher than Au-NPs at the doses of treatment.

6.3 Biodistribution of Au-NPs

6.3.1 Optical microscopy

6.3.1.1 Light microscopy (LM): Direct observation

The interaction between Au-NPs and visible light results in colours ranging from reddish to bluish, from smaller to bigger NP sizes. Based on these optical properties, we could track Au-NPs in *C. elegans* by direct observation using light microscopy (**Figure 82**). About ~15 min after the beginning of the exposure, Au-NPs were already visible inside the worm. We observed that NPs were introduced gradually through the alimentary system and they concentrated in the intestinal lumen for up to 24 h. Using transmitted light, the 11-nm Au-NPs were viewed in pink inside the intestinal lumen of *C. elegans* while the 150-nm Au-NPs appeared blue. In contrast, 40-nm Au-NPs were observed inside *C. elegans* either pink or blue depending on the worm, and colour transition occurred also within single worms remaining pink close to the mouth and turning into blue in more posterior regions. Such colour change was not observed in the case of Au-NPs between 5 to 20 nm, which appeared pink, hence it indicates that the interaction between 40-nm Au-NPs with *C. elegans* can modify the optical properties of the material likely due to NP aggregation or confinement inside the intestinal lumen. In this thesis, we studied into detail the *in vivo* behaviour of 11-nm and 150-nm Au-NPs, however intermediate sizes around 40 nm deserve further investigation to better understand the changes in their optical properties.

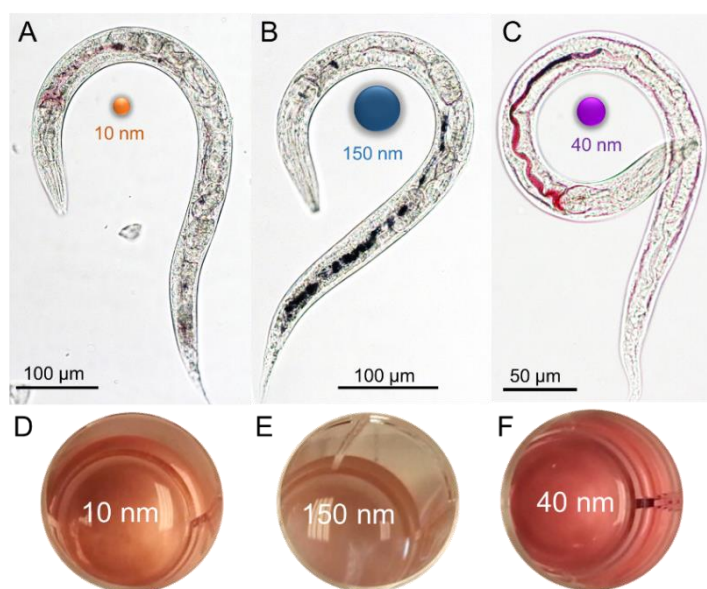


Figure 82. Light microscopy images under transmitted light of A) 11-nm, B) 150-nm and C) 40-nm Au-NPs treated worms. D-F) Images of the respective nanoparticles in dispersion.

Biodistribution map

Using the same methodology as for SPIONs, we evaluated the predominance (frequency) of Au-NPs visualisation in the different regions of the *C. elegans* anatomy under light microscopy in young adult worms (n=30). The resulting colour map (**Figure 83**) evidence that 11-nm Au-NPs show a clear gradient being more frequently observed in the posterior regions of the intestine than in the more anterior ones, suggesting facile passage through the intestine. This biodistribution pattern is in good agreement with previous findings.^[197] The pharyngeal content of 11-nm Au-NPs was generally not sufficient to confer visible pink colour to that anatomical structure. In contrast, 150-nm Au-NPs were more frequently observed in the pharynx than 11-nm Au-NPs, probably due to their bigger size facilitating the visualization, and tended to remain either close to the entry portal (anterior gut) or to the exit portal (posterior gut). These observations might indicate that large particles are less stable in biological environments leading to aggregation or precipitation inside *C. elegans*.

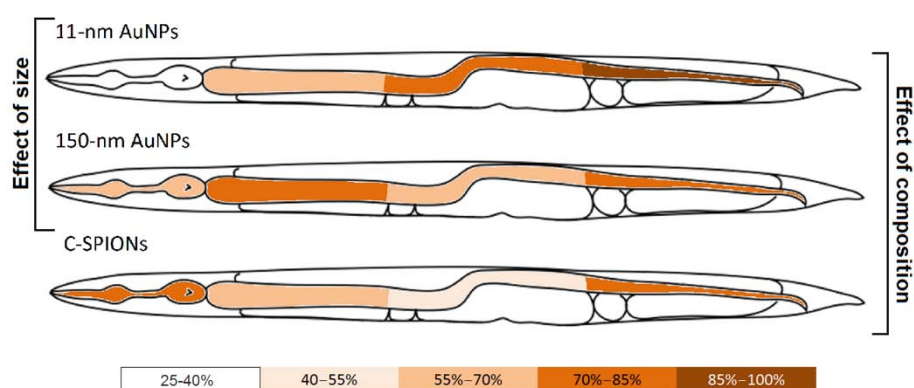


Figure 83 Biodistribution map of 11-nm Au-NPs, 150-nm Au-NPs and C-SPIONs.

Remarkably, both SPIONs and Au-NPs exhibited an uptake gradient towards the posterior gut where they accumulated most. However, SPIONs were more frequently visualized in the pharynx than Au-NPs. The differences in concentration exposure and NP size could contribute to the differences observed. However, to evaluate NP distribution more accurately, techniques with superior spatial resolution such as TEM are required.

6.3.1.2 Dark-Field Hyperspectral imaging

Hyperspectral dark-field microscopy (HDFM) is an advanced visualization technique that combines hyperspectral imaging with state-of-the-art optics and computer software to enable the rapid identification of materials at the micro- and nanoscales. This technique can be used to screen for the presence of nanomaterials, but also to locate, identify, and characterise them. We performed HDFM using a CytoViva microscope, which allowed us to study Au-NP distribution inside treated *C. elegans* at both larval and adult stages. Both Au-NPs were constrained to the alimentary system, located inside the intestinal lumen but apparently not internalised by the enterocytes either translocated to secondary organs such as the reproductive system or the eggs (**Figure 84**).

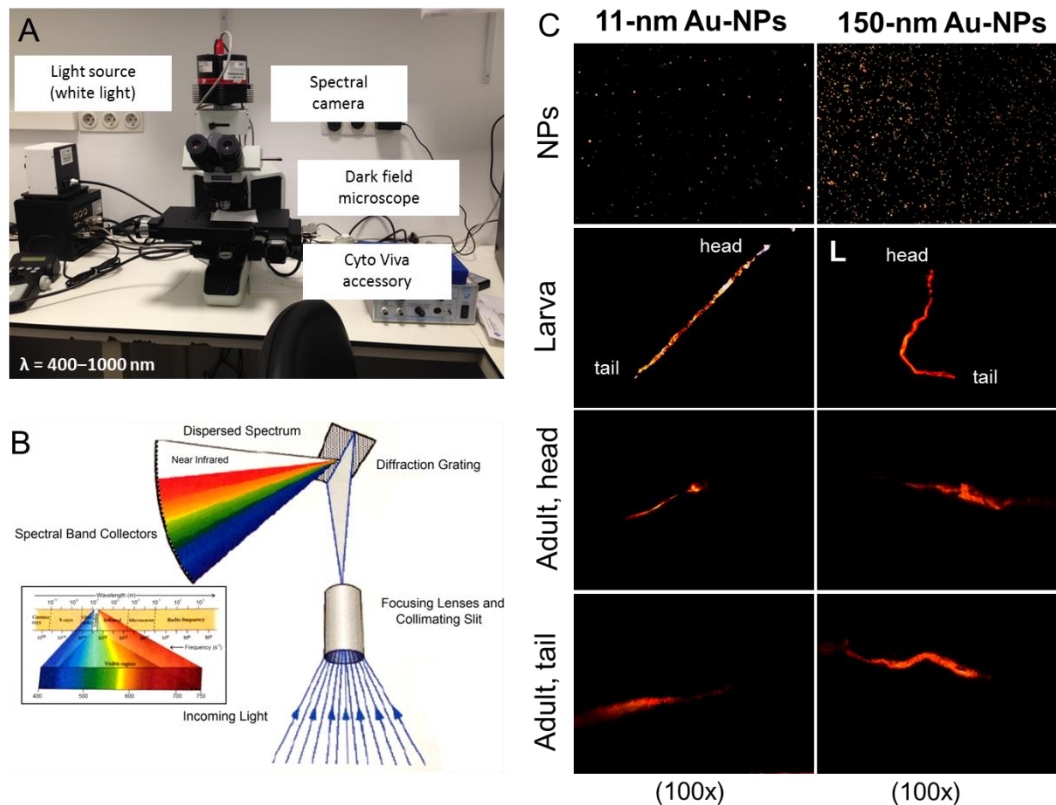


Figure 84. A) Hyperpsectral Dark-Field Microscope. B) Fundament of the technique. C) Hyperspectral images of larvae and adult worms treated with 11 and 150-nm Au-NPs. Nanoparticles are only observed in the digestive tract, but not inside the intestinal cells either translocated to secondary organs such as the reproductive system.

6.3.1.3 Two-Photon Luminescence Microscopy (TPLM)

Exploiting the luminescent properties of Au-NPs, we performed TPLM studies to track Au-NPs in individual worms. Under near-infrared pulsed illumination, Au-NPs luminesce via interband transitions induced by the absorption of two photons. This signal is strongly enhanced when the pulsed illumination spectrally overlap with the localized plasmon resonance of the Au-NP. TPLM provide better contrast than bright-field or dark-field microscopy, which are often hampered by the endogenous parasitic scattering of the worms. Furthermore, as multiphoton processes feature a nonlinear dependence on the excitation intensity, TPLM is intrinsically confocal and offers three-dimensional imaging capabilities with improved spatial resolution. Therefore, this technique was superior in resolution than our previous attempts of Au-NP localization in *C. elegans* and remarkably, to our knowledge it was the first time that TPLM was used to localize Au-NPs inside *C. elegans*.

TPLM revealed Au-NPs presence solely in the *C. elegans* intestine and specifically confined to the intestinal lumen. By scanning the sectioning plane of the TPLM images, TPLM tomography offered a three-dimensional reconstruction of the entire worms, confirming the absence of Au-NPs adsorbed onto the cuticle and excluding topical entrance of Au-NPs. Moreover, TPLM also provides semi-quantitative information

regarding Au-NP uptake based on the optical properties of the material, as shown in **Figure 85**: the luminescent signal is proportional to the number of NPs in the area.

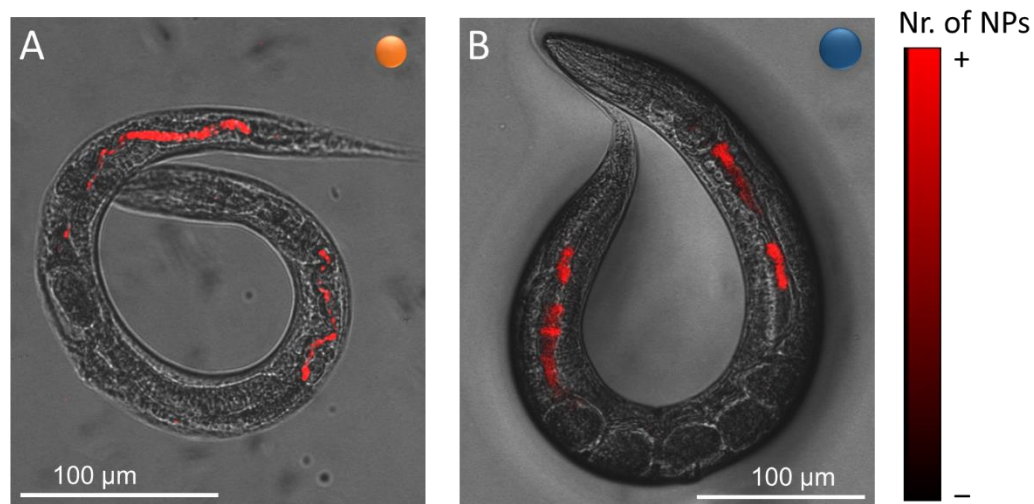


Figure 85. TPLM images of 11-nm and 150-nm Au-NP treated worms. Dark-Field micrographs were merged with the luminescent signal from the Au-NPs pseudo-colored via a Look Up Table expressing NP uptake as number of NPs, according to the colour bar presented on the right. Image processing was performed using ImageJ software.

Overall, according to our optical microscopy studies, Au-NPs were constrained to the *C. elegans* intestine, which might determine their biological effects. Besides NP localization, their status (aggregation, surface area, etc.) in the intestinal lumen may also play a determining role in the *in vivo* behaviour of Au-NPs in *C. elegans*, as studied in Section 6.4.

6.3.2 Electron microscopy

6.3.2.1 Interaction between Au-NPs and the cuticle

The interaction between the external part of *C. elegans* and Au-NPs was investigated using SEM-EDX (**Figure 86A**). EDX quantitative analysis revealed that Au-NPs did not attach to the external surface of the animal, based on the absence of gold. The negative charge of both the cuticle and the citrate-capped Au-NPs could explain the lack of affinity between them. Hence, these results exclude entrance of NPs by the dermal route and indicate that the alimentary tract of the animal is the unique portal of NP entry into the body of the worm, in good agreement with the TPLM observations.

The interaction between the pharyngeal cuticle and the Au-NPs was investigated by TEM as shown in **Figure 86BC**. We did not observe adhesion either attachment of Au-NPs to the pharyngeal cuticle and the nanoparticles were distributed inside the pharyngeal lumen.

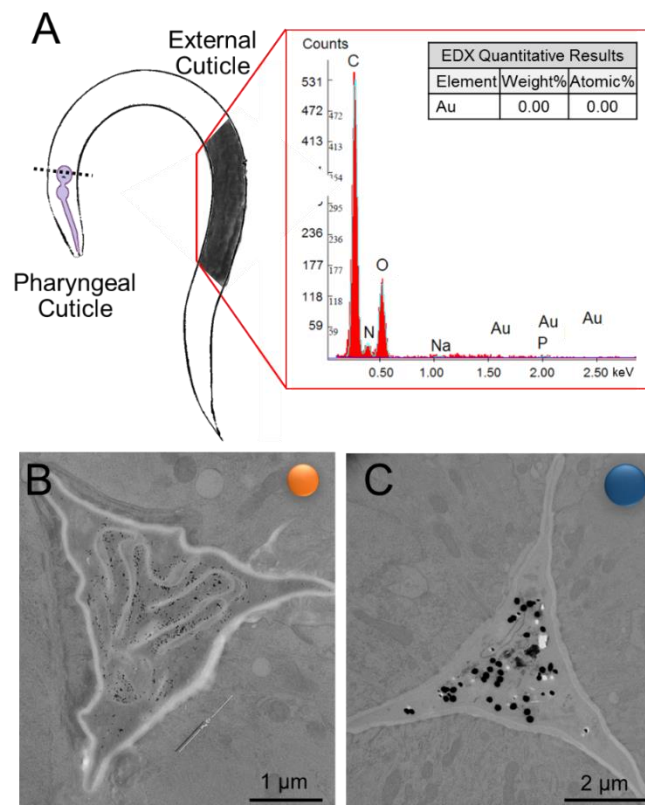


Figure 86. A) Representative SEM-EDX analysis of the external cuticle of a Au-NP treated animal showing no traces of gold on the outer surface of *C. elegans*. B) TEM image of the pharynx of a 11-nm Au-NP treated *C. elegans* showing individual NPs inside the lumen. C) TEM image of the pharynx of a 150-nm Au-NP treated *C. elegans* showing individual NPs inside the lumen. Adapted from Gonzalez-Moragas *et al.*

6.3.2.2 Study of *C. elegans* cross-sections with single particle resolution

We studied cross-sections of the anterior and posterior regions of *C. elegans* exposed to Au-NPs by TEM to reach nanometric resolution. We confirmed that Au-NPs were restricted to the intestinal lumen and not internalised by the intestinal cells based on the absence of endosomes with NPs inside (**Figure 87**). Moreover, Au-NPs remained separated from the microvilli by the glycocalyx at all times. Interestingly, Au-NPs preserved their monodispersity in the intestinal environment with no apparent necking between individual NPs, suggesting that the citrate coating is preserved inside the *C. elegans*. These results suggest, therefore, a strong electrostatic interaction between the metallic core of the NP and the surfactant.

We also observed the cross-sections by HAADF STEM which enhances the contrast between Au ($Z=79$) and C ($Z=6$) and confirmed the absence of NP endocytosis and translocation, as Au-NPs were only visualized in the lumen (**Figure 88**).

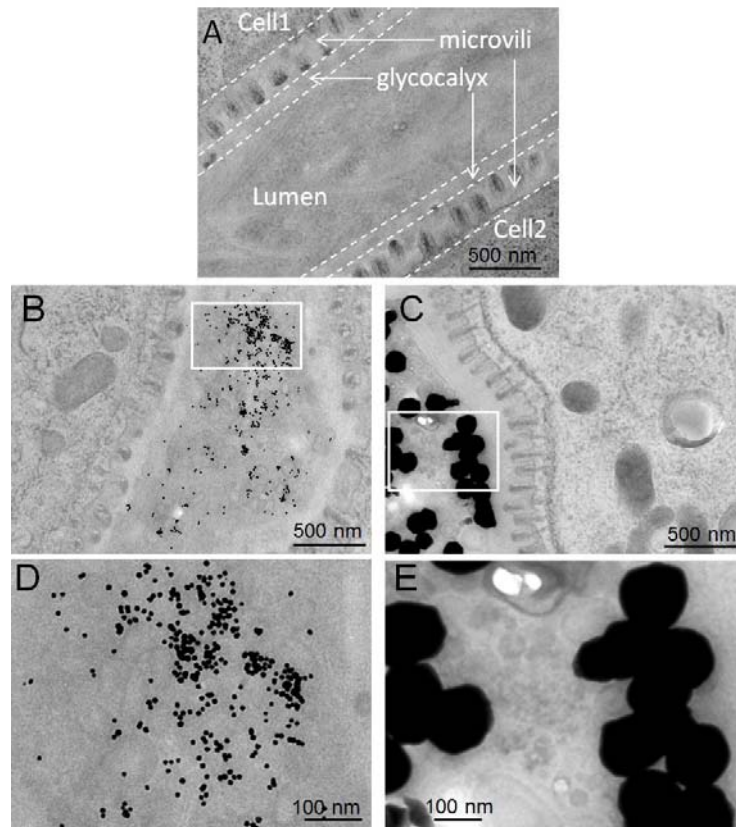


Figure 87. TEM images of the anterior part of the intestine of A) control nematodes, and nematodes treated with B) 11-nm and C) 150-nm Au-NPs.

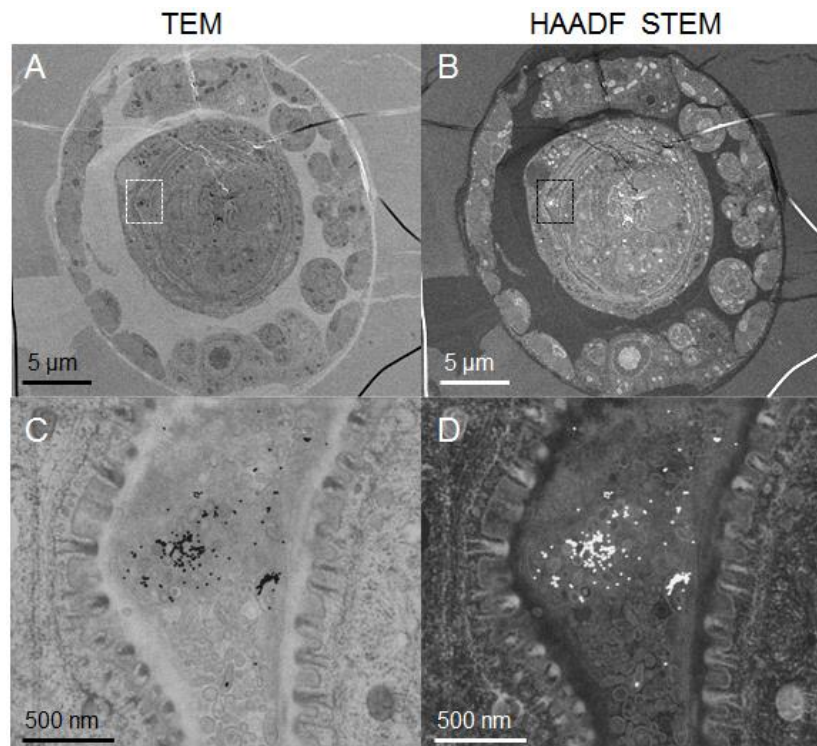


Figure 88. TEM and HAADF STEM images of a 11-nm Au-NP treated worm. Upper panels show the entire width of the worm. Lower panels show a magnification 9 of the selected area, corresponding to the intestinal lumen. Au-NPs appear dark by TEM and bright by HAADF STEM.

The absence of internalisation of Au-NPs by the intestinal cells of *C. elegans* could be attributed to the lower transcytotic capacity of the *C. elegans* intestine compared to that of vertebrates. In contrast, the observation of endocytosis in the case of SPIONs might be attributed to the essential role of iron in the *C. elegans* biology, triggering internalisation mechanisms such as endocytosis, whereas the non-essential nature of gold would not promote accumulation strategies. The mechanistic studies described in Section 5.6 analyse into more detail the molecular response of *C. elegans* to Au-NPs.

Recent studies in mammals have revealed that the Microfold cells (or M cells) present in the intestinal barrier, which lack the glycocalyx covering and have a poorly organized brush border, are necessary for the absorption of NPs that are administered orally (**Figure 89**).^[277, 278] While little translocation occurs through the enterocytes, especially for negatively charged particles, the coexistence of enterocytes and M cells can increase NP absorption by up to 50-fold. The absence of M cells in *C. elegans* might explain the composition-specific endocytosis of SPIONs and the lack of Au-NP internalisation.

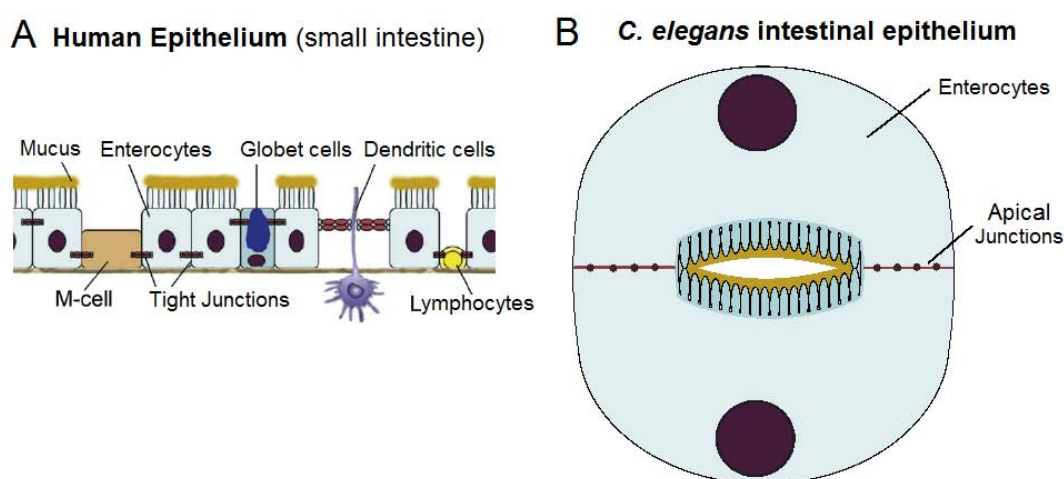


Figure 89. Schematic drawing of the intestinal structure of A) humans and B) *C. elegans*. There are intrinsic differences in tissue architecture between *C. elegans* and humans. Human intestine shows different types of accessory cells between the enterocytes, among them M-cells, absent in the *C. elegans*' intestine which is formed exclusively by enterocytes that delimit the intestinal rings.

6.4 NP status inside *C. elegans*

We combined the analysis of NP status by TEM analysis, absorbance micro-spectroscopy and evaluation of excreted Au-NPs to study changes in NP size aggregation and optical properties inside *C. elegans*.

6.4.1 Nanoparticle size inside *C. elegans*

We evaluated the TEM sizes of 11-nm and 150-nm Au-NPs in the cross-sections of treated *C. elegans* and did not observe a significant size reduction inside *C. elegans* after 24 h (**Figure 90**), confirming the superior chemical inertness of Au-NPs compared to other compositions such as iron oxide, ZnO-NPs or Ag-NPs.^[190, 199, 258] However, minimal

corrosion and ion leakage would be plausible *in vivo* according to recent *in vitro* work of Sabella *et al* using 4-nm Au-NPs.^[254]

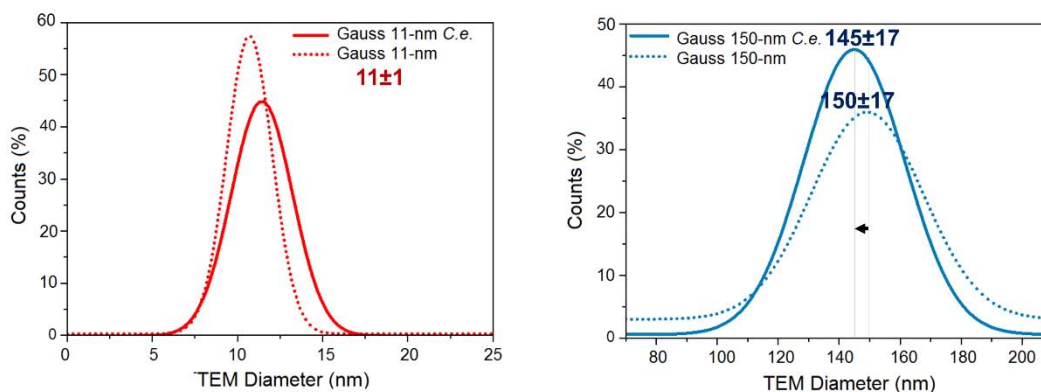


Figure 90. Size distribution of Au-NPs as synthesised (dotted lines) and inside *C. elegans* (solid lines). The results indicate that no size decrease occur inside *C. elegans*, which confirms the inertness of these materials and their resistance to oxidative dissolution *in vivo*.

6.4.2 Aggregation status and optical characterisation

Aggregation of Au-NPs induces coupling of the gold nanoparticle's plasmon resonance modes, which results in a red shift and broadening of the plasmon resonance. Absorbance μ -spectroscopy allows us the study of the aggregation status of Au-NPs inside *C. elegans*, where interparticle distances between the nanoparticles can be modified due to space constrictions or due to the conditions of the intestine lumen (i.e. ionic strength, acidic pH, secreted enzymes...). In collaboration with the group of Dr. Romain Quidant from ICFO, we applied absorbance μ -spectroscopy to characterise Au-NP treated worms using a home-made setup consisting of a UV-Vis spectrometer coupled to an optical microscope.

We acquired the spectra of targeted areas of individual animals with 10- μ m precision. The shift of the plasmon resonance peak was used to evaluate the aggregation level of the Au-NPs in the different anatomical regions (**Figure 91**). We have observed that interparticle distance changed according to the physioanatomical properties and pH of the different areas of the intestinal tract, inducing specific degrees of aggregation in each region as discussed below. In all cases, we detected a broadening of the absorption band and a red-shift of the peak maxima. In agreement with our previous results, Au-NPs were not detected in the reproductive system either in the eggs by spectroscopy.

In the grinder, the 150-nm Au-NPs showed the highest peak shift, due to the space constriction of the pharyngeal lumen at this specific structure. The grinder is made up of three pairs of muscle cells that rotate when the muscles contract and act as "teeth" that macerate food.^[119] When closed, the pharyngeal lumen is constrained to a diameter of only a few hundred nanometers. In the grinder, the 11-nm Au-NPs showed smaller peak shift based on their smaller volume, three orders of magnitude smaller than the volume of the 150-nm Au-NP. In the anterior intestine, both NPs showed the smallest peak shift, which confirms that Au-NPs can redisperse when the intestinal lumen becomes a few microns wide. In this region, the presence of other biomolecules can result in the

formation of a protein corona that may enhance the stability of the NPs in this anatomical area.^[119] Remarkably, the aggregation experienced by the Au-NPs was not irreversible, but associated with their surrounding environment.

After 24 h Au-NPs feeding, a significant amount of NPs accumulated in the posterior region of the gut, promoting low interparticle distance in such narrower space, which resulted in a red-shift corresponding to ca. 5% of the initial peak position. The transit to the posterior intestine might be determined by the pumping mechanisms of *C. elegans* rather than to the Au-NPs' properties.

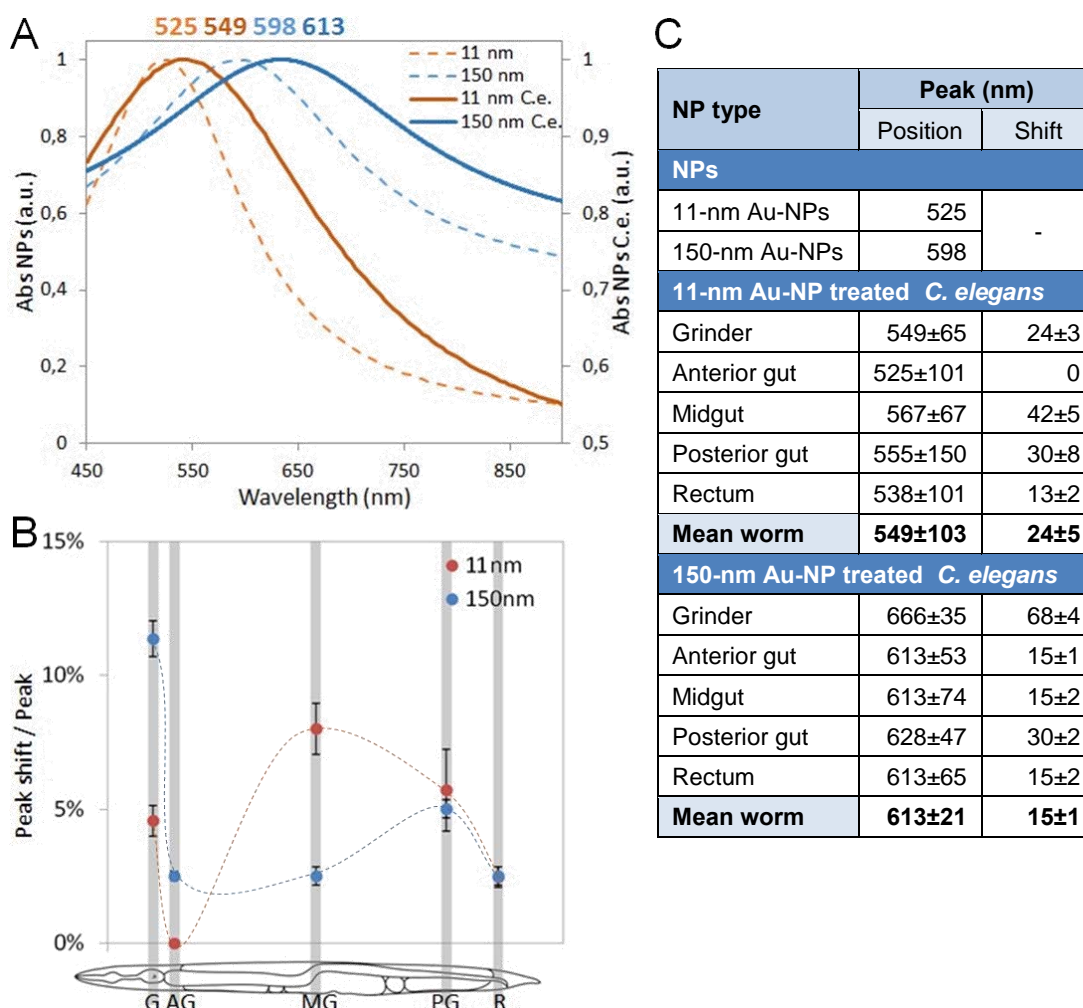


Figure 91. A) Absorbance spectra of Au-NPs in dispersion (dotted lines) and inside *C. elegans* (solid lines). The mean spectra of the different anatomical areas of *C. elegans* is plotted. B) Relative peak shift of the Au-NP in the different anatomical areas (G: Grinder. AG: Anterior gut. MG: Mid-gut. PG: posterior gut. R: rectum). C) Absolute peak position and peak shift. Adapted from Gonzalez-Moragas *et al.* {Gonzalez-Moragas, 2016 #1042}

The effect of the pH on NP status should also be considered. While in the most anterior region of the gut the pH is close to 6, it decreases to ca. 3.5 in the posterior part.^[152] We investigated the effects of pH and ionic strength *in vitro* using citrate buffer at pH 4.6 and observed aggregation and precipitation of the Au-NPs, suggesting that the combination of these two factors in the *C. elegans* intestine could act against the stability of the Au-NPs, as detailed in Section 6.4.4.

6.4.3 Evaluation of NP excretion

When treated worms were transferred to a bacterial lawn and started to feed on bacteria, they quickly excreted the intestinally confined NPs in the form of micrometric ejections which appeared the same colour as inside the worm (**Figure 92**), indicating that the size and optical properties of the Au-NPs did not significantly change inside *C. elegans*. However, the aspect of such ejections suggests that NPs were mixed with the intestinal content of the worm; typically food debris and endogenous secretions. After 2 h of food resumption, Au-NPs were no longer observed inside treated *C. elegans*. In contrast, when treated worms were washed but kept in fresh media or transferred to NGM plates without food, after two hours the NPs were still accumulated inside the intestine.

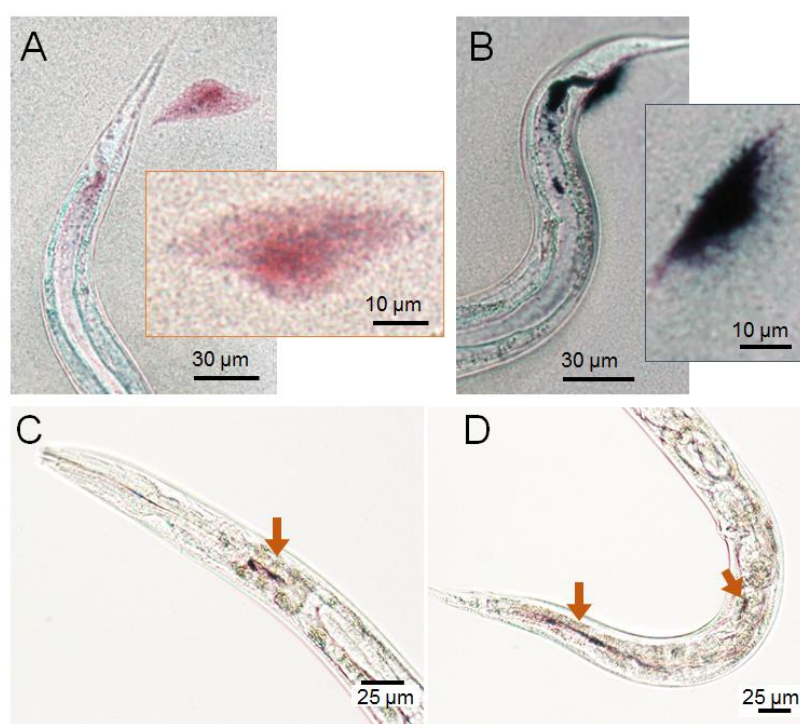


Figure 92. A,B) Au-NPs are excreted when treated *C. elegans* are transferred to plates with food. Blow-ups show NP ejections at higher magnification. Excreted Au-NPs maintain the same colour as inside the worms: 11-nm NPs appear pink and 150-nm NPs, blue. C,D) 11-nm Au-NPs inside *C. elegans* (head and tail, respectively) 2 h after washing in the absence of food.

6.4.4 Comparison with *in vitro* experiments

We mimicked the intestinal *C. elegans* microenvironment by incubating 11-nm Au-NPs for 24 h in citrate buffer at pH 4.6 (CB) with and without 10% fetal bovine serum (FBS). DLS measurements showed that Au-NPs aggregated in CB ranging from an initial hydrodynamic mean size of 10 ± 2 nm to 900 ± 300 nm. In contrast, when 10% FBS was incorporated into the system, Au-NPs aggregated to a much lesser extent (180 ± 60 nm). UV-Vis spectroscopy revealed a 59-nm red-shift of the maximum absorbance peak when Au-NPs were incubated without protein, and a mere 6-nm peak shift when FBS was

added, close to the peak position of 11-nm Au-NPs inside *C. elegans* (**Figure 93**). TEM analysis further confirmed the aggregation degree suggested by DLS and UV-Vis.

This *in vitro* study validates our hypothesis that the pH of the specific region of the intestine and the biomolecules present (i.e. proteins) enhance the stability of the Au-NPs and prevent the formation of large irreversible aggregates, as observed *in vivo* in the *C. elegans* intestine, resulting in reversible aggregation determined by the confinement in the biological environment.

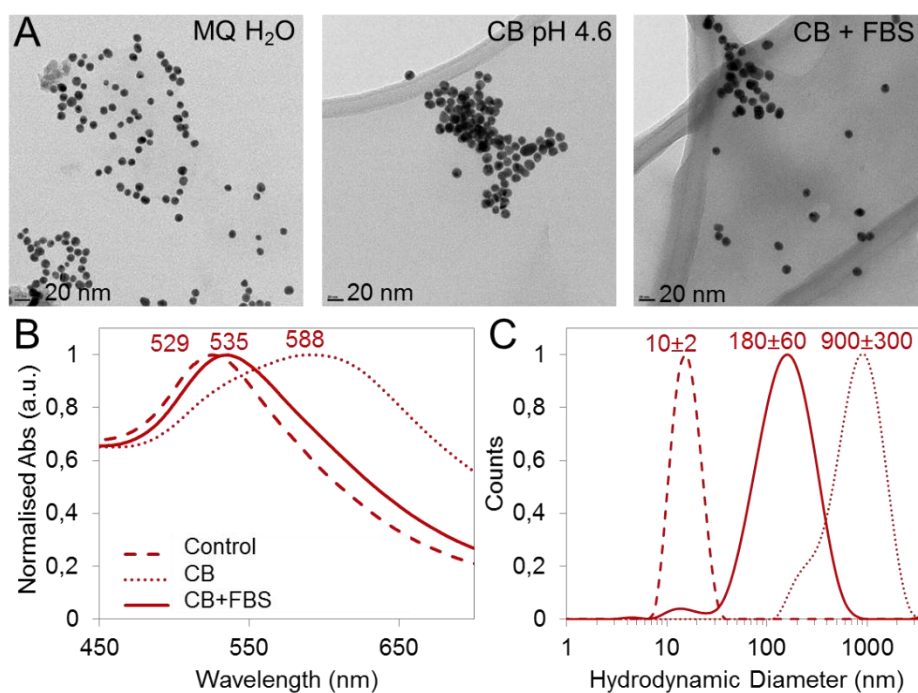


Figure 93. Characterisation of 11-nm Au-NPs at 100 µg/mL *in vitro* after 24 h incubation in citrate buffer pH = 4.6 (CB) with and without 10% fetal bovine serum (FBS) to mimic the *C. elegans* intestine regarding pH and the presence of biomolecules. A) TEM images of 11-nm Au-NPs in water (left panel), CB pH 4.6 (central panel) and CB pH 4.6 + 10% FBS (right panel). B) UV-Vis spectra of 11-nm Au-NPs in water, CB and CB-FBS after 24 h incubation. C) DLS measurement of 11-nm Au-NPs in water, CB and CB-FBS after 24 h incubation. Adapted from Gonzalez-Moragas *et al.* {Gonzalez-Moragas, 2016 #1042}

6.5 Biological mechanisms

6.5.1 Gene expression analysis of 11-nm Au-NP treated *C. elegans*

6.5.1.1 Study of selected pathways

We used two different exposure conditions: i) acute exposure (24 h) of young adults to 100 µg/ml (200 µg in total) in liquid exposure; and ii) prolonged (48 h) exposure of L1 worms in NGM agar plates with food (40 µg/plate). We aimed to evaluate the effects of NP exposure and to compare acute treatment *versus* prolonged treatment.

Gene expression after acute exposure: Effects compared to unexposed worms

Figure 94A shows the gene expression levels after 24 h exposure to 100 µg/ml 11-nm Au-NP in 50% M9 buffer. NP exposure significantly affected genes related to metal

detoxification and oxidative stress (*mtl-2*, *pcs-1* and *sod-3*), suggesting a potential role of these pathways in the *in vivo* effects of Au-NPs in *C. elegans*. Interestingly, iron homeostasis genes were also activated upon treatment, which could act as a stress mechanism in *C. elegans*^[162] and also in higher model organisms.^[279] In good agreement with our TEM observations, endocytosis and intestinal structure were not significantly affected (except the expression of *act-5*) confirming the absence of cell internalisation of Au-NPs and the non-harmful character of Au-NPs over the intestinal barrier. We attribute the activation of *act-5* to the presence of Au-NPs in close contact to the microvilli.

Gene expression after prolonged exposure: Effects versus unexposed worms

Figure 94B shows the gene expression levels after 48 h exposure of L1 larvae to 40 µg/plate 11-nm Au-NPs in NGM agar plates with food. We did not find a significant increase in the lethality of treated *C. elegans* compared to untreated worms after 48 h exposure in the presence of food, emphasizing the influence of the exposure conditions in the toxicological profile of the test material. Prolonged treatment to Au-NPs affected to a much greater extent than acute exposure the metal detoxification and antioxidant pathways, indicating enhanced biological activity of Au-NPs under this exposure regime. The expression of iron homeostasis genes was significantly affected compared to unexposed worms and to a similar extent than after acute exposure, suggesting that ferritins and metal transporters can respond to chemical compositions other than iron.^[280] The expression of genes involved in the microvilli structure and the integrity of the intestinal barrier was also affected by prolonged Au-NP exposure. Similarly, Au-NPs affected the expression of genes related to endocytosis (*dyn-1*, *eps-8*), which might indicate that Au-NPs are more bioavailable after prolonged treatment with food. However, the basal expression of *chc-1* does not suggest clathrin-dependent endocytosis of Au-NP even after prolonged treatment in the presence of food, in opposition to previous findings using 4-nm Au-NPs.^[186]

Effects of exposure system

Comparing acute and prolonged treatment of *C. elegans* to 11-nm Au-NPs, the effects on metal and antioxidant responses shows dependence on the exposure conditions (**Figure 94C**). Moreover, the expression of iron homeostasis genes was also dependent on the regime: even though these genes were modulated after both acute and prolonged exposures, their response was different, suggesting that the underlying biological mechanisms are also different. The intestinal effects, however, did not show significant differences comparing the two exposure systems.

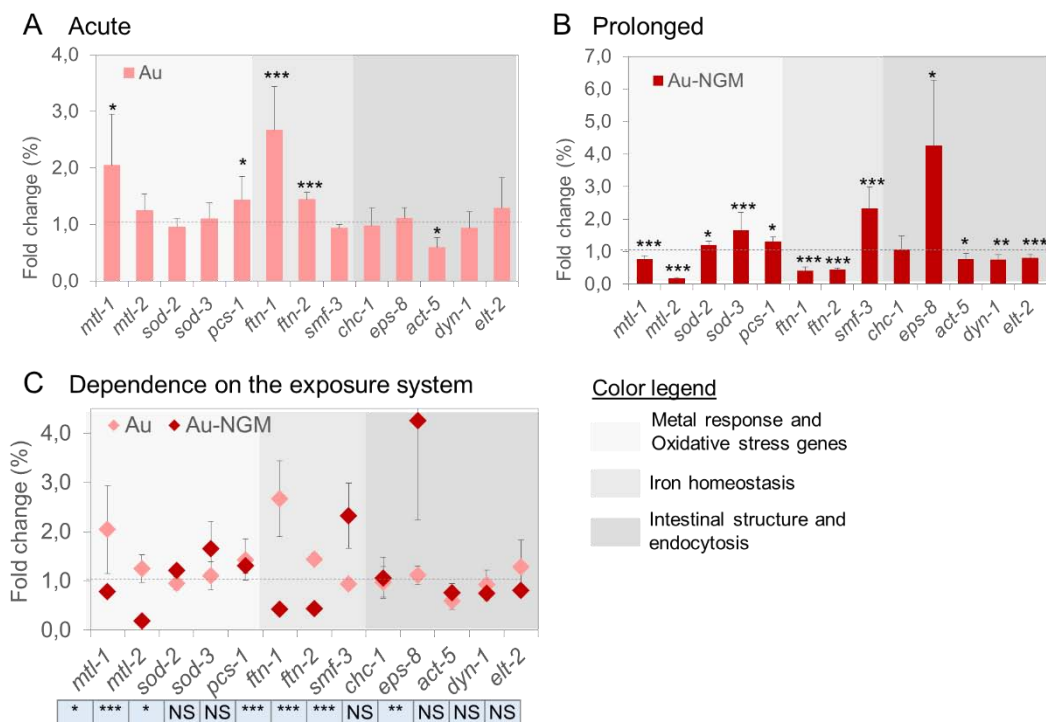


Figure 94. Gene expression levels of selected pathways after Au-NP treatment in A) liquid media for 24 h (100 µg/ml) and B) solid media for 48 h. C) Effect of the exposure system.

Interaction between factors

The two-way ANOVA of the results revealed significant effects of Au-NP treatment in gene expression depending on the exposure system and the gene under study. We found that the changes in gene expression significantly depended on the specific gene under study ($p < 0.001$), which indicates that the changes in the level of expression were gene-specific and did not follow a general trend (i.e. all down-regulated or all up-regulated). No significant effect of the exposure system was detected in a global level despite that significant differences were found when the results were compared in pairs using T test. Overall, the effects on gene expression depended on the interaction between the gene under study and the exposure regime ($p < 0.001$).

6.5.1.2 Study of most affected transcripts identified by Microarrays

The expression of the most responsive genes after 6-nm C-SPION treatment, presented in Section 5.6.3.3, was investigated in 11-nm citrate Au-NP treated worms to discern whether the molecular mechanisms triggered by nanoparticle treatment were composition-specific or general for materials with similar size and surface properties. The expression levels are presented in **Figure 95**. We did not find significant differences between 11-nm Au-NP treated and untreated animals except for *F55G11.8* and *F49F1.5* genes, involved in innate immune response and engulfment of apoptotic cell respectively, indicating that the most affected genes after C-SPION treatment do not respond to Au-NPs in a similar manner. These results suggest that the biochemical pathways affected by

Au-NPs are distinctive and deserve further investigation by studying the whole genome of Au-NP treated worms.

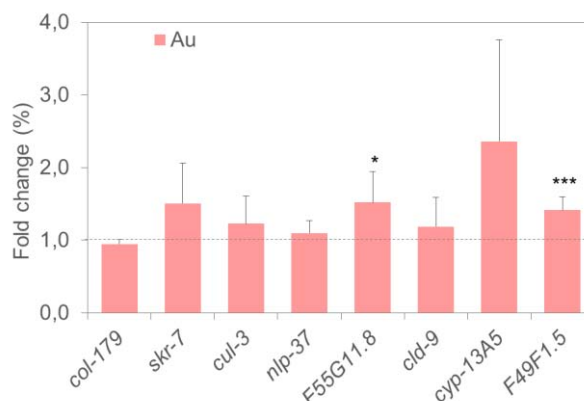


Figure 95. Study of most responsive transcripts after C-SPION exposure in 11-nm Au-NP treated nematodes.

6.5.1.3 Remarks

Gold is the least corrosive and most biologically inert of all metals together with platinum, however it can be gradually dissolved at extremely small levels to form Au^{1+} that can be oxidized to Au^{3+} inside the lysosomes resulting in pro-inflammatory and toxic effects due to the oxidant properties of Au^{3+} salts.^[253, 281-283] Although we did not detect size reduction of Au-NPs inside *C. elegans* by TEM, minute amounts of surface gold atoms could be complexed with biomolecules contributing with its consequent biological impact. In this direction, the higher surface area of the smaller nanoparticles could account for the higher toxicity of 11-nm Au-NPs compared to SPIONs based on their superior solubility. Recent work published by Sabella *et al* reported ion release from 4-nm Au-NPs *in vitro* at pH 4.5 after 24 h by ICP-MS.^[254] A similar level of ion leakage inside the intestine of *C. elegans* would lead to a size decrease too small to be robustly confirmed by TEM size distribution analysis. Furthermore, we believe that such level of dissolution could not explain alone the bioactivity of Au-NPs, therefore we propose that some nano-specific effect other than ion release might operate and determine the *in vivo* effects observed. However, to date it has not been possible to postulate and confirm such hypothetical mechanism neither *in vitro* nor *in vivo*.

6.5.2 Comparison of the effects of 11-nm Au-NPs and 6-nm SPIONs

Figure 96 presents the comparison of gene expression in worms treated with 6-nm SPIONs and 11-nm Au-NPs at concentrations with similar survival rates (500 and 100 $\mu\text{g}/\text{ml}$, respectively) both coated with citrate. The analysis of the selected pathways (panels A and B) shows significant differences in their metal detoxification and oxidative stress responses, except for *mtl-1*, both after acute and prolonged exposure. Similarly, the effects on iron homeostasis and intestinal-related genes is very dependent on NP composition irrespective of the exposure system. These results highlight the very different

in vivo behaviour of Au-NPs and SPIONs in *C. elegans*. It is remarkable that despite their similar sizes, Au-NPs do not trigger clathrin-mediated endocytosis while SPIONs do, hence we propose that this activation is composition-dependent.

The expression of the most affected genes after SPION treatment in comparison to Au-NPs (**Figure 96**) and confirms the very distinct bio-identity of the two materials *in vivo*. Only the expression of *skr-7* and *cul-3*, involved in morphogenesis and ubiquitination, respectively, was similar for the two treatments, while the other six genes responded very differently. Despite the effects on *skr-7*, no growth defects were observed after SPION either Au-NP treatment. Interestingly, in Chapter 5 we concluded that the activation of *cul-3* was coating-dependent, however the fact that it does not show composition-dependency might indicate that it is activated upon contact of *C. elegans* with inorganic nanoparticles, while the BSA coating may hide the NP core from *C. elegans* recognition based on their biomolecular nature.

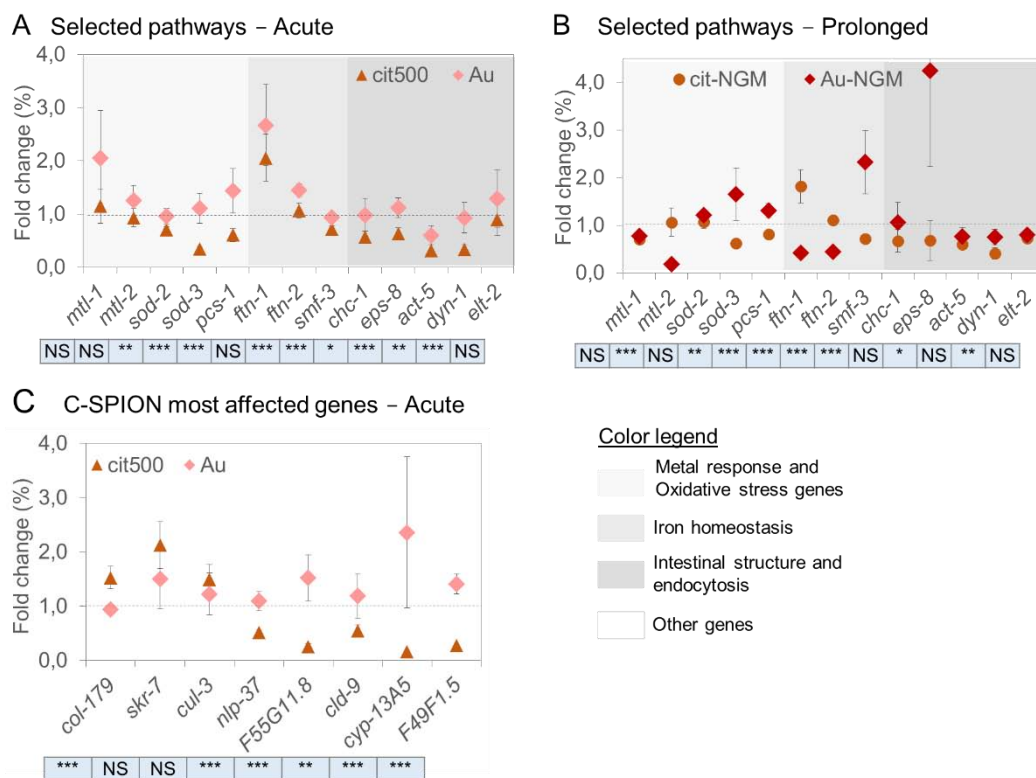


Figure 96. Comparison of the effects of 6-nm C-SPION and 11-nm citrate Au-NPs in the gene expression levels by qPCR. A,B) Selected pathways after A) acute and B) prolonged treatment. C) Expression of the most responsive genes to C-SPIONs after SPION and 11-nm Au-NP treatment.

6.6 Chapter conclusions

We exposed *C. elegans* to two sizes of in-house synthesised citrate-coated Au-NPs, 11-nm and 150-nm, to study the effects of size. We have also compared the effects of 11-nm Au-NPs with 6-nm C-SPIONs to discern the influence of composition in two nanoparticulate systems of similar size and surface coating. First, we studied the effects of NP treatment in the survival, locomotion, reproduction and growth of *C. elegans*. We found dose-dependent effects after Au-NP exposure and reported higher toxicity for the

smaller nanoparticles, in good agreement with previous findings. {Wu, 2012 #477}{Roh, 2010 #918; Meyer, 2010 #901; Ellegaard-Jensen, 2012 #905; Contreras, 2014 #904} In particular, we observed a significant decrease on brood size and lethality at 100 µg/ml in the case of 11-nm Au-NPs, but not in the case of 150-nm Au-NPs. The final length of treated animals was not affected by Au-NP treatment. The locomotion behaviour was only slightly affected at 100 µg/ml (25% decrease), and higher doses (300 µg/ml) were required to significantly decrease *C. elegans* motility. These results suggest that acute exposure to Au-NPs at concentrations up to 100 µg/ml can be considered safe as the physiological status of the survivors is not significantly compromised.

We quantified NP uptake and found that *C. elegans* ingested 500 times more 11-nm particles than the big ones, likely due to their volume four orders of magnitude smaller, although the gold content of treated worms was seven times higher in the case of the 150-nm Au-NPs. Compared to SPIONs, 11-nm Au-NP treated worms contained 5 times more metal in their body than SPION-treated animals, nonetheless it corresponded to similar surface area of the ingested NPs in contact with *C. elegans*.

In the biodistribution studies by optical and electron microscopy, we found that both Au-NPs types were contained in the intestinal lumen of *C. elegans* and no endocytosis was detected. Both materials remained monodisperse under the intestinal microenvironment, however with specific degree of confinement depending on the intestinal region (grinder, anterior gut, mid-gut and posterior gut) and NP size. Both Au-NPs kept their luminescent properties and SPR *in vivo* although with a mean red shift of ~20 nm of the peak position. We did not find clear evidence of Au-NP degradation, consistent with their chemical inertness *in vitro*, however minute dissolution to Au^{1+/3+} is plausible, which could enter the cells and trigger biochemical pathways and contribute to the biological effects observed. We did not find evidence of Au-NP entrance through the dermal route (that is, across the cuticle) or other body openings, either translocation to secondary organs such as the reproductive system in the nanoparticulate form.

The mechanistic studies confirmed that stress responses, including oxidative stress, metal detoxification and iron homeostasis, were disrupted by 11-nm Au-NPs treatment, however clathrin-mediated endocytosis was not induced. We found that Au-NPs had a more pronounced effect after prolonged exposure with food, resulting in higher stress responses than the acute treatment, and also affected to a greater extent intestine-related genes (*eps-8*, *act-5*, *dyn-1*, *elt-2*) except clathrin. We did not perform a genome-wide analysis of Au-NPs, however we studied if the most responsive genes after C-SPION treatment were also affected upon 11-nm Au-NP exposure and found that they were barely responsive, indicating that the biological responses of *C. elegans* depend on the composition of NPs even when they have similar sizes and surface properties.

Overall, we report higher toxicity of 11-nm Au-NPs than 150-nm Au-NPs, size-dependent uptake after 24 h, and similar biodistribution of the two sizes of Au-NPs with no apparent endocytosis. We propose that the higher toxicity of 11-nm Au-NPs compared to

150-nm Au-NPs could be attributed to the higher surface area of ingested NPs and the higher number of surface atoms in contact with the worms. Furthermore, we could hypothesise that soluble gold ions might form in trace amounts after Au-NP treatment, which would be able to cross the intestinal barrier and trigger different biological responses. Ion release would occur in a size-dependent manner given the superior solubility of the smaller NPs. The molecular mechanisms activated by Au-NPs could be general of nanoparticulate materials (i.e. stress responses) but also composition-dependent, based on the different gene expression response observed in respect to SPIONs.

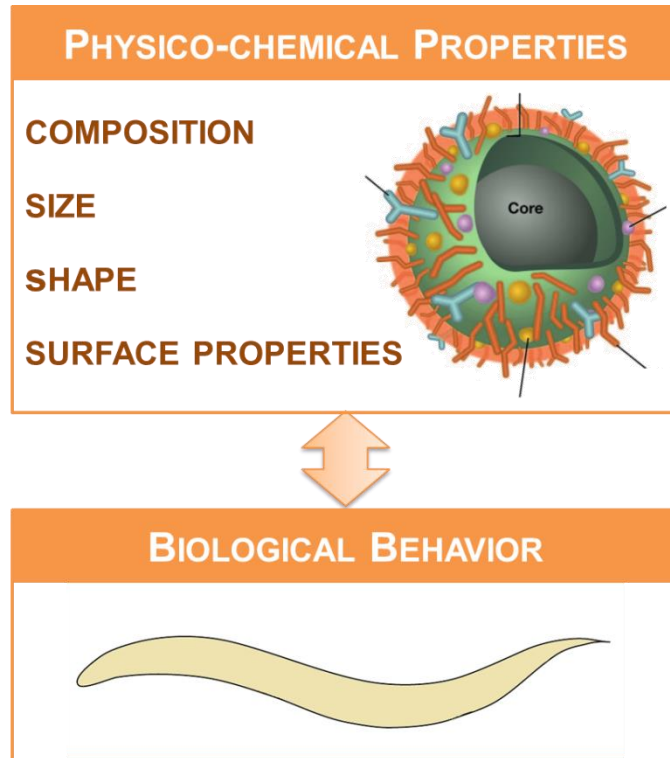
6.6.1 Effects of composition

We have compared the *in vivo* behaviour of C-SPIONs and 11-nm Au-NPs in *C. elegans* as nanoparticulate systems of different composition but comparable size and surface coating at the concentrations at which they induced a significant decrease on the survival and the brood size assays, which corresponds to 500 µg Fe/ml for the SPIONs and 100 µg Au/ml for the 11-nm Au-NPs. The comparison between 6-nm SPIONs and 11-nm Au-NPs sheds light on the different *in vivo* effects that are somehow influenced by the composition of the material core in a simple model organism. Interestingly, we have observed that the uptake of inorganic NPs, their biodistribution and the effects on molecular mechanisms have composition-dependent traits. A summary of the findings is presented in **Table 37**.

Table 37. Comparison between the *in vivo* and *in vitro* behaviour of iron oxide and gold nanoparticles of similar sizes and same surface coating.

	6-nm SPIONs	11-nm Au-NPs
Behaviour in <i>C. elegans</i>		
Biocompatibility	High	3~5 times more toxic at the same metal dose
Biodegradability	Yes (~15% size decrease)	Undetectable by TEM
Subproducts	Fe ³⁺ release	Au ^{1+/3+} salts (hypothetical)
Entrance route	Oral feeding. Dermal route is excluded.	
Biodistribution	Alimentary system (lumen+cells). No translocation to secondary organs.	Alimentary system (lumen only). No translocation to secondary organs.
Cell internalisation	Clathrin-mediated endocytosis confirmed.	No cell internalisation detected.
<i>In vivo</i> status and properties	- Monodisperse. - Superparamagnetic at room temperature.	- Monodisperse. - Red shift of the maximum absorbance peak (24 nm). - Luminescent.
<i>In vitro</i> stability		
Acid pH	Degradation	Aggregation / Precipitation. Degradation not detected.
High ionic strength	High stability	
Protein presence	Enhanced stability	

CHAPTER 7. Conclusions and future work



CHAPTER SUMMARY

This chapter summarises the main conclusions of the thesis and proposes future experiments to complement the present findings.

CHAPTER INDEX

7.1 Conclusions	163
7.2 Conclusiones	167
7.3 Conclusions	171
7.4 Future work	175
7.4.1 Future experiments	175
7.4.2 Challenges and Prospects	176

7.1 Conclusions

- 1- We have synthesised citrate- and BSA-coated 6-nm SPIONs using a microwave-assisted thermal decomposition reaction that yields monodisperse water soluble nanoparticles with good magnetic properties ($M_s=76$ emu/g Fe_2O_3 at 5 K) and high colloidal stability in biological media (22% polydispersity). We have also proved that the synthetic process can be scale-up up to 10-fold maintaining the properties of SPIONs.

We have also synthesised 11-nm citrate Au-NPs using the Frens-Turkevich method and produced 150-nm citrate Au-NPs by seeded growth through two intermediate sizes of 32 and 75 nm. The as-synthesised materials were also monodisperse, water soluble and exhibited SPR at the expected wavelengths,^[284] however they were less stable than SPIONs in biological media.

In summary, as the starting point of a comprehensive biological evaluation of NPs in C. elegans, we have produced SPIONs and Au-NPs in-house with controlled properties (surface coating and size) by means of robust reactions. We have extensively characterised the physicochemical properties of the as synthesised materials confirming good monodispersity, water solubility, good magnetic and optical properties respectively, and batch reproducibility. Finally, we have studied their colloidal stability in biological media and optimized the assay conditions for their in vivo evaluations in C. elegans.

- 2- We have proposed novel techniques to study the nano-bio interactions in *C. elegans* based on an extensive literature review and adopted the existing protocols to characterise the NP status *in vivo* by transmission electron microscopy, magnetometry, two-photon luminescence microscopy and absorbance micro-spectroscopy. We have combined these techniques with other well-established methodologies including the analysis of toxicity endpoints,^[220] chemical techniques, imaging and gene expression analysis. As a result, we have been able to draw solid conclusions of NP effects, uptake, fate, metabolism and mechanisms of action in *C. elegans*.

In conclusion, we have set up materials science techniques to complement the toolkit available for the NP assessment in C. elegans and we have confirmed the technical feasibility and information-rich nature of the experiments to advance in the evaluation of the interaction between nanomaterials and C. elegans.

- 3- We have studied in depth the interaction of 6-nm SPIONs (citrate-coated and BSA-coated) and citrate-coated Au-NPs (of 11 nm and 150 nm) over a wide dose range in the model organism *C. elegans* to understand the portals of entry and exit of NPs,

their biodistribution and metabolism, their status *in vivo*, and their biological and molecular effects. We have also investigated the influence of NP size, composition and surface properties in *C. elegans*.

- a. We have studied the biocompatibility of SPIONs and Au-NPs after 24 h treatment to doses up to 500 µg/ml and reported lower LD₅₀ for SPIONs (600 *versus* 350 µg/ml), indicating the higher tolerance of *C. elegans* to iron oxide and confirming the high biocompatibility of both materials at expected clinical doses, which are far below the reported LD₅₀. Furthermore, the biological functions of the surviving animals such as their reproduction ability were not dramatically impaired after cessation of the exposure and animals could recover upon transfer to standard culture conditions. Remarkably, the study up to high doses has been possible due to the lack of ethical regulations over the use of *C. elegans*, which results very advantageous at the early stages of discovery compared to the use of mammalian model organism.
- b. We have observed differences in the effects of SPIONs depending on their surface coating, resulting BSA-SPIONs less harmful than C-SPIONs. We hypothesise that BSA may minimize the interaction between the *C. elegans* cells and the SPION core and reduce the recognition of BSA-SPIONs as a foreign body by acting as a biomimetic shell. We have also found differences in the effects of Au-NPs depending on their size, being the smaller particles the most damaging. We propose that the higher surface area of the smaller Au-NPs exposed to the worm can lead to superior reactivity and bioactivity compared to the 150-nm Au-NPs.
- c. We reported NP entrance solely during the feeding processes of *C. elegans* through the alimentary system, but neither through the cuticle (dermal route) nor through other body openings such as the excretory pore or the vulva. We found differences on nanoparticle biodistribution depending on the composition: SPIONs were located in the intestinal lumen and also intracellularly in the lysosomal compartment of the intestinal cells of *C. elegans* (although it corresponded to a small fraction compared to the lumen loading), while Au-NPs were restricted to the intestinal lumen and not internalised by the intestinal cells (**Table 38**). Indeed, Au-NPs were observed separated from the microvilli by the glycocalyx at all times whereas individual SPIONs were observed within the glycocalyx. We attribute the differences in the internalisation to the composition of the NPs: while the essential nature of iron for *C. elegans* could trigger some pathways in favour of iron storage, the non-essential property of gold and their chemical inertness could not activate such mechanisms, as confirmed in the gene expression analysis. We did not detect NP translocation to secondary organs for any of the NPs.

Table 38. Biodistribution of inorganic nanoparticles in the model organism *C. elegans*.

	Citrate coated Au-NPs		6-nm SPIONs	
	11 nm	150 nm	Citrate coated	BSA coated
Intestine – lumen	✓	✓	✓	✓
Intestine – glycocalyx	✗	✗	✓	✓
Intestine – cells	✗	✗	✓	✓
Reproductive organs / Eggs	✗	✗	✗	✗
Cuticle	✗	✗	✗	✗

✓ NPs detected in the area ✗ NPs not detected in the area

- d. We characterised the NP status (size and aggregation) inside *C. elegans* and found a superior resistance to degradation of Au-NPs compared to SPIONs. C-SPIONs and BSA-SPIONs showed similar level of agglomeration inside *C. elegans*, however C-SPIONs were degraded to a greater extent than BSA-SPIONs *in vivo*. Interestingly, both SPIONs maintained their superparamagnetism inside the worm.

We characterised the absorbance of Au-NPs inside *C. elegans* and observed a ~20 nm red peak shift of the SPR, indicative of particle confinement. Interestingly, We found that such aggregation was reversible and determined by the properties of the surrounding environment, mainly pH and presence of biomolecules. By TEM, We could not detect a significant size variation of the Au-NPs inside *C. elegans*; however, we do not discard minute ion release of Au^{1+/3+} in the intestinal microenvironment of *C. elegans*.

- e. We have compared the *in vivo* results with *in vitro* experiments using intestinal and lysosomal simulated conditions, which yielded very similar results than the *in vivo* experiments confirming that the biological environment of the NPs inside *C. elegans* can determine the nano-bio interaction to a great extent.
- f. We detected that oxidative stress and metal detoxification mechanisms were affected by NP treatment. By gene expression analysis, We found disruption of these molecular mechanisms in NP-treated *C. elegans*, although not consistently in all the conditions and genes studied, suggesting that they might be involved in the responses triggered by NP exposure. However, they may not be general nano-toxicity mechanisms governing NP *in vivo* effects. Based on my experimental results, we propose that the biochemical routes responsive to NP exposure might be determined by a combination of NP size, coating and composition. Finally, ion release can also have an influence on the *in vivo* effects of NPs.

This in-depth study of inorganic NPs in C. elegans confirms the potential of C. elegans as a model organism for NP evaluation within the synthetic laboratory, revealing correlation of NP initial properties with their in vivo effects. Remarkably, we were able

to characterise the effects and status of NPs in C. elegans at different biological levels (organism, organ, cellular and subcellular), to track their fate with single particle resolution, and to study the molecular mechanisms responsive to NP exposure.

All in all, this thesis has contributed to: i) extend the toolkit of techniques available for the characterisation of nano-bio interactions in *C. elegans*; ii) a systematic and comprehensive evaluation of the interaction of inorganic nanoparticles with the model organism *C. elegans*, starting from the synthesis of the material; and iii) study the influence of NP properties such as size, surface coating and composition on their *in vivo* effects.

7.2 Conclusiones

- 1- Hemos sintetizado nanopartículas superparamagnéticas de óxido de hierro de 6 nm de diámetro recubiertas de citrato y BSA a través de una reacción de descomposición termal asistida por microondas, obteniendo nanopartículas solubles en agua con buenas propiedades magnéticas (M_s de 76 emu/g Fe_2O_3 a 5 K) y una elevada estabilidad coloidal en medio biológico (polidispersidad del 22%). También hemos demostrado que esta reacción sintética puede ser escalada 10 veces manteniendo la misma calidad de producto.

Hemos sintetizado también nanopartículas de oro de 11 nm de diámetro recubiertas de citrato mediante el método de Frens-Turkevich y obtenido nanopartículas de 150 nm por crecimiento a través de los tamaños intermedios de 32 y 75 nm. Estas nanopartículas eran también monodispersas, solubles en agua y exhibían su resonancia plasmónica de superficie a la longitud de onda esperada,^[284] sin embargo su estabilidad en medio biológico es inferior a la de las nanopartículas de óxido de hierro.

*En resumen, como punto de partida de una evaluación biológica completa de nanopartículas en *C. elegans*, hemos producido nanopartículas de óxido de hierro y de oro controlando su tamaño y recubrimiento superficial empleando reacciones de síntesis robustas. Hemos caracterizado de forma extensa las propiedades fisicoquímicas de los materiales obtenidos, confirmando su monodispersión, solubilidad en agua, sus buenas propiedades magnéticas y ópticas respectivamente, y la reproducibilidad entre lotes. Finalmente, hemos estudiado su estabilidad coloidal en medio biológico y optimizado las condiciones experimentales para la evaluación *in vivo* en *C. elegans*.*

- 2- Hemos propuesto nuevas técnicas para el estudio de la interacción nano-bio en *C. elegans* en base a una extensa revisión bibliográfica, y hemos adaptado los protocolos existentes para la caracterización del estado de las NP *in vivo* a través de microscopía electrónica de transmisión, magnetometría, microscopía de luminiscencia de dos fotos y micro-espectroscopía de absorbancia. Hemos combinado estas técnicas con ensayos de parámetros toxicológicos,^[220] análisis químicos, técnicas de imagen y análisis de la expresión génica. Como resultado, hemos sido capaz de llegar a conclusiones sólidas acerca de los efectos de las nanopartículas, la ingesta, la localización, el metabolismo y los mecanismos de acción en *C. elegans*.

*En conclusión, hemos utilizado técnicas de ciencia de materiales para complementar el abanico de herramientas disponibles para evaluar nanopartículas en *C. elegans* y he confirmado su viabilidad técnica y el carácter altamente informativo de los*

experimentos para avanzar en el estudio de la interacción entre nanomateriales y C. elegans.

- 3- Hemos estudiado en profundidad la interacción de las SPIONs de 6 nm (recubiertas de citrato y de BSA) y de las Au-NPs (de 11 nm y 150 nm) sintetizadas en un amplio rango de dosis en el modelo animal *C. elegans* para entender las vías de entrada de NPs al cuerpo y de salida, su biodistribución y metabolismo, su estado *in vivo*, y sus efectos toxicológicos y moleculares. También hemos estudiado la influencia de diferentes parámetros fisicoquímicos en *C. elegans*: su tamaño, composición y propiedades superficiales.
 - a. Hemos evaluado la biocompatibilidad de las SPIONs y de las Au-NPs tras 24 h de tratamiento de dosis hasta los 500 µg/ml y observado que la dosis letal 50 (LD₅₀) de lo SPIONs era mayor que la del oro (600 *versus* 350 µg/ml), lo cual indica una elevada tolerancia de *C. elegans* al óxido de hierro y confirma la elevada biocompatibilidad de ambos materiales a las dosis clínicas previstas en humanos, muy inferiores a los valores LD₅₀ encontrados. Además, las funciones biológicas de los animales supervivientes tales como su fertilidad no se vieron afectadas de forma drástica una vez cesó el tratamiento y se pudieron recuperar en condiciones estándar de cultivo. Cabe destacar que el estudio de dosis altas en *C. elegans* es posible gracias a que el uso de *C. elegans* no se encuentra sometido a regulaciones éticas, lo cual resulta muy ventajoso en etapas iniciales de desarrollo de nuevos materiales comparado con el uso de mamíferos.
 - b. Hemos detectado diferencias en los efectos de las SPIONs según su recubrimiento, siendo las recubiertas de BSA menos perjudiciales que las recubiertas de citrato. Mi hipótesis es que el BSA puede minimizar la interacción entre las células de *C. elegans* y las SPIONs y reducir el reconocimiento de las BSA-SPIONs como un agente externo, actuando como un recubrimiento biomimético. También hemos encontrado diferencias en los efectos de las Au-NPs según su tamaño, siendo las nanopartículas pequeñas las más nocivas. Es posible que la mayor área superficial de las Au-NPs de 11 nm expuesta al gusano resulte en una reactividad y un impacto biológico superior de éstas en comparación con las Au-NPs de 150 nm.
 - c. Hemos observado entrada de nanopartículas en *C. elegans* únicamente durante el proceso de alimentación a través del sistema alimentario, pero no a través de la cutícula (vía cutánea) ni a través de otros orificios del cuerpo como el poro excretor o la vulva. Hemos detectado diferencias en la biodistribución de las nanopartículas según su composición: las SPIONs se encontraban en la luz intestinal y una pequeña fracción también en el compartimento lisosomal de las células intestinales de *C. elegans*, mientras que las Au-NPs sólo se

localizaban en la luz intestinal y no eran internalizadas por las células intestinales (Table 39). De hecho, las Au-NPs fueron siempre observadas separadas del microvilli por el glicocálix mientras que SPIONs individuales sí que fueron observadas en el interior del glicocálix. Mi hipótesis es que las diferencias en internalización son atribuibles a la diferente composición química de las NPs: mientras que el hierro es un metal esencial para *C. elegans* que puede activar rutas bioquímicas específicas para aumentar el almacenamiento del hierro, el animal no dispone de rutas que favorezcan la acumulación de oro dada su naturaleza no esencial. Sin embargo, en ningún caso detecté translocación de NPs a órganos secundarios.

Table 39. Biodistribución de las SPIONs y las Au-NPs estudiadas en *C. elegans*.

	Au-NPs recubiertas de citrato		SPIONs de 6-nm	
	11 nm	150 nm	Recubiertas de citrato	Recubiertas de BSA
Intestino – luz	✓	✓	✓	✓
Intestino – glicocálix	×	×	✓	✓
Intestino – células	×	×	✓	✓
Órganos reproductores / Huevos	×	×	×	×
Cutícula	×	×	×	×

✓ NPs detectadas en esa zona × NPs no detectadas en esa zona

- d. Hemos caracterizado el estado de las NPs (tamaño y agregación) dentro del cuerpo de *C. elegans* y detectado una mayor resistencia a la degradación de las Au-NPs comparado con las SPIONs. Los dos tipos de SPIONs mostraron niveles similares de aglomeración dentro de *C. elegans*, sin embargo las SPIONs recubiertas de citrato se degradaron en mayor medida *in vivo* que las recubiertas de BSA. Cabe destacar que ambas NPs mantuvieron su carácter superparamagnético dentro del gusano.

Hemos caracterizado la absorbancia de las Au-NPs dentro de *C. elegans* y observado un desplazamiento del pico de SPR de unos 20 nm hacia el rojo, lo cual indica el confinamiento de las NPs en *C. elegans*. Es destacable que la agregación detectada es de tipo reversible y puede venir determinada en gran parte por las propiedades del entorno de las NPs, en especial por el pH y la presencia de biomoléculas. Empleando TEM no detecté un cambio significativo del tamaño de las Au-NPs dentro de *C. elegans*, sin embargo no descarto la hipótesis de que cantidades mínimas de oro puedan liberarse de las Au-NPs en forma de iones debido al microambiente intestinal de *C. elegans*.

- e. Hemos comparado los resultados obtenidos *in vivo* con los resultados de experimentos *in vitro* simulando las condiciones lisosomales e intestinales de *C. elegans*, obteniendo resultados muy similares en ambos casos, lo cual

confirma que las características del entorno en el que se encuentran las NPs en el interior de *C. elegans* pueden determinar en gran parte la interacción nano-bio.

- f. Hemos visto que los mecanismos de estrés oxidativo y de detoxificación de metales se ven afectados por el tratamiento con NPs. A través del análisis de la expresión génica, detecté alteración de estas rutas en gusanos tratados con SPIONs y Au-NPs, aunque no de forma uniforme en todas las condiciones y genes estudiados, lo cual sugiere que pueden estar implicadas en la respuesta de *C. elegans* a la exposición a NPs. Sin embargo, estos mecanismos pueden no ser generales de todas las nanopartículas ni ser los que determinan los efectos de las NPs *in vivo*. En base a mis resultados experimentales, sugiero que las rutas bioquímicas activadas por el tratamiento con NPs pueden venir determinadas por una combinación de sus parámetros fisicoquímicos incluyendo tamaño, recubrimiento y composición. Finalmente, también es plausible que se liberen iones de las NPs que también influyan los efectos *in vivo* de las NPs.

Este estudio detallado de NPs inorgánicas en C. elegans confirma el potencial de C. elegans como modelo animal para la evaluación de NPs en el laboratorio sintético y evidencia correlación entre las propiedades iniciales de las NPs y sus efectos in vivo. Es destacable el hecho de haber podido caracterizar los efectos y el estado de las NPs en C. elegans en diferentes escalas biológicas (a nivel de organismo, de órgano, de célula y subcelular), haber podido monitorear la localización de las NPs con resolución espacial nanométrica, y haber explorado los mecanismos moleculares afectados por la exposición a NPs.

En conclusión, esta tesis ha contribuido a: i) ampliar el conjunto de técnicas disponibles para caracterizar la interacción nano-bio en *C. elegans*; ii) una evaluación sistemática y completa de la interacción de nanopartículas inorgánicas con el modelo animal *C. elegans*, empezando desde la síntesis del material; y iii) estudiar la influencia de las propiedades de las NPs tales como tamaño, superficie y composición en sus efectos *in vivo*.

7.3 Conclusions

- 1- Hem sintetitzat nanopartícules superparamagnètiques d'òxid de ferro de 6 nm de diàmetre recobertes de citrat i BSA a través de una reacció de descomposició termal assistida per microones, obtenint nanopartícules solubles en aqua amb bones propietats magnètiques (M_s de 76 emu/g Fe_2O_3 a 5 K) i una elevada estabilitat col·loïdal en medi biològic (polidispersitat del 22%). També hem demostrat que aquesta reacció sintètica pot ser escalada 10 vegades mantenint l'elevada qualitat del producte final.

Hem sintetitzat també nanopartícules d'or de 11 nm de diàmetre recobertes de citrat mitjançant el mètode de Frens-Turkevich i obtingut nanopartícules de 150 nm per creixement a través de les mides intermèdies de 32 i 75 nm. Aquestes nanopartícules eren també monodisperses, solubles en aqua i exhibien la seva ressonància plasmònica de superfície a la longitud d'ona esperada,^[284] no obstant la seva estabilitat en medi biològic és inferior a la de les nanopartícules d'òxid de ferro.

*En resum, com a punt de partida per l'avaluació biològica completa de nanopartícules en *C. elegans*, hem produït nanopartícules d'òxid de ferro i d'or controlant la seva mida i el seu recobriment superficial a través de reaccions de síntesi robustes. Hem caracteritzat de forma extensa les propietats fisicoquímiques dels materials obtinguts, confirmant la seva monodispersió, solubilitat en aqua, les seves bones propietats magnètiques i òptiques respectivament, i la reproductibilitat entre lots. Finalment, hem estudiat la seva estabilitat col·loïdal en medi biològic i optimitzat les condicions experimentals per l'avaluació in vivo en *C. elegans*.*

- 2- Hem proposat noves tècniques per l'estudi de la interacció nano-bio en *C. elegans* en base a una extensa revisió bibliogràfica i hem adaptat els protocols existents a la caracterització de l'estat de les NP *in vivo* a través de microscòpia electrònica de transmissió, magnetometria, microscòpia de luminescència de dos fotos i micro-espectroscòpia d'absorbància. Hem combinat aquestes tècniques amb assajos de paràmetres toxicològics,^[220] anàlisis químics, tècniques d'imatge i anàlisis de l'expressió gènica. Com a resultat, hem estat capaç d'assolir conclusions sòlides dels efectes de les nanopartícules, la ingesta, la localització, el metabolisme i els mecanismes d'acció en *C. elegans*.

*En conclusió, hem utilitzat tècniques de ciència de materials para complementar el ventall d'eines disponibles per avaluar nanopartícules en *C. elegans* i hem confirmat el seu viabilitat tècnica i el caràcter altament informativa dels experiments per avançar en l'estudi de la interacció entre nanomaterials i *C. elegans*.*

- 3- Hem estudiat en profunditat la interacció de les SPIONs de 6 nm (recobertes de citrat i de BSA) i de les Au-NPs (de 11 nm i 150 nm) sintetitzades en un ampli rang de dosis en el modelo animal *C. elegans* per entendre les vies d'entrada de NPs al cos, la seva biodistribució i metabolisme, el seu estat *in vivo*, i els seus efectes toxicològics i moleculars. També hem estudiat la influència de diferents paràmetres fisicoquímics en *C. elegans*: la seva mida, composició i propietats superficials.
- Hem avaluat la biocompatibilitat de les SPIONs i de les Au-NPs després de 24 h de tractament de dosis fins els 500 µg/ml i observat que la dosis letal 50 (LD₅₀) dels SPIONs era més elevada que la de l'or (600 *versus* 350 µg/ml), cosa que revela una elevada tolerància de *C. elegans* a l'òxid de ferro i confirma l'elevada biocompatibilitat d'ambdós materials a les dosis clíniques previstes en humans, molt inferior als valors LD₅₀ trobats. A més, les funcions biològiques dels animals supervivents com la seva capacitat reproductiva no es van veure afectats de forma dràstica una cop els cucs tractats es van transferir a condicions de cultiu estàndard, en absència de NPs. És destacable que l'estudi de dosis altes en *C. elegans* és possible gracies a que el uso de *C. elegans* no es troba sotmès a regulacions ètiques, cosa que resulta molt beneficiós en les etapes inicials del desenvolupament de nous materials en comparació amb l'ús de mamífers.
 - Hem detectat diferències en els efectes de les SPIONs en funció del seu recobriment, sent les recobertes de BSA menys perjudicials que les recobertes de citrat. La meua hipòtesi és que el BSA pot minimitzar la interacció entre les cèl·lules de *C. elegans* i les SPIONs i reduir el reconeixement de les BSA-SPIONs com un agent extern, actuant com una capa protectora biomimètica. També hem trobat diferències en els efectes de les Au-NPs depenent de la seva mida, sent les nanopartícules petites les mes nocives. És possible que el fet que les 11-nm Au-NPs tinguin una àrea superficial més gran exposada al cuc resulti en una reactivitat i un impacte biològic superior que en el cas de les Au-NPs de 150 nm.
 - Hem observat entrada de nanopartícules al cos de *C. elegans* únicament durant el procés d'alimentació a través del sistema alimentari, però no a través de la cutícula (via cutània) ni a través d'altres orificis del cos como el porus excretor o la vulva. Hem detectat diferències en la biodistribució de les nanopartícules segons la seva composició: les SPIONs es trobaven en la llum intestinal i, en petita proporció, també en el compartiment lisosomal de les cèl·lules intestinals de *C. elegans*, mentre que les Au-NPs només es localitzaven en la llum intestinal i no eren internalitzades per les cèl·lules intestinals (**Table 40**). De fet, les Au-NPs sempre es trobaven separades del microvilli pel glicocàlix mentre que sí que s'observaven SPIONs individuals en l'interior del glicocàlix. La meua hipòtesi és que les diferències en internalització són atribuïbles a la diferent composició

química de les NPs: mentre que el ferro és un metall essencial per *C. elegans* que pot activar rutes bioquímiques específiques per augmentar l'emmagatzemament del ferro, l'animal no disposa de rutes que afavoreixin l'acumulació d'or donat que no es tracta d'un metall essencial. En qualsevol cas, no hem detectat translocació de NPs a òrgans secundaris ni en el cas de les SPIONs ni de les Au-NPs.

Table 40. Biodistribució de les SPIONs i les Au-NPs estudiades en *C. elegans*.

	Au-NPs recobertes de citrat		SPIONs de 6-nm	
	11 nm	150 nm	Recobertes de citrat	Recobertes de BSA
Intestí – llum	✓	✓	✓	✓
Intestí – glicocàlix	×	×	✓	✓
Intestí – cèl·lules	×	×	✓	✓
Òrgans reproductors / Ous	×	×	×	×
Cutícula	×	×	×	×

✓ NPs detectades en aquella zona × NPs no detectades en aquella zona

- d. Hem caracteritzat el estat de les NPs (mida i agregació) dins del cos de *C. elegans* i detectat una resistència superior a la degradació de les Au-NPs comparat amb les SPIONs. Els dos tipus de SPIONs van exhibir nivells similars d'aglomeració dins de *C. elegans*, no obstant les SPIONs recobertes de citrat es degradaven en major proporció *in vivo* que les recobertes de BSA. Cal destacar que ambdues NPs van mantenir el seu caràcter superparamagnètic dins el cuc. Hem caracteritzat l'absorbància de les Au-NPs dins de *C. elegans* i observat un desplaçament del pic de SPR d'uns 20 nm cap al vermell, cosa que indica el confinament de les NPs en *C. elegans*. És destacable que l'agregació detectada és reversible i pot venir determinada en gran part per les propietats de l'entorno de les NPs, en especial pel pH i la presència de biomolècules. Mitjançant TEM no hem detectat un canvi significatiu de la mida de les Au-NPs dins de *C. elegans*, tot i això no descarto la hipòtesis que quantitats mínimes d'or es puguin alliberar de les Au-NPs en forma de ions degut al microambient intestinal de *C. elegans*.
- e. Hem comparat els resultats obtinguts *in vivo* amb els resultats d'experiments *in vitro* simulant les condicions lisosomals i intestinals de *C. elegans*, obtenint resultats molt similars en ambdós casos, cosa que confirma que les característiques de l'entorno en el que es troben les NPs a l'interior de *C. elegans* poden determinar en gran part la interacció nano-bio.
- f. Hem detectat que els mecanismes d'estrés oxidatiu i de detoxificació de metalls s'afecten pel tractament amb NPs. A través de l'anàlisi de l'expressió gènica, hem detectat alteració d'aquestes rutes en cucs tractats amb SPIONs i Au-NPs, tot i que no de manera uniforme en totes les condicions i gens estudiats, cosa que

suggereix que poden estar implicades en la resposta de *C. elegans* a l'exposició a NPs. No obstant, aquests mecanismes poden no ser generals de tots les nanopartícules ni ser els que determinen els efectes de les NPs *in vivo*. En base als meus resultats experimentals, suggereixo que les rutes bioquímiques activades pel tractament amb NPs poden venir determinades per una combinació dels seus paràmetres fisicoquímics incloent mida, recobriment i composició. Finalment, també es plausible que s'alliberin ions de les NPs que també influeixin en els efectes *in vivo* de les NPs.

Aquest estudi detallat de NPs inorgàniques en C. elegans confirma el potencial de C. elegans com a modelo animal per l'avaluació de NPs en el laboratori sintètic i evidencia correlació entre les propietats inicials de les NPs i els seus efectes in vivo. És destacable el fet d'haver pogut caracteritzar els efectes i el estat de les NPs en C. elegans en diferents escales biològiques (a nivell d'organisme, d'òrgan, de cèl·lula i subcel·lular), haver pogut monitoritzar la localització de les NPs amb resolució espacial nanomètrica, i haver també explorat els mecanismes moleculars afectats per l'exposició a NPs.

En conclusió, aquesta tesis ha contribuït a: i) ampliar el conjunt de tècniques disponibles per caracteritzar la interacció nano-bio en *C. elegans* ; ii) una avaluació sistemàtica i completa de la interacció de nanopartícules inorgàniques amb el model animal *C. elegans* , començant des de la síntesi del material; i iii) estudiar la influència de les propietats de les NPs (mida, superfície i composició) en els seus efectes *in vivo*.

7.4 Future work

7.4.1 Future experiments

We aim to perform further experiments on SPION-treated *C. elegans* to track the fate of the BSA coating *in vivo* in order to monitor their stability in different locations of the *C. elegans* intestine and determine whether the BSA coating is preserved inside the lysosomal compartment, which could account for the different biological effects observed between C- and BSA-SPIONs. To this aim, we plan to prepare ultrathin cross-sections of treated nematodes and perform immunolabelling using a primary anti-BSA antibody and a secondary antibody linked to a 10-15 nm Au-NPs that specifically binds to the primary antibody. TEM observations of the as prepared samples can shed light on the stability of the BSA coating in a three-dimensional complex biological environment. **Figure 97** shows the technique fundament and expected results. These experiments will be performed in collaboration with the Electron Microscopy Core Facility at EMBL, Heidelberg. Complementarily, we plan to try immunostaining experiments using the same cross-sections and primary antibody as in the case of immunogold, but using a secondary fluorescently-labelled antibody with the aim to apply super-resolution microscopy to the samples, in collaboration with Dr. Lorenzo Albertazzi from Institute for Bioengineering of Catalonia (IBEC), Barcelona.

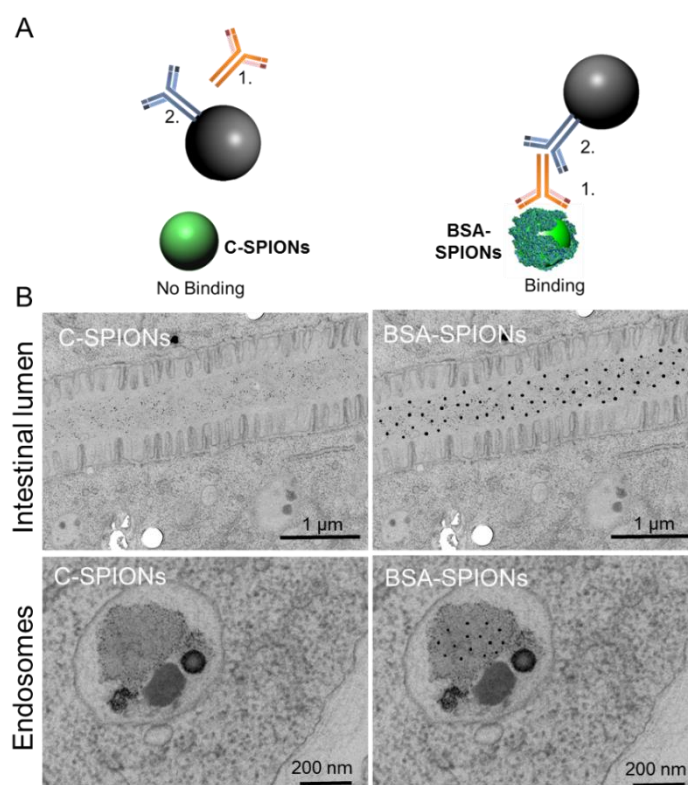


Figure 97. A) Fundamentals of immunolabeling. 1. Primary antibody (anti-BSA) 2. Secondary antibody linked to a Au-NP. D) Expected results in C-SPIION and BSA-SPIION treated worms. We hypothesise that the BSA coating is preserved inside the intestinal lumen of *C. elegans* and also inside endosomes until the enzymes and the acidic pH completely degrade the coating.

Regarding the evaluation of gold nanoparticles in *C. elegans*, it would be interesting to perform microarray experiments to compare the effects of 11-nm Au-NPs versus C-SPIONs in a genome-wide manner and conclude composition-specific effects on the activation of molecular mechanisms. In addition, samples consisting of the RNA of 150-nm Au-NP treated worms could also be prepared and analysed using microarrays in order to study the effect of size at the transcriptome level by comparing with the gene expression levels of 11-nm AuNP treated worms. In addition, to confirm the effects of the BSA coating, a monolayer of BSA could be adsorbed onto the surface of 11-nm Au-NPs. I applied the BSA adsorption protocol reported by Yu *et al*^[85] to 11-nm Au-NPs and observed the formation of an organic layer around the metallic NP core that did not alter the initial optical properties of the 11-nm Au-NPs (**Figure 98**). This material could be further evaluated in *C. elegans*.

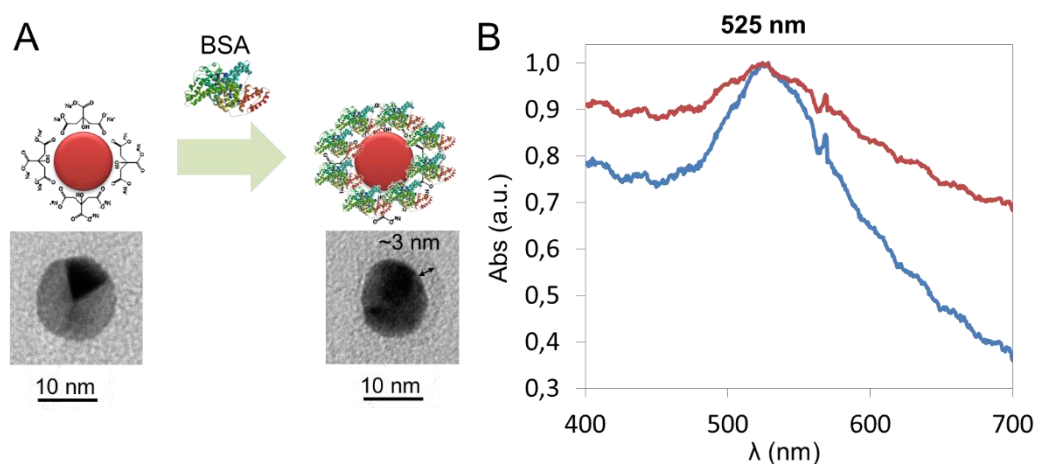


Figure 98. TEM images and UV/Vis spectra of C-Au-NPs and BSA-Au-NPs.

Finally, the study of inorganic nanoparticles in *C. elegans* could be extended to other compositions including titania or silver nanoparticles based on the expertise of the group in NP synthesis.

7.4.2 Challenges and Prospects

Despite the numerous advantages of the use of simple model organisms to evaluate new materials, these experiments can be extremely challenging considering the lack of standardized protocols and the need to adapt some techniques before applying them in *C. elegans* samples.

To advance in the field, the toolkit of techniques to characterise small animals treated with NPs could be further extended and the suitability of the novel techniques to extract meaningful information should be investigated. Some of the tools that we propose to be assayed are: microbeam analysis (i.e. infrared μ -spectroscopy or transmission X-ray microscopy), advanced imaging techniques such as light sheet microscopy, or more physicochemical approaches by means of NMR spectroscopy, thermogravimetric analysis, among others. Their use would allow us to gather more information about nano-bio interactions in small organisms following a top-down approach, from organism level

down to the nanometric resolution of the cell compartments, taking advantage of the high spatial resolution and high sensitivity of these techniques, among other promising features. At the same time, they would provide relevant information about the nanomaterials' properties *in vivo* and their fate, contributing to the correlation between the nanomaterials' initial properties and their behavior in a multicellular animal.

From the *C. elegans* perspective, given that the assay conditions vary from laboratory to laboratory, the definition of standardized protocols to perform NP evaluation in *C. elegans* would be highly recommended, as attempted by the recent publication of Maurer *et al*{Maurer, 2015 #1027}. In addition, *C. elegans* has its genome sequenced and it is used to perform robust genetic investigations. In this sense, we can find in the *Caenorhabditis* Genetics Center and within the *C. elegans* community mutant strains with specific deletions and also knock out animals, which offer specific characteristics and sensitivities that could be exploited to track down the biological effects of nanomaterials in *C. elegans*. The availability of mutants, together with the easy genetic manipulation of the worms (i.e. by RNA interference), allow scientists to dissect molecular pathways with precision. Therefore, *C. elegans* results in a very convenient biological platform to identify nanotoxicity mechanisms and to validate biochemical routes affected by NP exposure in human cells or other animals.

In a similar manner, the use of *C. elegans* as a terrestrial model organism can contribute to shedding light on controversial findings with environmental relevance. For instance, very recently Maher *et al* reported that airborne nanoparticles from industrial air pollution were able to get to the human brain contributing to the development of neurodegenerative diseases such as Alzheimer.{Maher, 2016 #1041} In this direction, *C. elegans* allows a rapid evaluation of the impact of nanoparticles in neurons and neurosignalling pathways, in the accumulation of β -amyloid or the ageing process. Hence, *C. elegans* could provide worthy evidence to validate or refute such alarming conclusions faster than using higher animals or clinical trials.

To sum up, we truly believe that a joint effort of the *C. elegans* community and material scientists, pushed by the desire to better understand nano-bio interactions, will make a substantial leap forward in the field of nano-bio interactions.

THESIS REFERENCES

1. Ramsden, J.J., *Chapter 1 - What is Nanotechnology?*, in *Nanotechnology*. 2011, William Andrew Publishing: Oxford. p. 1-14.
2. Ramsden, J.J., *Chapter 2 - The Nanoscale*, in *Nanotechnology*. 2011, William Andrew Publishing: Oxford. p. 15-34.
3. Kreyling, W.G., M. Semmler-Behnke, and Q. Chaudhry, *A complementary definition of nanomaterial*. *Nano Today*, 2010. **5**(3): p. 165-168.
4. Ramsden, J.J., *Chapter 12 - The Impact of Nanotechnology*, in *Nanotechnology*. 2011, William Andrew Publishing: Oxford. p. 227-246.
5. Vance, M.E., et al., *Nanotechnology in the real world: Redeveloping the nanomaterial consumer products inventory*. *Beilstein Journal of Nanotechnology*, 2015. **6**: p. 1769-1780.
6. Ramsden, J.J., *Chapter 11 - Bionanotechnology*, in *Nanotechnology*. 2011, William Andrew Publishing: Oxford. p. 213-225.
7. Silva, G.A., *Introduction to nanotechnology and its applications to medicine*. *Surgical Neurology*, 2004. **61**(3): p. 216-220.
8. Jain, K.K., *Future of nanomedicine: impact on healthcare & society*. *Nanomedicine (Lond)*, 2015. **10**(21): p. 3199-202.
9. Lammers, T., et al., *Theranostic Nanomedicine*. *Accounts of Chemical Research*, 2011. **44**(10): p. 1029-1038.
10. Prabhu, P. and V. Patravale, *The Upcoming Field of Theranostic Nanomedicine: An Overview*. *Journal of Biomedical Nanotechnology*, 2012. **8**(6): p. 859-882.
11. Nahar, M., et al., *Functional polymeric nanoparticles: an efficient and promising tool for active delivery of bioactives*. *Crit Rev Ther Drug Carrier Syst*, 2006. **23**(4): p. 259-318.
12. Jain, K., N.K. Mehra, and N.K. Jain, *Potentials and emerging trends in nanopharmacology*. *Curr Opin Pharmacol*, 2014. **15**: p. 97-106.
13. Colvin, V.L., *The potential environmental impact of engineered nanomaterials*. *Nat Biotechnol*, 2003. **21**(10): p. 1166-70.
14. Oberdorster, G., E. Oberdorster, and J. Oberdorster, *Nanotoxicology: An emerging discipline evolving from studies of ultrafine particles*. *Environmental Health Perspectives*, 2005. **113**(7): p. 823-839.
15. Zellner, R., *Biological responses to nanoscale particles*. *Beilstein Journal of Nanotechnology*, 2015. **6**: p. 380-382.
16. Ramsden, J.J., *Chapter 4 - The Nano/Bio Interface*, in *Nanotechnology*. 2011, William Andrew Publishing: Oxford. p. 53-71.
17. Gormley, A.J. and H. Ghandehari, *Evaluation of Toxicity of Nanostructures in Biological Systems*, in *Nanotoxicity*. 2009, John Wiley & Sons, Ltd. p. 115-159.
18. Stone, V., et al., *Nanomaterials for environmental studies: Classification, reference material issues, and strategies for physico-chemical characterisation*. *Science of The Total Environment*, 2010. **408**(7): p. 1745-1754.
19. Chan, V.S.W., *Nanomedicine: An unresolved regulatory issue*. *Regulatory Toxicology and Pharmacology*, 2006. **46**(3): p. 218-224.
20. Demetzos, C., *Regulatory Framework for Nanomedicines*, in *Pharmaceutical Nanotechnology: Fundamentals and Practical Applications*. 2016, Springer Singapore: Singapore. p. 189-203.
21. Irache, J.M., et al., *Nanomedicine: Novel approaches in human and veterinary therapeutics*. *Veterinary Parasitology*, 2011. **180**(1-2): p. 47-71.
22. Muthu, M.S., et al., *Nanotheranostics - Application and Further Development of Nanomedicine Strategies for Advanced Theranostics*. *Theranostics*, 2014. **4**(6): p. 660-677.
23. Barenholz, Y., *Doxil(R)--the first FDA-approved nano-drug: lessons learned*. *J Control Release*, 2012. **160**(2): p. 117-34.
24. Sekhon, B.S. and S.R. Kamboj, *Inorganic nanomedicine-Part 1*. *Nanomedicine-Nanotechnology Biology and Medicine*, 2010. **6**(4): p. 516-522.
25. Sekhon, B.S. and S.R. Kamboj, *Inorganic nanomedicine-Part 2*. *Nanomedicine-Nanotechnology Biology and Medicine*, 2010. **6**(5): p. 612-618.

26. Hall, J.B., et al., *Characterization of nanoparticles for therapeutics*. *Nanomedicine*, 2007. **2**(6): p. 789-803.
27. Jain, K.K., *Nanomedicine: Application of nanobiotechnology in medical practice*. *Medical Principles and Practice*, 2008. **17**(2): p. 89-101.
28. Arvizo, R., R. Bhattacharya, and P. Mukherjee, *Gold nanoparticles: opportunities and challenges in nanomedicine*. *Expert Opinion on Drug Delivery*, 2010. **7**(6): p. 753-763.
29. Wang, Y.-X.J., *Superparamagnetic iron oxide based MRI contrast agents: Current status of clinical application*. *Quantitative Imaging in Medicine and Surgery*, 2011. **1**(1): p. 35-40.
30. Stanwix, H., *First clinical trial of gold nanoshells for treating lung cancer to be carried out in the USA*. *Nanomedicine*, 2013. **8**(1): p. 10-10.
31. Kharlamov, A.N. and J.L. Gabinsky, *Plasmonic photothermal and stem cell therapy of atherosclerotic plaque as a novel nanotool for angioplasty and artery remodeling*. *Rejuvenation Res*, 2012. **15**(2): p. 222-30.
32. Ma, J.K.H. and B. Hadzija, *Basic physical pharmacy*. 2013, Burlington, MA: Jones & Bartlett Learning.
33. Bieri, N.R., et al., *Towards Nanosized Particles in Pharmaceutical Industry*. *Nsti Nanotech 2008, Vol 2, Technical Proceedings*, ed. M. Laudon and B. Romanowicz. 2008. 194-197.
34. Chapman, P., *Nanotechnology in the pharmaceutical industry*. *Expert Opinion on Therapeutic Patents*, 2005. **15**(3): p. 249-251.
35. Stolarczyk, E.U. and K. Stolarczyk, *Perspectives of nanotechnology in medicine and pharmacy and its influence on pharmaceutical industry*. *Przemysl Chemiczny*, 2007. **86**(8): p. 797-799.
36. Morgan, S., et al., *The cost of drug development: A systematic review*. *Health Policy*, 2011. **100**(1): p. 4-17.
37. Kennedy, T., *Managing the drug discovery/development interface*. *Drug Discovery Today*, 1997. **2**(10): p. 436-444.
38. Hay, M., et al., *Clinical development success rates for investigational drugs*. *Nat Biotech*, 2014. **32**(1): p. 40-51.
39. DiMasi, J.A., R.W. Hansen, and H.G. Grabowski, *The price of innovation: new estimates of drug development costs*. *Journal of Health Economics*, 2003. **22**(2): p. 151-185.
40. Dickson, M. and J.P. Gagnon, *Key factors in the rising cost of new drug discovery and development*. *Nat Rev Drug Discov*, 2004. **3**(5): p. 417-429.
41. Farokhzad, O.C. and R. Langer, *Nanomedicine: Developing smarter therapeutic and diagnostic modalities*. *Advanced Drug Delivery Reviews*, 2006. **58**(14): p. 1456-1459.
42. Emerich, D.F., *Nanomedicine - prospective therapeutic and diagnostic applications*. *Expert Opinion on Biological Therapy*, 2005. **5**(1): p. 1-5.
43. Singh, S., *Nanomedicine-Nanoscale Drugs and Delivery Systems*. *Journal of Nanoscience and Nanotechnology*, 2010. **10**(12): p. 7906-7918.
44. Venugopal, J., et al., *Nanotechnology for nanomedicine and delivery of drugs*. *Current Pharmaceutical Design*, 2008. **14**(22): p. 2184-2200.
45. Chen, G., et al., *Nanochemistry and Nanomedicine for Nanoparticle-based Diagnostics and Therapy*. *Chemical Reviews*, 2016. **116**(5): p. 2826-2885.
46. Cragg, G.M., D.J. Newman, and K.M. Snader, *Natural products in drug discovery and development*. *Journal of Natural Products*, 1997. **60**(1): p. 52-60.
47. Molinski, T.F., et al., *Drug development from marine natural products*. *Nature Reviews Drug Discovery*, 2009. **8**(1): p. 69-85.
48. Thirumurugan, P., D. Matosiuk, and K. Jozwiak, *Click Chemistry for Drug Development and Diverse Chemical-Biology Applications*. *Chemical Reviews*, 2013. **113**(7): p. 4905-4979.
49. Chong, C.R. and D.J. Sullivan, *New uses for old drugs*. *Nature*, 2007. **448**(7154): p. 645-646.
50. Howie, L.J., B.R. Hirsch, and A.P. Abernethy, *A Comparison of FDA and EMA Drug Approval: Implications for Drug Development and Cost of Care*. *Oncology-New York*, 2013. **27**(12): p. 1195-+.

51. Wang, T., et al., *ICH guidelines: inception, revision, and implications for drug development*. Toxicol Sci, 2010. **118**(2): p. 356-67.
52. Caron, M., M.-P. Emery, and W. Maier, *Post-Marketing Requirements: An Overview of the Therapeutic Areas Targeted by the EMA and the FDA*. Pharmacoeconomics and Drug Safety, 2013. **22**: p. 87-87.
53. Ohno, Y., *ICH Guidelines—Implementation of the 3Rs (Refinement, Reduction, and Replacement): Incorporating Best Scientific Practices into the Regulatory Process*. ILAR Journal, 2002. **43**(Suppl 1): p. S95-S98.
54. Etheridge, M.L., et al., *The big picture on nanomedicine: the state of investigational and approved nanomedicine products*. Nanomedicine, 2013. **9**(1): p. 1-14.
55. Hauptman, A. and Y. Sharan, *Envisioned developments in nanobiotechnology-Nano2Life expert survey report*. 2006, Interdisciplinary Center for Technology Analysis and Forecasting, Tel-Aviv University: Tel-Aviv, Israel.
56. Pautler, M. and S. Brenner, *Nanomedicine: promises and challenges for the future of public health*. International Journal of Nanomedicine, 2010. **5**: p. 803-809.
57. Sartain, F., et al., *Emerging nanomedicine applications and manufacturing: progress and challenges*. Nanomedicine, 2016. **11**(6): p. 577-580.
58. Kendall, M. and I. Lynch, *Long-term monitoring for nanomedicine implants and drugs*. Nat Nano, 2016. **11**(3): p. 206-210.
59. Gupta, A.K. and M. Gupta, *Synthesis and surface engineering of iron oxide nanoparticles for biomedical applications*. Biomaterials, 2005. **26**(18): p. 3995-4021.
60. Sun, Y.G. and Y.N. Xia, *Shape-controlled synthesis of gold and silver nanoparticles*. Science, 2002. **298**(5601): p. 2176-2179.
61. Marko, Z., *Dimensional analysis and scale-up in theory and industrial application*, in *Pharmaceutical Process Scale-Up, Third Edition*. 2011, CRC Press. p. 1-57.
62. Frans, L.M., A.G. Kathryn, and E.R. Graham, *Understanding scale-up and quality risks on the interface between primary and secondary development*, in *Pharmaceutical Process Scale-Up, Third Edition*. 2011, CRC Press. p. 70-108.
63. Felton, L.A., *Pharmaceutical Process Scale-Up, 3rd edition*. Drug Development and Industrial Pharmacy, 2012. **38**(4): p. 512-512.
64. Steven, O., *Scale-up and process validation*, in *Pharmaceutical Process Scale-Up, Third Edition*. 2011, CRC Press. p. 109-116.
65. Fernando, J.M., *Engineering approaches for pharmaceutical process scale-up, validation, optimization and control in the PAT era*, in *Pharmaceutical Process Scale-Up, Third Edition*. 2011, CRC Press. p. 58-69.
66. Lin, P.-C., et al., *Techniques for physicochemical characterization of nanomaterials*. Biotechnology advances, 2014. **32**(4): p. 711-726.
67. Powers, K.W., et al., *Characterization of Nanomaterials for Toxicological Evaluation*, in *Nanotoxicity*. 2009, John Wiley & Sons, Ltd. p. 1-27.
68. Soenen, S.J., et al., *Cellular toxicity of inorganic nanoparticles: Common aspects and guidelines for improved nanotoxicity evaluation*. Nano Today, 2011. **6**(5): p. 446-465.
69. Mout, R., et al., *Surface functionalization of nanoparticles for nanomedicine*. Chemical Society Reviews, 2012. **41**(7): p. 2539-2544.
70. Nam, J., et al., *Surface engineering of inorganic nanoparticles for imaging and therapy*. Adv Drug Deliv Rev, 2013. **65**(5): p. 622-48.
71. Carezza, E., et al., *Rapid synthesis of water-dispersible superparamagnetic iron oxide nanoparticles by a microwave-assisted route for safe labeling of endothelial progenitor cells*. Acta Biomaterialia, 2014. **10**(8): p. 3775-3785.
72. Iavicoli, I., et al., *Toxicological effects of titanium dioxide nanoparticles: a review of in vitro mammalian studies*. Eur Rev Med Pharmacol Sci, 2011. **15**(5): p. 481-508.
73. Ramsden, J.J., *Chapter 5 - Nanometrology*, in *Nanotechnology*. 2011, William Andrew Publishing: Oxford. p. 73-100.
74. Kagan, V.E., H. Bayir, and A.A. Shvedova, *Nanomedicine and nanotoxicology: two sides of the same coin*. Nanomedicine : nanotechnology, biology, and medicine, 2005. **1**(4): p. 313-6.

75. Simak, J., *Nanotoxicity in Blood: Effects of Engineered Nanomaterials on Platelets*, in *Nanotoxicity*. 2009, John Wiley & Sons, Ltd. p. 191-225.
76. Duncan, R. and S.C.W. Richardson, *Endocytosis and Intracellular Trafficking as Gateways for Nanomedicine Delivery: Opportunities and Challenges*. *Molecular Pharmaceutics*, 2012. **9**(9): p. 2380-2402.
77. Kou, L., et al., *The endocytosis and intracellular fate of nanomedicines: Implication for rational design*. *Asian Journal of Pharmaceutical Sciences*, 2013. **8**(1): p. 1-10.
78. Murday, J.S., et al., *Translational nanomedicine: status assessment and opportunities*. *Nanomedicine-Nanotechnology Biology and Medicine*, 2009. **5**(3): p. 251-273.
79. Gornati, R., et al., *In Vivo and In Vitro Models for Nanotoxicology Testing*, in *Nanotoxicity*. 2009, John Wiley & Sons, Ltd. p. 279-302.
80. Jeong, J., et al., *In Vitro and In Vivo Toxicity Study of Nanoparticles*, in *Nanotoxicity*. 2009, John Wiley & Sons, Ltd. p. 303-334.
81. Yu, K.O., et al., *In Vitro and In Vivo Models for Nanotoxicity Testing*, in *Nanotoxicity*. 2009, John Wiley & Sons, Ltd. p. 335-348.
82. Ma, Y., *In Vitro Models for Nanotoxicity Testing*, in *Nanotoxicity*. 2009, John Wiley & Sons, Ltd. p. 349-377.
83. Freshney, R.I., *Defined Media and Supplements*, in *Culture of Animal Cells*. 2010, John Wiley & Sons, Inc. p. 99-114.
84. Freshney, R.I., *Serum-Free Media*, in *Culture of Animal Cells*. 2010, John Wiley & Sons, Inc. p. 115-132.
85. Yu, S.-M., A. Laromaine, and A. Roig, *Enhanced stability of superparamagnetic iron oxide nanoparticles in biological media using a pH adjusted-BSA adsorption protocol*. *Journal of Nanoparticle Research*, 2014. **16**(7).
86. Lynch, I., A. Salvati, and K.A. Dawson, *Protein-nanoparticle interactions: What does the cell see?* *Nat Nano*, 2009. **4**(9): p. 546-547.
87. Nazarenus, M., et al., *In vitro interaction of colloidal nanoparticles with mammalian cells: What have we learned thus far?* *Beilstein J Nanotechnol*, 2014. **5**: p. 1477-90.
88. Bargheer, D., et al., *The fate of a designed protein corona on nanoparticles in vitro and in vivo*. *Beilstein J Nanotechnol*, 2015. **6**: p. 36-46.
89. O'Shaughnessy, J.A., et al., *Weekly nanoparticle albumin paclitaxel (Abraxane) results in long-term disease control in patients with taxane-refractory metastatic breast cancer*. *Breast Cancer Research and Treatment*, 2004. **88**: p. S65-S65.
90. Mariam, J., S. Sivakami, and P.M. Dongre, *Albumin corona on nanoparticles - a strategic approach in drug delivery*. *Drug Deliv*, 2015: p. 1-9.
91. Arbab, A.S., et al., *A model of lysosomal metabolism of dextran coated superparamagnetic iron oxide (SPIO) nanoparticles: implications for cellular magnetic resonance imaging*. *Nmr in Biomedicine*, 2005. **18**(6): p. 383-389.
92. Canton, I. and G. Battaglia, *Endocytosis at the nanoscale*. *Chemical Society Reviews*, 2012. **41**(7): p. 2718-2739.
93. Yu, S.-M., et al., *Bio-identity and fate of albumin-coated SPIONs evaluated in cells and by the C. elegans model*. *Acta Biomaterialia*. **43**: p. 348-357.
94. Shukla, R., et al., *Biocompatibility of gold nanoparticles and their endocytotic fate inside the cellular compartment: A microscopic overview*. *Langmuir*, 2005. **21**(23): p. 10644-10654.
95. Feliu, N., et al., *In vivo degeneration and the fate of inorganic nanoparticles*. *Chem Soc Rev*, 2016. **45**(9): p. 2440-57.
96. Freshney, R.I., *Subculture and Cell Lines*, in *Culture of Animal Cells*. 2010, John Wiley & Sons, Inc. p. 187-206.
97. Freshney, R.I., *Laboratory Design, Layout, and Equipment*, in *Culture of Animal Cells*. 2010, John Wiley & Sons, Inc. p. 25-36.
98. Freshney, R.I., *Equipment and Materials*, in *Culture of Animal Cells*. 2010, John Wiley & Sons, Inc. p. 37-56.
99. Freshney, R.I., *Aseptic Technique*, in *Culture of Animal Cells*. 2010, John Wiley & Sons, Inc. p. 57-70.
100. Freshney, R.I., *Contamination*, in *Culture of Animal Cells*. 2010, John Wiley & Sons, Inc. p. 299-315.

101. Corporation, S.-A., *Cell Culture Manual: 2008-2009*. 2008: Sigma-Aldrich.
102. Oprea, T.I. and J. Gottfries, *Toward minimalistic modeling of oral drug absorption*. Journal of Molecular Graphics & Modelling, 1999. **17**(5-6): p. 261-+.
103. Hou, T., et al., *ADME evaluation in drug discovery. 7. Prediction of oral absorption by correlation and classification*. Journal of Chemical Information and Modeling, 2007. **47**(1): p. 208-218.
104. Khan, M.T.H., *Predictions of the ADMET Properties of Candidate Drug Molecules Utilizing Different QSAR/QSPR Modelling Approaches*. Current Drug Metabolism, 2010. **11**(4): p. 285-295.
105. Poater, A., et al., *Computational methods to predict the reactivity of nanoparticles through structure-property relationships*. Expert Opin Drug Deliv, 2010. **7**(3): p. 295-305.
106. Tejeda-Benitez, L. and J. Olivero-Verbel, *Caenorhabditis elegans, a Biological Model for Research in Toxicology*, in *Reviews of Environmental Contamination and Toxicology, Vol 237*, P. DeVoogt, Editor. 2016. p. 1-35.
107. Woodhead, A.D., *Nonmammalian Animal Models for Biomedical Research*, in *Animal Models*. 1990, CRC Press: Boca Raton, FL.
108. Wang, B.D., *Sourcebook of Models for Biomedical Research*. The Quarterly Review of Biology, 2010. **85**(3): p. 381-381.
109. Hulme, S.E. and G.M. Whitesides, *Chemistry and the Worm: Caenorhabditis elegans as a Platform for Integrating Chemical and Biological Research*. Angewandte Chemie-International Edition, 2011. **50**(21): p. 4774-4807.
110. Bohnsack, J.P., et al., *The primacy of physicochemical characterization of nanomaterials for reliable toxicity assessment: a review of the zebrafish nanotoxicology model*. Methods in molecular biology (Clifton, N.J.), 2012. **926**: p. 261-316.
111. Chakraborty, C., et al., *Zebrafish: A Complete Animal Model for In Vivo Drug Discovery and Development*. Current Drug Metabolism, 2009. **10**(2): p. 116-124.
112. Arya, U., C.K. Das, and J.R. Subramaniam, *Caenorhabditis elegans for preclinical drug discovery*. Current Science, 2010. **99**(12): p. 1669-1680.
113. Hedges, S.B., *The origin and evolution of model organisms*. Nat Rev Genet, 2002. **3**(11): p. 838-849.
114. Gonzalez-Moragas, L., A. Roig, and A. Laromaine, *C. elegans as a tool for in vivo nanoparticle assessment*. Advances in Colloid and Interface Science, 2015. **219**(0): p. 10-26.
115. Choi, J., et al., *A micro-sized model for the in vivo study of nanoparticle toxicity: what has Caenorhabditis elegans taught us?* Environmental Chemistry, 2014. **11**(3): p. 227-246.
116. Zhao, Y., et al., *Translocation, transfer, and in vivo safety evaluation of engineered nanomaterials in the non-mammalian alternative toxicity assay model of nematode Caenorhabditis elegans*. Rsc Advances, 2013. **3**(17): p. 5741-5757.
117. Liebsch, M., et al., *Alternatives to animal testing: current status and future perspectives*. Archives of Toxicology, 2011. **85**(8): p. 841-858.
118. Riddle, D.L., et al., *C. elegans II*. *C. elegans II*, ed. D.L. Riddle, et al. 1997, Cold Spring Harbor NY: Cold Spring Harbor Laboratory Press.
119. Hall, D.H. and Z.F. Altun, *C. elegans atlas*. 2008, Cold Spring Harbor, N.Y.: Cold Spring Harbor Laboratory Press.
120. Swanson, M.M., M.L. Edgley, and D.L. Riddle, *The nematode Caenorhabditis elegans*. Genetic maps - 1984. A compilation of linkage and restriction maps of genetically studied organisms. Volume 3., ed. S.J. O'Brien. 1984. 286-300.
121. Kaletta, T. and M.O. Hengartner, *Finding function in novel targets: C. elegans as a model organism*. Nat Rev Drug Discov, 2006. **5**(5): p. 387-98.
122. Bird, D.M., et al., *The Caenorhabditis elegans genome: A guide in the post genomics age*. Annual Review of Phytopathology, 1999. **37**: p. 247-265.
123. Hashmi, S., et al., *A C. elegans model to study human metabolic regulation*. Nutrition & Metabolism, 2013. **10**.
124. Sato, K., et al., *C. elegans as a model for membrane traffic*. WormBook : the online review of C. elegans biology, 2014: p. 1-47.
125. Kirienko, N.V., K. Mani, and D.S. Fay, *Cancer models in Caenorhabditis elegans*. Dev Dyn, 2010. **239**(5): p. 1413-48.

126. Sengupta, P. and A.D.T. Samuel, *C. elegans: a model system for systems neuroscience*. Current opinion in neurobiology, 2009. **19**(6): p. 637-643.
127. Leung, M.C., et al., *Caenorhabditis elegans: an emerging model in biomedical and environmental toxicology*. Toxicol Sci, 2008. **106**(1): p. 5-28.
128. Kutscher, L.M. and S. Shaham, *Forward and reverse mutagenesis in C. elegans*, in *WormBook*, T.C.e.R. Community, Editor., WormBook.
129. San-Miguel, A. and H. Lu, *Microfluidics as a tool for C. elegans research*, in *WormBook*, T.C.e.R. Community, Editor., WormBook.
130. Artal-Sanz, M., L. de Jong, and N. Tavernarakis, *Caenorhabditis elegans: a versatile platform for drug discovery*. Biotechnol J, 2006. **1**(12): p. 1405-18.
131. Contag, P.R., *Whole-animal cellular and molecular imaging to accelerate drug development*. Drug Discovery Today, 2002. **7**(10): p. 555-562.
132. Pomper, M.G. and J.S. Lee, *Small animal imaging in drug development*. Current Pharmaceutical Design, 2005. **11**(25): p. 3247-3272.
133. Stiernagle, T., *Maintenance of C. elegans*, in *WormBook*, T.C.e.R. Community, Editor., WormBook.
134. Hu, P.J., *Dauer*, in *WormBook*, T.C.e.R. Community, Editor., WormBook.
135. Emmons, S.W., *Male development*, in *WormBook*, T.C.e.R. Community, Editor., WormBook.
136. Barr, M.M. and L.R. Garcia, *Male mating behavior*, in *WormBook*, T.C.e.R. Community, Editor., WormBook.
137. Hodgkin, J., *Introduction to genetics and genomics*, in *WormBook*, T.C.e.R. Community, Editor., WormBook.
138. Walhout (ed.), A.J.M. and S.J. Boulton (ed.), *Biochemistry and molecular biology*, in *WormBook*, T.C.e.R. Community, Editor., WormBook.
139. Corsi, A.K., *A biochemist's guide to Caenorhabditis elegans*. Analytical Biochemistry, 2006. **359**(1): p. 1-17.
140. Kohara, Y., *Functional genomics of the nematode C. elegans*. Tanpakushitsu kakusan koso. Protein, nucleic acid, enzyme, 1997. **42**(17 Suppl): p. 2907-13.
141. Lai, C.H., et al., *Identification of novel human genes evolutionarily conserved in Caenorhabditis elegans by comparative proteomics*. Genome Res, 2000. **10**(5): p. 703-13.
142. McGhee, J.D., *The C. elegans intestine*, in *WormBook*, T.C.e.R. Community, Editor., WormBook.
143. Sternberg, P.W., *Vulval development*, in *WormBook*, T.C.e.R. Community, Editor., WormBook.
144. Hobert, O., *Specification of the nervous system*, in *WormBook*, T.C.e.R. Community, Editor., WormBook.
145. Kerr, R.A., *Imaging the activity of neurons and muscles*, in *WormBook*, T.C.e.R. Community, Editor., WormBook.
146. Page, A.P. and I.L. Johnstone, *The cuticle*, in *WormBook*, T.C.e.R. Community, Editor., WormBook.
147. Chisholm, A.D. and S. Xu, *The Caenorhabditis elegans epidermis as a model skin. II: differentiation and physiological roles*. Wiley Interdiscip Rev Dev Biol, 2012. **1**(6): p. 879-902.
148. Chisholm, A.D. and T.I. Hsiao, *The C. elegans epidermis as a model skin. I: development, patterning, and growth*. Wiley interdisciplinary reviews. Developmental biology, 2012. **1**(6): p. 861-878.
149. Altun, Z.F.a.H., D. H. . *Handbook of C. elegans Anatomy*. In *WormAtlas*. . 2005; Available from: <http://www.wormatlas.org/ver1/handbook/contents.htm>.
150. Avery, L. and Y.-J. You, *C. elegans feeding*, in *WormBook*, T.C.e.R. Community, Editor., WormBook.
151. Avery, L., *Food transport in the C. elegans pharynx*. Journal of Experimental Biology, 2003. **206**(14): p. 2441-2457.
152. Chauhan, V.M., et al., *Mapping the Pharyngeal and Intestinal pH of Caenorhabditis elegans and Real-Time Luminal pH Oscillations Using Extended Dynamic Range pH-Sensitive Nanosensors*. Acs Nano, 2013. **7**(6): p. 5577-5587.
153. Take-uchi, M., et al., *An ion channel of the degenerin/epithelial sodium channel superfamily controls the defecation rhythm in Caenorhabditis elegans*. Proc Natl Acad Sci U S A, 1998. **95**(20): p. 11775-11780.

154. Pispa, J., et al., *C. elegans dss-1 is functionally conserved and required for oogenesis and larval growth*. BMC Dev Biol, 2008. **8**: p. 51.
155. Jain, K., N.K. Mehra, and N.K. Jain, *Nanotechnology in Drug Delivery: Safety and Toxicity Issues*. Curr Pharm Des, 2015. **21**(29): p. 4252-61.
156. Auer, J.A., et al., *Refining animal models in fracture research: seeking consensus in optimising both animal welfare and scientific validity for appropriate biomedical use*. BMC Musculoskeletal Disorders, 2007. **8**(1): p. 1-13.
157. Oh, E., et al., *Meta-analysis of cellular toxicity for cadmium-containing quantum dots*. Nat Nano, 2016. **11**(5): p. 479-486.
158. Krug, H.F., *Nanosafety Research-Are We on the Right Track?* Angewandte Chemie-International Edition, 2014. **53**(46): p. 12304-12319.
159. Dhawan, R., D.B. Dusenbery, and P.L. Williams, *A comparison of metal-induced lethality and behavioral responses in the nematode Caenorhabditis elegans*. Environmental Toxicology and Chemistry, 2000. **19**(12): p. 3061-3067.
160. Dhawan, R., D.B. Dusenbery, and P.L. Williams, *Comparison of lethality, reproduction, and behavior as toxicological endpoints in the nematode Caenorhabditis elegans*. Journal of Toxicology and Environmental Health-Part a-Current Issues, 1999. **58**(7): p. 451-462.
161. Ganio, K., et al., *Accurate biometal quantification per individual Caenorhabditis elegans*. Analyst, 2016. **141**(4): p. 1434-1439.
162. Chen, P., et al., *Metal-induced neurodegeneration in C. elegans*. Frontiers in Aging Neuroscience, 2013. **5**.
163. James, S.A., et al., *Direct in vivo imaging of essential bioinorganics in Caenorhabditis elegans*. Metallomics, 2013. **5**(6): p. 627-635.
164. Qu, Y., et al., *Full Assessment of Fate and Physiological Behavior of Quantum Dots Utilizing Caenorhabditis elegans as a Model Organism*. Nano Letters, 2011. **11**(8): p. 3174-3183.
165. Lim, S.F., et al., *In vivo and scanning electron microscopy imaging of upconverting nanophosphors in Caenorhabditis elegans*. Nano Lett, 2006. **6**(2): p. 169-174.
166. Ma, H., et al., *TOXICITY OF MANUFACTURED ZINC OXIDE NANOPARTICLES IN THE NEMATODE CAENORHABDITIS ELEGANS*. Environmental Toxicology and Chemistry, 2009. **28**(6): p. 1324-1330.
167. Meyer, J.N., et al., *Intracellular uptake and associated toxicity of silver nanoparticles in Caenorhabditis elegans*. Aquatic Toxicology, 2010. **100**(2): p. 140-150.
168. Rui, Q., et al., *Biosafety assessment of titanium dioxide nanoparticles in acutely exposed nematode Caenorhabditis elegans with mutations of genes required for oxidative stress or stress responset*. Chemosphere, 2013. **93**(10): p. 2289-2296.
169. Wang, H., R.L. Wick, and B. Xing, *Toxicity of nanoparticulate and bulk ZnO, Al₂O₃ and TiO₂ to the nematode Caenorhabditis elegans*. Environ Pollut, 2009. **157**(4): p. 1171-7.
170. Mohan, N., et al., *In Vivo Imaging and Toxicity Assessments of Fluorescent Nanodiamonds in Caenorhabditis elegans*. Nano Lett, 2010. **10**(9): p. 3692-3699.
171. Zanni, E., et al., *Graphite nanoplatelets and Caenorhabditis elegans: insights from an in vivo model*. Nano Lett, 2012. **12**(6): p. 2740-4.
172. Wu, Q., et al., *Crucial role of the biological barrier at the primary targeted organs in controlling the translocation and toxicity of multi-walled carbon nanotubes in the nematode Caenorhabditis elegans*. Nanoscale, 2013. **5**(22): p. 11166-11178.
173. Wu, Q., et al., *Comparison of toxicities from three metal oxide nanoparticles at environmental relevant concentrations in nematode Caenorhabditis elegans*. Chemosphere, 2013. **90**(3): p. 1123-31.
174. Sanches Moraes, B.K., et al., *Clozapine-Loaded Polysorbate-Coated Polymeric Nanocapsules: Physico-Chemical Characterization and Toxicity Evaluation in Caenorhabditis elegans Model*. Journal of Nanoscience and Nanotechnology, 2016. **16**(2): p. 1257-1264.
175. Colmenares, D., et al., *Delivery of dietary triglycerides to Caenorhabditis elegans using lipid nanoparticles: Nanoemulsion-based delivery systems*. Food Chemistry, 2016. **202**: p. 451-457.

176. Miyako, E., et al., *In Vivo Remote Control of Reactions in Caenorhabditis elegans by Using Supramolecular Nanohybrids of Carbon Nanotubes and Liposomes*. *Angewandte Chemie-International Edition*, 2015. **54**(34): p. 9903-9906.
177. Huang, H., et al., *Remote control of ion channels and neurons through magnetic-field heating of nanoparticles*. *Nat Nanotechnol*, 2010. **5**(8): p. 602-6.
178. Charan, S., et al., *Development of lipid targeting Raman probes for in vivo imaging of Caenorhabditis elegans*. *Chemistry*, 2011. **17**(18): p. 5165-70.
179. Wu, Q., et al., *Small sizes of TiO₂-NPs exhibit adverse effects at predicted environmental relevant concentrations on nematodes in a modified chronic toxicity assay system*. *J Hazard Mater*, 2012. **243**: p. 161-8.
180. Roh, J.-y., et al., *Ecotoxicity of Silver Nanoparticles on the Soil Nematode Caenorhabditis elegans Using Functional Ecotoxicogenomics*. *Environmental Science & Technology*, 2009. **43**(10): p. 3933-3940.
181. Gao, Y., et al., *Mapping technique for biodistribution of elements in a model organism, Caenorhabditis elegans, after exposure to copper nanoparticles with microbeam synchrotron radiation X-ray fluorescence*. *Journal of Analytical Atomic Spectrometry*, 2008. **23**(8): p. 1121.
182. Collin, B., et al., *Influence of Natural Organic Matter and Surface Charge on the Toxicity and Bioaccumulation of Functionalized Ceria Nanoparticles in Caenorhabditis elegans*. *Environmental Science & Technology*, 2014. **48**(2): p. 1280-1289.
183. Hoess, S., et al., *Size- and Composition-Dependent Toxicity of Synthetic and Soil-Derived Fe Oxide Colloids for the Nematode Caenorhabditis elegans*. *Environmental Science & Technology*, 2015. **49**(1): p. 544-552.
184. Dawlatsina, G.I., R.T. Minullina, and R.F. Fakhrullin, *Microworms swallow the nanobait: the use of nanocoated microbial cells for the direct delivery of nanoparticles into Caenorhabditis elegans*. *Nanoscale*, 2013. **5**(23): p. 11761-9.
185. Kim, J., et al., *Effects of a potent antioxidant, platinum nanoparticle, on the lifespan of Caenorhabditis elegans*. *Mech Ageing Dev*, 2008. **129**(6): p. 322-331.
186. Tsyusko, O.V., et al., *Toxicogenomic Responses of the Model Organism Caenorhabditis elegans to Gold Nanoparticles*. *Environmental Science & Technology*, 2012. **46**(7): p. 4115-4124.
187. Jung, S.-K., et al., *Multi-endpoint, High-Throughput Study of Nanomaterial Toxicity in Caenorhabditis elegans*. *Environmental Science & Technology*, 2015. **49**(4): p. 2477-2485.
188. Carvalho, R.N., et al., *Mixtures of Chemical Pollutants at European Legislation Safety Concentrations: How Safe Are They?* *Toxicological Sciences*, 2014. **141**(1): p. 218-233.
189. Yang, X., et al., *Silver Nanoparticle Behavior, Uptake, and Toxicity in Caenorhabditis elegans: Effects of Natural Organic Matter*. *Environmental Science & Technology*, 2014. **48**(6): p. 3486-3495.
190. Yang, X., et al., *Mechanism of Silver Nanoparticle Toxicity Is Dependent on Dissolved Silver and Surface Coating in Caenorhabditis elegans*. *Environmental Science & Technology*, 2012. **46**(2): p. 1119-1127.
191. Maurer, L.L., et al., *Intracellular trafficking pathways in silver nanoparticle uptake and toxicity in Caenorhabditis elegans*. *Nanotoxicology*, 2016. **10**(7): p. 831-5.
192. Ahn, J.-M., et al., *Comparative toxicity of silver nanoparticles on oxidative stress and DNA damage in the nematode, Caenorhabditis elegans*. *Chemosphere*, 2014. **108**: p. 343-352.
193. Starnes, D.L., et al., *Impact of sulfidation on the bioavailability and toxicity of silver nanoparticles to Caenorhabditis elegans*. *Environmental Pollution*, 2015. **196**: p. 239-246.
194. Starnes, D.L., et al., *Distinct transcriptomic responses of Caenorhabditis elegans to pristine and sulfidized silver nanoparticles*. *Environmental pollution (Barking, Essex : 1987)*, 2016. **213**: p. 314-21.
195. Kim, S.W., J.I. Kwak, and Y.-J. An, *Multigenerational Study of Gold Nanoparticles in Caenorhabditis elegans: Transgenerational Effect of Maternal Exposure*. *Environmental Science & Technology*, 2013. **47**(10): p. 5393-5399.

196. Kim, J., T. Shirasawa, and Y. Miyamoto, *The effect of TAT conjugated platinum nanoparticles on lifespan in a nematode Caenorhabditis elegans model*. Biomaterials, 2010. **31**(22): p. 5849-54.
197. Pluskota, A., et al., *In Caenorhabditis elegans Nanoparticle-Bio-Interactions Become Transparent: Silica-Nanoparticles Induce Reproductive Senescence*. Plos One, 2009. **4**(8).
198. Scharf, A., A. Piechulek, and A. von Mikecz, *Effect of Nanoparticles on the Biochemical and Behavioral Aging Phenotype of the Nematode Caenorhabditis elegans*. Acs Nano, 2013. **7**(12): p. 10695-10703.
199. Polak, N., et al., *Metalloproteins and phytochelatin synthase may confer protection against zinc oxide nanoparticle induced toxicity in Caenorhabditis elegans*. Comparative Biochemistry and Physiology C-Toxicology & Pharmacology, 2014. **160**: p. 75-85.
200. Li, Y., et al., *Chronic Al₂O₃-nanoparticle exposure causes neurotoxic effects on locomotion behaviors by inducing severe ROS production and disruption of ROS defense mechanisms in nematode Caenorhabditis elegans*. J Hazard Mater, 2012. **219-220**: p. 221-30.
201. Zhao, Y., et al., *The in vivo underlying mechanism for recovery response formation in nano-titanium dioxide exposed Caenorhabditis elegans after transfer to the normal condition*. Nanomedicine-Nanotechnology Biology and Medicine, 2014. **10**(1): p. 89-98.
202. Le Trequesser, Q., et al., *In situ titanium dioxide nanoparticles quantitative microscopy in cells and in C. elegans using nuclear microprobe analysis*. Nuclear Instruments & Methods in Physics Research Section B-Beam Interactions with Materials and Atoms, 2014. **341**: p. 58-64.
203. Lim, D., et al., *Oxidative stress-related PMK-1 P38 MAPK activation as a mechanism for toxicity of silver nanoparticles to reproduction in the nematode Caenorhabditis elegans*. Environmental Toxicology and Chemistry, 2012. **31**(3): p. 585-592.
204. Ellegaard-Jensen, L., K.A. Jensen, and A. Johansen, *Nano-silver induces dose-response effects on the nematode Caenorhabditis elegans*. Ecotoxicology and Environmental Safety, 2012. **80**: p. 216-223.
205. Contreras, E.Q., et al., *SIZE-DEPENDENT IMPACTS OF SILVER NANOPARTICLES ON THE LIFESPAN, FERTILITY, GROWTH, AND LOCOMOTION OF CAENORHABDITIS ELEGANS*. Environmental Toxicology and Chemistry, 2014. **33**(12): p. 2716-2723.
206. Roh, J.-Y., H.-J. Eom, and J. Choi, *Involvement of Caenorhabditis elegans MAPK Signaling Pathways in Oxidative Stress Response Induced by Silver Nanoparticles Exposure*. Toxicological research, 2012. **28**(1): p. 19-24.
207. Kim, S.W., S.-H. Nam, and Y.-J. An, *Interaction of Silver Nanoparticles with Biological Surfaces of Caenorhabditis elegans*. Ecotoxicology and Environmental Safety, 2012. **77**: p. 64-70.
208. Roh, J.Y., et al., *Ecotoxicological investigation of CeO₂ and TiO₂ nanoparticles on the soil nematode Caenorhabditis elegans using gene expression, growth, fertility, and survival as endpoints*. Environ Toxicol Pharmacol, 2010. **29**(2): p. 167-72.
209. Gupta, S., et al., *Optimization of ZnO-NPs to Investigate Their Safe Application by Assessing Their Effect on Soil Nematode Caenorhabditis elegans*. Nanoscale Research Letters, 2015. **10**.
210. Arnold, M.C., et al., *Cerium oxide nanoparticles are more toxic than equimolar bulk cerium oxide in Caenorhabditis elegans*. Arch Environ Contam Toxicol, 2013. **65**(2): p. 224-33.
211. Wu, Q., et al., *Evaluation of environmental safety concentrations of DMSA Coated Fe₂O₃-NPs using different assay systems in nematode Caenorhabditis elegans*. Plos One, 2012. **7**(8): p. e43729.
212. Donkin, S.G. and P.L. Williams, *INFLUENCE OF DEVELOPMENTAL STAGE, SALTS AND FOOD PRESENCE ON VARIOUS END-POINTS USING CAENORHABDITIS-ELEGANS FOR AQUATIC TOXICITY TESTING*. Environmental Toxicology and Chemistry, 1995. **14**(12): p. 2139-2147.

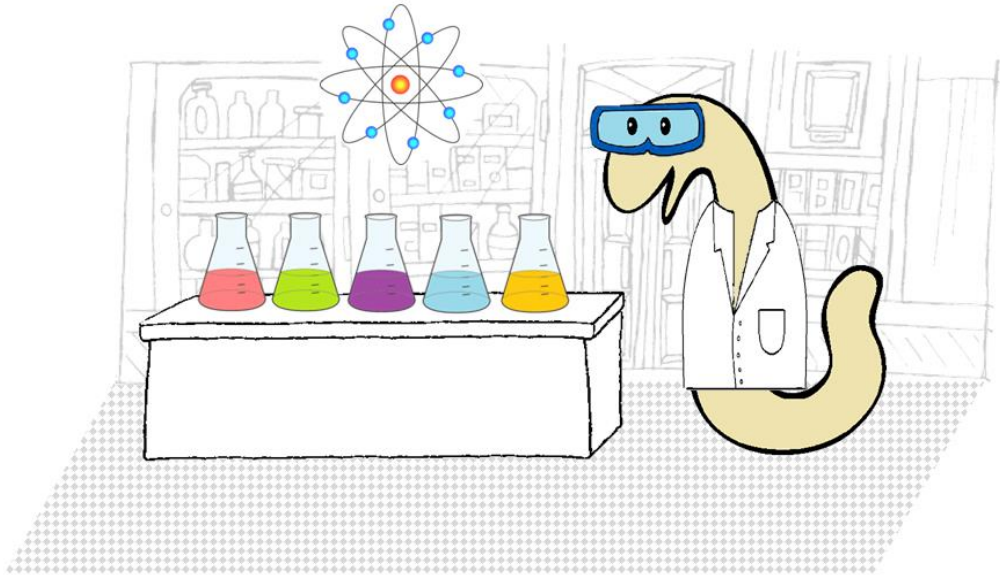
213. Zhao, Y., et al., *In vivo translocation and toxicity of multi-walled carbon nanotubes are regulated by microRNAs*. *Nanoscale*, 2014. **6**(8): p. 4275-4284.
214. Fang-Yen, C., L. Avery, and A.D.T. Samuel, *Two size-selective mechanisms specifically trap bacteria-sized food particles in Caenorhabditis elegans*. *Proceedings of the National Academy of Sciences*, 2009. **106**(47): p. 20093-20096.
215. Aksu, B., *Quality By Design: QbD and Quality Risk Management*. *Marmara Pharmaceutical Journal*, 2015. **19**(1): p. 12-18.
216. Hoess, S., K. Schlottmann, and W. Traunspurger, *Toxicity of Ingested Cadmium to the Nematode Caenorhabditis elegans*. *Environmental Science & Technology*, 2011. **45**(23): p. 10219-10225.
217. Jackson, B.P., et al., *Evidence for biogenic pyromorphite formation by the nematode Caenorhabditis elegans*. *Environmental Science & Technology*, 2005. **39**(15): p. 5620-5625.
218. Asati, A., et al., *Surface-Charge-Dependent Cell Localization and Cytotoxicity of Cerium Oxide Nanoparticles*. *ACS Nano*, 2010. **4**(9): p. 5321-5331.
219. Basketter, D.A., et al., *A roadmap for the development of alternative (non-animal) methods for systemic toxicity testing - t4 report**. *Altex*, 2012. **29**(1): p. 3-91.
220. Maurer, L.L., et al., *Caenorhabditis elegans as a Model for Toxic Effects of Nanoparticles: Lethality, Growth, and Reproduction*, in *Current Protocols in Toxicology*. 2015, John Wiley & Sons, Inc.
221. Pascu, O., et al., *Surface Reactivity of Iron Oxide Nanoparticles by Microwave-Assisted Synthesis; Comparison with the Thermal Decomposition Route*. *The Journal of Physical Chemistry C*, 2012. **116**(28): p. 15108-15116.
222. Liu, G., et al., *Applications and Potential Toxicity of Magnetic Iron Oxide Nanoparticles*. *Small*, 2013. **9**(9-10): p. 1533-1545.
223. Singh, R., *Unexpected magnetism in nanomaterials*. *Journal of Magnetism and Magnetic Materials*, 2013. **346**: p. 58-73.
224. Carezza, E., et al., *In vitro angiogenic performance and in vivo brain targeting of magnetized endothelial progenitor cells for neurorepair therapies*. *Nanomedicine*, 2014. **10**(1): p. 225-34.
225. Cai, X.W., F. Yang, and N. Gu, *Applications of Magnetic Microbubbles for Theranostics*. *Theranostics*, 2012. **2**(1): p. 103-112.
226. Erogbogbo, F., et al., *Biocompatible Magnetofluorescent Probes: Luminescent Silicon Quantum Dots Coupled with Superparamagnetic Iron(III) Oxide*. *Acs Nano*, 2010. **4**(9): p. 5131-5138.
227. Nasongkla, N., et al., *Multifunctional polymeric micelles as cancer-targeted, MRI-ultrasensitive drug delivery systems*. *Nano Letters*, 2006. **6**(11): p. 2427-2430.
228. Hwu, J.R., et al., *Targeted Paclitaxel by Conjugation to Iron Oxide and Gold Nanoparticles*. *Journal of the American Chemical Society*, 2009. **131**(1): p. 66-+.
229. Medarova, Z., et al., *In vivo imaging of siRNA delivery and silencing in tumors*. *Nature Medicine*, 2007. **13**(3): p. 372-377.
230. Salunkhe, A.B., V.M. Khot, and S.H. Pawar, *Magnetic hyperthermia with magnetic nanoparticles: a status review*. *Curr Top Med Chem*, 2014. **14**(5): p. 572-94.
231. Wang, Y.X.J., *Current status of superparamagnetic iron oxide contrast agents for liver magnetic resonance imaging*. *World Journal of Gastroenterology*, 2015. **21**(47): p. 13400-13402.
232. Laurent, S., et al., *Magnetic Iron Oxide Nanoparticles: Synthesis, Stabilization, Vectorization, Physicochemical Characterizations, and Biological Applications (vol 108, pg 2064, 2008)*. *Chemical Reviews*, 2010. **110**(4): p. 2574-2574.
233. Niederberger, M. and G. Garnweitner, *Organic Reaction Pathways in the Nonaqueous Synthesis of Metal Oxide Nanoparticles*. *Chemistry – A European Journal*, 2006. **12**(28): p. 7282-7302.
234. Kelly, P.M., et al., *Mapping protein binding sites on the biomolecular corona of nanoparticles*. *Nat Nano*, 2015. **10**(5): p. 472-479.
235. Yu, S., et al., *Albumin-coated SPIONs: an experimental and theoretical evaluation of protein conformation, binding affinity and competition with serum proteins*. *Nanoscale*, 2016.

236. Kolen'ko, Y.V., et al., *Large-Scale Synthesis of Colloidal Fe₃O₄ Nanoparticles Exhibiting High Heating Efficiency in Magnetic Hyperthermia*. Journal of Physical Chemistry C, 2014. **118**(16): p. 8691-8701.
237. Ibarra-Sánchez, J.J., et al., *Key Parameters for Scaling up the Synthesis of Magnetite Nanoparticles in Organic Media: Stirring Rate and Growth Kinetic*. Industrial & Engineering Chemistry Research, 2013. **52**(50): p. 17841-17847.
238. Bowman, M.D., et al., *Approaches for Scale-Up of Microwave-Promoted Reactions*. Organic Process Research & Development, 2008. **12**(1): p. 41-57.
239. Kremsner, J.M., A. Stadler, and C.O. Kappe, *The scale-up of microwave-assisted organic synthesis*, in *Microwave Methods in Organic Synthesis*, M. Larhed and K. Olofsson, Editors. 2006. p. 233-278.
240. Kremsner, J.M., A. Stadler, and C.O. Kappe, *The Scale-Up of Microwave-Assisted Organic Synthesis*. 2006. **266**: p. 233-278.
241. Ángel, D.-O., et al., *Reproducibility and Scalability of Microwave-Assisted Reactions*. Microwave Heating. 2011.
242. Gonzalez-Moragas, L., et al., *Scale-up synthesis of iron oxide nanoparticles by microwave-assisted thermal decomposition*. Chemical Engineering Journal, 2015. **281**: p. 87-95.
243. Pedrosa, P., et al., *Gold Nanotheranostics: Proof-of-Concept or Clinical Tool?* Nanomaterials, 2015. **5**(4): p. 1853-1879.
244. Baptista, P., et al., *Gold nanoparticle-based theranostics: Disease diagnostics and treatment using a single nanomaterial*. Nanobiosen. Dis. Diagn, 2015. **4**(11).
245. Conde, J., et al., *Revisiting 30 years of biofunctionalization and surface chemistry of inorganic nanoparticles for nanomedicine*. Frontiers in chemistry, 2014. **2**: p. 48.
246. Zhang, X., J.G. Teodoro, and J.L. Nadeau, *Intratumoral gold-doxorubicin is effective in treating melanoma in mice*. Nanomedicine: Nanotechnology, Biology and Medicine, 2015. **11**(6): p. 1365-1375.
247. Gabizon, A., H. Shmeeda, and Y. Barenholz, *Pharmacokinetics of pegylated liposomal doxorubicin*. Clinical pharmacokinetics, 2003. **42**(5): p. 419-436.
248. Conde, J., et al., *Design of Multifunctional Gold Nanoparticles for In Vitro and In Vivo Gene Silencing*. ACS Nano, 2012. **6**(9): p. 8316-8324.
249. Turkevich, J., P.C. Stevenson, and J. Hillier, *A study of the nucleation and growth processes in the synthesis of colloidal gold*. Discussions of the Faraday Society, 1951. **11**(0): p. 55-75.
250. Frens, G., *Controlled Nucleation for the Regulation of the Particle Size in Monodisperse Gold Suspensions*. Nature Physical Science, 1973. **241**: p. 20-22.
251. Bastús, N.G., J. Comenge, and V. Puntes, *Kinetically Controlled Seeded Growth Synthesis of Citrate-Stabilized Gold Nanoparticles of up to 200 nm: Size Focusing versus Ostwald Ripening*. Langmuir, 2011. **27**(17): p. 11098-11105.
252. Anderson, C.P. and E.A. Leibold, *Mechanisms of iron metabolism in Caenorhabditis elegans*. Frontiers in Pharmacology, 2014. **5**: p. 113.
253. Merchant, B., *Gold, the Noble Metal and the Paradoxes of its Toxicology*. Biologicals, 1998. **26**(1): p. 49-59.
254. Sabella, S., et al., *A general mechanism for intracellular toxicity of metal-containing nanoparticles*. Nanoscale, 2014. **6**(12): p. 7052-7061.
255. Buser, C. and P. Walther, *The structure and behavior of liquid water*. Journal of Microscopy, 2008. **230**(2): p. 268-277.
256. Swain, S.C., et al., *C. elegans metallothioneins: new insights into the phenotypic effects of cadmium toxicosis*. J Mol Biol, 2004. **341**(4): p. 951-59.
257. Swain, S., et al., *Linking toxicant physiological mode of action with induced gene expression changes in Caenorhabditis elegans*. BMC Syst Biol, 2010. **4**: p. 32.
258. Gonzalez-Moragas, L., et al., *Protective Effects of Bovine Serum Albumin on Superparamagnetic Iron Oxide Nanoparticles Evaluated in the Nematode Caenorhabditis elegans*. ACS Biomaterials Science & Engineering, 2015. **1**(11): p. 1129-1138.
259. Sinnecker, H., K. Ramaker, and A. Frey, *Coating with luminal gut-constituents alters adherence of nanoparticles to intestinal epithelial cells*. Beilstein J Nanotechnol, 2014. **5**: p. 2308-15.

260. Dosio, F., et al., *Preparation, characterization and properties in vitro and in vivo of a paclitaxel–albumin conjugate*. *Journal of Controlled Release*, 1997. **47**(3): p. 293-304.
261. Kolotuev, I., et al., *Targeted ultramicrotomy: a valuable tool for correlated light and electron microscopy of small model organisms*. *Methods Cell Biol*, 2012. **111**: p. 203-22.
262. Levy, M., et al., *Degradability of superparamagnetic nanoparticles in a model of intracellular environment: follow-up of magnetic, structural and chemical properties*. *Nanotechnology*, 2010. **21**(39).
263. Lunov, O., et al., *Lysosomal degradation of the carboxydextran shell of coated superparamagnetic iron oxide nanoparticles and the fate of professional phagocytes*. *Biomaterials*, 2010. **31**(34): p. 9015-9022.
264. Soenen, S.J.H., et al., *Intracellular Nanoparticle Coating Stability Determines Nanoparticle Diagnostics Efficacy and Cell Functionality*. *Small*, 2010. **6**(19): p. 2136-2145.
265. Malvindi, M.A., et al., *Toxicity Assessment of Silica Coated Iron Oxide Nanoparticles and Biocompatibility Improvement by Surface Engineering*. *Plos One*, 2014. **9**(1).
266. Li, Z., et al., *Fabrication of coated bovine serum albumin (BSA)-epigallocatechin gallate (EGCG) nanoparticles and their transport across monolayers of human intestinal epithelial Caco-2 cells*. *Food Funct*, 2014. **5**(6): p. 1278-85.
267. Caracciolo, G., et al., *Surface adsorption of protein corona controls the cell internalization mechanism of DC-Chol–DOPE/DNA lipoplexes in serum*. *Biochimica et Biophysica Acta (BBA) - Biomembranes*, 2010. **1798**(3): p. 536-543.
268. Frazer, D.M. and G.J. Anderson, *The regulation of iron transport*. *Biofactors*, 2014. **40**(2): p. 206-214.
269. Unrine, J., P. Bertsch, and S. Hunyadi, *Bioavailability, Trophic Transfer, and Toxicity of Manufactured Metal and Metal Oxide Nanoparticles in Terrestrial Environments*, in *Nanoscience and Nanotechnology*. 2008, John Wiley & Sons, Inc. p. 345-366.
270. Wohlschläger, T., et al., *Methylated glycans as conserved targets of animal and fungal innate defense*. *Proceedings of the National Academy of Sciences*, 2014. **111**(27): p. E2787-E2796.
271. Shi, H., J. Tan, and H. Schachter, *N-glycans are involved in the response of *Caenorhabditis elegans* to bacterial pathogens*. *Methods Enzymol*, 2006. **417**: p. 359-89.
272. Zhu, S., et al., **Caenorhabditis elegans* triple null mutant lacking UDP-N-acetyl-D-glucosamine:α-3-D-mannoside β1,2-N-acetylglucosaminyltransferase I*. *Biochemical Journal*, 2004. **382**(Pt 3): p. 995-1001.
273. Merlot, A.M., D.S. Kalinowski, and D.R. Richardson, *Unraveling the mysteries of serum albumin—more than just a serum protein*. *Frontiers in Physiology*, 2014. **5**(299).
274. Cui, Y., et al., *Toxicogenomic analysis of *Caenorhabditis elegans* reveals novel genes and pathways involved in the resistance to cadmium toxicity*. *Genome Biol*, 2007. **8**(6): p. R122.
275. Hsu, P.C., et al., *Quantum dot nanoparticles affect the reproductive system of *Caenorhabditis elegans**. *Environ Toxicol Chem*, 2012. **31**(10): p. 2366-74.
276. Hart (ed.), A.C., *Behavior*, in *WormBook*, T.C.e.R. Community, Editor., WormBook.
277. Hillyer, J.F. and R.M. Albrecht, *Gastrointestinal persorption and tissue distribution of differently sized colloidal gold nanoparticles*. *J Pharm Sci*, 2001. **90**(12): p. 1927-36.
278. Frohlich, E. and E. Roblegg, *Models for oral uptake of nanoparticles in consumer products*. *Toxicology*, 2012. **291**(1-3): p. 10-7.
279. Mahler, G.J., et al., *Oral exposure to polystyrene nanoparticles affects iron absorption*. *Nat Nano*, 2012. **7**(4): p. 264-271.
280. VanDuyn, N., et al., *The metal transporter SMF-3/DMT-1 mediates aluminum-induced dopamine neuron degeneration*. *J Neurochem*, 2013. **124**(1): p. 147-57.
281. Thakor, A.S., et al., *Gold nanoparticles: A revival in precious metal administration to patients*. *Nano Letters*, 2011. **11**(10): p. 4029-4036.

282. Khlebtsov, N. and L. Dykman, *Biodistribution and toxicity of engineered gold nanoparticles: A review of in vitro and in vivo studies*. Chemical Society Reviews, 2011. **40**(3): p. 1647-1671.
283. Shaw lii, G.F., et al., *Redox Chemistry and [Au(CN)₂(-)] in the Formation of Gold Metabolites*. Metal-Based Drugs, 1994. **1**(5-6): p. 351-362.
284. Huang, X. and M.A. El-Sayed, *Gold nanoparticles: Optical properties and implementations in cancer diagnosis and photothermal therapy*. Journal of Advanced Research, 2010. **1**(1): p. 13-28.
285. Maher, B.A., et al., *Magnetite pollution nanoparticles in the human brain*. Proceedings of the National Academy of Sciences, 2016.
286. Akbulut, O., et al., *Separation of Nanoparticles in Aqueous Multiphase Systems through Centrifugation*. Nano Letters, 2012. **12**(8): p. 4060-4064.
287. Mace, C.R., et al., *Aqueous Multiphase Systems of Polymers and Surfactants Provide Self-Assembling Step-Gradients in Density*. Journal of the American Chemical Society, 2012. **134**(22): p. 9094-9097.
288. Vanfleteren, J.R., *Oxidative stress and ageing in Caenorhabditis elegans*. Biochemical Journal, 1993. **292**(2): p. 605-608.
289. Clokey, G.V. and L.A. Jacobson, *THE AUTOFLUORESCENT LIPOFUSCIN GRANULES IN THE INTESTINAL-CELLS OF CAENORHABDITIS-ELEGANS ARE SECONDARY LYSOSOMES*. Mech Ageing Dev, 1986. **35**(1): p. 79-94.

APPENDIX 1. Working with *C. elegans* in the synthetic laboratory



APPENDIX SUMMARY

This chapter describes the equipment required to host *C. elegans* in the chemical laboratory, the standard protocols used to grow and maintain *C. elegans* and the procedures use to prepare the desired population for NP treatment.

APPENDIX INDEX

1.1 Set-up of the <i>C. elegans</i> facility in a Materials Science laboratory.....	195
1.1.1 Equipment	195
1.1.2 Working under sterile conditions	195
1.2 Maintenance of <i>C. elegans</i>	196
1.2.1 Obtaining <i>C. elegans</i>	196
1.2.2 Preparation of Nematode Growth Media (NGM).....	196
1.2.3 Preparation of the bacterial food source	197
1.2.4 Transference of worms.....	198
1.2.5 Freezing bacteria stocks	198
1.2.6 Freezing worm stocks	199
1.2.7 Preparation of other Media (M9 Buffer, S Basal, K-medium).....	199
1.2.8 Bleaching for cleaning and synchronizing worms	199
1.2.9 Obtaining the desired worm population.....	200

1.1 Set-up of the *C. elegans* facility in a Materials Science laboratory

The standard wild-type laboratory strain of *C. elegans* is Bristol N2. It is typically grown in Petri dishes on Nematode Growth Media (NGM) agar seeded with a lawn of *Escherichia coli* as bacterial food source. It can be also grown using liquid culture strategies with *E. coli* or axenically, and even in fermentor-like devices.

1.1.1 Equipment

The following equipment was acquired to set-up the *C. elegans* facility (**Figure 99**):

- Laminar flow cabinet, to work under sterile conditions. It is equipped with nitrogen and vacuum lines, and also has a germicidal UV lamp. If not available, an alcohol lamp could be used instead.
- Incubator: Worms were kept at $20\text{ }^{\circ}\text{C} \pm 1\text{ }^{\circ}\text{C}$. Humidity was maintained by placing a tray with deionizer water inside the incubator. Otherwise we realized that agar dried up very quickly due to the air flow inside the incubator.
- Nutating agitator, to maintain the eggs under agitation overnight after applying the bleaching protocol resulting in increased aeration which enhances the survival of L1.
- Stereoscope (7.5x-50x) to monitor *C. elegans*.

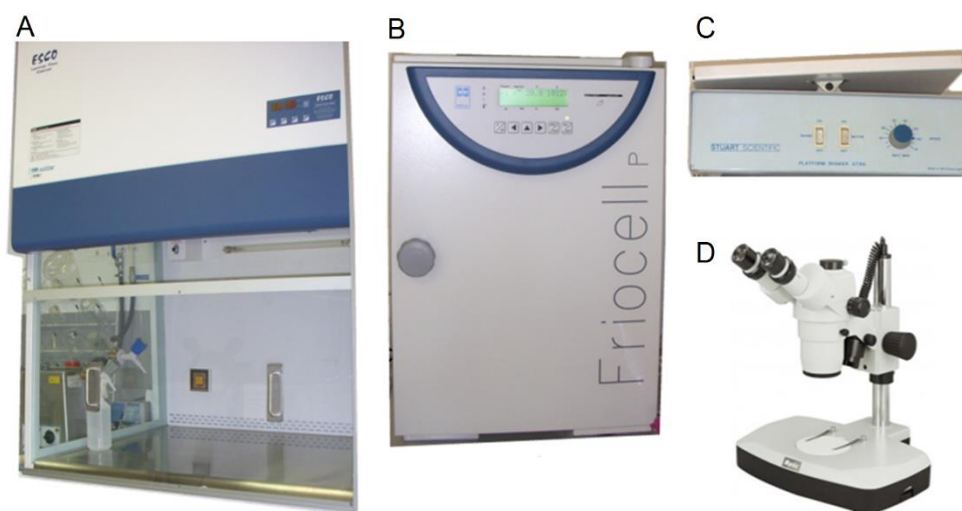


Figure 99. Equipment of the *C. elegans* facility in our lab. A) Laminar flow cabinet; B) Incubator; C) Nutating agitator; D) Stereomicroscope.

1.1.2 Working under sterile conditions

As *C. elegans* stocks can become contaminated with bacteria, yeast or mold, it is necessary to use sterile techniques when working with the stock plates (i.e. while transferring worms...) and with the reagents/media that will be used in such cultures (i.e. while preparing media components or bacterial cultures, seeding plates...). The laminar flow cabinet allowed us to work under sterile conditions. In order to preserve sterility, the bench inside the cabinet was cleaned with 70% ethanol before placing any objects inside, and fan was switched on 3 minutes before use so that the air flow stabilized. Once the

cabinet was in operation, sterility was maintained inside thanks to an ULPA-filtered laminar airflow. After work, fan was switched off and the bench was cleaned with 70% ethanol again. Finally, the cabinet was closed with its front cover, and sterilized by UV light (lamp on about 15 min.).

When working at the lab bench, the work area was cleaned with 70% ethanol in advance, and there was an alcohol lamp on all the time. The flame from the lamp creates an updraft that pushes airborne contaminants away. However, the lamp must be placed in a safe place so that cannot set things on fire, even if it is bumped accidentally. The flame was also used to sterilize objects by flaming them, in particular the worm picker between transfers, to avoid contaminating the worm stocks; and the spatula (previously dipped on alcohol) when transferring worms by chunking.

Regarding the sterilization of liquids, autoclaving was used for LB broth, LB agar and NGM agar; and sterile filtration (0.2 μm pore size) was used for most media components and test media. For handling sterile liquids, sterile plastic disposable serological pipettes were used.

1.2 Maintenance of *C. elegans*

C. elegans stocks are best maintained between 16 °C and 25 °C, most typically at 20 °C. They can be kept for months between transfers, as worms enter the dauer form. *C. elegans* and bacteria stocks can also be stored frozen (either in liquid nitrogen or at – 80 °C) with good viability. The maintenance of *C. elegans* involves the following steps: i) Preparation of Nematode Growth Media (NGM); ii) Preparation of the bacterial food source; iii) Transference of *C. elegans*.

1.2.1 Obtaining *C. elegans*

C. elegans wild-type (strain N2) was obtained from the *Caenorhabditis* Genetics Center (CGC) from the Massachusetts University, as well as its bacterial food source *Escherichia coli* strain OP50. The worms were maintained at 20 °C. A wide range of mutant strains and food sources can be purchased. They are sent in NGM plates by post.

1.2.2 Preparation of Nematode Growth Media (NGM)

To prepare NGM agar, we weighted 2.5 g peptone, 3 g NaCl and 17 g agar in 2 L Erlenmeyer flask, added 975 ml Milli-Q water, then autoclaved (121 °C, 40 minutes) and added 1 ml 1M CaCl₂, 1 ml (5 mg/ml) cholesterol in ethanol, 1 ml 1 M MgSO₄, and 25 ml 1 M KPO₄ buffer. We poured a volume of agar into Petri plates according to their sizes, as indicated in **Table 41**.

Table 41. Amount of NGM poured into the plates depending on their diameter.

Plate diameter	15 cm	10 cm	6 cm
Volume of NGM agar	100 ml	35 ml	12 ml

Agar solidifies at 32–40 °C. Plates (**Figure 100**) were left at room temperature for 2–3 days before use to allow for detection of contaminants, and to allow excess moisture to evaporate. Plates stored at room temperature remained usable for several weeks.

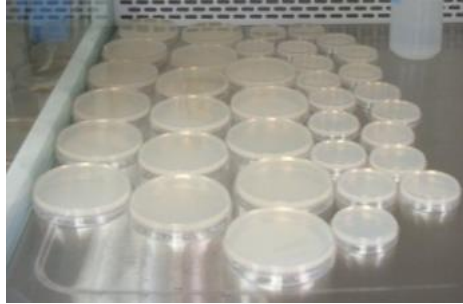


Figure 100. NGM plates inside the laminar flow cabinet, upside down.

1.2.3 Preparation of the bacterial food source

To prepare the bacterial food source for *C. elegans*, we first prepared an OP50 streak plate in LB agar. For that, we streaked bacteria from our frozen stock at -80 °C at the top end an LB agar plate in a zig-zag horizontal pattern. The plate was incubated overnight at 37 °C. Once cool, the streak plate was stored at 4 °C and used to prepare bacterial liquid cultures. Streak plates remained usable for several months.

The lawn of OP50 in NGM plates was prepared by transferring an aliquot of an OP50 liquid culture in the center of such plates according to their size (**Table 42**).

Table 42. Amount of bacterial culture used to seed NGM plates according to their diameter.

Plate diameter	15 cm	10 cm	6 cm
Volume of OP50	5 ml	0.6 ml	0.3 ml

Bacterial liquid cultures were prepared by transferring a colony from the streak plate to 20 ml of LB broth in a 50-ml centrifugal tube, and allowing it to grow overnight (**Figure 101**). Liquid cultures were stored at 4 °C, and used to seed NGM plates. Liquid cultures remained usable for several weeks.

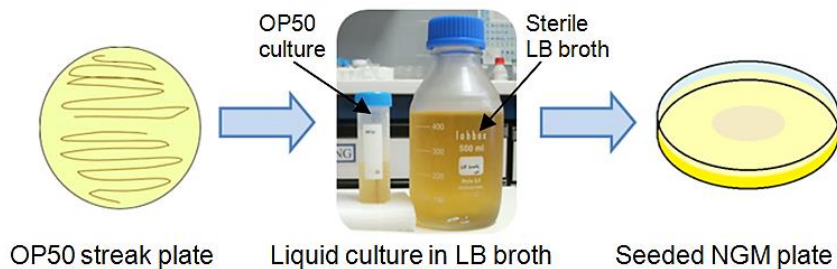


Figure 101. Preparation of the bacterial food source for *C. elegans*.

Seeded plates remained usable for 2-3 weeks. The growth of OP50 is limited on NGM plates, as it is a uracil auxotroph. The result is a limited bacterial lawn, which is desirable for easier observation of the worms.

Recipes

- LB agar [10 g tryptone, 5 g yeast extract, 10 g NaCl, 7,5 g agar in 1 L H₂O. Sterilize by autoclave (121 °C, 40 min)];
- LB broth [10 g tryptone, 5 g Yeast extract, 5 g NaCl, 1 ml 1 N NaOH in 1L water. Sterilize by autoclave (121 °C, 40 min)].

1.2.4 Transference of worms

Worms were transferred from old plates to fresh plates either by chunking or by worm picking (**Figure 102**), according to the purpose of such transference, as described below.

By chunking: 'Chunking' consists on moving a chunk of agar from an old plate to a fresh plate using a sterilized spatula. In the new plate, worms crawl out of the chunk and spread out onto the bacterial lawn.^[133] Chunking was used for transferring worms when food was scarce and starvation was not desired. The old plates used for chunking must not be contaminated. Otherwise, contaminants will be transferred to the new plate within the chunk (i.e. spores of yeast, bacterial cells).

By worm picking: Single animals can be picked by means of a worm picker.^[133] To pick a worm, we got a blob of *E. coli* OP50 on the end of the picker before gently touching the top of the chosen worm. The worm stuck to the bacteria. We could also pick several animals at a time by this method. However, it took a bit of experience with a worm picker to avoid poking holes in the agar. Worms crawl into the holes, making it difficult to see or to pick them. To put a picked worm on a fresh plate, we put a drop of water, then lowered the tip of the worm picker inside the drop, and held it there to allow the worm to crawl off of the picker onto the drop. The drop soaked into the plate and the worms remained in the surface of the agar of the fresh plate. It is important to avoid having worms for too long on the picker or they will desiccate and die. Worm picking was used to pick a worm identified under the microscope, i.e. a worm with a concrete phenotype. In our case, we used this method to pick gravid adults to perform bleaching in a drop, and to pick the desired number of worms in the assays described in this thesis.

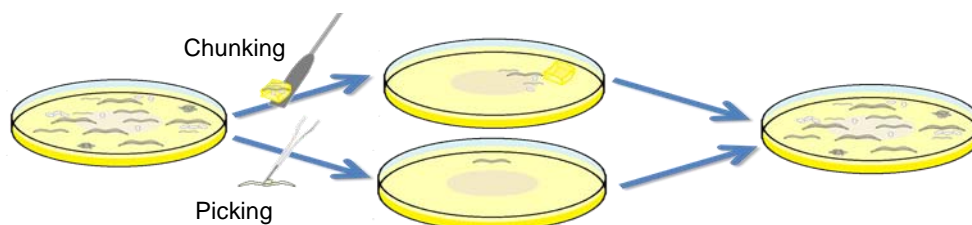


Figure 102. Scheme of the transference of worms. The upper procedure shows transference by chunking. The lower part corresponds to transference by picking.

1.2.5 Freezing bacteria stocks

We prepared cryovials of *E. coli* OP50 from the CGC. For this, we centrifuged a bacterial liquid culture, removed supernatant, added the same volume of glycerol, and

transferred 1 ml of the resulting mixture to 1.8-ml cryovials. Cryovials were stored at -80°C .

1.2.6 Freezing worm stocks

We rinsed a plate full of freshly starved L1-L2 with S basal, and mixed it (1:1) with 30% glycerol in S basal. We transferred 1 ml of the resulting mixture to 1.8-ml cryovials. Cryovials were stored at -80°C .

1.2.7 Preparation of other Media (M9 Buffer, S Basal, K-medium)

The following recipes were used to paper M9 buffer, S basal and K-medium:

- M9 buffer [3 g KH_2PO_4 , 6 g Na_2HPO_4 , 5 g NaCl, 1 ml 1 M MgSO_4 , Milli-Q water to 1 litre. Sterilize by filtration (0.2 μm pore size)].
- S Basal [5.85 g NaCl, 1 g K_2HPO_4 , 6 g KH_2PO_4 , 1 ml cholesterol (5 mg/ml in ethanol), H_2O to 1 litre. Sterilize by autoclaving.]
- K-Medium [2.36 g KCl, 3 g NaCl, Milli-Q water to 1 litre. Sterilize by filtration (0.2 μm pore size)].

1.2.8 Bleaching for cleaning and synchronizing worms

C. elegans stocks can become contaminated with other bacteria, yeast or mold. Most contaminants do not hurt the worms, but it is much easier to score phenotypes and transfer worms when the stocks are clean. Bacterial contaminants and yeast are easily removed by treating with a hypochlorite solution, which will kill the contaminant and all worms not protected by the egg shell. In contact with the alkaline hypochlorite solution, *C. elegans* tissue dissolve and, in the case of gravid adults, eggs are released. Embryos inside egg shells survive due to its relative resistance to the alkaline pH.

To perform bleaching (**Figure 103**), the worms of a stock plate containing gravid adults are collected in M9 in a centrifugal tube. Freshly prepared bleach prep consisting on 5N NaOH and household bleach (1:2) was added to a final concentration (1:10). The tube is vortexed every 2 min, and the reaction is monitored under the microscope. When eggs are obtained, M9 is added to stop the reaction. The tube is centrifuged at 1.300 xg to get an egg pellet. The supernatant is removed, fresh M9 is added, and the tube is centrifuged again. The procedure is repeated three times in total to remove excess of the bleach prep. The egg pellet is diluted with M9 was added to 1 ml and incubated overnight in a nutating agitator. The absence of food make that even embryos hatch, they cannot develop further than L1 larva. When the starved L1 are transferred to seeded NGM plates, synchronous growth begin due to the reintroduction of food. Animals should be monitored using the stereomicroscope and used at the desired stages.

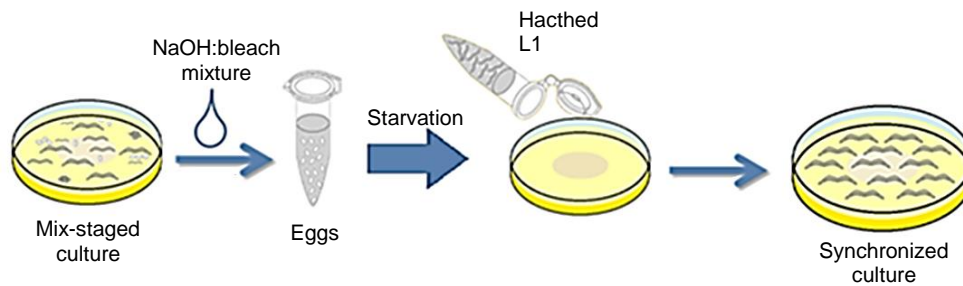


Figure 103. Bleaching protocol.

1.2.9 Obtaining the desired worm population

During this thesis we worked with three different types of *C. elegans* populations. For initial screenings, we used mixed-stage cultures. For separation on adults and larva based on size, we fractionated mixed-stage cultures using a 40- μm cell strainer. Indeed, most studies were performed with synchronized populations which means that all worms were in the same stage of the life cycle.

Synchronous cultures: Several chunks were performed from a stock plate to NGM plates seeded with OP50. After a few days, when a considerable number of gravid adults were observed under the microscope, the plates were rinsed with M9 buffer and bleached as described before in order to get an egg prep. When a large population of worms was required, we used 15-cm diameter plates, while 6- or 10-cm plates were adequate to perform experiments that required a smaller amount of worms.

Mixed-stage cultures: The work with mixed-staged cultures was performed using several 10-cm diameter NGM plates where the worms were in the presence of OP50. When the number of worms was considerate adequate for the purposes of the experiments, worms were collected in Milli-Q water, centrifuged 1 min at 1300 xg, and washed three times to remove any remaining bacteria and debris from the plate.

Fractioning mixed-staged populations of worms (Figure 104): A mixed-staged population of worms could be separate into juveniles (L1-L4) and adults using a cell strainer of 40 μm diameter (BD Falcon) on top of a 50-ml Falcon tube, based on the difference of size of the individuals according to their developmental stage. Larvae passed through the filter, while adults were retained by the mesh. In order to recuperate the adults, the filter was placed upside down in a 6-cm Petri dish and washed three times with Milli-Q water.

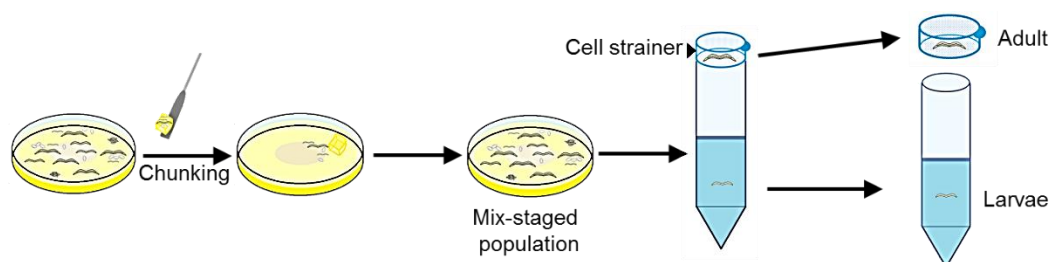
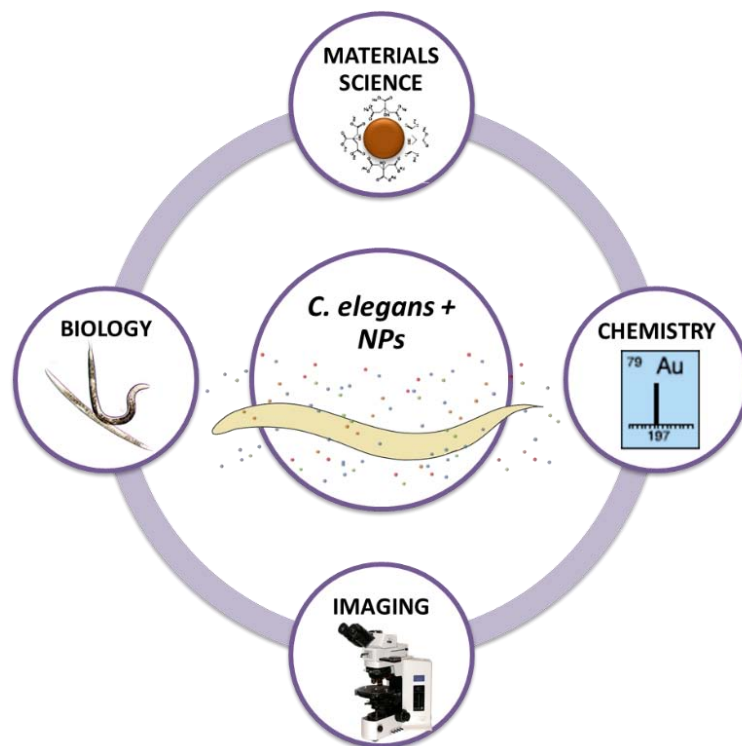


Figure 104. Fractioning of *C. elegans* mixed-stage cultures using a 40- μm cell-strainer.

APPENDIX 2. Open avenues between *C. elegans* and the nano-world



APPENDIX SUMMARY

This chapter illustrates the potentialities of the animal model *C. elegans* in combination with materials sciences techniques, presenting some preliminary work with potential for further experimentation.

APPENDIX INDEX

2.1	Introduction.....	203
2.2	Promising techniques for future work	203
2.2.1	Magnetic separation	203
2.2.2	Magnetic Resonance Imaging.....	203
2.2.3	Hyperthermia.....	204
2.2.4	Fluorescence microscopy.....	205
2.2.5	Gradient centrifugation to study stress responses	206
2.4	Chapter conclusions	207

2.1 Introduction

C. elegans hold great promise in the materials science laboratory, where many protocols and techniques could be adapted to perform studies in this small animal model. During this thesis, we performed some preliminary experiments using different materials science techniques. This chapter presents preliminary results obtained in NP-treated *C. elegans* specimens.

2.2 Promising techniques for future work

2.2.1 Magnetic separation

Magnetically-labelled worms can be separated from unlabelled using a simple magnet. Exposures for 24 h in liquid media were led to rapid attraction (**Figure 105**). Because of the magnetization increases with size, the magnetization of *C. elegans* treated with 9-nm and 12-nm SPIONs was greater with 6-nm SPIONs-treated worms although it was also efficient. The use of magnetized worms could be useful in the *C. elegans* community, i.e. to separate mutants with feeding impairments. Magnetic labelling could also be applied to the immobilization of worms by applying a magnetic field under the microscope. For these applications, it is noteworthy the biocompatible properties of SPIONs, as well as the possibility of excretion of the labelling by food resumption within less than 2 h.

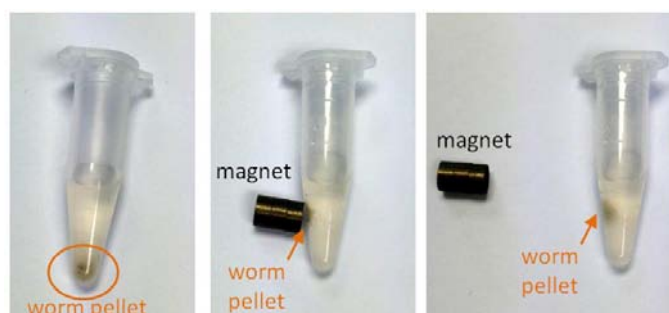


Figure 105. SPION-treated worms respond to the application of a magnetic field. A) Pellet of treated worms. B) When a magnet is located near the tube, treated worms are attracted by the magnet. C) After the magnet is removed, the worm pellet can be seen close to the prior magnet location.

2.2.2 Magnetic Resonance Imaging

We were able to detect the MRI signal arising from C-SPION treated worms using a Bruker 7T MRI BioSpec 70/30 USR (**Figure 106**). The signal increased with increasing number of labelled animals. Their T_2 value (49 ± 13 ms) was lower than that of control worms (66 ± 11 ms) (**Figure 107**), as expected.

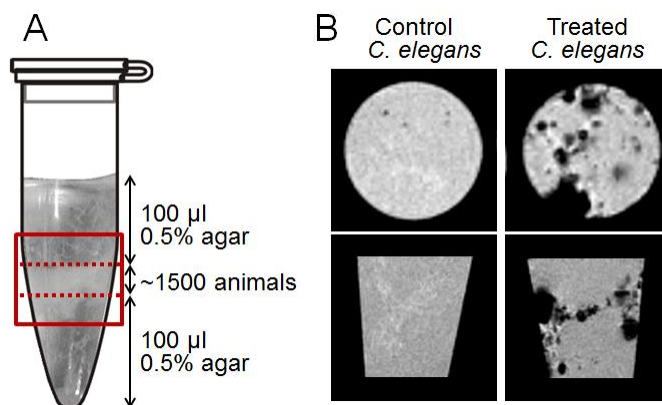


Figure 106. Magnetic Resonance Imaging of control and SPION-treated *C. elegans*. A) Sample composition. The square indicates the part of the sample shown in Panel B. B) MRI T2w* images of control worms (left) and worms treated with 500 µg/ml SPIONs for 24 h (right). C) T2 values of control and treated worms obtained from the axial slices shown in Panel B.

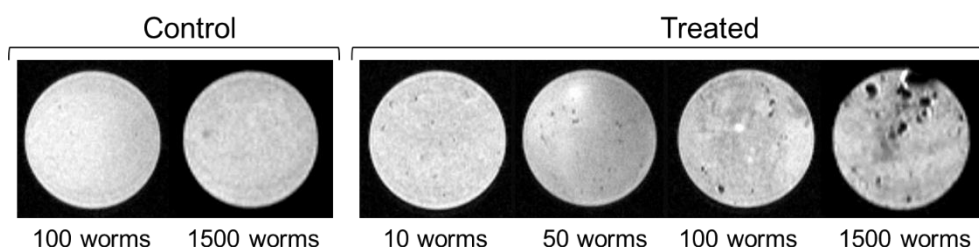


Figure 107. Magnetic Resonance Imaging of control and SPION-treated *C. elegans*.

2.2.3 Hyperthermia

The use of SPIONs to manipulate *C. elegans* by applying a magnetic field have already been reported by Huang *et al*, confirming that it is definitely possible to excite SPIONs inside the *C. elegans*.^[177] In their study, they used to heat induced to alter the motor behaviour of *C. elegans*, and calculated a local temperature of 42 °C in the targeted neurons after application of the magnetic field. By switching on and off the magnetic field, they could manipulate the locomotion of treated worms. However, this experimental system required the use of targeted functionalized SPIONs and the use of a transgenic strain, hence involved a big effort. Our experimental approach was rather simpler, consisting on the use of SPION-treated worms to study whether magnetic hyperthermia treatment changed the biodistribution of the NPs, induced a delay in the life cycle, or triggered higher stress, than SPION-treated worms not exposed to the magnetic field.

In collaboration with the group of Dr. Jesús de la Fuente at INA-UNIZAR, Zaragoza, we tried to use SPIONs-treated worms to induce a local increase of the temperature by magnetic hyperthermia using a Nanoscale Biomagnetics hyperthermia device. We initially used our 6-nm citrate NPs but could not observe any difference regarding the biodistribution of the NPs after the hyperthermia, neither on the lifecycle resumption of *C. elegans*. Given the low calorimetric ability of our small NPs (SAR <5 W/g

aT 260 kHz), we moved to 12-nm SPIONs provided by the group of Dr. Jesús de la Fuente with a SAR of 325 W/g but obtained very similar results.

The difficulty of these experiments was related to the finding of a good indicator of heat generation. Given the small increase of temperature, measuring the temperature of the media was not informative as NP heating could not induce an increase of this temperature. We hypothesised that gut autofluorescence would give us clues, as it is used as a stress indicator, but we could not find any differences between treatment conditions. These results could be related to the fact that no significant heat is being generated inside the *C. elegans*. In order to get a positive control of heat stress, we incubated *C. elegans* for 30 min at 37 °C, and observed a 1.4-fold increase in the gut autofluorescence comparing the thermally treated worms with untreated animals. Even though the worms looked very stressed (they barely moved), the change in the autofluorescence increase was not profound, considering a standard deviation of 25%. We hypothesise that magnetic hyperthermia of 6-nm and 12-nm SPION treated worms does not result in a temperature increase strong enough to produce a noticeably increase of the intrinsic autofluorescence of the worm, whose increase is related to stress responses. We propose that the use of mutants with *hsp* fused to GFP (i.e. *hsp-70:gfp* mutants) could bring promising results in the evaluation of magnetic hyperthermia treatment of SPION-exposed worms, as *hsp* genes are very sensitive to heat stress.

Similarly, the application of a laser at the excitation wavelength of the SPR of gold nanoparticles could result in heat generation in *C. elegans*, as have been previously reported with other simple organisms.

2.2.4 Fluorescence microscopy

The use of fluorescent nanoparticles have allowed the study of the particle sizes that can enter the body of the worm by feeding, and provided information of the size-exclusion mechanisms of the worm's pharynx. Fang-Yen *et al* concluded that particules larger than 3 µm could not enter *C. elegans* pharynx, while smaller particles did enter through the alimentary system and accumulated in the *C. elegans* intestine.^[214] Using 100 and 500-nm fluorescent latex beads, we were able to confirm that these NP size range are able to be ingested, and were located only in the intestinal lumen of the *C. elegans* after 24 h exposure (**Figure 108**).

However, the potential of fluorescence microscopy in *C. elegans* has yet to be completely exploited. Advanced techniques such STORM could allow single-NP localization of fluorescently-modified NPs in *C. elegans*, but these labels should comply with the specific requirements of STORM of photoswitching. Based on the high autofluorescence of *C. elegans*, STORM attempts should be better performed using the laser at 647 nm, i.e. by using CY5 and Alexa Fluor. For instance, the coating of SPIONs with CY5-BSA would allow us to track the *in vivo* coating fate by direct visualization of BSA-SPION treated *C. elegans*.

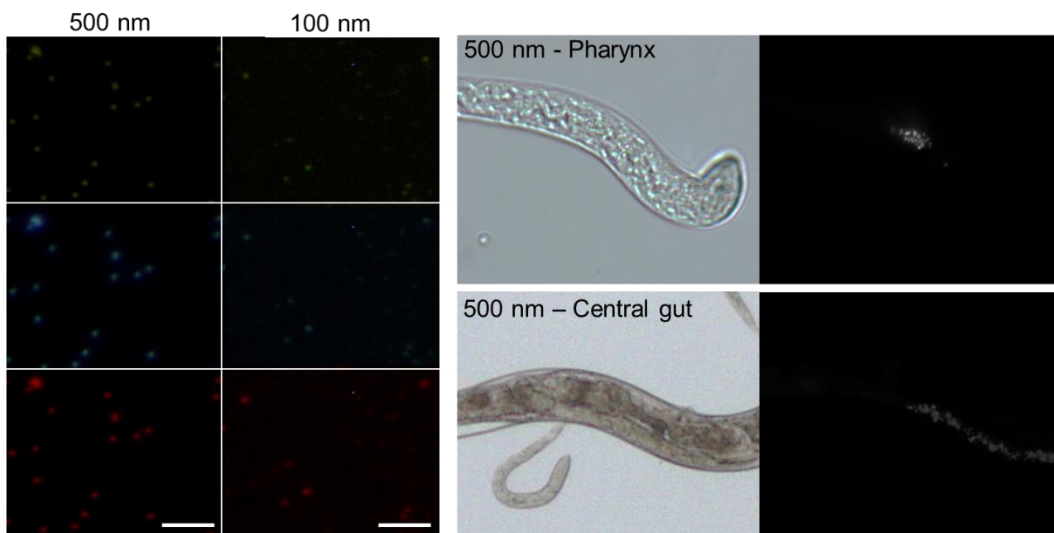


Figure 108. Images of different sizes of fluorescent latex beads (100 nm, 500 nm and 5 μm Tetraspeck® from Invitrogen) in the green, blue and red channels. Scale bar: 10 μm .

2.2.5 Gradient centrifugation to study stress responses

These experiments were done in collaboration with Gökay Avci from Sabanci University, Istanbul, during his short stay in our lab. By studying the density of *C. elegans* treated with SPIONs, we aimed to study NP uptake. For this, we used aqueous two-phase systems (ATPS) composed of Dextran and Ficoll at different concentrations.^[286, 287] Unexpectedly, we found that NP treated worms appeared to be less dense than non-treated worms. Based on these findings, our hypothesis was that nanoparticle triggered stress response in *C. elegans*, resulting in the accumulation of lipofuscin granules which are highly composed of fat, which would reduce the density of the treated nematodes even compensating NP uptake. To further investigate this issue, we performed the same experiments using Paraquat (PQ) treatment to deliberately stress the worms. Paraquat is known to induce oxidative stress in *C. elegans* and promote lipofuscin accumulation.^[288, 289] PQ treated worms appeared to be significantly less dense, confirming that stress does reduce the density of the worms probably by increasing fat content, similarly as what happens during ageing of *C. elegans*.

We assayed different concentrations to try to relate the degree of stress of NP treated worms with that of PQ treated worms. Although we observed some dose-effect response (**Figure 109**), most worms did not successfully entered the two-phase system but stayed on top. To solve this, higher densities would have been required, however a Three-Phase System would have been required for this aim. Therefore, aqueous multiphase systems may allow the study of stress responses in NP-treated *C. elegans*. However, it is required to find the appropriate composition of biocompatible polymers and the right densities, to optimize centrifugation time and speed, and to define a systematic method for image capturing and processing.

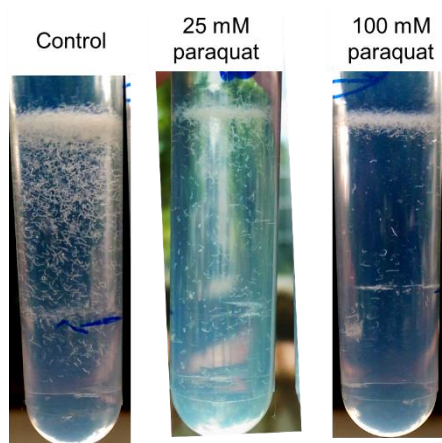
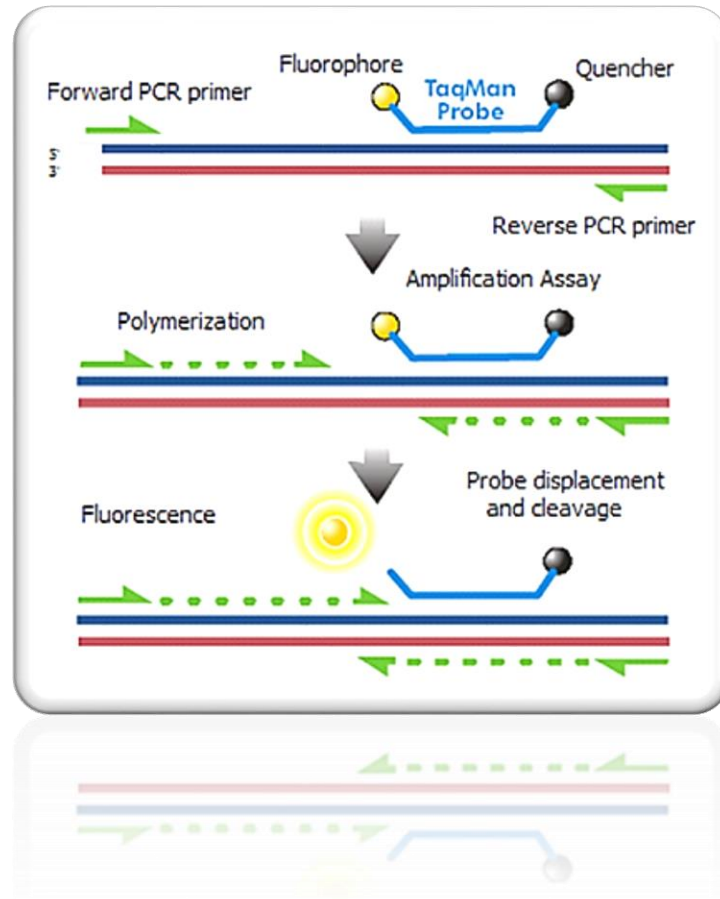


Figure 109. Centrifugation of control and PQ-worms using ATPS at 18% Dextran and 18% Ficoll (density=1.055-1.065).

2.3 Chapter conclusions

We have explored different promising joint efforts combining materials sciences and the use of *C. elegans*, including MRI, magnetic hyperthermia, fluorescence microscopy and gradient centrifugation. However, optimization of the experimental set-up is required before successfully applying these techniques to NP-treated *C. elegans* specimens yielding robust results.

APPENDIX 3. Primers and probe combinations of qPCR analysis



APPENDIXSUMMARY

This appendix includes the gene sequence of each of the gene studied by qPCR, the combination of primer-probe used in the assays, and the resulting amplicon size.

APPENDIX INDEX

3.1 Primers (and probe combination) already available in the lab	211
3.2 Primers (and probe combination) designed during my stay	214
3.3 Primers (and probe combination) designed for the validation of the microarrays	221

3.1 Primers (and probe combination) already available in the lab

sod-2

spliced + UTR (870 bp)

atatgtttctgcgaattgtaaaaattatattgactattgaatatttaattattgcagccgaaaATGCTTCAAAACACCGTTTCGCT
 GTGTCTCAAAGCTTGTTC AACCGATCACAGGAAGTCGCTGCTGTTTCGCTCGAAAGCACTCGCTGC
 CAGATTACCATACGACTATGCTGATTTGGAGCCTGTAATCAGTCACGAGATTATGCAACTTCA
 TCATCAAAAGCATCATGCCACTTATGTGAACAATCTCAACCAAATTGAGGAAAAGCTTCACGAG
 GCGGTCTCCAAAGGAAACGTCAAAGAAGCTATCGCTCTTCAGCCAGCTCTCAAGTTCAATGGA
 GGAGGACATATCAACCACTCCATCTTCTGGACTAATTTGGCAAAGGACGGAGGAGAACCATCG
 GCGGAGTTGCTCACCGCAATTAAGAGCGACTTCGGATCTCTGGATAATCTTCAAAAACAGCTTT
 CGGCATCAACTGTCGCTGTTCAAGGATCAGGATGGGGATGGTTGGGATACTGTCCAAAGGGAA
 AGATCTTGAAGGTTGCCACATGTGCCAATCAGGATCCACTTGAGGCAACAACCTGGACTTGTTC
 ACTGTTCCGAATTGACGTCTGGGAGCACGCTTACTACTTGCAGTACAAGAATGTTTCGACCAGAT
 TATGTCAATGCTATTTGGAAGATCGCCAACTGGAAGAACGTCAGCGAGCGTTTTGCAAAGGCCA
 CAGCAATAAatgagctgaatcacaagaattaatcgcaaatgtagcagtagaagttgactcccattgtttgtaactattttgttctaatta
 tttcgaatgtaaattttcaaaccttttcaaatgaaaagtttcaccgaaa

Primers:

FOR 5'TTGTTCAACCGATCACAGGA3'
 REV 5'GTAAATCTGGCAGCGAGTGC3'

Amplicon size: 60 ba

Probe:

#150

sod-3

spliced + UTR (833 bp)

gttcgagaaaagtgaccgtttgtcaaatcttctaattttcagtgataaaaATGCTGCAATCTACTGCTCGCACTGCTTCAA
 AGCTTGTTC AACCGTTGCGGGAGTTCTCGCCGTCGCTCCAAGCACTCTCCCAGATCTCC
 CATTCGACTATGCAGATTTGGAACCTGTAATCAGCCATGAAATCATGCAGCTTCATCATCAAAA
 GCATCATGCCACCTACGTGAACAATCTCAATCAGATCGAGGAGAACTTCACGAGGCTGTTTCG
 AAAGGGAATCTAAAAGAAGCAATTGCTCTCCAACCAGCGCTGAAATTC AATGGTGGTGGACACA
 TCAATCATTCTATCTTCTGGACCAACTTGGCTAAGGATGGTGGAGAACCTTCAAAGGAGCTGAT
 GGACACTATTAAGCGCGACTTCGGTCCCTGGATAACTTGCAAAAACGCTTTTCTGACATCACT
 ATTGCGGTTCAAGGCTCTGGCTGGGGATGGTTGGGATATTGCAAGAAAGACAAAATCTTGAAG
 ATCGCCACCTGTGCAAACCAGGATCCTTTGGAAGGAATGGTCCCACTTTTTGGAATTGACGTTT
 GGGAGCACGCCTACTACTTGCAGTACAAAAATGTCCGCCAGACTATGTCCATGCTATTTGGAA
 GATTGCCAACTGGAAGAATATCAGCGAGAGATTTGCCAATGCTCGACAATAAaagcaggaatattgg
 aattttcggttttacgaaaatattgaagataattcagatgtagtttaaacgctgagaattgtattttgtaattgttaataaaagaacgcacagt
 ttttctatg

Primers:

FOR 5'CACTGCTTCAAAGCTTGTTC A3'
 REV 5'ATGGGAGATCTGGGAGAGTG3'

Amplicon size: 77 ba

Probes:

#152

pcs-1

spliced + UTR (1364 bp)

ctaaattccaattcacttctaa**ATGTCGCAACGAAGACACTTCAAAATGTCGGTAACCGCAAAAAATTTCTA**
CCGAGAGCCGCTTCCAGAGACGTGATTGAGTTTTCCAGTGAGCTTGGCAAGAACTTTTCAC
CGAGGCATTGGTTGAGGATCAGCGAATATTTATTCAAGTTGGCATCTCAATTTTCGGACACAA
GATGAGCCAGCATATTGTGGTTTGGACACATTAGTGATGGTTCTGAATGCGTTGGAAGTGGATC
CTGAAAAAGTTTGGAAAGCGCCGTGGAGATTCTATCACGAGTCGATGCTGGATTGTTGTGTGC
CTTTGGAAAAATTAGAAAAGTGGAAATCAATCTACAACAATTCTCCTGCCTTGCAAAATGTAAT
CGTCTAAAATCTACAGTAAGCTACGGTGACAATTCTCCAGATTTTCTCAAAAAATTCGGGACATC
GCTCGTGAATTCAGTTTCAAGTGATGATCAAGTTCTGGTAGCCAGCTACGATCGGAGTGTGCTT
GGTCAAACGGGATCAGGTCACTTTTACCACCTGCGCCTATCACGAGGATTCTGATCAAGTTC
TGATTATGGACGTTGCAAGATTCAAGTATCCACCTCATTGGGTGAAATTGGAGACTCTTCAGAA
GGCATTGTGCTCCGTTGATGTTACAACAAAACCTACCACGTGGGCTCGTGGAGCTCGAACTAAA
AAAAGGAACGAGGCCCTCTGATAATGTATGGATTGAAAGCCTATGTGAACATCAATGATCCGAT
TTTGCCACGTCAGTGATCTCGTGGAAATCAATTCTTATTATGTGATCCATTAGAAGACGACGAAG
AAGAATTCGAATTGTGCTGTGCAAGTTTCGGGCAATGTTTTGCTCCCCACGCAATGTGCTGCAC
TCAGAAAACTTTGACGCGAGATCAAAAAAACTCGTGTACAGAATGCTCAACCGATCAGAATGAG
GCTTGCAAGATGATTTGTTTCGAAATACGAAGAACCCGATTTGCCGAAGTGTCTCTAGTTCCGG
CGGTTGCTGCTCTTCTCATAGCGTGGCCATTCGAAAAAGGATATTCAGAACGAAGTGATCGAAT
AGGAAATCTTGGCGAAAAATATAAAATGAATTTTCGGCAGAGACTATGAATGAAATGAACCAA
CTGACAACCCAGATCCGAACGTTAATCAGTTGTTTCGAAGCCACCTGTCGTGATCAATATCAACA
AACCGGACGCCACAAGCAACAAATGCTGTAAAAACAAAATCGGGCAATCATGTGCGTGTGCGA
ATGATGTTAATTTATAAtttgggaattttatgaaattcattttattaacgagataaaataaaaaacatgcattt

Primers:

FOR 5' **AAGCGCCGTGGAGATTCTA3'**

REV 5' **GTTGTAGATTGATTCCA**CTT3'

Amplicon size: 87 ba

Probes:

#159

mtl-1

spliced + UTR (375 bp)

agctcaattgactgctgaaattaagaaatc**ATGGCTTGCAAGTGTGACT**GCAAAAACAAGCAATGCAAGTGC
GGAGACAAATGTGAATGCAGTGGAGACAAGTGTGTTGTGAGAAGTACTGCTGTGAGGAGGCCAG
TGAGAAAAAATGCTGTCCAGCTGGATGTAAGGGAGACTGCAAGTGTGCAAACTGTCATTGTGC
AGAGCAGAAGCAGTGCGGAGACAAGACCCATCAACACCAGGGAAGTCTGCGGCTCATTAAaa
tgtttcagagttgaaatctgaaaaataccacaattcctactaaactgtgaacatcctactaaattgtaattacctccgagatttatgtaaactaataaa
tgtgtatattactgtga

Primers:

FOR 5' **CATGGCTTGCAAGTGTGACT3'**

REV 5' **CACAGCAGTACTTCTCACAAC3'**

Amplicon size: 94 ba

Probes:

#86

mtl-2

spliced + UTR (315 bp)

aagcttcaaaggcttactcaaaa**ATGGTCTGCAAGTGTGA**CTGCAAAAACCAAATTGTTCTGCAACAC
CGGAACTAAAGATTGCGATTGCTCCGACGCCAAGTGCTGTGAGCAATACTGCTGCCCAACTGC
CAGTGAGAAGAAATGCTGCAAATCTGGATGTGCCGAGGATGCAAGTGTGCCAACTGCGAATG
TGCTCAGGCTGCTCATTAAttgaaattaactcttcccttgaacaaattcctactaattgatattgtcgagggttttcttgaagc
 tgaataaatgttaaatattattgt

Primers:

FOR 5'AAAAATGGTCTGCAAGTGTGA3'

REV 5'GGCAGTTGGGCAGCAGTA3'

Amplicon size: 111 ba

Probes:

#100

rla-1

spliced + UTR (498 bp)

actttcttcagcgttctatcaaacggttctcttggagctaaggcaaaccgcgcaacttacgattgaaga**ATGGCTTGAACCAA**
GAACTGGCTTTCGTCTACGCTGCTCTCATCCTTCAAGATGACGAGGTCGCCATCACCGGCGAG
AAGATCGCTACCCTTCTCAAGGCCGCCAACGTCGAGTTCGAGCCATACTGGCCAGGACTCTT****
CGCCAAGGCTCTCGAGGGAGTTGATGTGAAGAACCTCATCACTTCTGTCTCTTCCGGAGCCGG****
ATCTGGACCAGCTCCAGCCGCCGCCGCTGCTGCTCCAGCTGCTGGAGGAGCCGCCCCAGCTG
CCGAGACCAAGAAGAAGGAGGAGCCAAAGGAGGAATCCGATGACGACATGGGCTTCGGTCTC
TTCGACTAAagatctgttattgtttcaataaatctgttaacaacaccaagaaagtgttatggcttcaaaagtgaaaaaggagggtatt
 ttgg

Primers:

FOR 5'ACGTCGAGTTCGAGCCATA3'

REV 5'CCGGAAGAGACAGAAGTGATG3'

Amplicon size: 91 ba

Probes:

#162

3.2 Primers (and probe combination) designed during my stay

act-5

spliced + UTR (1344 bp)

```
cATGGAAGAAGAAATCGCCGCCCTCGTTGTCGACAATGGATCCGGAATGTGCAAGGCCGGATT
CGCCGGAGACGATGCTCCACGCGCGTCTTCCCGTCCATCGTCCGACGCCACGTCATCAGG
GAGTGATGGTCGGTATGGGACAGAAGGACTCGTATGTCGGAGATGAAGCACAATCCAAGAGA
GGAATCCTCACCTTGAAGTACCCAATCGAGCACGGAATCGTCACCAACTGGGATGATATGGAG
AAAACTGGCATCACACATTCTACAACGAGCTTCGTATCGCCCCAGAGGAACACCCAGTTCTCC
TTACCGAGGCTCCATTGAACCCAAAGAGCAACAGAGAAAAGATGACACAGATCATGTTTGAGAC
CTTCAACACTCCAGCCATGTACGTCAACATTCAGGCTGTGCTTTCCTTGTACGCTTCCGGAAGA
ACCACCGGAATCGTTTTGGACACCGGAGATGGTGTCACTCACACCGTTCCAATCTATGAAGGA
TATGCCCTCCACATGCCATCCAACGTCTCGATCTTGCCGGACGCGACTTGACCGACTACATG
ATGAAGATCCTCACCGAGCGCGGTTACACTTTTACCACCACCGCCGAACGCGAAATCGTCCGG
GACATCAAAGAGAAGCTTTGCTACGTCGCCACGACTTCGAGTCCGAGCTCGCCGCCGCCGC
CTCCTCCTCCTCCCTCGAGAAGAGCTACGAGCTTCCCGACGGACAGGTTATCACCATCGGAAA
CGAGAGATTCCGCTGCCCAGAAGTCCTCTTCCAGCCTGCCTTCATCGGAATGGAAGGTGCCGG
AATCCACGAGACCACCTACCAATCCATCATGAAGTGCATGTCGACATCAGAAAGGATCTCTAC
GCCAACACTGTTCTCTCCGGAGGTACCTCCATGTTCCAGGAATCGCTGATCGTATGCAAAAAG
GAGATTCAACATTTGGCTCCAAGCACAATGAAGATCAAGATTATTGCTCCACCAGAGCGCAAGT
ACTCCGCTGGATCGGAGGATCTATTCTTGCTTCCCTCTCAACCTTCCAGCAAAATGTGGATCTC
CAAGCAGGAGTACGACGAGTCCGGCCCATCGATTGTTACCGAAAAGTGCTTCTAAgctgattttttca
aattttttttcaacatgtgcctccatttctagcgaaacacgattttacttgacacaaatccatgagatactcattttcttatattatggttcttaa
catgaataaaactgtaggaccacttgctacttgggaattgagtaaaatgatggtactgtgtattattcccctcatttttaaaatataat
```

Primers:

FOR 5' CCAATCTATGAAGGATATGCC 3'

REV 5' CATCATGTAGTCGGTCAAGTC 3'

Amplicon size: 80 ba

Probe:

#158

chc-1

spliced + UTR (5396 bp)

gtatataatttattgtaagaagttttccattctacacacagtttcaagATGGCGCTCCCAATCAAATTTACGAGCACCT
 GCAGCTTCCGAATGCTGGAATTCGGGTGCCCAACATTACATTCTCCAATGTCACAATGGAATCT
 GATAAGAACATTGTTGTTTCGTGAGATGATTGGTGATCAACAACAGGTTGTGATTATTGATTTGGC
 CGACACAGCGAATCCAACCTCGTCGTCCAATTTCTGCTGACTCAGTAATCATGCACCCAACCTGCC
 AAAATTTCTTGCTTTGAAATCTGGCAAGACACTTCAAATTTTCAATATTGAGTTGAAAAGCAAAGT
 GAAAGCTCATCAGAATGTAGAAGATGTAGTTTATTGGAAGTGATCAGTGAGAAAACGATTGCA
 CTCGTTTCCGACACAGCCGTCTATCATTGGTTCGATCGAGGGTGATGCAGCTCCAGTCAAGATG
 TTCGATAGACATCAGTCGTTGGCCGGAACCTCAAATCATAAATTATCGCGCTGATGCCGAAAACA
 AGTGGCTCGTTCTTATTGGAATTTCCGCAAAAGACTCCCGTGTGTTGGAAGTATGCAATTGTA
 CAGTACCGAGAGAAAAGTATCGCAGCCAATCGAAGGCCATGCCGCTTGTTCGTTTCGATTCAA
 GGTTCGATGGAAACCAAACCCATCTAACTTATTCTGTTTTCCGTCAAACCCGATAATGGAGGA
 AAATTGCACGTTATTGAAGTAGGAACCCAGCTGCTGGAAACACTCCTTTCCAAAAGAAGAATG
 TTGATGTTCCATATACCGCTGACACAGCTGGCGATTTTCCAGTGTCTATGCAGGTATCTGCGAA
 GCAAGGAATTTTACCTGGTAACAAAAGCAAGGATATGTTTCATCTTTATGATGTCGAGTCTGGAA
 CACGGATTTATTGCAATCGAATTTGACTGATACCGTATTTGTGACCTGTGAATACACAGCTACA
 GGAGGAATAATGGGAATTAACAGAAAGGGACAAGTTCTTTCCGTCTCTATCGATGAAGCTAACT
 TGGTCCGTTTCGTTACGAACCAGCTGCAAAATCCAGATTTGGCTTTGAAGTTGGCCGTGCGTTG
 TGATCTGCCTGGAGCTGAAGAGTTGTTGTTTCGCAAATCAACTGTTGTTTCAGCAACGGACAG
 TTTGGAGAATCAGCCAAGGTTGCTGCATCGGCTCCACAAGGAATTTGAGAACCAGCCACC
 ATTCAAAAGTCCAGCAGTGCCTGCTACTGGTCCAGGACCATCTCCACTTCTTCAATATTTCCG
 GAATTTCTTCGATCAAGGAAAGTTGAATAAATACGAAACACTCGAGCTGTGTCGTCGCGTCTT
 GGCACAAGGAAGAAAGGAGTTGATAACGAAGTGGCTCAATGATCAGAAGTTGGAGTGTGTGA
 AGAATTGGGAGATCTCATTAAAGCCGCACGATGTGAATACTGCTCTTTCAGTCTATTTGCGTGA
 AATGTCCCGCACAAGGTTGTTCAATCTTTGCTGAAACTGGACAATTCGACAAGATCGTAATGT
 ATGCCAAGCGTGTGCGATTCCAACCAGACTATTTGTTCCAACCTCGTCAAATTTCCGTAATTC
 GAATCCTGATCATGGAGCAAAATTCGCTCAACTTCTGTCTCTGAGAGCGAAAACGGAGAACCA
 CTTGCTGATCTTTCACAGATCATTGACTGTTTCATGGAGGTTCAAGCTGTTCAACCATGCACTTC
 ATTCTTCTCGAAGTTTTGAAGGGTGATAAGCCGGAGGAAGGACATCTGCAAACGAGACTTCTT
 GAAATGAATCTGCTCGCTGCCCCAGCTGTTGCCGATGCTATTCTAGCCAACAAGATGTTCTCTC
 ACTACGATCGTGCCGCTATCGGACAACCTCTGCGAAAAGGCTGGACTTCTCAAAGAGCTCTCG
 AACACTTCACTGACCTCTACGACATTAAGCGAACTGTTGTTACACCCCATCTTCTCAAGCCTGAT
 TGGCTCGTTGGATATTTCCGAAAGCCTTTCTGTTGAAGATTCGGTTCGAATGCTTGAAGCCATGC
 TCACTCAGAATATCCGACAGAACCTCCAAGTCGTTGTGCAGATTGCATCCAAGTATCATGAACA
 GCTCGGAGCTGACAAGCTGATTGAGATGTTGAAAAATCACAAGTCATACGAAGGCTTTTTCTAC
 TTCTTGGTTTCGATTGTCAACTTCAGCCAGGACCCAGAAGTTCACCTTCAAGTACATTCAAGCTG
 CCACGCGCACAGGGCAAATTAAGAGGTTGAGCGTATCTGTAGAGAGTCGCAATGTTATGATG
 CCGAACGTGTCAAGAATTTCTTAAGGAAGCCAAGCTCAACGATCAACTTCTTTGATCATTGT
 CTGCGATCGTCATAACATGGTTCATGATCTTGTCTTTACCTGTACAGAAACCAGCTCCAGAAG
 TACATTGAAGTCTTTGTTCAAAGGTTAATGCCGCCGCTTCCGATCGTTGTTGGTGCTCTTCT
 AGATGTTGATTGTAGTGAAGATGCTATCAAACAATTGATCATTAACTCCTGGAAAGTTTGACA
 TTGATGAGCTTGTGAGGAAGTTGAGAAACGCAATCGTTTGAAGCTTTTGAATCACTGGCTTGA
 ATCGAAAATCCAGGAGGAGCGACTGATGCTGCTACCCACAATGCGATGGCCAAGATTTACAT
 AGATTCTAAACAATCCCGAACGATTCTTGAAGGAAAATCCCTACTACGATAGCAAAGTTGTT
 GGAAAGTACTGCGAAAAGCGTGATCCTCACTACGCCTTCTTGTACATACGAACGCGGACAGTGC
 GACGCTGAATTGATCAACGTGTGCAACGAGAATTCATATTCAAGAATCTTGCAAGATATTTGG
 TGAAGAGAAGAGACTTCACTCTGTGGGAGCAAGTTCTCAACGAAGAGAATGTTTCATCGTAGACA
 GCTGATAGATCAAGTGGTTCAAACCTGCTTTTCCGAAACTCAAGATCCCGAAGACATCTCTGTG
 ACTGTTAAGGCATTGATGGCTGCCGATTTGCCGAACGAACCTTATTGAACTTTTGGAAAAGATTG
 TTCTCGATAACTCTGCATTCTCGGAGCACCGTAATCTTCAAATCTGCTCATTGACTG**CAATG**
AGAGCCGATAGAACTCGTGTGATGGAGTACATTCAAAGCTTGACAACATATGATGCTCCAGAT
 ATTGCTAACATTGCTATAACTTCTGAACTCTACGAAGAAGCGTTTGCCATTT**CAAGAAAATCGA**
TGTGAACTCAAGTGCCATCAATGTTCTTATCGAGAACGTGAACAATTTGGATCGTGTACGAA
 TTTGCTGAAAAGTGAACCCAGTCAGATGTCTGGGCATCTTTAGCCAAGGCACAGCTCCAACAA
 ATTTGGTGAAGGAGGCTGTGATTCGTTTATCAAGGCCGATGATCCAGGAGCGTACATGGAGG
 TTGTGAACAAATGTTCTCAAACGGAGCACTGGGAAGATCTGTTTCGTTACCTTCAAATGGCTCG

CAAGAAGAGTCGTGAGTCATACATCGAAACGGAACCTCGTTTTTGCTCTGGCCAAGACTGGTCCG
TCTCACTGAACTTGAAGAGTTTATCGCTGGACCAAATCACGCTCAAATCGGACAAATTGGAGAT
CGTTGCTTTGACAATGGAATGTTTCGATTCCGCTAAGATCCTTTCAACAATGTTCCAACCTCGC
CAAACCTTTCCGTTACTCTTGTTCTGCTTTGGAGAATATCAAGGAGCTGTCGATGCTGCACGCAA
GCCAACAGCACGAAGACATGGAAACAAGTGTGCTTCTCTTGTCGAGAATGGAGAGTTCCGG
CTTGCCCAGATGTGTGGACTTCACATCGTTGTCCACGCTGATGAGCTTGAGGAATTGATCAACT
TCTACCAAGATCGTGGACATTTTGAAGAGCTCATTGCTCTTCTCGAAGCTGCATTGGGTCTTGA
ACGGGCTCACATGGGAATGTTACCCGAACCTCGCGATTTTGTACTCGAAGTATAAGCCAGAGAA
GATGCGTGAGCATTGGAATTGTTCTGGAGCCGTGTTAATATTCCAAAAGTTCTTCGTGCTGCC
GAGCAGGCTCATCTTTGGTCCGAGTTGGTGTCTTGTACGATAAATACGAAGAATATGATAACG
CCGCACTGACAATGATGCAGCATCCAACCTGAATCTTGGAGAGAGCAACATTTCAAGGAAGTCAT
CGCTAAAGTCGCTAATGTTGAGCTATACTACAAAGCAATGCAGTTCTACCTGGATTATAAGCCA
CTTCTCCTGAATGACCTTCTTACTGTGCTATCGCCTCGGTTGGATCATTCCGCGCACAGTTTTGT
CTTCAATAAGCTGAAGCAAATCCCACTGGTCAAGCCTTACTTGAGACAAGTTCAAAAAGTTGAAC
AACAAAGGCTATCAACGAGGCTTTGAATCAGTTGCTCATTGATGAGGAGGATCACGCCGGGCTT
CGTTCTTCTATTGAGGCTCAAGACAACCTTTGACAATATCACTTTGGCCCAACAACCTTGAGAAGC
ACCCACTTGTGGAATTCAGAAGAATTTCCGCATACTTGTTCAGGGAAACAACAGATGGAAGCA
ATCGATCGAGCTTTGCAAAAAAGACAAGCTGTACAAGGATGCCATGGAATACGCTGCAGAATC
GAGAAACGGAGAACTCGCCGAAGAGCTCTTGTCACTTCTCCTGGATGAGAACTTTATGATTGT
TTTGCCGCCTCCCTTTACCATTGTTATGATCTCCTTACCCCGATGTCATCATGGAGCTCGCTT
GGAAGCATAAGATTATGGATTACGCCATGCCTTACATGATCCAAGTTATGAGAGATTATCAGAC
GAGACTTGAGAAGTTGGAGCGTTCTGAGCATGAGAGGAAAGAGGAGAAGGCTGAGCAGCAAC
AAAACAATGGAATGACCATGGAACCACAACCTTATGCTTACCTATGGTGCCCTGCCCAACAAT
GACTTATCCAGGAACAACCTGGTGGCTATGGCGGACAGCCTGCTTACGGTCAACCTGGACAACC
AGGATATAATGCCCTGGATTTATGTAA

ttcgatagttttatccccatttctacccccacccccctcactttctccccgatcaa
taattatattgtaattatgcttgatgtctatacacttttttgttaaatgatattctatttctatttattcgtcccctatgaaattgtgatggtgtattct
aatccgtgaacttatacctaaaggtgtgtccgatgtgtcgtctctcagttctgcccgtttcaaaaaaagttgatcacaactctttaaacac
cagaacctcatgaataaattaattcgttgta

Primers:

FOR 5' CAATGAGAGCCGATAGAACTC 3'
REV 5' TTGAGTTCACATCGAATTTCTTG 3'
Amplicon size: 144 ba

Probe:

#50

dyn-1

spliced + UTR (3266 bp)

cagccATGTCGTGGCAAAACCAGGGAATGCAGGCGTTGATCCCTGTGATCAATCGTGTCAGGA
CGCCTTCTCCAGCTGGGCACATCTGTCAGCTTCGAACTTCCACAGATCGCCGTCGTCGGAGG
ACAGTCCGCTGAAAAGTCGTCGGTGTGGAGAATTTTGTGCGAAAAGACTTCTTGCCACGTGG
ATCAGGAATCGTAACACGTCGTCCTACTTATTTTGCAGCTTATTCAAGATCGCAATGAGTACGCC
GAGTTCCTACACAAGAAGGGTTCATCGCTTTGTGGATTTGATGCAGTTCGGAAAAGAGATTGAGG
ATGAGACTGATCGTGTCACTGGACAGAATAAGGGAATCAGTCCACATCCAATCAACTTGCGTGT
CTTTTCTCCAAATGTTCTAAATCTGACACTCATCGATTTGCCCGGTCTCACAAAAGTGCCCGTC
GGAGATCAACCAGCAGATATTGAGCAACAGATCCGTGACATGATTCTCACATTCATCAACCCTG
AGACTTGCCCTATTCTTGCCGTCCTCCGGCCAACAGCGATCTCGCCACTTCGGATGCGTTGA
AACTTGCGAAGGAAGTCGATCCACAGGGTCTTCGCACGATTGGAGTCCACCAAACCTTGACT
TGATGGACGAGGGAACCGATGCTCGCGAGATCCTCGAGAACAAGCTGTTACACTTCGTCGTG
GCTACGTCGGAGTTGTCAATCGTGGGCAGAAGGATATTGTGCGTGCAGGATATTAGAGCTG
CTTTGGACGCCGAGAGAAAAGTTCTTATCTCACACCCATCCTACCGACATATGGCTGATCGGTT
GGGAACAAGCTACCTTCAACACACTCTTAATCAACAGCTCACCAATCATATCCGTGATACACTG
CCAACACTTCGTGATAGTCTTCAAAGAAGATGTTTGTATGGAAAAGGATGTGGCCGAGTACA
AGAACTACCAGCCAAATGATCCAGGCCGCAAGACCAAGGCTCTTTTGCAAATGGTTACCCAGTT
CAATGCTGACATTGAGCGCTCCATTGAAGGTTCTCTGCAAAGCTGGTTTCAACCAATGAGCTC
AGTGGAGGAGCCCGTATCAATCGGCTTTCCATGAGCGTTTCCATTTGAGATTGTTAAAATGG
AAATTGACGAGAAAAGAAATGCGCAAAGAAATCCAGTATGCCATCAGAAACATTCACGGTATCCG
CGTCGGTCTCTTCACTCCGGATATGGCGTTGAGGCAATTGCCAAAAGCAAATCACCCGCTCT
GAAGGAGCCATCGTTGAAATGCGTTGATCTGGTGGTCAACGAGTTGGCTAATGTGATCAGACA
GTGCGCTGACACTATGGCTAGATATCCACGTCTTCGTGACGAGCTGGAAAAGAAATCGTCGTCTC
GCATATGCGTGAACGTGAGCAAATTGCCAAGCAGCAAATTGGGCTCATTGTTGACTACGAACTC
GCTTATATGAACACAAACCATGAGGATTTTATTGGATTCAGCAATGCTGAAGCAAAGCCTCCC
AAGGACAATCAGCGAAGAAGAATCTTGGAAACCAGGTGATCAGAAAAGGGCTGGCTCTCACTGA
GCAACGTATCGTTTGTGCGTGGCTCCAAGGACAATTGGTTTGTGCTCATGTCGGACAGTTTGA
GTTGGTACAAAGATGATGAGGAGAAGGAGAAGAAGTACAT**GCTCCATTGGATGGTGTCAAGC**
TGAAGGATATTGAGGGTGGATTTATGTCTCGTAACCACAAGTTTGTCTGTTCTACCCCGACGG
AAAG**AACATCTACAAGGATTACAAGCAGC**TTGAGTTGGGATGCACCAATTTGGACGAAATTGA
TGCGTGGAAAGGCTTCATTCTTGCCTGCTGGTGTCTATCCAGAAAAGCAGAAGGCACAGGAAGA
TGAGTCCCAACAAGAGATGGAGGATACCTCGATTGATCCACAACCTTGAGAGACAGGTGGAGAC
AATCCGTAATTTGGTTGATTCTTACATGAGAATCATTACCAAGACAATTAAGGACCTGGTTCCAA
AGGCGGTGATGCATTTGATTGTTAACCAGACAGGTGAGTTCATGAAAGATGAACTTTTGGCCCA
TCTCTACCAATGCGGCGACACTGATGCTCTCATGGAGGAATCTCAAATAGAAGCCCGAGAAGCG
CGAGGAGATGCTCCGAATGTACCATGCTTGCAAGGAGGCGCTCCGCATTATCTCTGAAGTCAA
CATGAGCACCCCTTGCGACACAGCCGCGCCATTGCCGATGTCTGACTACCGCCACACCCAT
CTGGACCTTACCCGGTGCCGCGTCCGGCTCCTGCTCCACCAGGCGGACGTCAGGCCCAATG
CCACCACGCGGAGGACCCGGTGCCCCACCACCACCAGGCATGAGACCACCACCAGGTGCGC
CAGGAGGCGGCGGTGGCATGTACCCACCGTTGATTCCAAC**AAGAGTACCGACACCATCCAAC**
GGAGCACCAAGATTCCAGCTCGCCCGCAAGTCCCAAGAGACCTTTCTAAatgcttttacatctccatcc
tagctcactgtcatactattaccgttcccatagtaattgtacaatgccccgtttatcaagcattctttttttgagaattttaaattaatcaatat
cccgagttctccaccttttgagcaagtctcgttgaggattgcattggtcccagcgtactaggcgtcaattcatccacctctccattctctccc
gttccaactgtgtttctgtcagcggcgaatttccacaaccaatcgagtcctattctctttttcccccactccaataattttattgcatgtttta
taaactcactttgtcaataatttattgattttttctatgattgaaactttacattttctactctctatagcaatactttgtcactacaataacc
ccccccccagctcgcctataattttagatgtctttatggccaccaatgtataaacttttagtgacattgtaggtctttctctcatcccaccaat
tccccctccaccacaatcccagttttgatttttaagcccatattataagaagtaaatattatagattttcttagattataagctcttaggtt
ttccctcgtgagaagaatgatctgaaaagcctaattatagattttgaaacgtattgtgagaattgtattattcgtgaaagtggaataaagt
taaacgg

Primers:
FOR 5' GCTCCATTGGATGGTGT 3'
REV 5' GCTGCTTGTAACTCCTTGTAGATGTT 3'
Amplicon size: 116 ba

Probe:
#161

elt-2

spliced + UTR (1568 bp)

agaATGGATAATAACTACAATGATAATGTCAACGGCTGGGCCGAAATGGAACCATCTCAACCAAT
GGGAGGTCTGCGCCTACCAACTCAGAACATGGATCCACCAGAGCAAAAATAATGAGTCACAATT
GAGTGAACACTACCGAGAATGAAAATTGATAATGATTACGCATCTCCAATTGAACGGCAAAGTGTT
ATCACAAAGTGGCACAATAACTATGAGCCGAAAAGTGGAAAAGTGTACATCATTTTTCCATACTG
GCATAGACTACTCAAACCTTTGGAATGTTGGACCAAACCTACCATGCAACCGTTTTATCCTCTTTAC
AGTGGAATTCCTGTAACACTCTTGGAACTTTTTCGGGATATACAACTCCATATACGACAAAACC
CTCTCTGTACGACCCAGTATTCCTACCATTAACATCCCTTCTACTTATCCAACCTGTGGCTCCAA
CTTACGAATGCGTCAAATGCTCACAAGTTGTGGGGCCGGGATGAAGGCAGTAAACGGAGGA
ATGATGTGCGTCAACTGTTCAACACCAAAAACCACGTATTCTCCTCCAGTCGCGTATAGCACTT
CTTTGGGACAACCCTCGATTCTGGAATACCTTCAGAGCAGCCAACCTGCTAAAATTGCCAAGC
AATCCTCTAAAAAGTCAAGTAGCTCAAATAGGGGGTCAAACGGATCTGCGTCCCGTCGGCAGG
GACTTGTGTGCTCCAATTGCAATGGTACCAACACAACCTCTCTGGAGAAGAAAATGCTGAAGGAGA
TCCGGTCTGCAATGCTTGGGGCTTTACTTCAAACCTCATCACATCCCTCGGCCGACCTCAATG
AAGAAAAGAAGGTGCTTTACAGACAAGAAAAGAGAAAATCAAAAAGCGGAGACTCTTCCACACCAT
CAACGTCACGGGCCCGAGAAAGGAAGTTTGAGAGAGCCTCTTCTTCGACCGAAAAGGCTCAAA
GGTCATCTAACCGCGTGCAGGAAAGTCAAAGCAGACCGAGAAGTGAAGCACTGCTGCCGTC
GCAGCTGCGACTGCCACATATGTGTCACATGCCGACTTGTATCCCGTTTCCTCAGCTGCCGTC
ACCTTGCCAGATCAAACGTACAGTAATTACTATCAATGGAACACTGCCGCTACAGCTGGGTTGA
TGATGGTTCCAAACGATCAAAAACACTACGTGATGCAGCAACAACTACCAGACTGGCCTAAGACC
TGCCGATAACATCCAAGTTCATGTGATGCCAGTTCAGGATGATGAAACCAAAAGCTGCCGGCTCG
CGATTTGGAAGCGGTGACGGAGATTCTTAAacatatagaaatattgctcagctctccaaagttgccatitaaatgcata
gtttgtattctcaaaaaaaaaaacatattgtattattatcactgattgcaataactgccttttaaaagtgtttcaagtggtcatcactatgtat
agtttcaaatgttttaaatatcttctctaaataactaactaataattatacaaacatgtgtaccctacttttagtttaataaaattattatggtctg
aaaa

Primers:

FOR 5' AGTAAACGGAGGAATGATGTG 3'

REV 5' GGTTGTCCCAAAGAAGTGCTA 3'

Amplicon size: 90 ba

Probe:

#25

ftn-1

spliced + UTR (657 bp)

gtataatattatctcccaaaaaacaaatcaagtcattatatttctgccaagtaaatcgctATGTCTCTAGCTCGTCAAAACTATC
ACGATGAAGTCGAAGCGGCCGTCAATAAACAGATTAACGTAGAAGTCTACGCCTCCTATGTCTA
TCTATCGATGTCTGCACACTTCGATCGTGATGATATCGCACTTCGGAACATTGCCAAAATTTTTCA
AGGAGCAATCGGATGAGGAGCGTGGCCATGCCACAGAGCTCATGAGAATTCAGCTGTCCGT
GGAGGACGTGTTGCCATGCAGAACATTGAGAAGCCAGAGAAAAGACGAGTGGGGAAGTGTCCCT
GAAGCATTGAAGCCGCACTTGCTCTAGAGAGAGCCAATAATGCATCTTTGTTGAAGCTTCATG
GAATCGCCGAACAACGCAATGACGCGCACTTGACAAATTACATTGAGGAGAAGTATTTGGAAG
AGCAGGTACATTGATCAATGAATTTGCTCGCTACATTGCAAAATATCAAGAGAGCCGGCCAG
GACTCGGAGAATATTTGTTGACAAAAGAGGAATTTTCTGATTAAtaattttattgatgtattatgtacatatggat
gaaattgtatatttactgaaatgaaacacattgaaaactcaaaaaa

Primers:

FOR 5' GACGCGCACTTGACAAATTA 3'

REV 5' CATTGATCGAATGTACCTGCTC 3'

Amplicon size: 64 ba

Probe:

#2

ftn-2

spliced + UTR (670 bp)

attgagcagtattgcagcctaccagccacaaactaccatcaataATGTCTCTCGCTCGTCAAAACTACCACTCCGAG
 GTTGAAGCTGCCGTTAACAAAGCAGATCAACATTGAGCTCTATGCCTCATACGTCTACCTTTCAA
 TGTCATTCTATTTTCGATCGTGACGATGTTGCCCTTCCAAACATTGCCAAGTTCTTCAAGGAACAA
 TCGGATGAGGAGCGTGAGCATGCTACCGAGCTCATGCGTGTGCAGAATCTTCGTGGAGGACG
 TGTCTGTGCTTCAGGACATCCAGAAGCCAGAGAATGATGAGTGGGGAACCGCCTTGAAGGCTT
 TTGAAGCCGCGTTGGCTCTCGAGAAGTTCAACAACGAGTCGCTTCTGAAGTTGCACTCGACAG
 CCGGAAACCACAACGACGCGCATCTCACTGACTTTATCGAGGAGAAATATTTGGACGAGCAGG
 TCAAATCTATCAACGAATTCGCCCGCATGGTTGCCAACCTCAAGAGAGTCGGACCAGGAGTTG
 GAGAGTACGTCTTCGATAAGGAACACTTTTCCGATTAAttaatatatatctatctgctcatcgcatctctttgttctct
 gtacataattatttgcgaaaatttacaacatgccacaatctgcaaatgaaaagtattgatcgaa

Primers:
 FOR 5' CGTGCTTCAGGACATCCA 3'
 REV 5' CGGCTTCAAAGCCTTCA 3'
 Amplicon size: ba

Probe:
 #106

smf-3

spliced + UTR (1839 bp)

agataatatttcacaATGGAGGGTGAAATGAAATGTCCGATAGAAGAAATTAGGGAAAAGCCTGAGAT
 GCGAAAAGCTCAGCAAACCTATGAAGTTCAGGTGCAAGTTGAAGATACTCCAGATACAACCTTC
 AGTTGGCGTAAGCTCTGGGCATTACAGGCCCCCGGTTTCTAATGTCAATCGCCTACCTGGAC
 CCGGAAACATTGAAAGCGACCTTCAAGCCGAGCAATTTCTACTTTAAGCTCATCTGGGTG
 CTCCTAGTGGCCACATAATGGGTCTCTGCTCCAAAGACTTGCTGCAAGACTTGGAGTGGTG
 TCTGGAAGCATATGGCGGAAATTGCGTTCAGTTATTACCCGAAAATTCCTCGTTTGGTACTGT
 GGATGTTGGTAGAGTCGGCGATTGTTGGAAGTGACATGCAGGAAGTCATCGGAAGTCCATCT
 CGTTTTATTTGCTTTCTAACGGAGTAATCCCTCTCTGGGCAGGTGTCTTAATTACAATCTGCGAT
 ACCTTCACCTTCTTGTTCCTGGAAAAGTACGGAGTGCAGAAAGTTTGAAGCATTCTTCTGTTTTCT
 GATCACTTGTATGGCAATTACTTTTGGTTATGAGTTTGGAGTTAGTCTCCTGATGCGGGAAAA
 ATGTTCTCCGGAATGTTTGTGCCATGGTGAATGGCTGCGACAATAACATGGTGTATGCAAGGG
 GTAGCGATTATTGGTGTGTAATTATGCCACATAACTTCTACCTTCACTCGGCACCTGTCAAGA
 GCCGAAGAGTGGACCGCCGGAGAGCTGAAAAGTGACAGAAGCGAATAAATATTTTTTCATTG
 AAAGTGCTTTTTGCTCTTTTTGTGTCGTTTATTATTAACACTTTGGTCATATCGGTTTTTGCACAAG
 GAATGTATGGAAAGACGAATCAGGATATTCGCGACACCTGCTACAACAATACTCACAATGGAAT
 GCCGGATTTCTATAAAGTAGAGTTCCAGCAACAATGATGCTGCTCAATCGGATATCTATCAT
 GCCGGAATCTTTCTTGGATGCACCTTTGGAATCTTTGCACTTTATGTGTGGGCGGTGGGGATTC
 TGGCCGCTGGACAATCTTCTACAATGACCGGACTTATGCTGGACAGTTTGCTATGGAGGGCT
 TTATCCAATCAAACCTCCCAATGGAAGCGTATCCTTATCACCCGATCTTTGGCAATCCTTCC
 AACTCTTGCTGTAGTGATCTTCTCCGGCGGAATCGATAATATCTCAAGTTTGAATGATTTTTTGA
 ATTGCTTGCAGCTGATTCAACTTCCGTTTCGCTTAAATCCAGTGCTGACATTTGTATCGGATAGA
 AATATTATGCACGAGTATAAGCTAGCAAGTGTCTCCAAAGTGGTCTCCATTGTGATTTCTTGTAT
 AATTTTATTCATCAACTTTTATTTCTTATACTCTTGGATTGGATCAACATTTGGTTATAATGCAGTT
 TCTATTCCAATCACTATTTTTTGCGCGATTTTCTACATTATTTTCATCGCATATTTGACGTATTATT
 GCCTTGTGCAATGGAATTCATCTCACCCATTCAAACAAAATGGCTCGCGGAGCCCATCTACCA
 CGATTTTCGATGCTCCTTGGCTGGAGGACTCGGAAAATCCATCGACGAAAAATACAATTTCCGAC
 GACGAAGTGTCTATGCGATATTGAttatgtaataattttataataatatatgtattttgaaacaaaaaatttcgaaaatttca
 aatgtaataacctaatttataatcaatttatatgatctcctatgcaaaaaatcaataaatatctccgatttc

Primers
 FOR 5' GCTATGGAGGGCTTTATCCA 3'
 REV 5' GCCAAAGATCGGGTGATAAG 3'
 Amplicon size: 68 bp

Probe:
 #60

eps-8

spliced + UTR (3090 bp)

ccagtcaaatgccattgcttaaaaaagcgaggaattatcatcagtgagaagtgtaaaacatctataaaaatgATGCGTTCGAGG
TGGATCGATGGGTCCACCGAGCGGGGATCCATATCAGAGTCGCCCATCCCCGGAGGCTACT
ACTACAACCGTTCAACGCCTGGTGGTCAGCCAGCTCCATCACCCCTCACACAGTCAACAATCCG
CATCTTCACATCATCCAAGAGGAGTGCCTAATGTCACAACCAATCGCCCGCCGATCGGACTACC
GTA CTGGAAGTGAACAAATGACTCCACGATCCGATCATCGTGGCCCATCGATGGGTACGGTA
ATGGGGGTTCTGTGGATCAACGTGTGATGACGTCAGCCGTCCTACTACGTGGAACATCTTG
CCACGTTTGCAGTTGGAAGACAGTTGGACTCACTTTTCCAGCCGATGGCATCAGAAAGTTGAA
ACAAATGGAAAAGAATTCAGCCATTTGGGCGCAACCTCTAATTCTTCGTTTCGACACAACGCA
GTGACGGTAGAAGACGACAACGGGGAGCTCGTCGAGCAATTTCCGTTGGAATTAATCGAGCAG
CCGACGGCTCACGTGAGCAATGATTCTCGTGAGACTTACAACAATGTGCTCCTTTTTGTTGTC
GGGAGGACCGGAAGAGGATGAGCACGCCACCGAGATGCACATTTTCCAGTGTATCCGTGTAT
CCGCTACCGATGTGGCCGAGGACCTCAAAAACTACGTACAAGGTCAATTCCGTCGTGTGCGTA
ATGGCCGACGTACCGCCGCGCCGACGCATCTTCAAGCTCAACAACAACAAATGCCATTCTACC
CACCGGACGACGCTTCAATCAGCAGTGAACATCTGAAATGTTGGAACGAGATGTGAATACACT
GAATCGTTGTTTCGATGATATCGAACGATTTGTGGCGAGAATTCAATCGGCCGCACTGGCTCAG
CGAGAAATTGAGCAACAGAATCATAGATATCGAACCGCAATCGTCGGGACAAGAAGAACCG
CAGCCACCAGATCCGAATGGCATCCTATTTATGAGAGCTCAACTTCCATTGGAGTCTGAATTTG
TCGATATTTGAAGAAGTTCAAGCTCTCCTTAATCTACTGGCCAACTCAAAAAACCACATCCAC
GAGCCAAATGCTCCGGAACTTTTGCACTTTCTTTCACGCCACTAGCTGTGATCCTTGAAGCAT
GCCACTGGGGGCTCGGAAGAAATGTTGCTCCAAGTGTGCTCGCCGCTGCTCTCGTTGGAAG
CTCGTGAGCTCATGCAAACTGTTTGACAAGTCATGAGAGTGACATTTGGATGAGCCTCGGAG
AAGCCTGGGAACTCCACCAGAGGACTGGACAAAACCACTTCCACCACCATATCGTCCAATCTT
CAATGATGGGTTTGCCCTTACGGGGTTCGCCGACAGAGCCATGGCAACTCCAAATCAAATCCA
TCGTGGACATTCTGCTCCGCCAGAGCACTTCCGTCAGCCACCGCCAGAGAGGAATATGGT
GGATACGCTCGAATTCGATCGATTAACCTGGAACCGGAGCGACTCGAATTTGAAAAGGCAAA
GATTATGGAAGGGGAGAGTCGTTTGGAGCATGAGGAGAAGCAGATTGAAGATGAAAAGCGACG
AATGCACGCCGAGAAGGATCTCATCAAAAAGAGACAACAACCAAGTTCCACCACCAGCTGC
AGTCGTTACACATCAACCAATCACAAGCGATATGATCCACCAATTTCCATCTCTCCACCACCA
CAACGTAACAATATTACACGTGAAGGTTACTGTAGATTCTGACACATCGCCACGTCAGCAGG
CATTCAATGATGACATCGTGGCAAAAAGGTGGCAAGTTGGCAGTGGTCACCTATGATAGAGGAG
GTCAGAATACGAAGGAGCTGACTGTTCAAGGGGGAGTATTTGGAGTTATCTTCGACGAGC
GCAACTGGTGGGAGTGCAAGAATATGCATCAAAGAGTCGGATACGTTCCACACACAATTTGTC
AATGGTGCCATTTGAGCAACAACAATATGCGTCACCAAAACCATCACAACAATTCCTCATCAACC
GGTGGCTACAACAACGGACATCATCAAGGCCAGCGCAAAACGTCTATCGTCCACCCCCACCA
CCACTAGTATCCGATGCAGGTGTCCAGGTGCAAAATCCGCCGGGAACATGTTGCTCCGCCACCA
CCTCCAGTTGTAATTCACCACCACCACCAGTGCAGTCCAACTATGGAAGAGTTGCTC
CGCATGCAACAACAACAACAGCAGAAGCAGAGAAAACCACAGTTGAAGAACCAGTCTACCAA
CCGCAACCCGCTCAACGTGCCGGATTGGAAATCTGGAGACGGAATCAGAATCCTCAATTGATT
CAAGAAGTGACTGAAACTGTGGGACAACACAGTGGAGACATTTTAAGACCAGCAATGCAAAGG
GCCACTCGAGTGGCAATCAACGAAAAGTCTTCTCCGGAAGACGTGACTCGTTGGTTACAGGAG
AAGGGATTCTACCAAGAGTAATTGACCTATTGGATGGTCAAGATGGTGCCAATCTATTCTCCT
TGTCAAAATTGCATCTGCAACAAGCTTGTGGAAGAGATGAGGGTGGATATTTGTACAGTCAATT
GTTGGTTCAGAAGAAAAGAAGTGGA TTCCGAACTCACACTGGCGATGAATTGAAAGCAATTCTC
AATCACAGACGAACCCAGTGAATTATCAAATGAAGCTGCAGCTGATGAACCTGTATTCACTA
TTAACCCAATTCTCTAGgttttcaaatctgtctactttccaacgacaaaaatccaatttcacaaaaaaatattgattaaat
tatttcgtaattctttggctagctcaacaataagaaatccccgattttccagatgaatactcattccaactactttcaatattgtaattactg
cctccgttaatcattttgttcagatttgaatttcaacattttaaattgaattatgtttcaataaatgcttctcgaata

Primers:

FOR 5' ATATCAGAGTCGCCCATCC 3'
REV 5' GACTGTGTGAGGGTGTATGGA 3'

Amplicon size: 86 ba

Probe:

#131

3.3 Primers (and probe combination) designed for the validation of the microarrays

col-179

spliced + UTR (914 bp)

aacaccgaatagtgc**ATGGAAGACAAAGCAAAGTTTGCGTACGCAGCCGACCTTAAAAAGTTTGCTT**
TCTTTGGAGTTGCGGTCTCAACCGTAGCTACATTGATTGCAATCATTGCTATTCCACTTTTCTGT
GTTTCATATGCAATCCGTTACATCTGGCCTTTCTGAAGAGCTTCTCTTCTGCAAGTCTAAGAATG
TGTATATTAAGGGAGAAATCGAACAACCTTTCTGTTACTCGTGAAGCTGGAAGACAGAAACGTC
AAACTCCACAAACTTGCTGTTTCATGCGGTATTGGAGAACTGGACCAGCTGGAGTTCCAGGAC
AAGAAGGAGCCCCTGGAAATGACGGAAAAGCTGGACAACCAGGAGCACCAGGAGCTGACGCT
GATGAGCAAGGTTTCCATTACAAGGCTCCAGAGTTTTGCTTCGACTGCCAGCTGGACCACCA
GGAGCCGTTGGAGGACCAGGACCAAGGGACCACCAGGACCACCAGGAGGTCCAGGAGAGC
TTGGAGGACCAGGACGTGGAGGAAACCGCGGACCACCAGGACCACGTGGGCCACCAGGAGA
GGCCGGACCAGACGGAGAAGGAGGACGTCCAGGACAAGCCGGACAACTCGCTCAGCTCCAT
CTCCACCAGGACAACCAGGACAACCAGGAGAACCAGGATCGCCAGGAGAGCCAGGACCAGAT
GGACGTGCTGGACATCCAGGACGTAACGGACCACCAGGACCACCAGGAGACAATGGAGGTCA
AGGAGAGCCAGGAAAGGACGGAGAAGATGGAGAGAACGGAGCTGCTGGAGCCGCTGGACCA
AAGGGATCTTGCATCACTGCCACCTCCACGCACTGCCCCAGGATATTAtaggttttcatagtgtatta
gacgtttaataaaaagttttat

Primers

FOR 5'CGAACAACCTTTCTGTTACTCGTG3'

REV 5'GCAAGTTTGTGGAGTTTGACG3'

Amplicon size: 61 ba

Probe:

#11

skr-7

spliced + UTR (660 bp)

aaatcaccctaactttcaaaa**ATGTCTGCTGAAGCCGCCCGCCGTCGAAGTTCAAGCCAACGAGGCTCCA**
ATTGTGCCCCAATCATGTACAAGGTCGAATCAAGTGATGGACAAGTCTATGAAATCAGTGATG
AAGCAGTAAAGCAGTCGAACACCCTCTCCAATCTGATTTCTACATGTGTTGCCAATGATGTTGC
TTCAATGGATCCAATTCCAATTACCAATGTCACCGGAAACATCATGAAGATGGTCATTGAGTGG
TGTGAGAAACACAAAGGAGAAACACTTCCAGTTGAAGATGACAGTGTTCCTCAAGAACATCACTG
TTCCAGAATGGGATACCAACTTCTTAAAAATCGACAACGACGTGCTCTTCGACTTGATTGTTGC
CTCCAACCTTCTTGATGTGCCTGGATTGATGAGCTATGCATGCAAGATGGTCGCCAACATGGCT
ATCGGAAAGTCCCCTGATGAGATGAGAGTTCTCTTTGCAATTCCAACTGATGAGGAGGATGAAG
CTGCCGAGAAGGCTGCAAAGGAGAAGGCTGAAGCTGAGAAAAAGGCAATCACAGAGAAGGA
CGCAGCTGAACCATCAACTTCCAAGTAActcccagttctaaatttccgagttttgatcaaataaattcatttcgctgtc

Primers:

FOR 5'CGAGAAGGCTGCAAAGGA3'

REV 5'GCTGCGTCCTTCTCTGTGAT3'

Amplicon size: 63 ba

Probe:

#41

cul-3

spliced + UTR (2522 bp)

tgtgcacgaaaaacgagcgagattctgacttgaccagttcgttcggaatcgactcattttggag **ATGAGCGGACGCTCCGGTA**
ATGGTGGACAACAAAAAATGAGAATTCGCCATTTATGGCCACAATAGACGAGCAATATGTGAC
ACAGACATGGGAACTTTTGAAGCGTGCCATACAGGAAATCCAACGCAAAAAACAATTCGGGCTT
GAGTTTCGAGGAGCTCTACCGCAACGCATATACAATGGTGCTCCACAAGCACGGAGAACGTCT
CTATAATGGCCTGAAAGACGTGATTCAGGATCATATGGCGTCGGTTCGAATTCGAATTATCGAA
TCAATGAATTCTGGAAGCTTCTGGAGACTGTCGCCGAATCGTGGGCTGATCACACTGTCGCC
ATGGTCATGATTCGTGATATTCTGATGTATATGGATCGGATCTACGTGGCACAGAATAATCACG
TCCTGCCGGTCTATAATCTGGGTCTCGACGCGTATCGGACGGAAATCTGCGGCAAAACGGGA
TTGGCGACCGAATTCGCGATGCTCTTCTGGAGCTTATCAAATTGGATCGAAAATCGAATCAAAT
CAATTGGCACGGAATAAAAAACGCGTGTGATATGCTCATCTCGCTAGGAATCGATAGCCGGAC
GGTTTATGAGGACGAATTTGAGAGGCCACTTCTGAAGGAGACTAGTGATTACTATCGGGATGT
GTGCAAGAATTGGCTTTCTGGCGACAATGACGCGTGCTTCTATCTGGCACAGGTGGAGATTGC
GATGCACGACGAGGCGAGCCGAGCGTGCAGATATCTTGACAAAATGACAGAGGCCAAAATCCT
GCAGGTGATGGATGATGTGATGGTTGCTGAGCATATTCAGACGATTGTCTACATGCAGAATGGT
GGTGTGAAGTTTATGTTGGAGCACAGAAGATTGAGGATTTGACTCGCATTTCCTGATTTTCAA
ACGTATCGGAGATTCGGTGACAGTACCGGGTGGTGGATTGAAGGCGCTGCTTAAGGCGGTTA
GCGAATATCTCAACGAAACCGGCTCGAACATTGTAAAAATGAGGATCTGCTCAAAAACCCCGT
CAATTTTGTCAACGAATTGCTCCAGCTCAAAGACTACTTCTCCAGTCTGCTCACCCTGCGTTT
GCCGACGATCGTGACTTTAAGAATCGTTCAGCATGATTCGAGACGTTCTCAACTCGAATC
GCCAATCGCCGGAATTTGTGGCCCTCTACATGGACGATATGCTGCGAAGCGGTCTGAAATGTG
TGTCGGACGCCGAAATGGACAATAAGCTCGACAATGTGATGATCTTGTCCGCTATCTACAGGA
GAAGGATGTATTCGAGAAGTATTTCAAGCAATACCTCGCCAAACGTCTCTTGCTCGACAAATCG
TGCTCCGACGATGTGGAGAAGGCTCTGCTGGCAAAGCTGAAGACAGAGTGTGGTTGCCAGTTT
ACTCAGAAGCTTGAGAATATGTTTCAGAGACAAGGAGCTTTGGCTGACACTGGCCACAAGCTTC
AGAGACTGGCGAGAGGCTCAGCCGACCAAAATGAGCATTGACATATCGCTTAGAGTTTTGACC
GCGGGCGTTTGGCCGACGTTTCAAGTGAATCCGTTTGTGTTGCCGCAAGAGTTGTGCGTTGC
CTATGAGATGTTACACAATACTACACTGAAAAGCACACTGGCCGTAAGCTGACAATCAACACA
CTTCTCGGAAACGCTGACGTCAAAGCCACATTCTATCCACCACCAAAAGCATCCATGTCAAACG
AGGAAAATGGTCTGACCGTTCGAGCAGTGGAGAGTGCATGAAAGAACGAAAACCGGAGCAC
AAGATTCTCCAGGTCAATACGCATCAGATGATCATTCTCCTTCAGTTCAACCATCACAATCGGAT
CTCATGTGACGAGCTGATGGATGAGCTTAAGATTCCCGAGCGAGAGTTGAAGAGGAATTTGCA
GTCGCTGGCTCTCGGAAAAGCGTGCAGCGGATTTTGGTCAGAAAAGAATAAGGGAAAAGATGC
GATAGACATGAGTGACGAGTTCGCCGTCAACGACAACCTCCAATCGAAGCTGACACGTGTCAA
AGTGCAAATGGTGACAGGAAAAGTGAATCGGAGCCCAGATTTCGTGAAACTCGCCAGAAAGT
TGAGGATGATCGAAAGTTGGAAGTGGAGGCGGCGATTGTTTCGTATTATGAAGGCCCGAAAGA
AGTTGAATCACAATAATCTGGTGGCAGAGTGACCCAACAACCTGCGCCACCGCTTCATGCCG
TCACCAATCATCATCAAGCAACGCATCGAAACACTGATCGAGCGAGAATATTTGGCTCGCGATG
AGCACGATCATCGTGCCTATCAATACATTGCCTAGggtcgatttttcggttggttccaatgattttcactctcatctgctct
ccatttactttgctatattctcttaaacacagcaacaacgattgttcataatacgttaattctgtagaaa

Primers:

FOR 5'CGAAAGAAGTTGAATCACAATAATCT3'
REV 5'GATTGGTGACGGCATGAAG3'

Probe:

#53

Amplicon size: 78 nt

nlp-37

spliced + UTR (574 bp)

agATGAGCTCTCGAATTTCCGGTCTCCCTATTGCTGCTTGCTGTAGTGGCAACCATGTTCTTCACA
 GCCAATGTTGTTGATGCGACCCCAAGATCACAAGGAAACATGATGCGTTACGGCAACTCTCTT
 CCAGCGTACGCCCCACATGTCTTATACCGTTTTTACAACCTCAAGACAGTTTGCTCCAATAAACA
 AGAGAAACAACGCCGAAGTAGTGAACCATATTCTCAAAAATTTTGGAGCTCTGGATCGACTTGG
 AGACGTTGGCAAGTAAaagtcacacggatctgataatttctaaaagcactgtagttgaacactattcactttgaaagttggcat
 agttttgagacctgaacaattgccaattctatgtttactttgcatccataatattttcaccattctcaaattctctgattctgactgaggctacc
 acaaaaaccgattttactttgctttaatcgatattttcgtaactgtgctgattctttatgtcacctgtgacaccgaaacctgtgaaaataaaatgc
 tactgttcaataaacgcttattcagtt

Primers: Probe
 FOR 5'ATGATGCGTTACGGCAACT3' #11
 REV 5'TGTA AAAACGGTATAAGACATGTGG3'
 Amplicon size: 61 ba

F55G11.8

spliced + UTR (1143 bp)

atgcttttctgaaaacattgtcatccaggtgtgtttatatattcagttccagaacgtgaaagttctcaacaaaATGTTACAAAAATTAT
 TAATTTATTTGGCTATTGCTGCTATAGTTTCGGCTACGGGAAATGGTTGCAAACCTTGGTAATGCA
 ATCAATAAGCCCGTTATTGATGGTCAGCCTTTTTATTGGCCAGCTTCATGGAACGAAACCCAAC
 CAGCTCCTCAGCTTGAGAAGGAGCAGTCGTGCAGTTGGATTGTGACAATTCCACGTGGATATT
 ATGCAAAAACCTGATAATCAGTGGAAAGACAACCTGACAAGGATTCAAGATTCCAAAACCTGTCGATTC
 TGCAGGAAATCTTATTCAAACAACCCACGAGAAAATGGAACCTTATTACTTTCCGGCTTCAAAGT
 TCACTCTTGCTGTCTCCAACGAAGGATTTGCTACACTTGGTTTTCAAAGTTGTCTGGTTTTCTCTT
 CCATCAGTGAATACCAACTATGGCGTTGGAGCTGTTGGAGCAGTTTTGGATGTAACAAATGAG
 GTTCTTGCCATTGAATATGGTTCAACTGGTGGACTCACTTTAATGGCCTTCCCTGCAGACGATA
 AAAAAATCATTCTGTTGAGAAGCGCTCTCATATTGAAAGGAAATGGTCTGCAAAGTGGAAACTA
 CATTTCGAATCTTTACTTACTCTACCAGTCGAAGAAGCAATGGGTATCAAGTCAAGACAGTATTG
 TAATAGTGAACCTCGACGCTAGTCAGGTTAACGATAAACTTCTCATCCAAGCATCTAGATACTTG
 ACTGGAATCAGTGAGACGGTGGAAATCCACCCGAGTTGAACTCAACCTATAATGTAAGTGTAA
 ACGGAGGGACACGCATGTCTTCTTGTGCTGTTTCCGATATCACAATGCACATGGTTGATGT
 TCAGATGAAAGATGAATCTACCGTCACAGTCTACGATGGTTCTCCAAGCGCATTACATTTGATA
 AAACCTATACCAAAAACACAACCTTAAGAACGCATTCCCACTGTCGTTCCGGCGGATATTTTGTGCA
 GTTTGTGGTCAGCAGTGGCAAAGCTGTTTTACGTTCAAGAGCTAAttttaaatgtttttataataagacct
 acaaatcata

Primers: Probe
 FOR 5'CGAAGGATTTGCTACACTTGG3' #144
 REV 5'CCAACGCCATAGTTGGTATTC3'
 Amplicon size: 75 ba

F35E12.8 (or cld-9)

spliced + UTR (1604 bp)

agtttgattggccaaagtgcagaaatcagc**ATGTCTAGTCAAACAACGTTTTGACATTTGCTTTATTTCTTTTA**
TTTTCTGCAAAATATTTCCAAATCCGTCAATTTACATGTCCGCAAAATCCGATTGTGGGTGGAAC
TGGAACATTTCCACCTGATTACAGCAGCAAGGTTCCAGTTTCCGATAAATTATCATTGTAAAATAC
AATTTAAAATTCAAGATGGATTTGTAGTGAGACTTACGTTTTCTTCAAAGCAACTGCGGCAGAT
TCTATCATTGTGAGCAACGTGCTCGGATCGTCTTACGCTTACAATCAAGGTTCTGGTACCTTCTT
TGCTCCGGCAACAGCAGCTACTGTCTCAATCGACACCTCAACTGCAACGTCTGAATTTGGTTC
AGTTATGATTATCAAAACC**TGCTTTGTTTGAACAAAATCCTACGCTGCCAACCGGAACCTCTCT**
TAATCTCAACCTTCAACCTACACAAACATACACACTTGAGTCTCCCACCAACGATAATGTTGTCA
TAAATGTGGCTCTAGTTGATCAAATTGGAAAACTGATATAGTTATAAAATTAATTTATGTTTATG
ACGGTCCCAATGTTAACTCGCGATTCTGTTGGGCAACTTGTATGATTACGTGAATTCTCCGACGCT
CATGAAATCAAGTGGAAATTCGACTACATTGGTTAACTATTATGGGCCAACAAAGTAATTCCTACG
CATTGGCAAATGATTTCAAATCGCTTTCTTCTGTTTGAAGAGTACACATTTGTTGCATTCTCCAAA
AATGTAACAGTTCCTAAAACTTCAAAGTGAAGGTATACCATTACGTCAAGTGCCTTACGTT
CTTGTGTAATCTAGTATGGTTTATCTCACTGATTTGAATTTGGAGCAAATGGACACAAAG
TTGATGTACAAACACTGACACCTTCGGATAATCAGATAACTTATCTCACTTATTTAGCAACTGAT
GCAGTGCAGAACTCAATGCCTCAAATGATTCGGGCAAAGCTATTCAGTATGGTAACACTAGGCC
CAGAACTTTCATTGACTTTGTCTTCTACTGCTGATAATTGGTTAACCCCTTATAATGGAAGGAAA
GGAAGTATTTTCTCATCATCTCTATGGACACCT**GAAGCAACATCAGGATACAATCATACTTTG**
TATCAACTAATGTCATGACATTTACTTTCAATATTAAGGCCATTATTCATCAGGCTGGAGAA
CAGATGCATGTTCAAGTTGGACTACCAGGATTTAAACCATCGAGTTTGACATTCACCTAACAGTG
TTTCGGATCAAAGTCGACTTGCCAATGGAACCTATTTAATGATTGAATACATAGGCGATTCAACT
TCTTCATCATCCATTGTCACATTTGAAATGGCCAATGCAAACGGAGAGCAGGGGACAAGTTATT
TACCAAGTAAATCTACAAGTTCTTCTATTCAATCAACTACTAAATCGGGATTGAAGAATACATTTG
GTATTGCAAGTGAATTAGTCTGTTGATTGCTTTATTTTTGAACTGTTGActataaaatcttaattttctaatat
tcgaagaactcaataaattattgcat

Primers:

FOR 5'GAAGCAACATCAGGATACAATCA3'
REV 5'TTAAATCCTGGTAGTCCAACCTGA3'

Amplicon size: 131 ba

Probe

#19

cyp-13A5

spliced + UTR (1667 bp)

gaaacactatattttgtccaaaatATGAGTTTAAGTATACTTATTGCTGGTGCTTCGTTTATTGGACTTTTGA
 CATATTATATCTGGATTTGGTCATTTTGGATCAGGAAAGGAGTCAAAGGACCCCGTGGATTTCC
 ATTTTTGGAGTGATTCACGAGTTCCAAGACTATGAAAAATCCAGGACTGTTGAAATTGGGAGAA
 TGGACAAAAGAATACGGACCAATATATGGTATTACTGAAGGAGTCGAAAAAACTTTGATTGTGT
 CTAATCCAGAATTTGTTTCATGAAGTATTTGTGAAACAGTTTGATAATTTCTATGGAAGAAAAGACA
 AATCCCATTC AAGGAGACCCAAATAAAAAACAAAAGAGCACATCTTGTCTCGGCTCAAGGGCACC
 GTTGAAGCGGTTGAGA ACTCTGT CATCACCTACGTTTTCAAATAAAAAACCTCAGAAAAATTATG
 AGTACTGTAGAAGAACTGTAGTAGAGTTGATGAGACATTTGGACGATGCAAGTGCAAAAAGGAA
 AAGCTGTAGATTTATTAGACTACTACCAAGAATTCACTCTTGACATCATTGGAAGAATTGCAATG
 GGTCAAACAGAATCGCTGATGTTTAGAAAATCCAATGCTTCCTAAGGTGAAAGGAATTTCAAAG
 ATGGTCGTAAACTACCTTCTAGTTTTCTGGTATTTTCCCGATAGCGGGA ACTATGTTCCGCGA
 ATTCTTCATGAGATTTCCCATCTATAACAACAGCCTTCGATATTATGAGTACTGTGAAAAAGCTT
 TGAATAAACGACTGGAACAAAAGAGCCGCAGACGAAAAAGCTGGAATTGAGCCATCTGGTGAAC
 CACAAGATTTCAATTGATTTGTTCTAGACGCAAGAGCAAATGTAGATTTCTTTGAAGAGGAATCC
 GCACTAGGATTTGCTAAAACAGAAATTGCGAAAGTTGATAACA ACTGACATTTGATGAAATTAT
 TGGCCAATTGTTGTTTTCTGTTAGCTGGATATGATACA ACTGCCCTTTCCCTCTCATATTCTT
 CATATCTCCTGGCAAGACATCCAGAGATTCAGAAGAAATTACAAGAAGAAAGTGGATAGAGAATG
 CCCAAATCCTGAAGTCACTTTTGATCAAATATCAAATTTGAAGTACATGGAATGTGTGGTAAAGG
 AAGCTCTACGAATGTATCCATTAGCATCCATCGTTCACAACCGAAAGTGCATGAAGGAAACGAA
 TGTACTTGGAGTTCAAATAGAGAAAAGGAACAAATGTTCAAGTGGATACATGGACACTTCATTAT
 GATCCAAAAGTTTGGGGAGAGGATGCAAATGAGTTTAGGCCAGAGAGATGGGAATCTGGAGA
 CGAACTATTTTATGCAAAAAGGAGGATATCTTCCATTCGGTATGGGACCAAGAATTTGTATTGGAA
 TGCGATTGGCAATGATGGAAAAAAAATGCTTTTGACCCACATCCTGAAAAAGTACACATTCGA
 AACTTCTACGCAAACAGAAATTCATTAATAATTGGTCGGATCCGCCACA ACTGCACCAAGAAGT
 GTTATGCTCAAGTTGACACCAAGACATTCCAATTAAttcctaattttagttgtataataaattatgcatatgtgtacctattg
 gtttttgattaataaattgttcaaatcgata

Primers: Probe:
 FOR GGACACTTCATTATGATCCAAAAGTT #55
 REV CGTCTCCAGATTCCCATCTCT
 Amplicon size: 78 ba

F49F1.5

spliced + UTR (528 bp)

aattcaagATGCTCCAACAATGCCTCATTGTTCTATTTTTCTGGGTGCCTGCTCAAGTCAATGCAT
 GGACACTTCACTGTCTTGCCCTGACCAAGTGATCGCTTGCTTTGAACCTTCTGTGCAAAGTGAA
 TGTCCGTATAGCTGTGCCACTTGTGAGTTTACCCGAATGAGTGTGTGGACAGAAACACCCAA
 GTCAGACTCTGAAGGTCTTCTGTGATGATCCGAAGAATAGCGAGCAATGCCAGGAAAGCTGT
 GGAATATGTGTGCCACTAGAAAAATAACATCTACTTTGCGACCGGTACATGTTGGTACACAAA
 CGACTACAGTAAAGCCA ACTAGTCCTAAGACTTCATCAACAGCTTCAGA ACCATGCTACGAAAA
 TCCAATTTGTCCGCATTGGGCGGCTAATGGCTTCTGCACCAACCCCTTCTACTCGCCGGAGCA
 CAGAAAGAAGTACTGCGGGAAGACATGTAATCTGTGTTGAattatggtatgttgtgatgataaaataatt
 tataactttc

Primers: Probe:
 FOR 5'GATCCGAAGAATAGCGAGCA3' #72
 REV 5'CCGGTCGCAAAGTAGATGTT3'
 Amplicon size: 82 ba

CV and Publications

a. Curriculum vitae	228
b. Publications	231

Curriculum vitae

Laura Gonzalez Moragas

DATE AND PLACE OF BIRTH: 20/12/1989. Barcelona, Spain

CONTACT INFORMATION: ☎ +34 630 72 87 55

✉ lauragonzalezmoragas@gmail.com



Education

- **PhD in Material Sciences**
Universitat Autònoma de Barcelona, Spain. Apr 2013 – Currently
Thesis title: 'Evaluating of inorganic nanoparticles in the living organism *Caenorhabditis elegans*'
Stays abroad: 2016 – 14 weeks at King's College London, London (UK)
2015 – 6 weeks at the European Molecular Biology Laboratory, Heidelberg (Germany)
- **MSc in Industrial Management and Organization**
Universitat Autònoma de Barcelona, Spain. Set 2014 – Jul 2015
Thesis title: 'Business plan of a GMP pilot plant for the manufacture of iron oxide nanoparticles'
GPA: 9.12/10 Honors Grade
- **Postgraduate Certificate in Quality Systems in the Pharmaceutical Industry and Research**
Universitat de Barcelona, Spain. Nov 2012 – May 2013
- **BSc+MSc in Pharmacy**
Universitat de Barcelona, Spain. Set 2007 – Set 2012
GPA: 9.32/10 Honors Grade

Work experience

- **PhD candidate**
Institut de Ciència de Materials de Barcelona, ICMA-B-CSIC. Apr 2013 – Currently
- **Technical Management Officer**
Laboratorios Salvat SA, Barcelona. Abr 2012 – Mar 2013
- **Intern at the Clinical Pharmacy and Pharmacotherapy unit**
Universitat de Barcelona, Spain. Feb – Jun 2012
- **Pharmacist**
Local pharmacies in Barcelona. Jun – Set 2010 and Oct 2011 – Jul 2012

Publications

- Gonzalez-Moragas *et al.* *C. elegans* as a tool for *in vivo* nanoparticles assessment. *Advances in Colloids and Interface Science*, 2015, 219, 10–26
- Gonzalez-Moragas *et al.* *Scale-up synthesis of iron oxide nanoparticles by microwave-assisted thermal decomposition*. *Chemical Engineering Journal*. 2015, 281, 87–95
- Gonzalez-Moragas *et al.* *Protective effects of Bovine Serum Albumin on superparamagnetic iron oxide nanoparticles evaluated in the nematode Caenorhabditis elegans*. *ACS Biomaterials Science & Engineering*, 2015, 1 (11), 1129–1138
- Yu, S.M. *et al.* *A. Bio-identity and fate of albumin-coated SPIONs evaluated in cells and by the C. elegans model*. *Acta Biomaterialia*, 2016, 43, 348–357
- Gonzalez-Moragas *et al.* *In vivo testing of gold nanoparticles using the Caenorhabditis elegans model organism*. Submitted.
- Gonzalez-Moragas *et al.* *Evaluating the effect of iron oxide nanoparticles in the transcriptome of C. elegans: a genome-wide study*. In preparation.
- Gonzalez-Moragas *et al.* *Impact of metal and metal oxide nanoparticles in C. elegans: a review*. In preparation

Awards and Scholarships

- [BoosterWe Fellowship 2016](#)
Fellowship to cover a 6-12 week placement in an international start-up. Awarded by Red Emprendia.
- [PhD Travel Grant 2016](#)
Travel grant awarded by the Spanish Ministry of Education to cover a 3-month stay at King's College London in the Toxicogenomics group under the supervision of Dr. Stephen Sturzenbaum.
- [Short Term Scientific Mission 2015](#)
Travel grant awarded by the GENIE COST ACTION to cover a 3-week stay (December 2015) at the Electron Microscopy Core Facility at EMBL in collaboration with Dr. Yannick Schwab.
- [1st National Award for the Excellent Performance at University 2015](#)
First National Award for Health Graduates. Awarded by the Spanish Ministry of Education.
- [Christian Boulin Fellowship 2015](#)
Travel grant awarded by the European Molecular Biology Laboratory to cover a 3-week stay (summer 2015) at the Electron Microscopy Core Facility in collaboration with Dr. Yannick Schwab.
- [4-year PhD Scholarship 2013-17](#)
Awarded by the Spanish Ministry of Education.
- [Scholarship for Graduate Programs for Health Professionals 2012-13](#)
Awarded by Assistència Sanitària Col·legial.
- [Student-Faculty Collaborative Scholarship 2011-12](#)
Awarded by the Spanish Ministry of Education.
- [Best Students' Scholarship 2007-08](#)
Awarded by Caixa Manresa.

Contribution to Conferences and Seminars

- [2nd Scientific Meeting of BNC-b Students](#) – ORAL. Best Oral Presentation Award.
Universitat Autònoma de Barcelona, Spain. 29-20 Jun 2016
- [Impact of microbes in *C. elegans* life traits \(Workshop\)](#) – ORAL
University College of London (UCL), UK. 25 – 26 Feb 2016
- [HINTBCN Scientific Workshop on Biomedical, Health and Bio-Related applications of Hybrid Materials](#) – POSTER
Institut Català de Nanociència i Nanotecnologia (ICN2), Spain. 7 – 8 Jun 2015
- [1st Scientific Meeting of BNC-b Students](#) – POSTER
Universitat Autònoma de Barcelona, Spain. 20-21 May 2015
- [4th International Conference on Multifunctional, Hybrid and Nanomaterials](#) – ORAL
Sitges, Spain. 9 – 13 Mar 2015
- [V Spanish Worm Meeting 2015](#) – ORAL
Salamanca, Spain . 4 – 6 Mar 2015
- [3rd Workshop on Nanomedicine UAB^{CEI}](#) – POSTER
Universitat Autònoma de Barcelona, Spain. 27 Nov 2014
- [Nanomedicine Conference](#) – POSTER
Heriot-Watt University Edinburgh, United Kingdom. 26 – 27 Mar 2014
- [2nd Workshop on Nanomedicine UAB^{CEI}](#) – POSTER
Universitat Autònoma de Barcelona, Spain. 8 Oct 2013

Other Scientific Merits

- [64th Lindau Nobel Laureate Meeting in Physiology/Medicine 2014](#) – Spanish representative.
Lindau, Germany. 28 Jun – 5 Jul 2014
- [BRIGHT Students' Conference 2012](#) – Representative of Universitat de Barcelona.
Organized by the League of European Research Universities, LERU.
Universiteit van Amsterdam, The Netherlands. 13 – 17 Ago 2012

Technical skills

- Dynamic Light Scattering (DLS), Spectroscopy (UV-Vis), Light microscopy (LM), Scanning Electron Microscopy (SEM), Transmission Electron Microscopy (TEM), Quantitative Polymerase Chain Reaction (qPCR): self-use
- *C. elegans* culture techniques
- Bacterial culture
- Scale-up of synthetic reactions by microwave-assisted reaction to pilot scale

Languages

- Spanish: Native
- Catalan: Native
- English: C2 (CEFR)

Publications



Historical perspective

C. elegans as a tool for in vivo nanoparticle assessment



L. Gonzalez-Moragas, A. Roig, A. Laromaine*

Institut de Ciència de Materials de Barcelona, Campus UAB, 08193 Bellaterra, Spain

ARTICLE INFO

Available online 15 February 2015

Keywords:*Caenorhabditis elegans*

Nanoparticles

Nanoscience and nano-bio interfaces

Model organism

ABSTRACT

Characterization of the in vivo behavior of nanomaterials aims to optimize their design, to determine their biological effects, and to validate their application. The characteristics of the model organism *Caenorhabditis elegans* (*C. elegans*) advocate this 1 mm long nematode as an ideal living system for the primary screening of engineered nanoparticles in a standard synthetic laboratory. This review describes some practicalities and advantages of working with *C. elegans* that will be of interest for chemists and materials scientists who would like to enter the “worm” community, anticipates some drawbacks, and offers relevant examples of nanoparticle assessment by using *C. elegans*.

© 2015 Elsevier B.V. All rights reserved.

Contents

1. Introduction	10
2. The <i>C. elegans</i> model	11
2.1. Cuticle and epidermis	13
2.2. Pseudocoelom	13
2.3. Alimentary system	14
2.3.1. Metabolism	14
2.3.2. Excretory system	14
2.4. Reproductive system	15
2.5. Nervous system	15
3. Practical considerations, parameters and techniques	15
3.1. Life cycle	15
3.2. <i>C. elegans</i> mutants	15
3.3. Physiological features of <i>C. elegans</i>	17
3.4. Biochemical assays for <i>C. elegans</i>	17
3.5. Microtechniques	17
3.6. Chemistry-nanoparticle techniques	18
4. Nanoparticle assessment in <i>C. elegans</i>	19
4.1. Nanoparticles in the worm	19
4.1.1. Cuticle	19
4.1.2. Alimentary system	21
4.1.3. Reproductive system	22
4.1.4. Absorption and translocation pathways	23
4.1.5. Nervous system	23
4.2. Nanoprobes for optical imaging in <i>C. elegans</i> : an example	24
5. Conclusions and perspectives	25
Acknowledgments	25
References	25

1. Introduction

Nanometer-scale materials have unique structural and functional properties that can lead to new engineering systems potentially useful

* Corresponding author.

E-mail address: alaromaine@icmab.es (A. Laromaine).

for sensors, catalysis, transport, and other applications in medicinal and engineering sciences. Among the plethora of nanomaterials, nanoparticles (NPs) exhibit great potential in numerous biomedical applications: magnetic NPs for medical imaging, separation tags, or for thermal ablation therapy; [1] gold NP conjugates as biosensors; [2] inorganic or polymeric NPs for drug delivery; [3] and semiconductor NPs as components of sun creams [4], to name a few.

Future materials systems developed for biotechnology could include a variety of metals that assemble, reconfigure, disassemble, and react specifically with the surrounding biological media. The ability to predict and control the reactivity of these systems in biologically relevant conditions, i.e., the degradation of the NPs, the release of unwanted products, and the interaction with biological tissues, would help to create safe materials that have near limitless applications.

The structure, chemical composition, and properties of NPs are usually well characterized and controlled; however the interaction of NPs with biological fluids and organisms has not been assessed in depth. Typically, such biological assessment is performed during the late stages of NP development and not in conjunction with their synthesis. Consequently, any adjustments to structure and composition of the NPs to optimize them for biological application are delayed, which increases the price and translation time of the products to market. Performing well-planned and information-rich experiments *in vitro* with simple animals is fundamental to reduce the number of materials before screening them in high-order animals. Assays that provide useful biological information at lower cost during the early stages of NP development are in high demand [5] (Fig. 1).

Caenorhabditis elegans (*C. elegans*) is a 1-mm long free-living nematode that was postulated as an animal model in 1965 by Sydney Brenner [6,7]. The ability to grow hundreds of animals on a single Petri dish feeding on bacteria, their transparency, a rapid-life cycle (3 days), a short lifespan (2–3 weeks), and facile and inexpensive growth in the laboratory make this worm an ideal model [7]. Advances in genetics and molecular biology have allowed the identification of all 959 cells of *C. elegans* and its complete genome, which demonstrated a high conservation of biological mechanisms between the worm and vertebrates [8]. *C. elegans* does have some limitations as an experimental model, because it lacks some specific tissues (i.e. bones), organs (i.e. eyes and ears), and systems (i.e.

the circulatory system). Although, since its establishment as a model organism, the impact of *C. elegans* has extended from biology to other fields including chemistry [9,10], materials science, and medicine [11].

The invertebrate *Drosophila melanogaster* receives similar attention as a model organism, because it offers a completely sequenced genome and facile and inexpensive culture, although it is not transparent. In addition, the invertebrate model earthworm is a common name that refers to various species used primarily in environmental sciences as a model of soil invertebrates. It is bigger than *C. elegans* and lacks most of its experimental advantages, but offers higher complexity, i.e. blood vessels and a primitive kidney. *Hydra vulgaris* is a freshwater polyp used as an invertebrate animal model for nanotoxicology, in particular for regeneration studies. Vertebrate models such as *Danio rerio* (commonly known as zebrafish) and mice are widely exploited in the laboratory and offer higher homology to humans than invertebrates, but their manipulation is much more complex and they have longer life cycles [10,11] (Table 1).

Based on its features and requirements, we advocate *C. elegans* as a suitable animal model for chemists and materials scientists to perform initial biological screenings of nanomaterials in chemical synthesis laboratories. Immediate *in vivo* characterization of NPs after synthesis opens opportunities for rapid design optimization, eliminates the need for time-consuming cell-culture-based assays, and overcomes the difficulties involved in the use of mammalian models. It is worth noting that the use of *C. elegans* complies with the widely accepted ethical principles, known as Three Rs, for animal experiments, which are: Reduction of the use of higher animals, Refinement of current techniques, and ultimately Replacement of animals with alternative methods.

This tutorial review offers, in the next section, a general description of the anatomy of *C. elegans* and highlights the main features that lend this animal to be an excellent *in vivo* platform. In the second section, we expose some practicalities and parameters commonly used in experimental research that facilitate work with *C. elegans*. Finally, we present recent examples of the evaluation of NPs by using “the worm”.

2. The *C. elegans* model

C. elegans was the first multicellular organism for which the genome was fully sequenced (1998) [7]. Its genome size is approximately 100

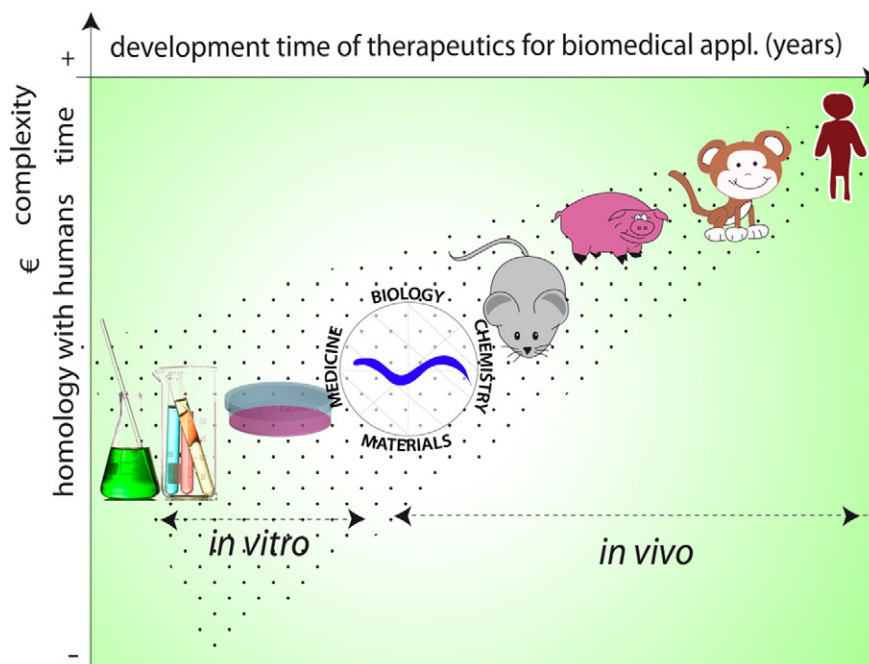







Fig. 1. Typical methodologies to screen drugs, from *in vitro* processes to increasing complexity of the model organisms. The use of *C. elegans* to evaluate NPs could impact different disciplines.

Table 1
Main features of simple animal models widely used in the evaluation of drugs, chemicals and new materials.

	Invertebrates			Vertebrates	
	<i>Caenorhabditis elegans</i>	<i>Hydra vulgaris</i>	<i>Drosophila melanogaster</i>	<i>Danio rerio</i>	<i>Mus musculus</i>
					
Common name	Worm	Hydra	Fruit fly	Zebrafish	Mouse
Habitat	Terrestrial (soil)	Aquatic (freshwater)	Terrestrial	Aquatic (freshwater)	Terrestrial
Cultivation	Inexpensive and easy	Inexpensive and easy	Inexpensive and easy	Inexpensive and easy	Expensive
Space	Hundreds of animals in a 10-cm Petri dish in an incubator in the laboratory	20-L aerated aquaria	Bottles in a dedicated room	45-L aerated aquaria in a dedicated room	Cages in a dedicated room
Food	Bacteria	Shrimp larvae	Fly food (water, agar, sugar, corn meal, yeast ...)	Adult shrimp	Pelleted mouse feed
Environmental conditions	16–25 °C	18–21 °C	18–29 °C	25–31 °C	18–23 °C; 40–60% humidity
Adult size (length × width)	~1 mm × 70–90 μm	Column: 2–10 × 0.3–1.8 mm; tentacles (6–9): ~¼ column	~3 mm × ~2 mm	~4.5 cm × ~1 cm	~17 cm (9-cm tail)
Adult weight	~4 μg ^a	~400 μg	200–250 μg	150–250 mg	17–25 g
Gender	Hermaphrodite and ♂ ~0.1%	Hermaphrodite	♀ and ♂	♀ and ♂	♀ and ♂
Lifecycle	Short (2–3 days)	They do not undergo senescence and can regenerate	Short (10 days)	Long (2–4 months)	Long (2–3 months)
Embryogenesis	18 h at 20 °C	Budding predominates over sexual reproduction	24 h at 25 °C	48–72 h at 28.5 °C	19–21 days
Lifespan	2–3 weeks; up to months as dauer larva	'Biologically immortal'	~30 days	2–3 years	2–3 years
Number of offsprings (per animal)	~300	~112/year, mainly clonal offspring	~400	100–200 eggs/clutch	40–100
Year genome sequenced	1998	Ongoing	2000	2013	2002
% Homology with humans	60–80%	Some functional conservation has been reported	50–80%	70%	Up to 99%
Automated high throughput assays	Possible at all stages	Possible at all stages	Only possible with larvae	Only possible with embryos	Not possible
Other features	Transparency Storage by freezing Many mutants available	Biological indicator of water pollution	Difficulty of conservation of mutants	Transparent and small embryo	Strong bioethical issues

^a Calculated according to Andrassy's formula [12,13].

million base pairs long and, although it is notably smaller than the human genome, both genomes have a similar number of genes (worms 20 000 genes; humans 23 000). There is substantial overlap between *C. elegans* and humans with respect to genes and biochemical pathways. Bioinformatics analyses suggest that 60–80% of the genes of the worm are homologous to human [10]. The reduced number of cells, together with the invariant cell number and fate within the somatic tissues, enabled the identification of every cell [6].

C. elegans are predominantly hermaphroditic, and males arise spontaneously with a frequency of approximately 0.1%, therefore we will focus on the features of hermaphrodite worms. Their body is essentially a tube, the alimentary tract inside another tube, the cuticle, and epidermis. Between the two tubes there is a fluid-filled body cavity, the pseudocoelom. The anatomy of *C. elegans* includes the following systems: an alimentary system, a reproductive system, a nervous system, and an excretory system all protected by the cuticle. (Fig. 2). *C. elegans* does not have a circulatory system, and relies on passive diffusion in the pseudocoelomic fluid for the transport of O₂, CO₂, and nutrients [6].

Here, we describe some parts of the anatomy of *C. elegans*, its structure and composition, and emphasize similarities to humans. From this section, the reader will be able to evaluate how convenient *C. elegans* is for the study of specific functions, and how NPs can be evaluated in the worm.

2.1. Cuticle and epidermis

The cuticle is the tough extracellular surface of the worm, which protects the animal from the environment, maintains the morphology and integrity of the body, and has a critical role in locomotion by acting as an external skeleton. (Fig. 2). The adult cuticle is $\approx 0.5 \mu\text{m}$ thick and comprises five layers based mostly on collagen, lipids, and some glycoproteins. The cuticle prevents leakage of internal solutes into the environment, and blocks the entry of some molecules from the environment, although it allows some specific diffusion. At each larval stage, an entirely new cuticle is generated and the old cuticle is shed, which permits growth. Cuticles at different stages differ significantly in their surface protein expression, layer number, relative thickness and composition [14].

In humans, the skin is composed of three primary layers; epidermis, dermis, and hypodermis. It functions as a protective barrier to the environment similar to the cuticle of *C. elegans*. Human skin is rich in keratin, collagen, and elastin (structural proteins), with flexibility provided by glycosaminoglycans (a type of carbohydrate). The innermost layer, the hypodermis, is mainly made of fat and connective tissue [15]. The combination of structural proteins and lipids is present in both human skin and *C. elegans* cuticle, whereas other components lead to different properties. Table 2 presents an analysis of *C. elegans* cuticle and human skin.

The epidermis of invertebrates is, in its structure and function, the primitive forerunner of human skin and of all other vertebrate animals [16]. Thus, the cuticle and epithelial system of *C. elegans* can be used as a simplified skin (epidermis) model for NP assessment to study possible adverse effects (i.e. abrasion), and to assess adsorption or absorption mechanisms of NPs.

2.2. Pseudocoelom

The pseudocoelom is a fluid-filled body cavity that bathes the internal organs of the nematode and includes the alimentary system and reproductive system. The pseudocoelom carries out many of the functions normally performed by the circulatory system or the respiratory system in higher animals. The pseudocoelomic fluid helps to establish an ionic equilibrium by balancing the hydrostatic pressure of the whole worm, acts as a lubricant between tissues, and provides a medium for intercellular signaling and for nutrient and oxygen transport. The pseudocoelom also offers a path for the translocation of materials from the alimentary to the reproductive system and even to the progeny. For instance, yolk protein is synthesized in the intestine of adult worms and is secreted to the pseudocoelom as free particles up to 1 μm in diameter. Yolk is finally shuttled to the reproductive tract and enters into the growing embryos. Thus, yolk granules provide a model from which the transport mechanism of materials from the alimentary to the reproductive system can be studied [14].

In humans a straightforward structure comparable to the pseudocoelom does not exist, although the study of NPs in the pseudocoelom can be related to endocytosis mechanisms. The

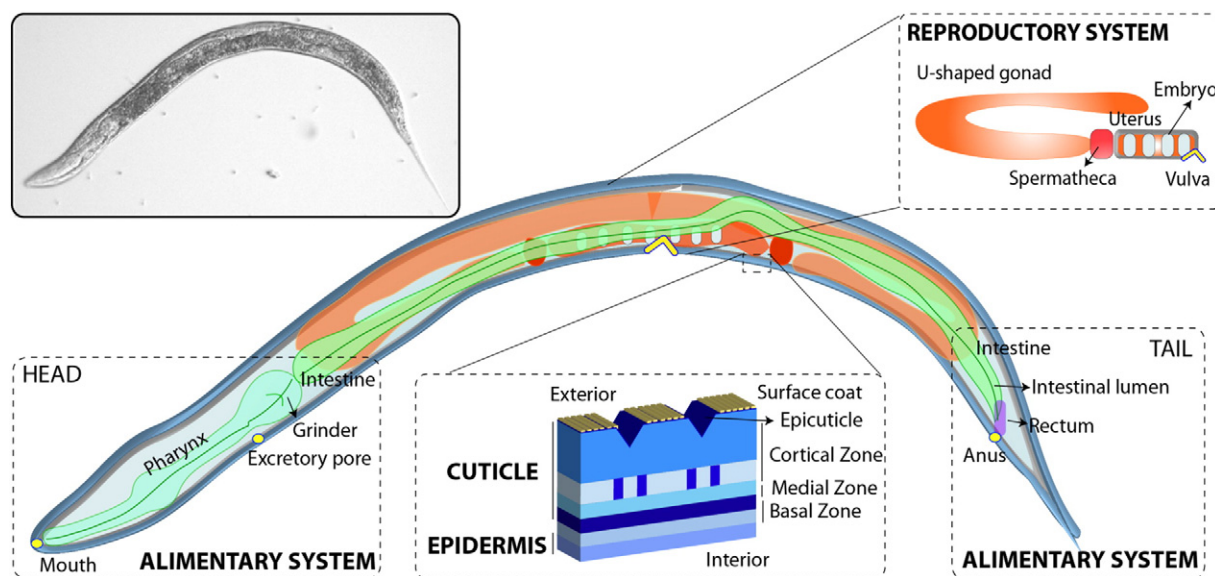


Fig. 2. *C. elegans* anatomy. In the left upper part, a light microscopy image of *C. elegans*. Below, a schematic representation of *C. elegans* anatomy showing the parts of interest for NPs assessment. Legend: Cuticle and epidermis in blue; Alimentary system in green; Reproductive system in orange; Pseudocoelom in light blue; Portals of entry (mouth) and exit (excretory pore, vulva, anus) indicated in yellow. The cuticle comprises five layers (from outermost to innermost): a surface coat of glycoproteins; the epicuticle, formed of lipids; the cortical layer, that consists in collagens and other proteins; the medial layer, which is a fluid-filled layer with "struts" of collagen; and the basal layer made of collagen fibrils. The alimentary system consists of the mouth, buccal cavity, pharynx, intestine, rectum, and anus. The reproductive system is formed by two symmetrical U-shaped gonads that are joined to a common uterus and egg-laying apparatus in the mid-body.

Table 2Analysis of Epidermal Layers in *C. elegans* and mammals.Adapted with permission from: A. D. Chisholm and T. I. Hsiao, *Wiley Interdisciplinary Reviews-Developmental Biology*, 2012, 1, 861–878. Copyright 2012 Wiley Periodicals, Inc.

	<i>C. elegans</i>	Mammals
Epidermal epithelia	Simple epithelium; largely syncytial	Stratified epithelium
Dimensions, in adult	~0.1 mm ² , ~230 nuclei	2 m ² , 10 ¹¹ cells (human)
Embryonic origin	AB, C blastomeres	Surface ectoderm
Major morphogenetic processes	Ventral enclosure; elongation	?
Post-embryonic growth	Four molts; seam cells; polyploidization	Basal epidermal stem cells
Apical surface matrices	Flexible collagenous cuticle; epicuticle (lipid); surface coat	Stratum corneum
Major cytoskeletal elements	Cytoplasmic intermediate filaments, actin, microtubules	Keratins, hemidesmosomes
Junctional complexes	Hemidesmosomes; CCC, DAC	Desmosomes, focal adhesions, hemidesmosomes
Permeability barrier	Cuticle or epicuticle	Stratum corneum
Fate specification pathways	ELT-1/GATA	BMP signaling; p63; Grhl
Innate immune response pathways	TIR-1, p38 MAPK pathway, TGF β pathway	EGFR transactivation
Epidermal antimicrobial factors	p38 MAPK pathway, <i>nlp</i> , <i>cnc</i> genes	Defensins, cathelicidins
Wound closure pathways	Calcium signals	Re-epithelialization
Sensory functions	Embedded touch neurons and sensilla	Mechanoreceptors, thermoreceptors, nociceptors
Appendages	Lateral alae	Hair, nails, teeth, glands

pseudocoelom contains coelomocytes, which continuously endocytose fluid from the pseudocoelom. In particular, coelomocyte uptake assays have identified new components of the endocytosis machinery that are conserved between *C. elegans* and mammals, such as RME-1, a protein involved in membrane recycling to the plasma membrane [17]. Therefore mechanisms of NPs endocytosis could be extrapolated to a certain extent to the different endocytosis mechanisms in humans and be critical to the evaluation of how surface functionalization of NPs or NP shape influence endocytosis mechanisms.

2.3. Alimentary system

C. elegans feeding involves food ingestion, digestion, nutrient absorption and defecation. Metabolism is also intimately related to the alimentary process. *C. elegans* is a filter feeder: it draws bacteria suspended in liquid into its pharynx, traps the bacteria, and ejects the liquid. The alimentary system promotes intake and efflux of fluids and nutrients through the mouth and anus, respectively. Two motions are involved in the feeding behavior of *C. elegans*: pharyngeal pumping and isthmus peristalsis. Pumping is a contraction–relaxation cycle in which particles and liquid are sucked in. During relaxation, liquid is ejected to the exterior and bacteria are retained in the pharynx and transported into the intestine [14]. (Fig. 2).

Bacteria reside in the intestine of *C. elegans* for fewer than 2 min, much shorter than the 2-hour digestion in humans [18]. Although digestion is not completely understood in *C. elegans*, it seems to start with passage of bacteria through the grinder, which damages the bacterial cells. Next, the bacterial cell wall and the plasma membrane are degraded by secreted lysozymes and saposins/amoebapores in the intestine, and the contents of the bacteria pass to the intestinal lumen. Hydrolysis of the macromolecules is performed by secreted peptidases and lipases in the anterior gut. Finally, the absorption of nutrients mostly occurs in the apical part of the intestinal cells owing to the presence of microvilli, which increase surface area contact between the cell and the intestinal lumen, and also contains peptide transporters and nucleosides transporters, among others that are involved in absorption [14]. The pH of intestinal lumen of *C. elegans* ranges from ≈ 6 in the anterior pharynx to 3.6 in the posterior intestine, in which enzymes are released and provide the acidity required for enzymatic activity [14,19].

In humans, the pH of the intestinal tract ranges from acidic in the stomach (pH = 3 or even lower during digestion) to pH 6.8 in the first section of the small intestine, so the pH range in humans is similar to that of the worm, although the change is in the opposite direction. Swallowing in humans is equivalent of pharyngeal pumping in *C. elegans*, although humans choose what they ingest, whereas *C. elegans* simply filters food through the pharynx. The mechanical processing of food in humans occurs in the mouth, in which food is

chewed, and continues through the churning action of the stomach. Chemical digestion begins in the mouth with food mixing with saliva, continues in the stomach, and finishes in the small intestine. Several enzymes, including amylases, lipases, lysozymes, proteases, esterases, and nucleases, break down complex molecules into simple structures. Most of these types of enzymes are also found in *C. elegans*. Absorption occurs mainly in the small intestine, in which nutrients pass from the digestive system into the blood stream by active transport or diffusion. The primary surface for nutrient absorption in humans is the microvilli, as in the worm, which are located in the apical surface of the intestinal cells that increase dramatically the cellular surface area for absorption and the number of digestive enzymes that can be present on the cell surface.

Digestion finishes with defecation, which is the removal of undigested materials from the digestive tract. In *C. elegans*, the waste material is discarded through the opening of the anus in 50-second cycles (Fig. 2). In each cycle, 47% of the total intestinal volume is expelled to the exterior. Defecation is under the control of the nervous system, and is achieved through rhythmic activation of a cycle of muscle contractions. When the intestinal contents press near the posterior end of the intestine, the enteric muscles contract promoting defecation. In *C. elegans*, defecation is temperature independent, but it is slow when food is scarce (the cycle increases to 80 s), and even can be inhibited as feeding ceases, being only resumed when food is available [7]. In humans, when the rectum is full, the waste stimulates receptors in the rectal walls, which are under the control of the nervous system, resulting in the desire to defecate, like in the worm. By contrast, in humans, relaxation of the external anal sphincter is under voluntary control.

2.3.1. Metabolism

There is high conservation of the metabolism between *C. elegans* and vertebrates, which allows the study of metabolic pathways and routes, such as lipid metabolism, in this simple organism. Conservation of the factors that control energy metabolism between mammals and the worm provide a powerful platform to study the genetic and molecular pathways that could be applied to human metabolism. For instance, insulin signaling is an active area of investigation in *C. elegans* because it plays an important role in lipid metabolic disorder, which is an important risk factor for diseases such as obesity and diabetes, represents a major public health concern, and it is highly conserved between the worm and humans [9].

2.3.2. Excretory system

The excretory system consists of four distinctive cell types which participate in osmotic/ionic regulation. Despite being rather simple, the function of the excretory system in *C. elegans* is analogous to the renal system of higher animals and it is critical for the animal's survival

[14]. When the excretory system is compromised, worms inflate with excess fluid resulting quickly in a “rod-like” lethal phenotype, which is easily recognized [20].

Although the excretory system of *C. elegans* is not comparable with the mammalian kidney in terms of anatomy, it may serve as a valuable tool to study electrolyte and osmotic homeostasis on a molecular level, and various studies have demonstrated the conserved role of kidney disease genes in *C. elegans*. Therefore, the excretory system of *C. elegans* is a tool to study various aspects of renal function, development and disease [21].

2.4. Reproductive system

The reproductive system produces mature gametes (gametogenesis) and provides the structure and environment for fertilization and egg-laying. (Fig. 2). Spermatogenesis begins during the L4 larval stage and it is completed in the young adult shortly after molting. When sperm production stops, sperm stored in the spermatheca fertilizes the oocytes [14]. Hermaphrodites produce ≈ 300 embryos by self-fertilization. Fertilized eggs move into the uterus and are laid outside through the vulva. Egg-laying is facilitated by contraction of the sex muscles, which are regulated by the nervous system [6]. Several parameters can be studied in *C. elegans* including number of eggs or progeny, effects on the development of the progeny, or effects on the reproduction of different filial generations [22]. Thus, *C. elegans* facilitates experimentation and enables rapid initial results in the field of reprotoxicity.

In humans, reproduction also involves spermatogenesis and oogenesis, which correspond to the gametogenesis in males and females, respectively. A number of mechanisms and factors to establish germline and gametogenesis are remarkably conserved not only among mammals but also between more evolutionarily distant species. Some conserved genes between *C. elegans* and humans have already been reported. For instance, the protein encoded by *C. elegans dss-1* gene is required for embryogenesis, larval growth, and oogenesis. It is 71% similar and 46% identical to the human *DSS1* gene product, and it is functionally conserved in humans [23]. Mammals have four *Foxo* genes that are highly conserved but redundant in some contexts, which control multiple aspects of development, metabolism, reproduction, and tissue stem-cell function. *C. elegans* has a single ancestral *Foxo* homolog that is required for maintenance of the germline, which demonstrates that *Foxo* functions are quite ancient and functionally conserved [24]. Therefore, *C. elegans* can be used as a model organism to study the effects of NP exposure on oogenesis and its molecular mechanisms.

2.5. Nervous system

C. elegans are extensively used as model organisms in neuroscience. Adult *C. elegans* have 302 neurons and 7000 synapses that belong to two distinct and independent nervous systems: a large somatic system (282 neurons) and a small pharyngeal system (20 neurons). *C. elegans* development is reproducible among individuals and each neuron has been individually identified. Moreover, by reconstructing the entire connectivity of the nervous system through electron microscopy and by sequencing the *C. elegans* genome it was confirmed that almost all families of genes involved in neuron function in mammals are present in the worm. [14] The transparency of this animal allows us to visualize the regeneration of neurons or any damage by simple optical microscopy. The ability to distinguish between each neuron allows us to identify the damage inflicted on a neuron.

In mammals, the nervous system contains 100 billion neurons and thousands times more synapses than *C. elegans*. Each single neuron in mammals receives thousands of inputs from tens of neuronal subtypes. The challenging complexity of the human brain promotes the use of simple nervous systems, such as *C. elegans*, to understand neuronal growth and regeneration [25].

3. Practical considerations, parameters and techniques

In this section, we will describe some practical considerations of working with *C. elegans* and some common evaluation parameters possible from this model organism. We present some indicators of *C. elegans*, which we have divided into different categories according to whether they are involved in life cycle, genetic modifications, physiological features, biochemical assays, microtechniques, or chemical analysis and techniques suited to NPs. However, the majority of publications combine both practicalities and multiple methodologies to obtain information about the worm.

3.1. Life cycle

C. elegans has a rapid life cycle: at 25 °C, embryogenesis lasts 14 h, and postembryonic development to adult lasts 36 h. The postembryonic development progresses through four larval stages – known as L1, L2, L3, and L4 – before becoming an egg-laying adult. *C. elegans* stocks can best be maintained at 16–25 °C, typically at 20 °C. The growth rate differs at different temperatures: growth is 2.1 times faster at 25 than 16 °C, and 1.3 times faster at 20 than 16 °C. Stock plates can be kept for months even with scarce food supply, because *C. elegans* is able to enter an alternative larval stage, called dauer, which is adapted to survive under harsh environmental conditions [14]. (Fig. 3).

The ability to control the life cycle and development of *C. elegans* as a function of temperature and time, allows the use of worms at specific development stages from eggs to larva or adults, which represents the whole life cycle of the worm of just two or three weeks. Such control makes possible to study chronic or acute exposure of *C. elegans* to NPs, estimate how aging of the worm affects NP uptake, degradation, and toxicity and extrapolate to the aging process in humans.

3.2. *C. elegans* mutants

Full sequencing of the genome, together with a highly engaged worm community, and the ability to acquire *C. elegans* mutants of almost each gene, allows logical experiments to be performed to elucidate whether certain mechanisms of toxicity occur or not.

C. elegans is highly attractive for functional genetics because of the broad genetic tools available. There are two main strategies for genetic studies in this animal model: forward and reverse genetics. In forward genetic studies, individuals are treated with mutagens to induce DNA lesions, and mutants with a particular phenotype are sought (i.e. increased sensitivity to oxidative stress). The efficiency of mutagenesis, in which several chemical mutagens work efficiently on the worm, i.e. ethyl methane sulfonate or ionizing radiation, together with easy frozen storage of mutants promotes continuous growth of the number of mutants. After a mutant with the phenotype of interest is found, the gene mutated is identified through molecular techniques, typically PCR-based screens. Detailed studies of the mutant phenotype coupled with molecular analyses of the gene allow elucidation of the gene's function [26,27].

Reverse genetics provides a way to manipulate gene activity; the gene is altered and the effect on development or behavior of the organism is analyzed. In most organisms, the majority of genes have not yet been mutated, but the complete genome sequence in *C. elegans* combined with reverse genetics techniques allow every gene to be targeted in this organism. The main method to perturb gene function in *C. elegans* is RNA interference, which creates a knock-down of gene function without altering the organism's DNA within few hours and allows rapid screening of loss-of-function phenotypes [28]. The ability to propagate mutant animals with severe impairments of different function benefits the identification of neuronal functions, metabolic pathways, stress-response behaviors, and related proteins.

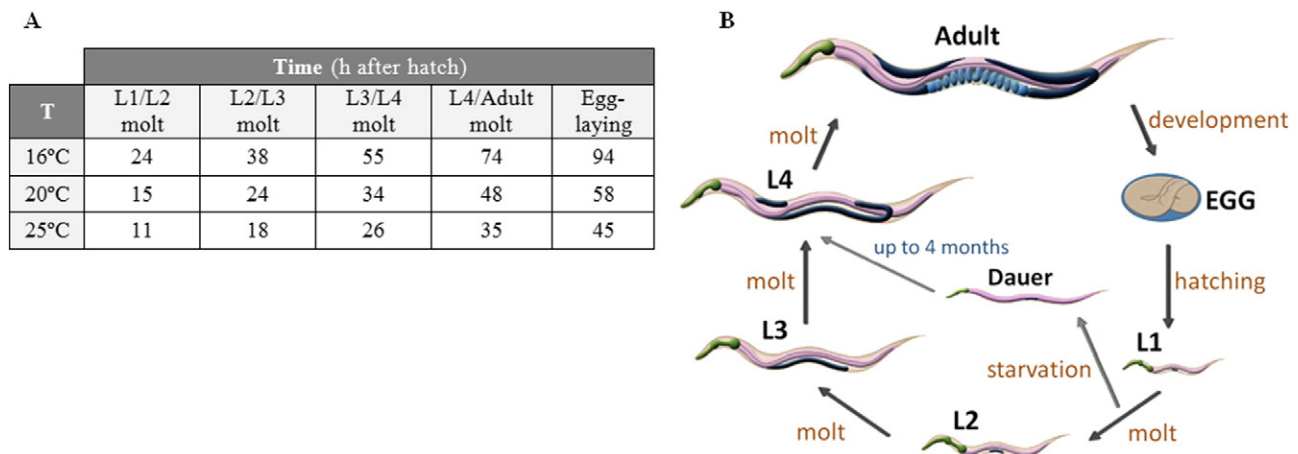


Fig. 3. (A) Table presenting the growth rate under different temperatures and (B) Life cycle of *C. elegans*. Adapted from WormAtlas.

Another essential tool in *C. elegans* research is the generation of transgenic strains. Genetically modified *C. elegans* can over-express genes or express tagged proteins. Transgenic nematode strains can be generated by microinjection or gene bombardment. In the first method, a transgene is injected into the gonad usually by using pRF4 plasmid as the DNA vector. The second method, gene bombardment, consists of “shooting” the transgene bound onto gold particles into living worms with a “gene gun” [29].

In Table 3 we present the main mutations used in NP research. We detail the name of the mutant, the impairment, and the main aim for which this mutation has been performed. This methodology allows us to select a suitable mutant for a given hypothesis. Mutants with reported or expected sensitivity to specific mechanisms of toxicity can be used to investigate particular mechanisms and molecular pathways involved in nanotoxicity. For instance, mutations on enzymes involved in

antioxidant defense can be used to study the importance of oxidative stress in nanotoxicity. Superoxide dismutases (SOD) are one such antioxidant enzyme. *Sod-2* and *sod-3* *C. elegans* mutants are reportedly more susceptible than wild-type worms to oxidative stress for several types of NPs [31,32]. Through SOD-3 overexpression, the adverse effects of NPs are prevented, which confirms that worms were susceptible to oxidative stress [32]. The use of DNA repair-deficient strains (i.e. *nth-1* and *xpa-1* mutants) can provide evidence as to whether DNA damage is a biologically relevant mechanism in the toxicity of NPs or not. The use of *mlt-2* mutants, which carries a mutation in one of the two identified *C. elegans* metallothioneins, can help to elucidate if metallothionein has a protective role against nanotoxicity. Metallothionein could protect *C. elegans* against metal toxicity by binding to the metal ions released and scavenging the reactive oxygen species (ROS) produced. The protective effects of metallothioneins would suggest that particle

Table 3
C. elegans deletion mutants and transgenic strains used in the literature to assess NP toxicity.

Mutants				
Gene	Gene function	Mutant phenotype	Mechanism of toxicity investigated	Ref
<i>sod-2</i>	They encode superoxide dismutases, involved in protection against oxidative stress.	Hypersensitive to oxidative stress	Oxidative stress	[30–32]
<i>sod-3</i>	It encodes a protein involved in DNA repair.	Mildly mutation-prone	DNA damage	[30]
<i>nth-1</i>	It encodes a protein involved in DNA repair.	Loss of DNA repair, growth inhibition following UVC radiation, sensitive to chemical induced helix-distorting DNA damage	DNA damage	[30]
<i>xpa-1</i>	It encodes a protein involved in DNA repair.	Sensitive to metal toxicity	Metal toxicity due to intracellular release of metal ions from metallic NPs	[30]
<i>mlt-2</i>	It encodes a metallothionein, which protect <i>C. elegans</i> against metal toxicity.	Hypersensitive to oxidative stress	Oxidative stress	[30]
<i>mev-1</i>	It encodes a succinate dehydrogenase, which acts as a source of superoxide in the mitochondrial respiratory chain.			
Transgenic strains				
Transgene	Transgene description.	Transgenic phenotype.	Aim	Ref
<i>Ex(Psod-3-sod-3)</i>	Gene encoding SOD-3 fused onto the <i>sod-3</i> gene promoter	SOD-3 overexpression	Oxidative stress	[32]
<i>Phsp-16.2::gfp</i>	Gene encoding GFP fused onto the <i>hsp-16.2</i> heat-shock promoter.	GFP is expressed when a toxic stress triggers a stress response, which induces the synthesis of heat-shock proteins.	Stress response	[32]
<i>mlt-2::gfp</i>	Gene encoding GFP fused onto the metallothionein-2 gene promoter	GFP is expressed in a concentration-dependent manner when <i>C. elegans</i> is exposed to metal ions.	Metal toxicity due to intracellular release of metal ions from metallic NPs	[33]
<i>daf-16::gfp</i>	GFP is fused to the C terminus of DAF-16, as a stress response reporter.	Under normal conditions, GFP is primarily distributed in the cytoplasm. In response to stress, GFP translocates into the nuclei.	Stress response mediated by the conserved DAF-16/FOXO pathway	[34]
<i>gcs-1::gfp</i>	Gene encoding GFP fused onto the <i>gcs-1</i> promoter	When exposed to a toxic stress (i.e. arsenic), intestinal GFP increases dramatically	Stress response mediated by the conserved SKN-1 pathway	[34]

dissolution plays an important role in the toxicity of metallic nanoparticles. The examples presented illustrate how each strain can facilitate a better understanding of the nanotoxicity mechanisms in vivo.

3.3. Physiological features of *C. elegans*

Indicators used to assess the biocompatibility and effects of NPs in *C. elegans* can be divided into evaluation of the physiological status of the treated worms, and toxicity to reproduction and the next generations of worms (Table 4).

The physiology evaluation could include monitoring of the following parameters: survival rate, which can also be expressed as lethality or lethal concentration; [31,33,35] growth or length, as a measure of the development of treated worms; [31,35] and lifespan [36]. Identifying dead worms typically involves touching each nematode to evaluate their response to external stimulus. Motility, or locomotion, has also been extensively quantified as an indicator of the viability of nematodes [31,33], because it can be easily automated. Evaluation of specific locomotive movements (turns, pirouettes, bending angles ...) can provide additional information, because locomotion involves many anatomical parts and systems, including the muscles and the nervous system. Among other physiological indicators, the level of ROS or lipofuscin accumulation in the gut can reveal age-related degeneration, and such indicators are often highlighted as nano-specific toxicity mechanisms [31,36].

The state of the alimentary system, such as pumping rate or defecation cycle can also help to evaluate the effects of NPs on *C. elegans*. NPs uptake depends on the rate of pharyngeal pumping, which is modulated by both internal and external factors, including temperature, presence or absence of food, quality of food, and nutritional status of *C. elegans*. For instance, in the absence of food the pharynx pumping rate is four times slower than in the presence of food. Also, a well-fed worm pumps only in the presence of bacteria, whereas starved worms keep pumping in the absence of food and accelerate their pumping in the presence of lower amounts of bacteria relative to a well-fed worm [7,14]. The duration of the defecation cycle has been also used to evaluate the effects of NP exposure in *C. elegans* [31]. The integrity of the intestinal barrier (i.e. state of the microvilli) can be assessed by electron microscopy. Compromised integrity of the intestinal epithelium may result in infection of exposed worms by undigested bacteria, or in translocation of NPs to other locations from the intestinal lumen.

Evaluation of the effects of NP exposure over reproduction and subsequent generations of *C. elegans* are undoubtedly important parameters, and include: evaluation of the fertility of treated worms (i.e. number of eggs or offspring); presence of abnormalities in the reproductive system such as bag-of-worm (BOW) phenotype, in which hatching occurs inside the body of the pregnant worm, and correlates with age-related degeneration of the reproductive organs; and effects on the offspring (growth, fertility ...) [37]. Several generations could remain affected by exposure to NPs, and this issue could be addressed

by designing appropriate multigenerational tests, which so far have not been evaluated in depth [22].

3.4. Biochemical assays for *C. elegans*

Biochemical assays, commonly translated from cell cultures, are already in place to evaluate *C. elegans*' activity and biology upon NP exposure. (Table 4). For instance, the oxidative stress induced by NP exposure can be assessed through ROS detection by using 5-(and-6)-chloromethyl-2,7-dichlorodihydrofluorescein diacetate, acetyl ester. Alternative assays that provide similar information include: quantification of SOD/catalase activity; [32,36] paraquat assay [36], which assesses oxidative stress resistance; lipofuscin accumulation in the gut promoting gut autofluorescence [31,36]; detection of carbonylated proteins, which reflects oxidative damage [32]; or treating NP-exposed *C. elegans* with ascorbate or N-acetyl-L-cysteine (antioxidants) [32] to inhibit the formation of oxidative stress and observe if nanotoxic effects can be counteracted. This example also illustrates the ease of use of *C. elegans*, in which a single parameter (i.e. oxidative stress) can be assessed with multiple assays and techniques.

3.5. Microtechniques

The size of the worm and its transparency facilitates their manipulation on the microscale (i.e. by microinjection [34]) and the application of microtechniques such as microfluidics. Microfluidics is a miniaturized system of multi-well plates in which standard high-throughput screening is carried out. Microfluidics can control the placement and movement of the worms, and allow individual recording and evaluation of the animals in a high-throughput manner [42]. In microfluidic devices, multiple animals can be held in a single device with each worm in a single chamber being provided a different feeding solution and the effects can be visualized from the same chip. Motility assays are facile to combine with microfluidics devices, but other parameters, such as sinusoidal movement, activity and latency period, or pumping rate of the pharynx can also be monitored [43]. Microfluidic immobilization of *C. elegans* has been used to perform laser microsurgery for in vivo studies of neuronal regeneration [25].

Microfluidics can be applied to other small multicellular organisms, including *D. melanogaster* or *D. rerio*, although most of the microfluidic devices developed for *Drosophila* and zebrafish research were used mainly for the culture and development of embryos. The size of the embryo makes them suitable for integrated chip-based systems, whereas the adult size (>2000 μm) is above the size range of these technologies. By contrast, *C. elegans* adults match perfectly the size requirements for microfluidics, which makes it possible to sort and analyze large numbers of living *C. elegans* adult or larvae in microfluidic systems [44].

Table 4
Biological parameters of *C. elegans* that can be evaluated after nanoparticle treatment.

	Parameters	Effects	Method of measurement	Quantitative	Ref
Survival	Lethality	Increase	Dissecting microscope	Yes	[31,33,35,38]
	Lifespan	Increase [36] or decrease		Yes	[34,36,39,40]
Behavioral	Pharyngeal pumping	Decrease in rate		Yes	[31,41]
	Locomotion	Decrease in rate		Yes	[31–33]
	Defecation	Decrease in rate		Yes	[31]
	Development	Body size		Decrease in length	Yes
Reproduction	Reproductive system abnormalities	Increase		Yes	[22,37,40]
	Progeny production	Increase [40] or decrease		Yes	[31,33,34,38–40]
	Larval development	Decrease [39] or unaffected [40]		Yes	[39,40]
Biochemical	Lipofuscin accumulation	Decrease [36] or increase	Fluorescence microscope	Semi	[22,31,36]
	ROS levels	Decrease [36] or increase	Biochemical assays	Yes	[31,32,34,36]
	Protein carbonylation	Increase in levels		Yes	[32]
	Enzymatic activity (i.e. SOD/catalase activity)	Decrease [32] or increase [36]		Yes	[32,36]
Genetics	Gene expression (i.e. <i>sod-2</i> and <i>sod-3</i>)	Decrease	Microarray	Yes	[32]

3.6. Chemistry-nanoparticle techniques

Colloidal chemistry procedures to *C. elegans* can be used to modify the external surface of this animal model [45]. Modification of the surface charge can be assessed by measuring the zeta potential of the worms before and after treatment. In our group we measured successfully the change in surface charge in *C. elegans* cuticle once they were functionalized with cationic species (prothamine) and polyelectrolyte multilayers (prothamine/polyacrylic acid/prothamine). This strategy can modulate the interaction of the external surface of *C. elegans* with NPs, which enhances control over NP distribution, and could be used to achieve the desired surface status or to functionalize worms with specific molecules or materials. Zeta potential measurements also can be expanded to the evaluation of the cuticle surface.

All the above-mentioned parameters related to the biology of *C. elegans* (locomotion, pharyngeal pumping ...) (Table 4) are intimately related to the toxicity upon exposure to NPs or chemicals. By tracing NPs inside the body of the worm, any correlation between particle distribution in the worm's metabolism and organ function can be appraised. The biodistribution and status of NPs along the body of *C. elegans* have been studied by fluorescence microscopy, spectroscopy, microbeam synchrotron radiation X-ray fluorescence (μ -SRXRF) or microbeam X-ray absorption near edge structure (μ -XANES). Inductively coupled plasma mass spectrometry (ICP-MS) has been used to quantify the metal levels of worms exposed to Cu NPs [46] and Pt NPs [36], and also to study the uptake and distribution of metals such as Mn [47]. NPs can behave unexpectedly in vivo with respect to their fluorescence emission or radiation scattering as a result to their interaction with *C. elegans*, and can even have a different structure (i.e. as a result of the release of ions owing to digestion by *C. elegans*). Thus, the use of different techniques to localize NPs inside the worm can provide more accurate results to understand the NP's fate [39,48].

The size and transparency of the worm allows examination at the cellular level in living preparations by differential interference contrast (DIC) microscopy, and facilitates visualization of NPs with optical microscopy, either by direct observation or by using dyes. For instance,

Fe_2O_3 NPs appear brown along the alimentary system of exposed *C. elegans*, and blue if stained with Prussian blue, which confirms the presence of iron [49]. UV-Vis spectroscopy could provide colorimetric results, i.e. for Au NP exposed nematodes, based on the optical properties of Au NPs and their well-known color changes according to NP status and size (Fig. 4). Fourier transform infrared spectroscopy can also help to characterize the NP's status inside the worm, whereas techniques such as transmission electron microscopy, scanning electron microscopy or X-ray analysis would be useful to visualize and assess the state of the NPs in *C. elegans* [38,50].

C. elegans may degrade NPs at different rates to produce different degradation products than those observed in vitro (typically in cells and cell culture media). All this information allows chemists and materials scientists to improve NP design and their study in vivo. Recently, two new microscopy techniques have been employed in *C. elegans* to obtain complex information including quantification and characterization of the NP's status inside the worm, and its biodistribution and degradation [30,51–53]. The spectral features of AgNPs were investigated by using darkfield hyperspectral imaging microscopy. The spectra remained unchanged in the presence and absence of *C. elegans*, except for their relative intensities, which suggests that AgNPs are not significantly altered as a result of their interaction with *C. elegans* [30]. The technique has also been applied to investigate worms fed with nanoceria to show the presence of accumulated CeO_2 NPs in the intestinal tract and on the cuticle [53]. Nuclear MicroProbe analysis has been successfully applied to the quantitative study of titanium oxide nanoparticles in *C. elegans* and human skin cells. The use of a microbeam allows in situ chemical imaging and quantification of trace elements, which enables the study of worm morphology and its internal structure, and investigation of the elemental composition of defined anatomical structures to address questions of bio-accumulation and bio-persistence [52]. Other chemical techniques such as high-performance liquid chromatography, mass spectrometry, elemental analysis, or nuclear magnetic resonance spectroscopy could help our understanding of how *C. elegans* modifies the NP's chemical composition or size. In the case of magnetic NPs, magnetic characterization of exposed worms can provide valuable

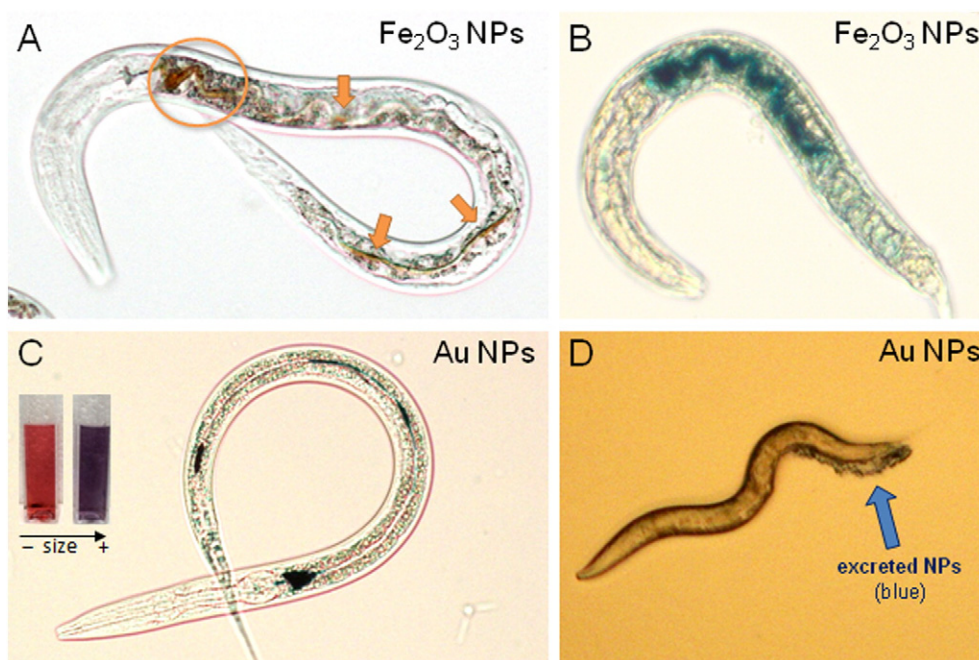


Fig. 4. Worms treated with Fe_2O_3 NPs (A, B) and Au NPs (C, D). (A) Fe_2O_3 NPs can be seen inside the body of treated worms in brown by direct observation. (B) When treated worms are stained with Prussian Blue (an iron staining), NPs appear in blue and facilitates the visualization, (C) Au NPs appear blue within the alimentary system of treated worms, indicating aggregation of the NPs relative to the stock solution (red) due to the interaction with *C. elegans*. (D) When food is reintroduced, worms excreted Au NPs through the anus, which appear also blue.

Table 5
Summary of proposed techniques to study the interaction between nanoparticles and *C. elegans*.

Aim	Parameter	Technique/measurement	Aim	Parameter	Technique/measurement
Characterization of NPs in the test media	Surface status, dispersity, aggregation	<ul style="list-style-type: none"> • Electron microscopy • DLS • Zeta potential • AFM • NMR • Darkfield hyperspectral imaging microscopy 	NPs quantification	Internalization/uptake	<ul style="list-style-type: none"> • ICP • Fluorescence quantification • Magnetic measurements • Darkfield hyperspectral imaging microscopy
NPs toxicity	Effects on exposed worms	Quantitative: <ul style="list-style-type: none"> • Lethality assay • Length • Locomotion • Pharyngeal pumping • Defecation cycle Qualitative: <ul style="list-style-type: none"> • Microvilli status • Locomotion behavior 	NPs biodistribution	NPs localization/intracellular uptake	<ul style="list-style-type: none"> • Electron microscopy • Optical microscopy • Fluorescence microscopy • Raman spectroscopy • μ-SRXRF • ICP-MS • Nuclear microprobe analysis • Darkfield hyperspectral imaging microscopy
	Effects on reproduction	<ul style="list-style-type: none"> • Number of eggs/offspring • Brood size • Anatomical abnormalities • BOW phenotype 			
	Toxicity mechanisms	<ul style="list-style-type: none"> • Biochemical assays • Fluorescence microscopy (autofluorescence) • Use of different strains 	NPs degradation	Size, surface status, dissolution	<ul style="list-style-type: none"> • DLS • Zeta potential • Electron microscopy • μ-XANES • NMR • Nuclear microprobe analysis • Darkfield hyperspectral imaging microscopy

DLS: Dynamic Light Scattering; AFM: Atomic force microscopy; NMR: Nuclear magnetic resonance; BOW: bag-of-worm; μ -SRXRF: microbeam synchrotron radiation X-ray fluorescence; ICP-MS: Inductively coupled plasma mass spectrometry; μ -XANES: microbeam X-ray absorption near edge structure.

information NP status and behavior inside the body and after excretion. (Table 5).

Additionally, it is important to mention that the experimentation with *C. elegans* generate a large amount of data that needs to be processed, therefore bioinformatics tools, data management tools, and statistics software are necessary to analyze the data.

4. Nanoparticle assessment in *C. elegans*

In this section, we summarize recent and key literature that aids in the evaluation of the interaction of NPs and *C. elegans*. These works combine the advantages of *C. elegans* and use techniques mentioned in previous sections. We have structured this section according to the part of the *C. elegans* anatomy evaluated. We believe these studies constitute examples for the next chemists and materials scientists to use the *C. elegans* model.

The assessment of the interaction between NPs and *C. elegans* provides information of the in vivo behavior and biocompatibility in a multicellular organism of some NPs to evaluate their fate and toxicity. Processes such as aggregation, agglomeration, adsorption to surface, interaction with the molecules present in the environment, dissolution of the NPs upon interaction with biological systems, toxicity of non-modified NPs, or evaluation of the effects of subsequent NPs' modifications can also be assessed in vivo in *C. elegans*.

C. elegans can be readily used in oral exposures, topical applications, and microinjection to particular organs, and allows acute, prolonged and chronic regimes of treatment. In general, the fate of NPs in *C. elegans* includes interaction with the cuticle; entrance to the alimentary system through the pharynx during feeding; and translocation to secondary organs, mainly the reproductive system (with its subsequent effects). Most of the time experiments were not performed under the same conditions, therefore comparison and extrapolation of data is complicated.

The following Table 6 lists some examples of NPs assessed by using *C. elegans*. The characterization of the NPs, the assay system, and the purpose of the study are also indicated.

4.1. Nanoparticles in the worm

The main route of uptake of NPs in *C. elegans* is the alimentary system: the worms ingest NPs actively during feeding. NPs could also passively diffuse through the cuticle during exposure or the vulva, anus, and excretory pore, because these openings connect the body of the worm to its environment. To our knowledge, there are no reported examples of entry of NPs through the cuticle, the anus or the excretory pore, even though it has been reported that some chemicals can enter through the cuticle [61].

4.1.1. Cuticle

Metal toxicity and adverse physical effects can be evaluated by using the dermal route in *C. elegans*. Adverse physical effects include epithelial thinning [62], a decreased number of pseudocoelom cells [63], and molting disruption [64], which affects the survival rate of exposed nematodes [65]. *C. elegans* treated with 50-nm citrate Ag NPs exhibited epidermal fissuring at 10 mg/L and serious burst effects at 100 mg/L after 24-h exposure (Fig. 5), which suggests a concentration-dependent effect, although no lethal effects were attributed to molting disruption induced by NPs exposure [38].

The outermost layer of the cuticle of *C. elegans* is mostly glycoproteins that provide the worms with a negative surface charge. This surface charge could interact electrostatically with nanomaterials, thus potentially influencing the effect of the NP on the worm (i.e. little interaction with negatively-charged NPs or adsorption of positively-charged NPs onto the cuticle). Minullina et al. used bilayers of polyelectrolytes to electrostatically modify the external surface of *C. elegans* with gold and magnetic NPs [45]. The possibility of tailoring the charge of the *C. elegans* cuticle offers potential to mimic surface barriers in physiology

Table 6
Selected examples of NPs assessment in *Caenorhabditis elegans*.

NPs	Characterization of NPs						Assay conditions				Worm population			Purpose	Ref
	Assynthesized			In test media			NPs conc (mg/L)	Exposure duration	Media	Food source	Synchr.	Stage	Mutants/transgenic strains		
	Ø (nm)	Surface	ZP (mV)	DLS (nm)	DLS (nm)	ZP (mV)									
Ag	1, 28	Citrate, PVP	−62	--	190	−39	0.5–10	24,48, 72 h	Liquid	Yes/no	Yes	L2	Yes	Toxicity; NPs dissolution	[54]
			−43	--	350	−35									
	3, 13, 76	Citrate, PVP	−23	--	1000–1600	--	0.5–50	Lifetime	Liquid	Yes	Yes	L1	Yes	Toxicity; NPs dissolution	[30]
	50	Nile red	--	--	--	--	0.0025 µM	30 min	Liquid	No	--	--	No	Toxicity; Imaging	[48]
	<100	Citrate	−31	--	--	--	10–1000	24, 48 h	Solid	--	Yes	L3	No	Toxicity; NPs dissolution	[38]
Al ₂ O ₃	60	--	33.1	763	--	--	10–408	24 h, 5 days	Liquid	Yes	Yes	L1	No	Toxicity; metal analysis	[35]
	60	--	34.2	--	--	--	0.01–23	6, 48 h, 10 days	Solid liquid	Yes	Yes	YA	Yes	Toxicity	[32]
Au	10	--	--	--	--	--	12.5 µg	48 h	Solid	Yes	Yes	L3	No	Toxicity	[22]
Cu	20	Citrate	--	--	--	--	7000	30 min	Liquid	No	Yes	YA	No	Toxicity; imaging	[45]
	23.5	--	--	--	--	--	100 µM	36 h	Solid	Yes	Yes	L1	No	Biodistribution; metal analysis	[46]
Fe ₂ O ₃	9	DMSA	--	--	85	−69	0.5–100	24 h	Liquid	Yes	Yes	L4	Yes	Toxicity	[31]
Fe ₃ O ₄	15	PAH	--	--	--	--	500	30 min	Liquid	No	Yes	YA	No	Toxicity; imaging	[45]
MnFe ₂ O ₄	6–8	Streptavidin	--	--	--	--	0.1% (v/v)	4–6 h	Liquid	No	--	YA	Yes	Toxicity; imaging	[56]
Pt	2.4	TAT	--	--	--	--	0.1–50 µM	Lifetime	Liquid	Yes	Yes	L4	No	Biological activity	[36]
TiO ₂	50	--	−19	550	--	--	24–240	24 h, 5 days	Liquid	Yes	Yes	L1	No	Toxicity; metal analysis	[35]
	10	--	--	--	97	−24	0.0001–1 µg/L	~3.5 days	Liquid	Yes	Yes	L1	Yes	Toxicity mechanisms	[57]
	10	--	--	--	97	−24	20 µg/L	24 h/0.48, 5.71 h	Liquid	Yes	Yes	YA	Yes	Toxicity mechanisms	[58]
ZnO	1.5	--	--	--	--	--	5–1625	4, 24, 72 h	Liquid	Yes	Yes	A	Yes	Toxicity	[33]
ZnO	20	--	0.02	759	--	--	0.4–8.1	24 h, 5 days	Liquid	Yes	Yes	L1	No	Toxicity; metal analysis	[35]
	FNDs	Bare, dextran, BSA	--	120	--	--	300 µg	2–3 h	Solid	No	No	YA/L4	Yes	Imaging; toxicity	[34]
CdSe@ZnS QD	5	MPA, MEA	−64	--	--	--	0.02, 0.2 µM	12 h, 16 days	Solid	Yes	Yes	L1,A	Yes	Biodistribution	[39]
			−19	--	--	--									
CdTe QD	5	MPA	−51	--	--	--	0.02, 0.2 µM	12 h, 16 days	Solid	Yes	Yes	L1,A	Yes	Biodistribution	[39]
	(NaYF ₄ :Yb,Er)UCNP	Bare, PEI, OA	--	--	--	--	1000–5000	3, 24 h	Liquid	No	--	--	No	Toxicity; imaging	[59]
PS	30 to 3000	--	--	--	--	--	0.1% (v/v)	--	Liquid	No	Yes	All	Yes	Imaging	[60]
	50	Unmodified, carboxy	--	--	--	--	12.5 µg	O/N, lifetime	Solid	Yes	No	YA/L4	No	Biodistribution; toxicity	[37]
SiO ₂	50	--	--	--	--	--	12.5–250 µg	O/N, lifetime	Solid	Yes	No	YA/L4	No	Biodistribution; toxicity	[37]
	50	--	−50	~50	--	--	12.5–250 µg	Lifetime	Solid	Yes	Yes	YA	No	Toxicity; biodistribution	[41]

Ø: diameter; DLS: Dynamic Light Scattering; ZP: Zeta potential; conc: concentration; Synchr.: synchronized population; Stage: Developmental stage at which the incubation with nanoparticles begins; h: hours; d: days; PVP: polyvinylpyrrolidone; DMSA: dimercaptosuccinic acid; FNDs: fluorescent nanodiamonds; QD: quantum dots; UCNP: upconverting nanophosphors; PS: polystyrene; PAH: Poly(allylamine hydrochloride); TAT: HIV-1 TAT fusion protein; BSA: bovine serum albumin; MPA: 3-mercaptopropionic acid; MEA: 2-mercaptoethylamine; PEI: polyethylenimine; OA: oleic acid; Carboxy: Carboxy groups; O/N: overnight; YA: young adults; --: Non-described.

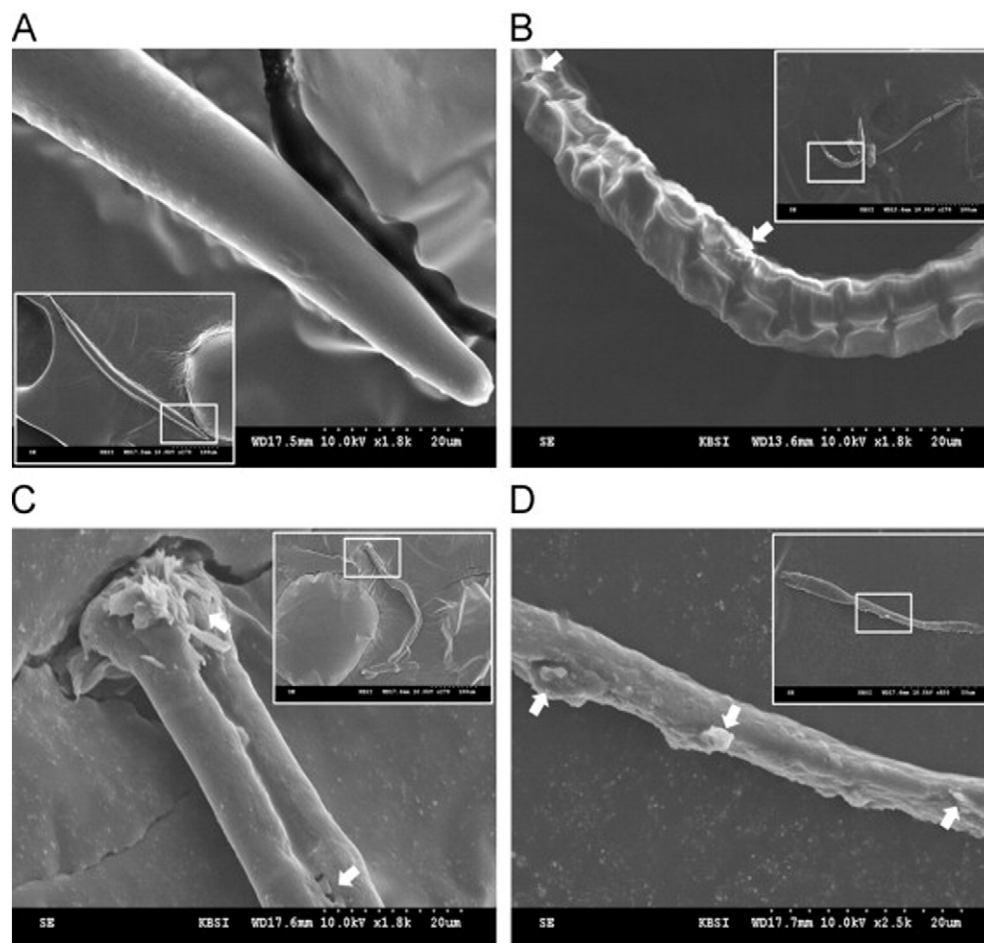


Fig. 5. Scanning electron micrograph of *C. elegans* exposed to citrate Ag NPs: (A) control, (B) 10 mg/L, and (C and D) 100 mg/L. The white arrows indicate epidermal divisions and necrosis. Reprinted with permission from S. W. Kim, S.-H. Nam and Y.-J. An, *Ecotoxicology and Environmental Safety*, 2012, 77, 64–70. Copyright 2011 Elsevier Inc. [38]

studies; to selectively heat worms with microwave or infrared irradiation; or to manipulate magnetically-modified worms for precise positioning, to name some potential applications.

4.1.2. Alimentary system

The interaction of NPs with the alimentary tract is limited for the pharynx mechanisms. The pharynx specifically catches and transports particles of a size range corresponding to most soil bacteria (0.5–3 μm). Particles that enter to the pharynx pass through the grinder on their way to the intestine. Polystyrene beads of different sizes (30 nm to 3 μm) appeared unaffected by their grinder and adhered to the inner structures of the pharynx [60]. Therefore, NPs interact with the pharyngeal epithelium, and can attach to it or be taken up by the epithelial cells. Exposure to CdTe and CdSe@ZnS quantum dots (QDs) of 5 nm diameter revealed adherence of the NPs to the epithelium: not only was the pharynx lumen filled with QD, but other structures, such as the pharyngeal intestinal valve, were also labeled [39].

Particles larger than 3 μm cannot enter the buccal cavity of young adults, whereas particles of diameters 500 nm or smaller are ejected with the liquid [60]. Thus, we would expect that NPs in dispersion will be expelled with the fluids towards the exterior, however, it has been demonstrated that NPs are efficiently taken up by *C. elegans* when NPs are mixed with food [30,37,39], and also when the NPs are freely suspended in aqueous media [45,48,55]. Therefore, NPs enter into the alimentary system and concentrate in the intestine even though there is a backward flow during the pumping. Dawlatsina et al. described that feeding *C. elegans* with nano-coated *E. coli* resulted in a more even distribution of NPs in the body than when feeding worms with NPs in dispersion [66].

Pharyngeal pumping reflects the health status of the worm and can be used as an indicator to evaluate the toxic effects of NPs in *C. elegans*. The concentrations of Fe_2O_3 NPs coated with dimercaptosuccinic acid showed different adverse effects on pharyngeal pumping according to the developmental stage of the exposed worms and the duration of the exposure. Exposure to 100 mg/L altered the pharyngeal pumping of L4-larva after exposure for 24 h, whereas concentrations higher than 500 mg/L were required to observe adverse effects on nematodes exposed from L1-larvae to adult [31].

Once in the intestine, the NPs enter the digestion cycle of *C. elegans*. Markers such as mineral oil or latex beads pass through the intestine of a rapidly feeding adult in 3–10 min. The pH of the intestinal lumen could promote the degradation of NPs and release of sub-products, which could be of importance in assessing the degradation mechanisms of NPs.

Experiments can be performed in the presence of bacteria, *C. elegans'* food, or without bacteria. Bacteria can metabolize drugs, which reduces their concentration in the media and consequently reduce the levels of NP exposure or promote the release of ions from NPs as well as affect the biodistribution and excretion of NPs [67]. Additionally, the presence of food introduces considerable bacterial surface area, which may adsorb a proportion of the NPs and reduce their concentration in free suspension. Ag NPs of different sizes (3, 13, and 76 nm) and different coating (citrate and polyvinylpyrrolidone) caused toxicity to *C. elegans* in the absence of food by extra-organismal release of dissolved (ionic) silver species, intraorganismal dissolved Ag, and through a nano-specific effect owing to size-specific interactions [30]. A similar bioavailability of ZnO NPs and ZnCl_2 also suggested that intracellular biotransformation (i.e. dissolution) might have occurred after ingestion of the NPs

by the worm in the absence of bacteria [33]. The influence of particle dissolution was further studied for ZnO, Al₂O₃, and TiO₂ NPs in the presence of food, and it was found that the dissolution rate in aqueous media was slightly faster for NPs than the bulk materials, which accounts for the effects on the release of ions [35]. After exposure to Cu NPs in the presence of food, an increase in the Cu⁺ concentration was also detected which suggests metabolism of the NPs [46].

From these experiments, release of ions has been observed both in the absence and presence of bacteria, which suggests metabolism of live bacteria has little influence. To further investigate the effects of food, Ellegaard-Jensen et al. analyzed the toxicity of Ag NPs after exposing worms with and without *E. coli* and obtaining a LC50 more than three times lower in the presence of food. The authors proposed that the presence of bacteria changed the way worms were exposed to the NPs: NPs were adsorbed onto the bacterial surface, which led to enhanced oral uptake and gut exposure that resulted in higher toxicity [54]. Exposure to CdTe and CdSe@ZnS QDs together with *E. coli* resulted in ingestion of a large quantity of NPs through the digestive tract. Many QDs were retained in the initial part of the intestine and separated from bacteria in the middle intestine [39]. Ingestion of silica and polystyrene NPs together with food also followed an uptake-gradient with decreasing concentrations from the anterior to the posterior regions of intestine. Similar uptake patterns were previously described in the presence of food and chemicals [37].

The movement of NPs along the alimentary system has been tracked in worms exposed to upconverting nanophosphors of 150–200 nm diameter. NPs were retained up to 24 h in the digestive system when the worms were deprived of food, and no apparent change in the phosphors was observed. Worms only excreted the NPs when feeding resumed and the phosphors were secreted in 2 h [68]. Excretion of NPs was also found to be dependent on food availability for fluorescent nanodiamonds [34] and in our experiments for Fe₂O₃ NPs and Au NPs. Moreover, even in the presence of food, NPs can increase the duration of the defecation cycle to 80 s [31]. All these experimental results corroborate that caution must be taken in the evaluation of NPs with or without the presence of food in the experimental setup.

Lipid metabolism in *C. elegans* was studied by using Nile red coated Ag NPs which allowed visualization of the intestinal granules of *C. elegans* through Raman spectroscopy and confocal microscopy. When *C. elegans* ingested Nile red coated Ag NPs, the Raman band in the CH stretching region was greatly enhanced and a Raman image could be obtained by confocal microscopy. Moreover, the fluorescence

signal of Nile red was observed with a 488 nm excitation source, which confirms the distribution of the lipid-targeting Raman probes in the intestine [48] (Fig. 6).

To study how metabolism of *C. elegans* affects NP distribution the correct technique must be chosen to understand the complete process. Fluorescence and elemental distribution of CdSe@ZnS QDs matched perfectly when worms were exposed for 12 h, whereas after 24 h exposure no fluorescence signal was observed at the rectal part of the intestine, in which Se and Zn elements were largely present. This finding suggests fluorescence quenching and may be attributed to the collapse of the core/shell structure as a result of destruction of the ZnS coating during digestion. Based on those results, optical fluorescence imaging did not reflect the actual distribution in vivo after 24-h exposure to CdSe@ZnS QDs; consequently it was not an appropriate technique, whereas elemental distribution was more appropriate [39].

4.1.3. Reproductive system

Scharf et al. described two entry portals for rhodamine-labeled SiO₂ NPs of 50-nm diameter: through the pharynx to the intestinal system, and through the vulva to the reproductive system [41]. (Fig. 7). Generally, the reproductive system is described as a secondary organ where NPs are localized solely after translocation from the alimentary system [22,30,37], and is sometimes portal of exit of NPs owing to ejection to the exterior through the vulva [39]. NPs can also be delivered to the reproductive system by microinjection to the gonads to study NPs in a specific location of the body of the worm [34].

NPs of different sizes and compositions, such as SiO₂ [37], Ag [30,38], Au [22] or CdTe and CdSe@ZnS [39], can translocate and affect the reproductive system, and some even transfer to the progeny. Duration of exposure has an important influence on the effects of NPs exposure on the reproductive system. After a short exposure (12 h) to CdTe and CdSe@ZnS QDs, most were excreted through the anus and vulva to the exterior, and only a few were observed in the reproductive system without entering the eggs. Exposure of 12 h to 3 days indicated transference and accumulation of QDs from the alimentary to the reproductive system, but surprisingly no obvious adverse effect was observed. After chronic exposure (16 days), a large quantity of QDs transferred into and accumulated in the uterus and vulva and resulted in adverse effects on the reproductive system and damaged the eggs [39]. The increase in embryo mortality and egg-laying defects could be attributed to disrupted transmission across neural synapses in motor neurons [40]. These results add to the controversy of whether QDs are toxic or not,

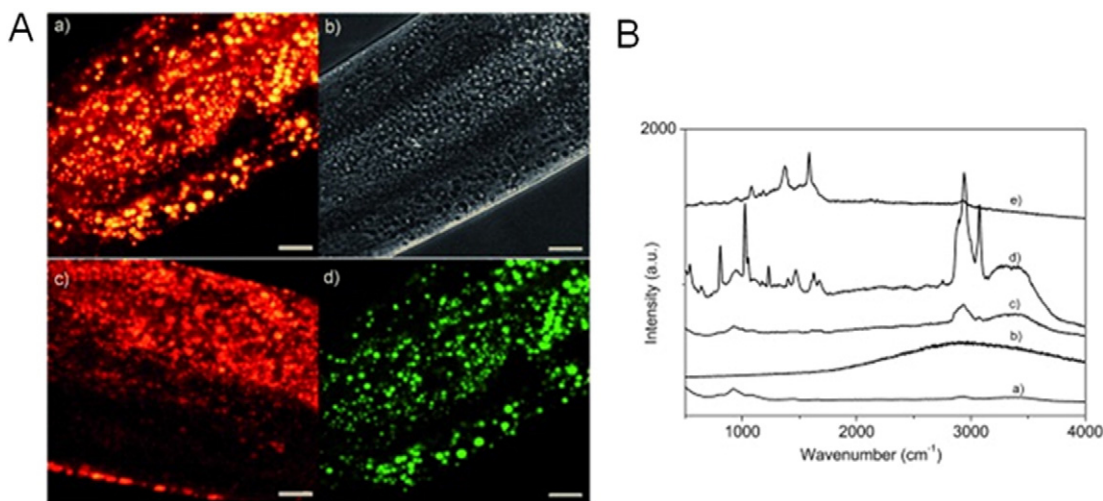


Fig. 6. Panel A shows (a) confocal and (b) DIC images of worms labeled with Raman probes, (c) confocal image of *C. elegans* labeled with Nile red dye, and (d) confocal image of worms labeled with Raman probes by using signals in the CH stretching region. Bar: 10 μ m. Panel B shows the Raman spectra of a) worms without Ag NPs, b) worms stained with Nile red dye, c) worms with Ag NPs, d) worms with Raman probes, and e) Raman probe outside worms. Reprinted with permission from S. Charan, F. C. Chien, N. Singh, C. W. Kuo and P. Chen, *Chemistry*, 2011, 17, 5165–5170. Copyright 2011 WILEY-VCH Verlag GmbH & Co. KGaA, Weinheim [48].

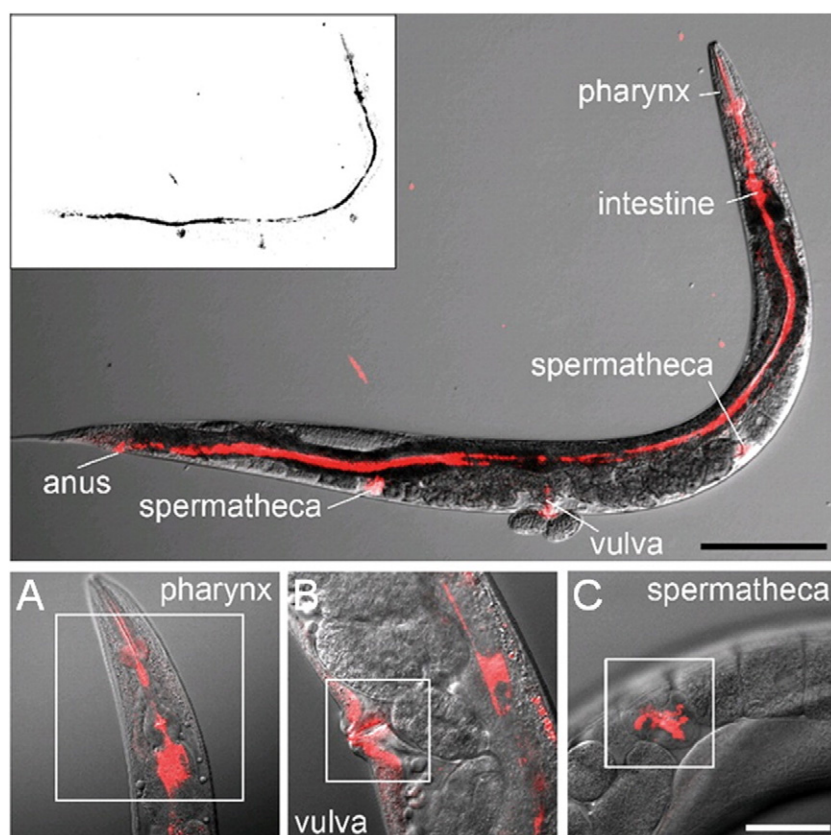


Fig. 7. Fluorescence micrographs of representative 2-day adult *C. elegans* that were treated with 2.5 mg/mL rhodamine-labeled silica NPs (red color) for 24 h. Bar, 100 μ m. NPs are localized in all the structures of the pharynx (A), in the vulval cells (B) and in the spermatheca (C). Bar, 10 μ m.

Adapted with permission from A. Scharf, A. Piechulek and A. von Mikecz, *ACS Nano*, 2013, 7, 10,695–10,703. Copyright 2013 American Chemical Society [41].

and how their toxicity depends on the metal core or the surface coating. Large number of replicates and different conditions with *C. elegans* could bring light to this issue.

Microinjection of fluorescent nanodiamonds of \approx 120-nm diameter to the gonads of gravid adults resulted in incorporation of the NPs into the embryo within 30 min. Fluorescence persisted throughout embryogenesis, although no abnormal embryonic development was observed. NPs were localized into the cytoplasm of many cells in the early embryos but predominantly to the intestines of the late embryos [34].

Exposure to Au NPs for 48 h resulted in multigenerational effects. The reproduction rate was clearly affected in the second generation but not in the progeny of exposed worms, and then gradually recovered in subsequent generations to normal levels. Abnormalities of the reproductive system were observed in all the generations studied, such as abnormal uterus, no egg, and no vulva, among others. The effects on the second generation may be attributed to the impairment of the reproductive cells of the first filial generation in which they were developing embryos inside the exposed worms [22].

SiO₂ NPs (50 nm) exposed worms showed a reduction of progeny production, a significant increase in abnormalities of the reproductive system, and BOW phenotype. These results indicate that long-term exposure of young adults induced age-related degeneration of the reproductive organs in *C. elegans* [37]. Citrate Ag NPs promoted abnormalities in the reproductive system (mainly BOW) and NPs transferred to the fertilized eggs within 24-h exposure of young adults. These abnormalities were not observed after exposure to PVP-coated Ag NPs which indicates protection by the PVP layer and the importance of coating modification of NPs [30]. Experiments like this one help evaluate the coating layer of the NPs and not just the metal core.

Based on the absence of fluorescent emission from the progeny of worms exposed for 20 h to 35-nm diameter PEI coated upconverting

nanophosphors, the authors proposed that the NPs do not cause any side effects on the oogenesis and embryonic development [59]. Given the limited resolution of fluorescence microscopy, study of the intracellular translocation of NPs would be required (i.e. by electron microscopy) to conclude that NPs have no effect on the reproduction of exposed *C. elegans*.

4.1.4. Absorption and translocation pathways

There are still many details missing in the description and understanding of the internalization pathway of NPs by the intestinal cells in *C. elegans*. Results suggest different routes according to the cellular location of NPs after absorption. Intracellular uptake occurred for Ag NPs, even with different coatings (citrate and PVP), and they were located in the cytosol [30]. Intracellular localization of QDs in lysosomes was confirmed by feeding worms simultaneously with lysosomal tracker and QDs [39]. Fluorescently labeled SiO₂ NPs of 50-nm diameter were localized throughout the cytoplasm and the cell nucleus in single intestinal and reproductive cells, although they were not detected in the developing egg [41].

4.1.5. Nervous system

Magnetic-field heating of NPs has been used to remotely control the behavior of *C. elegans*. Streptavidin-conjugated MnFe₂O₄ NPs of 6–8 nm were targeted to a specific neuronal region located in the head of the worms. When a magnetic field was turned on, most of the worms reversed their course of crawling and initiated backward locomotion when the worms felt a temperature of 34 °C. This temperature is the same threshold that in nature promotes the thermal avoidance reaction in *C. elegans* [56]. These experiments demonstrate that magnetic-field heating of NPs can be used in vivo to trigger behavioral responses.

4.2. Nanoprobes for optical imaging in *C. elegans*: an example

Nanosciences have enabled the emergence of a class of biological labels that have strong luminescence, good photostability, narrow emission spectra, and even tunable luminescence colors dependent on size and composition, which has resulted in extensive applications. *C. elegans* have been used to prove in vivo non-bleaching, biocompatible, resistance to digestive enzymes, and nontoxic properties of different imaging probes, which makes them as ideal candidates for biolabeling in multicellular organisms. [68] This example illustrates how *C. elegans* can facilitate analysis of the toxicity of these nanoprobes and how NPs could help acquire new biological information and elucidate pathways not yet understood.

Rare earth upconversion nanophosphors (UCNPs) emit bright green fluorescence under near-infrared light excitation, which is safe to the body and can penetrate tissue. Long incubation times, high UCNP concentrations, and small UCNP size promoted much brighter and more continuous in vivo fluorescence along the body of *C. elegans*. Worms ingested small amounts of UCNP of irregular shapes, 150–200 nm diameter and unmodified surface. These large UCNP aggregated in the intestinal lumen of *C. elegans*, which prevented endocytosis by the intestinal cells as a result of large aggregates. By contrast, worms ingested higher quantities of 35-nm diameter spherical UCNPs with different capping ligands, oleic acid (OA) and polyethylenimine (PEI), which resulted in continuous fluorescence along the alimentary system of the exposed worms with little influence on the in vivo fluorescent signal of the capping ligand [59].

After the worms' resumed feeding, the UCNPs were excreted and no OA-coated UCNPs were seen in the intestinal cells. By contrast, PEI coated UCNPs showed little luminescent signal in the intestinal cells around the gut cavity. This result indicates that endocytosis by intestinal cells was sensitive to the size of the NPs and also to the capping ligand. The electrostatic attraction between the net positive charge of PEI, which provides amino groups to the UCNPs surface, and the negative charge of cells can facilitate cell-binding and endocytosis by the intestinal cells, and indicates the potential use of PEI coating to increase nanoparticulate cellular uptake [59].

The size and the coating of the surface of fluorescent nanodiamonds (FNDs) also influenced the absorption of NPs by intestinal cells. Bare FNDs of ≈ 120 nm were fed in the absence of bacteria, and retained in the intestinal lumen even after 12 h without visualizing any translocation into the intestinal cells. However, dextran- and BSA-bioconjugated FNDs of 290 and 170 nm, respectively, were mostly absorbed into the intestinal cells, with very few still remaining in the gut lumen region. A plausible explanation is that bare-FNDs aggregate in the intestinal lumen and the bigger size impedes translocation. Upon resumption of feeding the worms with *E. coli*, bare FNDs were pushed down through the gut lumen and excreted in less than an hour (Fig. 8), but bioconjugated FNDs absorbed into the cells were retained even after recovery on bacteria for 24 h. It is likely that the surface modifications make FNDs disperse better in solution, which prevents their aggregation inside the gut and helps their uptake through endocytosis by the intestinal cells. Additionally, bioconjugation may

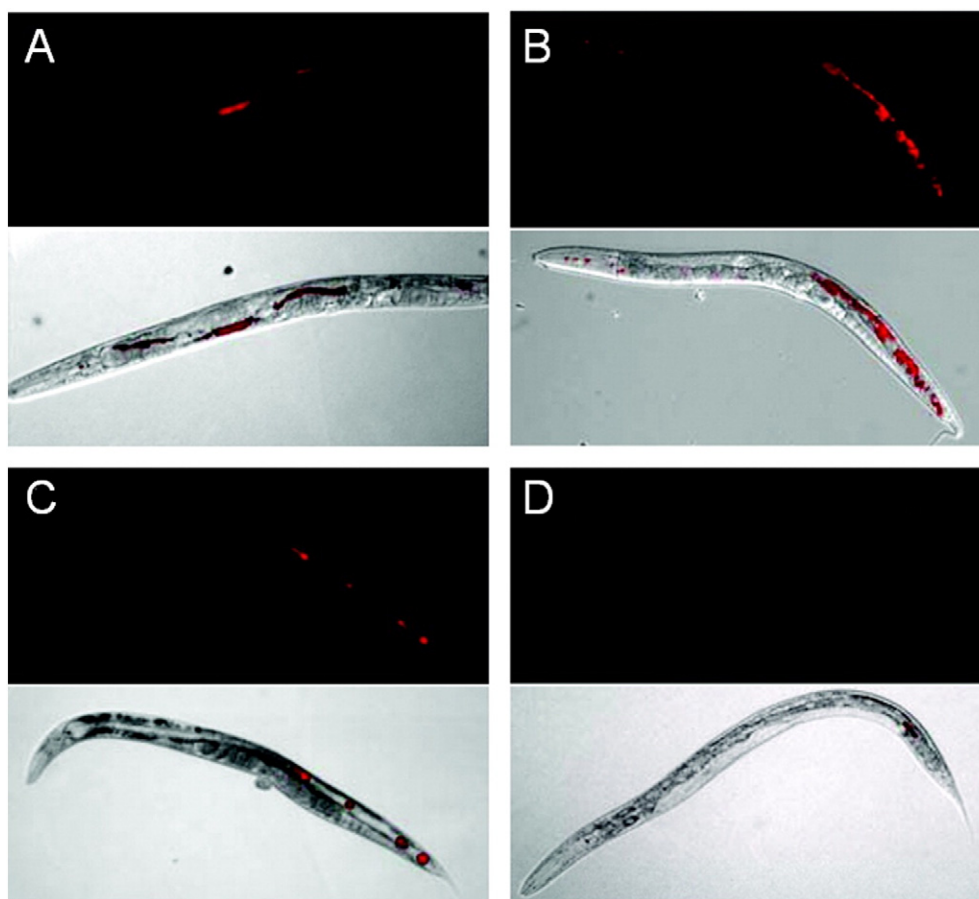


Fig. 8. Epifluorescence and epifluorescence/DIC-merged images of wild-type *C. elegans*. Worms fed with bare FNDs for 2 h (A) and 12 h (B). The FNDs stayed inside the gut and were not excreted out when the worms were deprived of food. Excretion of FNDs occurred when worms were provided with *E. coli* for 20 min (C) and 40 min (D). The upper panels show the epifluorescence images and the lower panels show the epifluorescence/DIC-merged images.

Reprinted with permission from N. Mohan, C. S. Chen, H. H. Hsieh, Y. C. Wu and H. C. Chang, *Nano letters*, 2010, 10, 3692–3699. Copyright 2010 American Chemical Society [34].

activate some receptor-mediated endocytosis pathway(s) that facilitate absorption of FNDs into the intestinal cells from the lumen [34].

5. Conclusions and perspectives

In this review, we have illustrated how *C. elegans* can be used in nanoscience as a powerful biological platform to validate nanoparticles in vivo. To facilitate understanding of the *C. elegans* model, we include here a table that summarizes the main advantages and drawbacks of *C. elegans* (Table 7).

This model animal facilitates the identification of low-toxic sizes, compositions and biocompatible surface modifications to enable optimization of NP design in the laboratory. The availability of biochemical tests and genetic analysis tools for *C. elegans* opens the doors to study the molecular and genetic basis of nanotoxicity. The large range of mutants that can be purchased or produced by genetic manipulations offers large experimental advantages relative to the use of other model animals. Screening of mutant strains with particular features (i.e. resistance to oxidative stress) can provide information to unravel conserved signaling pathways that control nanotoxicity across the animal kingdom. The anatomy of *C. elegans* allows understanding of the interaction of NPs and different biological surfaces with similarities to mammals (i.e. skin; intestinal barrier). If NPs damage the integrity of such biological barriers, it would be possible to explain the translocation of NPs through different organs and tissues, and a distribution path could be discerned. Moreover, studies at a cellular level would help elucidate the specific subcellular and molecular mechanism of entrance of NPs (i.e. through activated receptors, endocytosis ...) to different types of cells (i.e. epithelial or intestinal cells) and their intracellular localization (i.e. cytosol, nucleus, and lysosomes). The short and prolific lifecycle of *C. elegans* offers potential to study the development/reproductive toxicity and intergenerational effects/transfer after NP exposure, which constitutes a controversial point in the evaluation of

chemicals and drugs. Future assays in rodent and non-rodent vertebrate model animals will be necessary, but are more time-consuming, expensive, and involve ethical issues. From the examples given, it can be concluded that *C. elegans* has great potential for NPs assessment in vivo, and will enable chemists and materials scientists to speed up the in vivo characterization of their materials with few requirements and within synthetic chemistry laboratories.

Until now, the interaction between *C. elegans* and NPs has been mostly evaluated by using parameters related to the biology of the worm, and few or no parameters related to the NPs have been explored, including size change after interaction with *C. elegans*, NPs degradation, or chemical analysis of sub-products. Chemistry and NPs characterization techniques could provide useful information to improve the design of NPs, and to achieve a better understanding of the dynamics and behavior of NPs in complex organisms. Collaboration of chemists and materials scientists with the worm community will open up new avenues for deeper understanding of the physico-chemical properties of NPs after exposure to *C. elegans*. Compilation of the results obtained from NP assessment in *C. elegans* with mammals, as well as in vitro, would help unquestionably to improve NPs development by using biological systems of increasing complexity. Moreover, the data analysis combination from biologists (including in vitro and in vivo) and physico-chemical characterization for a wide range of engineered nanomaterials would contribute to the establishment of mathematical models to predict negative effects of new engineered nanomaterials in a similar manner to quantitative structure–activity relationship models.

Chemists and material scientists have to undergo thorough NPs assessment from a multidisciplinary approach during all of the development of their product to insure a controlled synthesis and well-characterized nanomaterial that exhibits low toxicity, biocompatibility and efficiency in its application. We have described how the tiny *C. elegans* can help in this complicated process, and encourage the reader to take advantage of the experimental features and possibilities offered by “the worm”.

Table 7

Advantages and drawbacks of *C. elegans* as a model organism.

Advantages
<p>Easy and Inexpensive Cultivation.</p> <ul style="list-style-type: none"> ✓ Few requirements of cultivation. ✓ Easy to adapt any laboratory to work with <i>C. elegans</i>. <p>Small Size, hermaerochroite, Short Life Cycle, Large Number of Offspring.</p> <ul style="list-style-type: none"> ✓ Large number of animals in a reduced space. <p>Temperature-Dependent Development.</p> <ul style="list-style-type: none"> ✓ Developmental stage can be controlled adjusting the temperature. <p>Two to Three Weeks Lifespan.</p> <ul style="list-style-type: none"> ✓ It facilitates ageing studies. <p>Genome Sequenced, High Homology with Humans, Availability of Mutants.</p> <ul style="list-style-type: none"> ✓ Molecular mechanisms may be conserved in humans. ✓ Powerful platform to perform genetic studies. <p>Transparency.</p> <ul style="list-style-type: none"> ✓ Facile visualization of specimens by using simple instrumentation. <p>Online Resources.</p> <ul style="list-style-type: none"> ✓ Available information on <i>C. elegans</i> anatomy, physiology, genetics, methods... ✓ Engaged scientific community. <p>No Bioethical Concerns.</p> <ul style="list-style-type: none"> ✓ No restriction of use derived from bioethical regulations.
Drawbacks
<p>Lack of Particular Organs.</p> <ul style="list-style-type: none"> ✗ It is not possible to study adverse effects on specific organs such as heart, kidneys, bone, eye, and ear. <p>Lack of Circulatory System.</p> <ul style="list-style-type: none"> ✗ Nanoparticles cannot be administered intravenously. <p>Lower Conservation of Biological Pathways with Humans Relative to Vertebrate Model Organisms.</p> <ul style="list-style-type: none"> ✗ Vertebrate models and in particular <i>Mus musculus</i> have higher homology with humans than <i>C. elegans</i>. <p>It is not used in Regulatory Tests.</p> <ul style="list-style-type: none"> ✗ The use of <i>C. elegans</i> is restricted to early stages of product development (discovery).

Acknowledgments

This research was funded by the People Program of the European Commission (grant agreement n° 303630, cofunded by the European Social Fund) and the Spanish Ministry of Economy (MAT 2012-35324). The authors also acknowledge the support from the Generalitat de Catalunya (2014SGR213), the COST Action MP1202 (COST-MP1202-101212-07606), the Ramon y Cajal grant RYC-2010-06082 (AL), and the FPU fellowship FPU12/05549 (LGM).

References

- [1] Carenza E, Barcelo V, Morancho A, Levander L, Boada C, Laromaine A, et al. *Nanomedicine* 2014;10:225–34.
- [2] Laromaine A, Koh LL, Murugesan M, Ulijn RV, Stevens MM. *J Am Chem Soc* 2007; 129:4156–7.
- [3] Murillo-Cremaes N, Lopez-Periago AM, Saurina J, Roig A, Domingo C. *Supercrit J. Fluids* 2013;73:34–42.
- [4] Singh P, Nanda A. *Int J Cosmet Sci* 2014;36:273–83.
- [5] Sahu SC, Casciano DA. *Nanotoxicity: from in vivo and in vitro models to health risks*. Ltd, USA: John Wiley and Sons; 2009.
- [6] Wood WB. *The nematode Caenorhabditis elegans*. Cold Spring Harbor Laboratory; 1988.
- [7] Riddle DL. *C. elegans* II. Cold Spring Harbor Laboratory Press; 1997.
- [8] Shaye DD, Greenwald I. *PLoS One* 2011;6:e20085.
- [9] Corsi AK. *Anal Biochem* 2006;359:1–17.
- [10] Hulme SE, Whitesides GM. *Angew. Chem.-Int. Edit*, 50; 2011 4774–807.
- [11] Leung MC, Williams PL, Benedetto A, Au C, Helmcke KJ, Aschner M, et al. *Toxicol Sci* 2008;106:5–28.
- [12] Andrassy I. *Arch Zoologicum Budapest* 1956;2:1–15.
- [13] Freckman DW. *Parameters of the nematode contribution to ecosystems*; 1982.
- [14] Hall DH, Altun ZF. *C. elegans* atlas. Cold Spring Harbor Laboratory Press; 2008.
- [15] Jablonski NG. *Skin: a natural history*. University of California Press; 2006.
- [16] Chisholm AD, Hsiao TI. *Wiley Interdiscip Rev Dev Biol* 2012;1:861–78.
- [17] Fares H, Greenwald I. *Genetics* 2001;159:133–45.

- [18] Ghafouri S, McGhee JD. *Nematology* 2007;9:87–91.
- [19] Chauhan VM, Orsi G, Brown A, Pritchard DI, Aylott JW. *ACS Nano* 2013;7:5577–87.
- [20] Liegeois S, Benedetto A, Michaux G, Belliard G, Labouesse M. *Genetics* 2007;175:709–24.
- [21] Barr MM. *J Am Soc Nephrol* 2005;16:305–12.
- [22] Kim SW, Kwak JI, An Y-J. *Environ Sci Technol* 2013;47:5393–9.
- [23] Pispas J, Palmen S, Holmberg CI, Jantti J. *BMC Dev Biol* 2008;8(51):1–13.
- [24] Tarnawa ED, Baker MD, Aloisio GM, Carr BR, Castrillon DH. 101–111. *Biol Reprod* 2013;88:103.
- [25] Yanik MF, Rohde CB, Pardo-Martin C. *Annu Rev Biomed Eng* 2011;13:185–217.
- [26] Hodgkin J. *WormBook*. In: T. C. e. R. Community, editor. *WormBook*; 2005.
- [27] K. Kempfues, in *WormBook*, ed. T. C. e. R. Community, *WormBook*
- [28] Ahringer J. *WormBook*; 2006.
- [29] T. C. Evans (Ed.), in *WormBook*, ed. T. C. e. R. Community, *WormBook*.
- [30] Meyer JN, Lord CA, Yang XY, Turner EA, Badireddy AR, Marinakos SM, et al. *Aquat Toxicol* 2010;100:140–50.
- [31] Duan S-m, Wu Q, Li Y, Tang M, Wang D. *PLoS One* 2012;7:e43729.
- [32] Li Y, Yu S, Wu Q, Tang M, Pu Y, Wang D. *J Hazard Mater* 2012;219–220:221–30.
- [33] Ma H, Bertsch PM, Glenn TC, Kabengi NJ, Williams PL. *Environ Toxicol Chem* 2009;28:1324–30.
- [34] Mohan N, Chen CS, Hsieh HH, Wu YC, Chang HC. *Nano Lett* 2010;10:3692–9.
- [35] Wang H, Wick RL, Xing B. *Environ Pollut* 2009;157:1171–7.
- [36] Kim J, Shirasawa T, Miyamoto Y. *Biomaterials* 2010;31:5849–54.
- [37] Pluskota A, Horzowski E, Bossinger O, von Mikecz A. *PLoS One* 2009;4:e6622.
- [38] Kim SW, Nam S-H, An Y-J. *Ecotoxicol Environ Saf* 2012;77:64–70.
- [39] Qu Y, Li W, Zhou Y, Liu X, Zhang L, Wang L, et al. *Nano Lett* 2011;11:3174–83.
- [40] Hsu PCL, O'Callaghan M, Al-Salim N, Hurst MRH. *Environ Toxicol Chem* 2012;31:2366–74.
- [41] Scharf A, Piechulek A, von Mikecz A. *ACS Nano* 2013;7:10695–703.
- [42] Hulme SE, Shevkopylas SS, McGuigan AP, Apfeld J, Fontana W, Whitesides GM. *Lab Chip* 2010;10:589–97.
- [43] Lockery SR, Hulme SE, Roberts WM, Robinson KJ, Laromaine A, Lindsay TH, et al. *Lab Chip* 2012;12:2211–20.
- [44] Hwang H, Lu H. *Biotechnol J* 2013;8:192–205.
- [45] Minullina RT, Osin YN, Ishmuchametova DG, Fakhruilin RF. *Langmuir* 2011;27:7708–13.
- [46] Gao Y, Liu N, Chen C, Luo Y, Li Y, Zhang Z, et al. *J Anal At Spectrom* 2008;23:1121–4.
- [47] McColl G, James SA, Mayo S, Howard DL, Ryan CG, Kirkham R, et al. *PLoS One* 2012;7:e32685.
- [48] Charan S, Chien FC, Singh N, Kuo CW, Chen P. *Chemistry* 2011;17:5165–70.
- [49] L. Gonzalez-Moragas, S. M. Yu, E. Carenza, A. Laromaine and A. Roig, 2015. Submitted.
- [50] Ami D, Natalello A, Zullini A, Doglia SM. *FEBS Lett* 2004;576:297–300.
- [51] Yang X, Jiang C, Hsu-Kim H, Badireddy AR, Dykstra M, Wiesner M, et al. *Environ Sci Technol* 2014;48:3486–95.
- [52] Le Trequesser Q, Saez G, Devès G, Michelet C, Barberet P, Delville M-H, et al. *Nucl Instrum Methods Phys Res, Sect B* 2014;341:58–64.
- [53] Arnold MC, Badireddy AR, Wiesner MR, Di Giulio RT, Meyer JN. *Arch Environ Contam Toxicol* 2013;65:224–33.
- [54] Ellegaard-Jensen L, Jensen KA, Johansen A. *Ecotoxicol Environ Saf* 2012;80:216–23.
- [55] Chatterjee N, Eom HJ, Choi J. *Environ Mol Mutagen* 2014;55:122–33.
- [56] Huang H, Delikanli S, Zeng H, Ferkey DM, Pralle A. *Nat Nanotechnol* 2010;5:602–6.
- [57] Wu Q, Zhao Y, Li Y, Wang D. *Nanomedicine* 2014;10:1263–71.
- [58] Rui Q, Zhao Y, Wu Q, Tang M, Wang D. *Chemosphere* 2013;93:2289–96.
- [59] Chen J, Guo C, Wang M, Huang L, Wang L, Mi C, et al. *J Mater Chem* 2011;21:2632–8.
- [60] Fang-Yen C, Avery L, Samuel AD. *Proc Natl Acad Sci U S A* 2009;106:20093–6.
- [61] Artal-Sanz M, de Jong L, Tavernarakis N. *Biotechnol J* 2006;1:1405–18.
- [62] Cunha L, Campos I, Montiel R, Rodrigues A, Morgan AJ. *Ecotoxicol Environ Saf* 2011;74:25–32.
- [63] Homa J, Olchawa E, Sturzenbaum SR, Morgan AJ, Plytycz B. *Environ Pollut* 2005;135:275–80.
- [64] Dabrunz A, Duester L, Prasse C, Seitz F, Rosenfeldt R, Schilde C, et al. *PLoS One* 2011;6:e20112.
- [65] Meli VS, Osuna B, Ruvkun G, Frand AR. *Mol Biol Cell* 2010;21:1648–61.
- [66] Dawlatsina GI, Minullina RT, Fakhruilin RF. *Nanoscale* 2013;5:11761–9.
- [67] Zheng S-Q, Ding A-J, Li G-P, Wu G-S, Luo H-R. *PLoS One* 2013;8:e56877.
- [68] Lim SF, Riehn R, Ryu WS, Khanarian N, Tung CK, Tank D, et al. *Nano Lett* 2006;6:169–74.



Scale-up synthesis of iron oxide nanoparticles by microwave-assisted thermal decomposition



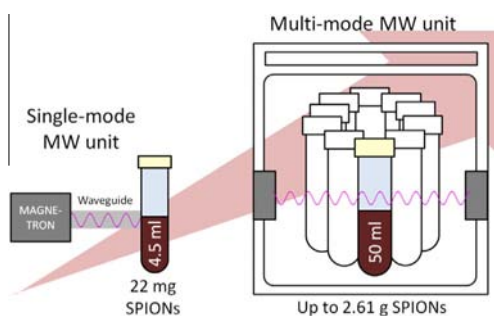
Laura Gonzalez-Moragas¹, Si-Ming Yu¹, Nerea Murillo-Cremaes, Anna Laromaine, Anna Roig*

Institut de Ciència de Materials de Barcelona (ICMAB-CSIC), Campus de la UAB, Bellaterra, Catalonia E-08193, Spain

HIGHLIGHTS

- Scale-up of SPIONs to 3 g/batch with a multi-mode microwave unit is demonstrated.
- SPIONs are dispersible in water, monodisperse with high saturation magnetization.
- Energy and cost-efficient scaled-up microwave-assisted SPIONs synthesis is validated.

GRAPHICAL ABSTRACT



ARTICLE INFO

Article history:

Received 19 April 2015

Received in revised form 5 June 2015

Accepted 13 June 2015

Available online 19 June 2015

Keywords:

Microwave

Multi-mode

Scale-up

Superparamagnetic iron oxide nanoparticles

Water dispersible

ABSTRACT

We report the multi-gram production of water-dispersible superparamagnetic iron oxide nanoparticles (SPIONs) by microwave-assisted reaction. A laboratory-scale reaction performed in a single-mode microwave unit (4.5 mL, producing 22 mg of Fe_2O_3) was scaled-up in a multi-mode equipment (up to 500 mL, corresponding to 2.61 g Fe_2O_3). The quality of the final material in terms of size, colloidal stability and magnetic properties, and the yield of the reaction (~80%) were not compromised in the large-scale setup. Hence, these results reinforce the potential of microwave irradiation in industrial laboratories to synthesize high quality nanoparticles readily dispersible in water and in a short time.

© 2015 Elsevier B.V. All rights reserved.

1. Introduction

Superparamagnetic iron oxide nanoparticles (SPIONs), due to their ultra small size, excellent magnetic properties,

Abbreviations: SPIONs, superparamagnetic iron oxide nanoparticles; NPs, nanoparticles; $\text{Fe}(\text{acac})_3$, iron (III) acetylacetonate; Na_3Cit , trisodium citrate dihydrate; MQ, MilliQ water; MW, microwave; RT, room temperature; LS, laboratory-scale; SU, scale-up.

* Corresponding author at: Institut de Ciència de Materials de Barcelona (ICMAB-CSIC), Campus de la UAB, Bellaterra, Catalonia E-08193, Spain. Tel.: +34 935801853x325; fax: +34 935805729.

E-mail address: roig@icmab.es (A. Roig).

URL: <http://www.icmab.es/nn> (A. Roig).

¹ Equal contribution.

biocompatibility and low toxicity, [1,2] have been extensively studied and used for magnetic resonance imaging (MRI), hyperthermia therapy and drug delivery [3–5]. To date, many methods have been established for the synthesis of SPIONs, including co-precipitation, microemulsion, hydrothermal synthesis, thermal decomposition, and microwave-assisted synthesis [6]. Each of those methods displays advantages as well as some drawbacks, which are detailed in Table 1. In the last few years, microwave-assisted synthesis of SPIONs has attracted considerable interest since it is a facile and fast synthetic route to produce monodisperse nanoparticles with good magnetic properties under moderate temperature, as we recently reported [7,8]. Moreover, considering 1 g of SPIONs, we showed that microwave synthesis

Table 1
Advantages and drawbacks of the main synthetic routes for SPIONs [6].

Method	Advantages	Drawbacks
Co-precipitation	<ul style="list-style-type: none"> • Simple • Aqueous media • Large amounts of NPs can be synthesized (grams) • Size and morphology control • Generally performed at RT • Easy surface functionalization 	<ul style="list-style-type: none"> • Broad size distribution • Poor crystallinity • Basic pH is required • Long reaction times (hours)
Microemulsion	<ul style="list-style-type: none"> • Narrow size range • High crystallinity • Uniform physical properties • Size and morphology control 	<ul style="list-style-type: none"> • Low yield ($\leq 3\%$ per mass of microemulsion) • Requires large amounts of organic solvents
Hydrothermal synthesis	<ul style="list-style-type: none"> • Aqueous media • Size control 	<ul style="list-style-type: none"> • High temperature (≥ 200 °C) • High pressure (≥ 2000 psi) • Special reactors or autoclaves are required
Thermal decomposition	<ul style="list-style-type: none"> • Narrow size distribution (high monodispersity) • High crystallinity • High yield ($\sim 80\%$) • Size and morphology control 	<ul style="list-style-type: none"> • High temperature (~ 300 °C) • Long reaction times (hours) • Requires organic solvents • Hydrophobic particles; ligand-exchange is required to transform them into hydrophilic but aggregation may occur.
Microwave-assisted synthesis	<ul style="list-style-type: none"> • Narrow size distribution (high monodispersity) • High crystallinity • High yield ($\sim 80\%$) • Water dispersible • Short reaction times (minutes) • Moderate temperature (160 ~ 210 °C) • Efficient heating, resulting in low energy consumption • Easy surface functionalization after synthesis 	<ul style="list-style-type: none"> • Safety issues • Requires organic solvents • Limited penetration depth of the microwave

reduced 10 times the energy consumption, and decreased 40% the overall fabrication cost compared to the high temperature thermal decomposition approach [7].

As the number of applications of SPIONs for nanomedicine increases, larger amounts of material at reasonable cost will be in high demand. Microwave-assisted synthesis results in top quality SPIONs, however, the typical reaction vessel volume ranges from 1 to 5 mL leading to yields of less than 20 mg of SPIONs [7]. As an example, the FDA-approved MRI contrast agent *Gastromark*[®] requires 52.5 mg Fe per a single adult dose. Therefore, efforts to turn a laboratory milligram-scale synthesis into a gram-scale production are of great value.

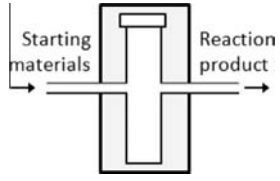
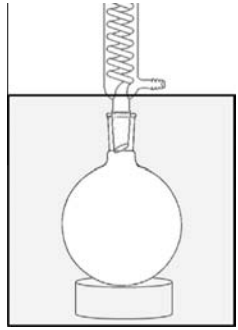
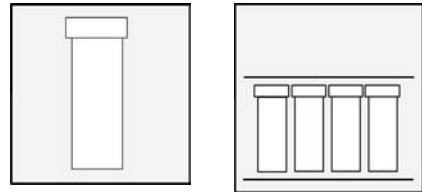
Attempts to demonstrate large-scale synthesis of SPIONs have already been published. Co-precipitation was used by Kolen'ko et al. to scale-up the synthesis of SPIONs using $\text{FeCl}_3 \cdot 4\text{H}_2\text{O}$ and $\text{FeCl}_3 \cdot 6\text{H}_2\text{O}$ as iron precursors [9]. However, the yield was relatively low (68%) and the resulting nanoparticles had poor monodispersity (polydispersity was 46%). Ibarra-Sánchez et al. evaluated the high temperature decomposition of $\text{Fe}(\text{acac})_3$ in a large scale and found the reaction was sensitive to several conditions; the stirring rate, the stirring periods and the reaction temperature [10]. Unfortunately, SPIONs obtained by thermal decomposition are hydrophobic, and require of a ligand exchange before can be used *in vivo*. Based on the potential applications of SPIONs, the synthetic methods to scale-up should not only be simple, safe, and energy and cost efficient, but also yield water dispersible, biocompatible and high saturation magnetization NPs. All these requirements could be achieved by scaling up a microwave-assisted reaction.

To the best of our knowledge, no previous attempts have been performed on the scale-up of microwave synthesis of SPIONs. Many factors as increased heat loss, changes in absorption, limited penetration depth of the radiation into the reaction medium and the additional reflection of the microwaves, make the scaling-up not straightforward [11]. Based on the scale-up of

microwave-assisted organic reactions, two main approaches could be used to scale-up SPIONs production: a flow approach and a batch-type approach [11]. In the flow method, the reaction mixture is pumped in and out of the reaction vessel using a peristaltic pump. Although it avoids the limitations of small vessel volumes and offers complete automatization, this approach is unsuitable for handling heterogeneous mixtures, viscous liquids and particulate materials. The batch-type approach consists of a MW equipment with a larger cavity than the one used in the previous method where reactions can be performed either in one open large vessel or in multiple sealed vessels. In the open-vessel configuration, standard glassware can be employed (i.e. round-bottom flask) and it is usually attached to a condenser to control any vapours produced [12]. Using this strategy, considerable scale-up can be achieved, but penetration depth of the irradiation and power density can become important issues as the vessel size increases. By contrast, the use of sealed vessels allows carrying out reactions in heterogeneous conditions, in the presence of solvents and under pressure. The limiting factor here, for safety concerns, is the vapour pressure generated by a superheated solvent [11]. Characteristic features of the microwave scale-up approaches are summarised in Table 2. In the last couple of years, a new generation of microwave devices that offer scale-up capabilities in a single large vessel (≤ 1 L) under pressure have been also developed and are commercially available (i.e. Masterwave BTR from Anton-Paar or SYTHwave from Milestone). Despite their great potential in increasing the productivity with minimal reaction optimization requirements, they are not widely implemented in synthetic laboratories compared to routinely used single-mode units or multi-mode systems.

This work aims to demonstrate SPIONs scale-up production in a multi-mode unit for multigram quantity, which is a challenge objective. For this purpose, we evaluate the impact of different microwave-specific factors (equipment, reaction time,

Table 2
Main features of the different well-established microwave scale-up approaches.

	Flow approach	Batch-type approach	
		Large batch synthesis	Parallel synthesis
Scheme (MW-irradiated area in grey)			
Conditions	Continuous-flow or Stop-flow	Open vessel	Sealed vessel
Automatisation	Yes	No	No
Microwave Equipment	Single-mode or multi-mode	Multi-mode (≤ 5 L)	Single-mode
Vessel type	Typically Teflon or glass vessels	Standard glassware	Thick-wall vessel
Batch size	High throughput	Limited (≤ 5 L)	Limited (≤ 1 L)
Temperature and pressure	Moderate/High	Moderate	High
Reaction parameter reoptimization	Minimal	May be required	Generally required
Heterogenous mixtures	Not supported	Not recommended	Supported
Safety issue	Less concern	Higher concern	Higher concern

temperature and power) on the reaction product, and we focus on the reproducibility between the lab-scale synthesis and the scaled-up synthesis. At industrial level, the control of microwave-specific variables must result in high quality water dispersible SPIONs with low batch-to-batch variability and good scalability with respect to the previously optimized lab-scale process.

2. Materials and methods

2.1. Materials

Iron (III) acetylacetonate ($\text{Fe}(\text{acac})_3$, $\geq 97.0\%$) and trisodium citrate dihydrate (Na_3Cit), were purchased from Sigma–Aldrich. Benzyl alcohol was obtained from Scharlau. Acetone was bought from Panreac. All materials were used as received if not stated otherwise.

2.2. Laboratory-scale synthesis of SPIONs in a single-mode MW unit

Single-mode CEM Discover reactor (Explorer 12-Hybrid) at a frequency of 2.45 GHz and 300 W was used to perform more than thirty laboratory-scale synthesis of SPIONs. Briefly, 123.6 mg $\text{Fe}(\text{acac})_3$ were dissolved completely in 4.5 mL anhydrous benzyl alcohol (78 mM $\text{Fe}(\text{acac})_3$) in a 10-mL glass tube and vortexed for 30 s. Reaction tubes were capped and transferred to the microwave reactor, heated for 5 min at 60 °C and 10 min at 180 °C, and further cooled down to 50 °C in 3 min using compressed nitrogen. Temperature was monitored by an IR sensor located underneath the reaction vessel. Right after the cooling, 150 μL 10 wt.% Na_3Cit was added to reaction MW-tube and sonicated for 1 min. SPIONs were precipitated with acetone (50 mL) and centrifuged at 6000 rpm for 30 min. After removing the supernatant, 150 μL 10 wt.% Na_3Cit were added to each centrifugal tube and sonicated for 1 min. The washing step was repeated twice. Collected SPIONs pellets were dried completely in a 60 °C oven overnight, and redispersed in MQ H_2O . TEM and DLS were used to assess consistency and reproducibility of the materials obtained in the different reactions. More thorough characterization was done for a representative batch.

2.3. Scaled-up synthesis of SPIONs in a multi-mode MW unit

Six scaled-up synthesis of SPIONs were performed in a multi-mode Milestone ETHOS One unit at a frequency of 2.45 GHz and 500 W. Briefly, 1.373 g $\text{Fe}(\text{acac})_3$ were dissolved completely in 50 mL anhydrous benzyl alcohol in a 100 mL Teflon vessel (78 mM $\text{Fe}(\text{acac})_3$) and vortexed for 30 s. The reaction vessel was placed into a protective sleeve, sealed with a screw-top, and transferred to the microwave reactor. The heating ramp was 3 min from RT to 60 °C, 5 min at 60 °C, 5 min to the maximum temperature (either 180 °C or 210 °C), and 10 to 20 min reaction at maximum temperature (as indicated in Table 4). The reaction vessel was cooled down to 85 °C within 15 min through a high airflow over the vessels, and then to RT in an ice bath (~ 10 min). Direct temperature monitoring and control was achieved using a thermocouple probe (type K) inserted into the reaction vessel. 1.7 mL 10 wt.% Na_3Cit was added to the reaction vessel and sonicated for 5 min. Then an aliquot of the as synthesized SPIONs was washed twice with acetone following the same procedure described for single-mode. Collected SPIONs pellets were dried and redispersed in MQ H_2O . Once more, TEM and DLS were used to assess consistency and reproducibility of the as-obtained materials in the different reactions. More thorough characterization was done for a representative batch.

2.4. Dynamic light scattering (DLS) measurements

DLS measurements were performed to monitor the water dispersability and colloidal stability of SPIONs in MQ H_2O . Hydrodynamic diameter of the SPIONs was determined by using a Zetasizer Nano ZS (Malvern) equipment with a He/Ne 633 nm laser at 25 °C. For each sample, 3 independent measurements were performed with 15 scans for each measurement and hydrodynamic diameters were obtained from the average of the volume-weighted particle size distribution of those measurements.

2.5. Transmission electron microscope (TEM)

Size distribution, morphology and selected area electron diffraction patterns (SAED) of SPIONs were collected in a JEOL

JEM-1210 electron microscope at an operating voltage of 120 kV. TEM samples were prepared by placing one drop of the corresponding SPIONs aqueous dispersion on a holey carbon-coated copper grid (200 mesh, Monocomp) for few seconds, blotting the copper grid with a filter paper and letting the water evaporate completely at room temperature. Typically, about 200 to 300 different SPIONs were counted to depict the size distribution histogram and calculate the SPIONs mean size using the ImageJ software.

2.6. Iron content determination

To determine the iron concentration, samples were sonicated for 10 min in an ultrasound bath. An aliquot of the sample was diluted with HCl (1%), and the iron content of the resulting solution was determined by flame absorption spectroscopy (air-acetylene) with a Perkin-Elmer 2100 spectrometer in triplicate. The yield of the reactions was determined based on the iron concentration of the SPIONs dispersions.

2.7. Superconductive quantum interference device (SQUID)

The magnetic characterization was performed with a Quantum Design MPMS5XL Magnetometer. 150 μ L of SPIONs of known concentration were first dried in a polycarbonate capsule at 60 °C overnight, and then transferred to the SQUID sample holder. Magnetization curves of SPIONs at 300 K were recorded as a function of applied magnetic field up to 5 Tesla. Zero-field-cooling and field cooling magnetization (ZFC-FC) as a function of temperature in a magnetic field of 50 Oe was also recorded.

2.8. X-ray diffraction (XRD)

Powder X-ray diffraction patterns of the nanoparticles were measured with a PANalytical X'PERT PRO MPD diffractometer using $\text{Cu}_{K\alpha}$ incident radiation in the 2θ range of 10–70°.



3. Results and discussion

Following the pioneering work on inorganic nanoparticles synthesis using microwave by Niederberger's group [13–15], we recently reported the fast synthesis of water-dispersible citrate coated SPIONs [8]. Monodisperse SPIONs were characterized by TEM, DLS, and SQUID. The roughly spherical SPIONs had a mean diameter of 5.7 ± 0.9 nm (Fig. 1a and b), a hydrodynamic mean diameter of 17 nm (Fig. 1c), and a saturation magnetisation of 62 emu/g Fe_2O_3 at 300 K (Fig. 1d). This material will be considered the reference material for the scale-up experiments and hereinafter will be referred as laboratory-scale batch (LS).

Even though water dispersible SPIONs with high magnetic response have been successfully synthesized in a single-mode microwave oven, only 22 mg of product (in terms of the Fe_2O_3 content) can be prepared in each vessel. For multi-gram scale-up, the approach chosen involves synthesizing SPIONs inside sealed vessels in a multi-mode microwave system. This choice followed the decision diagram presented in Fig. 2.

When a synthesis developed at the lab-scale is used as a starting point, scale-up typically begins with processing a 50 mL reaction mixture, corresponding to a 10- to 100-fold scale-up of the lab-scale reaction [16]. We started the scale-up trials processing a 50 mL reaction mixture in a 100-mL Teflon vessel in the multi-mode platform Milestone ETHOS ONE, corresponding to a \sim 10-fold scale-up of the synthesis compared to the single-mode CEM Discover unit. It is noteworthy that the ETHOS ONE equipment, as most multi-mode units, can be used for scale-up purposes in any synthetic laboratory considering its benchtop dimensions and standard electrical requirements (Table 3). Hence, no special laboratory settings were required (see Supporting Information for a detailed description of the single-mode and multi-mode equipments). Morphological and structural characterizations of the scaled-up batches (henceforth, referred as SU) were performed using transmission electron microscopy, selected area electron diffraction and X-ray diffraction. Dynamic Light Scattering was used to monitor the hydrodynamic size and the stability of the SPIONs dispersion in H_2O . The magnetic properties were recorded

Table 3
Main features of the equipment used in the experiments, the CEM Discover unit and the Milestone ETHOS One.

	CEM discover	Milestone ETHOS ONE
		
Cavity	Focused single mode cavity	Large microwave cavity (43 L)
Magnetron	2.45 GHz magnetron	Dual magnetron system (2.45 GHz) with pyramid-shaped diffuser
Power	Up to 300 W. Automated power control based on temperature feedback	Up to 1600 W. Automated power control based on temperature feedback. (PID Algorithm)
Temperature	Up to 300 °C	Up to 300 °C
Pressure	Up to 30 bar	Up to 100 bar
Weight	17 kg	90 kg
External dimensions	36 × 43 × 28 cm	55 × 55 × 65 cm
Electrical requirements	220/240 V, 50 Hz	230 V, 50–60 Hz

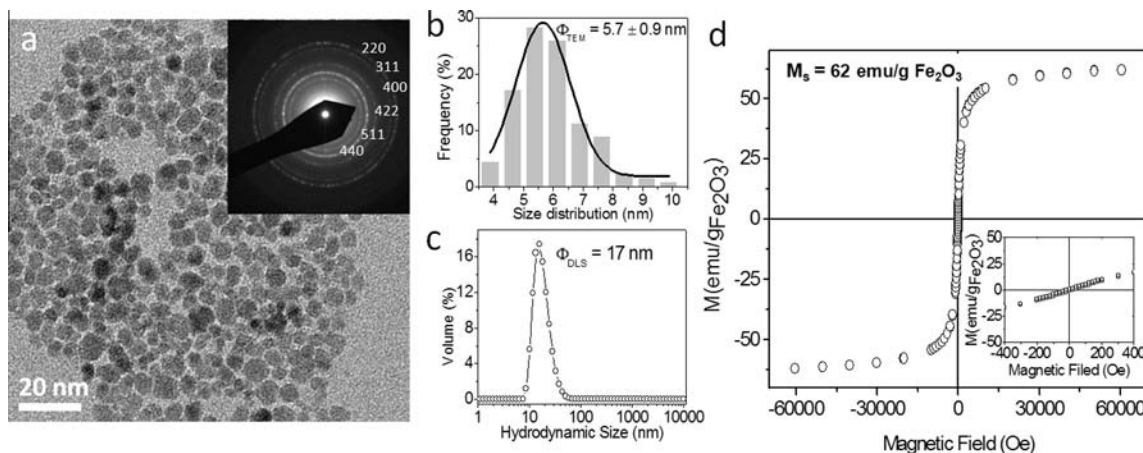


Fig. 1. (a) TEM image of SPIONs obtained by using a single-mode microwave equipment. Inset is the select area electron diffraction (SAED) patterns. (b) Size distribution of SPIONs determined by TEM. (c) Volume-weighted size distribution of SPIONs in MQ H₂O. (d) Magnetization curve of SPIONs as a function of the external magnetic field at 300 K. Inset presents a blow-up at small fields indicating the lack of remanence and coercivity of the M(H) loop.

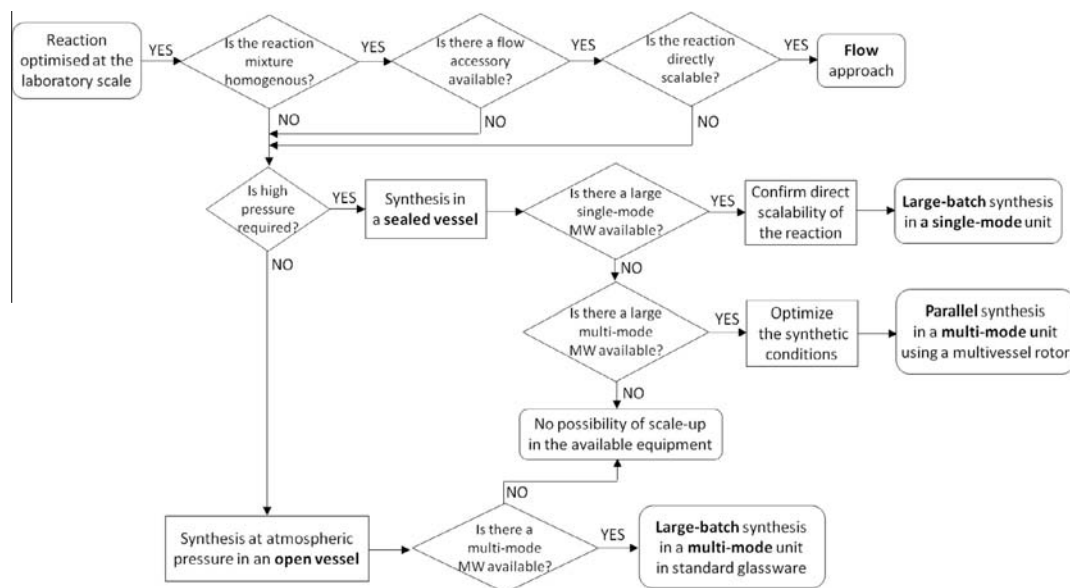


Fig. 2. Decision tree on the scale-up approaches for microwave-promoted reactions performed in solution. Because our reaction system becomes heterogeneous when SPIONs are produced, we foresaw some difficulties regarding the direct scalability using the flow approach and discarded it. Within the batch-type approach, based on our reaction conditions ($\geq 180^\circ\text{C}$), we chose the use of sealed vessels (parallel synthesis) and discarded the use of open-vessels (large-batch synthesis).

in a SQUID device and the yields of the reactions were determined by flame absorption spectroscopy.

When going to larger scale with previously optimized reactions for the lab scale synthesis, a major issue is the direct scalability of the method [16]. As a first approximation, we used the same reaction temperature and irradiation time than in the small-scale synthesis to investigate whether the laboratory scale conditions could be applied directly for the large-scale synthesis of SPIONs. It was not possible to directly compare single-mode and multi-mode experiments using identical output power, as heating rates are lower when processing larger volumes [16]. Hence, higher microwave power was required in the case of multi-mode equipment (500 W) than the single-mode unit (300 W). Using these operational conditions, SPIONs (referred as SU-1) with a mean core size of 3.8 ± 0.8 nm were obtained (Fig. 3a and c), which were smaller than LS. Hydrodynamic diameter displayed a similar value to that of the LS (Fig. 5a), this might be due to the formation of small SPIONs aggregates (Fig. 3a).

Re-optimization of the reaction parameters is typically required when methods are transferred from small-volume, single-mode systems, to larger-volume multi-mode systems [11]. To increase the size of SPIONs by microwave heating, synthesis parameters such as precursor concentration [17], temperature, reaction time and microwave frequency [17–19] can be considered. Here we focused on size control of SPIONs by adjusting some of the microwave-specific parameters, specifically reaction time and reaction temperature, apart from the already reoptimized microwave power. Many studies have determined that MW irradiation time is the most general and simple way for size control. By prolonging the irradiation time from 5 min to 35 min, Bilecka et al. observed that the size of ZnO NPs could be tuned from 3.5 nm to 7 nm [17]. From our experience simply extending the microwave heating time from 10 min to 20 min in the single-mode microwave oven, afforded 1.5-nm increase in size of SPIONs. Following this strategy, we doubled the reaction time while the rest of the reaction parameters remained unchanged. Extended reaction time

Table 4
Reaction conditions for each synthesis.

	Vessel material	Vessel volume (mL)	Starting materials		Time to 60 °C	Time at 60 °C (min)	Max. Temp (°C)	Time to max. T	Time at Max. T (min)	Max power (W)	Cooling (min)
			Fe(acac) ₃	Benzyl alcohol (mL)							
LS	Closed, glass	10	123.6 mg (78 mM)	4.5	N.C.	5	180	N.C.	10	300	3
SU-1	Sealed, Teflon	100	1.373 g (78 mM)	50	3 min	5	180	5 min	10	500	25
SU-2	Sealed, Teflon	100	1.373 g (78 mM)	50	3 min	5	180	5 min	20	500	25
SU-3	Sealed, Teflon	100	1.373 g (78 mM)	50	3 min	5	210	5 min	20	500	25

N.C.: Not controlled.

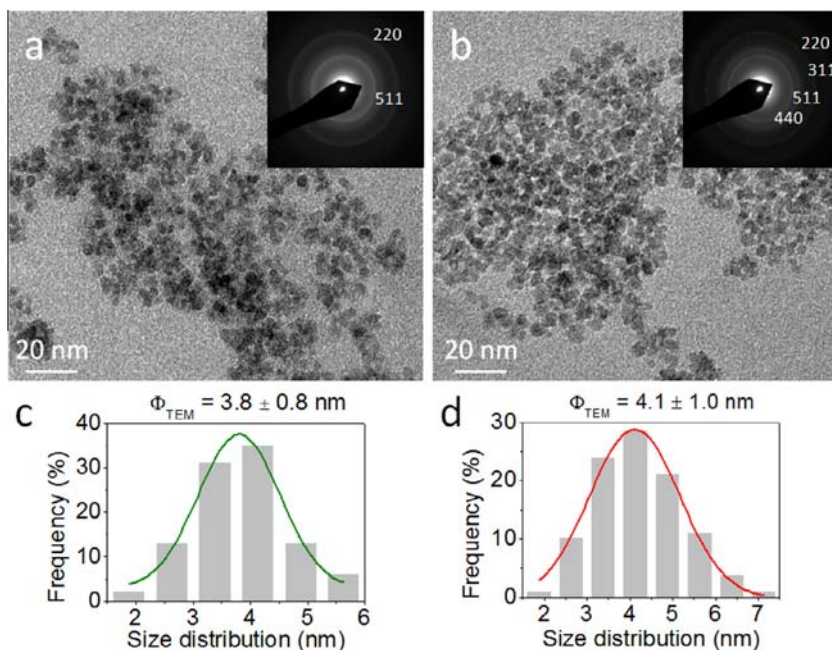


Fig. 3. Characterisation of the scale-up batches by TEM. Panels a and b show TEM images of: (a) SU-1, (b) SU-2. Panels c and d show the size distribution histogram of the scale-up batches: (c) SU-1, (d) SU-2.

(sample referred as SU-2) resulted in a 0.3 nm increase in SPIONs diameter, which had a mean core size of 4.1 ± 1.0 nm (Fig. 3b, d), and similar hydrodynamic size to that of the LS (Fig. 5a). Due to the larger volume of the reaction mixture, a 10-min prolongation in the reaction time did not seem enough for complete growth of the SPIONs, and particle size increased only slightly. Previous work in the single-mode equipment showed that an increase of the maximum reaction temperature from 180 °C to 210 °C lead to a size increase of about 2 nm of the SPIONs. Therefore, we increased the maximum reaction temperature in the multi-mode equipment to 210 °C, while maintaining the irradiation time at 20 min. Interestingly, we obtained SPIONs (sample referred as SU-3) with similar TEM size (5.9 ± 1.4 nm) and polydispersity (24%) as those prepared by the single-mode equipment, but in a reaction volume ten times larger (Fig. 4). Similar results to that of LS were found for the hydrodynamic size too (Fig. 5a). We ascribed this size increase of ~ 2 nm to the faster crystal growth rate of SPIONs observed at higher temperature [17]. Although the morphological shape is slightly irregular, the obtained SPIONs were crystalline and showed good monodispersity. The XRD patterns of SU-3 (Fig. 4d) were coincident with those of maghemite and confirmed a good degree of crystallinity.

These results indicate a good reproducibility between the small-scale reaction and the large-scale process, after re-optimization, in terms of size and colloidal stability of the reaction product. The colloidal stability of SU-3 was re-measured

6 months after its fabrication. Fig. 5b shows that the scale-up material stored at room temperature remained stable in water, since no size increase was observable. This is an extremely interesting information when considering the 'shelf-time' of those nanoparticles. A summary of the reaction parameters used is provided in Table 4. As shown, the heating ramp necessary to yield comparable size of NPs had to be adjust when shifting from the laboratory scale to the large scale (Fig. 6). In the first case, the heating ramp was 5 min at 60 °C and 10 min at 180 °C. In the latter, the heating ramp was 5 min at 60 °C and 20 min at 210 °C. According to the classical LaMer mechanism, the preparation of monodisperse nanoparticles requires a fast nucleation followed by a controlled growth of the existing nuclei [20]. In our microwave mediated route, the pre-heating at 60 °C is used to facilitate the dissolution of the precursor in the solvent [15]. We believe that nucleation occurs after the decomposition of Fe(acac)₃ at 186 °C [21]. The last step involves the growth of particles at constant temperature, in which Ostwald ripening among other growth mechanisms are involved [22–24]. Time resulted a determinant factor to control the growth of NP nucleus to the desired size and form a crystalline structure while keeping narrow particle size distribution, although the temperature had a stronger impact to control microwave-assisted chemistry reaction. Similar findings have been reviewed by Kremnser et al. [16]. Obermayer et al. indicated that differences in the reaction temperature could arise from the system used to control the temperature [25]. In the multi-mode unit,

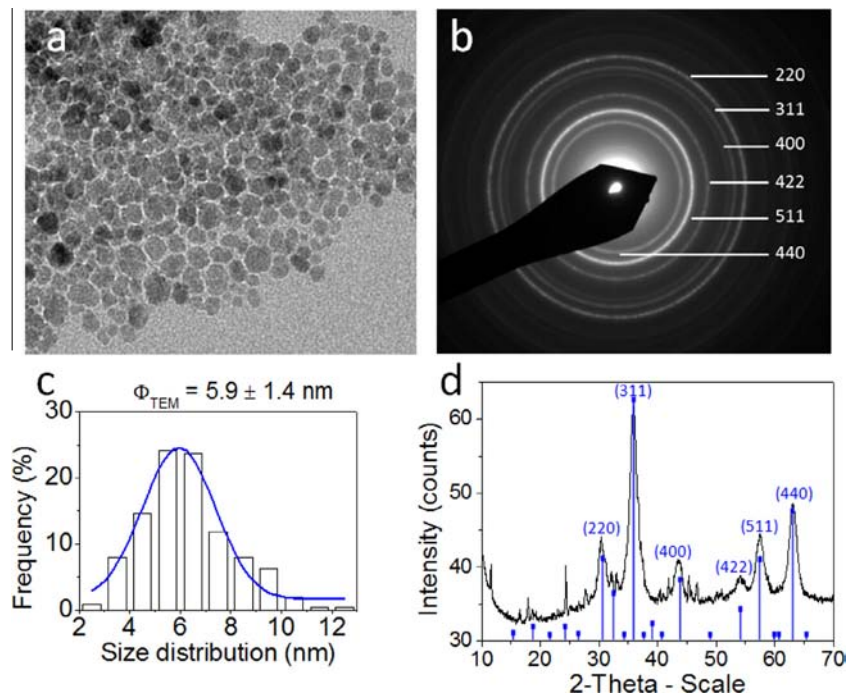


Fig. 4. Characterisation of the SU-3 batch: (a) TEM image. (b) SAED pattern indexed to maghemite iron oxide phase. (c) Size distribution histogram and mean size value, (d) XRD diffractogram indexed for maghemite iron oxide phase.

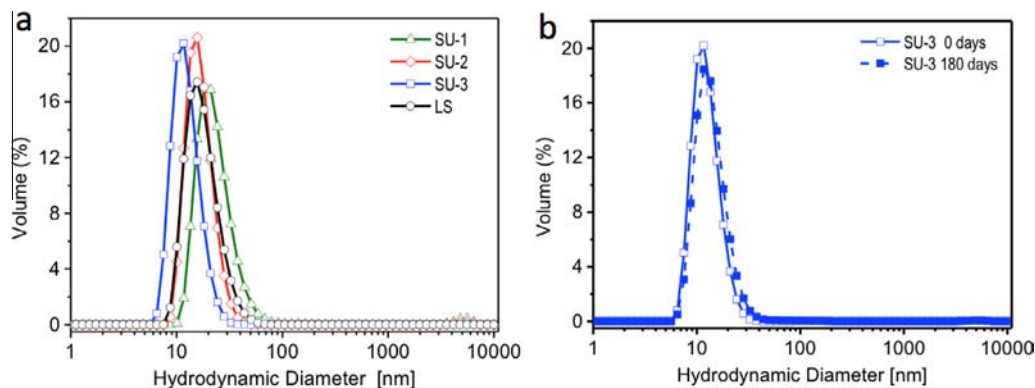


Fig. 5. DLS measurements. (a) Volume-weighted size distribution of the as-synthesized scale-up and laboratory batches in MQ H₂O. (b) Volume-weighted size distribution of SU-3 in MQ H₂O 6 months after synthesis.

temperature is measured using an optic fiber probe immersed in the reaction vessel whereas in the single-mode equipment, an infrared (IR) sensor monitors the outside surface temperature of the glass vessel. As the thermal decomposition temperatures of Fe(acac)₃ is slightly higher than 180 °C [21], the IR sensor of the single-mode equipment could underestimate the temperature inside the reaction mixture. Moreover, IR temperature control results in some delay, as the vessel is warmed from the inside. This delay, typically in the order of a few seconds, can lead to an overheating of the reaction mixture by applying more power than necessary. Hence, the use of internal optic fiber probe allows the monitoring and control of the heating behaviour in a much more accurate way, [25] due to the direct contact with the reaction mixture. On the other hand, different cooling times did not affect the final product. In the laboratory scale, the cooling time was very short (~3 min) due to the use of compressed nitrogen. In the SU batches, the increased cooling time could be attributed to the larger reaction volume, the use of Teflon vessels (as Teflon is an insulating material), and the use of a different cooling system (first,

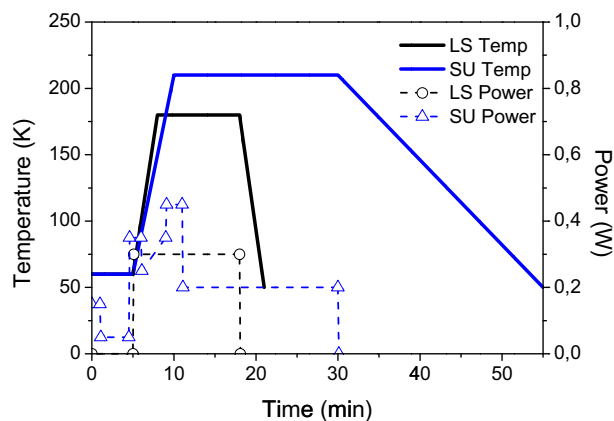


Fig. 6. Heating ramps of the laboratory scale synthesis (LS, in black solid line) and of the optimized scaled-up synthesis (SU-3, in blue solid line). Power is also shown in dotted lines (expressed in KW).

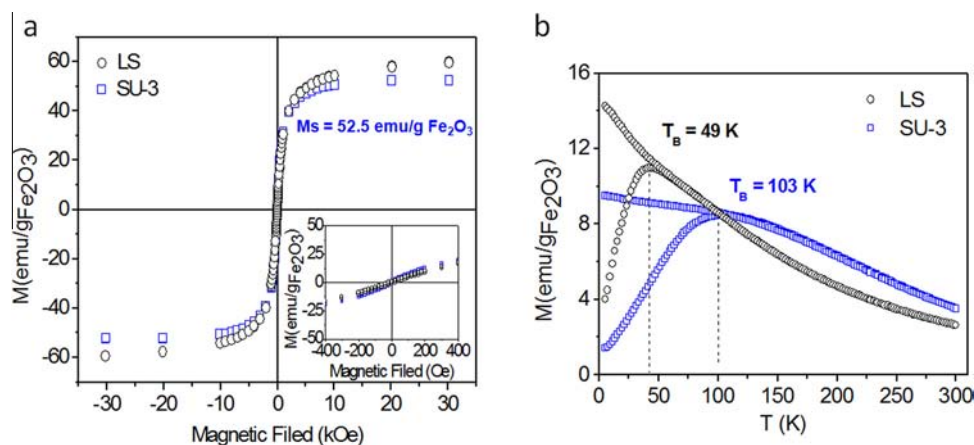


Fig. 7. (a) Magnetization curve $M(H)$ at room temperature of LS and SU-3. (b) ZFC-FC curve of LS and SU-3 measured with a 50 Oe field.

15 min with high airflow and then, 10 min in an ice bath). After cooling, sodium citrate was added to both LS and SU batches to confer water dispersability to the as-synthesized material based on the electrostatic repulsion of the citrate coated particles.

We characterised the magnetic properties of LS and SU-3 SPIONs (Fig. 7). Neither remnant magnetization nor coercivity were observed at room temperature (inset of Fig. 7a), as corresponds to magnetization loops of superparamagnetic materials. A saturation magnetization of 53 emu/g Fe_2O_3 was determined at 300 K, which was slightly lower than the value of the reference material (62 emu/g Fe_2O_3), that could indicate a slightly less crystalline structure. Even though, the high value of the saturation magnetization for the SU-3 system at room temperature is a strong indication of the crystallinity of the material since poorly crystalline samples would show a much lower value. Superparamagnetism of SPIONs for all batches was confirmed by the ZFC-FC measurements. The blocking temperature correlates very well with the mean size of the nanoparticle determined by TEM and DLS with the lowest T_B for the smallest particles (SU-1) (Fig. S1). The blocking temperature (T_B) of the scale-up batch was higher than that from the lab-scale batch (103 K and 49 K, respectively) (Fig. 7b), which can be attributed to the slightly larger size and size distribution of SU-3 SPIONs. Still, this increase on T_B do not compromise the superparamagnetic behaviour of the final material as it is far below room temperature. Thus, SU-3 nanoparticles are superparamagnetic at room temperature. These results indicate that the use of single-mode and multi-mode equipments is comparable regarding the magnetic properties of the final material.

Finally, we computed the yield of the scale-up process through the iron concentration measured by flame absorption spectroscopy. Under the optimal conditions of the scale-up experiments, a yield of 84% was obtained, which was slightly higher than the 79% yield of the small-scale synthesis in the single-mode equipment. Interestingly, Panzarella et al. found that the rate of nucleation was more rapid in a multi-mode oven than in a single-mode unit with a more uniform field, which could account for the higher yield observed [26]. The physicochemical characterization of laboratory scale product (LS) and the optimized scaled-up (SU-3) are summarised in Table 5. Upon irradiating one single vessel, we synthesized 261 mg Fe_2O_3 nanoparticles, corresponding to more than 10 times the amount obtained in the laboratory scale synthesis (22 mg). Using the optimized reaction conditions, our synthesis could be further scaled-up 10 times using the parallel synthesis approach by integrating a multi-vessel rotor system in the multi-mode instrument. These would allow us to produce ~ 3 g of nanoparticles in 30 min with a low energy consumption (<1 kWh). Using the single-mode equipment, producing

Table 5
Physicochemical characterization of the laboratory-scale (LS) and the scale-up (SU) batches.

	Lab-scale (LS)	Scale-up (SU)
TEM size (nm)	5.7 ± 0.9	5.9 ± 1.4
Hydrodynamic size (nm)	17	16
Saturation magnetisation at 300 K (emu/g Fe_2O_3)	62	53
Blocking temperature at 50 Oe (K)	49	103
Yield (% Fe)	79%	84%
Mass of NPs per vessel (mg Fe_2O_3)	22	261

Table 6
Cost estimate to produce 10 g of SPIONs by microwave-assisted reaction.

	Lab-scale (LS)	Scale-up (SU)
Time ^a (hours)	136	2
Energy consumption (kWh)	40.9	1.1
Energy cost ^b (€)	3.75	0.10
Reagents price ^c (€)	86.36	80.61
Labour cost ^d (€)	3231.82	49.94
Total cost (€)	3321.93	130.65

^a Calculated by considering the necessary time used in one batch and adding the required batches to yield 10 g of material.

^b A 0.0917 €/kWh energy price was assumed according to Eurostat (<http://ec.europa.eu/eurostat>, 2014).

^c For the reagents, supplier prices from 2014 were used.

^d A 23.7 €/hour labour cost was assumed according to Eurostat (<http://ec.europa.eu/eurostat>, 2013).

the same amount would require 36 h of MW irradiation and imply a 40-fold increase in the energy consumption and cost. Table 6 compares the costs associated with the production of 10 g Fe_2O_3 NPs using the lab-scale and the scale-up procedures. Hence, the reported scale-up approach notably shortens the synthesis time and reduces the energy consumption compared to the lab-scale process without significantly altering the physicochemical properties of our high quality water dispersible SPIONs.

4. Conclusions

In a previous work, we showed some advantages of the microwave-assisted synthesis of iron oxide nanoparticles compared to the thermal decomposition route regarding cost, time and energy consumption using laboratory scale equipment. In this work, we focused on the scale-up of microwave assisted synthesis

of SPIONs. Attempting larger scale nanomaterials fabrication with reactions previously optimized at the laboratory scale is a big challenge that involves defining a new process setup being able to achieve good reproducibility in comparison with the lab-scale product. In particular, MW-assisted reactions are not easily scalable and optimization steps are generally required. We have assessed the effects of reaction temperature, time, and power on the properties, yield and quality of the final product. The use of a multi-mode equipment allowed us to increase the reaction volume from 4.5 mL to 50 mL (10-fold scale-up), yielding SPIONs with very similar size, colloidal stability and magnetic properties to those produced in the lab-scale synthesis. Hence, we report good reproducibility between two different designs of microwave equipments, a single-mode platform and a multi-mode unit, after reaction parameter re-optimization. Among the advantages of multi-mode equipment, the possibility of simultaneous irradiation of several vessels (parallel synthesis) notably reduces the time and energy cost for production of large amounts of SPIONs. Our large-scale set up allows us the fabrication of up to 3 g SPIONs per reaction in less than 1 h by means of implementing a multivessel rotor system. These results are of great value from an industrial viewpoint, as multi-mode equipments can overcome the bottleneck in productivity associated with single-mode microwave systems, where reactions must be processed sequentially, and make multigram production of SPIONs by MW-assisted synthesis feasible. Finally, the colloidal stability in water of the nanoparticles was measured 6 months after its fabrication. The material stored at room temperature remained stable in water and no size increase was observable. This is an extremely interesting information when considering the 'shelf-time' of the nanoparticles.

Acknowledgments

This research has been partially funded by the Spanish Ministry of Economy (MAT 2012-35324), the Generalitat de Catalunya (2014SGR213), the People Program (Marie Curie Actions) of the European Union's Seventh Framework Program (FP7/2007-2013) under REA grant agreement n° 303630 and cofunded by the European Social Fund. Authors also acknowledge the funding from the Ramon y Cajal grant RYC-2010-06082 (AL), China Scholarship Council fellowship 201206150053 (SMY) and FPU fellowship FPU12/05549 (LGM) and the COST Action MP1202. We are very grateful to Gomensoro S.L. for letting us to perform our experiments with an ETHOS ONE demonstration unit, and specifically to S. Estany, A. Palma and J. Garcia for their advice and support during the experiments. We also want to acknowledge A. May-Masnou for her critical reading of the manuscript.

Appendix A. Supplementary data

Supplementary data associated with this article can be found, in the online version, at <http://dx.doi.org/10.1016/j.cej.2015.06.066>.

References

- [1] L.-H. Shen, J.-F. Bao, D. Wang, Y.-X. Wang, Z.-W. Chen, L. Ren, X. Zhou, X.-B. Ke, M. Chen, A.-Q. Yang, One-step synthesis of monodisperse, water-soluble ultra-small Fe₃O₄ nanoparticles for potential bio-application, *Nanoscale* 5 (2013) 2133–2141.

- [2] E. Carenza, V. Barceló, A. Morancho, J. Montaner, A. Rosell, A. Roig, Rapid synthesis of water-dispersible superparamagnetic iron oxide nanoparticles by a microwave-assisted route for safe labeling of endothelial progenitor cells, *Acta Biomater.* 10 (2014) 3775–3785.
- [3] E. Carenza, V. Barcelo, A. Morancho, L. Levander, C. Boada, A. Laromaine, A. Roig, J. Montaner, A. Rosell, In vitro angiogenic performance and in vivo brain targeting of magnetized endothelial progenitor cells for neurorepair therapies, *Nanomed. Nanotechnol. Biol. Med.* 10 (2014) 225–234.
- [4] R. Hergt, S. Dutz, Magnetic particle hyperthermia—biophysical limitations of a visionary tumour therapy, *J. Magn. Magn. Mater.* 311 (2007) 187–192.
- [5] A.D. Grief, G. Richardson, Mathematical modelling of magnetically targeted drug delivery, *J. Magn. Magn. Mater.* 293 (2005) 455–463.
- [6] S. Laurent, D. Forge, M. Port, A. Roch, C. Robic, L.V. Elst, R.N. Muller, Magnetic iron oxide nanoparticles: synthesis, stabilization, vectorization, physicochemical characterizations, and biological applications, *Chem. Rev.* 108 (2008) 2064–2110.
- [7] O. Pascu, E. Carenza, M. Gich, S. Estradé, F. Peiró, G. Herranz, A. Roig, Surface reactivity of iron oxide nanoparticles by microwave-assisted synthesis, comparison with the thermal decomposition route, *J. Phys. Chem. C* 116 (2012) 15108–15116.
- [8] S.-M. Yu, A. Laromaine, A. Roig, Enhanced stability of superparamagnetic iron oxide nanoparticles in biological media using a pH adjusted-BSA adsorption protocol, *J. Nanopart. Res.* 16 (2014).
- [9] Y.V. Kolen'ko, M. Bañobre-López, C. Rodríguez-Abreu, E. Carbó-Argibay, A. Sailsman, Y. Piñeiro-Redondo, M.F. Cerqueira, D.Y. Petrovykh, K. Kovnir, O.I. Lebedev, J. Rivas, Large-scale synthesis of colloidal Fe₃O₄ nanoparticles exhibiting high heating efficiency in magnetic hyperthermia, *J. Phys. Chem. C* 118 (2014) 8691–8701.
- [10] J.J. Ibarra-Sánchez, R. Fuentes-Ramírez, A.G. Roca, M. del Puerto Morales, L.I. Cabrera-Lara, Key parameters for scaling up the synthesis of magnetite nanoparticles in organic media: stirring rate and growth kinetic, *Ind. Eng. Chem. Res.* 52 (2013) 17841–17847.
- [11] D.-O. Ángel, d.I.H. Antonio, A. Jesús, C.J. R., H.M. Antonia, M.J.d. M., P. Pilar, C.A. de, Reproducibility and Scalability of Microwave-Assisted Reactions, 2011.
- [12] M.D. Bowman, J.L. Holcomb, C.M. Kormos, N.E. Leadbeater, V.A. Williams, Approaches for scale-up of microwave-promoted reactions, *Org. Process Res. Dev.* 12 (2007) 41–57.
- [13] I. Bilecka, M. Kubli, E. Amstad, M. Niederberger, Simultaneous formation of ferrite nanocrystals and deposition of thin films via a microwave-assisted nonaqueous sol-gel process, *J. Sol-Gel. Sci. Technol.* 57 (2011) 313–322.
- [14] I. Bilecka, M. Niederberger, New developments in the nonaqueous and/or non-hydrolytic sol-gel synthesis of inorganic nanoparticles, *Electrochim. Acta* 55 (2010) 7717–7725.
- [15] I. Bilecka, M. Niederberger, Microwave chemistry for inorganic nanomaterials synthesis, *Nanoscale* 2 (2010) 1358–1374.
- [16] J.M. Kremsner, A. Stadler, C.O. Kappe, The scale-up of microwave-assisted organic synthesis 266 (2006) 233–278.
- [17] I. Bilecka, P. Elser, M. Niederberger, Kinetic and thermodynamic aspects in the microwave-assisted synthesis of ZnO nanoparticles in benzyl alcohol, *ACS Nano* 3 (2009) 467–477.
- [18] X. Hu, J.C. Yu, J. Gong, Q. Li, G. Li, α -Fe₂O₃ Nanorings prepared by a microwave-assisted hydrothermal process and their sensing properties, *Adv. Mater.* 19 (2007) 2324–2329.
- [19] E.K. Nyutu, C.-H. Chen, P.K. Dutta, S.L. Suib, Effect of microwave frequency on hydrothermal synthesis of nanocrystalline tetragonal barium titanate, *J. Phys. Chem. C* 112 (2008) 9659–9667.
- [20] C. Niederberger, Re: heat shock factor Y chromosome (HSFY) mRNA level predicts the presence of retrievable testicular sperm in men with nonobstructive azoospermia, *J. Urol.* 187 (2012) 627–628.
- [21] Q. Song, Y. Ding, Z.L. Wang, Z.J. Zhang, Tuning the thermal stability of molecular precursors for the nonhydrolytic synthesis of magnetic MnFe₂O₄ spinel nanocrystals, *Chem. Mater.* 19 (2007) 4633–4638.
- [22] J.A. Marqusee, J. Ross, Kinetics of phase-transitions – theory of ostwald ripening, *J. Chem. Phys.* 79 (1983) 373–378.
- [23] J.A. Marqusee, J. Ross, Theory of ostwald ripening – competitive growth and its dependence on volume fraction, *J. Chem. Phys.* 80 (1984) 536–543.
- [24] P. Dagtepe, V. Chikan, Quantized ostwald ripening of colloidal nanoparticles, *J. Phys. Chem. C* 114 (2010) 16263–16269.
- [25] D. Obermayer, C.O. Kappe, On the importance of simultaneous infrared/fiber-optic temperature monitoring in the microwave-assisted synthesis of ionic liquids, *Org. Biomol. Chem.* 8 (2010) 114–121.
- [26] I. Bilecka, I. Djerdj, M. Niederberger, One-minute synthesis of crystalline binary and ternary metal oxide nanoparticles, *Chem. Commun.* (2008) 886–888.

Protective Effects of Bovine Serum Albumin on Superparamagnetic Iron Oxide Nanoparticles Evaluated in the Nematode *Caenorhabditis elegans*

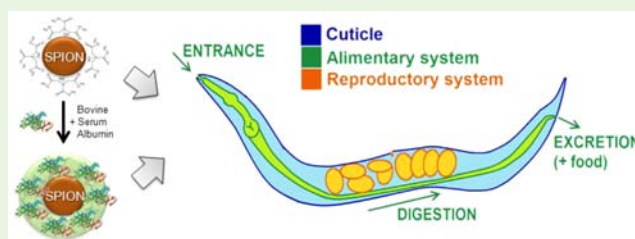
Laura Gonzalez-Moragas, Si-Ming Yu, Elisa Carena, Anna Laromaine,* and Anna Roig

Institut de Ciència de Materials de Barcelona, CSIC, Campus UAB, 08193 Bellaterra, Spain

S Supporting Information

ABSTRACT: Nanomaterials give rise to unique biological reactivity that needs to be thoroughly investigated. The quest for enhanced magnetic nanomaterials of different shapes, magnetic properties, or surface coatings continues for applications in drug delivery, targeting therapies, biosensing, and magnetic separation. In this context, the use of simple in vivo models, such as *Caenorhabditis elegans*, to biologically evaluate nanoparticles is currently in increasing demand as it offers low-cost and information-rich experiments. In this work, we evaluated how surface modification (citrate- and protein-coated) of superparamagnetic iron oxide nanoparticles (C-SPIONs and BSA-SPIONs, respectively) induces changes in their toxicological profile and biodistribution using the animal model *C. elegans* and combining techniques from materials science and biochemistry. The acute toxicity and nanoparticle distribution were assessed in two populations of worms (adults and larvae) treated with both types of SPIONs. After 24 h treatment, nanoparticles were localized in the alimentary system of *C. elegans*; acute toxicity was stronger in adults and larvae exposed to C-SPIONs rather than BSA-SPIONs. Adult uptake was similar for both SPION types, whereas uptake in larvae was dependent on the surface coating, being higher for BSA-SPIONs. Nanoparticle size was evaluated upon excretion, and a slight size decrease was found. Interestingly, all results indicate the protective effects of the BSA to prevent degradation of the nanoparticles and decrease acute toxicity to the worms, especially at high concentrations. We argue that this relevant information on the chemistry and toxicity of SPIONs in vivo could not be gathered using more classical in vitro approaches such as cell culture assays, thus endorsing the potential of *C. elegans* to assess nanomaterials at early stages of their synthetic formulations.

KEYWORDS: *Caenorhabditis elegans*, superparamagnetic iron oxide nanoparticles, bovine serum albumin, nano-bio interfaces, protein corona, surface modification, magnetometry



INTRODUCTION

The study of the interaction between nanoparticles (NPs) and biological environments has been the focus of recent investigations.^{1–3} This evaluation is vital to improve the design of biocompatible NPs that effectively carry out diagnostic, therapeutic, or theranostic functions in vivo and have a harmless toxicological profile.^{4,5} Along this line, detailed information about the effects of NP coating, their chemistry, the structure of the NPs, and their toxicity mechanisms is crucial to predict NP behavior.^{6–11} Surface modifications on NPs induce changes in their toxicological profile both in vitro and in vivo. For instance, magnetite (Fe₃O₄) cores (25 nm) functionalized with positive polyethylenimine (PEI) and negative poly(acrylic acid) (PAA) did not show differences in the viability of human neuroblast SH-SY5Y cells, but the uptake of PEI NPs was 4.5-fold larger than that of PAA NPs after 2 h incubation.¹² Polyvinylpyrrolidone (PVP)-coated silver NPs (28 nm) reduced the reprotoxicity in *Caenorhabditis elegans* and avoided NP transference to the growing embryo and in the subsequent generations compared to 1 nm citrate-coated silver

NPs.¹³ Sulfidation of PVP-coated silver NPs (37 nm) decreased the toxicity of silver NPs in zebrafish (*Danio rerio*).¹⁴

From the plethora of inorganic NPs available, superparamagnetic iron oxide NPs (SPIONs) show potential because of their biocompatibility and magnetic properties. SPIONs are approved by the U.S. Food and Drug Administration as magnetic resonance imaging (MRI) contrast agents, and their application in magnetic hyperthermia is already at the clinical stage (phase II).^{15,16} SPIONs are also investigated for drug delivery, targeting therapies, biosensing, and magnetic separation to name only few applications.^{17,18} Therefore, the quest for enhanced magnetic nanomaterials of different shapes, magnetic properties, or surface coatings continues.^{19,20}

In order to facilitate the optimization of NPs and mitigate most of the difficulties associated with the use of complex animal models, we assessed the surface functionalization of superparamagnetic iron oxide nanoparticles (SPIONs) in *C.*

Received: June 12, 2015

Accepted: September 27, 2015

Published: September 28, 2015

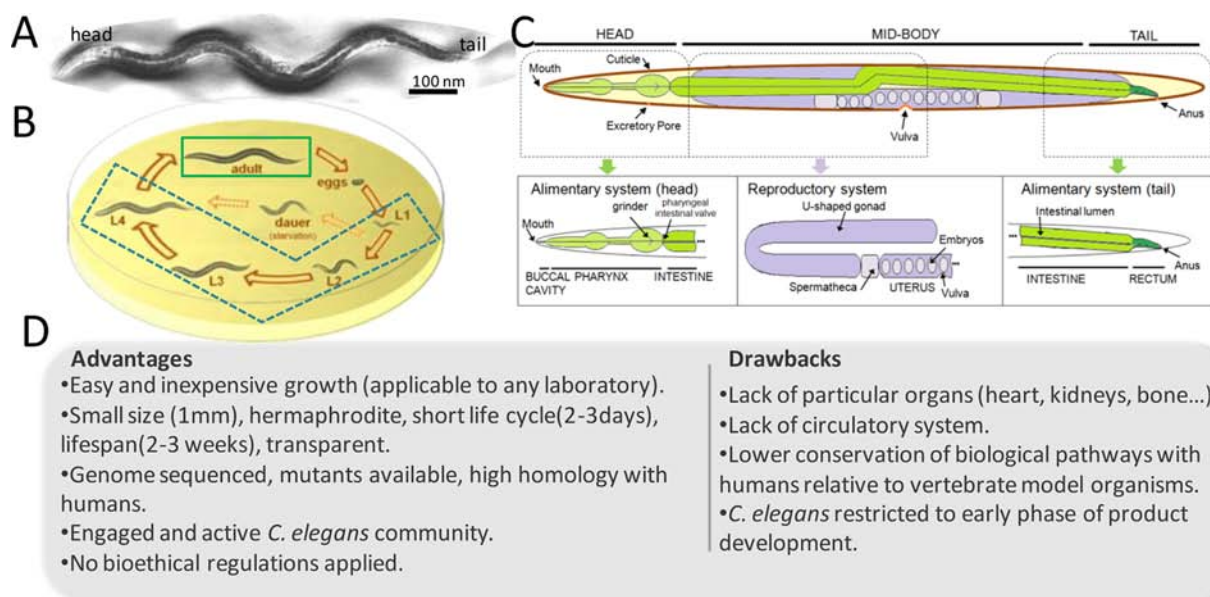


Figure 1. Main biological features of *C. elegans*. (A) Light microscopy image of *C. elegans*. (B) Life cycle progress through four larval stages (L1–L4) before reaching adulthood. Larval stages are marked with a dotted blue box. Adults are marked with a green box. (C) General anatomy of *C. elegans*. (D) Table listing the advantages and drawbacks of working with *C. elegans*.

elegans. The evaluation in simple animals at the early stages of the synthesis can reduce the number of candidate materials and facilitate the research before screening them in mammalian models, minimizing ethical issues and avoiding high costs and delayed results.²¹ *C. elegans* is a 1 mm long soil nematode with a rapid life cycle (3 days) and short lifespan (2–3 weeks) that is facile and inexpensive to grow.²² Its small size and transparency permit the observation of NP uptake and distribution at the cellular, tissue, and organism levels, combining techniques and procedures from different fields such as materials science and biochemistry (Figure 1).^{23–26} A detailed comparison of *C. elegans* and mammalian models can be found in the existing literature.^{21,27,28} Advantages and drawbacks of using *C. elegans* for the evaluation of nanomaterials are summarized in Figure 1D.

In this work, citrate-coated SPIONs (C-SPIONs) and SPIONs coated with bovine serum albumin (BSA-SPIONs) were chosen as a model system. The different surface functionalizations were investigated in order to determine whether they lead to different uptake, biodistribution, or in vivo properties in adult and larvae populations of the model organism *C. elegans*.

MATERIALS AND METHODS

Materials. *C. elegans* Bristol strain N2 and *Escherichia coli* OP50 were obtained from the Caenorhabditis Genetic Center (CGC) stock collection, University of Minnesota, St. Paul, MN, USA. Benzyl alcohol ≥99% was bought from Scharlau. Peptone, yeast extract, bacteriological agar, and tryptone were purchased from Conda Lab. All other reagents used were bought from Sigma-Aldrich, if not stated otherwise.

Nanoparticle Synthesis. Citrate-coated SPIONs were synthesized by using microwave-assisted thermal decomposition, as described previously.²⁹ Iron(III) acetyl acetonate (0.35 mmol) was dissolved in anhydrous benzyl alcohol (4.5 mL) in a microwave tube and mixed with a vortex mixer for 30 s. The reaction tubes were transferred into a microwave CEM Discover reactor (Explorer 12-Hybrid; 2.45 GHz; 300 W). A heating ramp was used for 5 min at 60 °C and 10 min at 180 °C, before cooling to 50 °C in 3 min by using compressed nitrogen. Then, sodium citrate (150 μL; 10 wt %) was added to each

reaction tube and sonicated for 1 min. Acetone was added to precipitate the particles and centrifuged at 6000 rpm for 30 min. The supernatant was discarded, and the washing step was repeated twice. The final black precipitate was dried overnight in an oven at 60 °C and redispersed in Milli-Q water (2 mL). The dispersion was adjusted to pH 7.4 by the addition of HNO₃ (0.1 M).

BSA-SPIONs were synthesized by using the BSA adsorption protocol described previously.²⁹ In brief, synthesized C-SPIONs were dispersed in Milli-Q water (2 mg/mL). The dispersion was first adjusted to pH 11 by adding NaOH (0.01 M), and then equal volumes of the C-SPION dispersion (2 mg/mL) and BSA solution (5 mg/mL) were rapidly mixed and stirred with a vortex mixer for 10 min. Finally, the mixture was adjusted to pH 7.4 by adding HNO₃ solution (0.05 mM) and a BSA-SPIONs dispersion (1 mg/mL) was obtained.

To determine the iron concentration, C-SPIONs were sonicated for 10 min in an ultrasound bath. An aliquot of the sample was diluted with HCl (1%), and the iron content of the resulting solution was determined by flame absorption spectroscopy (air–acetylene) with a PerkinElmer 2100 spectrometer in triplicate. The concentration of SPIONs expressed throughout the text refers to the concentration of iron in the SPIONs.

Dynamic Light Scattering and Transmission Electron Microscopy Analysis. Dynamic light scattering (DLS) and zeta-potential measurements were performed with a Zetasizer Nano ZS (Malvern) with a He/Ne 633 nm laser at 25 °C. For each sample, three independent measurements were performed.

Transmission electron microscopy (TEM) samples were prepared by placing one drop of the corresponding SPION dispersion on the copper grid, blotting the copper grid with a filter paper, and letting it evaporate completely at room temperature. C-SPIONs were imaged with a JEOL JEM-1210 electron microscope at an operating voltage of 120 kV. About 200 different particles were computed to depict the size distribution and the mean size of C-SPIONs.

Adsorption of BSA on C-SPIONs was visualized by performing negative staining TEM.²⁹ A drop of BSA-SPIONs was placed on a carbon-coated grid and then blotted with filter paper. Subsequently, uranyl acetate (5 μL; 2%) was placed on the grid for 1 min before being blotted. The grid was then placed in a 2011 JEOL electron microscope. About 200 different particles were counted to depict the size distribution and the mean size of the BSA-SPIONs.

Magnetometry. A magnetometer from Quantum Design MPMS5XL was used to perform magnetization measurements.

Magnetization versus applied field was measured at 5 K. The zero-field-cooled/field-cooled magnetization (ZFC-FC) was measured with a 50 Oe applied field in the range of 4–300 K.

Worm Growth and Maintenance. Nematodes were grown on nematode growth medium (NGM) and fed *E. coli* OP50 according to the standard protocol at 20 °C.³⁸

Preparation of the Adult and Larvae Populations. Mixed-stage well-fed worms with OP50 were rinsed with Milli-Q water and transferred into a 15 mL centrifuge tube. Worms settled down in 10 min, and then the supernatant was changed to clean Milli-Q water. We washed the worms three times to remove any remaining bacteria. Adult worms were filtered by using a 40 μm pore size nylon mesh (BD Falcon) and washed three times with Milli-Q water to remove any remaining juvenile stages. The retentate worms were collected in Milli-Q water and used as the adult population (less than 10% larvae). The filtrate was used as the larvae population.

Iron Determination. Around 1×10^4 adults and 4×10^4 larvae in triplicate were treated with 500 μg of SPIONs/mL for 24 h, transferred to a polycarbonate capsule, dried for 48 h at 60 °C, and used for magnetometry measurements. The quantity of SPIONs in the worms was evaluated by measuring the value of the remanence magnetization (M_R) at 5 K of the treated worms ($M_{R, \text{worms}}$). The $M_{R, \text{worms}}$ (emu) divided by the total number of worms gives the magnetization per worm (emu/worm). To know the amount of iron per worm, the magnetization per worm was divided by the value of the remanence magnetization of the SPIONs ($M_{R, \text{SPIONs}}$) (emu/g Fe) also at 5 K. This value is not affected by any diamagnetic or paramagnetic components in the sample. Calculation was performed according to the following formula:

$$\text{NP uptake (pg Fe/worm)} = \frac{M_{R, \text{worms}} \text{ (emu/worm)}}{M_{R, \text{SPIONs}} \text{ (emu/pg Fe)}}$$

Nanoparticle uptake was normalized by worm body volume, dividing the NP uptake (pg Fe/worm) by the body volume of worms (either adults or larvae) expressed in nanoliters, as follows

$$\text{NP uptake (pg Fe/nL worm)} = \frac{\text{NP uptake (pg Fe/worm)}}{\text{body volume (nL/worm)}}$$

Scanning Electron Microscopy–Energy-Dispersive X-ray Spectroscopy Analysis. A mixed-stage worm population was treated with 500 μg of SPIONs/mL for 24 h and fixed with 4% paraformaldehyde in Milli-Q water for 2 h at room temperature. Fixed worms were washed three times with Milli-Q water and concentrated to 100 μL. A sample (20 μL) was transferred to a piece of carbon tape placed on a aluminum stub and left to dry at room temperature. Scanning electron microscopy–energy-dispersive X-ray spectroscopy (SEM-EDX) analyses were carried out with a scanning electron microscope (QUANTA FEI 200 FEG-ESEM) equipped with an EDX system. SEM was used under low-vacuum conditions, an acceleration voltage of 10 kV, and an electron beam spot of 3.0.

Biodistribution Assay. Two populations of worms (adults and larvae) were treated with 500 μg Fe/mL SPIONs for 24 h and fixed with 4% paraformaldehyde in Milli-Q for 2 h at room temperature. Fixed worms were washed three times with Milli-Q water, mounted on a glass slide, and observed under the microscope. For Prussian Blue staining, fixed worms were incubated with a mixture of Perl's solution (4% KFeCN/4% HCl), incubated in the dark for 1 h, and washed three times. The worms were then mounted on a glass slide and observed under the microscope. To study the biodistribution of the SPIONs within the alimentary system of the treated worms, the alimentary system was divided into four segments—pharynx, anterior gut, central gut, and posterior gut—and the number of worms of the total 50 animals that presented SPIONs in the given segment was counted. Results were expressed as a percentage of worms with NPs in the pharynx, anterior gut, central gut, and posterior gut, respectively. Percentages of worms with NPs are represented as a color map, establishing different intervals; 45–55% pale orange, 55–65% light orange, 65–75% orange, 75–85% dark orange. Scale with colors and percentages are included in Figure 6.

Toxicological Assays. We assessed two different parameters in order to evaluate the effects of SPIONs in *C. elegans*: survival and brood size. In the survival assay, the adult and larval populations were treated separately with C-SPIONs, BSA-SPIONs, and Fe(NO₃)₃ in a final volume of 100 μL in 96-well plates for 24 h. The assay was performed in triplicate. The plates were tapped, and the worms that moved were counted as alive. Each well contained between 9 ± 3 adult worms and 25 ± 8 larvae. The concentration range assayed was 0–500 μg/mL. To study the brood size, individual young adult worms nontreated and treated with C- and BSA-SPIONs (concentration range: 100–500 μg/mL) were transferred to a NGM plate seeded with an OP50 lawn at 20 °C. The number of progeny was scored after 72 h of food resumption. Results are expressed as % of brood size with respect to the nontreated (control) worms. The reprotoxicity assay was performed per triplicate.

Excretion of the Internalized SPIONs. After treatment with 500 μg Fe/mL SPIONs for 24 h, few adult worms were transferred to a NGM plate either with or without *E. coli* OP50. Plates were monitored for 12 h to check if food resumption or absence would induce excretion of the internalized SPIONs.

A mixed-stage population consisting of 6×10^3 well-fed worms was treated with 500 μg Fe/mL BSA-SPIONs and C-SPIONs in Milli-Q water in a 24-well plate for 24 h. After treatment, worms were collected in 1.5 mL Eppendorfs and centrifuged at 1400g for 2 min, and the supernatant was discarded. The worms were washed three times with Milli-Q water to remove any remaining SPIONs in the media. The worm pellet was diluted to 100 μL with Milli-Q water and incubated with a freshly prepared mixture of household bleach (20 μL) and NaOH (5 N; 1:1). After 20 min, Milli-Q water (1.5 mL) was added to stop the reaction, and the Eppendorfs were centrifuged for 45 min at 1400g. After centrifugation, a brown pellet of NPs was visible at the bottom of the Eppendorf. The supernatant was removed, fresh Milli-Q water was added up to a volume of 100 μL, and the Eppendorf was sonicated for 5 min. Finally, a drop was deposited onto a TEM grid and observed with a JEOL JEM-1210 electron microscope at an operating voltage of 120 kV. More than 100 different particles were measured to describe the size distribution and the mean size of internalized C-SPIONs and BSA-SPIONs. Diluted C-SPIONs (100 μg/mL) were also treated with bleach and used as control samples for the TEM observations.

To further characterize the effect of bleach treatment on the NPs, we monitored the changes in the hydrodynamic mean diameter of diluted citrate SPIONs (100 μg/mL) by DLS before and after the bleach treatment and after NP redispersion.

Magnetometry of the Internalized SPIONs. The dependence of the magnetic moment on the temperature (4–300 K) at an applied magnetic field of 50 Oe was investigated for the superconducting quantum interference device samples prepared as previously described. From the variation of the blocking temperature of the NPs internalized inside the worms, their size decrease was calculated according to the Néel–Arrhenius equation:

$$\tau_N = \tau_0 \exp\left(\frac{KV}{k_B T}\right); V_2 = \frac{V_1 T_{2B}}{T_{1B}}; \% \text{decrease} = \frac{r_1 - r_2}{r_1} \times 100$$

in which τ_N is the Néel relaxation time; τ_0 is the attempt time; K is the magnetic anisotropy energy density; V is the NP volume; k_B is the Boltzmann constant; T is the temperature; T_B is the blocking temperature; r is the NP radius; 1 refers to as-obtained NPs; and 2 refers to the internalized NPs.

Statistical Analysis. Past 3.03 was used for all statistical analyses. For the survival and brood size assays, statistical significance between groups was assessed using ANOVA followed by the Tukey's post-hoc test. Survival and brood size data were fitted to four linear regression equations: adults/C-SPIONs, adults/BSA-SPIONs, larva/C-SPIONs, and larva/BSA-SPIONs. Differences between the behaviors of C- and BSA-SPIONs were studied using ANCOVA. For iron uptake, intergroup differences were assessed using Student's *t* test, and the interaction between SPION type and *C. elegans* developmental stage was evaluated using a two-way ANOVA. Three levels of statistical

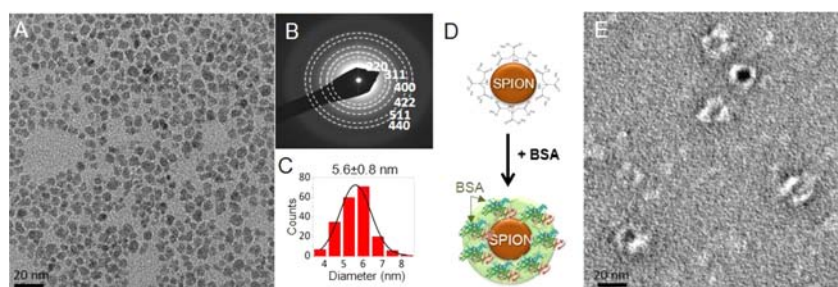


Figure 2. Characterization of SPIONs. (A) TEM image of C-SPIONs. (B) Diffraction pattern. (C) Histogram of TEM size distribution. (D) Scheme of BSA-SPION preparation. (E) Negative staining TEM image of BSA-SPIONs.

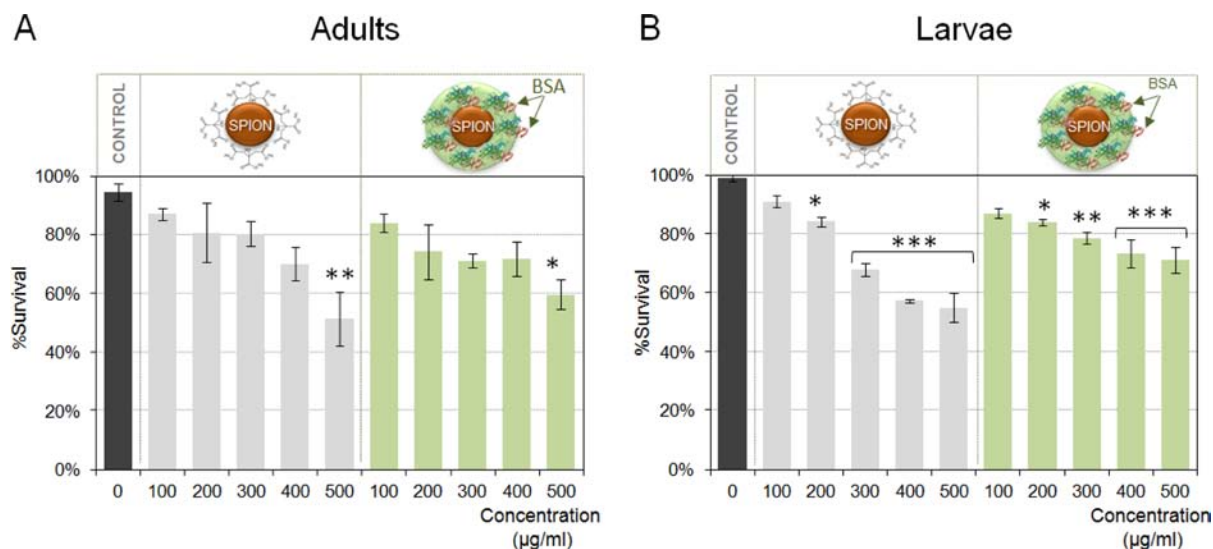


Figure 3. Effect of C-SPIONs and BSA-SPIONs on the acute toxicity of *C. elegans*. (A) Adult worms and (B) larvae treated with 0–500 $\mu\text{g/mL}$ C-SPIONs and BSA-SPIONs. Three replicates per concentration were performed. Error bars indicate standard error; $p < 0.05$ (*), $p < 0.01$ (**), and $p < 0.001$ (***).

significance were considered in all cases: $p < 0.05$ (*), $p < 0.01$ (**), and $p < 0.001$ (***).

RESULTS AND DISCUSSION

Monodisperse C-SPIONs synthesized by using a microwave-assisted thermal decomposition method were characterized by TEM, DLS, and zeta-potential measurements. C-SPIONs had a diameter of 5.6 ± 0.8 nm, a hydrodynamic mean diameter of 17 nm, and a zeta-potential of -41 mV. The same SPIONs when protein-coated (BSA-SPIONs) exhibited a hydrodynamic mean diameter of 25 nm and a zeta-potential of -26 mV. TEM observations performed with negative staining and the increase in hydrodynamic diameter indicated that a single monolayer of BSA was coating the SPION surface (Figure 2).^{29,30} We chose BSA since it builds a protein corona around NPs, controlling their aggregation, and improving their colloidal stability. Full characterization of the C-SPIONs and BSA-SPIONs are summarized in the Figure S1 and by Yu et al.²⁹

Previous studies of NPs in *C. elegans* have been mainly performed in solid media, mixing the NPs with the agar, this exposure route bears high ionic strength and leads to NP instability and precipitation and uneven exposure of *C. elegans* to the NPs, increasing the variability and compromising the reproducibility of the results.^{23,31–35} Exposure of the worms to NPs in liquid media, as used in these experimental studies, can minimize the above-mentioned drawbacks.^{23,36} In order to balance the stability of our NPs and the survival rate of *C.*

elegans, we evaluated Milli-Q water and M9 medium as *C. elegans* standard media. The high ionic strength of M9 medium promoted the aggregation of C-SPIONs, while in Milli-Q water, they remained stable; the *C. elegans* survival was identical in both media after 24 h; therefore, we selected Milli-Q water as the exposure media. The use of liquid media ensured the even distribution of NPs, a homogeneous and free contact with the worms, and allowed us to monitor the physicochemical properties of the SPIONs during exposure. *C. elegans* were exposed to SPIONs for 24 h without food, which allowed us to maintain the SPIONs inside the *C. elegans* intestine without being excreted.^{32,37} Prior to the incubation with NPs, *C. elegans* were fed on OP50 according to the standard practices.³⁸ The exclusion of bacteria during the incubation with NPs prevented SPIONs from being adsorbed on the bacteria and avoided the active metabolism of live bacteria from decreasing the concentration of SPIONs and generating NP subproducts. Any potential starvation effects in the animals due to absence of food were taken into account with appropriate controls (Figure 3).

We evaluated the survival rate in adult and larval populations of *C. elegans* treated with 0–500 $\mu\text{g/mL}$ C-SPIONs and BSA-SPIONs after 24 h (Figure 3). The survival of adults at 24 h for both types of SPIONs was higher than 70% at doses below 400 $\mu\text{g/mL}$ and decreased significantly at 500 $\mu\text{g/mL}$ to 60% ($p < 0.05$) and 51% ($p < 0.01$) in the case of BSA-SPIONs and C-SPIONs, respectively. In the case of larvae, survival was higher

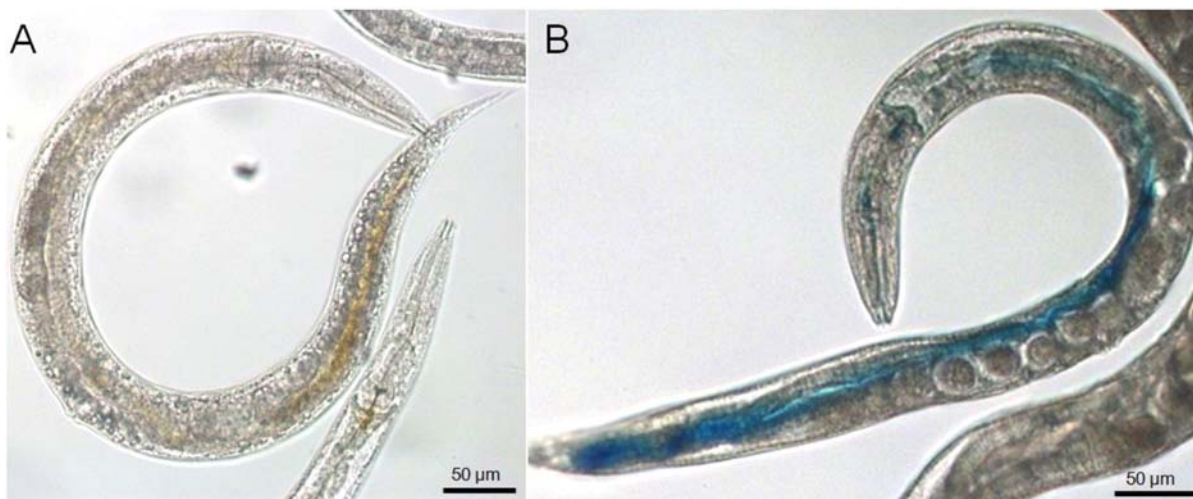


Figure 4. Light microscopy images of SPION-treated *C. elegans*. (A) Direct observation of C-SPIONs inside fixed *C. elegans*. SPIONs appear brown. (B) Prussian Blue stained worms where SPIONs appear blue.

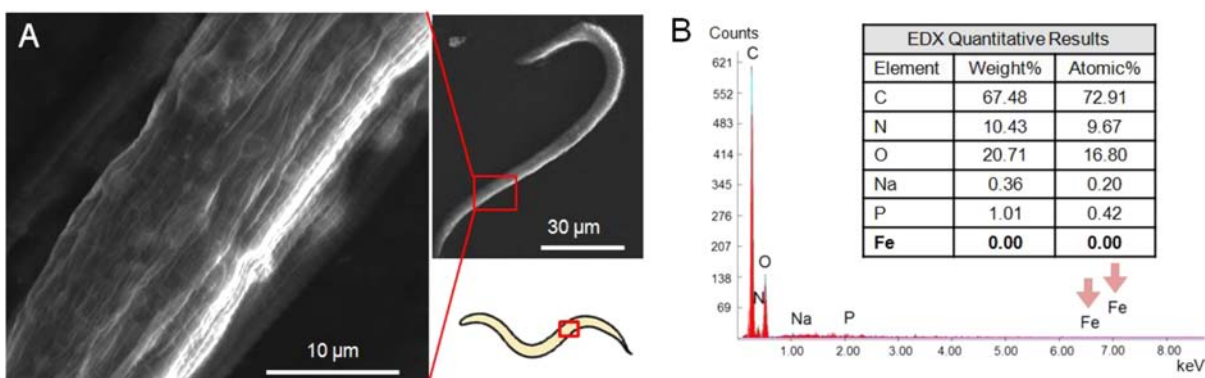


Figure 5. SEM-EDX analysis of treated *C. elegans*. (A) SEM image of treated *C. elegans* that does not show SPIONs adsorbed onto the cuticle. (B) Representative EDX measurement of the cuticle of treated *C. elegans*. The presence of iron is not detected in the cuticle of treated *C. elegans*.

than 70% at all BSA-SPIONs concentrations, whereas the lethality of the C-SPIONs increased rapidly at concentrations $>200 \mu\text{g/mL}$ ($p < 0.05$). The higher sensitivity of larvae to SPION treatment indicates that the toxic effects of SPIONs are stronger in the early stages of worms. Adult survival showed no differences with respect to the type of SPIONs, whereas statistical differences on larval survival were found at concentrations $>400 \mu\text{g/mL}$ ($p < 0.05$) depending on the treatment they received, either C-SPIONs or BSA-SPIONs. The survival of *C. elegans* after 24 h was fitted to a linear regression, revealing a linear dose–response relationship of the short-term mortality over the range of concentrations studied (Table S1). The value of the slopes shows that the mortality increases quicker in the case of worms treated with C-SPIONs than in the case of treatment with BSA-SPIONs, although the differences are only statistically significant for larvae ($p < 0.01$).

To investigate the influence of dissolved iron on the toxic effects of SPIONs, we studied the survival of *C. elegans* adult and larvae treated with Fe^{3+} at the same concentrations and time as that for SPION exposure (Figure S2A). Under these conditions, dose dependence between the Fe^{3+} concentration and *C. elegans* mortality was not observed, and a significant difference between the survival of treated and control worms was not noted. These results suggest that the toxicity exerted by SPIONs cannot be explained solely by the release of metal ions, but SPIONs, at high concentrations, must exert some toxicity

through a nanospecific mechanism due to the small size of the NPs, their high surface area-to-volume ratio, or their high reactivity. The tolerance of *C. elegans* to high concentrations of ferric ions may arise from the iron homeostasis of the worm, which maintains cellular iron content within a narrow range to avoid the adverse consequences of iron depletion or excess.³⁹

Additionally, we evaluated the number of progeny in adults at the same concentrations that we performed the survival assay as a sublethal end point. The brood size also indicated BSA-SPIONs and C-SPIONs mildly affected *C. elegans* (Figure S3). Statistical differences between treated and nontreated worms were found only at $500 \mu\text{g/mL}$, which caused the greater decrease in the number of progeny (brood size), 19% and 18% for the C-SPIONs and BSA-SPIONs, respectively. No statistical differences could be found between the effects of BSA-SPION and C-SPION treatment on the brood size.

Hereinafter, we used $500 \mu\text{g/mL}$ as the exposure concentration for 24 h because, at this concentration, we found statistical differences between treated and control worms, and it allowed us to visualize SPIONs inside the worms using an optical microscope. Exposure of worms for shorter time (i.e., 6 h) did not allow us to visualize the nanoparticles inside the *C. elegans*. As mentioned, the use of Milli-Q water as exposure media ensured that the colloidal stability of both C-SPIONs and BSA-SPIONs was preserved upon incubation with *C. elegans* for 24 h (Figure S4). Hence, our experimental design

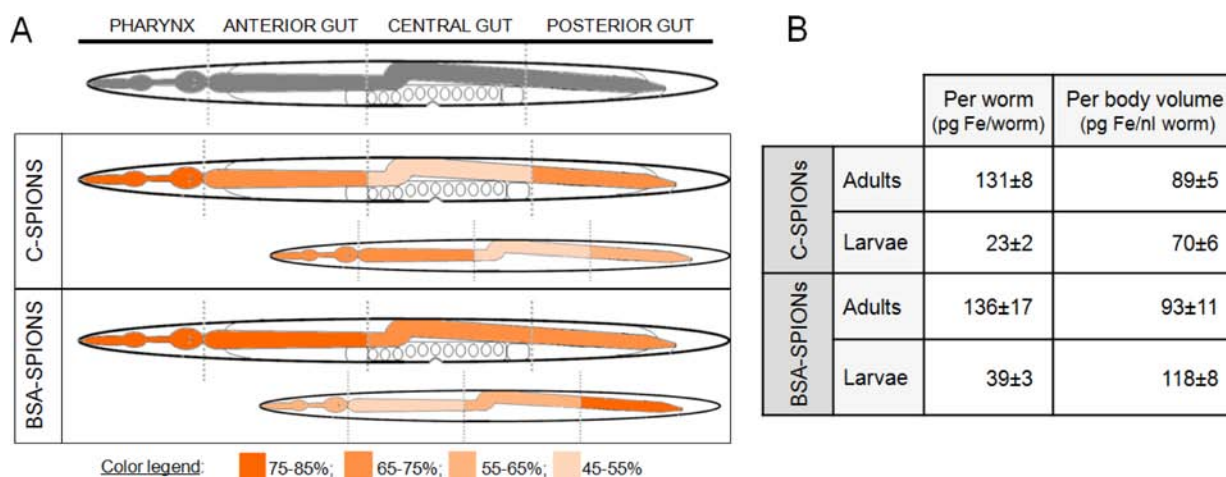


Figure 6. Biodistribution of C-SPIONs and BSA-SPIONs in adult and larval *C. elegans* after 24 h exposure to 500 $\mu\text{g}/\text{mL}$. (A) Scheme of the division of the alimentary system: pharynx, anterior gut, central gut, and posterior gut. Color map of the biodistribution of C-SPIONs and BSA-SPIONs in treated *C. elegans* adults and larvae. Color legend refers to the percentage of worms with NPs in the pharynx, anterior gut, central gut, and posterior gut (of 50 animals per sample). Bright orange indicates a percentage of 75–85% of *C. elegans* with SPIONs present in that region, and light orange indicates a percentage of 45–55% of *C. elegans* with SPIONs present in that region of the all animals analyzed. (B) Iron content of *C. elegans* treated with 500 $\mu\text{g}/\text{mL}$ during 24 h ($n = 3$). The values are given with their standard deviation and relative errors.

allowed us to perform controlled and well-characterized exposures, which are parameters of vital importance to evaluate the interaction with NPs.²¹

In all cases, SPIONs were located in the alimentary tract, which indicates that SPIONs entered the worms primarily through the intestinal tract by ingestion.⁴⁰ We studied SPION biodistribution in treated worms by using Perl's Prussian Blue to stain the iron present in *C. elegans* since it enhances its contrast and facilitates its visualization (Figure 4).⁴¹ Interestingly, the use of Prussian Blue revealed the presence of SPIONs in areas in which they were not visible by direct observation.

Translocation into the reproductive system was not observed within 24 h, even though it has been reported for several types of NPs, including gold, silica, and silver NPs.^{13,35,42} It is well-accepted that enterocytes, the intestinal epithelial cells, have a limited endocytic capacity in both *C. elegans* and mammals; therefore, it supports the finding of the absence of translocation through this epithelial barrier.⁴³ The lack of translocation allows us to have a confined and astringent environment in the *C. elegans*, where we can evaluate the modification of our SPIONs for 24 h in such biological conditions.^{32,37} Entrance of SPIONs into the vulva by passive diffusion was observed in less than 5% of the worms (Figure S5), whereas for silica NPs, it has been reported as a main entry pathway together with the pharynx.³⁴ Adsorption of SPIONs (either C- and BSA-SPIONs) in the cuticle of *C. elegans*²⁵ was discarded because we did not detect iron in the *C. elegans* cuticle by EDX (Figure 5).

More than 50 animals at both adult and larvae stages were stained with Prussian Blue and analyzed (Figure 6). We computed the predominance of SPIONs in the different regions (pharynx, anterior gut, central gut, posterior gut). Adults presented SPIONs in the pharynx region more frequently than larvae, independently of the SPION type. BSA-SPIONs were more homogeneously distributed from the pharynx to the posterior gut in adults than C-SPIONs, and they were predominantly retained in the posterior gut relative to C-SPIONs in larvae, thus suggesting a more facile transit of BSA-SPIONs through the intestine.

We propose that, because BSA-SPIONs retain monodispersity for longer time, muscle contractions of *C. elegans* move

BSA-SPIONs forward easily in the intestinal lumen relative to C-SPIONs (Figure 6A and Figure S6). Reported *in vitro* experiments using CaCO-2 cells, intestinal epithelial cells, concluded that pretreatment of NPs with BSA reduced the adherence of the NPs to the cells by enhancing the NP colloidal stability and alleviating adherence.⁴⁴ In this line, cell studies of FDA-approved Abraxane, an antitumoral active principle (paclitaxel) bound to human albumin, demonstrated that the presence of albumin facilitated the transport of paclitaxel through the endothelial cells, enhancing the accumulation of paclitaxel in the tumor.⁴⁵ Hence, BSA-coated NPs appear to interact less with biological environments than their noncoated counterparts, which could make BSA coating suitable for NPs as drug carriers because BSA-coated NPs could travel within an organism to reach specific tissues efficiently (quickly) and harmlessly (with low unspecific interactions).

The SPION uptake by *C. elegans* was quantified by using magnetometry. ZFC-FC plots showed that SPIONs kept their superparamagnetism after being internalized by the *C. elegans*. We measured the remanence magnetization of treated worms at 5 K ($\approx 1 \times 10^4$ adults and $\approx 4 \times 10^4$ larvae per sample) after exposure to 500 $\mu\text{g}/\text{mL}$ SPIONs for 24 h and compared these values to the remanence magnetization of SPIONs at the same temperature. The amount of iron uptake per worm showed dependence on the stage of the worms for both types of SPIONs ($p < 0.001$) (Figure 6B) and was ≈ 4 –6 times higher in adults than in larvae. Differences between the uptake of the two types of SPIONs in adults were not significant (131 pg/worm for C-SPIONs and 136 pg/worm for BSA-SPIONs). However, larvae showed uptake of BSA-SPIONs (39 pg/worm) significantly higher than that of C-SPIONs (23 pg/worm) ($p < 0.01$).

If we assume that the entrance of NPs into *C. elegans* occurs only through the alimentary system by ingestion, the lower NP uptake in larvae relative to adults may be attributed to differences in body and pharynx size. Larvae (L1–L4) are on average 2–3 times smaller than a newly molted adult with respect to both length and width and 4.4 times smaller in volume.⁴⁶ Considering this, we normalized NP uptake relative to body volume of adults and larvae. After normalization, BSA-

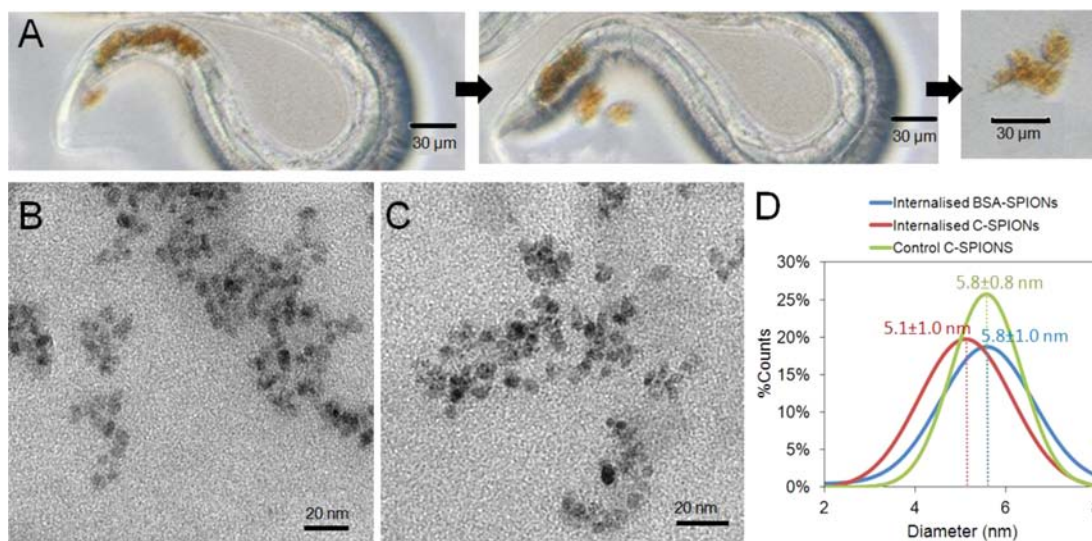


Figure 7. Characterization of internalized SPIONs. (A) Light microscopy images of excretion of SPIONs upon food resumption of treated *C. elegans*. (B) TEM image of internalized C-SPIONs. (C) TEM image of internalized BSA-SPIONs. (D) Gaussian distribution of TEM size for the internalized C-SPIONs, internalized BSA-SPIONs, and control C-SPIONs as-obtained.

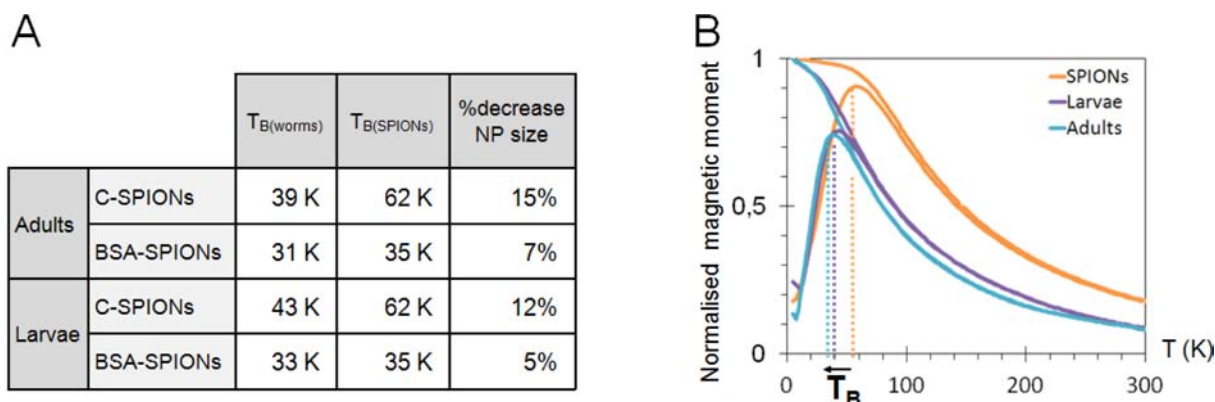


Figure 8. Characterization of internalized SPIONs from their blocking temperature. (A) Size decrease of internalized SPIONs can be calculated from the variation of the blocking temperatures of SPIONs upon interaction with *C. elegans*. (B) ZFC-FC graphs of control C-SPIONs and internalized C-SPIONs by adults and larvae.

SPION uptake remained slightly higher for adults than C-SPION uptake and significantly higher for larvae ($p < 0.01$) (Figure 6B and Table S2). The analysis of the two variables—developmental stage and SPION type—using a two-way ANOVA indicated that SPION type significantly influenced the NP uptake ($p < 0.001$), whereas the development stage did not, thus reinforcing the influence of the BSA coating on the NP uptake in *C. elegans*.

To investigate whether any modifications occurred with the NPs that had been internalized by *C. elegans* after 24 h, we analyzed the excreted NPs and the ZFC-FC plots in detail.

We transferred the magnetically treated worms onto nematode growth medium plates with food, and within 2 min of food resumption, the worms began to excrete NPs through the anus in the form of micrometric agglomerates. SPIONs were excreted over a 2 h period (Figure 7A and video S1).^{32,37,47} In contrast, treated worms that were transferred to NGM plates without food still had SPIONs in their intestinal lumen after 12 h (Figure S7), which confirms that excretion is dependent upon food availability. In effect, we are able to modulate uptake and excretion of NPs in *C. elegans* based on the presence or absence of a food source. Recovery of the

internalized NPs in the treated worms was difficult because the excreted material was spread over the bacterial lawn and mixed with bacteria, which hindered their subsequent characterization. Therefore, we adapted a standard bleaching procedure to dissolve the worm tissue and recover the internalized SPIONs (see Materials and Methods).⁴⁸ The procedure did not affect the initial size caused by aggregation of SPIONs (Figure S8), thus any change in NP status could be attributed to interactions with *C. elegans*. We measured the diameter of internalized NPs by TEM (Figure 7B–D) and analyzed more than 100 particles. The diameter was found to be smaller for C-SPIONs (10% reduction of the initial diameter; 0.6 nm), whereas for the BSA-SPIONs, the diameter remained unchanged.

ZFC-FC plots also showed that SPIONs decreased in diameter upon interaction with *C. elegans* of 14 and 6% for C-SPIONs and BSA-SPIONs, respectively, calculated from the variation of the blocking temperatures, which correspond to the maximum value of the ZFC curve (Figure 8A). The size reduction in adults was higher than that for larvae for both types of SPIONs. The sharp increase of the FC curve at low temperatures indicated the presence of a paramagnetic component in the system, which could likely arise from the

release of Fe³⁺ ions (Figure 8B). The slight decrease in the size of the SPIONs and the subsequent release of Fe³⁺ could occur during both ingestion and intestinal residence time.

In *C. elegans*, the buccal cavity and its associated structures act as a size-selective filtering mechanism that efficiently traps bacteria (that is their food) into the pharynx. The particles trapped in the pharynx pass through the grinder.⁴⁹ Although the grinder impairs physical damage to bacterial cells (0.5–1 μm), polystyrene beads of up to 3 μm diameter appeared unaffected by their passage through the grinder.^{40,49} Hence, we hypothesize that size reduction of the SPIONs occurs during the residence time inside the gut because of the mild acidic conditions and the presence of digestive enzymes in the intestinal microenvironment, which results in their partial digestion. The acidity of the intestinal lumen of *C. elegans* ranges from pH 6, in the anterior pharynx, to pH 3.6 in the posterior intestine, and many digestive enzymes are secreted in the anterior part of the gut, including amylases, lipases, lysozymes, proteases, esterases, and nucleases.^{26,50} The acidic conditions in the posterior intestine could partially dissolve the C-SPIONs and result in the release of Fe³⁺ ions.⁵¹ Our results are consistent with those reported for other metallic and metal oxide NPs in *C. elegans*.⁵² Silver NPs of different sizes (3, 13, and 76 nm) and coatings (citrate and PVP) were toxic to *C. elegans* as a result of different mechanisms, in which intraorganismal dissolved Ag was important.¹³ Similar bioavailability of ZnO NPs and ZnCl₂ also suggested that biotransformation (i.e., dissolution) occurred after ingestion of the NPs by the worm.³⁶ After exposure to Cu NPs, an increase in the Cu⁺ concentration was also detected, which suggests metabolism of the NPs.³¹

In the case of BSA-SPIONs, digestion of the protein layer is required before the iron oxide core is accessible to the environmental conditions and contacts the intestinal cells, which suggests that BSA acts as a protective coating that prevents the direct interaction between SPIONs and the biological environment and thus decreases the potential toxicity of the SPIONs.⁵³ In vitro experiments in simulated digestive fluid showed that, although proteinases could digest the BSA, it still delayed the contact between the core of the NP and the intestinal microenvironment, provided an additional barrier for diffusion, and decreased the accessibility or digestibility of NPs by digestive enzymes.⁵⁴ Similarly, our findings indicate that the BSA coating improved the stability of SPIONs in the gastrointestinal tract of *C. elegans* and protected BSA-SPIONs from digestion compared to C-SPIONs.

In conclusion, SPION exposure in liquid media allowed us to combine materials science, chemistry, and physical approaches to quantitatively assess the uptake and the modification of SPIONs in *C. elegans* after 24 h. The different coatings of the SPIONs, citrate and BSA, exhibited different short-term mortality and biodistribution in *C. elegans*. BSA-SPIONs were associated with lower mortality than C-SPIONs in a broader range of concentrations and more remarkably at high concentrations, hence suggesting that the BSA coating layer has a protective role not only for the material itself but also for the nematodes. The evaluation of the fate of SPIONs within *C. elegans* was achieved due to the transparency of the worm and the staining with Prussian Blue. SPIONs were localized only in the alimentary tract of the *C. elegans*, indicating ingestion as the main entry portal. BSA-SPIONs offered a more homogeneous distribution within the alimentary tract of *C. elegans* compared to the C-SPIONs, which could be

attributed to their enhanced stability in biological environments and their reduced interaction with the intestinal cells, as demonstrated in previous work.^{29,44} Therefore, if we aim to develop a nanotherapeutic agent that should pass through the intestinal tract with minor biological interactions, the BSA coating would rather facilitate this process.

Magnetometry allowed us to quantitatively compute the amount of SPIONs ingested by the worms, which was higher for BSA-SPIONs in the two development stages under study. This technique in combination with TEM let us evaluate the decrease in diameter for C-SPIONs during digestion in the intestinal microenvironment of *C. elegans*. This size decrease was not observed for the BSA-SPIONs, indicating the protective role of the BSA coating on the material itself.

The results of this work open interesting avenues to evaluate different coatings of synthesized NPs using *C. elegans* as an in vivo system in synthetic laboratories, by combining materials science and chemistry. Future work will focus on the study of the molecular pathways triggered by C-SPIONs and BSA-SPIONs to advance in the nanotoxicological mechanisms involved in NPs with different coatings at different developmental stages of *C. elegans*.

■ ASSOCIATED CONTENT

📄 Supporting Information

The Supporting Information is available free of charge on the ACS Publications website at DOI: 10.1021/acsbomaterials.5b00253.

Excretion of SPIONs by *C. elegans* (AVI)

Characterization of SPIONs before and after exposure to *C. elegans*, instrumentation used for the characterization, and additional images of the exposure of SPIONs with *C. elegans* (PDF)

■ AUTHOR INFORMATION

Corresponding Author

*E-mail: alaromaine@icmab.es.

Author Contributions

A.L., A.R., and L.G. conceived and designed the experiments; L.G., S.M.Y., and E.C. performed the experiments; A.L., A.R., and L.G. analyzed the data; S.M.Y. and E.C. contributed reagents/materials/analysis tools; and A.L., A.R., and L.G. wrote the paper.

Notes

The authors declare no competing financial interest.

■ ACKNOWLEDGMENTS

C. elegans N2 and *E. coli* OP50 were provided by the CGC, which is funded by NIH Office of Research Infrastructure Programs (P40 OD010440). The research leading to these results has received funding from the People Program (Marie Curie Actions) of the European Union's Seventh Framework Program (FP7/2007-2013) under REA Grant Agreement No. 303630 and cofunded by the European Social Fund. Authors acknowledge the funding from Spanish Ministry of Economy MAT 2012-35324 and FEDER funds, the Generalitat de Catalunya 2014SGR213, the COST Action MP1202, Ramon y Cajal Grant RYC-2010-06082 (A.L.), China Scholarship Council fellowship (S.M.Y., 201206150053), and FPU fellowship FPU12/05549 (L.G.M.).

■ ABBREVIATIONS

BSA, bovine serum albumin; BSA-SPIONs, BSA-coated SPIONs; CGC, Caenorhabditis Genetic Center; C-SPIONs, citrate-coated SPIONs; DLS, dynamic light scattering; EDX, energy-dispersive X-ray spectroscopy; M_R , remanence magnetization; NGM, nematode growth medium; MRI, magnetic resonance imaging; NPs, nanoparticles; PAA, poly(acrylic acid); PEI, polyethylenimine; PVP, polyvinylpyrrolidone; SEM, scanning electron microscopy; SPIONs, superparamagnetic iron oxide NPs; ZFC-FC, zero-field-cooled/field-cooled magnetization

■ REFERENCES

- (1) Monopoli, M. P.; Walczyk, D.; Campbell, A.; Elia, G.; Lynch, I.; Bombelli, F. B.; Dawson, K. A. Physical-chemical aspects of protein corona: relevance to in vitro and in vivo biological impacts of nanoparticles. *J. Am. Chem. Soc.* **2011**, *133* (8), 2525–34.
- (2) Walczyk, D.; Bombelli, F. B.; Monopoli, M. P.; Lynch, I.; Dawson, K. A. What the Cell "Sees" in Bionanoscience. *J. Am. Chem. Soc.* **2010**, *132* (16), 5761–5768.
- (3) Singh, R.; Nalwa, H. S. Medical Applications of Nanoparticles in Biological Imaging, Cell Labeling, Antimicrobial Agents, and Anticancer Nanodrugs. *J. Biomed. Nanotechnol.* **2011**, *7* (4), 489–503.
- (4) Jain, T. K.; Reddy, M. K.; Morales, M. A.; Leslie-Pelecky, D. L.; Labhasetwar, V. Biodistribution, clearance, and biocompatibility of iron oxide magnetic nanoparticles in rats. *Mol. Pharmaceutics* **2008**, *5* (2), 316–327.
- (5) Reddy, L. H.; Arias, J. L.; Nicolas, J.; Couvreur, P. Magnetic Nanoparticles: Design and Characterization, Toxicity and Biocompatibility, Pharmaceutical and Biomedical Applications. *Chem. Rev.* **2012**, *112* (11), 5818–5878.
- (6) Krug, H. F.; Wick, P. Nanotoxicology: An Interdisciplinary Challenge. *Angew. Chem., Int. Ed.* **2011**, *50* (6), 1260–1278.
- (7) Etheridge, M. L.; Campbell, S. A.; Erdman, A. G.; Haynes, C. L.; Wolf, S. M.; McCullough, J. The big picture on nanomedicine: the state of investigational and approved nanomedicine products. *Nanomedicine* **2013**, *9* (1), 1–14.
- (8) Hassan, S.; Singh, A. V. Biophysicochemical perspective of nanoparticle compatibility: a critically ignored parameter in nanomedicine. *J. Nanosci. Nanotechnol.* **2014**, *14* (1), 402–14.
- (9) Saptarshi, S. R.; Duschl, A.; Lopata, A. L. Interaction of nanoparticles with proteins: relation to bio-reactivity of the nanoparticle. *J. Nanobiotechnol.* **2013**, *11*, 26.
- (10) Albanese, A.; Tang, P. S.; Chan, W. C. The effect of nanoparticle size, shape, and surface chemistry on biological systems. *Annu. Rev. Biomed. Eng.* **2012**, *14*, 1–16.
- (11) Wu, Q. L.; Li, Y. P.; Tang, M.; Wang, D. Y. Evaluation of Environmental Safety Concentrations of DMSA Coated Fe₂O₃-NPs Using Different Assay Systems in Nematode *Caenorhabditis elegans*. *PLoS One* **2012**, *7* (8), e43729.
- (12) Calatayud, M. P.; Sanz, B.; Raffa, V.; Riggio, C.; Ibarra, M. R.; Goya, G. F. The effect of surface charge of functionalized Fe₃O₄ nanoparticles on protein adsorption and cell uptake. *Biomaterials* **2014**, *35* (24), 6389–99.
- (13) Meyer, J. N.; Lord, C. A.; Yang, X. Y.; Turner, E. A.; Badireddy, A. R.; Marinakos, S. M.; Chilkoti, A.; Wiesner, M. R.; Auffan, M. Intracellular uptake and associated toxicity of silver nanoparticles in *Caenorhabditis elegans*. *Aquat. Toxicol.* **2010**, *100* (2), 140–50.
- (14) Levard, C.; Hotze, E. M.; Colman, B. P.; Dale, A. L.; Truong, L.; Yang, X. Y.; Bone, A. J.; Brown, G. E., Jr.; Tanguay, R. L.; Di Giulio, R. T.; Bernhardt, E. S.; Meyer, J. N.; Wiesner, M. R.; Lowry, G. V. Sulfidation of silver nanoparticles: natural antidote to their toxicity. *Environ. Sci. Technol.* **2013**, *47* (23), 13440–8.
- (15) Christen, T.; Ni, W.; Qiu, D.; Schmiedeskamp, H.; Bammer, R.; Moseley, M.; Zaharchuk, G. High-resolution cerebral blood volume imaging in humans using the blood pool contrast agent ferumoxytol. *Magn. Reson. Med.* **2013**, *70*, 705.
- (16) Laurent, S.; Dutz, S.; Haefeli, U. O.; Mahmoudi, M. Magnetic fluid hyperthermia: Focus on superparamagnetic iron oxide nanoparticles. *Adv. Colloid Interface Sci.* **2011**, *166* (1–2), 8–23.
- (17) Shubayev, V. I.; Pisanic, T. R., II; Jin, S. Magnetic nanoparticles for theragnostics. *Adv. Drug Delivery Rev.* **2009**, *61* (6), 467–477.
- (18) Veisoh, O.; Gunn, J. W.; Zhang, M. Design and fabrication of magnetic nanoparticles for targeted drug delivery and imaging. *Adv. Drug Delivery Rev.* **2010**, *62* (3), 284–304.
- (19) Hao, R.; Xing, R.; Xu, Z.; Hou, Y.; Gao, S.; Sun, S. Synthesis, Functionalization, and Biomedical Applications of Multifunctional Magnetic Nanoparticles. *Adv. Mater.* **2010**, *22* (25), 2729–2742.
- (20) Mahmoudi, M.; Sant, S.; Wang, B.; Laurent, S.; Sen, T. Superparamagnetic iron oxide nanoparticles (SPIONs): Development, surface modification and applications in chemotherapy. *Adv. Drug Delivery Rev.* **2011**, *63* (1–2), 24–46.
- (21) Gonzalez-Moragas, L.; Roig, A.; Laromaine, A. C. *elegans* as a tool for in vivo nanoparticle assessment. *Adv. Colloid Interface Sci.* **2015**, *219*, 10.
- (22) Wood, W. B. *The Nematode Caenorhabditis Elegans*; Cold Spring Harbor Laboratory, 1988.
- (23) Kim, S. W.; Nam, S.-H.; An, Y.-J. Interaction of Silver Nanoparticles with Biological Surfaces of *Caenorhabditis elegans*. *Ecotoxicol. Environ. Saf.* **2012**, *77*, 64–70.
- (24) Wu, Q.; Li, Y.; Li, Y.; Zhao, Y.; Ge, L.; Wang, H.; Wang, D. Crucial role of the biological barrier at the primary targeted organs in controlling the translocation and toxicity of multi-walled carbon nanotubes in the nematode *Caenorhabditis elegans*. *Nanoscale* **2013**, *5* (22), 11166–78.
- (25) Kaletta, T.; Hengartner, M. O. Finding function in novel targets: *C. elegans* as a model organism. *Nat. Rev. Drug Discovery* **2006**, *5* (5), 387–98.
- (26) Wu, Q.; Yin, L.; Li, X.; Tang, M.; Zhang, T.; Wang, D. Contributions of altered permeability of intestinal barrier and defecation behavior to toxicity formation from graphene oxide in nematode *Caenorhabditis elegans*. *Nanoscale* **2013**, *5* (20), 9934–43.
- (27) Corsi, A. K. A Biochemist's Guide to *C. elegans*. *Anal. Biochem.* **2006**, *359* (1), 1–17.
- (28) Hall, D. H.; Altun, Z. F. *C. elegans Atlas*; Cold Spring Harbor Laboratory Press, 2008.
- (29) Yu, S. M.; Laromaine, A.; Roig, A. Enhanced stability of superparamagnetic iron oxide nanoparticles in biological media using a pH adjusted-BSA adsorption protocol. *J. Nanopart. Res.* **2014**, *16* (7), 2484–2499.
- (30) Rucker, C.; Potzl, M.; Zhang, F.; Parak, W. J.; Nienhaus, G. U. A quantitative fluorescence study of protein monolayer formation on colloidal nanoparticles. *Nat. Nanotechnol.* **2009**, *4* (9), 577–580.
- (31) Gao, Y.; Liu, N.; Chen, C.; Luo, Y.; Li, Y.; Zhang, Z.; Zhao, Y.; Zhao, B.; Iida, A.; Chai, Z. Mapping technique for biodistribution of elements in a model organism, *Caenorhabditis elegans*, after exposure to copper nanoparticles with microbeam synchrotron radiation X-ray fluorescence. *J. Anal. At. Spectrom.* **2008**, *23* (8), 1121–1124.
- (32) Mohan, N.; Chen, C. S.; Hsieh, H. H.; Wu, Y. C.; Chang, H. C. In vivo imaging and toxicity assessments of fluorescent nanodiamonds in *Caenorhabditis elegans*. *Nano Lett.* **2010**, *10* (9), 3692–9.
- (33) Qu, Y.; Li, W.; Zhou, Y.; Liu, X.; Zhang, L.; Wang, L.; Li, Y. F.; Iida, A.; Tang, Z.; Zhao, Y.; Chai, Z.; Chen, C. Full assessment of fate and physiological behavior of quantum dots utilizing *Caenorhabditis elegans* as a model organism. *Nano Lett.* **2011**, *11* (8), 3174–83.
- (34) Scharf, A.; Piechulek, A.; von Mikecz, A. Effect of Nanoparticles on the Biochemical and Behavioral Aging Phenotype of the Nematode *Caenorhabditis elegans*. *ACS Nano* **2013**, *7* (12), 10695–10703.
- (35) Pluskota, A.; Horzowski, E.; Bossinger, O.; von Mikecz, A. In *Caenorhabditis elegans* Nanoparticle-Bio-Interactions Become Transparent: Silica-Nanoparticles Induce Reproductive Senescence. *PLoS One* **2009**, *4* (8), e6622.
- (36) Ma, H.; Bertsch, P. M.; Glenn, T. C.; Kabengi, N. J.; Williams, P. L. Toxicity of manufactured zinc oxide nanoparticles in the nematode *Caenorhabditis elegans*. *Environ. Toxicol. Chem.* **2009**, *28* (6), 1324–1330.

- (37) Lim, S. F.; Riehn, R.; Ryu, W. S.; Khanarian, N.; Tung, C. K.; Tank, D.; Austin, R. H. In vivo and scanning electron microscopy imaging of upconverting nanophosphors in *Caenorhabditis elegans*. *Nano Lett.* **2006**, *6* (2), 169–174.
- (38) Brenner, S. The genetics of *Caenorhabditis elegans*. *Genetics* **1974**, *77* (1), 71–94.
- (39) Anderson, C. P.; Leibold, E. A. Mechanisms of iron metabolism in *Caenorhabditis elegans*. *Front. Pharmacol.* **2014**, *5*, 113.
- (40) Fang-Yen, C.; Avery, L.; Samuel, A. D. Two size-selective mechanisms specifically trap bacteria-sized food particles in *Caenorhabditis elegans*. *Proc. Natl. Acad. Sci. U. S. A.* **2009**, *106* (47), 20093–6.
- (41) Carenza, E.; Barcelo, V.; Morancho, A.; Levander, L.; Boada, C.; Laromaine, A.; Roig, A.; Montaner, J.; Rosell, A. In vitro angiogenic performance and in vivo brain targeting of magnetized endothelial progenitor cells for neurorepair therapies. *Nanomedicine* **2014**, *10* (1), 225–34.
- (42) Kim, S. W.; Kwak, J. I.; An, Y.-J. Multigenerational Study of Gold Nanoparticles in *Caenorhabditis elegans*: Transgenerational Effect of Maternal Exposure. *Environ. Sci. Technol.* **2013**, *47* (10), 5393–5399.
- (43) Audus, K. L.; Raub, T. J. *Biological Barriers to Protein Delivery*; Springer, 1993; DOI: [10.1007/978-1-4615-2898-2](https://doi.org/10.1007/978-1-4615-2898-2).
- (44) Sinnecker, H.; Ramaker, K.; Frey, A. Coating with luminal gut-constituents alters adherence of nanoparticles to intestinal epithelial cells. *Beilstein J. Nanotechnol.* **2014**, *5*, 2308–2315.
- (45) Dosio, F.; Brusa, P.; Crosasso, P.; Arpicco, S.; Cattel, L. Preparation, characterization and properties in vitro and in vivo of a paclitaxel-albumin conjugate. *J. Controlled Release* **1997**, *47* (3), 293–304.
- (46) Knight, C. G.; Patel, M. N.; Azevedo, R. B.; Leroi, A. M. A novel mode of ecdysozoan growth in *Caenorhabditis elegans*. *Evol. Dev.* **2002**, *4* (1), 16–27.
- (47) Laaberki, M. H.; Dworkin, J. Role of spore coat proteins in the resistance of *Bacillus subtilis* spores to *Caenorhabditis elegans* predation. *Journal of bacteriology* **2008**, *190* (18), 6197–203.
- (48) Stiernagle, T. Maintenance of *C. elegans*. In *WormBook*, 2006; DOI: [10.1895/wormbook.1.101.1](https://doi.org/10.1895/wormbook.1.101.1).
- (49) Avery, L.; You, Y.-J. *C. elegans* Feeding. In *WormBook*, 2012, DOI: [10.1895/wormbook.1.150.1](https://doi.org/10.1895/wormbook.1.150.1).
- (50) Chauhan, V. M.; Orsi, G.; Brown, A.; Pritchard, D. I.; Aylott, J. W. Mapping the Pharyngeal and Intestinal pH of *Caenorhabditis elegans* and Real-Time Luminal pH Oscillations Using Extended Dynamic Range pH-Sensitive Nanosensors. *ACS Nano* **2013**, *7* (6), 5577–5587.
- (51) Huang, G.; Chen, H.; Dong, Y.; Luo, X.; Yu, H.; Moore, Z.; Bey, E. A.; Boothman, D. A.; Gao, J. Superparamagnetic iron oxide nanoparticles: amplifying ROS stress to improve anticancer drug efficacy. *Theranostics* **2013**, *3* (2), 116–26.
- (52) Zhao, Y.; Wu, Q.; Li, Y.; Wang, D. Translocation, transfer, and in vivo safety evaluation of engineered nanomaterials in the non-mammalian alternative toxicity assay model of nematode *Caenorhabditis elegans*. *RSC Adv.* **2013**, *3* (17), 5741–5757.
- (53) Malvindi, M. A.; De Matteis, V.; Galeone, A.; Brunetti, V.; Anyfantis, G. C.; Athanassiou, A.; Cingolani, R.; Pompa, P. P. Toxicity assessment of silica coated iron oxide nanoparticles and biocompatibility improvement by surface engineering. *PLoS One* **2014**, *9* (1), e85835.
- (54) Li, Z.; Ha, J.; Zou, T.; Gu, L. Fabrication of coated bovine serum albumin (BSA)-epigallocatechin gallate (EGCG) nanoparticles and their transport across monolayers of human intestinal epithelial Caco-2 cells. *Food Funct.* **2014**, *5* (6), 1278–1285.



Full length article

Bio-identity and fate of albumin-coated SPIONs evaluated in cells and by the *C. elegans* model



Si-Ming Yu^{a,1,2}, Laura Gonzalez-Moragas^{a,1}, Maria Milla^a, Androniki Kolovou^b, Rachel Santarella-Mellwig^b, Yannick Schwab^b, Anna Laromaine^{a,*}, Anna Roig^{a,*}

^a Institut de Ciència de Materials de Barcelona (ICMAB-CSIC), Campus de la UAB, Bellaterra, Catalonia E-08193, Spain

^b European Molecular Biology Laboratory (EMBL), Electron Microscopy Core Facility, 69117 Heidelberg, Germany

ARTICLE INFO

Article history:

Received 25 April 2016

Received in revised form 3 July 2016

Accepted 13 July 2016

Available online 15 July 2016

Keywords:

Iron oxide nanoparticles

Protein corona

Cytotoxicity

C. elegans

Biodistribution

ABSTRACT

Nanoparticles which surface adsorb proteins in an uncontrolled and non-reproducible manner will have limited uses as nanomedicinal products. A promising approach to avoid nanoparticle non-specific interactions with proteins is to design bio-hybrids by purposely pre-forming a protein corona around the inorganic cores. Here, we investigate, *in vitro* and *in vivo*, the newly acquired bio-identity of superparamagnetic iron oxide nanoparticles (SPIONs) upon their functionalization with a pre-formed and well-defined bovine serum albumin (BSA) corona. Cellular uptake, intracellular particle distribution and cytotoxicity were studied in two cell lines: adherent and non-adherent cells. BSA decreases nanoparticle internalization in both cell lines and protects the iron core once they have been internalized. The physiological response to the nanoparticles is then *in vivo* evaluated by oral administration to *Caenorhabditis elegans*, which was selected as a model of a functional intestinal barrier. Nanoparticle biodistribution, at single particle resolution, is studied by transmission electron microscopy. The analysis reveals that the acidic intestinal environment partially digests uncoated SPIONs but does not affect BSA-coated ones. It also discloses that some particles could enter the nematode's enterocytes, likely by endocytosis which is a different pathway than the one described for the worm nutrients.

Statement of Significance

Unravelling meaningful relationships between the physiological impact of engineered nanoparticles and their synthetic and biological identity is of vital importance when considering nanoparticles biomedical uses and when establishing their nanotoxicological profile. This study contributes to better comprehend the inorganic nanoparticles' behavior in real biological milieus. We synthesized a controlled pre-formed BSA protein corona on SPIONs to lower unspecific cell uptake and decrease nanoparticle fouling with other proteins. Such findings may be of relevance considering clinical translation and regulatory issues of inorganic nanoparticles. Moreover, we have advanced in the validation of *C. elegans* as a simple animal model for assessing biological responses of engineering nanomaterials. The physiological response of BSA coated SPIONs was evaluated *in vivo* after their oral administration to *C. elegans*. Analyzing ultra-thin cross-sections of the worms by TEM with single-particle precision, we could track NP biodistribution along the digestive tract and determine unambiguously their translocation through biological barriers and cell membranes.

© 2016 Acta Materialia Inc. Published by Elsevier Ltd. All rights reserved.

1. Introduction

The biological identity of a synthetic nanoparticle (NP) is modified by the proteins and other biomolecules (i.e., DNA, lipids and sugars) adsorbed on its surface when placed in biological milieus. NP synthetic identity includes the size, shape, and surface chemistry, while biological identity includes the structure and composition of the protein corona, along with the size and aggregation

* Corresponding authors.

E-mail addresses: alaromaine@icmab.es (A. Laromaine), roig@icmab.es (A. Roig).

¹ Equal contribution.

² Current address: Key Laboratory of Biomaterials of Guangdong Higher Education Institutes, Department of Biomedical Engineering, Jinan University, Guangzhou 510632, China.

state of the nanoparticles in a physiological environment. Biological response includes the triggering of signaling pathways, NP fate, and NP toxicity. Protein adsorption onto NPs in biological media is a determining factor that influences both their uptake and cytotoxicity [1–6]. An increasing number of publications have studied the impact on cytotoxicity and cellular uptake of aggregates of NPs in protein-rich media [7–10]. In addition, when those aggregates flocculate, the consequence is a heterogeneous distribution of the NPs in cell media that adds more variability in the uptake at the single-cell level and hinders the understanding of the population-wide biological response [11]. Nevertheless, particle aggregation in cell media can also be advantageous [12]. Aggregates of iron oxide NPs increase cell uptake and enhance cell contrast in magnetic resonance imaging (MRI) without compromising on cell viability [13]. Protein–nanoparticle aggregates were proposed as biocompatible drug carriers [14] and their use was suggested to increase the cell viability of some nanomaterials [15,16]. However, adsorption of proteins by NPs in an uncontrolled and non-reproducible manner will have limited applications in nanomedicine. A recurring and successful approach to avoid the out-of-control formation of a protein corona is grafting a protein-resistant polymer on the surface, such as polyethylene glycol (PEG), which increases their stealth character and blood circulation time [17–20]. Although this strategy is effective at lowering the nonspecific interactions of nanomaterials with proteins and cells, it suffers several drawbacks: PEG can be oxidized in a physiological environment, either spontaneously or by enzyme action [21] and even high PEG densities can't prevent protein adsorption and macrophage uptake [22,23]. Moreover, PEGylated nanomaterials can induce the production of antibodies against them [6]. Some studies have monitored, with radiolabels, the fate of the grafted polymer after cell uptake both *in vitro* and *in vivo* [24,25]. For a particular case, authors reported the loss of polymer integrity [24], making difficult the correlation of the potential toxic effects of the polymer fragments or the NPs themselves. Other studies also suggest preclinical evidence that PEGylation can lead to storage diseases interfering with kidney, spleen or liver function in the long term and high dosed therapies [26,27].

A different approach to safeguard the stability of engineered nanoparticles in biofluids is to pre-form a protein corona around the inorganic core in a controlled and reproducible mode, commonly labeled as hard-corona in contraposition of weaker bound biomolecules, soft-corona [28]. Such systems demonstrate enormous potential, not only because they show longer blood circulation and superior stealth than when bare nanoparticles are used but also because the protein can be exploited as a theranostic vehicle, where a drug [29–31], an imaging probe [32], or a non-masked targeting agent can be anchored. We have followed this latter approach by performing a well-defined bovine serum albumin (BSA) hard corona on the surface of superparamagnetic iron oxide nanoparticles (SPIONs) and, subsequently exposing the BSA-SPIONs to other biomolecules, cells, and living organisms to investigate their newly acquired bio-identity. Albumin is a non-immunogenic and nontoxic endogenous protein, while engineered SPIONs are extensively used in preclinical studies as contrast agents in magnetic resonance imaging (MRI), magnetic hyperthermia, and as drug-delivery vehicles [33,34]. In addition, the use of SPIONs for cell labeling to guide and image their engraftment in target tissues has also been reported [35]. Besides applications in nanomedicine, SPIONs offer other advantages that help to address standing questions related to their biological identity, since precise quantification of NP uptake in cells and small organisms can be done using magnetometry techniques, while Prussian blue staining can easily be used to confirm the homogeneity of their uptake. Quantification of NP uptake is not straightforward for other inorganic nanomaterials.

In a previous work, we showed that SPIONs synthesized in a microwave oven can be readily stabilized in water without tedious ligand exchanges mandatory in colloidal organic routes [36], while a second step allowed us to compactly coat the NPs with a monolayer of BSA [37]. In addition, *C. elegans* were used to monitor the SPIONs *in vivo* [38]. This animal model encompasses simplicity, transparency, short lifecycle, sequenced genome, small body size (1 mm long), and ease of cultivation, which makes it a very convenient host in the materials science laboratory for initial NP biological evaluation [39]. It has been long used as an animal model in development, neurobiology and functional genomics, and is currently emerging as a promising alternative model organism in toxicology [40,41]. In this work, we take advantage of its anatomical complexity and in particular, of the functional and structural similarities between the *C. elegans* alimentary system and the human [42,43] to evaluate the nano/bio interaction of orally administered NPs and study the NP *in vivo* behavior with or without protein pre-coating. This simple animal allows materials scientists to perform information-rich experiments before using superior models that require higher infrastructure and dedicated laboratories.

Here, we thoroughly investigate the synthetic and the biological identity, and the physiological responses of albumin precoated iron oxide nanoparticles, BSA-SPIONs, using *in vitro* and *in vivo* assays and comparing the results with SPIONs stabilized with citrate, protein uncoated particles, C-SPIONs. For the *in vitro* studies we use electron microscopy and magnetometry to image and quantify the effect of the pre-formed protein corona on the nanoparticles, their subcellular localization, and uptake in two different cell lines. We also study the digestion kinetics of the NPs in a solution that mimics the lysosomal environment. The physiological response of BSA-SPIONs is evaluated by their oral administration to *C. elegans*; a model for the mammalian intestinal barrier. By analyzing thin cross-sections of the worms by transmission electron microscopy (TEM) we visualize the NPs and track their biodistribution with subcellular precision. We focus on two different regions of the body of the *C. elegans*: an anterior region of the intestine (pH = 6) and a region of the posterior intestinal segment (pH = 3.6). Most particles are visualized inside the intestinal lumen although we identify nanoparticles that crossed the lumen and they were endocytosed by the enterocytes. BSA-SPIONs were taken-up by the digestive cells in a similar magnitude regarding endosome size and number as the C-SPIONs.

2. Experimental section, materials and methods

2.1. SPIONs: synthesis and characterization

2.1.1. Chemicals

Iron (III) acetylacetonate ($\geq 97.0\%$) and trisodium citrate dihydrate (Na_3Cit) were purchased from Sigma–Aldrich. Benzyl alcohol was obtained from Scharlau. Acetone was bought from Panreac. Fetal bovine serum (FBS), cell-culture medium developed in the Roswell Park Memorial Institute (RPMI) with Glutamax, phosphate-buffered saline (PBS), Alamar Blue, and MTT were obtained from Invitrogen. All materials were used as received if not stated otherwise.

2.1.2. Synthesis of C-SPIONs and BSA-SPIONs

C-SPIONs were synthesized using microwave-assisted thermal decomposition [36,37] BSA-SPIONs were fabricated by performing a BSA adsorption protocol [37]. The pH of the C-SPIONs dispersion was adjusted to 11 with 0.01 M NaOH, then 100 μL BSA (18 mg/mL) solution were added dropwise under mild vortex. BSA and C-SPIONs were incubated for 1 h at room temperature. Finally,

the pH of the solution was adjusted to 7.4 by adding 0.05 mM HNO₃. The final concentration of BSA-SPIONs dispersion was maintained at 1 mg/mL (in terms of Fe₂O₃). Note that BSA and HSA (human serum albumin) are 76.36% identical (based on the alignment of their sequences using UNIPROT tool). No significant differences between the two proteins should be expected on the nano/bio assays presented here. In addition, *C. elegans* does not have albumin and lack albumin-receptors; hence no species-dependent reaction could occur.

2.1.3. Dynamic light scattering (DLS) and zeta-potential analysis

DLS measurements were performed in a Zetasizer Nano ZS (Malvern) equipped with a He/Ne 633 nm laser at 25 °C. For each sample, three independent measurements were performed with 15 scans for each measurement.

2.1.4. Superconductive quantum interference device (SQUID) analysis

Magnetometry was performed with a Quantum Design system (MPMS5XL) to determine the magnetization of SPIONs. 150 µL SPIONs at known concentration were dried in a polycarbonate capsule in a 60 °C oven overnight. Magnetization curves at 5K were recorded as a function of applied magnetic field up to 6 T.

2.1.5. Negative staining TEM

BSA-SPIONs were visualized by performing negative-staining TEM. One drop of the purified BSA-SPIONs was placed on a carbon-coated grid and blotted with filter paper. Subsequently, 5 µL of 2% uranyl acetate was placed on the grid for 1 min before draining off. The grid was then placed in a 2011 JEOL electron microscope at the working voltage 100 kV.

2.1.6. Flame absorption spectroscopy

To determine the iron concentration of C-SPIONs, samples were sonicated for 10 min in an ultrasound bath. An aliquot of the sample was diluted with HCl (1%) and the iron content of the resulting solution was determined by flame absorption spectroscopy (air–acetylene) with a Perkin-Elmer 2100 spectrometer in a triplicate assay.

2.2. SPIONs: degradation study

2.2.1. Color intensity determination

20 mM citrate buffer (CB; pH 4.6) was prepared by mixing equal volumes of 10 mM citric acid and 10 mM sodium citrate monobasic solution. CB with 10% FBS (CB-FBS) was also prepared by adding the appropriate amount of FBS. C-SPIONs and BSA-SPIONs were dispersed in CB or CB-FBS to a final SPION concentration of 0.5 mg/mL. During the whole degradation process, digital images of the dispersions were taken every day, at the same time and with identical conditions, using a digital camera. To quantify the color intensity of each image, ImageJ software was used. Images in grayscale were analyzed and the mean color intensity of each image was determined by averaging the intensity of at least three different regions. For an accurate determination of the changes during the degradation process, the “gray” intensity of Fe³⁺ ions from a FeCl₃ solution in the same buffer was used as the reference for a fully digested system. The gray intensity of C-SPIONs or BSA-SPIONs dispersion at day 0 was labeled as I₀, those measured at different days during the degradation process were I_d, and that of FeCl₃ was labeled as I_{FeCl₃}. Intensity of gray in each image, and thus percentage of digestion, was calculated as:

$$\text{Gray intensity}(\%) = \frac{I_0 - I_d}{I_0 - I_{\text{FeCl}_3}} \times 100\%$$

2.2.2. Size-evolution determination using transmission electron microscopy

During the degradation process, 100 µL sample solutions were added to the copper grid for TEM measurements. SPIONs were imaged in a JEOL TEM-1210 electron microscope at an operating voltage of 120 kV. Size-distribution histograms were computed from 200 to 300 SPIONs and fitted to a Gaussian curve to obtain the mean nanoparticle size. Selected-area electron diffraction (SAED) was used to identify the crystallinity of SPIONs.

2.3. In vitro cell experiments

2.3.1. Cell viability

MDA-MB231 cells were cultured at a concentration of approximately 1 × 10⁶ cells/mL in a 96-well plate (0.2 mL per well), in complete medium (RPMI supplemented with 10% FBS and 6 mM GlutaMax) and allowed to grow for 24 h. HL60 cells were cultured in complete medium (RPMI medium supplemented with 10% FBS, 6 mM GlutaMax and 0.5 mM sodium pyruvate) at a concentration of 2 × 10⁶ cells/mL in a 96-well plate (0.1 mL per well). Both cell lines were obtained from American Type Culture Collection (ATCC, Manassas, VA), and grown at 37 °C in 5% CO₂ until reaching 70% confluence.

For MDA-MB231 cell lines, after 24 h growth with a confluence of 70%, the medium was replaced with fresh complete medium containing C-SPIONs or BSA-SPIONs, at a final SPION concentration of 40 µg/mL, 75 µg/mL, 100 µg/mL, and 150 µg/mL. Cells and SPIONs were co-incubated for another 24 h.

For HL60 cell lines, after 24 h growing with a confluence of 70%, another 0.1 mL fresh complete medium containing C-SPIONs or BSA-SPIONs, at concentrations double of those for MDA MB 231 cell line, was added to each well to reach a final volume of 200 µL. The final SPION concentration in each well was also maintained at 40 µg/mL, 75 µg/mL, 100 µg/mL, and 150 µg/mL. Cells were then allowed to co-incubate with SPIONs for another 24 h.

Cell viability after SPION exposure was evaluated using MTT (Biomedica) assays. The appropriate amount of reactive MTT (10% of the sample volume in each well, 20 µL) was added to each well, plates were incubated at 37 °C for 2–5 h and read in a microplate reader (Victor3, Perkin Elmer) at 450 nm, and at 620 nm as reference. Viability test was performed in a total of 20 samples for those cultures incubated with C-SPIONs for MDA MB 231 and HL60 cells, and in 14 and 10 samples incubated with BSA-SPIONs for MDA MB 231 and HL60 cells respectively. Experiments were compared with the control using one-way ANOVA and Tukey's test post hoc analysis, (*) p < 0.05; (***) p < 0.005.

2.3.2. Cellular uptake

Briefly, after 24 h incubation of cells with C-SPIONs and BSA-SPIONs, cell cultures were thoroughly washed three times with PBS, and counted. Cells were centrifuged and pellets obtained were dried overnight in polycarbonate capsules at 60 °C and 25–35 mmHg vacuum. Magnetization curve of samples was recorded on a superconductive quantum interference device (SQUID) measurement magnetometer (Quantum Design MPMS5XL). Magnetization curve of SPIONs at 5K was recorded as a function of applied magnetic field under 6 T. At temperatures lower than the blocking temperature, superparamagnetic particles are blocked in a ferromagnetic state and display remnant magnetization at zero applied magnetic field. The uptake of the SPIONs can be evaluated by measuring the remnant magnetization value of treated cells (M_{r cells}) after they were magnetized up to 6 T. M_{r cells} was obtained by dividing the measured M_r value of the cell sample by the number of counted cells. To know the amount of iron oxide per cell (g Fe₂O₃/cell), the remnant magnetization value of the SPIONs

($M_{r \text{ SPIONs}}$) ($\text{emu/g Fe}_2\text{O}_3$) was divided by the $M_{r \text{ cells}}$; the calculation is given below.

$$\text{Fe}_2\text{O}_3 \text{ uptake (pg/cell)} = \frac{M_{r \text{ cells}}(\text{emu/cell})}{M_{r \text{ SPIONs}}(\text{emu/g}_{\text{Fe}_2\text{O}_3})}$$

2.3.3. Intracellular localization

MDA MB 231 cells were seeded in a 96-well petri dish, grown, and treated with 75 and 150 $\mu\text{g}\cdot\text{ml}^{-1}$ BSA-SPIONs. After 24 h of incubation, cells were trypsinized, washed twice with PBS, and collected by centrifugation (1400 rpm, 5 min). Supernatants were discarded and 2 mL of 2% glutaraldehyde (served as fixation solution) in cacodylate buffer was added to the pellet. Cells were incubated in the fixation solution at 4 °C and further stained using 1% OsO₄. They were then dehydrated in an alcohol series and embedded in Epon resin. Ultrathin sections (70 μm) were transferred onto copper grids and analyzed by TEM, using a Jeol-JEM 1400 microscope operating at 200 kV.

2.4. In vivo *C. elegans* experiments

2.4.1. Growth and treatment of *C. elegans*

C. elegans were grown on NGM agar seeded with *E. coli* OP50 following standard practices [35]. A 48 h synchronous culture was either fed SPIONs at 100 $\mu\text{g}/\text{mL}$ in MilliQ water (treated worms) or incubated in MilliQ water (control worms) for 24 h at 20 °C.

2.4.2. Sample preparation

Control and treated worms were washed twice with 20% BSA in M9 buffer and then fixed by high-pressure freezing, freeze-substituted, flat-embedded in Epon resin and sectioned by following a targeted ultra-microtomy protocol, as described previously [36].

2.4.3. Visualization and analysis of *C. elegans* sections

60-nm cross-sections were examined by transmission electron microscopy (TEM), high-angle annular dark-field scanning

transmission electron microscopy (HAADF STEM), electron energy loss spectroscopy (EELS) and energy-dispersive X-ray spectroscopy (EDX). TEM was performed using a PHILIPS CM 120 microscope. HAADF STEM, EDX, and EELS were performed using a FEI Tecnai G2 F20 S-TWIN HR(S)TEM equipped with an EDX system and an EELS system.

3. Results and discussion

Citrate-coated SPIONs (C-SPIONs) were synthesized by microwave-assisted thermal decomposition of iron acetylacetonate to yield $\gamma\text{-Fe}_2\text{O}_3$ nanoparticles with a mean diameter of 6 ± 1 nm. Particles were readily stabilized in water at pH = 7 with a zeta potential, $\zeta = -44$ mV. Cryo-TEM confirmed the individual stability of the SPIONs. The anionic aqueous dispersion was stable for more than six months without any noticeable changes by DLS [36,37]. The system is superparamagnetic above 45K and displays a high saturation magnetization value of 85 $\text{emu/g Fe}_2\text{O}_3$ at 5K (Fig. S1 a–d). Further coating of the C-SPIONs using a BSA-adsorption protocol yields the BSA-SPION system in which each nanocrystal is coated with approximately ten proteins, electrostatically bonded to the citrate through the positively charged moieties of the protein (Fig. 1a) [44]. BSA forms a monolayer of a hard protein corona as seen in the negative staining TEM image of Fig. 1b. An increase of 7 nm in the hydrodynamic diameter (D_h) by DLS supports the side-on binding of the protein (Fig. 1c). BSA-SPIONs have an anionic character with a surface charge of $\zeta = -22$ mV (Fig. 1d).

C-SPIONs and BSA-SPIONs were investigated *in vitro*. For this purpose, we chose two cell lines: adherent cells, MDA-MB231 (MDA), and suspension cells, HL60. MDA cells are highly invasive human mammary epithelial tumor cells and show low nonspecific binding to BSA [45]. It is expected that suspension cells are the first cell type encountered by the NPs after intravenous administration of NPs and that suspension cell lines have different nanoparticle internalization behavior [46]. Thus, human HL60 promyelocytic

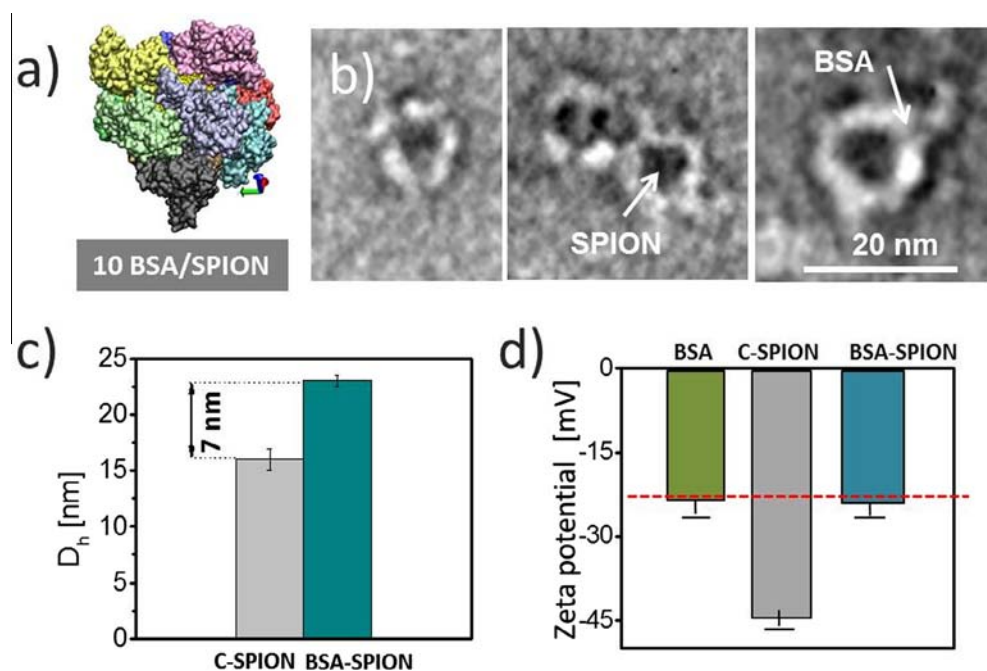


Fig. 1. a) Representation of a pre-formed protein corona coated nanoparticle BSA-SPION resulting from molecular dynamic modeling analysis, each protein is displayed with a different color [44], b) uranyl-stained TEM images; the inorganic SPIONs (dark) and the BSA hard protein corona (white) are marked with arrows, c) hydrodynamic diameter of the C-SPIONs (15 nm) and of the BSA-SPIONs (22 nm), d) zeta potential values for BSA, C-SPIONs, and BSA-SPIONs.

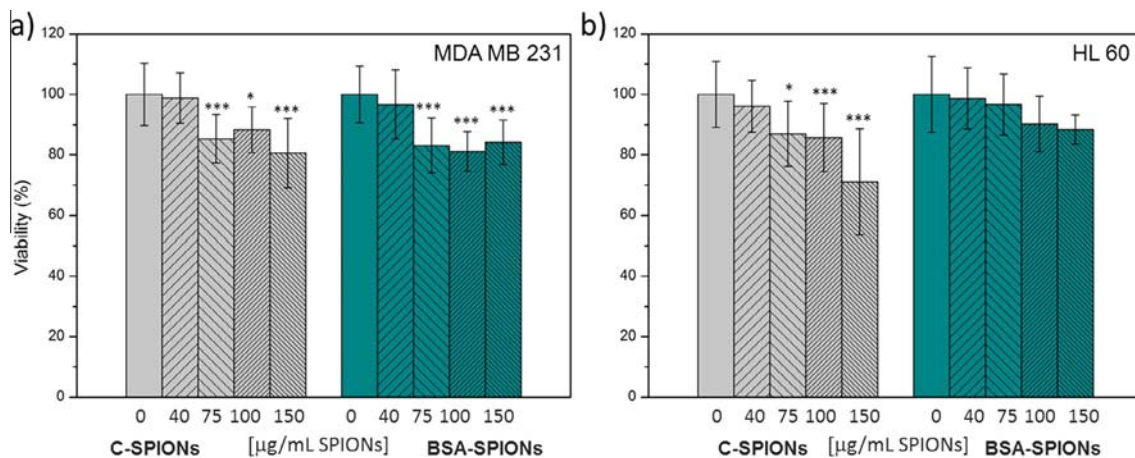


Fig. 2. Viability analysis (MTT assay) for two cell lines after 24 h incubation at increasing SPION concentration. Experiments were compared with the control, (*) $p < 0.05$; (***) $p < 0.005$.

leukemia cells were also selected. Fig. 2 displays the viability tests for the two cell lines upon 24 h exposure to C-SPIONs and BSA-SPIONs at different concentrations. In all cases, cell viability is higher than 80%, even for concentrations as high as 150 µg/mL. As expected, cytotoxic profiles are rather similar for the two systems since the experiments were carried out in a protein-rich media and therefore a protein corona also forms on the C-SPIONs. Even though, some differences between the two systems were identified; an increase in C-SPION concentration leads to a decrease in cell viability for MDA and HL60 cells ($p < 0.05$ and $p < 0.005$, respectively, when SPION concentration is higher than 75 µg/mL); in the case of BSA-SPION exposure, a significant decrease in cell viability is observed for MDA ($p < 0.005$ at BSA-SPION concentration higher than 75 µg/mL), while no significant changes in viability were observed for HL60 cell line at all concentrations studied. In short, the presence of BSA coating did not modify the viability of the cells for the adherent MDA cell line, while it moderately improved non-adherent HL60 cell viability.

SPION uptake after 24 h incubation for the two concentrations was quantified (g Fe_2O_3 /cell) by determining the remanent magnetization at 5K of a known number of cells (emu/cell) and the remanent magnetization of a given mass of nanoparticles (emu/g Fe_2O_3). Unsurprisingly a concentration-dependent process was found; higher concentrations of SPIONs resulted in an increased cellular uptake in all cases. Also, adherent cells internalized SPIONs (C-SPIONs and BSA-SPIONs) more efficiently than suspension cells. The iron oxide content of the labeled MDA cells was almost three fold higher than in the HL60 cells under the same incubation conditions (Fig. 3).

Cellular uptake of SPIONs was greatly affected by the presence of the BSA coating in both cell lines; a considerable lower uptake of BSA-SPIONs was observed than of the C-SPIONs (more than double). This finding clearly shows that the BSA coating modifies the interaction of SPIONs with cells by substantially decreasing unspecific cell internalization. Moreover, the BSA surface would enable the anchoring of cell-targeting specific moieties. A decrease in the cellular uptake of NPs with the BSA coating was previously reported [47,48]. Charge-mediated adhesion of nanoparticles to the plasma membrane leads to more efficient internalization. In our case, although both systems are negatively charged, BSA-SPIONs attach less to the plasma membrane, similarly to the neutrally charged PEG-nanoparticles (Fig. 4) [23]. After 24 h the colloidal stability and hydrodynamic sizes for the two systems are highly comparable as seen in Fig. S2. From Fig. 4, it appears that citrate-coated and protein-coated nanoparticles are taken up by

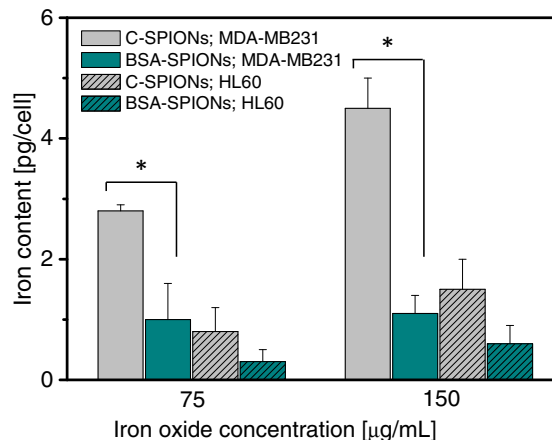


Fig. 3. Iron content versus two iron oxide concentrations for two cell lines: MDA (solid color) and HL60 (stripped pattern) and for the two systems: C-SPIONs (gray) and BSA-SPIONs (cyan). Statistical analysis by Anova: $p < 0.05$ (*). (For interpretation of the references to color in this figure legend, the reader is referred to the web version of this article.)

endocytosis. A characteristic feature of endosomal compartments for the BSA-SPIONs is the lower packing fraction, which we attribute again to the lesser affinity of those NPs to the cellular membrane compared to the C-SPIONs. Thus, we argue that differences in cellular uptake must be related to the nanoparticle surface and their level of “stickiness” to the cellular membrane rather than to particle aggregation or to different endosomal pathways.

To complete the *in vitro* investigations we followed the digestion process of the two NP systems in a solution that mimics a cell lysosome, for up to 30 days. We used a citrate buffer (CB) solution at a pH = 4.5. We also performed the same experiments in a buffer solution at a pH = 4.5 complemented with 10% FBS (CB-FBS) to better mirror the real lysosome environment. To monitor particle digestion, we analyzed the images of the solutions at fixed times; the results are shown in Fig. 5. For C-SPIONs incubated with CB, nanoparticles were digested fast during the first 4 days, and a complete degradation was observed at day 7. The addition of FBS in the buffer lowered the degradation rate; still, a complete dissolution was found by day 15. We thus assume that the FBS weakly adsorbs onto the C-SPIONs surface and hence slightly protects the SPIONs from degradation [18]. In contrast, BSA-SPIONs displayed completely different digestion profile. In CB, BSA-SPIONs are only

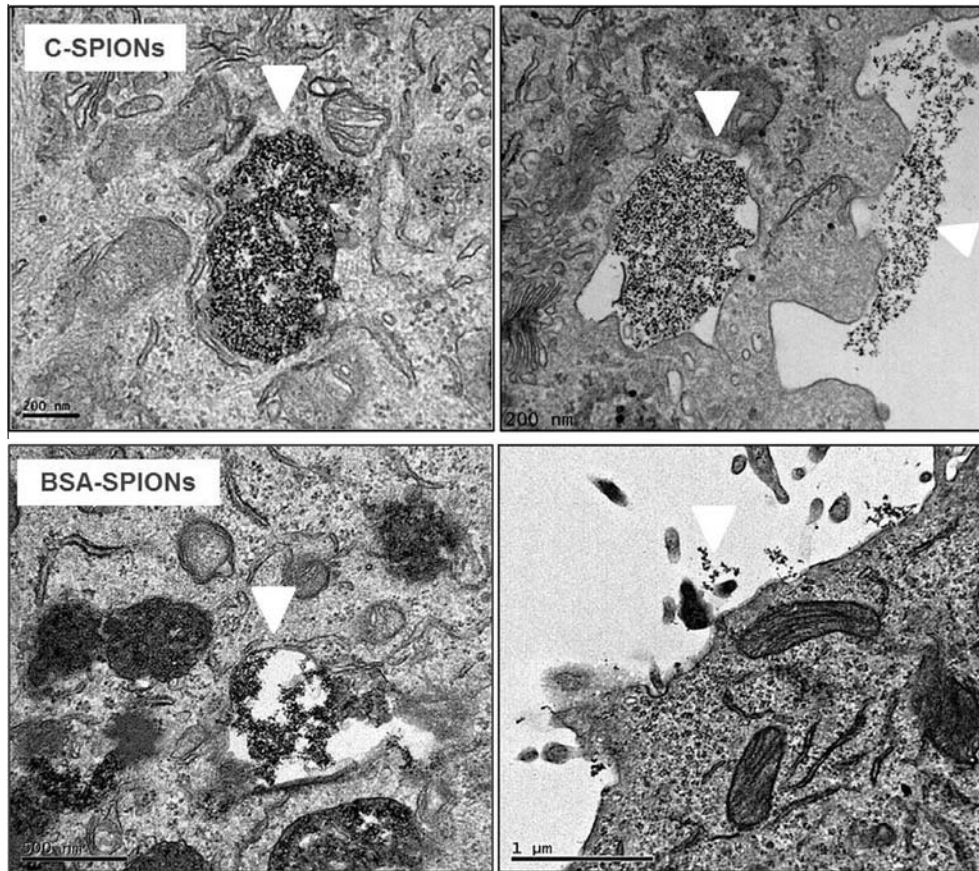


Fig. 4. TEM representative images of MDA cells after being incubated for 24 h with C-SPIONs (upper panels) and BSA-SPIONs (lower panels). Left panels show an endosome containing nanoparticles (marked with white arrow heads). The right panels show a fraction of the cell membrane; nanoparticle aggregates interacting with the plasma membrane are visible for the C-SPIONs (white arrow heads).

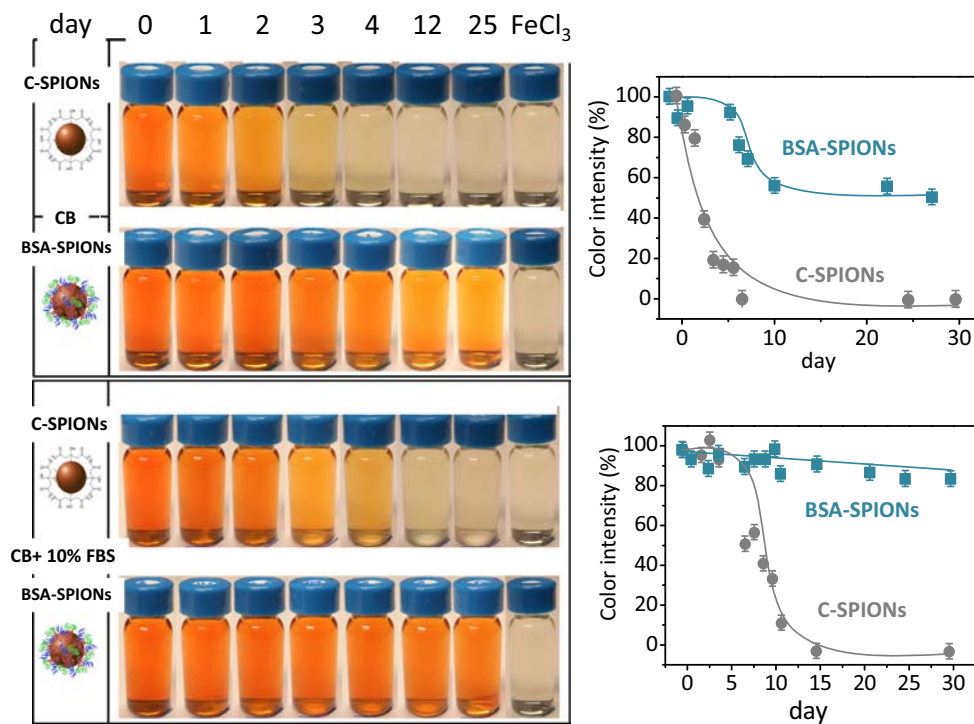


Fig. 5. Images of vials containing the same initial concentration of iron oxide as C-SPIONs or BSA-SPIONs in a citrate buffer (CB) at pH = 4.5 (two upper panels) and in a citrate buffer supplemented with 10% FBS (CB + 10% FBS) (two lower panels). Left figures represent the color intensity, directly linked to Fe³⁺ ions as a function of time for the two buffers. C-SPIONs are depicted in gray and BSA-SPIONs in blue. (For interpretation of the references to color in this figure legend, the reader is referred to the web version of this article.)

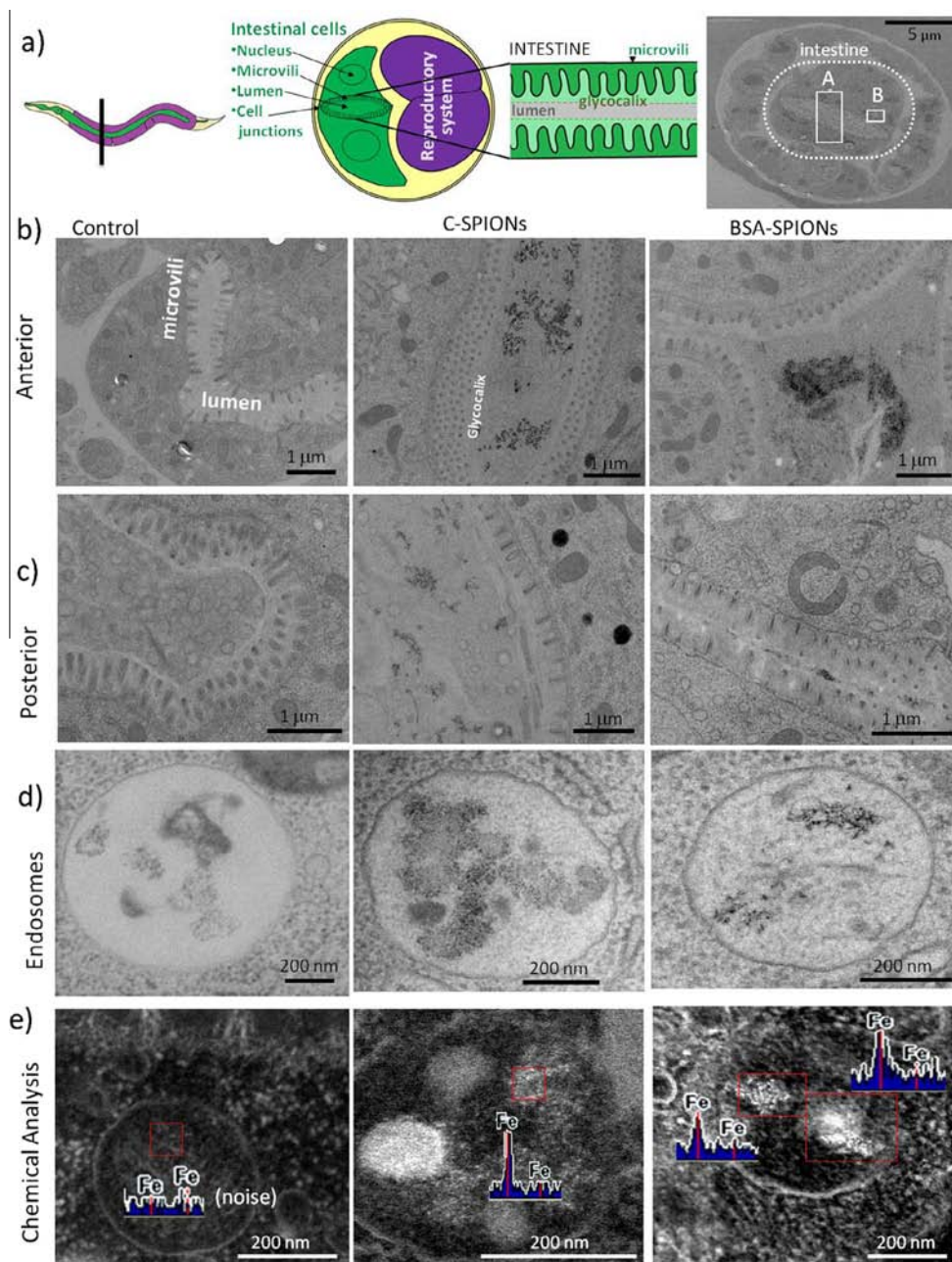


Fig. 6. a) Schematic drawing of the *C. elegans* anatomy and cross-section. b–d) TEM images of control *C. elegans* (first column), *C. elegans* treated with C-SPIONs (central column) and *C. elegans* treated with BSA-SPIONs (right column). *C. elegans* were cut at two body locations: b) anterior and c) posterior. d) Endosomes containing NP or NP-like content in treated and control worms, respectively. e) HAADF STEM images of endosomes. EDX analysis (insets) confirmed the absence or presence of iron in control and treated worms, respectively.

slightly digested during the first 7 days and 50% of the BSA-SPIONs remained after 30 day incubation. Remarkably, in the presence of FBS, there was only negligible degradation for BSA-SPIONs, even at day 30. Thus both the hard corona of the pre-formed BSA monolayer and the additional adsorbed soft FBS protein corona synergistically protected the SPIONs from being complexed and chelated by the free citrate ions present in the buffer. We further monitored the hydrodynamic diameter (D_h) by DLS and inorganic nanocrystal size by TEM (Figs. S4 and S5). Consistent with previous results, D_h for C-SPIONs incubated in CB displayed a gradual decrease with time, from the initial 17 nm to less than 3 nm at day 6. After 6 days, particle size was too small to be measured by DLS. Size reduction was also evident in the TEM images, where the loss of crystallinity is established from the fewer and less intense diffraction rings

visible at a greater number of days. However for BSA-SPIONs incubated in CB we could not detect differences in D_h over time, even after 30 day incubation. D_h is maintained at around 25 nm; even though 50% of the iron from BSA-SPIONs is in ionic form, the rest maintained their initial structure intact. This aspect will be studied in more detail in the future.

It is important to understand how the passage of nanoparticles through biological barriers and between compartments and organs is influenced by the protein corona [49]. The *in vivo* fate of orally administered SPIONs was evaluated in the model organism *Caenorhabditis elegans*. *C. elegans* has some key features that may allow it to become an alternative animal model for initial screening and evaluation of the oral delivery of nanomaterials. Because of its resemblances to the mammalian intestinal barrier, the *C. elegans*

intestine is proposed as a model for studying intestinal functions (Fig. 6a) [50–52]. In particular, the polarity of the intestinal cells is conserved, showing an apical membrane with microvilli that project to the lumen, and a basolateral membrane, both separated by apical junctions that also connect together adjacent cells. Such apical junctions are reminiscent of the apical junction complex found in mammals [53]. The mechanisms of biomolecule transport across the gastrointestinal barrier are also highly conserved. In addition, the pH value [54] and the variety of digestive enzymes [55] in the intestinal microenvironment of the worm allow us to investigate the nanoparticles' biodegradability after oral administration.

We studied the two iron oxide systems in *C. elegans*, where multiple parameters (i.e., ionic strength, pH value, diameter of the anatomical structures, etc.) could modify the NPs' original properties. We attempted to correlate the different bio-identity of C-SPIONs and BSA-SPIONs regarding cell internalization mechanisms. Previously, we reported on the similar uptake of C-SPIONs and BSA-SPIONs in *C. elegans* due to the rhythmic pharyngeal pumping that is responsible for nanoparticle entrance to *C. elegans* body during oral feeding. However, we observed coating-dependent toxicological effects in the worm, in which the BSA-SPIONs are more biocompatible than the uncoated particles, in particular at high dosage (500 µg/mL) [38]. Here, we evaluate the fate of SPIONs by TEM in ultrathin cross-sections of two different regions of the body of the *C. elegans*: an anterior region of the intestine (pH = 6), very close to the pharynx ending; and a more posterior region of the intestine (pH = 3.6; Fig. 6b and c) [54]. We have been able to observe that most particles are located inside the intestinal lumen and only a very small number of individual particles could be detected in the area surrounding the lumen; the glycocalyx, which appears to act as a buffer zone [56]. All along the intestine, SPIONs remained separated from the microvilli surface, and very few individual NPs were observed closer to the microvilli (Fig. S7). Remarkably, we detected endosomes loaded with particles in the enterocytes of worms treated with both SPION species (Fig. 6d and S8c), contrasting with our findings for 10-nm gold nanoparticles where all the NPs visualized where restrained to the intestinal lumen [57]. BSA-SPION treated worms contained slightly larger endosomes filled with NPs (600 ± 300 nm, $n = 19$) than C-SPION treated ones (470 ± 200 nm, $n = 17$). Control worms occasionally had endosomes that contained features resembling nanoparticle-like structures but both EDX and EELS confirmed the presence of iron in the endosomes of treated worms and not in the controls (Figs. 6e and S8d). The same cross-sections were further analyzed by HAADF STEM, where the intensity of the materials is approximately proportional to the square of the atomic number, Z^2 . In Figs. 6e and S8b–c, the high intensity of the SPIONs both inside the lumen and inside the endosomes can be attributed to Fe ($Z = 26$) whereas C ($Z = 6$) has lower intensity, thus SPIONs are seen as bright spots, not observed in the control worms. Both C-SPIONs and BSA-SPIONs remained monodispersed, both in the lumen and inside the endosomal/lysosomal compartment. A histogram with the nanoparticle size distribution showed that C-SPIONs in the lumen underwent a 10% size decrease after 24 h treatment in the anterior part of the intestine, while BSA-SPIONs remained unchanged (Fig. S9). In posterior regions, smaller clumps (<200 nm) of individual SPIONs were observed. In this area, C-SPIONs had a slightly smaller size than in the anterior, corresponding to a 15% size decrease compared to the as-synthesized SPIONs, while the size of the BSA-SPIONs again remained unchanged (Fig. S9). These observations support the hypothesis that C-SPIONs undergo a partial digestion under the intestinal conditions of *C. elegans* [38]. Note that the microvilli structure was not affected in the worm studies and that no apoptotic digestive cells were observed. The absence of food during NP treatment caused

cessation of defecation; TEM observations showed that no NPs were present in the lumen at the level of the excretory system (Fig. S10).

Overall, the observations on the fate of C-SPIONs and BSA-SPIONs in *C. elegans* suggest that the BSA coating protects the NP inorganic core from acidic degradation, in accordance with results in Fig. 5. Moreover, both NPs remained monodispersed in the worm intestine. However, NPs can be also endocytosed during their confinement in the intestine, and no remarkable differences have been observed regarding the number of endosomes, their size, or their loading in the two sections of the intestine studied. These findings indicate that nanoparticles are internalized by the cells through a different pathway than the nutrients feeding the worm. This point deserves further studies.

4. Conclusion

Unravelling meaningful relationships between the physiological impact of engineered nanoparticles and their synthetic and biological identity is rather complex but of vital importance when considering nanoparticle biomedical uses and when establishing their nanotoxicological profile. In this work, we focused on the acquired bio-identity, *in vitro* and *in vivo*, of anionic citrate-SPIONs (C-SPIONs) outfitted with a well-defined albumin corona (BSA-SPIONs). Cytotoxicity, intracellular particle distribution, and uptake were studied in two cell lines: adherent and suspension cells. The intracellular content of iron oxide in adherent cells is three-fold higher than in non-adherent while the uptake of the BSA-SPIONs was greatly reduced in both cell lines compared to the same particles without the pre-formed protein corona. Thus, the pre-formed corona substantially decreases unspecific cell internalization. Moreover, it protects the particles from acidic digestion. The fate of orally administered nanoparticles was then evaluated *in vivo* in the model organism *Caenorhabditis elegans*. Analysis of ultrathin cross-sections of the worm by transmission electron microscopy allowed us to screen the biodistribution of the particles showing that both nanoparticle systems remained monodispersed in the lumen microenvironment while we identify a small fraction that crossed the intestinal barrier by endocytosis of the intestinal cells. No remarkable differences were observed in the number of endosomes, their size or their loading, in either SPION coating. Observations on the NP fate in *C. elegans* suggest that the BSA coating protects the inorganic core from acidic degradation in the worm intestine and prevents the direct contact of the inorganic core with the worm's body which may result in a higher biocompatibility of the BSA-SPIONs.

The information gathered from the *in vitro* and the *in vivo* experiments on exactly the same NPs system with different surface coating is extremely relevant and complementary but the comprehensive analysis of results in an ensemble mode is challenging reflecting the complexity of this enterprise. Even though, we can conclude that the BSA coating did not significantly affect the cytotoxicity of NPs in the two cell lines studied it showed a marked influence on the *C. elegans* survival rates at high doses underpinning the need of NP evaluation in higher complex organisms [38]. Secondly, cell uptake was considerably reduced for BSA-SPIONs but the protein coating did not affect the NPs transit across the *C. elegans* intestinal barrier. Importantly both *in vitro* and *in vivo* studies identified endocytosis as the likely nanoparticle–cell invagination mechanism. Moreover, although the *in vitro* results show that uncoated SPIONs form aggregates in protein-rich media and stay monodispersed when precoated with BSA, we observed that both C-SPIONs and BSA-SPIONs retained their individuality in the biomolecule-rich intestinal microenvironment of the *C. elegans*. Finally, we observed that BSA-SPIONs are efficiently

protected from acidic media, both in the lysosome environment and in the *C. elegans* lumen, in contrast to the more easily digested uncoated SPIONs.

Acknowledgments

This research was partially funded by the Spanish Ministry of Economy (MAT2015-64442-R, Ramon y Cajal program (AL, RyC-2010-06082), FPU program (LGM, FPU12/05549), Severo Ochoa Program (SEV-2015-0496) co-funded by European Social Funds), the Generalitat de Catalunya (2014SGR213), People Program of the European Commission (grant agreement no. 303630, co-funded by the European Social Fund), the Chinese Fundamental Research Funds for the Central Universities (21616306), the Christian Boulton fellowship 2015 from EMBL (LGM), the COST Actions HINT (Action No. MP1202), and GENIE (Action No. BM1408-A). We thank Lorenzo Albertazzi (IBEC, Spain) for the critical reading of the manuscript.

Appendix A. Supplementary data

Supplementary data associated with this article can be found, in the online version, at <http://dx.doi.org/10.1016/j.actbio.2016.07.024>.

References

- [1] I. Lynch, K.A. Dawson, Protein-nanoparticle interactions, *Nano Today* 3 (2008) 40–47.
- [2] C. Roecker, M. Poetzel, F. Zhang, W.J. Parak, G.U. Nienhaus, A quantitative fluorescence study of protein monolayer formation on colloidal nanoparticles, *Nat. Nanotechnol.* 4 (2009) 577–580.
- [3] S. Ritz, S. Schoettler, N. Kotman, G. Baier, A. Musyanovych, J. Kuharev, K. Landfester, H. Schild, O. Jahn, S. Tenzer, V. Mailaender, Protein corona of nanoparticles: distinct proteins regulate the cellular uptake, *Biomacromolecules* 16 (2015) 1311–1321.
- [4] L. Assaud, E. Monyoncho, K. Pitzschel, A. Allagui, M. Petit, M. Hanbuecken, E.A. Baranova, L. Santinacci, 3D-nanoarchitected Pd/Ni catalysts prepared by atomic layer deposition for the electrooxidation of formic acid, *Beilstein J. Nanotechnol.* 5 (2014) 162–172.
- [5] M. Lundqvist, J. Stigler, G. Elia, I. Lynch, T. Cedervall, K.A. Dawson, Nanoparticle size and surface properties determine the protein corona with possible implications for biological impacts, *PNAS* 105 (2008) 14265–14270.
- [6] C.D. Walkey, W.C.W. Chan, Understanding and controlling the interaction of nanomaterials with proteins in a physiological environment, *Chem. Soc. Rev.* 41 (2012) 2780–2799.
- [7] A. Albanese, W.C.W. Chan, Effect of gold nanoparticle aggregation on cell uptake and toxicity, *ACS Nano* 5 (2011) 5478–5489.
- [8] M. Safi, J. Courtois, M. Seigneuret, H. Conjeaud, J.F. Berret, The effects of aggregation and protein corona on the cellular internalization of iron oxide nanoparticles, *Biomaterials* 32 (2011) 9353–9363.
- [9] X. Liu, Y. Chen, H. Li, N. Huang, Q. Jin, K. Ren, J. Ji, Enhanced retention and cellular uptake of nanoparticles in tumors by controlling their aggregation behavior, *ACS Nano* 7 (2013) 6244–6257.
- [10] A.R. Gliga, S. Skoglund, I.O. Wallinder, B. Fadeel, H.L. Karlsson, Size-dependent cytotoxicity of silver nanoparticles in human lung cells: the role of cellular uptake, agglomeration and Ag release, *Part Fibre Toxicol.* 11 (2014).
- [11] M.J. Ware, B. Godin, N. Singh, R. Majithia, S. Shamsudeen, R.E. Serda, K.E. Meissner, P. Rees, H.D. Summers, Analysis of the influence of cell heterogeneity on nanoparticle dose response, *ACS Nano* 8 (2014) 6693–6700.
- [12] D.R. Hristov, L. Rocks, P.M. Kelly, S.S. Thomas, A.S. Pitek, P. Verderio, E. Mahon, K.A. Dawson, Tuning of nanoparticle biological functionality through controlled surface chemistry and characterisation at the bioconjugated nanoparticle surface, *Sci. Rep.* 5 (2015).
- [13] E. Carenza, V. Barcelo, A. Morancho, J. Montaner, A. Rosell, A. Roig, Rapid synthesis of water-dispersible superparamagnetic iron oxide nanoparticles by a microwave-assisted route for safe labeling of endothelial progenitor cells, *Acta Biomater.* 10 (2014) 3775–3785.
- [14] P. Sanpui, A. Paul, A. Chattopadhyay, Theranostic potential of gold nanoparticle-protein agglomerates, *Nanoscale* 7 (2015) 18411–18423.
- [15] L. Landgraf, C. Christner, W. Storch, I. Schick, I. Krumbain, H. Daehring, K. Haedicke, K. Heinz-Herrmann, U. Teichgraber, J.R. Reichenbach, W. Tremel, S. Tenzer, I. Hilger, A plasma protein corona enhances the biocompatibility of Au@Fe₃O₄ Janus particles, *Biomaterials* 68 (2015) 77–88.
- [16] J.C.Y. Kah, J. Chen, A. Zubieta, K. Hamad-Schifferli, Exploiting the protein corona around gold nanorods for loading and triggered release, *ACS Nano* 6 (2012) 6730–6740.
- [17] S. Schoettler, G. Becker, S. Winzen, T. Steinbach, K. Mohr, K. Landfester, V. Mailaender, F.R. Wurm, Protein adsorption is required for stealth effect of poly(ethylene glycol)- and poly(phosphoester)-coated nanocarriers, *Nat. Nanotechnol.* 11 (2016) 372–377.
- [18] R. Gref, M. Luck, P. Quellec, M. Marchand, E. Dellacherie, S. Harnisch, T. Blunk, R.H. Muller, 'Stealth' corona-core nanoparticles surface modified by polyethylene glycol (PEG): influences of the corona (PEG chain length and surface density) and of the core composition on phagocytic uptake and plasma protein adsorption, *Colloids Surf. B* 18 (2000) 301–313.
- [19] Q. He, J. Zhang, J. Shi, Z. Zhu, L. Zhang, W. Bu, L. Guo, Y. Chen, The effect of PEGylation of mesoporous silica nanoparticles on nonspecific binding of serum proteins and cellular responses, *Biomaterials* 31 (2010) 1085–1092.
- [20] Q. Dai, C. Walkey, W.C.W. Chan, Polyethylene glycol backfilling mitigates the negative impact of the protein corona on nanoparticle cell targeting, *Angew. Chem. Int. Ed.* 53 (2014) 5093–5096.
- [21] F. Kawai, T. Kimura, M. Fukaya, Y. Tani, K. Ogata, T. Ueno, H. Fukami, Bacterial oxidations of polyethylene-glycol, *Appl. Environ. Microbiol.* 35 (1978) 679–684.
- [22] S. Stolnik, S.E. Dunn, M.C. Garnett, M.C. Davies, A.G.A. Coombes, D.C. Taylor, M. P. Irving, S.C. Purkiss, T.F. Tadros, S.S. Davis, L. Illum, Surface modification of poly(lactide-co-glycolide) nanospheres by biodegradable poly(lactide)-poly(ethylene glycol) copolymers, *Pharm. Res.* 11 (1994) 1800–1808.
- [23] B. Pelaz, P. del Pino, P. Maffre, R. Hartmann, M. Gallego, S. Rivera-Fernandez, J. M. de la Fuente, G.U. Nienhaus, W.J. Parak, Surface functionalization of nanoparticles with polyethylene glycol: effects on protein adsorption and cellular uptake, *ACS Nano* 9 (2015) 6996–7008.
- [24] D. Bargheer, J. Nielsen, G. Gebel, M. Heine, S.C. Salmen, R. Stauber, H. Weller, J. Heeren, P. Nielsen, The fate of a designed protein corona on nanoparticles in vitro and in vivo, *Beilstein J. Nanotechnol.* 6 (2015) 36–46.
- [25] W.G. Kreyling, A.M. Abdelmonem, Z. Ali, F. Alves, M. Geiser, N. Haberl, R. Hartmann, S. Hirn, D. Jimenez de Aberasturi, K. Kantner, G. Khadem-Saba, J.-M. Montenegro, J. Rejman, T. Rojo, I. Ruiz de Larramendi, R. Ufartes, A. Wenk, W.J. Parak, In vivo integrity of polymer-coated gold nanoparticles, *Nat. Nanotech.* 10 (2015). 619–+.
- [26] K. Klinker, M. Barz, Polypept(o) ides: hybrid systems based on polypeptides and polypeptoids, *Macromol. Rapid Commun.* 36 (2015) 1943–1957.
- [27] M.A. Young, A. Malavalli, N. Winslow, K.D. Vandegriff, R.M. Winslow, Toxicity and hemodynamic effects after single dose administration of MalPEG-hemoglobin (MP4) in rhesus monkeys, *Trans. Res.* 149 (2007) 333–342.
- [28] P.M. Kelly, C. Åberg, E. Polo, A. O'Connell, J. Cookman, J. Fallon, KrpeticZeljka, K.A. Dawson, Mapping protein binding sites on the biomolecular corona of nanoparticles, *Nat. Nanotechnol.* 10 (2015) 472–479.
- [29] Q. Peng, S. Zhang, Q. Yang, T. Zhang, X.-Q. Wei, L. Jiang, C.-L. Zhang, Q.-M. Chen, Z.-R. Zhang, Y.-F. Lin, Preformed albumin corona, a protective coating for nanoparticles based drug delivery system, *Biomaterials* 34 (2013) 8521–8530.
- [30] A. Aires, S.M. Ocampo, D. Cabrera, L. de la Cueva, G. Salas, F.J. Teran, A.L. Cortajarena, BSA-coated magnetic nanoparticles for improved therapeutic properties, *J. Mater. Chem. B* 3 (2015) 6239–6247.
- [31] J. Mariam, S. Sivakami, P.M. Dongre, Albumin corona on nanoparticles – a strategic approach in drug delivery, *Drug Delivery* (2015) 1–9.
- [32] X. Wang, X. Xing, B. Zhang, F. Liu, Y. Cheng, D. Shi, Surface engineered antifouling optomagnetic SPIONs for bimodal targeted imaging of pancreatic cancer cells, *Int. J. Nanomed.* 9 (2014) 1601–1615.
- [33] D. Ling, N. Lee, T. Hyeon, Chemical synthesis and assembly of uniformly sized iron oxide nanoparticles for medical applications, *Acc. Chem. Res.* 48 (2015) 1276–1285.
- [34] M. Colombo, S. Carregal-Romero, M.F. Casula, L. Gutierrez, M.P. Morales, I.B. Boehm, J.T. Heverhagen, D. Prosperi, W.J. Parak, Biological applications of magnetic nanoparticles, *Chem. Soc. Rev.* 41 (2012) 4306–4334.
- [35] E. Carenza, V. Barcelo, A. Morancho, L. Levander, C. Boada, A. Laromaine, A. Roig, J. Montaner, A. Rosell, In vitro angiogenic performance and in vivo brain targeting of magnetized endothelial progenitor cells for neurorepair therapies, *Nanomedicine* 10 (2014) 225–234.
- [36] O. Pascu, E. Carenza, M. Gich, S. Estrade, F. Peiro, G. Herranz, A. Roig, Surface reactivity of iron oxide nanoparticles by microwave-assisted synthesis: comparison with the thermal decomposition route, *J. Phys. Chem. C* 116 (2012) 15108–15116.
- [37] S.-M. Yu, A. Laromaine, A. Roig, Enhanced stability of superparamagnetic iron oxide nanoparticles in biological media using a pH adjusted-BSA adsorption protocol, *J. Nanopart. Res.* 16 (2014).
- [38] L. Gonzalez-Moragas, S.-M. Yu, E. Carenza, A. Laromaine, A. Roig, Protective effects of bovine serum albumin on superparamagnetic iron oxide nanoparticles evaluated in the nematode *Caenorhabditis elegans*, *ACS Biomater. Sci. Eng.* 1 (2015) 1129–1138.
- [39] L. Gonzalez-Moragas, A. Roig, A.C. Laromaine, *Elegans* as a tool for in vivo nanoparticle assessment, *Adv. Colloid Interface Sci.* 219 (2015) 10–26.
- [40] M.C.K. Leung, P.L. Williams, A. Benedetto, C. Au, K.J. Helmcke, M. Aschner, J.N. Meyer, *Caenorhabditis elegans*: an emerging model in biomedical and environmental toxicology, *Toxicol. Sci.* 106 (2008) 5–28.
- [41] L. Tejada-Benitez, J. Olivero-Verbel, *Caenorhabditis elegans*, A Biological Model for Research in Toxicology, in: W.P. de Voogt (Ed.), *Rev Environ Contam T. Cham*, Springer International Publishing, 2016, pp. 1–35.
- [42] D.H. Hall, Z.F. Altun, C. *Elegans Atlas*, Cold Spring Harbor Laboratory Press, 2008.
- [43] J.D. McGhee, The *C. elegans* Intestine. *WormBook: The Online Review of C elegans Biology*, 2007, pp. 1–36.

- [44] S. Yu, A. Peralvarez-Marin, C. Minelli, J. Faraudo, A. Roig, A. Laromaine, Albumin-coated SPIONs: an experimental and theoretical evaluation of protein conformation, binding affinity and competition with serum proteins, *Nanoscale* (2016). Advance article, <http://dx.doi.org/10.1039/C6NR01732K>.
- [45] A. Taherian, X. Li, Y. Liu, T.A. Haas, Differences in integrin expression and signaling within human breast cancer cells, *Bmc Cancer* (2011) 11.
- [46] J. Lin, Y. Yu, B. Li, H. Huang, S. Lin, C. Li, Y. Su, S. Feng, G. Chen, Y. Li, Z. Huang, H. Zeng, R. Chen, Electrical pulse - mediated enhanced delivery of silver nanoparticles into living suspension cells for surface enhanced Raman spectroscopy, *Laser Phys. Lett.* 9 (2012) 240–246.
- [47] G. Baier, C. Costa, A. Zeller, D. Baumann, C. Sayer, P.H.H. Araujo, V. Mailaender, A. Musyanovych, K. Landfester, BSA adsorption on differently charged polystyrene nanoparticles using isothermal titration calorimetry and the influence on cellular uptake, *Macromol. Biosci.* 11 (2011) 628–638.
- [48] C.A. Ruge, J. Kirch, O. Canadas, M. Schneider, J. Perez-Gil, U.F. Schaefer, C. Casals, C.-M. Lehr, Uptake of nanoparticles by alveolar macrophages is triggered by surfactant protein A, *Nanomedicine* 7 (2011) 690–693.
- [49] M.P. Monopoli, C. Aberg, A. Salvati, K.A. Dawson, Biomolecular coronas provide the biological identity of nanosized materials, *Nat. Nanotechnol.* 7 (2012) 779–786.
- [50] G. Gillard, M. Shafaq-Zadah, O. Nicolle, R. Damaj, J. Pecreaux, G. Michaux, Control of E-cadherin apical localisation and morphogenesis by a SOAP-1/AP-1/clathrin pathway in C-elegans epidermal cells, *Development* 142 (2015) 1684–1694.
- [51] M. Shafaq-Zadah, L. Brocard, F. Solari, G. Michaux, AP-1 is required for the maintenance of apico-basal polarity in the *C. elegans* intestine, *Development* 139 (2012) 2061–2070.
- [52] P. Martorell, S. Llopis, N. Gonzalez, F. Monton, P. Ortiz, S. Genoves, D. Ramon, *Caenorhabditis elegans* as a model to study the effectiveness and metabolic targets of dietary supplements used for obesity treatment: the specific case of a conjugated linoleic acid mixture (Tonalin), *J. Agric. Food Chem.* 60 (2012) 11071–11079.
- [53] G. Michaux, R. Legouis, M. Labouesse, Epithelial biology: lessons from *Caenorhabditis elegans*, *Gene* 277 (2001) 83–100.
- [54] V.M. Chauhan, G. Orsi, A. Brown, D.I. Pritchard, J.W. Aylott, Mapping the pharyngeal and intestinal pH of *Caenorhabditis elegans* and real-time luminal pH oscillations using extended dynamic range pH-sensitive nanosensors, *ACS Nano* 7 (2013) 5577–5587.
- [55] J.D. McGhee, The *Caenorhabditis elegans* intestine, *Wiley Interdiscip. Rev. Develop. Biol.* 2 (2013) 347–367.
- [56] V. Gobel, P.L. Barrett, D.H. Hall, J.T. Fleming, Lumen morphogenesis in *C-elegans* requires the membrane-cytoskeleton linker *erm-1*, *Dev. Cell* 6 (2004) 865–873.
- [57] L. Gonzalez-Moragas, P. Berto, C. Vilches, R. Quidant, A. Kolovou, R. Santarella-Mellwig, Y. Schwab, A. Roig, A. Laromaine, In vivo testing of gold nanoparticles using the *Caenorhabditis elegans* model organism, 2016, submitted for publication.

***In vivo* testing of gold nanoparticles using the *Caenorhabditis elegans* model organism**

Laura Gonzalez-Moragas¹, Pascal Berto², Clara Vilches², Romain Quidant², Androniki Kolovou³, Rachel Santarella-Mellwig³, Yannick Schwab³, Stephen Stürzenbaum⁴, Anna Roig^{1*}, Anna Laromaine^{1*}

1 Institut de Ciència de Materials de Barcelona, ICMAB-CSIC. Campus UAB. 08193 Bellaterra, Barcelona - Spain.

2 ICFO-Institut de Ciències Fotòniques. Av. Carl Friedrich Gauss, 3, 08860 Castelldefels, Barcelona - Spain

3 European Molecular Biology Laboratory, EMBL. Meyerhofstraße, 1, 69117 Heidelberg - Germany.

4 King's College London. Faculty of Life Sciences & Medicine, Analytical and Environmental Sciences Division, 150 Stamford Street, London SE1 9NH - United Kingdom.

Gold nanoparticles (Au-NPs) are present in many manmade products and cosmetics, and are frequently used by the food and medical industries. Tight regulations regarding the use of mammalian animals for product testing can hamper the study of the specific interactions between engineered nanoparticles and biological systems. The use of invertebrate models, such as the nematode *Caenorhabditis elegans* (*C. elegans*), can offer alternative approaches during the early phases of nanoparticle discovery.

Here, we report on the use of advanced optical techniques such as two-photon luminescence microscopy in *C. elegans*, together with an array of materials-science characterization techniques and state-of-the-art electron microscopy protocols to study and quantify the nano/bio interaction between *C. elegans* and orally administered monodisperse small and large citrate-coated Au-NPs. We thoroughly evaluate the biodistribution of Au-NPs inside the worm by microscopy at multiple scales, moving from micrometric to nanometric resolution and from organs to cells. These analyses are further complemented by investigating the effect of Au-NPs on the survival and reproductive performance of *C. elegans*, and correlating these effects with the uptake of Au-NPs in terms of their number, surface area, and metal mass. We determine NP status inside *C. elegans* by using absorbance microspectroscopy and relate the plasmonic properties of Au-NPs with NP confinement due to the biological traits of the *C. elegans* in their different anatomical areas. Finally, we assessed several molecular markers of endocytosis and intestinal barrier integrity and we did not find significant alteration in their expression levels compared to untreated worms.

Keywords: biological interactions, *Caenorhabditis elegans*, digestive system, enterocytes, gold nanoparticles.

Introduction

Many of the products used in our daily life contain nanoparticles, gold nanoparticles (Au-NPs) in facial creams,^[2] silver nanoparticles in preservatives,^[3] or zinc oxide nanoparticles and titanium dioxide nanoparticles in colorants and sunscreens^[4]. Colloidal Au-NPs hold great promise in cosmetics and as therapeutic and diagnostic agents due to their inertness, which limits their toxicity to cells, and unique optical and photothermal properties. The latter can be controlled and tuned by changing the size, shape, and surface functionalization of Au-NPs.^[5]

Gold nanoparticles have been selected by the Working Party on Manufactured Nanomaterials of the Organization for Economic Cooperation and Development (OECD) as manufactured nanomaterials which are either in commercialization or likely to enter the market in the near term.^[6] Indeed, some Au-NP formulations have already been proposed as novel tools for *in vitro* and *in vivo* molecular imaging and drug delivery.^[7] Au-NPs have, for example, attracted interest as carriers to enhance the oral absorption of

drugs and vaccines that are either poorly absorbed or are susceptible to gastrointestinal degradation.^[8] However, to our knowledge, only Au-NPs used for local heat generation in the plasmonic photothermal therapy of atherosclerosis and cancer have to date reached clinical stage (ClinicalTrials.gov Identifiers NCT01270139, NCT01679470, NCT00848042).^[9] In addition, Au-NPs are present in daily products such as anti-ageing creams and masks, toothpastes, and are even marketed as food supplements according to the Consumer Products Inventory, which is compiled by the Project on Emerging Nanotechnologies.^[10] On the other hand, the regulations on nanoparticles are being tightened and the use of animal-free alternatives to evaluate new materials is being actively promoted. For instance, in March 2013, EU regulations on Cosmetics and Household Products banned the use of animals to assess the safety of these products. The North American Food and Drug Administration (FDA) also supports the development and use of alternatives to animal testing to assess the safety of cosmetic products.^[11] Hence, there is a pressing need

to develop new platforms and approaches to evaluate Au-NP-containing products in particular to push forward the early stages of nanoparticle development in the cosmetic, food, and pharmaceutical industries. In this context, invertebrate models such as *Caenorhabditis elegans*, *Drosophila melanogaster* or *Danio rerio* allow scientists to obtain a first set of primary biological data on engineered nanomaterials in a facile experimental system, facing less strict regulations and ethical issues than in mammals. These simple model organisms allow high-throughput screenings and can be integrated into microfluidic technologies, which is an upward trend specifically in biomedical research that can, in turn, accelerate the path to the market.^[12] *C. elegans* exhibits 60-80% genome homology with humans and shares a multitude of biological traits in terms of physiology, anatomy, and metabolism (Figure 1).^[13] The use of worms grants a cost-effective initial biological assessment of nanomaterials within chemical laboratories.^[14] In addition, their transparency, small size, prolific and short lifecycle, and few requirements of maintenance facilitate the study of the interaction between nanomaterials and a multicellular organisms.^[14] The external part of the worm, the cuticle, can be used as a skin model based on its similar function and composition to human skin (Figure 1A).^[13a, 15] The *C. elegans* intestine also shares a similar cellular architecture with higher animals with respect to cell polarity of the intestinal cells (enterocytes) including the presence of apical and basolateral domains, cell junctions, and the presence of microvilli forming the brush border (Figure 1B). Setting aside some differences in the composition, both mammals and *C. elegans* encompass a peritrophic-like layer that protects the microvillar surface of the gut.^[13a, 16] Furthermore, the mechanisms of transport of biomolecules through the biological barriers are highly conserved.^[17] Therefore, *C. elegans* offers promising features and valuable tools to evaluate the delivery of topical and oral nanomaterials before moving to more complex model organisms.^[14, 18] *C. elegans* can be used to track NPs through different biological barriers (dermal and intestinal) and at multiple anatomical levels (organs, tissues, and cells). Here, we report on the use of advanced optical techniques such as two-photon luminescence microscopy (TPLM)^[11] in *C. elegans*, together with an array of materials-science characterization techniques and state-of-the-art electron microscopy protocols^[19]

to study and quantify the nano/bio interaction between *C. elegans* and orally administered monodisperse small and large citrate-coated Au-NPs. We thoroughly evaluate the biodistribution of Au-NPs inside the worm by microscopy at multiple scales, moving from micrometric to nanometric resolution and from organs to cells. These analyses are further complemented by investigating the effect of Au-NPs on the survival and reproductive performance of *C. elegans*, and correlating these effects with the uptake of Au-NPs in terms of their number, surface area, and metal mass. We determine NP status inside *C. elegans* by using absorbance microspectroscopy and relate the plasmonic properties of Au-NPs with NP confinement due to the biological traits of the *C. elegans* in their different anatomical areas. Finally, we assessed several molecular markers of endocytosis and intestinal barrier integrity and we did not find significant alteration in their expression levels compared to untreated worms.

Methods

Materials

Caenorhabditis elegans Bristol strain N2 and *Escherichia coli* OP50 were obtained from the *Caenorhabditis* Genetic Center (CGC) stock collection, University of Minnesota, St. Paul, MN, USA. Peptone, yeast extract, bacteriological agar and tryptone were purchased from Conda Lab. All other reagents were bought from Sigma-Aldrich, if not stated otherwise.

Nanoparticle synthesis

The 11-nm citrate-coated gold nanoparticles were synthesized by the Frens Turkevich synthesis, as described previously.^[20] 2 mL of an aqueous solution of trisodium citrate (Na₃C, 38.8 mM) were added to 20 mL of gold chloride (HAuCl₄·3H₂O, 1 mM) at 100 °C under stirring. The solution was kept at 100 °C for 10 min or until it turned deep red.

The 150-nm citrate-coated gold nanoparticles were synthesized by seeded growth of 11-nm Au-NPs. Two intermediate size steps were required (32 and 75 nm), as described previously.^[21]

NP characterization

Dynamic light scattering

Dynamic light scattering (DLS) and zeta potential measurements were performed with a Zetasizer Nano ZS (Malvern) with a He/Ne 633 nm laser at 25 °C. For each sample, three independent measurements were performed.

Transmission electron microscopy

Transmission electron microscopy (TEM) samples were prepared by placing one drop of the corresponding Au NP dispersion on the copper grid, blotting the copper grid with a filter paper, and allowing a complete evaporation at room temperature. C-SPIONs were imaged with a JEOL JEM-1210 electron microscope at an operating voltage of 120 kV. About 200 different particles were computed to depict the size distribution and the mean size of gold nanoparticles.

UV-Vis spectroscopy

Gold nanoparticles were sonicated for 10 min in an ultrasound bath. UV-Vis spectra were acquired using a Varian Cary 5000 UV-Vis-NIR spectrophotometer.

Exposure of the Au-NPs to *C. elegans*

Worm growth and exposure

Nematodes were grown on nematode growth medium (NGM) and fed *Escherichia coli* OP50 according to the standard protocol at 20 °C.^[22] Young adult specimens (1-day adults) were treated with 100 µg Au/mL for 24 h in MilliQ water.

Au-NP uptake

Worms were pelleted in a polycarbonate capsule and dried at 60 °C overnight. The sample was diluted with HCl (1%), and the gold content of the resulting solution was determined in duplicate using inductively coupled mass plasma spectrometry with an Agilent 7500ce spectrometer.

Zeta potential measurements

~25 young adult *C. elegans* were introduced in a Zeta potential cuvette filled with MilliQ water. The measurements were performed with a Zetasizer Nano ZS (Malvern) with a He/Ne 633 nm laser at 25 °C. For each sample, three independent measurements were performed.

Scanning electron microscopy–energy-dispersive X-ray spectroscopy analysis

Treated worms were fixed with 4% paraformaldehyde in MilliQ water for 2 h at room temperature, then washed three times with MilliQ water, and concentrated to 100 µL. A sample (20 µL) was transferred to a piece of carbon tape placed on an aluminum stub, and dried at room temperature. SEM-EDX analyses were carried out with a scanning electron microscope (QUANTA FEI 200 FEG-ESEM) equipped with an energy-dispersive X-ray (EDX) system. SEM was used under low-vacuum conditions,

an acceleration voltage of 10 kV, and an electron beam spot of 3.0.

Biodistribution assay

Treated worms were fixed with 4% paraformaldehyde in MilliQ water for 2 h at room temperature, then washed three times with MilliQ water, mounted on a glass slide with aqueous mounting media (Fluoromount®) and observed under the microscope. A Zeiss Axio Observer Optical Microscope in transmission mode was used to detect visible accumulation of Au-NPs inside treated *C. elegans*.

Two-photon luminescence microscopy

A TPLM based on a commercial Leica TCS SP5 confocal system, coupled to a MIRA 900F Ti:Sa laser source (Coherent), was used to acquire the two-photon luminescence of Au-NPs inside *C. elegans*. The femtosecond laser beam was tuned in the near infrared ($\lambda=800$ nm) and focused onto the sample by means of a microscope objective (HCX PL APO 10x/0.40 CS). The epi-collected luminescence signal was acquired in the 400–700 nm range with a hybrid detector (HyDs, Leica). Each image was taken in a 1024×1024 pixel format, and a scanning speed of 200 Hz. Z-stacks were collected in 6.5 µm step size and processed using Image J software. Average power in the sample plane was measured to be 12 mW. No endogenous autofluorescence of the worms was detected. Experiments were repeated with six worms per condition.

Absorbance microspectroscopy

C. elegans were mounted as described above, visualised using an Olympus BX51 microscope and spatially resolved absorbance spectroscopy was performed by fiber-coupling the signal to a spectrometer (Shamrock SR-303i-B with Andor Solis camera: iDus DV401A-BV). The sample, illuminated in bright field geometry, was imaged at the entrance of the optical fiber to reduce the collection area to a 10-µm spot size. Spectra were background subtracted against and normalized with a reference spectrum (the glass slide). The spectra of ten worms per condition were acquired using 1000 s accumulation per triplicate.

Toxicological assays

We assessed survival (lethal endpoint) and brood size (sub-lethal endpoint). In the survival assay, animals were treated in 100 µL MilliQ water (controls) or 100 µg Au/mL (treated worms) in 96-well plates for 24 h. The assay was performed in triplicate. The

plates were tapped and the worms that moved were counted as alive. Each well contained 9 ± 3 young adult worms. To study the brood size, individual untreated or treated young adult worms were transferred to a NGM plate seeded with an OP50 lawn at 20 °C. The number of progeny was scored after 72 h of food resumption. Results are expressed as percentage brood size in respect to the untreated (control) worms. The reprotoxicity assay was performed in triplicate.

Excretion of Au-NPs

After treatment for 24 h, few worms were transferred to an NGM plate with *E. coli* OP50. Excretion of the internalized Au-NPs was monitored up to 12 h after food resumption.

Correlative light electron microscopy (CLEM)

The cellular localization of Au-NPs in *C. elegans* was investigated by using correlated light and electron microscopy (CLEM). Control and treated animals were fixed by high-pressure freezing, flat-embedded in resin, and sectioned following a targeted ultra-microtomy protocol, as described previously.^[19] Imaging analysis was performed with a PHILIPS CM 120 transmission electron microscope.

High angle annular dark field scanning transmission electron microscopy (HAADF STEM)

The as prepared cross-sections of *C. elegans* were also visualized by means of HAADF STEM using the Magellan XHR SEM 400L at 20 kV in STEM mode.

Quantitative PCR

A minimum of 2000 synchronized worms were exposed to 500 µg/ml 11-nm Au-NPs for 24 h in 50% M9 buffer^[23] (treated worms), or without NPs (control worms). Total RNA was extracted using Tri-reagent (Sigma-Aldrich) according to the instructions of the manufacturer. We included an additional preliminary step consisting of 5-min vortexing with equal quantity of glass beads (Sigma). The total concentration of RNA was quantified using a Nanodrop ND1000 spectrometer (Thermo Scientific) and the quality of the RNA was evaluated by 0.8% agarose gel electrophoresis. cDNA was synthesized with 1000 ng of RNA by means of an oligo-dT primer. Quantitative PCR of *elt-2*, *eps-8*, *act-5*, *chc-1* and *dyn-1* was performed using an ABI Prism 7500 FAST platform (Applied BioSystems). All probes were purchased from the Universal ProbeLibrary (Roche) and primers were designed using the Assay Design from Roche (Table S1). Each PCR reaction contained 8.8 µL ROX (Roche), 2 µL cDNA (5 ng/µL), 0.1 µL of probe (10

µM), 0.4 µL of each primer (10 µM), and double-sterilised HPLC water to a final volume of 20 µL. Using standard ABI Prism cycling conditions (2 min at 50 °C, followed by 10 min at 95 °C, and 40 cycles of 15 s at 95 °C and 1 min at 60 °C), C_T (threshold cycle) values were determined. We applied the $\Delta\Delta CT$ method to calculate the fold change in gene expression for each gene. The gene *rla-1* was used as house-keeping gene to normalize gene expression; it encodes for an acidic ribosomal subunit protein P1 previously shown to be remain invariant after metal exposure.^[24] Three biological replicates were analyzed, and four technical repeats were used per sample.

Statistical analysis

Past 3.03 was used for all statistical analyses. For the toxicological assays, statistical significance between control and treated worms was assessed using the Student's t-test. Three levels of statistical significance were considered in all cases: $p < 0.05$ (*), $p < 0.01$ (**), and $p < 0.001$ (***)

Results and discussion

Characterization of the material

The 11-nm citrate-coated gold nanoparticles were synthesized by the Frens Turkevich reaction, as described previously.^[20] The 150-nm citrate-coated gold nanoparticles were obtained by seeded growth (Figure S1).^[21] The citrate coating is present in some commercial colloidal gold formulations.^[25] The two Au-NPs systems were characterized by transmission electron microscopy (TEM), dynamic light scattering (DLS) and UV-Vis spectroscopy. These techniques showed a nominal size for the Au-NPs of 11 ± 1 and 150 ± 17 nm; a hydrodynamic mean diameter of 16 ± 3 and 221 ± 49 nm; a zeta potential of -26.4 and -21.2 mV; and a maximum resonance plasmonic absorption band at 525 and 598 nm, respectively (Figure 2).

C. elegans exposure to the Au-NPs

C. elegans were fed with Au-NPs in aqueous dispersion for 24 h. During feeding, *C. elegans* pumps liquids by rhythmic contractions of the pharynx and subsequently to the lumen of the intestine.^[13a] Au-NPs were introduced gradually through the alimentary system and concentrated there for up to 24 hours. Toxicological effects were evaluated by means of survival and brood size assays. We quantified the ingestion of gold by means of inductively coupled plasma mass spectrometry (ICP-MS) and investigated the interaction between the external surface of

C. elegans, the cuticle, and the Au-NPs using scanning electron microscopy (SEM), energy-dispersive X-ray (EDX) spectroscopy, and zeta potential measurements. The pharyngeal cuticle was studied by TEM, Au-NP biodistribution evaluated by light microscopy (LM), TPLM, and TEM, from lower to higher spatial resolution. Remarkably, TEM investigations allowed us to track NP fate at the cellular and subcellular levels, and to evaluate the crossing of biological barriers at single-NP resolution. Finally, Au-NP optical status was determined by absorbance microspectroscopy on individual worms utilizing a custom-designed setup as described in the Experimental Section.

Toxicity and uptake

The biocompatibility of the material was evaluated by studying two toxicity endpoints, survival and reproductive performance (brood size) in young adults fed orally 0–500 µg/mL Au-NPs. We assessed Au-NPs in the concentration range 0–500 µg/mL and found that 100 µg/mL induced a significant decrease in the survival of 11-nm AuNP treated worms, compared to control animals (Figure S2), hence we selected this concentration to evaluate the effect of Au-NPs in *C. elegans*. Exposure to 100 µg/mL also significantly decreased the reproductive output of organisms treated with the small nanoparticles. Survival and brood size decreases were not statistically significant in the case of the big NPs (Figure 3A). Previous studies on Ag-NPs also reported toxicity for *C. elegans* survival and reproduction at similar metal doses,^[26] while other compositions such as iron oxide were more biocompatible (up to five fold in terms of metal weight).^[27] Similarly, other authors reported that smaller sizes of NPs (≤ 10 nm) were more toxic to *C. elegans* than larger sizes (≥ 50 nm).^[28]

We quantified the uptake of NPs by chemical analysis and found that treated worms ingested 500 times more 11-nm Au-NP than 150-nm ones. However, the gold mass contained in the worm's body was nearly seven times higher in the case of the large NPs due to the bigger volume of the ingested particles. Considering that the gold surface atoms are most reactive, worms treated with the 11-nm Au-NP were exposed to a surface area of ingested NPs double than worms treated with 150-nm Au-NP, which could account for the higher nanotoxicity of the smaller NPs (Figure 3B and Table S2). Studies on other inorganic NPs suggested that smaller particles (up to 10 nm) can

trigger oxidative stress to a greater extent than larger particles, mainly due to their larger surface area.^[28]

In terms of NP uptake per body mass, *C. elegans* ingested $6\text{--}42 \times 10^5$ µg/kg Au-NPs, which corresponds to metal doses 5–6 orders of magnitude above the anticipated human doses. For instance, MesoGold® is a 20-ppm dispersion of 3.2-nm Au-NPs, marketed as mineral supplement to enhance the body's immune system, the recommended adult daily dosage is 4–17 µg/kg. Given that the worm was treated with metal doses exceeding the human doses, these results suggests that the Au-NPs are highly biocompatible. Furthermore, this study emphasises the utility of *C. elegans* as a surrogate animal model as vertebrates could not be treated under these harsh conditions due to ethical concerns; *C. elegans* can thus fill a gap within toxicological evaluations, despite being a simple organism.

Interaction with the external and pharyngeal cuticle

The interaction between the external part of *C. elegans* and Au-NPs was investigated by SEM-EDX (Figure 4). The outer surface of *C. elegans* is covered by an extracellular cuticle, which separates the interior of the body from the environment and acts as an external skeleton.^[13a] The epidermis of invertebrates is the primitive predecessor of skin in humans and all other vertebrate animals, both structurally and functionally. Therefore, the cuticle and epithelia of *C. elegans* has been used as a simplified skin model for NP assessment *in vivo*.^[15] The cuticle comprises five layers, mostly consisting of collagen, lipids, and some glycoproteins (Figure 1A). Structural proteins and lipids are also present in human skin, whereas other components (i.e. keratin or elastin) are specific to mammals.^[13a] The two protective structures possess a negative surface charge, confirmed by a zeta potential of -20.1 mV for the *C. elegans* in MilliQ water. EDX quantitative analysis revealed that Au-NPs did not attach to the external surface of the animal, based on the absence of gold. The negative charge of both the cuticle and the citrate-capped Au-NPs may explain the lack of affinity between them.^[13a] Hence, these results imply that NPs do not enter via the dermal route and indicate that the alimentary tract is the main portal of NP entry into the body of the worm in our experiments. The *C. elegans* cuticle also covers the four major openings of the body to the exterior: the anus, the excretory pore, the vulva and the pharynx. However, unlike previous studies using fluorescent SiO₂-NPs^[29], we did not observe entrance of NPs through other body

openings. The interaction between the pharyngeal cuticle and the Au-NPs was investigated by TEM. Adhesion of Au-NPs to the pharynx was unlikely, as NPs were distributed inside the pharyngeal lumen and did not attach to the cuticle (Figure 4B,C).

Biodistribution

Au-NPs were introduced gradually to the alimentary system and accumulated for up to 24 h in the intestinal lumen. By light microscopy (LM) using transmitted light, the 11-nm Au-NPs were pink inside the intestinal lumen of *C. elegans* while the 150-nm Au-NPs are seen blue, consistent with their absorbance in the UV-Vis (Figure 5B–C and Figure S3). Although the intensity of the color was not homogenous along the body, no appreciable color change occurred inside the *C. elegans*. However, when using reflected light, both 11 and 150-nm Au-NPs appeared redder due to the complex color and scattering effects on the nanoscale depending on the light mode. To obtain a more precise analysis on the optical properties of Au-NPs inside the worm, absorbance microspectroscopy was employed.

Exploiting the luminescent properties of Au-NPs, we performed TPLM studies to analyze the NP uptake in individual worms at different segments of the intestinal tract: pharynx, anterior gut, mid-gut, posterior gut, and rectum (Figure 5A). We segmented the intestinal tract into those five parts since each of them exhibits a different pH value.^[30] Under near-infrared pulsed illumination, Au-NPs luminesce via interband transitions induced by the absorption of two photons. This signal is strongly enhanced when the pulsed illumination spectrally overlap with the localized plasmon resonance of the Au-NP.^[31] TPLM is of particular interest as it can provide a better Au-NP contrast than bright-field or dark-field microscopy, which are often hampered by the endogeneous parasitic scattering of the worms. Furthermore, as multiphoton processes feature a nonlinear dependence on the excitation intensity, TPLM is intrinsically confocal and offers three-dimensional imaging capabilities with improved spatial resolution.

TPLM allows us to visualize Au-NPs in a cellular environment,^[32] with single-particle sensitivity.^[33] This method has been widely used to image functionalized Au-NPs targeting cancer cells *in vitro*^[31e, 34] and Au-NPs distribution in mice *in vivo*,^[33, 35] but rarely to localize Au-NPs inside *C. elegans*.^[1] Here, TPLM images indicated the confinement of Au-

NPs in the *C. elegans* intestine and the absence of Au-NPs outside the intestinal lumen. By scanning the sectioning plane of the TPLM image, TPLM tomography allowed a three-dimensional reconstruction of the entire worms, confirming the absence of Au-NPs adsorbed onto the cuticle and excluding topical entrance of Au-NPs (Figure 5D,E, and Videos S1 and S2). Therefore, the toxicological effects of Au-NPs can only be attributed to the Au-NPs present in the digestive tract of *C. elegans*, and their status (aggregation, surface area, etc.) may play a determining role.

NP localization at the cellular scale

To study the possible crossing of the intestinal barrier by the Au-NPs, their subcellular localization, and their size inside *C. elegans*, we examined ultrathin cross-sections of treated worms by TEM. In all cases, Au-NPs were restricted to the intestinal lumen and preserved their monodispersity (Figure 6B–E). Au-NPs were not internalized by the intestinal cells; we did not visualize NP-containing endosomes, and they remained separated from the microvilli by a peritrophic-like membrane, the glycocalyx, which protects the intestinal cells against foreign materials, mechanical injury, and pathogens. This extracellular electron-lucent coating consists of highly modified glycoproteins, which localizes digestive enzymes and filters the molecules that reach the absorptive surface of the microvilli.^[16e, 36] Borgonie et al. investigated the passage of different molecules through this protective layer and observed only sparse crossing of ferritin molecules, while it allowed passage of fluorescein isothiocyanate, methyl red, neutral red, and acridine orange.^[16d] High-angle annular dark-field scanning transmission electron microscopy (HAADF STEM) of animal cross-sections confirmed the absence of NP endocytosis and translocation, as Au-NPs were only visualized in the lumen (Figure S4).

Endocytosis or translocation to secondary organs in *C. elegans* have been reported for oxide nanoparticles such as citrate-capped 6-nm Fe₂O₃-NPs^[37] 50-nm SiO₂-NPs,^[29b] and carbon nanomaterials including graphene oxide,^[38] bioconjugated nanodiamonds,^[39] or carbon nanotubes.^[40] Also, endocytic trafficking of metal NPs consisting on citrate-capped 7-nm Ag-NPs^[41] and 4-nm Au-NPs^[42] has been documented. We tracked Au-NPs of two different sizes by a range of techniques and in all cases concluded that no endocytosis occurred within the 24 h incubation period. The absence of internalization of NPs by the

intestinal cells of *C. elegans* could be attributed to the lower transcytotic capacity of the *C. elegans* intestine compared to that of vertebrates. Recent studies in mammals have revealed that the Microfold cells (or M cells) present in the intestinal barrier, which lack the glycocalyx covering and have a poorly organized brush border, are necessary for the absorption of NPs that are administered orally (Figure S5).^[43] While little translocation occurs through the enterocytes, especially for negatively charged particles, the coexistence of enterocytes and M cells can increase NP absorption by up to 50-fold.^[8, 44] The absence of M cells in *C. elegans* could explain the deficiency of Au-NP translocation. To support the lack of endocytosis of Au-NPs, we assessed molecular markers of endocytosis (*chc-1*, *dyn-1*, *eps-8*) and intestinal barrier integrity (*eps-8*, *act-5*, *elt-2*) by qPCR (Figure 7), genes previously reported to be affected by 4-nm Au-NP treatment in *C. elegans*.^[42] To validate the qPCR integrity of total RNA/cDNA, positive controls included two metal-responsive transcripts (*mtl-1*, *ftn-1*). We found no significant alteration in the gene expression patterns of the above mentioned endocytosis and intestine markers between control and treated worms, except for *act-5* (actin). The expression of *act-5* is limited to intestinal tissue and is essential for microvilli formation. It is conceivable that the down-regulation of *act-5* may be induced by the presence of Au-NP in the intestine, close to the microvilli. By contrast, the expression of *elt-2*, the dominant transcription factor controlling differentiation and function of the *C. elegans* intestine, was not significantly affected by NP treatment.^[45] The lack of endocytosis observed by TEM is supported by the basal expression of *dyn-1* (dynamin), involved in the early stages of endocytosis; *chc-1* (chlatrin), involved in vesicle formation during endocytic transit; and *eps-8*, located at the microvilli tips and associated with endocytosis. Based on the TEM images, no size decrease of the NP core was observed, which confirms that gold NPs are neither degraded nor digested in the intestinal microenvironment of *C. elegans*, at least within the first 24 h (Figure 6F,G). Other NPs such as iron oxide NPs or quantum dots are metabolized inside the *C. elegans* intestine and suffer size decrease or structural collapse.^[27b, 46] The unchanged size of the Au-NPs also indicates that both sizes of NPs passed unaffected through the grinder, suggesting that this pharyngeal structure is only able to damage biological entities such as bacteria but not inorganic materials,

which supports previous results obtained with 3- μ m latex beads.^[47]

The monodispersity of the Au-NPs inside *C. elegans* and the absence of necking between them suggest that the citrate coating was preserved inside the *C. elegans*, which hence indicates a strong electrostatic interaction between the metallic core of the NP and the surfactant. *In vitro* evaluation of Au-NPs in simulated *C. elegans* intestinal conditions confirmed those results. We mimicked the intestinal *C. elegans* microenvironment by incubating the Au-NPs for 24 h at pH 4.6 with and without 10% fetal bovine serum (FBS). DLS measurements showed that Au-NPs aggregated under the simulated conditions ranging from an initial hydrodynamic mean size of 10 \pm 2 nm to 900 \pm 300 nm. In contrast, Au-NP aggregation was comparatively less (180 \pm 60 nm) when FBS was incorporated into the system. UV-Vis spectroscopy revealed a 59-nm red-shift of the maximum absorbance peak when Au-NPs were incubated without protein, and a mere 6-nm peak shift when FBS was added. TEM analysis further confirmed the degree of aggregation suggested by DLS and UV-Vis (Figure S6). This *in vitro* study validates our hypothesis that the pH of the specific region of the intestine and the biomolecules present (i.e., proteins) enhance the stability of the Au-NPs and prevent the formation of large aggregates, as observed *in vivo* in the *C. elegans* intestine.

NP status inside *C. elegans*

Au-NPs have a strong tendency to form large aggregates, especially when they are exposed to highly ionic media. We wanted to evaluate the behaviour of citrate-capped Au-NPs *in vivo* in a multicellular biological environment (taking into account ionic strength, pH, space constriction, etc.) and to determine the resulting effects on the material. NP aggregation inside *C. elegans* was monitored by absorbance microspectroscopy measurements along the body of treated worms, in particular at the grinder, the anterior, central and posterior parts of the gut, and the rectum. Aggregation induces a coupling of the gold nanoparticle's plasmon resonance modes, which results in a red shift and broadening of the plasmon resonance.^[48] By using a home-made setup consisting of a UV-Vis spectrometer coupled to an optical microscope, we were able to acquire spectra of the Au-NPs in the targeted areas of individual *C. elegans* with 10- μ m precision. At least ten worms per

condition were analyzed and the mean spectrum for each part of the worm is plotted (Figure 8A).

Plasmon resonance peak shifts were used to evaluate the aggregation level of the Au-NPs when confined in the different anatomical regions. Interparticle distance changed according to the physioanatomical properties and pH of the different areas of the intestinal tract, inducing specific degrees of aggregation in each region (Figure 8B and Table S3). In all cases we observed a broadening of the absorption band and a red-shift of the peak maxima. No Au-NPs were detected by spectroscopy in the reproductive organs.

In the grinder, the 150-nm Au-NPs displayed the highest peak shift, due to the space constriction of the pharyngeal lumen at this specific structure. The grinder is made up of three pairs of muscle cells that rotate when the muscles contract and act as "teeth" that break up food.^[13a] When closed, the pharyngeal lumen is constrained to a diameter of only a few hundred nanometers. In the grinder, the 11-nm Au-NPs mediated peak shift was three times smaller than the 150-nm Au-NP. In the anterior intestine, the peak shift was small with both Au-NP, which confirms that Au-NPs can redisperse when the width of the intestinal lumen increases, returning to a lower degree of confinement. In this region, the presence of other biomolecules can result in the formation of a protein corona that may enhance the stability of the NPs,^[13a] a notion which warrants further investigations but is not within the scope of this work. Remarkably, the aggregation of Au-NPs is not irreversible, but associated with their temporary environment.

After 24 h of feeding, a significant amount of Au-NPs accumulated in the posterior region of the gut, promoting low interparticle distance as the space narrowed, which resulted in a red-shift corresponding to ca. 5% of the initial peak position with both Au-NPs. LM and TPLM studies showed that both NPs exhibited similar behavior in this region, which we believe is due to the mechanical pumping mechanism that governs the intestinal transit in *C. elegans* rather than to the Au-NPs' properties.

The effect of the pH on NP status should also be considered (Figure 5A). While the pH in the most anterior region of the gut is close to 6, it decreases to ca. 3.5 in the posterior part^[30] *In vitro* experiments showed that the combination of acidic pH and ionic strength of the citrate buffer pH 4.6 promoted the aggregation and precipitation of the Au-NPs (Figure S5). Therefore, these conditions can act against the

stability of the Au-NPs in the final part of the alimentary system.

In the rectal region, the presence of both Au-NPs was sparse, which was likely due to the absence of food and thus reduced intestinal activity. However, when worms were transferred to a bacterial lawn and feeding commenced, the intestinal NPs were rapidly excreted in the form of micrometric ejections which were identical in colour as observed inside the worm. The appearance of such ejections suggests that NPs were mixed with the intestinal content of the worm, typically food debris and endogenous secretions (Figure 9), and suggests that the size of the Au-NPs did not change. After 2 h of food consumption, Au-NPs were no longer observed inside treated *C. elegans*.

Conclusions

By employing a combination of microscopy techniques (light microscopy, two-photon luminescence microscopy, and electron microscopy), chemical analysis, absorbance micro-spectroscopy and key life cycle endpoints, we were able to screen the biodistribution of 11-nm and 150-nm citrate-capped gold nanoparticles in the model organism *Caenorhabditis elegans* at several levels, from organ down to subcellular resolution. We confirm that the nanoparticles did not cross the intestinal and dermal barriers, based on the absence of endocytosis and adsorption, respectively. In contrast from previous reports of other comparable sizes' metal nanoparticles.^[41-42] Moreover, our findings indicate that the AuNP status *in vivo* are influenced by the physiological properties and the anatomical structure of this model organism, in particular increasing the degree of aggregation and changing their optical properties inside the intestinal lumen where both acidic pH and the presence of biomolecules play an essential role. Quantitative PCR of *elt-2*, *eps-8*, *act-5*, *chc-*, *dyn-1*, markers of endocytosis and intestinal barrier integrity did not indicate any alteration in their expression levels compared to untreated worms.

This study highlights how *C. elegans* can advance our understanding of meaningful nano/bio interactions at different biological scales, from small animal down to cells. Here, we discern the effects of different gold nanoparticle sizes with potential applications as biocompatible nanomedicine products and safe cosmetics. This information is of particular relevance for the cosmetic, food, and pharmaceutical industries, as strict regulatory (and financial) guidelines restrict

their use of animals, especially during drug discovery and initial screening stages.

Acknowledgements

This research was partially funded by the Spanish Ministry of Economy (MAT2015-64442-R, Ramon y Cajal program (AL, RyC-2010-06082), FPU program (LGM, FPU12/05549), Severo Ochoa Program (SEV-2015-0496) co-funded by European Social Funds), the Generalitat de Catalunya (2014SGR213), People Program of the European Commission (grant agreement no. 303630, co-funded by the European Social Fund), the Christian Boulin fellowship 2015 from EMBL (LGM), the COST Actions HINT (Action No. MP1202), and GENIE (Action No. BM1408-A). We acknowledge Victor Fuentes for his collaboration in the synthesis of gold nanoparticles.

References

- [1] J. S. Donner, S. A. Thompson, C. Alonso-Ortega, J. Morales, L. G. Rico, S. I. C. O. Santos, R. Quidant, *Acs Nano* **2013**, *7*, 8666-8672.
- [2] M. Guix, C. Carbonell, J. Comenge, L. García-Fernández, A. Alarcón, E. Casals, *Contributions to sci.* **2010**, 213-217.
- [3] S. Kokura, O. Handa, T. Takagi, T. Ishikawa, Y. Naito, T. Yoshikawa, *Nanomedicine-Nanotechnology Biology and Medicine* **2010**, *6*, 570-574.
- [4] B. Gulson, M. McCall, M. Korsch, L. Gomez, P. Casey, Y. Oytam, A. Taylor, M. McCulloch, J. Trotter, L. Kinsley, G. Greenoak, *Toxicological Sciences* **2010**, *118*, 140-149.
- [5] a)X. Huang, M. A. El-Sayed, *Journal of Advanced Research* **2010**, *1*, 13-28; b)P. K. Jain, K. S. Lee, I. H. El-Sayed, M. A. El-Sayed, *The Journal of Physical Chemistry B* **2006**, *110*, 7238-7248.
- [6] O. E. C. D. Organization for Economic Co-operation and Development, in *Series on the Safety of Manufactured Nanomaterials. No. 27*, **2010**.
- [7] M. Bednarski, M. Dudek, J. Knutelska, L. Nowiński, J. Sapa, M. Zygmunt, G. Nowak, M. Luty-Błocho, M. Wojnicki, K. Fitzner, M. Tęšiorowski, *Pharmacological Reports* **2015**, *67*, 405-409.
- [8] J. F. Hillyer, R. M. Albrecht, *Journal of pharmaceutical sciences* **2001**, *90*, 1927-1936.
- [9] A. N. Kharlamov, A. E. Tyurnina, V. S. Veselova, O. P. Kovtun, V. Y. Shur, J. L. Gabinsky, *Nanoscale* **2015**, *7*, 8003-8015.
- [10] M. E. Vance, T. Kuiken, E. P. Vejerano, S. P. McGinnis, M. F. Hochella, D. Rejeski, M. S. Hull, *Beilstein Journal of Nanotechnology* **2015**, *6*, 1769-1780.
- [11] J. Suhag, H. Dureja, *Skinmed* **2015**, *13*, 191-194.
- [12] a)L. P. O'Reilly, C. J. Luke, D. H. Perlmutter, G. A. Silverman, S. C. Pak, *Advanced Drug Delivery Reviews* **2014**, *69-70*, 247-253; b)P. M. Valencia, O. C. Farokhzad, R. Karnik, R. Langer, *Nature Nanotechnology* **2012**, *7*, 623-629.
- [13] a)D. H. Hall, Z. F. Altun, *C. elegans atlas*, Cold Spring Harbor Laboratory Press, Cold Spring Harbor, N.Y., **2008**; b)D. L. Riddle, T. Blumenthal, B. J. Meyer, J. R. Priess, *C. elegans II*, Cold Spring Harbor Laboratory Press, Cold Spring Harbor NY, **1997**.
- [14] L. Gonzalez-Moragas, A. Roig, A. Laromaine, *Adv Colloid Interface Sci* **2015**, *219*, 10-26.
- [15] a)A. D. Chisholm, T. I. Hsiao, *Wiley interdisciplinary reviews. Developmental biology* **2012**, *1*, 861-878; b)A. D. Chisholm, S. Xu, *Wiley interdisciplinary reviews. Developmental biology* **2012**, *1*, 879-902.
- [16] a)O. Bossinger, M. Hoffmann, in *Current Frontiers and Perspectives in Cell Biology* (Ed.: S. Najman), **2012**; b)H. J. A. Egberts, J. Koninkx, J. E. Vandijk, J. Mouwen, *Veterinary Quarterly* **1984**, *6*, 186-199; c)J. Maury, C. Nicoletti, L. Guzzochambraud, S. Maroux, *European Journal of Biochemistry* **1995**, *228*, 323-331; d)G. Borgonie, M. Claeys, J. Vanfleteren, D. Dewaele, A. Coomans, *Fundamental and Applied Nematology* **1995**, *18*, 227-233; e)M. J. Lehane, *Annual Review of Entomology* **1997**, *42*, 525-550.
- [17] a)K. M. Balla, E. R. Troemel, *Cellular Microbiology* **2013**, *15*, 1313-1322; b)K. Sato, A. Norris, M. Sato, B. D. Grant, *WormBook : the online review of C. elegans biology* **2014**, 1-47; c)L. Wang, A. Audhya, *Methods* **2014**, *68*, 518-528.
- [18] Y. Zhao, Q. Wu, Y. Li, D. Wang, *Rsc Advances* **2013**, *3*, 5741-5757.
- [19] I. Kolotuev, D. J. Bumbarger, M. Labouesse, Y. Schwab, *Methods in cell biology* **2012**, *111*, 203-222.
- [20] a)J. Turkevich, P. C. Stevenson, J. Hillier, *Discussions of the Faraday Society* **1951**, *11*, 55-75; b)G. Frens, *Nature Physical Science* **1973**, *241*, 20-22.
- [21] C. Ziegler, A. Eychmüller, *The Journal of Physical Chemistry C* **2011**, *115*, 4502-4506.
- [22] S. Brenner, *Genetics* **1974**, *77*, 71-94.
- [23] D. R. Hitchcock, S. E. Law, J. Wu, P. L. Williams, *Archives of environmental contamination and toxicology* **1998**, *34*, 259-264.
- [24] a)S. C. Swain, K. Keusekotten, R. Baumeister, S. R. Sturzenbaum, *Journal of molecular biology* **2004**, *341*, 951-959; b)S. Swain, J. F. Wren, S. R. Sturzenbaum, P. Kille, A. J. Morgan, T. Jager, M. J. Jonker, P. K. Hankard, C. Svendsen, J. Owen, B. A. Hedley, M. Blaxter, D. J. Spurgeon, *BMC systems biology* **2010**, *4*, 32.

- [25] a)B. Sharma, A. Sharma, *International Journal of Pharmacy and Pharmaceutical Sciences* **2012**, *4*, 57-66; b)J.-h. Kim, C.-O. Hong, Y.-c. Koo, H.-D. Choi, K.-W. Lee, *Biological & Pharmaceutical Bulletin* **2012**, *35*, 260-264.
- [26] S. W. Kim, S. H. Nam, Y. J. An, *Ecotoxicol Environ Saf* **2012**, *77*, 64-70.
- [27] a)Q. Wu, Y. Li, M. Tang, D. Wang, *Plos One* **2012**, *7*, e43729; b)L. Gonzalez-Moragas, S.-M. Yu, E. Carenza, A. Laromaine, A. Roig, *ACS Biomaterials Science & Engineering* **2015**, *1*, 1129-1138.
- [28] a)Q. Wu, W. Wang, Y. Li, Y. Li, B. Ye, M. Tang, D. Wang, *Journal of hazardous materials* **2012**, *243*, 161-168; b)S. Gupta, T. Kushwah, A. Vishwakarma, S. Yadav, *Nanoscale Research Letters* **2015**, *10*.
- [29] a)A. Scharf, A. Piechulek, A. von Mikecz, *Acs Nano* **2013**, *7*, 10695-10703; b)A. Pluskota, E. Horzowski, O. Bossinger, A. von Mikecz, *PLoS ONE* **2009**, *4*, e6622.
- [30] V. M. Chauhan, G. Orsi, A. Brown, D. I. Pritchard, J. W. Aylott, *Acs Nano* **2013**, *7*, 5577-5587.
- [31] a)M. R. Beversluis, A. Bouhelier, L. Novotny, *Physical Review B* **2003**, *68*; b)P. Ghenuche, S. Cherukulappurath, T. H. Taminiau, N. F. van Hulst, R. Quidant, *Physical Review Letters* **2008**, *101*; c)J. P. Wilcoxon, J. E. Martin, F. Parsapour, B. Wiedenman, D. F. Kelley, *Journal of Chemical Physics* **1998**, *108*, 9137-9143; d)M. B. Mohamed, V. Volkov, S. Link, M. A. El-Sayed, *Chemical Physics Letters* **2000**, *317*, 517-523; e)N. Gao, Y. Chen, L. Li, Z. Guan, T. Zhao, N. Zhou, P. Yuan, S. Q. Yao, Q.-H. Xu, *Journal of Physical Chemistry C* **2014**, *118*, 13904-13911.
- [32] D. Yelin, D. Oron, S. Thiberge, E. Moses, Y. Silberberg, *Optics Express* **2003**, *11*, 1385-1391.
- [33] H. F. Wang, T. B. Huff, D. A. Zweifel, W. He, P. S. Low, A. Wei, J. X. Cheng, *Proceedings of the National Academy of Sciences of the United States of America* **2005**, *102*, 15752-15756.
- [34] N. J. Durr, T. Larson, D. K. Smith, B. A. Korgel, K. Sokolov, A. Ben-Yakar, *Nano Lett.* **2007**, *7*, 941-945.
- [35] J. Park, A. Estrada, K. Sharp, K. Sang, J. A. Schwartz, D. K. Smith, C. Coleman, J. D. Payne, B. A. Korgel, A. K. Dunn, J. W. Tunnell, *Optics Express* **2008**, *16*, 1590-1599.
- [36] J. D. McGhee, *Wiley Interdiscip Rev Dev Biol* **2013**, *2*, 347-367.
- [37] L. Gonzalez-Moragas, S.-M. Yu, A. Laromaine, A. Roig, **2015**.
- [38] Q. Wu, L. Yin, X. Li, M. Tang, T. Zhang, D. Wang, *Nanoscale* **2013**, *5*, 9934-9943.
- [39] N. Mohan, C.-S. Chen, H.-H. Hsieh, Y.-C. Wu, H.-C. Chang, *Nano Letters* **2010**, *10*, 3692-3699.
- [40] Q. Wu, Y. Li, Y. Li, Y. Zhao, L. Ge, H. Wang, D. Wang, *Nanoscale* **2013**, *5*, 11166-11178.
- [41] J. N. Meyer, C. A. Lord, X. Y. Yang, E. A. Turner, A. R. Badireddy, S. M. Marinakos, A. Chilkoti, M. R. Wiesner, M. Auffan, *Aquatic Toxicology* **2010**, *100*, 140-150.
- [42] O. V. Tsyusko, J. M. Unrine, D. Spurgeon, E. Blalock, D. Starnes, M. Tseng, G. Joice, P. M. Bertsch, *Environmental science & technology* **2012**, *46*, 4115-4124.
- [43] L. Kou, J. Sun, Y. Zhai, Z. He, *Asian Journal of Pharmaceutical Sciences* **2013**, *8*, 1-10.
- [44] E. Frohlich, E. Roblegg, *Toxicology* **2012**, *291*, 10-17.
- [45] a)J. D. McGhee, M. C. Sleumer, M. Bilenky, K. Wong, S. J. McKay, B. Goszczynski, H. Tian, N. D. Krich, J. Khattra, R. A. Holt, D. L. Baillie, Y. Kohara, M. A. Marra, S. J. Jones, D. G. Moerman, A. G. Robertson, *Dev Biol* **2007**, *302*, 627-645; b)J. D. McGhee, T. Fukushige, M. W. Krause, S. E. Minnema, B. Goszczynski, J. Gaudet, Y. Kohara, O. Bossinger, Y. Zhao, J. Khattra, M. Hirst, S. J. Jones, M. A. Marra, P. Ruzanov, A. Warner, R. Zapf, D. G. Moerman, J. M. Kalb, *Dev Biol* **2009**, *327*, 551-565.
- [46] Y. Qu, W. Li, Y. Zhou, X. Liu, L. Zhang, L. Wang, Y.-f. Li, A. Iida, Z. Tang, Y. Zhao, Z. Chai, C. Chen, *Nano Letters* **2011**, *11*, 3174-3183.
- [47] C. Fang-Yen, L. Avery, A. D. T. Samuel, *Proceedings of the National Academy of Sciences* **2009**, *106*, 20093-20096.
- [48] K. H. Su, Q. H. Wei, X. Zhang, J. J. Mock, D. R. Smith, S. Schultz, *Nano Letters* **2003**, *3*, 1087-1090.

Figures and Tables

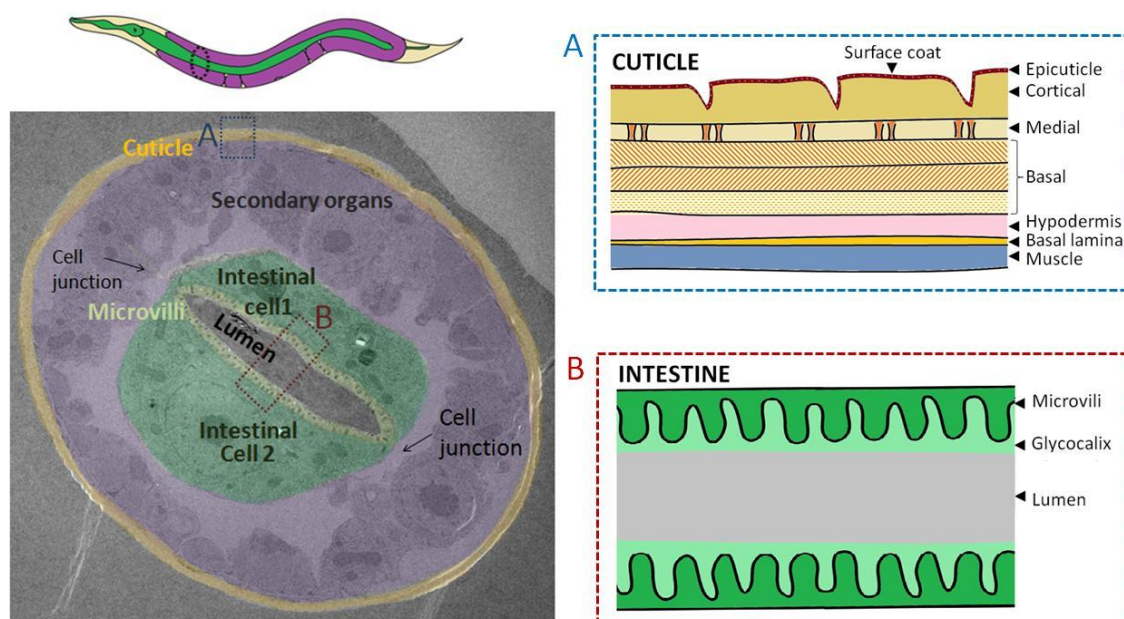


Figure 1. The anatomy of *C. elegans*: the alimentary system, the cuticle, and secondary organs, including the reproductive system. Left panel shows a modified TEM image of a *C. elegans* cross-section, as depicted in the schematic drawing above. Right panel shows a magnification of the (A) cuticle and (B) intestine, detailing their parts.

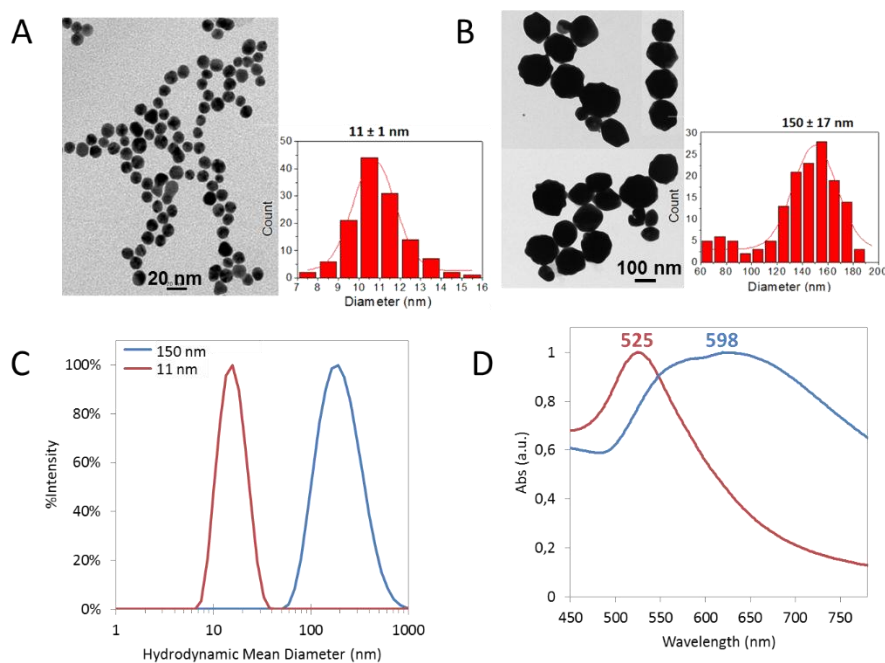


Figure 2. Characterization of small and large Au-NPs. (A) TEM images and size distribution of 11-nm Au-NPs. (B) TEM images and size distribution of 150-nm Au-NPs. (C) DLS. (D) UV-Vis spectroscopy.

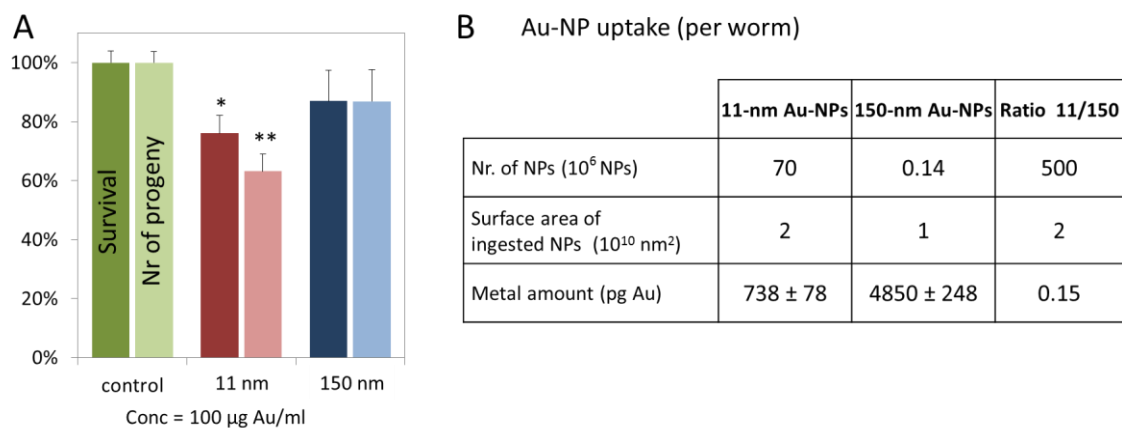


Figure 3. A) Survival (bold colors) and number of progeny (pale colors) evaluations for 100 µg/mL of 11 and 150-nm Au-NPs. Significant differences are only found for the 11-nm Au-NP. B) Au-NP uptake by chemical analysis. Results are indicated as number of nanoparticles per worm, surface area of ingested NPs, and gold mass. Legend: * $p < 0.05$ ** $p < 0.001$ *** $p < 0.005$.

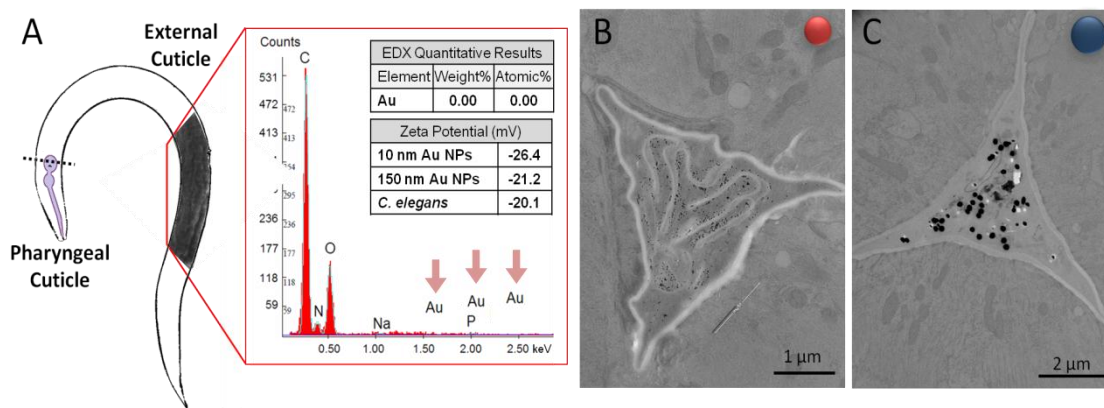


Figure 4. (A) Representative SEM-EDX analysis of the interaction between the external cuticle and Au-NP. After extensive washing of the worms with MQ water, no traces of gold are detected on the outer surface of *C. elegans*. (B,C) TEM images showing the interaction between the pharyngeal cuticle and 11- (red sphere) or 150-nm Au-NPs (blue sphere).

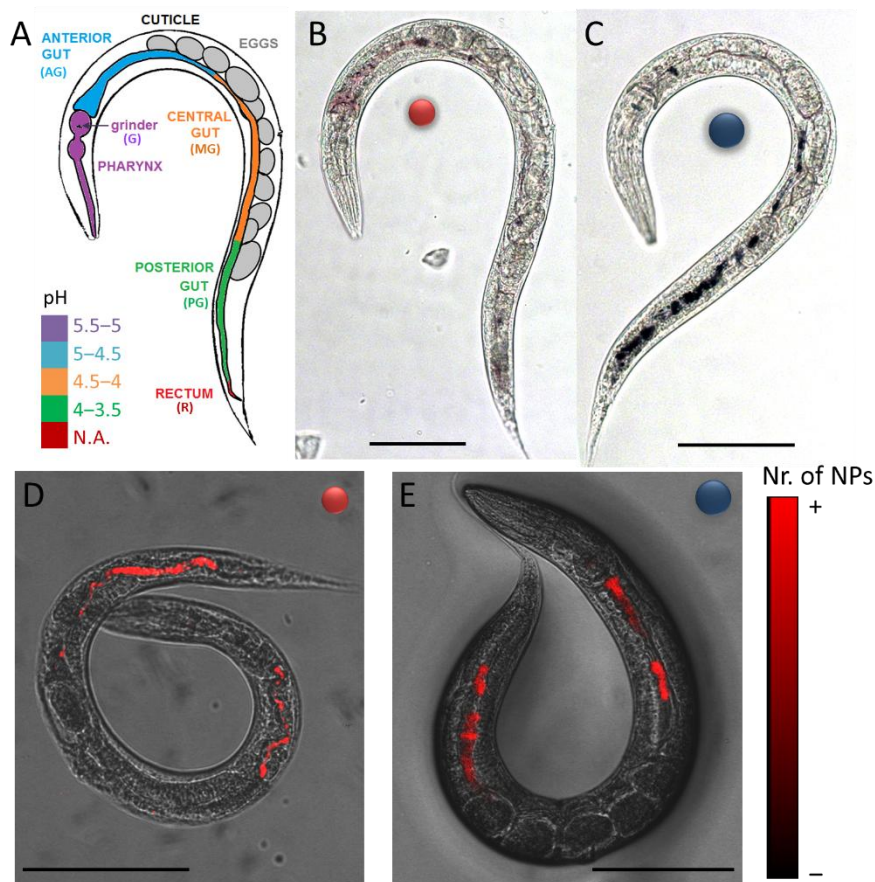


Figure 5. Panel A shows a schematic drawing of the anatomical parts under evaluation. The intestinal tract was segmented into five parts, depicted with various colors according to their pH: pharynx, which contains the specialized cuticle named grinder; the anterior part of the gut, mid part, the posterior part, and the rectum. Panels B and C are optical microscopy images of (B) 11-nm and (C) 150-nm Au-NP treated worms. 11-nm Au-NP appear pink, and 150-nm Au-NP appear blue. Panels D and E are TPLM images of (D) 11-nm and (E) 150-nm Au-NP treated worms, highlighting the areas with higher accumulation of nanoparticles. Scale bars correspond to 100 μm .

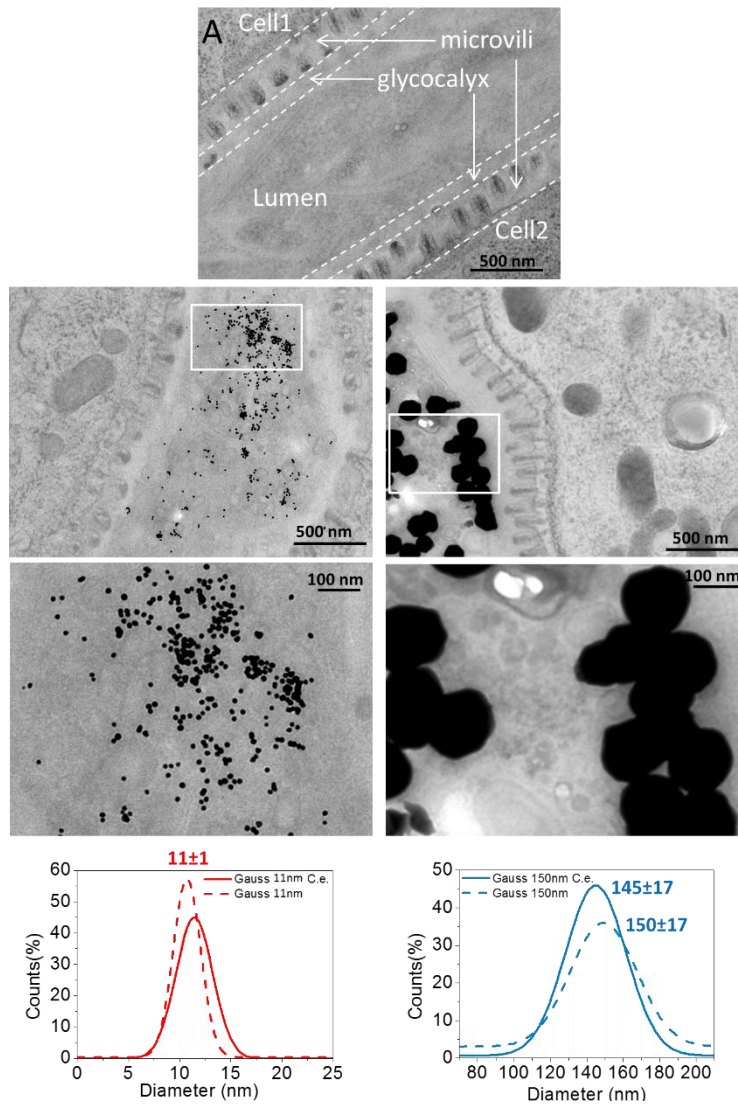


Figure 6. TEM sections of the anterior part of the intestine of control nematodes (A) and nematodes treated with 11-nm (B) and 150-nm GNPs (C). Images at higher magnification of 11-nm Au-NPs (D) and 150-nm Au-NPs (E). TEM size distributions of 11-nm Au-NPs as synthesized (dotted lines) and inside *C. elegans* (solid lines) (F) and 150-nm Au-NPs (G).

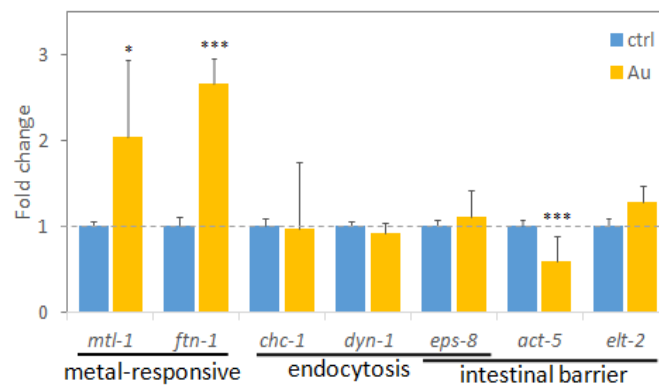


Figure 7. Gene expression fold change of metal-responsive genes (*mtl-1*, *mtl-2*, *ftn-1*, *ftn-2*), endocytosis genes (*chc-1*, *dyn-1*, *eps-8*) and intestinal barrier integrity genes (*eps-8*, *act-5*, *elt-2*) in unexposed worms and 11-nm Au-NP exposed worms

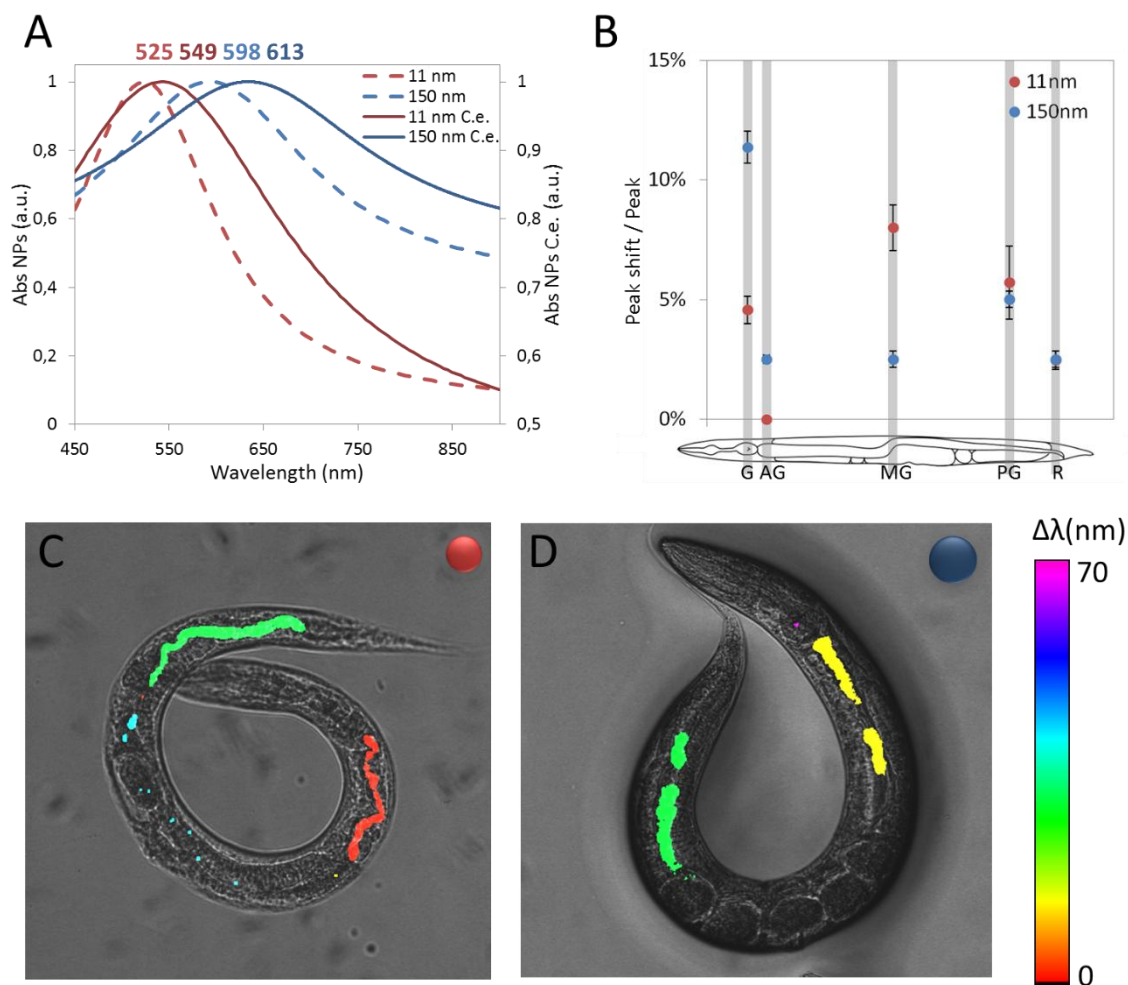


Figure 8. A) Absorbance spectroscopy of Au-NPs as-synthesized (in water) and inside *C. elegans*. The absorbance spectra of the Au-NPs inside *C. elegans* is expressed as the mean of the different anatomical areas analysed. B) Relative peak shift of the Au-NP in the different anatomical areas (G: Grinder. AG: Anterior gut. MG: Mid-gut. PG: posterior gut. R: rectum). C–D) Absolute peak shift of the (C) 11-nm and (D) 150-nm Au-NP in the different anatomical areas (generated by merging LM and TPLM images).

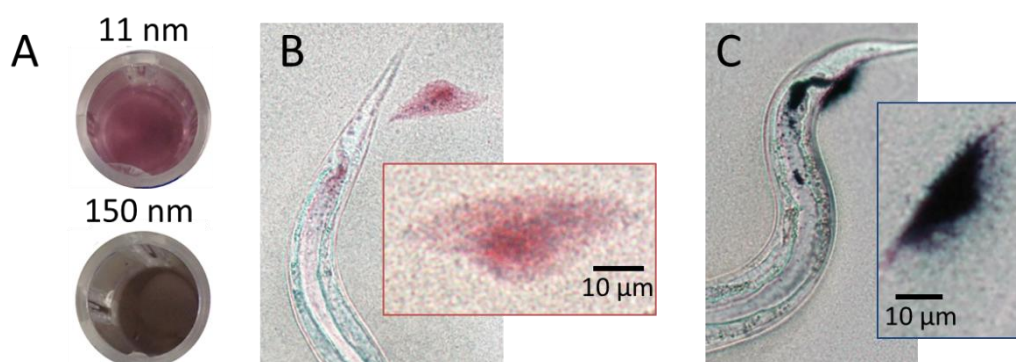


Figure 9. Excretion of Au-NPs onto the bacterial lawn when food is reintroduced. A) Colors of 11 and 150-nm Au-NPs at 100 $\mu\text{g}/\text{mL}$ (500 μL) in a 24-well plate. 11-nm Au-NPs are pink and 150-nm brownish in color. B–C) NP ejections after Au-NP-treated *C. elegans* are transferred to plates containing food. Au-NPs maintain the color observed inside the worms (B–C). The appearance of the ejections suggests that NPs are mixed with organic contents inside the intestine of *C. elegans*.

